Adolf W. Lohmann

Optical Information Processing

Optical Information Processing

Adolf W. Lohmann

Edited by Stefan Sinzinger

Universitätsverlag Ilmenau
2006

Impressum

Bibliographische Information der Deutschen Bibliothek
Die Deutsche Bibliothek verzeichnet diese Publikation in der Deutschen Nationalbibliographie; detaillierte bibliographische Angaben sind im Internet über http://dnb.ddb.de abrufbar.

Technische Universität Ilmenau – Universitätsbibliothek
Universitätsverlag Ilmenau
Langewiesener Str. 37
D-98693 Ilmenau/Thür.
http://www.tu-ilmenau.de/universitaetsverlag

Herstellung und Auslieferung
Verlagshaus Monsenstein und Vannerdat OHG
Am Hawerkamp 31
D-48155 Münster/Westf.
http://www.mv-verlag.de

ISBN 3-939473-00-6
1. Auflage 2006

The future cannot be predicted,
but futures can be invented.
Dennis Gabor, 1963

Contents

Preface to the 2006 edition

The idea to prepare a new edition of Adolf Lohmann's lecture notes came about a long time ago. Then the motivation mainly was to improve the handling. Due to the lack of an index and a comprehensive table of content it was quite difficult to find specific topics in those notes. Nevertheless, due to Adolf Lohmann's unique style of writing and presentation I could never do without the booklet with the "color of cognac" (third edition). Especially ever since I needed to prepare lectures on various fields of optics and information theory I have been using this booklet very frequently and always wanted to recommend it to the students for further studies. The more I was reading in the booklet, the more I was amazed about the numerous innovative ideas and visionary statements on future developments. These lecture notes, even nowadays, i.e. almost 40 years after the first edition has been published, are a treasure chest for students, teachers as well as researchers in the field of optics.

Being aware of the amount of work involved in re-editing the booklet, I always hesitated to accept the challenge. Early last year I realized that Adolf Lohmann's 80th birthday was approaching in 2006. Would not this be a good time to honour the great scientist and inspiring teacher by publishing a new edition with the additional motivation to make these excellent lecture notes accessible to new generations of optics-students and researchers? First attempts to scan the pages and use character recognition software to get it into a word processor were by far not satisfying. I hear Adolf Lohmann saying "why don't you use an *optical* pattern recognition system?". It became necessary to typeset everything anew. Now the question was how to typeset the new edition while maintaining the unique style of Adolf Lohmann. The compromise was to typeset all mathematical formulas, reinforce the format of chapters and sections while leaving the text body as well as the drawings, even though with some figure captions added, in their original form.

I would like to acknowledge the help of my secretary Martina Klein, not only for typing all the text body of the book but also for unconsciously maintaining the psychological pressure on me to typeset the formulas and finish the layout. Furthermore I am grateful to the Optical Scociety of America for the permission to reprint some of the papers refered to in the notes (see Appendix).

"Refraction is pretty much the same as what you experience when your left car wheel goes on ice."

This is one of the statements in Adolf Lohmanns lecture notes (see page: 356) which may help to illustrate his unique style of teaching. Other examples are the sections where he elaborates on the use of **nylon stockings** in portrait photography (page 290), the question on

"how many dB has a lens?" (page 264) or the similarity between mathematical calculations without visualization and **coffee grinding** (page 147).

These examples also illustrate that any attempt to edit the book in the sense of changing or adding sections would have been doomed to failure. Thus we exclusively focussed on reformatting and crosslinking the formulas, figures and chapters. As a consequence even sections which from a technical point of view might seem obsolete by now, like e.g. the section on the calculation of a Fourier transform by digital computers (Sec. 11.7), have been left unchanged since they certainly help to maintain the overall picture. I am convinced that precisely these sections are contributing significantly to the enjoyment of reading these lecture notes.

Obviousely science has made enormous progress since the first edition of theses lecture notes has been published. A significant portion of this progress is due to Adolf Lohmann himself. The list of his publications by now extends to more than 350 entries. The invention, among many others, which maybe is related closest to his name became famous as **Computer Holography**. It is, in fact, one of the milestones which mark the beginning of the success story of **diffractive optics**. As a matter of fact recent developments which led to the application of diffractive optical elements in photographic lenses show that this is still a very active area of research. It is my impression that Adolf Lohmann himself did not really consider Computer Holography his most important invention (which, by the way, might be a *necessary* but certainly not a *sufficient* condition for an invention to become famous with!). Consequently Computer Holography never made it into his lecture notes. I would therefore like to refer readers interested in the field of "Computer-Generated Holography" to an overview paper published by W. J. Dallas and Adolf Lohmann in the "Encyclopedia of Modern Optics", B. Guenther, D. Steel (Eds), Elsevier (2005). After having worked through the lecture notes you will certainly have no problems understanding this article.

Finally let me express my hope that this new edition of the lecture notes provides enjoyment to the huge family of Lohmann students around the world. However I also hope that it helps to transport some of the fascination of Humboldt's ideal of the combination of (interdisciplinary) research and academic teaching to todays generation of students as well as (university) teachers.

Thank you, Adolf Lohmann, and all the best to you and your wife, Carla, for many years to come.

Stefan Sinzinger Ilmenau, March 2006

Preface to the third edition

The third edition combines the formerly two volumes of the lecture notes on “Optical Information Processing”. These notes were written in 1967-71 for a two-semester course 205 A,B in the Department of Applied Physics and Information Science at the University of California in La Jolla. Course participants were seniors and first year graduate students in physics, electrical engineering and computer science.

The third edition is merely a polished version of the first edition, which came out 15 years ago. Why should anyone wish to buy this book? For two reasons: This book is unconventional, sometimes in the selection of topics, sometimes in the style of presentation, and overall in its aims, which are: teaching how to do optics and showing that optics is to a large degree an “information science”.

A second reason might be an interest in optical computing. That is the topic I am persuing right now, in research and in teaching. I intend to publish lecture notes on optical computing. In those new lecture notes this book on “Optical Information Processing” will be referenced frequently.

The first edition contained also reprints of some publications, as listed in the two separate tables of content for the two volumes. These publications are not reprinted here in order to keep the book compact. There are three exceptions, however, because those papers are not easily available in a normal library: “Electron Acceleration by Light Waves”, Vol. I, p. 98; “A New Fourier Spectrometer”, Vol. I, p. 111; and “The Space Bandwidth Product, Applied to Spatial Filtering and to Holography”, Vol. II, p. 90.

The cited publications, reprinted here or not, are not necessary for following the text of this book. It is recommended nevertheless to look at these publications since they contain pictures of experimental results and references to applications of the more fundamental lines of thought, as presented herein.

Adolf W. Lohmann

Erlangen, April 1986

Preface to volume 1

These are course notes, not a book. A book is usually a complilation of facts. But in these notes I have tried to show "how to do it yourself". Of course all the tricks in the world would not be of any use, if you did not have at least some facts in your head. Indeed, some facts are taught here. But for a more complete set of basic facts you should have, for example, Born and Wolf's Principles of Optics or Klein's Optics on your shelf. As a source of inspiration you might add Franon's Atlas of Optical Phenomena.

A "how to do it" course must be supplemented by homework problems. To keep up the suspense, these problems have not been included in these notes. But some reprints have been attached. Reading them prepares you for journal reading, and it shows you how some of the principles can be used for the solution of practical problems.

Curtis Shuman reorganized and polished the manuscript; Mrs. Linda Gail Chen typed it after eliminating the worst linguistic idiosyncrasies. She also inked the drawings. I am very grateful to both of them for their help and for having bugged me long enough that I finally wrote these notes.

1 Outline

This is a three-quarter course. Thereafter a seminar, APIS 294B, will be devoted to some special subjects in optical information processing. Instead of trying to cover the whole of physical optics in this course, we will concentrate on those aspects which are useful for information processing, such as holography. Another optics course, APIS 203, covers optical instrumentation and physiological optics, which is currently a very active field. Only recently did we begin to understand how colors are perceived, and how the brain gets information from the eyes. The brain constantly manipulates the eyes in order to optimize the acquisition of information. Optical instrumentation is perhaps not the most glamorous part of optics, but it is quite useful to know, since optical instruments are used in almost all parts of science. The laser and other quantum electronic subjects are treated in the course APIS 207. To understand the laser is worthwhile since lasers are used for so many projects, for example communication in space, microminiaturization, and making holograms.

APIS 205/114 contains a review of mathematical methods, fundamentals of physical optics, applications of physical optics to holography, and other optical data processing methods. In the mathematical treatment rigor is sometimes sacrificed for simple approximations. This approach is preferable to inflexible rigor if one wants to understand optics and to optimize optical methods.

Specifically, the following subjects will be treated in the three quarter terms :

- Optics I

  Fourier series. Moiré effects. Optical analog computer for Fourier transformation. "Delta-function". Fourier integral. Schwarz inequality. Fresnel transformation. Stationary phase method. Uncertainty. Sampling. What is light? Fraunhofer diffraction. Coherent image formation as a linear filter system. Some spatial filtering experiments.

- Optics II

  Waves boundaries. Interference. Coherence theory with applications to interferometry. Talbot fringes. Polarization and crystal optics. Holograms and Fresnel zones. Twin-image problem of holography. The pseudoscopic conjugate image. Classification of holographic setups. Influence of recording material. Space-bandwidth product. Holographic data storage.

- Optics III

  Generalized holograms. Penetration of fog and turbulence. Computer holograms. Spatial filtering. Other applications of holography. Other data processing methods. Utilization of *a priori* information.

As I said, the main goal of this course is to bring together *Physical Optics and Communications Theory*. Benefits will be derived for both fields: Optics had been treated in the past usually as "Transportation of *energy* from the object to the image". This is certainly valid, but insufficient, because in most cases we are more interested in the transfer of *information* rather than *energy*. Of course, no information can be transferred without any energy going along, but energy *per se* is not all we are interested in; its structure, distribution, or arrangement is important. In other words, the point of view which had been applied by communication theoreticians towards electronics shall now be applied to optics. This enables a new understanding of old optical schemes, and it is very suggestive for inventing some new optical schemes. Some of these new schemes might be very useful in communications and data processing technology. In fact, some data processing operations can be performed better by optical means than by elelctronic means. In that way we optical physicists might pay back for some of the benefits which we have received from the EE-community.

On page 19 I have outlined what I hope to cover in three terms of this year. As prerequisites we will need mainly *wave optics*, which in turn asks for familiarity with *Fourier transforms* as the most important mathematical tool. Since the background of the students is quite inhomogeneous, I will review these two fields, which might require about half of the first term.

A few words now about what I do not intend to cover: (1) *temporal phenomena*, like modulation and demodulation of a laser beam. From a systems point of view temporal modulation of light is not different from HF modulation, merely an extensions towards higher frequencies. Hence this aspect would fit most naturally into an EE lecture series, in which HF-modulation is covered.

Of course, the hardware used for emitting, modulating and detecting light beams is different from the hardware used in HF technology. A thorough understanding of the hardware used for temporal optics is best taught as part of a course on (2) *interaction of light and matter*.

A third topic not covered here is (3) *noise in optics*. Fortunately, spatial noise is generally not too severe a problem in time-stationary optics, but we will have to mention it occasionally. A treatment in the realm of classical physical optics is given by E. O'Neill in Introduction to Statistical Optics (Addison-Wesley 1963). A more complete treatment of noise in optics, which would probably be a full year's course, must take into account the quantum structure of matter and radiation. The books by W. Louisell on Quantum Theory of Radiation and Noise and by A. Yariv on Quantum Electronics cover this field, both in the notation of modern quantum theory. A. E. Siegman's book on Lasers and Masers, with Applications, uses a notation more familiar to EE students. Siegman does not indulge in mathematical elegance, but he covers all three of the "missing topics" quite well.

2 Fourier Series

2.1 Introduction

The main tools used here are Fourier series and Fourier integrals, which were published by Jean Baptiste Fourier in 1822, almost 150 years ago. Books on the same subject are still published at the rate of one per year. Franklin is cheap (pocket book), Bracewell (hard cover) is application oriented and well illustrated. EE-students might like A. Papoulis' System and Transforms with application in Optics.

A Fourier series is useful for representing a periodic function $f(x)$. Definition of periodic: $f(x) = f(x + md)$; $|m| = 0, 1, 2, \ldots$, where d: length of the period and ν: fundamental spatial frequency: $d = \frac{1}{\nu}$.

We want to put together some simple well know periodic functions, cosine and sine, such that they add up to the general function $f(x)$, which might be complex. x is real.

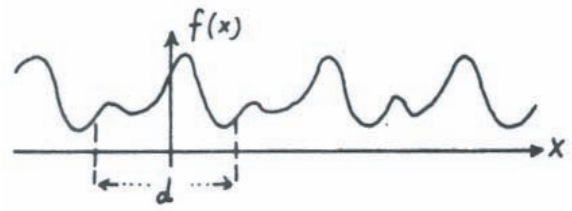

Figure 2.1: Example of a periodic function.

$$f(x) \stackrel{?}{=} \sum_{n=0}^{N} a_n \cos(2\pi n \nu_x) + b_n \sin(2\pi n \nu_x) = S_N(x) \tag{2.1}$$

What is the best choice of the coefficients a_n, b_n? Call the error $E_N = f(x) - S_N(x)$.

Tchebycheff approach: Look for $E_{\max}$ ($|E_N(x| \leq E_{\max}$) within a full period, and choose a_n, b_n such that $E_{\max}$ is minimized. While the Tchebycheff approach is intuitively appealing, it is not very practical for approximating a Fourier series, or any other expansion in terms

of orthogonal functions. Much handier is the *Gauss approach:* Compute the average of the squared error and minimize it. I.e.,

$$\sigma_N^2 = \frac{1}{d}\int_{-\frac{d}{2}}^{\frac{d}{2}} |E_N(x)|^2 \mathrm{d}x \to \text{minimum} \tag{2.2}$$

Since we will use the Fourier series so often, it is worth the trouble to perform this minimization process in detail. To make the problem more manageable we split $f(x)$ into its real part and its imaginary part:

$$f(x) = \mathrm{R}(x) + i\mathrm{I}(x) \tag{2.3}$$

Next we separate the symmetric and the antisymmetric parts:

$$\begin{aligned} \mathrm{R}(x) = \mathrm{RS}(x) + \mathrm{RA}(x) \quad ; \qquad \mathrm{RS}(x) = \frac{1}{2}[\mathrm{R}(x) + \mathrm{R}(-x)]; \\ \mathrm{RS}(x) = +\mathrm{RS}(-x); \mathrm{RA}(x) = -\mathrm{RA}(-x) \quad ; \qquad \mathrm{RA}(x) = \frac{1}{2}[\mathrm{R}(x) - \mathrm{R}(-x)] \end{aligned} \tag{2.4}$$

Correspondingly,

$$\mathrm{I}(x) = \mathrm{IS}(x) + \mathrm{IA}(x); \quad \mathrm{IS}(x) = \mathrm{IS}(-x); \quad \mathrm{IA}(x) = -\mathrm{IA}(-x) \tag{2.5}$$

Another way to split up $f(x)$ is:

$$f(x) = \underbrace{\mathrm{RS}(x) + i\mathrm{IS}(x)}_{f_S(x)=f_S(-x)} + \underbrace{\mathrm{RA}(x) + i(\mathrm{IA})(x)}_{f_A(x)=-f_A(-x)} \tag{2.6}$$

where now $f_S(x)$ and $f_A(x)$ are again complex functions.

We can guess already now that $f_S(x)$ will be approximated (if at all) by the cosine-part of $S_N(x)$, since both are symmetrical; while $F_A(x)$ might be approximated by the sine-portion of $S_N(x)$. Furthermore, when splitting the coefficients into real and imaginary parts, it is plausible to expect the following pairings:

$$\begin{aligned} a_n = \alpha_n + i\overline{\alpha}_n \quad ; \qquad b_n = \beta_n + i\overline{\beta}_n. \\ \mathrm{RS} \sim \alpha; \quad \mathrm{IS} \sim \overline{\alpha} \quad ; \qquad \mathrm{RA} \sim \beta; \quad \mathrm{IA} \sim \overline{\beta} \end{aligned} \tag{2.7}$$

In order to keep the formulas reasonably short we introduce the following abbreviation:

$$\frac{1}{d}\int_{-\frac{d}{2}}^{\frac{d}{2}} \varphi(x)\psi(x)\mathrm{d}x = \varphi\cdot\psi \tag{2.8}$$

This is sometimes called the scalar product of the two functions φ and ψ. It pays off to compute some frequently encountered special cases:

$$\begin{aligned}
\cos(2\pi n\nu x)\cdot\cos(2\pi m\nu x) &= \frac{(\delta_{n,m}+\delta_{n,m})}{2} \\
\sin(2\pi n\nu x)\cdot\sin(2\pi m\nu x) &= \frac{(\delta_{n,m}-\delta_{n,m})}{2} \\
\sin(2\pi n\nu x)\cdot\cos(2\pi m\nu x) &= 0 \qquad \text{“orthogonality“}
\end{aligned} \tag{2.9}$$

where we have used the Kronecker symbol :

$$\delta_{n,m} = \begin{cases} 1 & : \quad n = m \\ 0 & : \quad n \neq m \end{cases} \qquad (n, m \text{ are always integers}) \tag{2.10}$$

The last case, $\sin\cdot\cos = 0$ in Eq. 2.10, is a special case of $g_S(x)\cdot g_A(x) = 0$ wherein $g_S(x) = g_S(-x)$ and $g_A(x) = -g_A(-x)$. Obviously the product $g_S(x)\cdot g_A(x)$ is antisymmetrical, $g_S(x)\cdot g_A(x) = -g_S(-x)\cdot g_A(-x)$. Hence in the integral

$$\int_{-\frac{d}{2}}^{\frac{d}{2}} g_S(x)\cdot g_A(x)\mathrm{d}x \tag{2.11}$$

contributions from antisymmetrical places, x and $-x$ will cancel each other. In anticipation of many cancellations occurring in the following calculations, it is wise to split up $S_N(x)$ similarly to the way it was done with $f(x)$:

$$S_N(x) = \underbrace{\overbrace{S_{\mathrm{RS}}}^{\alpha_n} + i\overbrace{S_{\mathrm{IS}}}^{\overline{\alpha}_n}}_{\text{symmetrical}} + \underbrace{\overbrace{S_{\mathrm{RA}}}^{\beta_n} + i\overbrace{S_{\mathrm{IA}}}^{\overline{\beta}_n}}_{\text{antisymmetrical}} \tag{2.12}$$

When we calculate the mean square error σ_N^2 our “scalar product” abbreviation gives:

$$\sigma_n^2 = \frac{1}{d}\int_{-\frac{d}{2}}^{\frac{d}{2}} |E_N(x)|^2\mathrm{d}x = E_N(x)\cdot E_N^*(x) \tag{2.13}$$

with $E_N(x) = f(x) - S_N(x)$.

The following terms will drop out because they are special cases of $g_S(x) \cdot g_A(x) = 0$.

$$\begin{aligned} &\mathrm{RS}\cdot\mathrm{RA}, \quad S_{\mathrm{RS}}\cdot S_{\mathrm{RA}} \quad , \quad \mathrm{RA}\cdot S_{\mathrm{RS}}, \quad \mathrm{RS}\cdot S_{\mathrm{RA}} \\ &\mathrm{IS}\cdot\mathrm{IA}, \quad S_{\mathrm{IS}}\cdot S_{\mathrm{IA}} \quad , \quad \mathrm{IA}\cdot S_{\mathrm{IS}}, \quad \mathrm{IS}\cdot S_{\mathrm{IA}} \end{aligned} \tag{2.14}$$

What remains is:

$$\begin{aligned} \sigma_N^2 = {} & \mathrm{RS}\cdot\mathrm{RS} + \mathrm{RA}\cdot\mathrm{RA} + \mathrm{IS}\cdot\mathrm{IS} + \mathrm{IA}\cdot\mathrm{IA} + \\ & S_{\mathrm{RS}}\cdot S_{\mathrm{RS}} + S_{\mathrm{RA}}\cdot S_{\mathrm{RA}} + S_{\mathrm{IS}}\cdot S_{\mathrm{IS}} + S_{\mathrm{IA}}\cdot S_{\mathrm{IA}} \\ & -2\mathrm{RS}\cdot S_{\mathrm{RS}} - 2\mathrm{RA}\cdot S_{\mathrm{RA}} - 2\mathrm{IS}\cdot S_{\mathrm{IS}} - 2\mathrm{IA}\cdot S_{\mathrm{IA}} \end{aligned} \tag{2.15}$$

Since the terms in it do not involve the function $S_N(x)$, the first line is constant as far as $\alpha, \beta, \overline{\alpha}, \overline{\beta}$ are concerned. The terms in the second line are found, using the series expression for $S_N(x)$, to be:

$$\begin{aligned} S_{\mathrm{RS}}\cdot S_{\mathrm{RS}} &= \alpha_0^2 + \frac{1}{2}\sum_{n=1}^{N}\alpha_n^2 \quad ; \quad S_{\mathrm{RA}}\cdot S_{\mathrm{RA}} = \frac{1}{2}\sum_{n=1}^{N}\beta_n^2 \\ S_{\mathrm{IS}}\cdot S_{\mathrm{IS}} &= \overline{\alpha}_0^2 + \frac{1}{2}\sum_{n=1}^{N}\overline{\alpha}_n^2 \quad ; \quad S_{\mathrm{IA}}\cdot S_{\mathrm{IA}} = \frac{1}{2}\sum_{n=1}^{N}\overline{\beta}_n^2 \end{aligned} \tag{2.16}$$

In the third line we find:

$$\begin{aligned} \mathrm{RS}\cdot S_{\mathrm{RS}} &= \sum_{n=0}^{N}\alpha_n \mathrm{RS}\cos(2\pi n\nu x) \quad ; \quad \mathrm{RA}\cdot S_{\mathrm{RA}} = \sum_{n=1}^{N}\beta_n \mathrm{RA}\sin(2\pi n\nu x) \\ \mathrm{IS}\cdot S_{\mathrm{IS}} &= \sum_{n=0}^{N}\overline{\alpha}_n \mathrm{IS}\cos(2\pi n\nu x) \quad ; \quad \mathrm{IA}\cdot S_{\mathrm{IA}} = \sum_{n=1}^{N}\overline{\beta}_n \mathrm{IA}\sin(2\pi n\nu x) \end{aligned} \tag{2.17}$$

Now we are ready to calculate the coefficients $\alpha, \beta, \overline{\alpha}, \overline{\beta}$, which minimize the mean square error σ_N^2 of our attempt to approximate the general function $f(x)$ by means of a finite trigonometrical series $S_N(x)$. As is common when looking for a minimum we set the first derivatives equal to zero:

$$
\begin{aligned}
0 &= \frac{\partial\sigma_N^2}{\partial\alpha_0} = 2\alpha_0 - 2\mathrm{RS}\cdot\mathbf{1}; \quad \rightarrow \alpha_0 = \frac{1}{d}\int_{-\frac{d}{2}}^{\frac{d}{2}} \mathrm{RS}(x)\mathrm{d}x = \mathrm{RS}\cdot\mathbf{1} = \overline{\mathrm{RS}} \qquad (2.18)\\
0 &= \frac{\partial\sigma_N^2}{\partial\overline{\alpha}_0}; \quad \rightarrow \overline{\alpha}_0 = \overline{\mathrm{IS}}\\
0 &= \frac{\partial\sigma_N^2}{\partial\overline{\alpha}_m} \stackrel{m\neq 0}{=} \alpha_m - 2\mathrm{RS}\cdot\cos(2\pi m\nu x); \quad \rightarrow \alpha_m = 2\mathrm{RS}\cdot\cos(2\pi m\nu x)\\
0 &= \frac{\partial\sigma_N^2}{\partial\overline{\alpha}_m}; \quad \stackrel{m\neq 0}{\rightarrow} \overline{\alpha}_m = 2\mathrm{IS}\cos(2\pi m\nu x)\\
0 &= \frac{\partial\sigma_N^2}{\partial\overline{\beta}_m} = \beta_m - 2\mathrm{RA}\sin(2\pi m\nu x); \quad \rightarrow \beta_m = 2\mathrm{RA}\sin(2\pi m\nu x)\\
0 &= \frac{\partial\sigma_N^2}{\partial\overline{\beta}_m} = \overline{\beta}_m - 2\mathrm{IA}\sin(2\pi m\nu x); \quad \rightarrow \overline{\beta}_m = 2\mathrm{IA}\sin(2\pi m\nu x)
\end{aligned}
$$

We were very lucky that these $2(2N+1)$ equations for the $2(2N+1)$ unknowns $\alpha, \beta, \overline{\alpha}, \overline{\beta}$ came out so simple, completely separated. The reason for this is the orthogonality of cosine and sine, as expressed on top of Eq. 2.10. This feature has another nice consequence which is called "finality", because the coefficients determined for $S_N(x)$ do not change if we calculate for $S_{N+1}(x), S_{N+2}(x)$ and so forth.

We have to convince ourselves that our solution represents a minimum, and not a maximum, of σ_N^2. For this it is sufficient to show that all second derivatives are positive:

$$
\begin{aligned}
\frac{\partial^2\sigma_N^2}{\partial\alpha_0^2} &= 2 = \frac{\partial^2\sigma_N^2}{\partial\overline{\alpha}_0^2}; \qquad (2.19)\\
1 = \frac{\partial^2\sigma_N^2}{\partial\alpha_m^2} &= \frac{\partial^2\sigma_N^2}{\partial\overline{\alpha}_m^2} = \frac{\partial^2\sigma_N^2}{\partial\beta_m^2} = \frac{\partial^2\sigma_N^2}{\partial\overline{\beta}_m^2} \quad (\mathrm{m}\neq 0)
\end{aligned}
$$

Another remaining question is: how good is our approximation? Or, does the error σ_N^2 converge to zero if $N\rightarrow\infty$? In mathematical terms this question is equivalent to asking: is the set of function $\cos(2\pi n\nu x)$, $\sin(2\pi n\nu x)$ a complete set within the range $-\frac{d}{2} \leq x \leq \frac{d}{2}$? Before looking into that question we will somewhat simplify the results we have now.

$$
\alpha_0 + i\overline{\alpha}_0 = a_0 = \mathrm{RS}\cdot\mathbf{1} + i\mathrm{IS}\cdot\mathbf{1} = f_S\cdot\mathbf{1} = f\cdot\mathbf{1}; \quad (\mathrm{because} f_A\cdot\mathbf{1} = 0, \text{ anyway}) \qquad (2.20)
$$

$$
\begin{aligned}
\alpha_m + i\overline{\alpha}_m = a_m &= 2(\mathrm{RS} + i\mathrm{IS})\cdot\cos(2\pi m\nu x) = 2f_S\cdot\cos(2\pi m\nu x) = \qquad (2.21)\\
= 2f\cos(2\pi m\nu x) &\quad ; \qquad (\mathrm{because} f_A\cdot\cos = 0)
\end{aligned}
$$

$$\beta_m + i\overline{\beta}_m = b_m = 2(\mathrm{RA} + i\mathrm{IA}) \cdot \sin(2\pi m\nu x) = 2f_A \cdot \sin = 2f \cdot \sin \tag{2.22}$$

$$\begin{aligned} S_N &= a_0 + \sum_{n=1}^{N} [a_n \cos + b_n \sin] = \\ &= a_0 + \sum_{n=1}^{N} \left[\frac{(a_n - ib_n)}{2}\right] e^{2\pi i n\nu x} + \sum_{n=1}^{N} \left[\frac{(a_n + ib_n)}{2}\right] e^{-2\pi i n\nu x} \end{aligned} \tag{2.23}$$

The second term can be converted into a series with negative coefficients by changing $n \to -n$:

$$\sum_{-N}^{-1} \left[\frac{(a_{-n} + ib_{-n})}{2}\right] e^{+2\pi i n\nu x} \tag{2.24}$$

Making further use of symmetry properties we will arrive at the "complex form" of the Fourier series; noting that

$$a_{-n} = a_n;\ b_{-n} = -b_n\ \to \frac{(a_{-n} + ib_{-n})}{2} = \frac{a_n - ib_n}{2} \tag{2.25}$$

Call $C_n = \frac{(a_n - ib_n)}{2}$; $C_0 = a_0$. Then we arrive at the desired result:

$$\boxed{S_N = \sum_{-N}^{+N} C_n e^{2\pi i n\nu x}; \quad C_n = f(x) \cdot e^{-2\pi i n\nu x}} \tag{2.26}$$

Now let us return to the question of "how good is our approximation?" or "does $\sigma_N \to 0$ with $N \to \infty$"? Using the complex form, Eq. 2.12 becomes:

$$\begin{aligned} \sigma_N^2 &= \left(f - \sum_n C_n e^{2\pi i n\nu x}\right) \cdot \left(f^* - \sum_m C_m^* e^{-2\pi i m\nu x}\right) \\ &= f \cdot f^* - \sum_m C_m^* f e^{-m} - \sum_n C_n f^* \cdot e^{+n} \\ &+ \sum_m \sum_n C_n C_m^* \underbrace{e^{2\pi i n x}\, e^{-2\pi i m\nu x}}_{\delta_{n,m}} \end{aligned} \tag{2.27}$$

or:

$$\boxed{\sigma_N^2 = f \cdot f^* - \sum_{|n| \le N} |C_n|^2} \tag{2.28}$$

This relationship implies the desirable feature $\sigma_{N+1}^2 - \sigma_N^2 = -|C_{N+1}|^2 \le 0$. This means that the error σ_n can only decrease if more terms are added to the Fourier series as in $S_N \to S_{N+1}$. If $\sigma_N \to 0$, then $\sum_{|n| \le N} |C_n|^2 \to f \cdot f^*$.

The ultimate result, which holds for all healthy functions (and for some strange ones, too) is the *completeness relationship*:

$$f \cdot f^* = \sum_{-\infty}^{+\infty} |C_n|^2 \tag{2.29}$$

However, this relationship is not completely satisfactory, because it cannot always easily be checked, and it still allows $f(x)$ to be quite different from $\sum C_n e^{2\pi i n \nu x}$ at a finite number of points within each interval.

Example:

$$f(x) = \begin{cases} +1 & : \quad \text{in } 0 \le x \le \frac{d}{2} \\ -1 & : \quad \text{in } 0 > x > -\frac{d}{2} \end{cases} \tag{2.30}$$

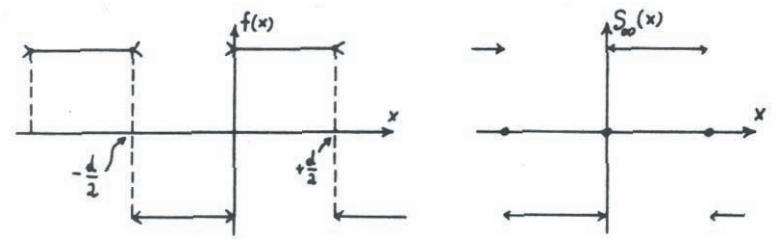

Figure 2.2: The periodic function $f(x)$ and its approximation through a discrete infinite series ("Dirichlet effect").

$f(x)$ can be represented in a series:

$$\sum_{-\infty}^{\infty} C_n e^{2\pi i \nu x}; \quad \text{with :} \quad C_n = \begin{cases} 0 & : \quad \text{if } n \text{ even} \\ \frac{2}{\pi i n} & : \quad \text{if } n \text{ odd} \end{cases} \tag{2.31}$$

i.e. $f(x) = \sum_{n=1,3,5,\ldots} \frac{4}{\pi n} \sin(2\pi n \nu x)$.

This series is certainly zero at $x = 0$, while $f(x) = +1$ at $x = 0$.

For functions with a finite number of discontinuities Dirichlet has shown, that, at discontinuous points of $f(x)$, the infinite Fourier series assumes the arithmetic mean of the right-hand limit and the left-hand limit:

$$\sum_{-\infty}^{+\infty} C_n e^{2\pi i n\nu x} = \lim_{\epsilon \to 0} \frac{1}{2}[f(x+\epsilon) + f(x-\epsilon)] \tag{2.32}$$

Fig. 2.2 shows how a square wave is perfectly represented by the infinite series, except at points of discontinuity, where the series assumes the mean value.

Another effect occurs when a discontinuous function $f(x)$ is approximated by a *finite* Fourier series $S_N(x)$. Figure 2.3 shows the so-called Gibbs-effect for the same square wave function $f(x)$ as was used for demonstrating the Dirichlet-effect.

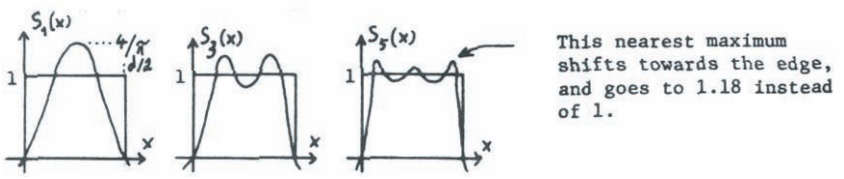

Figure 2.3: The periodic function $f(x)$ approximated through a discrete *finite* series.

The Gibbs-effect, which actually happens in some optical systems, does bother us occasionally. But the Dirichlet-effect is of no practical concern, because it cannot be measured. For example if $f(x)$ and $S(x)$ represent a distribution of energy, we will not be able to observe any difference between $f(x)$ and $S(x)$ because all detectors have a *finite* width W. Typically one measures:

$$\int_{x_0-\frac{W}{2}}^{x_0+\frac{W}{2}} f(x)\mathrm{d}x = \int_{x_0-\frac{W}{2}}^{x_0+\frac{W}{2}} S_\infty \mathrm{d}x \approx \int_{x_0-\frac{W}{2}}^{x_0+\frac{W}{2}} S_N(x)\mathrm{d}x \quad \text{if } W > \frac{2d}{N} \tag{2.33}$$

A sufficient condition for good convergence of $\lim_{n\to\infty} \sum |C_n|^2 \to f \cdot f^*$ is continuity of $f(x)$ and some of its integration by parts:

$$C_n = \frac{1}{d}\int f(x)e^{-2\pi i n\nu x}\mathrm{d}x = \left[\frac{f(x)e^{-2\pi i n\nu x}}{-2\pi i n}\right]_{\frac{-d}{2}}^{\frac{d}{2}} - \frac{1}{d}\int \frac{f'(x)e^{-2\pi i n\nu x}}{-2\pi i n\nu}\mathrm{d}x \tag{2.34}$$

The first term is zero if $f\left(\frac{d}{2}\right) = f\left(-\frac{d}{2}\right)$, which follows from the periodicity and assumed continuity. This leaves us with:

$$2\pi i n C_n = \int f'(x) e^{-2\pi i n \nu x} \mathrm{d}x \tag{2.35}$$

If some more derivatives are continuous, including $f^{(k-1)}(x)$, then by repeating the integration by parts one gets:

$$(2\pi i n \nu)^k C_n = \nu \int f^{(k)}(x) e^{-2\pi i n \nu x} \mathrm{d}x \tag{2.36}$$

If $f^{(k-1)}$ is continuous, f^k must be finite, say $|f^k(x)| \leq \frac{\varphi_k}{d^{(k-1)}} = \varphi_k \cdot \nu^{(k-1)}$. Hence

$$\nu \left| \int f^k(x) e^{-2\pi i n \nu x} \mathrm{d}x \right| \leq \varphi_k \nu^k \tag{2.37}$$

and also:

$$\left|(2\pi n \nu)^k C_n\right| \leq \varphi_k \tag{2.38}$$

This inequality is a very good guarantee that $\sum_{|n|<N} |C_n|^2$ converges when $N \to \infty$ because the $|C_n|^2$ terms decrease in proportion n^{-2k}.

2.2 Some Useful Properties of Fourier Series

So far we have seen why and how it is possible that a series of trigonometric functions can approximate any periodic function.

$$\begin{aligned} f(x) &\approx \sum_{n=-N}^{+N} C_n e^{2\pi i n \nu x}; \quad \text{in} \quad |x| \leq \frac{d}{2} \\ C_n &= \frac{1}{d} \int_{-\frac{d}{2}}^{\frac{d}{2}} f(x) e^{-2\pi i n \nu x} \mathrm{d}x; \quad d = \frac{1}{\nu} \end{aligned} \tag{2.39}$$

Now we want to list some useful properties, which can be derived very easily. If the function $f(x)$ has the Fourier coefficients A_n, and if $g(x)$ has the coefficients B_n, and if f and g are periodic with period $d/2$, then the follow properties in both Fourier-domains are equivalent.

$$\begin{aligned} [f(x)+g(x)] &\leftrightarrow [A_n+B_n] \\ f(x)=ag(x) &\leftrightarrow A_n=aB_n \\ f(x)=g(\mathrm{M}x) &\leftrightarrow A_{n\mathrm{M}}=B_n \qquad (\mathrm{M}:\ \text{fixed integer}, >0) \end{aligned} \tag{2.40}$$

The following two properties, which are quite important, are called the "shift theorem":

$$\begin{aligned} f(x)=g(x+c) &\leftrightarrow A_n=B_n e^{2\pi i n\nu c} \\ f(x)=g(x)e^{2\pi i\mathrm{M}\nu x}\ (\mathrm{M}\ \text{integer}) &\leftrightarrow A_n=B_{n-\mathrm{M}} \\ f(x)=g(-x);\ A_n=B_{-n} &\leftrightarrow f(x)=-g(-x);\ A_n=-B_{-n} \end{aligned} \tag{2.41}$$

The next two properties are sometimes called "reality symmetry" (or the functions are said to be Hermitian):

$$\begin{aligned} f(x)=g^*(x) &\leftrightarrow A_n=B^*_{-n} \\ f(x)=f^*(-x) &\leftrightarrow A_n=A^*_n \\ f(x)=-g^*(x) &\leftrightarrow A_n=-B^*_{-n} \\ f(x)=g_1(x)g_2(x) &\leftrightarrow A_n=\sum_{(m)} B^{(1)}_m B^{(2)}_{n-m} \\ f(x)=g(x)g^*(x) &\leftrightarrow A_n=\sum_{(m)} B_m B^*_{m-n} \\ f(x)=\frac{\mathrm{d}g(x)}{\mathrm{d}x} &\leftrightarrow A_n=2\pi i n\nu B_n \\ f(x)=\int_{-x}^{+x} g'(x)\mathrm{d}x' &\leftrightarrow A_n=\frac{(B_n+B_{-n})}{2\pi i n\nu};\quad (B_0=0\ \text{assumed}) \\ f(x)=\underbrace{\frac{1}{d}\int_{-\frac{d}{2}}^{\frac{d}{2}} g_1(x')g_2(x'-x)\mathrm{d}x'}_{\text{crosscorrelation}} &\leftrightarrow A_n=B^{(1)}_n B^{(2)}_{-n} \\ f(x)=\underbrace{\frac{1}{d}\int_{-\frac{d}{2}}^{\frac{d}{2}} g_1(x')g_2(x-x')\mathrm{d}x'}_{\text{convolution}} &\leftrightarrow A_n=B^{(1)}_n B^{(2)}_n \\ f(x)=\underbrace{\frac{1}{d}\int_{-\frac{d}{2}}^{\frac{d}{2}} g(x')g^*(x'-x)\mathrm{d}x'}_{\text{auto-correlation}} &\leftrightarrow A_n=|B_n|^2 \end{aligned} \tag{2.42}$$

$$f(x) = \underbrace{\frac{1}{d}\int_{-\frac{d}{2}}^{\frac{d}{2}} g(x')g(x-x')\mathrm{d}x'}_{\mathrm{auto-convolution}} \quad \leftrightarrow \quad A_n = B_n^2 \tag{2.43}$$

Now some specific examples:

- Periodic array of "rect"-functions:

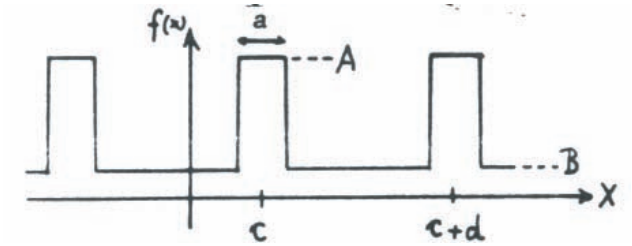

Figure 2.4: Grating: periodic array of rect functions.

$$\begin{aligned} A_0 &= B + \frac{a}{d}(A-B) \\ A_n &= \left[\frac{A-B}{d}\right] e^{2\pi i n\nu c} a\,\mathrm{sinc}(n\nu a) \\ \text{where : } \mathrm{sinc}(z) &= \frac{\sin(\pi z)}{\pi z} \end{aligned} \tag{2.44}$$

The sinc-function has the properties $\mathrm{sinc}(0) = 1$, $\mathrm{sinc}(m) = 0$, m : integer.

- Sinusoidal phase function:

$$f(x) = e^{iz\sin(2\pi i\nu x)}; \qquad A_n = J_n(z) \tag{2.45}$$

The $J_n(z)$ are the Bessel functions of first kind.

- "Dirac"-comb:

$$f(x) = \sum_{m=-\infty}^{+\infty} \delta(x - md - x_0); \qquad A_n = \frac{e^{-2\pi i n\nu x_0}}{d} \tag{2.46}$$

This is the so-called Dirac-comb. It has extremely sharp spikes at $x = md + x_0,\ |m| = 0, 1, 2, \ldots$. We will treat the "Dirac-delta-function" in more detail later.

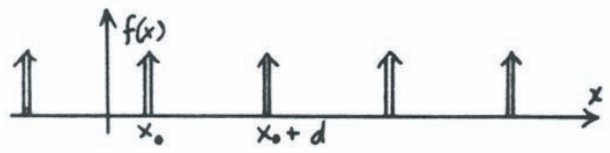

Figure 2.5: The "Dirac-comb".

Now we will treat another example in which we use several of the properties that had been derived in previous pages. The philosophy is to reduce the somewhat inconvenient problem into a simpler standard problem.

- "Sawtooth"-grating:

$$u(x) = \sum_{n=-\infty}^{+\infty} C_n e^{2\pi i n \nu x} \tag{2.47}$$

notice: B is negative here (Fig. 2.6).

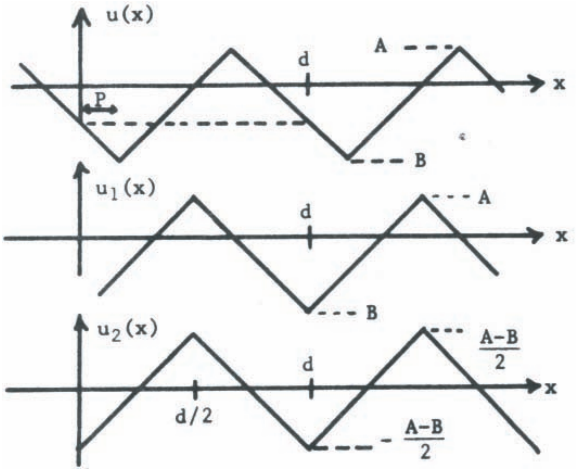

Figure 2.6: The "sawtooth"-grating.

Use of the shift theorem:

$$u(x) = u_1(x - P); \quad \text{hence} : C_n^{(1)} = C_n e^{2\pi i n \nu P} \tag{2.48}$$

$$u_2(x) = u_1(x) - \frac{A+B}{2}; \quad \text{hence} : C_n^{(2)} = C_n^{(1)} - \left[\frac{A+B}{2}\right] \delta_{n,0} \tag{2.49}$$

The next step is simply scaling:

$$u_3(x) = \frac{\frac{d}{2}}{A-B} u_2(x); \quad C_n^{(3)} = C_n^{(2)} \frac{\frac{d}{2}}{A-B} \tag{2.50}$$

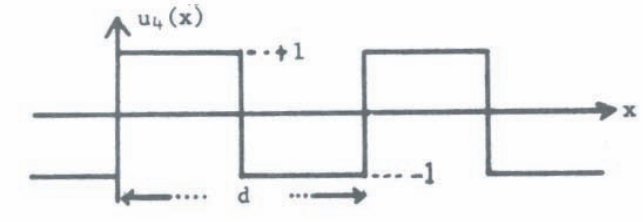

Figure 2.7: $u_4(x)$.

$$u_4(x) = \frac{\mathrm{d}u_3(x)}{\mathrm{d}x}; \quad C_n^{(4)} = 2\pi i n \nu C_n^{(3)} \tag{2.51}$$

$$C_n^{(4)} = \begin{cases} 0 & \text{if } n \text{ even} \\ \frac{2}{\pi i n} & \text{if } n \text{ odd} \end{cases}.$$

Now that $C_n^{(4)}$ is known for the simple case of a square wave we can go backwards from $C_n^{(4)}$ to C_n by way of $C_n^{(3)}$, $C_n^{(2)}$ and $C_n^{(1)}$:

$$\begin{aligned}
C_n^{(4)} &= \begin{cases} 0 & : \text{ if } n \text{ even} \\ \frac{2}{\pi i n} & : \text{ if } n \text{ odd} \end{cases}; \\
C_n^{(4)} &= 2\pi i n \nu C_n^{(3)}; \quad (\nu = \frac{1}{d}); \\
\Longrightarrow C_n^{(3)} &= \begin{cases} 0 & : \text{ if } n \text{ even} \\ -\frac{d}{(\pi n)^2} & : \text{ if } n \text{ odd} \end{cases}; \\
C_n^{(3)} &= C_n^{(2)} \frac{\frac{d}{2}}{A-B}; \\
\Longrightarrow C_n^{(2)} &= \begin{cases} 0 & : \text{ if } n \text{ even} \\ \frac{-2(A-B))}{(\pi n)^2} & : \text{ if } n \text{ odd} \end{cases}; \\
C_n^{(2)} &= C_n^{(1)} - \left[\frac{(A+B)}{2}\right] \delta_{n,0}; \\
\Longrightarrow C_n^{(1)} &= \begin{cases} \frac{A+B}{2} & : \text{ if } n = 0 \\ 0 & : \text{ if } n \text{ even but } n \neq 0 \\ -\frac{-2(A-B)}{(\pi n)^2} & : \text{ if } n \text{ odd} \end{cases}; \\
C_n^{(1)} &= C_n e^{2\pi i n \nu P};
\end{aligned} \tag{2.52}$$

So the final result is:

$$C_n = \begin{cases} \frac{A+B}{2} & : \quad \text{if } n = 0 \\ 0 & : \quad \text{if } n \text{ even but } n \neq 0 \\ -\frac{-2(A-B)}{(\pi n)^2} e^{-2\pi i n \nu P} & : \quad \text{if } n \text{ odd} \end{cases} ; \tag{2.53}$$

2.3 Fourier Series for Two-Dimensional Functions

An image is a two-dimensional message as a function of x and y. Hence for applications in optics it is important to extend our mathematical tools for work in two dimensions.

Definition of periodicity in x and in y:

$$u(x,y) = u(x + Nd_x, y + Md_y) \tag{2.54}$$

for every point (x,y) and for every pair (N,M) of integers. To reduce the new 2D-case to the old 1D-case we consider at first only $u(x,y)$ at one horizontal line y = constant. There $u(x,y)$ has an x-period of d_x, no matter which y = constant-line we choose. Hence:

$$\begin{aligned} u(x,y) &= \sum C_n(y) e^{2\pi i \nu x} \\ C_n(y) &= \frac{1}{d_x} \int_{-\frac{d_x}{2}}^{\frac{d_x}{2}} u(x,y) e^{-2\pi i n \nu x} \mathrm{d}x \end{aligned} \tag{2.55}$$

The coefficients $C_n(y)$ will be different for different y-levels, but the coefficients must be periodic in y themselves since $u(x,y)$ is period in y. Hence every $C_n(y)$ is in turn representable by a Fourier series in y:

$$\begin{aligned} C_n(y) &= \sum_m C_{nm} e^{2\pi i m \mu y}; \qquad \mu = \frac{1}{d_y} \\ C_{nm} &= \frac{1}{d_y} \int_{-\frac{d_y}{2}}^{\frac{d_y}{2}} C_n(y) e^{-2\pi i m \mu y} \mathrm{d}y \end{aligned} \tag{2.56}$$

We insert this result into the previous equations and get:

$$u(x,y) = \sum \sum C_{nm} e^{2\pi i (n\nu x + m\mu y)} C_{nm} \frac{1}{d_x d_y} \int_{-\frac{d_x}{2}}^{\frac{d_x}{2}} \int_{-\frac{d_y}{2}}^{\frac{d_y}{2}} u(x,y) e^{-2\pi i (n\nu x + m\mu y)} \mathrm{d}x \mathrm{d}y \tag{2.57}$$

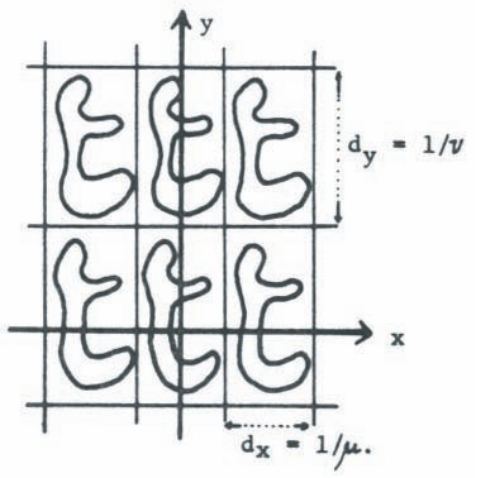

Figure 2.8: Periodic two-dimensional function.

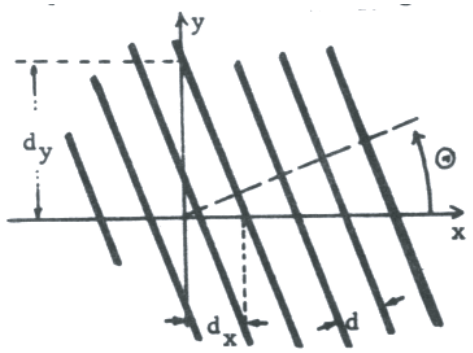

Figure 2.9: The Fourier Kernel (trigonometric function)

Interpretation of the 2D-trigonometric function $\cos[2\pi(\nu x + \mu y)]$:

$$
\begin{aligned}
d_x = \frac{1}{\nu} \qquad d_y = \frac{1}{\mu}; \qquad d = \frac{1}{\varrho} \\
\cos(\theta) = \frac{d}{d_x}; \qquad \tan(\theta) = \frac{d_x}{d_y} \\
\sin\theta = \frac{d}{d_y}; \qquad \tan(\theta) = \frac{\mu}{\nu} \\
\nu^2 + \mu^2 = \varrho^2; \qquad \nu = \varrho\cos(\theta); \qquad \mu = \varrho\sin(\theta)
\end{aligned}
\tag{2.58}
$$

From $\sin^2(\theta) + \cos^2(\theta) = 1$ it follows that $\frac{1}{d^2} = \frac{1}{d_x^2} + \frac{1}{d_y^2}$. If the space coordinates are also expressed in polar fashion the argument of the 2D trigonometric function assumes again a simple form :

$$\begin{aligned} x &= \mathbf{r}\cos(\varphi); \qquad y = \mathbf{r}\sin(\varphi) \\ \nu x + \mu y &= \mathbf{r}\varrho[\cos\varphi\cos\theta + \sin\varphi\sin\theta] = \mathbf{r}\varrho\cos(\varphi - \theta) \end{aligned} \tag{2.59}$$

Sometimes a vectorial abbreviation is handy:

$$\mathbf{x} = (x, y); \qquad \boldsymbol{\nu} = (\nu, \mu); \qquad \mathbf{x}\boldsymbol{\nu} = x\nu + y\mu \tag{2.60}$$

This means that results from 1D Fourier theory can simply be generalized into 2D-results by replacing:

$$x \to \mathbf{x} = (x, y); \qquad \nu \to \boldsymbol{\nu} = (\nu, \mu); \qquad x\nu \to \mathbf{x}\boldsymbol{\nu} = x\nu + y\mu \tag{2.61}$$

3 The Moiré Effect

3.1 Measurement of small shifts

Now we want to use the Fourier series formalism for studying the Moiré effect. Its best known version consists of the superposition of two gratings. In terms of physics we have to know nothing for this study but that the total transmittance of two superposed transparencies is the product of the two individual transmittances.

Two periodic masks may be defined by:

$$T_1(x) = \sum A_n e^{2\pi i n \nu_1 x} \quad \text{and} \quad T_2(x) = \sum A_m e^{2\pi i m \nu_2 x}; \quad \nu_1 \neq \nu_2 \tag{3.1}$$

These formulas say that the two masks have different spatial frequencies, but the same "groove shape" because their Fourier coefficients are alike. Now we superpose both masks, but shift one of them by x_0. The total transmittance will be:

$$T(x) = T_1(x)T_2(x - x_0) = \sum\sum A_n A_m e^{2\pi i \overbrace{[(n\nu_1 x + m\nu_2(x - x_0)]}^{(n\nu_1 + m\nu_2)x - m\nu_2 x_0}} \tag{3.2}$$

$T(x)$ contains many frequencies $n\nu_1 + m\nu_2$ in superposition, one for each (n, m) term of the double series. Let us assume the two fundamental frequencies to be almost alike, but not quite:

$$\nu_1 \approx \nu_2; \quad \nu_1 - \nu_2 = \Delta\nu << \nu_2; \quad \Delta\nu > 0. \tag{3.3}$$

Now let us sort the frequency components of $T(x)$ such that we begin with the very lowest ones: $(n = 0,\ m = 0)$; $(n = \pm 1,\ m = \pm 1))$

$$T(x) = A_0^2 + A_1 A_{-1} \underbrace{\cos[2\pi(\Delta\nu x - \nu_2 x_0)]}_{\cos[2\pi\Delta\nu(x - \frac{\nu_2}{\Delta\nu}x_0)]} + \ldots \tag{3.4}$$

This cosine-term is shifted by $\frac{\nu_2}{\Delta\nu_0}x_0$, although the physical shift of T_2 was only x_0. Hence we experience a "magnification" of $\frac{\nu_2}{\Delta\nu}$, which easily can be 10 or even 100 times.

The Moiré period is $\frac{1}{\Delta\nu}$.

When looking with our human eye at the joint transparency $T(x)$, we will not observe spatial frequencies larger than 10 mm^{-1} (10 full periods per millimetre). Our eye is a low-pass filter, which is another way of saying that the resolution is limited. The magnification effect is used for high precesion measurement of small shifts.

3.2 Moiré of two equal, rotating gratings

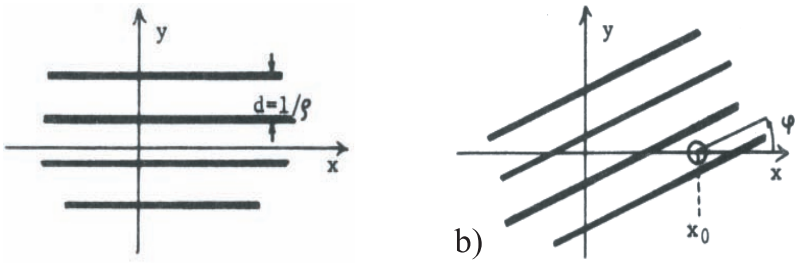

Figure 3.1: Moiré gratings with different orientations.

$$T(x,y) = \sum A_n e^{2\pi i n \varrho y} \tag{3.5}$$

Now rotate this grating around $(x_0, 0)$ (Fig. 3.1b):

$$T_+(x,y) \sum A_n e^{2\pi i n \varrho [y\cos\varphi + (x-x_0)\sin\varphi]} \tag{3.6}$$

Another grating like it is also rotated around $(x_0, 0)$, but in the opposite direction:

$$T_-(x,y) \sum A_n e^{2\pi i n \varrho [y\cos\varphi - (x-x_0)\sin\varphi]} \tag{3.7}$$

The total transmittance is:

$$\begin{aligned} T(x,y) &= T_+(x,y)T_-(x,y) = \sum\sum A_n A_m e^{2\pi i \varrho [\ldots]} \\ [\ldots] &= (n+m)y\cos\varphi + (n-m)(x-x_0)\sin\varphi \end{aligned} \tag{3.8}$$

Now we introduce separate spatial frequency components for the x and the y periodicity. Let us call

$$(n+m)\varrho\cos\varphi = \mu_{nm}; \qquad \varrho(n-m)\sin\varphi = \nu_{nm} \tag{3.9}$$

$$T(x,y) = \sum\sum A_n A_m e^{2\pi i(x\nu_{nm}+y\mu_{nm})} \tag{3.10}$$

The spatial frequencies can be visualized in the (ν,μ) domain with "Miller-indices" (n,m):

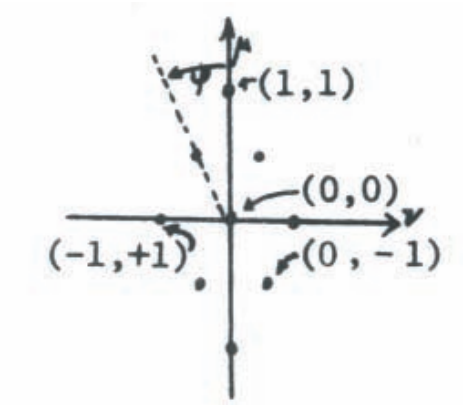

Figure 3.2: Miller indices.

For a specific application we want only the ν-frequencies contained in $T(x,y)$. In order to suppress the μ-frequency components we "smear" in the y-direction, which means mathematically an integration:

$$\frac{1}{\Delta y}\int_0^{\Delta y} T(x,y)\mathrm{d}y = T(x) \tag{3.11}$$

The range of integration Δy should be an integer multiple of the y-period, which is $\frac{1}{\varrho\cos\varphi}$.

Physically the process of "smearing" can be implemented for example by moving $T(x,y)$ in the y-direction while taking a photograph with sufficiently long exposure time. There are other ways, too, which will be mentioned somewhat later. Anyway, we compute now the result of the smearing operation ($\Delta y = \frac{M}{\varrho\cos\varphi}$):

$$\frac{1}{\Delta y}\int_0^{\Delta y} T(x,y)\mathrm{d}y = T(x)\sum\sum A_n A_{-n} e^{2\pi i 2n\varrho(x-x_0)\sin\varphi} \tag{3.12}$$

To get this result we made use of:

$$\frac{1}{\Delta y}\int_0^{\Delta y} e^{2\pi i\varrho(n+m)y\cos\varphi}\mathrm{d}y = \delta_{n,-m} \qquad \text{if } \Delta y = \frac{M}{\varrho\cos\varphi} \tag{3.13}$$

This tells us that we got a periodic target $T(x)$ with the fundamental frequency:

$$\nu = 2\varrho \sin\varphi \tag{3.14}$$

The frequency can be varied by rotation of the angels ($\pm\varphi$). The fringes are always vertical, since $\mu = 0$.

What can we do with such a variable grating? Many, many things; some of them will be discussed now, others later. But for many applications it is desirable that this periodic mask $T(x)$ is close to a pure sine-target. In other words, we want $A_0 A_0$ and $A_{+1}A_{-1}$ large, but all higher coefficients small. Now it is time to specify the "groove shape". Cheap and simple gratings are usually transparent or opaque:

$$T_1(y) = \begin{cases} +1 & : \text{ in } |y| \le \frac{a}{2} \\ 0 & : \text{ otherwise} \end{cases} \quad (\text{but of course still periodic, i.e. } T(y) = T(y+Md)) \tag{3.15}$$

$$A_0 = \frac{a}{d}; \qquad A_n = \frac{a}{d}\,\mathrm{sinc}(n\frac{a}{d}); \qquad \text{call} : \frac{a}{d} = \alpha \tag{3.16}$$

Such a "square-wave grating" is called a Ronchi-Ruling if $\alpha = \frac{1}{2}$, which means that the opaque bars are just as wide as the slits between them. Now let us assume that both gratings had the same period d, but different slit widths a and b respectively.

$$\begin{aligned} \frac{a}{d} = \alpha; \quad A_0 &= \alpha; \quad A_n = \alpha\,\mathrm{sinc}(n\alpha) \\ \frac{b}{d} = \beta; \quad B_0 &= \beta; \quad B_m = \beta\,\mathrm{sinc}(m\beta) \end{aligned} \tag{3.17}$$

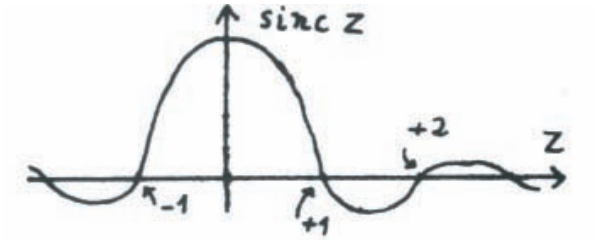

Figure 3.3: The shape of the sinc-function

With these assumptions we get:

$$T(x) = \alpha\,\beta \sum_{-\infty}^{+\infty} \mathrm{sinc}(n\alpha)\,\mathrm{sinc}(n\beta)\,e^{2\pi i(x-x_0)2n\varrho\sin\varphi} \tag{3.18}$$

The $\mathrm{sinc}(z)$ function has the property of being zero wherever z is an integer, except for $z = 0$, where $\mathrm{sinc}(0) = 1$. For a sinusoidal pattern $T(x)$ we want the second Fourier coefficient to vanish, which means $\mathrm{sinc}(n\alpha)\,\mathrm{sinc}(n\beta) = 0$ for $|n| = 2$. This is accomplished by choosing $\alpha = \frac{1}{2}$ or $a = \frac{d}{2}$. By the way, this choice of α eliminates some of the higher Fourier coefficients with $|n| = 4, 6, \ldots$. We still have β free, which we chose to eliminate the $|n| = 3$ term by means of $\beta = \frac{1}{3}$ or $b = \frac{d}{3}$. The first time where sinc sinc is not zero is at $n = 5$, but that term is fairly small because the sinc-function decreases like n^{-1}. The ratio of the fifth to the first Fourier coefficient of $T(x)$ is in this case:

$$\frac{\mathrm{sinc}(5\alpha)\,\mathrm{sinc}(5\beta)}{\mathrm{sinc}(\alpha)\,\mathrm{sinc}(\beta)} = \frac{1}{25}\frac{\sin(5n\alpha)\,\sin(5n\beta)}{\sin(n\alpha)\sin(n\beta)} \tag{3.19}$$

In practice this ratio of $5-$th harmonics to fundamental frequency is even smaller, because usually the edges of the gratings are not ideally sharp, which is equivalent to a reduction in higher harmonics' constants.

In order to find other periodic functions with no even harmonics ($|n| = 2, 4, \ldots$) it is useful to know that the set of all these functions is described by $f(x) + f(x + d/2) =$ constant.

Proof: We represent $f(x) + f(x + d/2)$ by its Fourier series, which by assumption is constant (= trivial case of a periodic function):

$$\sum A_n \left[1 + e^{2\pi i n\nu\frac{d}{2}}\right] e^{2\pi i n\nu x} = \mathrm{const} \tag{3.20}$$

The second term in the square bracket, which is actually $(-1)^n$ due to $\nu d = 1$, is a consequence of the shift theorem. If this Fourier series actually equals a constant, then all of its $(n \neq 0)$ Fourier coefficients $A_n[1 + (-1)^n]$ must be zero. For odd n this is guaranteed by the square brackets. Hence A_n (n odd) may be non-zero. But for even n it is necessary that $A_{2n} = 0$ in order to satisfy the assumptions $f(x) + f(x + d/2) = \mathrm{constant}$. The constant happens to be $2A_0$.

3.3 Moiré illustrations

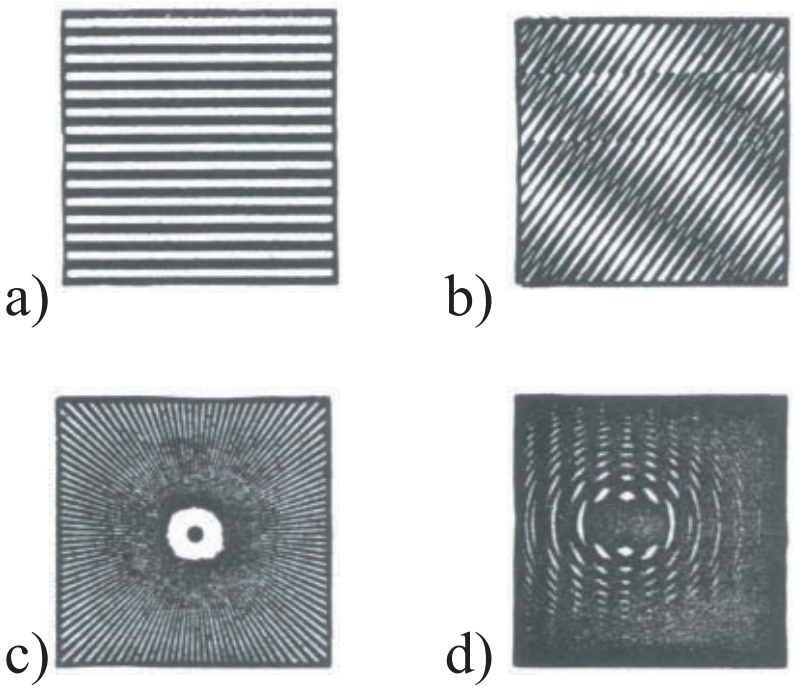

Figure 3.4: The Moiré effect: a) square wave grating; b) Moiré of a perfect grating and an imperfect grating; c) a pattern periodic in azimuth angle φ; d) Schuster fringes; Moiré of two FZPs.

4 An Optical Analog Computer for Fourier Transformation

Now we want to show that our Moiré system which consisted of the two rotating gratings can be used as an analog computer for calculating the coefficients of a Fourier series. Assume a periodic function (period Q) $f(x)$ has been measured and recorded on paper. Let us cut out one full period of this function, such that the hole in this "function mask" is described by $0 \leq y \leq f(x);\ 0 \leq x \leq Q$. Next we superpose our Moiré-mask $T(x,y)$ onto the function mask. Then we illuminate the masks with uniform brightness. Behind the masks we collect the light and measure it with some type of photodetector. We do this for various Moiré-angles φ, getting as photoelectric signal:

$$S(\sin\varphi) = \int_0^Q (x) \int (y) T(x,y) M(x,y) \mathrm{d}x \mathrm{d}y \tag{4.1}$$

Herein M stands for the "function mask":

$$M(x,y) = \begin{cases} +1 & : \text{ if } 0 \leq y \leq f(x) \text{ and if } 0 \leq x \leq Q \\ 0 & : \text{ elsewhere} \end{cases} \tag{4.2}$$

By $T(x,y)$ we mean the Moiré superposition of two rotated gratings which we discussed before:

$$\begin{aligned} T(x,y) &= \sum\sum A_n B_m e^{2\pi i \varrho[\ldots]}; \\ [\ldots] &= (n+m) y \cos\varphi + (n-m)(x-x_0)\sin\varphi \end{aligned} \tag{4.3}$$

$A_n \sim$ first grating at $+\varphi$ orientation; $A_n = \alpha \sin(n\alpha)$
$B_n \sim$ second grating at $-\varphi$ orientation; $B_n = \beta \sin(m\beta)$

The function mask M and parts of the two-grating patterns T are shown in the Fig. 4.1. Notice that the height $f(x)$ of the function mask is fairly large in comparison to the period d of the two gratings.

The limits of the y-integration in $S(\ldots)$ are 0 and $f(x)$, as expressed by $M(x,y)$. Hence $S(\sin\varphi)$ can be written also as:

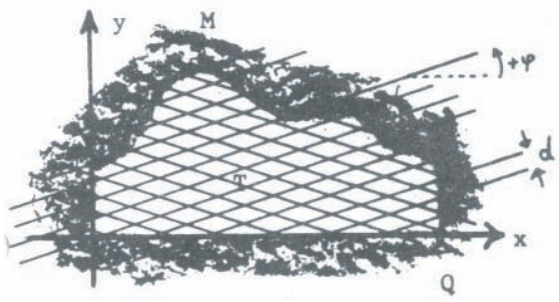

Figure 4.1: Superposition of the function mask M and the two grating patterns.

$$S(\sin\varphi) = \int_0^Q (x) \int_0^{f(x)} (y) T(x,y) \mathrm{d}y \mathrm{d}x \tag{4.4}$$

The function $f(x)$ of which we wish to get the Fourier transform appears as the integration limit. In order to get $f(x)$ down into the integrand we re-write $S(\sin\varphi)$ again:

$$S(\sin\varphi) = \int_0^Q (x) f(x) \left\{ \frac{1}{f(x)} \int_0^{f(x)} (y) T(x,y) \mathrm{d}y \right\} \mathrm{d}x \tag{4.5}$$

If $S(\sin\varphi)$ is really a Fourier transform of $f(x)$ then the content of the $\{\ldots\}$ bracket must be something like $e^{-2\pi i\nu x}$. This will turn out to be true. It is not surprising since the expression $F(x,\varphi) = \frac{1}{f}\int_0^f T(x,y)\mathrm{d}y$ is practically what we have called previously the "vertically smeared Moiré pattern". Inserting $T(x,y)$ we get:

$$F(x,\varphi) = \frac{1}{f} \sum\sum A_n B_m e^{2\pi i\varrho(n-m)(x-x_0)\sin\varphi} \int_0^f e^{2\pi i\varrho(n+m)y\cos\varphi} \mathrm{d}y \tag{4.6}$$

Herein the y-integral is:

$$\frac{1}{f}\int_0^f e^{2\pi i\varrho(n+m)y\cos\varphi}\mathrm{d}y = \begin{cases} +1 & : \text{ if } n+m=0 \\ (e^{2\pi i\overline{\mu}f}-1) & : \text{ if } n+m\neq 0 \end{cases} \tag{4.7}$$

$$\text{where} : \overline{\mu} = (n+m)\varrho\cos\varphi$$

This expression is almost equal to $\delta_{n,-m}$, because the result for $n+m \neq 0$ is very small:

$$\left|\frac{e^{2\pi i\overline{\mu}f}-1}{2\pi i\overline{\mu}f}\right| = |\mathrm{sinc}(\overline{\mu}f)| \leq |\pi\overline{\mu}f|^{-1} = \pi\left|\frac{d}{(n+m)f(x)\cos\varphi}\right| \tag{4.8}$$

In the worst case $|n+m|=1$; $f(x)=f_{\min}$; $\cos\varphi = 0.87$; $\sin\varphi = 0.5$; $\varphi = 30°$:

$$\frac{\pi d}{0.87 f_{\min}} = 3.5\frac{d}{f_{\min}} \leq 3.5\%;\ \text{if } f_{\min} \geq 100d;\ d = 0.1\mathrm{mm};\ f_{\min} \geq 1\mathrm{cm} \tag{4.9}$$

In might happen that the function $f(x)$ goes down to zero occasionally, or it may even be negative. In that case we add a constant to $f(x)$ such that $f(x)+$ constant ≥ 1 cm (in our example). Since we know beforehand how an additive constant influences a Fourier transformation we can easily subtract its effect. From now on let us assume that a good approximation is:

$$\frac{1}{f(x)}\int_0^{f(x)} e^{2\pi i(n+m)\varrho\cos\varphi}\mathrm{d}y = \delta_{n,-m} \tag{4.10}$$

From this it follows that:

$$F(x,\varphi) = \left(\frac{1}{f(x)}\right)\int_0^{f(x)} T(x,y)\mathrm{d}y = \sum A_n B_{-n} e^{2\pi i(x-x_0)2n\varrho\sin\varphi} \tag{4.11}$$

We will abbreviate $A_n B_{-n}$ as D_n. If T_1 and T_2 are real then A_n and B_n (and hence also D_n) satisfy the reality symmetry $A_n = A^*_{-n}$. Inserting this we get for the photoelectric signal:

$$\begin{aligned} S(\sin\varphi) &= \int_0^Q f(x)\sum D_n e^{2\pi i(x-x_0)2n\varrho\sin\varphi}\mathrm{d}x \\ &= \sum D_n e^{-4\pi i n x_0\varrho\sin\varphi}\int_0^Q f(x)e^{4\pi i n x\varrho\sin\varphi}\mathrm{d}x \end{aligned} \tag{4.12}$$

The integral is equal to QC_{-nm} if the angle φ is set such that $4\pi n x\varrho\sin\varphi = 2\pi nm\frac{x}{Q}$ Thus we get:

$$S\left(\frac{m}{2\varrho Q}\right) = Q\sum_{-\infty}^{+\infty}(n)D_n e^{-2\pi i n m\frac{x_0}{Q}}C_{-nm} \tag{4.13}$$

This result would be very nice, if only D_0 and $D_{\pm 1}$ would be non-zero and $D_{+1} = D_{-1} = |D_1|$. We know this can be done in fairly good approximation if $A_n = \alpha\,\mathrm{sinc}(n\alpha)$ and $B_n = \beta\,\mathrm{sinc}(n\beta)$ with $\alpha = \frac{1}{2}$ and with $\beta = \frac{1}{3}$. Then we have:

$$\frac{1}{Q}\,S\left(\frac{m}{2Q\varrho}\right) \rightarrow S_{C_m} = D_0C_0 + 2D_1|C_m|\cos(2\pi m\frac{x_0}{Q} + \gamma_m) \tag{4.14}$$

Herein we have set $C_m = |C_m|e^{i\gamma_m}$ and $C_m = C^*_{-m}$ due to $f(x)$ being *real*. Since the center of rotation x_0 is a parameter, which we are free to select, we might set it once so that $\frac{x_0}{Q}$ is an integer.

$$S\left(\frac{m}{2Q\varrho}\right) \rightarrow S_{C_m} = D_0C_0 + 2D_1|C_m|\underline{\cos\gamma_m} \tag{4.15}$$

During a second measurement we shift x_0 a little bit such that:

$$2\frac{mx_0}{Q} = -\frac{\pi}{2} + M2\pi;\ M \text{ integer} \tag{4.16}$$

In this case we get:

$$S\left(\frac{m}{2Q\varrho}\right) \rightarrow S_{S_m} = D_0C_0 + 2D_1|C_m|\underline{\sin\gamma_m} \tag{4.17}$$

Hence we get both the real part and the imaginary part of C_m.

Now let us assume that we cannot neglect the higher harmonics of our Moiré pattern; in other words, D_2, D_3 might not be negligibly small. We can cope with this either by computing the true coefficients C_m from the measured coefficients S_m, or we can employ an electronic trick.

First we will develop a mathematical recursion approach, which works if all Fourier coefficients C_n of the function $f(x)$ with $|n| > N$ (fixed) vanish. To avoid clumsiness we further simplify (although this is not necessary) as follows:

$$\begin{aligned} \gamma &= 0 \rightarrow C_{nm} = C_{-nm};\ D_n = D_{-n}; x_0 = 0 \\ S_m &= \sum D_nC_{nm};\ (|nm| \leq N) \\ S_m &= D_0C_0 + 2\sum_{n=1}^{n\leq N/m} D_nC_{nm} \end{aligned} \tag{4.18}$$

First let us take care of C_0. In this set of equations the D-coefficients describe the know Moiré, the S-coefficients are measured, and the C-coefficients are the desired Fourier coefficients of the function $f(x)$.

$$S_0 = D_0 C_0 + 2C_0 \sum_{n=1}^{N} D_n \rightarrow C_0 = \frac{S_0}{D_0 + 2\sum\limits_{n=1}^{N} D_n} \tag{4.19}$$

Now we will define two convenient abbreviations:

$$\frac{D_n}{D_1} = E_n; \quad \frac{(S_m - 2D_0 C_0)}{2D_1} = G_m \tag{4.20}$$

Thereby we simplify the old set of equations into a new form:

$$\begin{aligned} S_m &= D_0 C_0 + 2\sum_{(n)} D_n C_{nm} \qquad (1 \le n \le \frac{N}{m}) \\ G_m &= \sum_{(n)} E_n C_{nm} \qquad (1 \le n \le \frac{N}{m}; \quad nm \le N) \end{aligned} \tag{4.21}$$

The algorithm which leads to a simple sequential solution of this set of linear equations becomes apparent if we write this system down in some detail:

$$\begin{array}{lcccccccc} G_1 & = & E_1C_1 + & E_2C_2 + & E_3C_3 + & E_4C_4 + & \ldots + & E_N C_N \\ G_2 & = & & E_1C_2 + & & E_2C_4 + & \ldots + & E_{N'} C_{2N'} \\ G_3 & = & & & E_1C_3 + & & \ldots + & E_{N''} C_{3N'''} \\ \ldots & & & & & & & \\ G_{N-1} & = & & & & & E_1C_{N-1} & \\ G_N & = & & & & & & E_1C_N \end{array} \tag{4.22}$$

There are no contributions from below the diagonal. The last two equations and in fact all equations with $m > \frac{N}{2}$ have only one single term on the right hand side. Therefore we can solve these equations immediately, for $m > \frac{N}{2}$: $C_m = \frac{G_m}{E_f}$. Before going on to solve the other C_m values we have to state what is meant by N' and N'', which are integers in the second and third equations. For example the second equation with $m = 2$ is $G_2 = \sum E_n C_{2n}$. Since by assumption the Fourier-coefficients vanish if the coefficient is larger than N, this can occur for the second equation at $2n \rightarrow N + 2$ or $2n \rightarrow N + 1$, depending on whether N happens to be even or odd. Similarly N'' in the third equation is defined as:

$$3N'' = \left\{ \begin{array}{c} N \\ N-1 \\ N-2 \end{array} \right\} \text{ which ever is divisible by 3.} \tag{4.23}$$

Now we continue to solve our equation system:

$$G_m = \sum(n) E_n C_{nm};\ (1 \le n \le \frac{N}{M}) \tag{4.24}$$

We know already the C_m with $m > \frac{N}{2}$. These coefficients were easy to find since the corresponding equations had only one single term. Almost as simple are the equations with $\frac{N}{3} < m \le \frac{N}{2}$ since they can have at most *two* terms, the last one being known already. For this range of coefficients we get:

$$G_m = E_1 C_m + E_2 C_{2m} \tag{4.25}$$

From before we know $C_{2m} = \frac{G_{2m}}{E_1}$. Hence:

$$G_m = E_1 C_m + E_2 \frac{G_{2m}}{E_1};\quad C_m = \frac{G_m}{E_1} - E_2 \frac{G_{2m}}{E_1^2} \tag{4.26}$$

Next we would attack the range $\frac{N}{4} < m \le \frac{N}{3}$ and so on. A more elaborate treatment of this recursive algorithm is described by J. W. Coltman in JOSA 44, 468 (1954) and in even more generality by R. Röhler, Optik 19, 487 (1962). The electronic trick which we briefly mentioned as a means of avoiding the necessity to bother with the higher harmonic coefficients of the Moiré mask will be presented after we have learned enough about the Fourier integral.

5 Some More Moiré Effects

When we look at some of the patterns of Edmund's Moiré-kit it becomes obvious that these patterns are not strictly periodic in the sense of our first definition. But one hesitates to call these patterns "aperiodic". Actually they fall into the category of "quasi-periodic functions". In order to understand the Moiré effect of two quasi-periodic patterns in superposition we have to develop first some appropriate mathematical tools.

5.1 Fourier series representation of quasi-periodic functions

It is a wide-spread misconception that the application of a Fourier-series representation to describe a geometrical pattern $f(x)$ requires this pattern to be periodic like $f(x) = f(x + Md);\ |M| = 0, 1, 2, \ldots$. This is a *sufficient* condition, but not a *necessary* one. Assume for example the following pattern, which is "quasi-periodic": $g(x^3) = g(x^3 + Md)$. This function is not periodic in x, but in x^3. Hence it is possible to write:

$$g(x^3) = \sum_{-infty}^{+\infty} C_n e^{2\pi i n \frac{x^3}{d}};\ C_n = \frac{1}{d} \int_{-\frac{d}{2}}^{\frac{d}{2}} g(x^3) e^{-2\pi i n \frac{x^3}{d}} \, \mathrm{d}x^3 \tag{5.1}$$

An example of this set of quasi-periodic functions is $\cos(2\pi \frac{x^3}{d})$.

A more general definition of quasi-periodicity is:

$$f(\phi(x,y)) = f(\phi(x,y) + M);\ |M| = 0, 1, 2, \ldots \tag{5.2}$$
$$f(\phi(x,y)) = \sum C_n e^{2\pi i n \phi(x,y)}$$

A fruitful consequence is presented in Applied Optics 6, 1567 - 1570 (1967): "Variable Fresnel Zone Pattern".

5.2 Schuster fringes

Schuster fringes occur when two Fresnel zone plates are superposed. This subject was treated already in the reprint (Appl. Opt. 6, 1567, 1967). We now want to go deeper into the theory

of the Schuster fringes. This is justified in my opinion because this project is well suited for illustrating what spatial frequencies and quasi-periodic functions are. Furthermore I feel that there might be some applications of Schuster fringes still to be invented.

The Fresnel zone plate (abbreviated FZP) is a fairly simple example of a quasi-periodic function.

$$\begin{aligned} M(r^2) &= M(r^2 + mR_1^2); \qquad m = 1, 2, \ldots \\ M(r^2) &= \begin{cases} +1 & : \text{ if } |r^2 - (m + \frac{1}{2})R_1^2| \le \alpha R_1^2 \\ 0 & : \text{ otherwise; usually } \alpha = \frac{1}{4},\ m = 1, 2, \ldots \end{cases} \end{aligned} \tag{5.3}$$

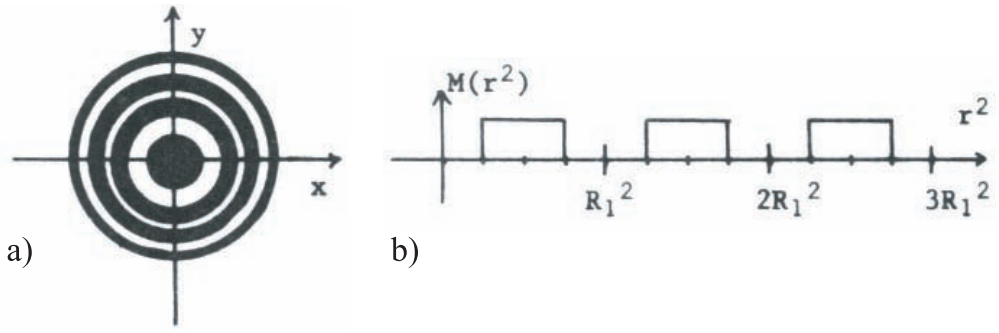

Figure 5.1: The Fresnel Zone Pattern as a quasi periodic function.

It does not do any harm if we formally continue $M(r^2)$ to negative r^2 if we never draw any conclusions about that half of the r^2-range where r would be imaginary. I mention this only so that you will not have scruples about representing $M(r^2)$ by a Fourier series, which formally is valid for the whole range $(-\infty, +\infty)$ of the argument.

$$\begin{aligned} M(r^2) &= \sum_{-\infty}^{\infty} A_n e^{2\pi i n \left(\frac{r}{R_1}\right)^2} \\ A_n &= \left(\frac{1}{R_1}\right)^2 \int_0^{R_1^2} M(r^2) e^{-2\pi i n (\frac{r}{R_1})^2} \mathrm{d}r^2 \end{aligned} \tag{5.4}$$

The equivalent formulas for more general quasi-periodic functions are:

$$
\begin{aligned}
F(x,y) &= f\{\phi(x,y)\} = f\{\phi(x,y)+m\} \\
f\{\phi(x,y)\} &= F(x,y) = \sum_{-\infty}^{\infty} A_n e^{2\pi i n\phi(x,y)} \\
A_n &= \int_0^1 F(x,y) e^{-2\pi i n\phi(x,y)} \mathrm{d}\phi(x,y)
\end{aligned}
\tag{5.5}
$$

This means a path-integral in the (x,y) domain from a point (x_0,y_0), where $\phi(x_0,y_0)=0$, to another point (x_1,y_1), where $\phi(x_1,y_1)=1$ (Fig. 5.2 a). This looks awfully impractical in the most general case. Fortunately in those particular cases in which we are interested, everything will be quite simple.

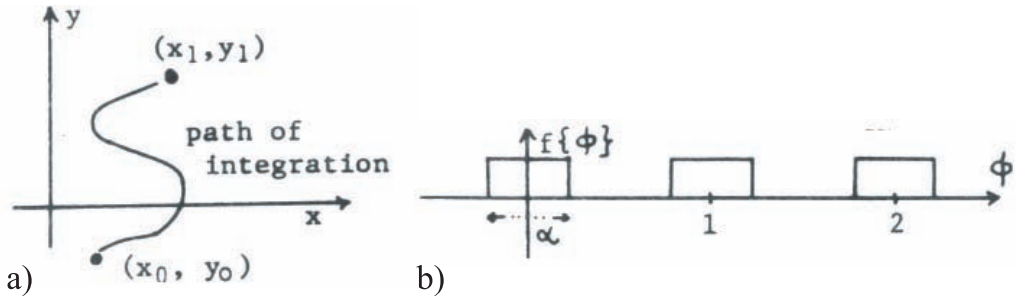

Figure 5.2: a) Path of integration; b) the general quasiperiodic function.

$$
\begin{aligned}
f\{\phi(x,y)\} &= \begin{cases} +1 & : \text{ if } |\phi - m| \le \frac{\alpha}{2}; \quad \mathrm{m}: \text{ integer} \\ 0 & : \text{ otherwise;} \end{cases} \\
f\{\phi\} &= \sum A_n e^{2\pi i n\phi}; \quad A_n = \alpha\,\mathrm{sinc}(n\alpha)
\end{aligned}
\tag{5.6}
$$

In the case of the Fresnel zone plate it was $\phi(x,y) = \frac{(x^2+y^2)}{R_1^2}$ and:

$$
M\{\phi(x,y)\} = \begin{cases} +1 & : \text{ if } |\phi(x,y) - \left(m+\frac{1}{2}\right)| \le \frac{\alpha}{2}; \quad \mathrm{m}: \text{ integer} \\ 0 & : \text{ otherwise;} \end{cases}
\tag{5.7}
$$

Hence $A_n = (-1)^n \alpha\,\mathrm{sinc}(n\alpha)$; ($(-1)^2$ due to the shift by $\frac{1}{2}$ period).

Now we are well prepared to study what happens if two FZP's are put on top of each other and shifted sidewise. In other words we study FZP-Moiré, which had been observed first by Schuster in 1924, treated theoretically in Optik 18, 514 (1961).

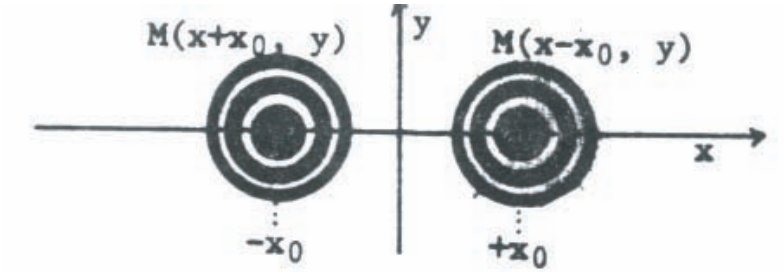

Figure 5.3: Two shifted Fresnel Zone Plates

The joint transmittance of the two symmetrically shifted FZP's is:

$$\begin{aligned} M_1(x-x_0,y)M_2(x+x_0,y) &= T(x,y,x_0);\ M_1 \sim A_n;\ M_2 \sim B_m \\ T &= \sum\sum A_n B_m e^{2\pi i[\ldots]\frac{1}{R_1^2}} \end{aligned} \tag{5.8}$$

where:

$$\begin{aligned} [\ldots] &= n\left\{(x-x_0)^2+y^2\right\} + m\left\{(x+x_0)^2+y^2\right\} = \\ &= (n+m)\{x^2+y^2+x_0^2\} - 2(n-m)xx_0 = \\ &= (n+m)\left\{\left(x-\frac{n-m}{n+m}x_0\right)^2+y^2\right\} + \frac{4nm}{n+m}x_0^2 \end{aligned} \tag{5.9}$$

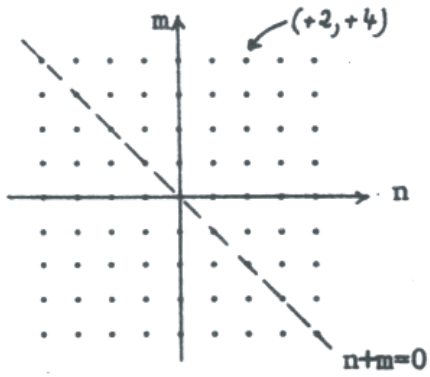

Figure 5.4: The symbolic index domain.

It will be obvious soon that these three different versions of the exponent of $T(x,y;x_0)$ are quite handy, if we want to discuss T. This T consists, mathematically, of a double sum:

$-\infty < n < \infty; -\infty < m < \infty$. We can assign points in a symbolic index domain (two-dimensional discrete space, Fig. 5.4).

The double sum $\sum \sum_{-\infty}^{\infty}(n,m)$ covers the whole plane. Instead of looking at the whole double sum it makes sense, physically, to consider partial sums, and ask what they mean.

$\boxed{N \neq 0,\ m = 0}$ ($\sim$ along the n-axis).

Look at the first version of the square bracket which describes the exponent of the joint transmittance $T(x, y, x_0)$. Only $n\left\{(x - x_0)^2 + y^2\right\}$ remains. In other words,

$$B_0 \sum A_n e^{2\pi i(n(x-x_0)^2+y^2)/R_1^2} = B_0 M_1(x + x_0, y) \tag{5.10}$$

When actually looking at the FZP-Moiré one still can concentrate and recognize M_1. In other words we really see this partial sum with $m = 0$.

$\boxed{n = 0, m \neq 0}$ by similar argument gives $A_0 M_2(x + x_0, y)$.

$\boxed{\text{n+m = 0}}$ This partial sum, which takes into account all points on the $-45°$ line through the center of the index plane, is best understood by looking at the second version of the square bracket in the T-exponent, which now becomes $-4nxx_0$, due $n + m = 0$, or $m = -n$. Hence this partial sum gives

$$\sum_{n+m=0} A_n B_{-n} e^{-2\pi i 4nxx_0/R_1^2} \tag{5.11}$$

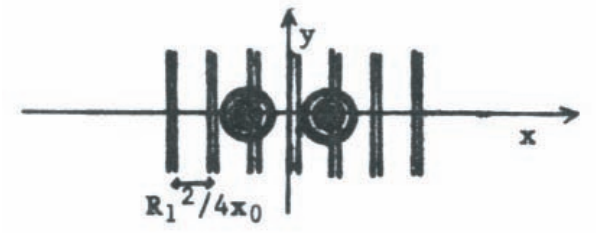

Figure 5.5: Schuster fringes.

This pattern, called "Schuster fringes", which is clearly visible for moderately small x_0, consists of vertical stripes with a spatial frequency:

$$\nu_{\text{Schuster}} = \frac{4x_0}{R_1^2} \tag{5.12}$$

One can see these fringes even more clearly if one wipes out all terms but those with $n+m=0$. This can be done by y-smearing, which corresponds to integration:

$$\frac{1}{\Delta y}\int\limits_{-\frac{\Delta y}{2}}^{\frac{\Delta y}{2}} T(x,y,x_0)\mathrm{d}y = \tag{5.13}$$

$$= \sum\sum A_n B_m e^{-4\pi i(n-m)xx_0/R_1^2}\cdot\frac{1}{\Delta y}\int\limits_{-\frac{\Delta y}{2}}^{\frac{\Delta y}{2}} e^{2\pi i(n+m)\{\ldots\}/R_1^2}\mathrm{d}y$$

Where $\{\ldots\}=x^2+y^2+x_0^2$. The y-integral is in essence:

$$\frac{1}{\Delta y}\int\limits_{-\frac{\Delta y}{2}}^{\frac{\Delta y}{2}} e^{2\pi i(n+m)y^2/R_1^2}\mathrm{d}y = \left\{\begin{array}{cc} +1 & \text{if } n+m=0 \\ \text{very small} & \text{if } n+m\neq 0 \text{ and } \Delta y >> R_1 \end{array}\right\} \approx \delta_{n,-m} \tag{5.14}$$

Let us postpone for a moment the proof that "very small ≈ 0" for $(n+m)\neq 0$. Then only the $(n+m=0)$ terms survive, hence $m=-n$, which leads us to:

$$\frac{1}{\Delta y}\int\limits_{-\frac{\Delta y}{2}}^{\frac{\Delta y}{2}} T(x,y,x_0)\mathrm{d}y \approx \sum A_n B_{-n} e^{-2\pi i 4xx_0/R_1^2} \tag{5.15}$$

Having considered so far the partial sums $\boxed{m=0;\ n=0}$ and $\boxed{n+m=0}$, it is obvious to ask, if $\boxed{n-m=0}$ yields anything noticable. We set $m=n$ in the $\sum\sum$ of $T(x,y;x_0)$ and get (see the second version of the square bracket of the T-exponent):

$$\sum A_n B_n e^{4\pi i n x_0^2/R_1^2} e^{4\pi i n(x^2+y^2)/R_1^2} \tag{5.16}$$

The term $e^{4\pi i n(x^2+y^2)/R_1^2}$ indicates a FZP pattern around $x=0, Y=0$, but with reduced scale (factor $\frac{1}{\sqrt{2}}$):

$$4\pi\frac{(x^2+y^2)}{R_1^2} = 2\pi\frac{(x^2+y^2)}{\left(\frac{R_1}{\sqrt{2}}\right)^2} \tag{5.17}$$

This ring system, or FZP pattern, at the center, between the two genuine FZPs $M_1(x-x_0,y)$ and $M_2(x+x_0,y)$ is easily observable if the two FZPs are separated enough. Upon

moving the two FZPs laterally in opposite directions (= changing x_0), one will observe that this in-between-FZP constantly changes its polarity, meaning a dark or bright center. This is due to the factor $e^{4\pi i n x_0^2/R_1^2}$, which is the phase factor of the joint "Fourier"-coefficient $A_n B_n e^{4\pi i n x_0^2/R_1^2}$. As we know from the shift theorem, a phase of the Fourier-coefficients means a shift of the function. The phase shift is proportional to the index n, as it should be according to the shift theorem. Hence the oscillation polarity is nothing but a shift of $M(r^2)$ along r^2-axis.

The third version of the square brackets in the T exponent becomes useful when considering the partial sums:

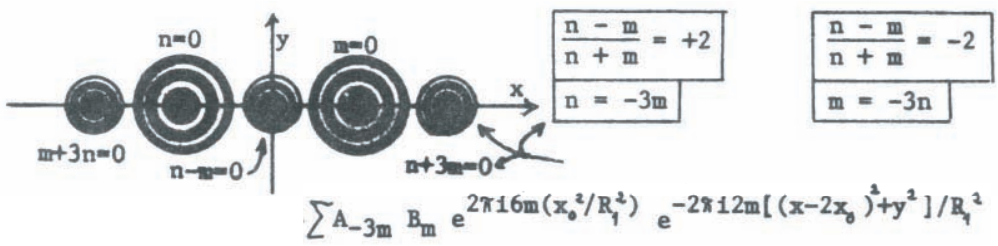

Figure 5.6: Schuster fringes part 2.

This is an FZP centered at $x = 2x_0$, $y = 0$, with reduced scale by $\frac{1}{\sqrt{2}}$, and with oscillating polarity.

Now we will return to the y-integral and prove that it is practically a Kronecker $\delta_{n,-m}$:

$$\frac{1}{\Delta y} \int_{-\frac{\Delta y}{2}}^{\frac{\Delta y}{2}} e^{2\pi i(n+m)y^2/R_1^2} \mathrm{d}y \tag{5.18}$$

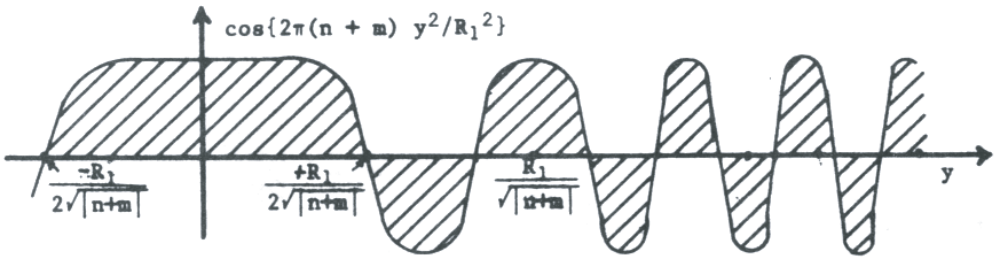

Figure 5.7: The function $\cos(\ldots y^2)$

For convenience we split the exponential function into cosine and sine. One might be tempted to discard the integral over the sine-function because $\sin y$ is asymmetric. However both $\cos(\ldots y^2)$ and $\sin(\ldots y^2)$ are even functions (because of the y-square). So one cannot simply discard the $\int \sin(\ldots y^2)$, although the range of integration is symmetrical around $y = 0$. Let us anyway restrict our considerations to the cosine case. The sine-case is very similar. First we plot the cosine-integrand:

The alternating patches become smaller and smaller. Hence for $C > 0$:

$$\int_{-\frac{R_1}{(2\sqrt{|n+m|}+C)}}^{\frac{R_1}{(2\sqrt{|n+m|}+C)}} \cos\left\{\frac{2\pi(n+m)y^2}{R_1^2}\right\}\mathrm{d}y < \int_{-\frac{R_1}{(2\sqrt{|n+m|})}}^{\frac{R_1}{(2\sqrt{|n+m|})}} \cos\left\{\frac{2\pi(n+m)y^2}{R_1^2}\right\}\mathrm{d}y \quad (5.19)$$

Hence the integral from $-\frac{\Delta y}{2}$ to $\frac{\Delta y}{2}$ with $\cos\{\ldots y^2\}$ is biggest if the range Δy covers only the central bump of the $\cos\{\ldots y^2\}$ function. Since furthermore $0 \leq \cos \leq 1$ in that region we arrive at a conservative estimate by replacing the cosine by $+1$ and the integration limits $\pm\frac{\Delta y}{2}$ by $\pm\frac{R_1}{2\sqrt{|n+m|}}$. So we see that:

$$\frac{1}{\Delta y}\int_{-\frac{\Delta y}{2}}^{\frac{\Delta y}{2}} \cos\left\{\frac{2\pi(n+m)y^2}{R_1^2}\right\}\mathrm{d}y < \frac{R_1}{\Delta y\sqrt{|n-m|}} \quad (5.20)$$

Since the sine-portion of the exponential function leads to an even smaller boundary we can safely state:

$$\frac{1}{\Delta y}\int_{-\frac{\Delta y}{2}}^{\frac{\Delta y}{2}} e^{2\pi i(n+m)y^2/R_1^2}\mathrm{d}y = \delta_{n,-m};\ \text{if } \Delta y >> R_1,\ \text{and } m \neq n \quad (5.21)$$

6 The Dirac or Delta "Function"

6.1 Introduction

It is not a proper function, just a "distribution" in the sense of Laurent Schwartz, but that shall not bother us. If you want to know exactly what δ is, and what you are allowed to do with it, look up for example Lighthill, Fourier Analysis and Generalized Functions (Cambridge University Press, 1960). In many books $\delta(x-t)$ is defined as:

$$\delta(x-t) = \begin{cases} +\infty & : \text{ if } x = t \\ 0 & : \text{ if } x \neq t \end{cases} \quad \text{such that} \int \delta(x-t)\mathrm{d}x = 1 \tag{6.1}$$

This is rather sloppy, which in itself does not bother me too much, but it is limited in scope, excluding certain useful approaches to δ. It is better to define δ such that for any function $f(x)$, which is continuous at $x = t,\ \delta$ has the effect of:

$$\int f(x)\delta(x-t)\mathrm{d}x = f(t) \tag{6.2}$$

This implicit definition is sometimes called the "sifting theorem". This indirect way of defining δ describes what *is used*, but leaves open what *really is*. Actually there is more than one form of δ which satisfies the implicit definition.

6.2 Several forms of $\delta(x)$

$$\delta(x-t) = \lim_{A\to\infty} \begin{cases} A & : \text{ if } |x| \leq \frac{1}{2A} \\ 0 & : \text{ if } |x| > \frac{1}{2A} \end{cases}$$

It is plausible that this form of delta satisfies the implicit definition if the rectangle gets narrower and higher, but maintains its area:

$$\int_{-\infty}^{\infty} f(x)\delta(x-t)\mathrm{d}x = \lim_{A\to\infty} \int_{-\infty}^{\infty} f(x) A \operatorname{rect}\left(\frac{x-t}{\frac{1}{A}}\right)\mathrm{d}x = f(x) \tag{6.3}$$

Herein we define:

$$\mathrm{rect}(x) = \begin{cases} 1 & \text{if } |x| \le \frac{1}{2} \\ 0 & \text{if } |x| > \frac{1}{2} \end{cases} \quad \text{hence : } \mathrm{rect}\left(\frac{x-t}{\frac{1}{A}}\right) \begin{cases} 1 & \text{if } |x-t| \le \frac{1}{2A} \\ 0 & \text{if } |x-t| > \frac{1}{2A} \end{cases} \tag{6.4}$$

We can also use:

$$\delta(x-t) = \left(\frac{1}{\sqrt{\pi}}\right) \lim_{\epsilon \to 0} \left\{ \frac{1}{\sqrt{\epsilon}} e^{-(x-t)^2/\epsilon} \right\} \tag{6.5}$$

The above is a Gauss-function of normalized area, getting very slim.
Another way:

$$\delta(x-t) = \frac{1}{\pi} \lim_{\epsilon \to 0} \left\{ \frac{\epsilon}{\epsilon^2 + (x-t)^2} \right\} \tag{6.6}$$

Here the limit process is applied to a Lorentzian. Other possibilities:

$$\begin{aligned}
\delta(x-t) &= \lim_{A\to\infty} \{A\,\mathrm{sinc}[A(x-t)])\} \qquad (6.7)\\
\delta(x-t) &= \lim_{A\to\infty} \left\{A\,\mathrm{sinc}^2[A(x-t)]\right\} \\
\delta(x-t) &= \lim_{A\to\infty} \{A\,\mathrm{trian}[1-A|x-t|]\} \text{ with } \mathrm{trian}(x) = \begin{cases} 1-|x| & \text{if } |x| \le 1 \\ 0 & \text{otherwise} \end{cases} \\
\delta(x-t) &= \frac{1}{\pi} \lim_{A\to\infty} \left\{ \frac{1-\cos[A\,(x-t)]}{A\,(x-t^2)} \right\} \\
\delta(x-t) &= \frac{1}{i\pi} \lim_{A\to\infty} \left\{ \frac{e^{iA(x-t)}}{(x-t)} \right\} \\
\delta(x-t) &= \lim_{A\to\infty} \int_{-A}^{A} e^{2\pi i \nu (x-t)} \mathrm{d}\nu = \lim_{A\,\to\infty} \{2A\,\mathrm{sinc}[(2A(x-t))]\} \\
\delta(x-t) &= \lim_{N\to\infty} \sum_{n=0}^{N} \varphi_n^*(x)\varphi_n(t);\ \text{if } \varphi_n \text{ are a compl. set of orthonorm. funct.} \\
\delta(x-t) &= \frac{1}{2}\frac{\partial}{\partial x} \{\mathrm{sign}(x-t)\}\,;\ \mathrm{sign}(x) = \begin{cases} 1 & \text{if } x > 0 \\ -1 & \text{if } x < 0 \end{cases} \\
\delta(x-t) &= \frac{1}{2}\frac{\partial^2}{\partial x^2} |x-t|
\end{aligned}$$

All definitions satisfy the implicit definition, and all forms are normalized $\int \delta(x-t)\mathrm{d}x = 1$. But not all forms of delta mean that $\delta(x-t) = 0$ whenever $x - t \neq 0$. Take for example:

$$A\,\mathrm{sinc}\{A(x-t)\} = \frac{\sin\{\pi A(x-t)\}}{\pi(x-t)} \tag{6.8}$$

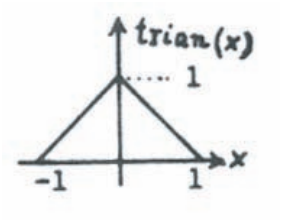

Figure 6.1: The trian function.

Even far away from $x - t = 0$ there will points where $\sin\{A(x-t)\} = 1$, hence it is possible that $A\ \mathrm{sinc}\{A(x-t)\} = \frac{1}{\pi}(x-t)$ (for any $A; x-t$). The reason why, in the sifting integral $\int f(x)\delta(x-t)\mathrm{d}x = f(t)$, this δ operates properly nevertheless, is that $A\mathrm{sinc}A(x-t)$ oscillates very rapidly if A is large. Hence there are no contributions of $f(x)$ from points $x - t \neq 0$ to the integral $\int f(x)\delta(x-t)\mathrm{d}x$. In other words:

$$\delta(x-t) = \lim_{A\to\infty} A\ \mathrm{sinc}\{A(x-t)\} \tag{6.9}$$

is indeed a legitimate representation of the δ-"function".

Now we want to discuss some properties of the Dirac-function:

$$\begin{aligned}
\delta(x) &= \delta(-x) = \delta^*(x) \\
\delta(x) &= \frac{1}{|A|}\delta\left(\frac{x}{A}\right) \\
\delta(x) &= \frac{\delta(x)}{|A|} \\
\delta(f(x)) &= \sum(n)\frac{\delta(x-x_n)}{\left|\frac{\mathrm{d}f(x)}{\mathrm{d}x}\right|_{x=x_n}}
\end{aligned} \tag{6.10}$$

where $f(x_n) = 0$; but $f'(x_n) \neq 0$. For proving it we represent $f(x)$ in the neighborohood of the zero point x_0 by a Taylor series $f(x) \approx 0 + f'(x)(x - x_0)$. Now we have reduced the delta function into a form which allows us to apply $\delta(Ax) = \frac{\delta(x)}{|A|}$.

$$\int \delta(x-t_1)\delta(x-t_1)\mathrm{d}x = \delta(t_1 - t_2) \tag{6.11}$$

Whenever our integrals had no limits specified we meant the range to extend from $-\infty$ to ∞. What happens if the limits of the integral are not $\pm\infty$.

$$\int_{t-\epsilon}^{t+\epsilon} f(x)\delta(x-t)\mathrm{d}x = f(t);\ \text{if } \epsilon \neq 0 \tag{6.12}$$

Now let the integral end just at the δ-peak itself. For this case two new functions are defined: δ_+ and δ_-.

$$\int_{-\infty}^{t} f(x)\delta(x-t)\mathrm{d}x = \frac{1}{2}f(t-0) = \int_{-\infty}^{\infty} f(x)\delta_-(x-t)\mathrm{d}x \tag{6.13}$$

$f(t-0)$ means "limit from the left", i.e.

$$f(t-0) = \lim\{f(t-\alpha)\} \text{ for } 0 \leq \alpha \to 0 \tag{6.14}$$

$$\int_{t}^{+\infty} f(x)\delta(x-t)\mathrm{d}x = \frac{1}{2}f(t+0) = \int_{-\infty}^{+\infty} f(x)\delta_+(x-t)\mathrm{d}x \tag{6.15}$$

Obviously, $\delta_+(x) + \delta_-(x) = \delta(x)$. This enable us now to generalize our original δ-definition, by allowing $f(x)$ to be discontinuous at $x = t$, in other words, it may be $f(t-0) \neq f(t+0)$.

$$\int_{-\infty}^{+\infty} f(x)\delta(x-t)\mathrm{d}x = \frac{f(t+0)+f(t-0)}{2} \tag{6.16}$$

A specific consequence of this "Dirichlet-property" of the delta function is related to the "step function", $H(x)$:

$$H(x)\int_{-\infty}^{t}\delta(x)\mathrm{d}x = \begin{cases} 1 & \text{if } t>0 \\ \frac{1}{2} & \text{if } t=0 \\ 0 & \text{if } t<0 \end{cases} \tag{6.17}$$

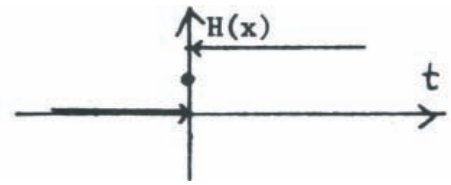

Figure 6.2: The step function.

Now let us consider the derivatives of delta:

$$\int_{-\infty}^{\infty} f(x)\delta'(x)\mathrm{d}x = [f(x)\delta(x)]_{-\infty}^{+\infty} - \int_{-\infty}^{\infty} \left(\frac{\mathrm{d}f(x)}{\mathrm{d}x}\right)\delta(x)\mathrm{d}x \tag{6.18}$$

(integration by parts)

Assume $f(\pm\infty)$ is finite, then $f(\pm\infty)\delta(\pm\infty) = 0$, hence:

$$\int_{-\infty}^{\infty} f(x)\delta'(x)\mathrm{d}x = -\left\{\frac{\mathrm{d}f(x)}{\mathrm{d}x}\right\}_{x=0} \tag{6.19}$$

Slightly more general,

$$\begin{aligned} \int f(x)\frac{\mathrm{d}\delta(x-t)}{\mathrm{d}x} &= -\int \frac{\mathrm{d}f(x)}{\mathrm{d}x}\delta(x-t)\mathrm{d}x = -\left\{\frac{\mathrm{d}f(x)}{\mathrm{d}x}\right\}_{d=t} \\ \int f(x)\frac{\mathrm{d}^n\delta(x-t)}{dx^n}\mathrm{d}x &= (-1)^n\left\{\frac{\mathrm{d}^n f(x)}{\mathrm{d}x^n}\right\}_{x=t} \end{aligned} \tag{6.20}$$

7 The Fourier Integral Transformation

Two functions are called Fourier transforms of each other if they are connected by:

$$f(x) = \int_{-\infty}^{\infty} \tilde{f}(x) e^{2\pi i \nu x} \mathrm{d}\nu \tag{7.1}$$

This definition tells us how to get $f(x)$ if we know $\tilde{f}(\nu)$ already. The next obvious question is, if we know $f(x)$, how do we find $\tilde{f}(\nu)$? In answering this question we use the following version of the δ-function.

$$\begin{aligned} \delta(x-t) &= \lim_{A\to\infty} \{a \,\mathrm{sinc}[A(x-t)]\} = \\ &= \lim_{A\to\infty} \int_{-\frac{A}{2}}^{\frac{A}{2}} e^{2\pi i \nu (x-t)} \mathrm{d}\nu \end{aligned} \tag{7.2}$$

which we write bluntly as $\int_{-\infty}^{+\infty} e^{2\pi i \nu (x-t)} \mathrm{d}\nu$. Now let us compute

$$\begin{aligned} \int_{-\infty}^{\infty} f(x) e^{-2\pi i \mu x} \mathrm{d}x &= \iint_{x\,\nu} \tilde{f}(\nu) e^{2\pi i x(\nu-\mu)} \mathrm{d}\nu \mathrm{d}x = \\ &= \int_{\nu} \tilde{f}(\nu) \left\{ \int_{x} e^{2\pi i x(\nu-\mu)} \mathrm{d}x \right\} \mathrm{d}\nu = \int_{\nu} \tilde{f}(\nu) \delta(\nu-\mu) \mathrm{d}\nu = \tilde{f}(\nu) \end{aligned} \tag{7.3}$$

$$\boxed{f(x) = \int \tilde{f}(\nu) e^{2\pi i \nu x} \mathrm{d}\nu; \;\; \tilde{f}(\nu) = \int f(x) e^{-2\pi i \nu x} \mathrm{d}x}$$

The equations in the box indicate that $f(x)$ and $\tilde{f}(\nu)$ are a "Fourier transform pair". You may call this a "proof" if you have no scruples about operating with the δ-function, and changing the order of integration: $\int_{(x)}\int_{(\nu)} \ldots = \int_{(\nu)}\int_{(x)} \ldots$

More common is the procedure to present the Fourier integral transformation as the limiting case of the Fourier series representation. Briefly the way to do this is like this:

$$f(x) = \sum A_n \, e^{2\pi i n x/d}; \text{ whereby } A_n = \frac{1}{d} \int_{-\frac{d}{2}}^{\frac{d}{2}} f(x) e^{-2\pi i n x/d} \mathrm{d}x \tag{7.4}$$

This representation of $f(x)$ has been proven to be possible for any reasonable function $f(x) = f(x + nd)$; $n = 0, \pm 1, \pm 2, \ldots$.

Now we assume that the period d becomes very large, hence the basic frequency $\frac{1}{d}$ very small; we will call it $\frac{1}{d} = \Delta\nu$ in order to indicate its smallness. Thereby the Fourier series representation assumes the form:

$$\frac{A_n}{\Delta\nu} = \int_{-\frac{d}{2}}^{\frac{d}{2}} f(x) e^{-2\pi i n \Delta\nu x} \mathrm{d}x; \quad f(x) = \sum \left(\frac{A_n}{\Delta\nu} \right) e^{2\pi i n \Delta\nu x} \Delta\nu \tag{7.5}$$

Now we perform the transition $d \to \infty$; $n\Delta\nu \to \nu$; $\frac{A_n}{\Delta\nu} \to A(\nu)$. The series goes over into an integral:

$$f(x) = \int A(\nu) e^{2\pi i \nu x} \mathrm{d}\nu; \quad A(\nu) = \int f(x) e^{-2\pi i \nu x} \mathrm{d}x \tag{7.6}$$

The whole motivation was to represent an *aperiodic* function by a superposition of many periodic elements $e^{2\pi i \nu x}$. This extension of the representability of *periodic* functions towards *aperiodic* functions is based upon the plausible argument that an *aperiodic* function is indeed periodic, just that its period is unusually long, namely infinity.

$$\begin{aligned} &\underline{\text{Periodic}}: && f(x) = f(x + md); \quad m \text{ integer} \\ &\underline{\text{Aperiodic}}: && f(x) = f(x + m\infty); \quad m \text{ integer} \end{aligned} \tag{7.7}$$

Although it does not make much sense to go from x to $x + \infty$, then to $x + 2\infty$, $x + 3\infty$, $\ldots$, $x + m\infty$, it does not create any logical disorder either. As long as something is logically consistent, we might as well base some arguments upon it.

Another approach to the Fourier-integral is more realistic. Let us assume that the variable x means something, for example length or time. In real life our knowledge, our access to things, and our interests cover only a *finite* range of x, let us say from $-\frac{d}{2}$ to $+\frac{d}{2}$. What is beyond this region is as good as non-existing in the sense of the positivistic philosophy. Hence we may assume $f(x) = 0$ in $|x| > \frac{d}{2}$. Furthermore let us assume that the function $f(x)$ does not show any periodicity within our range $|x| \leq \frac{d}{2}$. For practical purposes, then, this function is aperiodic. Hence we cannot use Fourier series representation. On the other hand, nothing can go wrong if we deal from now on with a hypothetical function $F(x)$, which is equal to

$f(x)$ within $|x| \leq \frac{d}{2}$, and which we define to be $f(x+md)$ outside of $|x| \leq \frac{d}{2}$. The function $F(x) = \sum\limits_{(m)} f(x+md)$ is periodic, hence it can be represented by Fourier series. Within our range of access $f(x) = F(x)$, hence from now on we just call $F(x) = f(x)$. Nothing can go wrong.

$$f(x) = \sum A_n e^{2\pi i n\varrho x}; \qquad A_n = \frac{1}{d}\int\limits_{-\frac{d}{2}}^{\frac{d}{2}} f(x)e^{-2\pi i n\varrho x}\mathrm{d}x; \qquad \varrho = \frac{1}{d} \tag{7.8}$$

What we have done here, namely to add something non-real to something real, in order to make both together a more tractable entity, is quite common. For example, instead of describing the oscillation of a voltage by $\cos(\omega t)$ one adds something non-real, or imaginary, namely $i\sin(\omega t)$:

$$\cos(\omega t) + i\sin(\omega t) = e^{i\omega t} \tag{7.9}$$

Thereby all mathematical manipulations become simpler. For example, $e^{i\omega_1 t} \cdot e^{i\omega_2 t} = e^{i(\omega_1+\omega_2)t}$ instead of $\cos(\omega_1 t) \cdot \cos(\omega_2 t) = \frac{1}{2}\{\cos[(\omega_1+\omega_2)t] + \cos[(\omega_1-\omega_2)t]\}$.

Actually $\cos(\omega t)$ itself is already unreal in some sense, because it is defined from time $(-\infty)$ till time $(+\infty)$, which certainly is an unrealistically long interval of time.

Now let us make another unrealistic step, which will have as a result that a series (which is not so handy) will be replaced by an integral (which is easier to handle). In the terminology of spatial frequencies a periodic function $f(x) = \sum A_n e^{2\pi i n\varrho x}$ contains the frequencies $0, \pm\varrho, \pm 2\varrho, \ldots$. In other words, the frequency domain is *discrete*, with ϱ-steps. However we prefer a *continuous* domain; let's call it ν. In it the frequency spectrum of $f(x)$ is $\sum A_n \delta(\nu - n\varrho)$. It is very spiky. Let's smooth it, but such that the smoothed spectrum $A(\nu)$ has the right value at every spike position $\nu = n\varrho$ except maybe for a constant factor c ($A(n\varrho) = cA_n$).

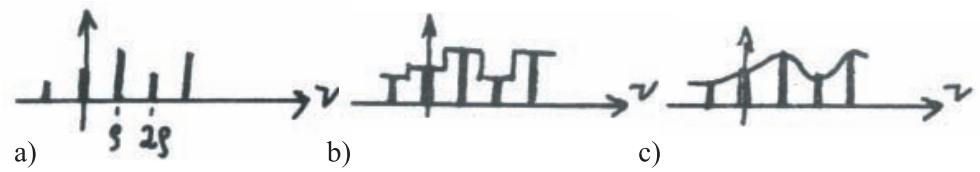

Figure 7.1: a) Discrete frequency spectrum (a) of a periodic object and its interpolation according to b) Eq. 7.10 (I) and c) Eq. 7.10(II)

This can be achieved in several ways:

$$\begin{aligned}
\text{(I)}: \quad A(\nu) &= c\sum A_n \text{rect}(\frac{\nu - n\varrho}{\varrho}) \\
\text{(II)}: \quad A(\nu) &= c\sum A_n \text{sinc}(\frac{\nu}{\varrho} - n) \\
\text{(III)}: \quad A(\nu) &= c\sum A_n \text{sinc}^2(\frac{\nu}{\varrho} - n)
\end{aligned} \tag{7.10}$$

There are even more possibilities. Which one is desirable? Obviously, we want our continuous frequency spectrum to be very suitable for representing the function $f(x)$:

$$\int A(\nu) e^{2\pi i \nu x} \mathrm{d}\nu = f(x) \tag{7.11}$$

When we insert the various smooth versions of $A(\nu)$ into the integral we find that the sinc-version produces the following result:

$$f(x)\text{rect}\left(\frac{x}{d}\right) = \begin{cases} f(x) & : \text{ if } |x| \le \frac{d}{2} \\ 0 & : \text{ if } |x| > \frac{d}{2} \end{cases} \tag{7.12}$$

This result is very nice, because it makes the function zero in the nonsensical range, but leaves it unchanged within the important range. From now we will use this nomenclature:

$$\boxed{f(x) = \int \tilde{f}(\nu) e^{2\pi i \nu x} \mathrm{d}\nu; \qquad \tilde{f}(\nu) = \int f(x) e^{-2\pi i \nu x} \mathrm{d}x} \tag{7.13}$$

$$\boxed{f(x) = f(x)\text{rect}\left(\frac{x}{d}\right); \qquad \tilde{f}(\nu) = \sum \tilde{f}(n\varrho)\ \text{sinc}\left(\frac{\nu}{\varrho} - n\right); \qquad \varrho\, d = 1} \tag{7.14}$$

The second line is the well-known *sampling theorem*. Ordinarily it is derived like this. The Fourier relationship $f(x) \leftrightarrow \tilde{f}(\nu)$ has been established already mathematically. Next the Fourier relationship is applied to the special function $f(x)$, which is zero outside of $|x| \le \frac{d}{2}$. Such a function satisfies the following identity:

$$f(x) = \text{rect}\left(\frac{x}{d}\right) \sum_{(m)} f(x + md) \qquad \text{This is "periodic continuation"}. \tag{7.15}$$

Applying a Fourier transformation to both sides of this equation, one gets the sampling theorem. The result is the same, differences are only of a philosophical nature. We will now perform the derivation in some detail because it provides a good opportunity for getting used to delta-functions. Furthermore this derivation is a good example for the significance of

changing skillfully the sequence of limit processing (= infinite series and integrals).

We apply $\int \ldots e^{-2\pi i\nu x}\mathrm{d}x$ to both sides of the identity $f(x) = \mathrm{rect}\left(\frac{x}{d}\right)\sum f(x + m\ d)$. On the left side we get of course $\tilde{f}(\nu)$. The right side is now:

$$\int \mathrm{rect}\left(\frac{x}{d}\right)\sum f(x + m\ d)e^{-2\pi i\nu x}\mathrm{d}x \tag{7.16}$$

Insert:

$$f(x + m\ d) = \int \tilde{f}(\nu)e^{2\pi im\mu d}e^{2\pi i\mu x}\mathrm{d}\mu \tag{7.17}$$

We do this because we expect $\tilde{f}$ to occur in the result. The summation applies only to one exponential term. The sum is actually the Fourier series of a delta-comb:

$$\sum_{(m)} e^{2\pi im\mu d} = \sum_{(n)} \delta(\mu d - n) = \frac{1}{d}\sum \delta\left(\mu - \frac{n}{d}\right) \tag{7.18}$$

Inserting this we arrive soon at the final result:

$$\begin{aligned} & \frac{1}{d}\sum \iint \mathrm{rect}\left(\frac{x}{d}\right)\tilde{f}(\mu)e^{2\pi ix(\mu-\nu)}\delta\left(\mu - \frac{n}{d}\right)\mathrm{d}x\ \mathrm{d}\mu = \\ = \ & \frac{1}{d}\sum \int \mathrm{rect}(\left(\frac{x}{d}\right)\tilde{f}\left(\frac{n}{d}\right)e^{-2\pi ix(\nu-\frac{n}{d})}\mathrm{d}x = \\ = \ & \frac{1}{d}\sum \tilde{f}\left(\frac{n}{d}\right)\frac{-2i\sin\left[\pi d\left(\nu - \frac{n}{d}\right)\right]}{-2\pi i\left(\nu - \frac{n}{d}\right)} \\ = \ & \sum \tilde{f}\left(\frac{n}{d}\right)\mathrm{sinc}(\nu d - n) = \tilde{f}(\nu) \end{aligned} \tag{7.19}$$

7.1 Some general properties

Since we generated our Fourier-integral transform as an extension of the Fourier-series transform for periodic functions, we can expect some of the same properties. In particular the Fourier-integral representation is optimized in the Gaussian sense:

$$\int \left| f(x) - \int \tilde{f}\nu e^{2\pi i\nu x}\mathrm{d}\nu \right|^2 \mathrm{d}x \rightarrow \text{ MINIMUM} \tag{7.20}$$

Hence it is plausible that also the Fourier integral exhibits the *Dirichlet effect*:

$$\int \tilde{f}(\nu) e^{2\pi i \nu x} \mathrm{d}\nu = \frac{f(x+0) + f(x-0)}{2} \tag{7.21}$$

Furthermore, whenever the Fourier-integral covers only a finite frequency range, $\int_{-\nu_0}^{\nu_0} \tilde{f}(\nu) e^{2\pi i \nu x} \mathrm{d}\nu$, this so-called "truncated Fourier-integral" will exhibit the *Gibbs*-phenomenon at discontinuities of the original function $f(x)$.

The convergence properties can be derived similarly as before:

$$\begin{aligned} \tilde{f}(\nu) = \int f(x) e^{2\pi i \nu x} \mathrm{d}x &= \left[f(x) \frac{e^{2\pi i \nu x}}{2\pi i \nu} \right]_{x=-\infty}^{x=+\infty} - \\ &- \frac{1}{2\pi i \nu} \int f'(x) e^{2\pi i \nu x} \mathrm{d}x \end{aligned} \tag{7.22}$$

We assume that $f(\pm\infty)$ is zero and that $\frac{\mathrm{d}f(x)}{\mathrm{d}x}$ has only a finite number of infinities due to discontinuities of $f(x)$ itself. Then will be $|\tilde{f}(\nu)| < \frac{\text{const.}}{|\nu|}$. If also $f^{(k-1)}(x)$ has only a finite number of discontinuities, then the convergence is even better: $|\tilde{f}(\nu)| < \frac{\text{const}}{|\nu|^k}$.

7.2 Some specific properties

$$\begin{aligned}
f(x) + g(x) &\leftrightarrow \tilde{f}(\nu) + \tilde{g}(\nu) \\
f(x) = a g(x) &\leftrightarrow \tilde{f}(\nu) = a \tilde{g}(\nu) \\
f(x) = g(mx) &\leftrightarrow \tilde{f}(\nu) = \frac{\tilde{g}\left(\frac{\nu}{m}\right)}{|m|} \\
f(x) = g(x+c) &\leftrightarrow \tilde{f}(\nu) = \tilde{g}(\nu) e^{2\pi i \nu c} \ \text{ shift theorem} \\
f(x) = g(x) e^{2\pi i \nu_0 x} &\leftrightarrow \tilde{f}(\nu) = \tilde{g}(\nu - \nu_0) \\
f(x) = g(-x) &\leftrightarrow \tilde{f}(\nu) = \tilde{g}(-\nu) \\
f(x) = -g(-x) &\leftrightarrow \tilde{f}(\nu) = -\tilde{g}(\nu) \\
f(x) = f^*(x) &\leftrightarrow \tilde{f}(\nu) = \tilde{f}^*(-\nu) \ \text{ reality symmetry} \\
f(x) = -f^*(x) &\leftrightarrow \tilde{f}(\nu) = \tilde{-} f^*(-\nu) \\
f(x) = g_1(x) g_2(x) &\leftrightarrow \tilde{f}(\nu) = \int \tilde{g}_1(\mu) \tilde{g}_2(\nu - \mu) \mathrm{d}\mu \ \text{ convolution} \\
\underbrace{f(x) = g(x) g^*(x)}_{\text{real nonnegative}} &\leftrightarrow \tilde{f}(\nu) = \int \tilde{g}(\nu) \tilde{g}(\mu - \nu) \mathrm{d}\mu \ \text{ auto} - \text{correlation} \\
f(x) = \frac{\mathrm{d}g(x)}{\mathrm{d}x} &\leftrightarrow \tilde{f}(\nu) = 2\pi i \nu \tilde{g}(\nu)
\end{aligned} \tag{7.23}$$

$$
\begin{aligned}
f(x) = \int_{-x}^{x} g(x')\mathrm{d}x' \quad &\leftrightarrow \quad \tilde{f}(\nu) = \frac{\tilde{g}(\nu) + \tilde{g}(-\nu)}{2\pi i \nu} \\
f(x) = \int g_1(x')g_2(x'-x)\mathrm{d}x' \quad &\leftrightarrow \quad \tilde{f}(\nu) = \tilde{g}_1(\nu)\tilde{g}_2(-\nu) \\
f(x) = \int g_1(x')g_2(x-x')\mathrm{d}x' \quad &\leftrightarrow \quad \tilde{f}(\nu) = \tilde{g}_1(\nu)\tilde{g}_2(\nu) \qquad (7.24) \\
f(x) = \int g(x')g^*(x'-x)\mathrm{d}x' \quad &\leftrightarrow \quad \tilde{f}(\nu) = |\tilde{g}(\nu)|^2 \\
f(x) = \int g(x')g(x-x')\mathrm{d}x' \quad &\leftrightarrow \quad \tilde{f}(\nu) = \tilde{g}^2(\nu) \\
f(x,y) = g(x+x_0, y+y_0) \quad &\leftrightarrow \quad \tilde{f}(\nu,\mu) = \tilde{g}(\nu,\mu)e^{2\pi i(x_0\nu + y_0\mu)} \\
f(x,y) = g(-x,-y) \quad &\leftrightarrow \quad \tilde{f}(\nu,\mu) = \tilde{g}(-\nu,-\mu) \\
\underbrace{f(x,y) = g(-x,y)}_{\text{inversion around the y}-\text{axis}} \quad &\leftrightarrow \quad \tilde{f}(\nu,\mu) = \tilde{g}(-\nu,+\mu) \\
f(x,y) = f^*(x,y) \quad &\leftrightarrow \quad \tilde{f}(\nu,\mu) = \tilde{f}^*(-\nu,-\mu) \\
f(x,y) = \iint g_1(x',y')g_2^*(x'-x,y'-y)\mathrm{d}x'\mathrm{d}y' \quad &\leftrightarrow \quad \tilde{f}(\nu,\mu) = \tilde{g}_1(\nu,\mu)\tilde{g}_2^*(\nu,\mu) \\
f(x,y) = \iint \nabla g_1(x',y')\ \nabla g_2^*(x',y')\, g^*(x'-x,y'-y)\mathrm{d}x'\mathrm{d}y' \ &\leftrightarrow \\
\leftrightarrow \tilde{f}(\nu,\mu) = (2\pi)^2(\nu^2+\mu^2)\tilde{g}_1(\nu,\mu)\tilde{g}_2^*(\nu,\mu)&
\end{aligned}
$$

where $\nabla = (\frac{\partial}{\partial x}, \frac{\partial}{\partial y}, \frac{\partial}{\partial z})$, so that $\nabla g(x,y) = \mathrm{grad}(g(x,y))$ is the gradient of $g(x,y)$.

7.3 Polar coordinates

$$f(r,\varphi) = \sum f_m(r)e^{im\varphi} \qquad (7.25)$$

The periodicity in φ is a consequence of the uniqueness of $f(r,\varphi)$:

$$
\begin{aligned}
f_m(r) &= \frac{1}{2\pi}\int_0^{2\pi} f(r,\varphi)e^{im\varphi}\mathrm{d}\varphi \qquad (7.26) \\
f_m(r) &= \int_{-\infty}^{\infty} \tilde{f}_m(\sigma)e^{2\pi i r\sigma}\mathrm{d}\sigma \\
f(r,\varphi) &= \sum e^{im\varphi}\int \tilde{f}_m(\sigma)e^{2\pi i r\sigma}\mathrm{d}\sigma
\end{aligned}
$$

The real part of $e^{i(m\varphi+2\pi r\sigma)}$ which is $\cos(m\varphi + 2\pi r\sigma)$ has maximum lines which form a set of spirals:

$$m\varphi + 2\pi r\sigma = N; \qquad N = 0, \pm 1, \pm 2, \ldots \tag{7.27}$$

Hence one may consider the expansion:

$$f(r,\varphi) = \sum e^{im\varphi} \int \tilde{f}_m(\sigma) e^{2\pi i r\sigma} \mathrm{d}\sigma \tag{7.28}$$

as a superposition of spirals. The sign of $m\sigma$ defines whether it is a left-turn spiral. The number m defines the multiplicity (in Fig. 7.2: 3). The quantity $\frac{2\pi\sigma}{m}$ determines the scale or the stretch of the spirals.

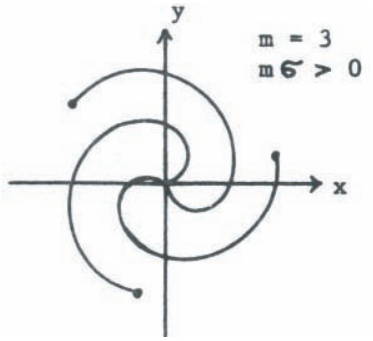

Figure 7.2: Spirals

Another approach to two-dimensional Fourier-representation is polar coordinates (compare page 36) takes the ordinary Fourier-elements but expresses them in polar coordinates:

$$\begin{aligned} \cos[2\pi(x\nu + y\mu)] &= \cos[2\pi r\varrho\cos(\varphi-\theta)] \\ x = r\cos(\varphi) & \qquad y = r\sin(\varphi) \\ \nu = \varrho\cos(\theta) & \qquad \mu = \varrho\sin(\theta) \\ x\nu = r\varrho\cos(\varphi)\cos(\theta) & \qquad y\mu = r\varrho\sin(\varphi)\sin(\theta) \\ \cos(\varphi)\cos(\theta) &+ \sin(\varphi)\sin(\theta) = \cos(\varphi-\theta) \end{aligned} \tag{7.29}$$

Now

$$f(x,y) = \iint_{-\infty}^{\infty} \tilde{f}(\nu,\mu) e^{2\pi i(\nu x + \mu y)} \mathrm{d}\nu \mathrm{d}\mu \tag{7.30}$$

goes over into:

$$f(r,\varphi) = \int_{\theta=0}^{2\pi} \int_{r=0}^{\infty} \tilde{f}(\varrho,\theta) e^{2\pi i r \varrho \cos(\varphi-\theta)} \varrho \mathrm{d}\varrho \mathrm{d}\theta \tag{7.31}$$

Actually I should have chosen new symbols for f and $\tilde{f}$, when going from cartesian to polar coordinates, because the functions f and $\tilde{f}$ are now different from before, assuming they describe still the same pattern. Let me explain this by means of some examples, because many students make mistakes when changing coordinates:

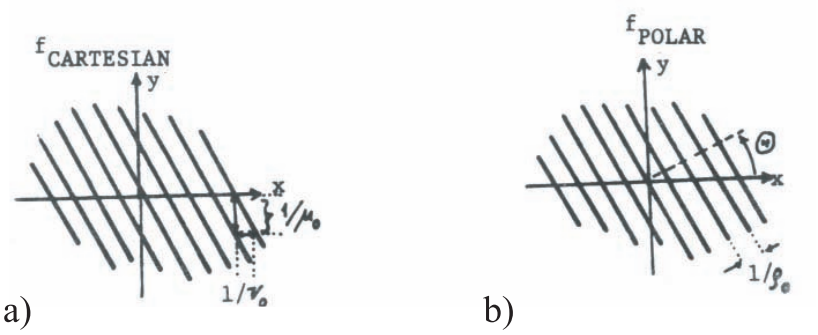

Figure 7.3: The functions described by Eq. 7.32.

$$f_{\mathrm{Cartesian}}(x,y) = e^{2\pi i(\nu_0 x + \mu_0 y)}; \qquad f_{\mathrm{Polar}}(r,\varphi) = e^{2\pi i r \varrho_0 \cos(\varphi-\theta)}; \tag{7.32}$$
$$\text{where}: \nu_0 = \varrho_0 \cos(\theta); \qquad \text{and}: \mu_0 = \varrho_0 \sin(\theta)$$

$$f_{\mathrm{Cartesian}}(r,\varphi) = e^{2\pi i(\nu_0 r + \mu_0 \varphi)} \tag{7.33}$$

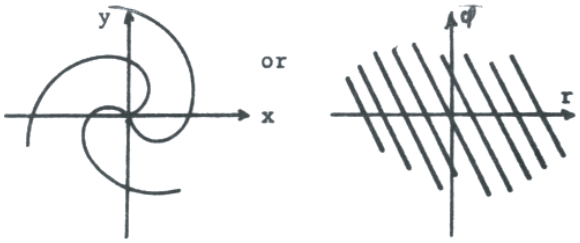

Figure 7.4: The function described by Eq. 7.33.

$$f_{\text{Polar}}(x,y) = e^{2\pi i x \varrho_0 \cos(y-\theta)} \tag{7.34}$$

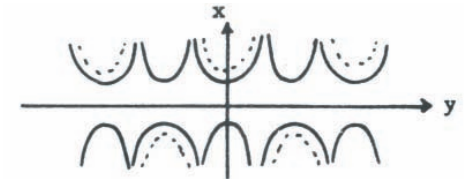

Figure 7.5: The function described by Eq. 7.34.

The second form be simplified, making use of the Bessel-function-generating series:

$$e^{iA\sin(\alpha)} = \sum_{-\infty}^{\infty} J_n(A)e^{in\alpha}; \quad \text{and}\cos(\varphi-\theta) = \sin\left(\frac{\pi}{2}+\varphi-\theta\right) \tag{7.35}$$

$$f(r,\varphi) = \sum \int_0^{\infty} J_n(2\pi r\varrho) \int_0^{2\pi} \tilde{f}(\varrho,\theta)e^{in\left(\frac{\pi}{2}+\varphi-\theta\right)}\varrho \mathrm{d}\theta\mathrm{d}\varphi \tag{7.36}$$

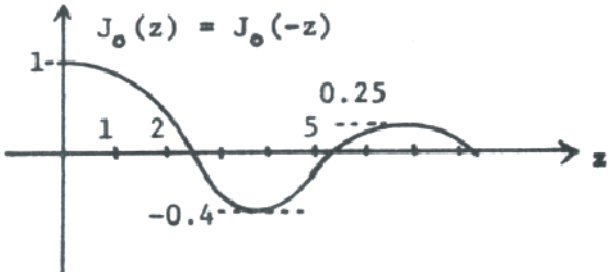

Figure 7.6: The Bessel-function $J_0(z)$.

We may also represent $\tilde{f}$ as a Fourier series: $\tilde{f}(\varrho,\theta) = \sum(m)\hat{f}_m(\varrho)e^{im\theta}$. Upon inserting it we encounter a Kronecker integral:

$$\hat{f}_m(\varrho) \int_0^{2\pi} e^{i\left\{m\theta+n\left(\frac{\pi}{2}+\varphi-\theta\right)\right\}}d\theta = \delta_{m,n}2\pi\hat{f}(\varrho)e^{in\left(\frac{\pi}{2}+\varphi\right)} \tag{7.37}$$

This leads us to:

$$f(r,\varphi) = \sum(n) 2\pi \int_0^\infty J_n(2\pi r\varrho)\hat{f}_n(\varrho) e^{in\left(\frac{\pi}{2}+\varphi\right)} \varrho \mathrm{d}\varrho \tag{7.38}$$

If $f(r,\varphi)$ does not depend on φ, then all $\hat{f}_n(\varrho)$, except $\hat{f}_0(\varrho)$ are zero. With $2\pi\hat{f}_0(\varrho) = \tilde{f}(\varrho)$ this results in the Bessel transformation:

$$\begin{aligned} f(r) &= \int_0^\infty J_0(2\pi r\varrho)\tilde{f}(\varrho)\varrho \mathrm{d}\varrho \\ \tilde{f}(\varrho) &= \int_0^\infty J_0(2\pi r\varrho) f(r) r \mathrm{d}r \end{aligned} \tag{7.39}$$

7.4 More about the Fourier-Integral transformation

Perhaps the most important formula is:

$$\iint f(x,y)g^*(x,y)\mathrm{d}x\mathrm{d}y = \iint \tilde{f}(\nu,\mu)g^*(\nu,\mu)\mathrm{d}\nu,\mathrm{d}\mu \tag{7.40}$$

or briefly:

$$f \cdot g^* = \tilde{f} \cdot \tilde{g}^* \qquad \text{PARSEVAL} \tag{7.41}$$

This formula is so important because most other formulas can be derived from it by specialization. For example:

$$\begin{aligned} g(x) &= \delta(x-x') & \tilde{g}(\nu) &= e^{-2\pi i\nu x'} \\ g^*(x) &= \delta(x-x') & g^*(\nu) &= e^{2\pi i\nu x'} \end{aligned} \tag{7.42}$$

When inserting this particular function g into the Parseval formula we get the Fourier transform:

$$\int f(x)\delta(x-x')\mathrm{d}x = \int \tilde{f}(\nu)e^{2\pi i\nu x'}\mathrm{d}\nu = f(x') \tag{7.43}$$

Now we set $f(x) = g(x)$ and get the PLANCHEREL-theorem:

$$\int |f(x)|^2 \mathrm{d}x = \int |\tilde{f}(\nu)|^2 \mathrm{d}\nu \tag{7.44}$$

And the WIENER-KHINTCHINE formula can be obtained in this way:

$$\begin{aligned} g(x) = f(x)e^{2\pi i\nu x}; \qquad & g^*(x) = f^*(x)e^{-2\pi i\nu' x} \\ \tilde{g}(\nu) = \tilde{f}(\nu-\nu'); \qquad & \tilde{g}^*(\nu) = \tilde{f}^*(\nu-\nu') \\ \int |f(x)|^2 e^{-2\pi i\nu' x}\mathrm{d}x = & \int \tilde{f}(\nu) f^*(\nu-\nu')\mathrm{d}\nu \end{aligned} \tag{7.45}$$

The same formula in two dimensions is:

$$\iint |f(x,y)|^2 e^{-2\pi i(x\nu'+y\mu')}\mathrm{d}x\mathrm{d}y = \iint \tilde{f}(\nu,\mu)\tilde{f}^*(\nu-\nu',\mu-\mu')\mathrm{d}\nu\mathrm{d}\mu \tag{7.46}$$

7.5 Now some examples

- the 1D and 2D rect-Function:

$$\begin{aligned} f(x) &= \mathrm{rect}\left(\frac{x}{a}\right) = \begin{cases} 1 & \text{if } |x| \le \frac{a}{2} \\ 0 & \text{otherwise} \end{cases} \\ \tilde{f}(\nu) &= a\,\mathrm{sinc}(a\nu) \\ f(x,y) &= f_1(x)f_2(y) \qquad \tilde{f}(\nu,\mu) = \tilde{f}_1(\nu)\tilde{f}_2(\mu) \\ f(x,y) &= \mathrm{rect}\left(\frac{x}{a}\right)\cdot \mathrm{rect}\left(\frac{y}{b}\right) \qquad \tilde{f}(\nu,\mu) = a\,b\,\mathrm{sinc}(a\nu)\,\mathrm{sinc}(b\mu) \end{aligned} \tag{7.47}$$

- The trian-function:

$$f(x) = \begin{cases} 1 - \frac{|x|}{a} & \text{if } |x| \le a \\ 0 & \text{if } |x| > 0 \end{cases} \tag{7.48}$$

i.e.

The computation of this Fourier transformation:

$$\tilde{f}(\nu) = \int f(x)e^{-2\pi i\nu x}\mathrm{d}x \tag{7.49}$$

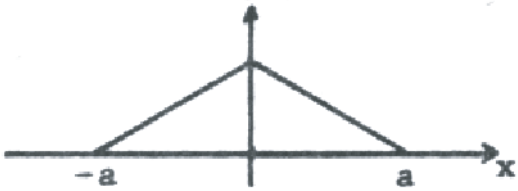

Figure 7.7: The "trian"-function, final example in Eq. 7.48.

is worth presenting in some detail. We will make use of the Wiener-Khintchine theorem

$$\int |f(x)|^2 e^{-2\pi i\nu' x}\mathrm{d}x = \int \tilde{f}(\nu)\tilde{f}^*(\nu-\nu')\mathrm{d}\nu \tag{7.50}$$

Let us first produce the inverse version of the Wiener-Khintchine theorem again by specializing the Parseval formula with $f(x)$ and $g^*(x) = f^*(x-x')$, if $g(x) = f(x-x')$, then

$$\tilde{g}(\nu) = \int f(x-x')e^{-2\pi i\nu x}\mathrm{d}x = \iint \tilde{f}(\nu')e^{2\pi i[x(\nu'-\nu)-x'\nu']}\mathrm{d}x\mathrm{d}\nu' \tag{7.51}$$

herein:

$$\int e^{2\pi ix(\nu'-\nu)}\mathrm{d}x = \delta(\nu'-\nu) \tag{7.52}$$

Hence:

$$\tilde{g}(\nu) = \int \tilde{f}(\nu')\delta(\nu'-\nu)e^{-2\pi ix'\nu'}\mathrm{d}\nu' = \tilde{f}(\nu)e^{-2\pi ix'\nu} \tag{7.53}$$

Therefore:

$$\tilde{g}^*(\nu) = \tilde{f}^*(\nu)e^{2\pi ix'\nu} \tag{7.54}$$

Now we insert these particular functions f and g into the Parseval formula $\int f(x)g^*(x)\mathrm{d}x = \int \tilde{f}(\nu)\tilde{g}^*(\nu)\mathrm{d}\nu$. Thereby we get the inverse Wiener-Khintchine theorem:

$$\int f(x)f^*(x-x')\mathrm{d}x = \int |\tilde{f}(\nu)|^2 e^{2\pi ix'\nu}\mathrm{d}\nu \tag{7.55}$$

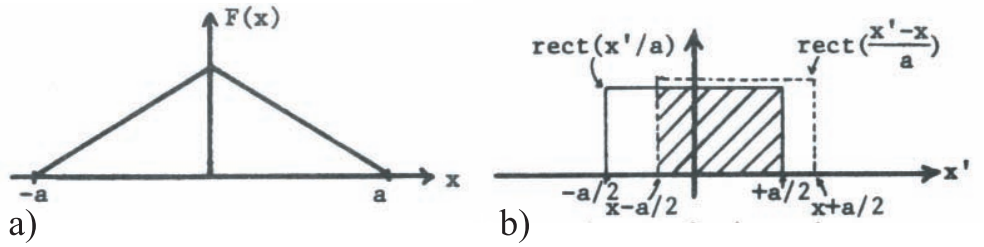

Figure 7.8: The "trian"-function as the autocorrelation of the rect-function.

Now comes the trick which simplifies the Fourier transformation of the triangular function, which can be constructed as the autocorrelation of two rectangular functions. The star on the second rect-function is not necessary, because the rect-function is real, but it does not hurt either. We put the star down only to make it obvious that we have here the inversion version of the W-K theorem, for the particular function $f(x) = \frac{1}{\sqrt{a}}\mathrm{rect}\left(\frac{x}{a}\right)$.

$$\int_{-\infty}^{\infty} \mathrm{rect}\left(\frac{x'}{a}\right) \mathrm{rect}\left(\frac{x'-x}{a}\right) \mathrm{d}x' = \int_{x-\frac{a}{2}}^{\frac{a}{2}} 1 \, \mathrm{d}x' = a - x \qquad (\text{if } x \geq 0) \quad (7.56)$$

For negative x the limits of the integral are $-\frac{a}{2}$ and $\left(\frac{a}{2} + x\right) = \frac{a}{2} - |x|$; hence $\int \mathrm{rect}\left(\frac{x'}{a}\right)$ $\mathrm{rect}\left(\frac{x'-x}{a}\right) \mathrm{d}x' = a - |x|$ for $|x| \leq a$. For $|x| > a$ the two rect-functions do not overlap, hence the integral become zero. We know already that $\mathrm{rect}\left(\frac{x}{a}\right)$ has $\mathrm{sinc}(a\nu)$ as Fourier transform, hence:

$$f(x) = \frac{1}{\sqrt{a}} \mathrm{rect}\left(\frac{x}{a}\right) \sim \tilde{f}(\nu) = \sqrt{a}\,\mathrm{sinc}(a\nu) \quad (7.57)$$

Now we insert all this into the inverse version of the W-K theorem.

$$\begin{aligned} F(x) = \int f(x')f^*(x'-x)\mathrm{d}x' &= \int |\tilde{f}(\nu)|^2 e^{2\pi i x\nu} \mathrm{d}\nu \qquad (7.58) \\ = \int \frac{\mathrm{rect}\left(\frac{x'}{a}\right)}{\sqrt{a}} \frac{\mathrm{rect}^*\left(\frac{x'-x}{a}\right)}{\sqrt{a}} \mathrm{d}x' &= \int \left|\sqrt{a}\,\mathrm{sinc}(a\nu)\right|^2 e^{2\pi i x\nu} \mathrm{d}\nu \\ = \begin{cases} 1 - \frac{|x|}{a} & \text{if } |x| \leq a \\ 0 & \text{if } |x| > 0 \end{cases} &= \int a\,\mathrm{sinc}^2(a\nu)\, e^{2\pi i \nu x} \mathrm{d}\nu \\ &= \int \tilde{F}(\nu) e^{2\pi i \nu x} \mathrm{d}\nu \end{aligned}$$

Comparing both sides we find:

$$F(x) = \begin{cases} 1 - \frac{|x|}{a} & \text{if } |x| \le a \\ 0 & \text{if } |x| > 0 \end{cases} \quad \longleftrightarrow \tilde{F}(\nu) = a\,\mathrm{sinc}^2(a\nu) \tag{7.59}$$

This trick for finding a Fourier transform, if the original function obviously is the autocorrelation of another function, might seem a little bit complicated, but there are realistic situations where this trick is almost essential for getting the solution of a specific Fourier integral.

- Another important pair of Fourier transforms is:

$$f(x) = e^{-\left(\frac{x}{a}\right)^2}; \quad \longleftrightarrow \quad \tilde{f}(\nu) = \sqrt{\pi} a e^{-(\pi\nu a)^2} \tag{7.60}$$

Proving this gives you a nice opportunity to test your skill in the art of integration by finding suitable substitutions of variables:

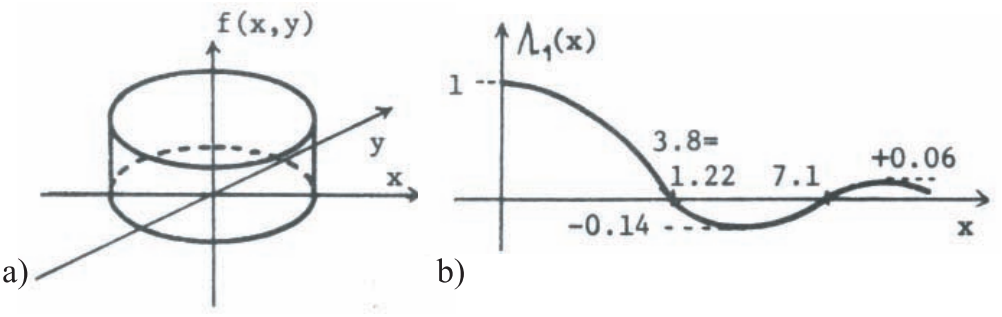

Figure 7.9: The 2D circular function and the Bessel function as its Fourier transform $\Lambda_1(x)$.

$$f(x) = \frac{e^{\frac{-|x|}{a}}}{2a}; \quad \longleftrightarrow \quad \tilde{f}(\nu) = \frac{1}{1 + (2\pi a\nu)^2} \tag{7.61}$$

$$f(x,y) = \frac{e^{-\frac{\sqrt{x^2+y^2}}{a}}}{2\pi a^2}; \quad \longleftrightarrow \quad \tilde{f}(\nu,\mu) = \frac{1}{(1 + (2\pi a)^2(\nu^2+\mu^2))^{\frac{3}{2}}}$$

$$f(x,y) = \begin{cases} 1 & \text{if } x^2 + y^2 \le a^2 \\ 0 & \text{otherwise} \end{cases} \quad \longleftrightarrow \quad \tilde{f}(\nu,\mu) = \tilde{f}(\varrho)$$

$$\text{where} \qquad \varrho^2 = \nu^2 + \mu^2$$

$$\tilde{f}(\varrho) = \frac{a^2}{2}\Lambda_1(2\pi a\varrho); \longleftrightarrow \Lambda_P(x) = P! \ \frac{J_P(x)}{\left(\frac{x}{2}\right)^P} \tag{7.62}$$

$$\Lambda_1(x) = \frac{2J_1(x)}{x} \tag{7.63}$$

The Λ_P-functions are called "diffraction-function" and the J_P are the Bessel functions (see for example Jahnke-Emde, Table of Functions).

- The following Fourier transform example is important for the theory of image formation:

$$\begin{aligned} g(x,y) &= \iint f\left(x'+\frac{x}{2}, y'+\frac{y}{2}\right) f^*\left(x'-\frac{x}{2}, y'-\frac{y}{2}\right) \mathrm{d}x'\mathrm{d}y' \\ \text{whereby :} \quad f(x,y) &= \begin{cases} 1 & \text{if } x^2+y^2 \le a^2 \\ 0 & \text{otherwise} \end{cases} \end{aligned} \tag{7.64}$$

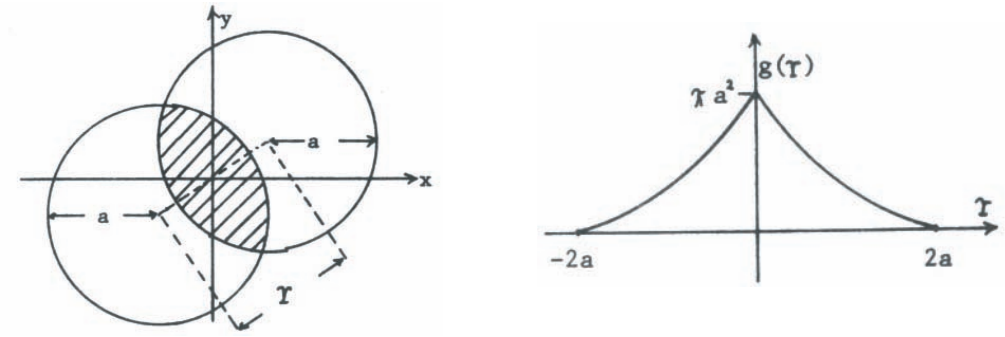

Figure 7.10: The calculation of the autocorrelation function $g(r)$.

$g(r)$ represents the joint area of two circles of radius a, whose centers are shifted by a distance T. Sometimes we will write the auto-correlation integral as $\int f\left(x'+\frac{x}{2}\right) f^*\left(x'-\frac{x}{2}\right)\mathrm{d}x'$, instead of $\int f(x')f^*(x'-x)\mathrm{d}x'$, which is obviously the same, just substitute $x' \to x'+\frac{x}{2}$, a change of variables. The limits of the integral are still $\pm\infty$. Of course, this does not prevent $f(x)$ from being zero outside of a finite range around $x=0$.

The exact form of $g(r)$, which is like a tent with finite tension on the ropes, can be found by looking at the geometry of the overlapping circles.

$$\underbrace{\frac{2\beta}{2\pi}\pi a^2}_{\text{circle element}} \quad \underbrace{-2\frac{\left(\frac{r}{2}\right) a\sin\beta}{2}}_{\substack{\text{two trinangles}\\ \text{which were the}\\ \text{excess}}} = \beta a^2 - \frac{ar}{2}\sin\beta \tag{7.65}$$

The angle β is defined by $\cos\beta = \frac{r}{2a}$.

$$g(r) = 2\beta a^2 - ar\sin(\beta); \quad g(r) = 0 \text{ if } r \geq 2a \tag{7.66}$$

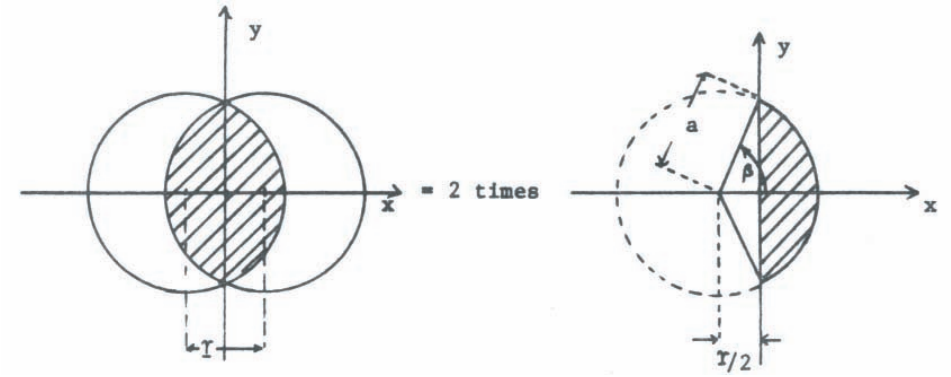

Figure 7.11: Calculation of the overlap integral.

8 Some Additions About the Analog Computer

Now that the Fourier-integral has been introduced, we can complete the treatment of the analog Computer (Chap. 4), which was based on the Moiré-effect of two gratings, rotating in opposite directions. Earlier we had assumed that the angle φ is increased step-wise. But a continuous motion is more practical, of course. Another drawback was a somewhat complicated algorithm for eliminating the higher harmonics. Furthermore the treatment was restricted to periodic functions $f(x) = f(x + mQ)$; m integer. Our goal is now to eliminate these restrictions and drawbacks.

Now $f(x)$ may be aperiodic, but zero outside of $|x| \leq \frac{Q}{2}$. Hence inside of this range nothing is changed. The setup is still as sketched in Fig. 4.1. However, $f(x)$ is centered around $x = 0$, extending from $-\frac{Q}{2}$ to $+\frac{Q}{2}$. The photoelectric signal recorded while the two gratings are in angular positions φ is as derived in Eq. 4.13:

$$\begin{aligned} S(\sin\varphi) &= \int_0^Q f(x) \sum D_n e^{2\pi i(x-x_0)2n\varrho\sin\varphi} \mathrm{d}x \\ &= \sum D_n e^{-4\pi i n x_0 \varrho \sin\varphi} \int_0^Q f(x) e^{4\pi i n x \varrho \sin\varphi} \mathrm{d}x \end{aligned} \tag{8.1}$$

where $D_n = A_n B_{-n}$, or $D_n = |A_n|^2$ if the two gratings are identical. In any case, $D_n = D_n^*$. Now we let φ change continuously with constant angular velocity; $\varphi = \omega t$. As long as $|\varphi| < 14°$, $\sin\varphi \approx \varphi$ (within 1%). Hence:

$$S(\sin\varphi) \longrightarrow S(\omega t) \tag{8.2}$$

Let us compute the spectrum $\tilde{S}(\nu)$ of temporal frequencies ν, because this will give us a clue for the elimination of the higher harmonic terms ($|n| > 1$):

$$\tilde{S}(\nu) = \int S(\omega t)e^{-2\pi i\nu t}\mathrm{d}t = D_0 \int\limits_{(x)}^{\frac{Q}{2}} \int\limits_{(t)}^{\infty} f(x)e^{-2\pi i\nu t}\mathrm{d}x\mathrm{d}t + \tag{8.3}$$

$$+ \sum_{n\neq 0} D_n \int\limits_{(x)}^{\frac{Q}{2}} \int\limits_{(t)}^{\infty} f(x)e^{2\pi it[-\nu+2n\varrho\omega(x-x_0)]}\mathrm{d}x\mathrm{d}t$$

The $(n = 0)$-term gives:

$$D_0\tilde{f}(\nu)\int e^{-2\pi i\nu t}\mathrm{d}t = D_0\tilde{f}(0)\delta(\nu) \tag{8.4}$$

where:

$$\tilde{f}(0) = \int f(x)\mathrm{d}x \tag{8.5}$$

In the $\sum(n \neq 0)$ we have:

$$\int e^{2\pi it[\ldots]}\mathrm{d}t = \delta([\ldots]) = \delta(-\nu + 2n\varrho\omega(x - x_0)) = \left|\frac{1}{2n\varrho\omega}\right| \delta\left(\left[\frac{-\nu}{2n\varrho\omega} + x - x_0\right]\right) \tag{8.6}$$

Hence integration over x changes the variable in the integrand $f(x)$ from x into $x_0 + \frac{\nu}{2n\varrho\omega}$.

$$\tilde{S}(\nu) = D_0\tilde{f}(0)\delta(\nu) + \sum_{n\neq 0} \frac{D_n}{|2n\varrho\omega|} f(x_0 + \frac{\nu}{2n\varrho\omega}) \tag{8.7}$$

Let us plot $\tilde{S}(\nu)$, remembering that $f(x)$ was non-zero only in $|x| \leq \frac{Q}{2}$, hence $f\left(x_0 + \frac{\nu}{2n\varrho\omega}\right)$ is non-zero only within $\left|x_0 + \frac{\nu}{2n\varrho\omega}\right| \leq \frac{Q}{2}$, or

$$|\nu + 2n\varrho\omega x_0| \leq |n\varrho\omega Q| \tag{8.8}$$

To separate the wanted first order term ($|n| = 1$) from the $(n = 0)$ term, and also to avoid overlapping between $n = +1$ and $n = -1$, it has to be true that

$$2\varrho\omega x_0 - \varrho\omega Q \geq 0 \longrightarrow \boxed{x_0 \geq \frac{Q}{2}} \tag{8.9}$$

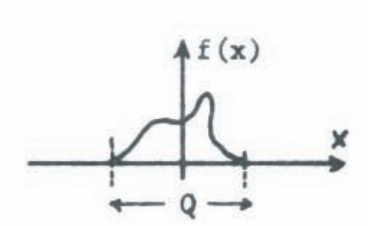

Figure 8.1: The example function $f(x)$).

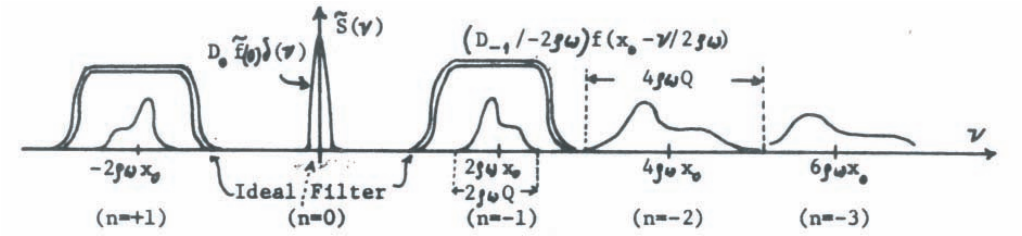

Figure 8.2: The Fourier transform of the photoelectric signal $\tilde{S}(\sin\nu)$.

To avoid a collision between the lower tail of the $(n=-2)$ term and the upper tail of the $(n=-1)$ term it should be true that:

$$4\varrho\omega x_0 - 2\varrho\omega Q \geq 2\varrho\omega x_0 + \varrho\omega Q \longrightarrow \boxed{x_0 \geq \frac{3Q}{2}} \tag{8.10}$$

The condition $|x_0| > \frac{Q}{2}$ has a very simple geometrical meaning, namely the center of the Moiré rotation has to be outside of the function mask, which extended from $\frac{-Q}{2}$ to $\frac{+Q}{2}$. In practice one would choose the location x_0 several times larger than $\frac{Q}{2}$, because the adjacent terms $(n=-1)$, $(n=-2)$ are even easier to separate then. The bandwidth of the $(n=1)$ term is $\Delta\nu_1 = 2\varrho\omega Q$, whereas the carrier frequency is $\nu_1 = 2\varrho\omega x_0$. From an electrical point of view it is desirable to have a small $\frac{\Delta\nu_1}{\nu_1} = \frac{Q}{x_0}$. That makes it easier to realize a bandpass filter, which is constant within $\nu_1 \pm \frac{\Delta\nu}{2}$, but zero for the higher harmonics.

Let us now assume that an electrical bandpass filter has eliminated everything but the $(n=\pm 1)$ terms:

$$\tilde{S}_1(\nu) = \frac{D_1}{2\varrho\omega}\, f\left(x_0 + \frac{\nu}{2\varrho\omega}\right) + \frac{D_{-1}}{2\varrho\omega}\, f\left(x_0 - \frac{\nu}{2\varrho\omega}\right) \tag{8.11}$$

We compute now the signal $S_1(t)$, which can be displayed on a CRT.

$$S_1(t) = \int \tilde{S}(\nu) e^{2\pi i \mu t} \mathrm{d}\mu \tag{8.12}$$

As part of this computation we need to know $\int f(x_0 \pm \frac{\nu}{2\varrho\omega}) e^{2\pi i \nu t} \mathrm{d}\nu$.
We insert $f(x) = \int \tilde{f}(\mu) e^{2\pi i \mu x} \mathrm{d}\mu$:
and get:

$$\iint \tilde{f}(\mu) e^{2\pi i [\nu t + \mu(x_0 \pm \frac{\nu}{2\varrho\omega})]} \mathrm{d}\nu \mathrm{d}\mu \tag{8.13}$$

Herein we recognize a delta-function:

$$\int e^{2\pi i \nu \left(t \pm \frac{\mu}{2\varrho\omega}\right)} \mathrm{d}\nu = \delta\left(t \pm \frac{\mu}{2\varrho\omega}\right) = 2\varrho\omega\delta(2\varrho\omega t \pm \mu) \tag{8.14}$$

This delta-function has the following effect:

$$2\varrho\omega \int \tilde{f}(\mu) e^{2\pi i \mu x_0} \delta(2\varrho\omega t \pm \mu) \mathrm{d}\mu = \tag{8.15}$$
$$2\varrho\omega \tilde{f}(\mp 2\varrho\omega t) e^{\mp 2\pi i 2\varrho\omega t x_0} = \int f\left(x_0 \pm \frac{\nu}{2\varrho\omega}\right) e^{2\pi i \nu t} \mathrm{d}\nu$$

We could have obtained this more quickly by using the shift theorem. - Now it is seen that:

$$\begin{aligned} S_1(t) &= D_1 \tilde{f}(-2\varrho\omega t) e^{-4\pi i \varrho\omega t x_0} + D_{-1} \tilde{f}(+2\varrho\omega t) e^{4\pi i \varrho\omega t x_0} \\ D_n &= D^*_{-n}; \qquad D_1 = D e^{i\vartheta}; \qquad D_{-1} = D e^{-i\vartheta}; \\ \tilde{f}(\mu) &= \tilde{f}^*(-\mu); \qquad \tilde{f} = |\tilde{f}| e^{i\varphi}; \qquad \tilde{f}(-\mu) = |\tilde{f}(+\mu)| e^{-i\vartheta\mu} \\ \text{or} \quad S_1(t) &= 2D|\tilde{f}(2\varrho\omega t)| \cos\{2\pi 2\varrho\omega x_0 t - \varphi(2\varrho\omega t) + \vartheta\} \end{aligned} \tag{8.16}$$

This trace can be observed on a CRT. The envelope represents the modulus $|\tilde{f}|$ of the Fourier transform. If $\tilde{f}(\mu)$ has a bandwidth $\Delta\nu$, which means that $\tilde{f}(\mu)$ is ≈ 0 for $|\mu| > \frac{\Delta\nu}{2}$, then $S_1(t)$ will go down to zero at $t_0 = \frac{\Delta\nu}{2\varrho\omega x_0}$. Naturally, we want many oscillation periods $\tau = \frac{1}{2\varrho\omega}$ to occur between $t = 0$ and t_0 so that the envelope is easy to abstract from the CRT trace. Hence we require:

$$1 \ll \frac{t_0}{\tau} = \frac{\frac{\Delta\nu}{2\varrho\omega}}{\frac{1}{2\varrho\omega x_0}} = x_0 \Delta\nu \tag{8.17}$$

For example $\Delta\nu = 10\mathrm{mm}^{-1}$ is probably as exact as the original recorder might have drawn $f(x)$. The inverse of the bandwidth $\Delta\nu$ is the accuracy or resolution $\delta x = \frac{1}{\Delta\nu}$, here

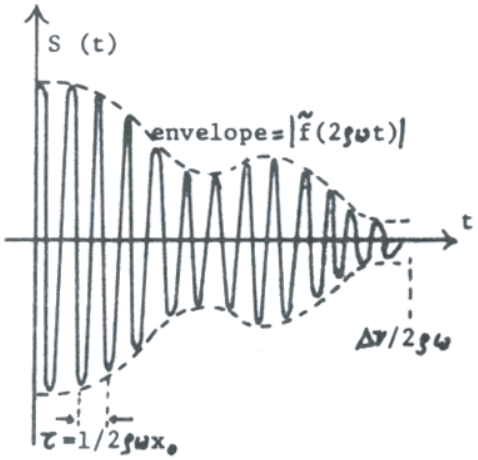

Figure 8.3: The signal $S_1(t)$.

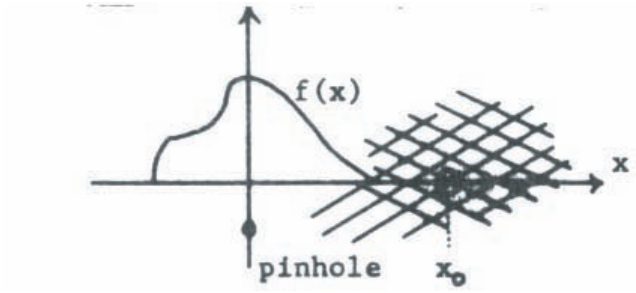

Figure 8.4: Filtering in the signal plane.

0.1 mm. In order to get 100 oscillations we must achieve $100 = \frac{t_0}{\tau} = x_0\Delta\nu = 10x_0$[mm]. Hence the pivot point x_0 should be at least 10 mm away from the center of $f(x)$.

Finally we have to indicate how the phase φ of the Fourier transform $\tilde{f}$ can be measured. For phase measurements it is necessary to have a phase reference signal; we get it by placing a pinhole below the center of the $f(x)$-mask. Behind the pinhole a second photocell picks up a photoelectrical signal which can be computed like before but with $\delta(x)$ for the pinhole instead of $f(x)$. This is the reference signal $S_R(t) = 2D\cos(2\pi 2\varrho\omega x_0 t + \vartheta)$. The main signal $S(t)$ is sent through an "amplitude equalizer" which converts $S_1(t)$ into $S_2(t) = 2D\cos\{2\pi 2\varrho\omega x_0 t - \varphi(2\varrho\omega t) + \vartheta\}$. Next the signals S_R and S_2 will be multiplied:

$$\frac{1}{2}\left(\frac{1}{D}\right)^2 S_2(t)\cdot S_R(t) = \cos\{4\pi 2\varrho\omega x_0 t - \varphi + 2\vartheta\} + \cos\varphi(2\varrho\omega t) \tag{8.18}$$

The first term represents a HF-signal, which is blocked out.

The method for phase measurement as described is possible but not always desirable since in most cases the experimenter wants to see on the CRT φ itself, not $\cos\varphi$ or $\sin\varphi$. This can be done by slightly modifying the method as described so far. The signals S_2 and S_R are "hardclipped" before being multiplied. "Hardclipping" is a nonlinear process to be explained in Chap. 9.

9 Nonlinear Transforms

The Fourier transformation is *linear*, which means that the processes of addition and transformation can exchange sequence and we still get the same result. Many other transformations are linear too. The property of "linearity" is mathematically popular since it makes things easy. Physically we can use linear transformations where the principle of linear superposition holds. In its most general form it says:

If	cause A	leads to	effect A'
and if	cause B	leads to	effect B'
then	cause (A+B)	will lead to	effect A' + effect B'

Hence, if the transition from the "cause-signal" to the "effect-signal" (or "input" to "output") obeys the law of linear superposition this transition can be described mathematically by a linear transformation.

As Charlie Brown once said to Snoopy, "Happiness is when all things are linear". Unfortunately the world of the experimentalist is not always linear. For the theoretician things are even worse, since most linear problems have been solved already because they are easier. What is left for today's Ph.D. candidates are mostly nonlinear problems, sometimes real problems, sometimes not. In any case we cannot pretend the world is all happiness. Therefore we want to study now some nonlinear transform problems. The only general statement one can make about nonlinear transform theory is that no statement is true in full generality. Hence we stick to some specific cases.

9.1 Graphical solution

The input function $f(x)$ is sketched in the lower part. The nonlinear transform assigns to each amplitude f an output amplitude F, which occurs on the same point x. Hence if we want to find for a given input amplitude $f(x)$ at x the output amplitude $F(x)$ for the same x, we draw a vertical line from $f-x$ diagram till it hits the $F(f)$ curve in the $F-f$ diagram. From there we go horizontally to the left into the $F-x$ diagram. The proper x-coordinate is found by going from the $x-f(x)$ point horizontally to the vertical x-axis. Then we travel along a circle to the x-axis of the $F-x$ diagram and continue vertically upwards till we meet the formerly drawn F-level curve. The crossing points is then $F(x)$.

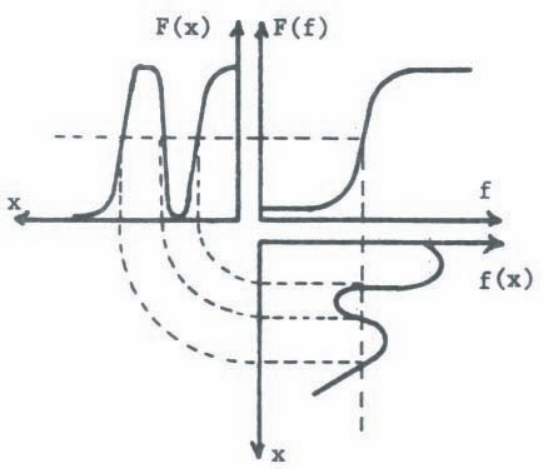

Figure 9.1: Graphical illustration of the nonlinear characteristic.

The nomenclature as used here is common. But it would have been better to call the "nonlinear characteristic" not $F(f)$ but for example $\mathrm{NL}(f)$ since $F(f)$ and $F(x)$ have different function structures (except in the trivial case of linearity). In summary we can describe this nonlinear transformation by:

$$f(x) \longrightarrow f \longrightarrow \mathrm{NL}(f) \longrightarrow \mathrm{NL}(f(x)) = F(x) \tag{9.1}$$

This type of nonlinearity is called "memoryless", or "amnesiac" or "point-to-point". A more general case is a combined convolution and nonlinearity.

$$F(x) = \int \mathrm{NL}(f(x - x'))\mathrm{d}x' \tag{9.2}$$

9.2 Polynomial Nonlinearity

$$f(x) \longrightarrow F(x) = \sum C_n f(x)^n \tag{9.3}$$

For example:

$$\begin{aligned} f(x) &= A(x)e^{i\varphi(x)} \longrightarrow f^n = A^n e^{in\varphi} \\ f(x) &= \sum B_m e^{2\pi i m\nu x} \\ f^2(x) &= \sum\sum B_m B_j e^{2\pi i(m+j)\nu x} = \sum(n)\{\sum(m)B_m B_{n-m}\}e^{2\pi in\nu x} \end{aligned} \tag{9.4}$$

Notice that the Fourier series with complex exponential is easier to handle than the form with sine and cosine.

9.3 FM-Nonlinearity

$$f(x) \longrightarrow F(x) = e^{if(x)} \tag{9.5}$$

For example:

$$f(x) = A(x)\sin(2\pi x + \varphi) \qquad F(x) = \sum J_n(A(x))e^{in(2\pi\nu x+\varphi)} \tag{9.6}$$

9.4 Hardclipping

$$f(x) \longrightarrow F(x) = \frac{1}{2} + \frac{1}{2}\text{signum}\{f(x)\} \tag{9.7}$$

Assume $f(x)$ to be bounded: $-\frac{1}{2} < f(x) < \frac{1}{2}$.

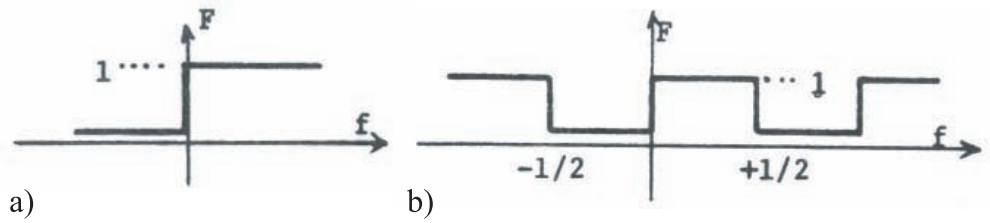

Figure 9.2: Hard clipping(a) and periodic continuation b).

The assumption is not very severe since all practical functions are bounded unless an explosion occurs. Now we use a trick which brings Fourier series into play. This is sometimes desirable since the Fourier representation usually reveals the frequency content of a signal. We replace the hard-clipping nonlinear characteristic by its periodic generalization. This does not make any difference since f was bounded.

$$\begin{aligned} F(f) &= \sum C_n e^{2\pi inf} \\ C_0 &= \frac{1}{2}; \qquad C_n = \frac{1}{2}(-i)^n \text{sinc}\left(\frac{n}{2}\right) \\ F(f(x)) &= \sum C_n e^{2\pi inf(x)} \end{aligned} \tag{9.8}$$

From here we can proceed easily to “multi-level-clipping”. Now we don’t assume anymore that f is bounded within $|f| < \frac{1}{2}$, at least within such narrow boundaries. The multi-level-clipping is (for example) described by the periodic $F(f)$ function which we just used. In that case we get as before $F(f(x)) = \sum C_n e^{2\pi inf(x)}$. In the case of a quadratic input function $f(x) = \left(\frac{x}{R}\right)^2$ this leads to a one-dimensional Fresnel zone plate. In other words our previous occupation with binary masks can be considered as a case of “multi-level-clipping”.

9.5 Amplitude height analysis

$$F(f) = \delta(f - f_0) \tag{9.9}$$

Assume both f and f_0 to be bounded, i.e., $|f|$, $|f_0| < \frac{1}{2}$. Under these circumstance we may add more delta-functions to F so that a delta-comb emerges.

$$F(x) = \sum(m)\delta(f - f_0 - m) = \sum(n)e^{2\pi in(f-f_0)} \tag{9.10}$$

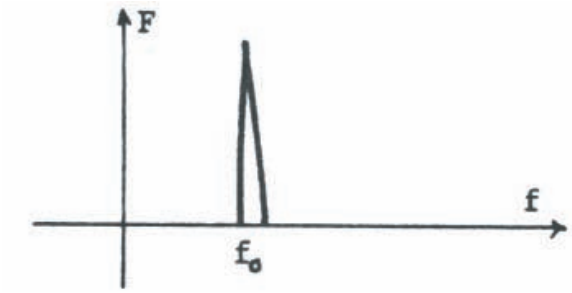

Figure 9.3: δ-shape nonlinearity.

For example:

$$F(x) = A\sin(x); \qquad f_0 < A < \frac{1}{2} \tag{9.11}$$

$$\begin{aligned} F(f(x)) &= \sum(n)e^{-2\pi inf_0}e^{2\pi inA\sin(x)} \\ &= \sum(m)\left\{\sum(n)J_m(2\pi nA)e^{-2\pi inf_0}\right\}e^{imx} \end{aligned} \tag{9.12}$$

10 Schwarz Inequality

The following integral I is certainly real and nonnegative:

$$I = \int |F(x) + zG(x)|^2 \, \mathrm{d}x; \qquad \text{for every z (which we assume to be real)} \quad (10.1)$$

But F and G might be complex. We introduce the following abbreviations:
$F \cdot F^* = A$; $F \cdot G^* + F^* \cdot G = B$; $G \cdot G^* = C$. $A,\ B,\ C$ are real, too.

$$I = A + Bz + z^2 C = I(z) \quad (10.2)$$

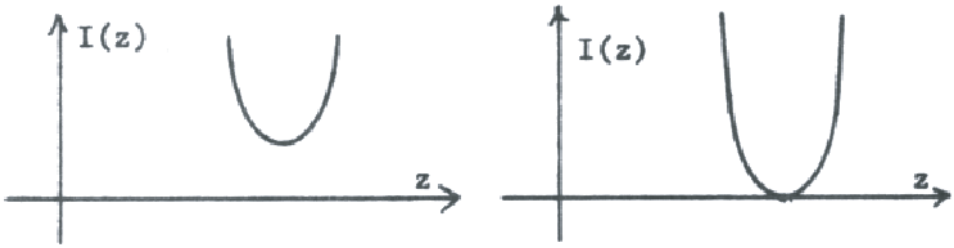

Figure 10.1: The parabolic shape of $I(z)$.

The inequality $I > 0$ means that the function $I(z)$ will never go below the z-axis. Since $I(z)$ is a parabola, this parabola must be opened upwards, which is due to $A > 0$. Furthermore the bottom of the parabola has to be above the z-axis, or on the z-axis, but not below it. The same property can be expressed in this way: The function $I(z)$ shall not have two zero-crossings. No zero-crossing or a "zero-touching" is compatible with $I \geq 0$. In both cases $I(z)$ is never negative. If $I(z)$ ever reaches zero then $I = 0 = A + Bz + z^2 C$. This is possible for:

$$z = \frac{1}{2A}[-B \pm \sqrt{B^2 - 4AC}] \quad (10.3)$$

No zero-crossing occurs if the root is imaginary, that is $4AC > B^2$. And "zero-touching" happens if the root is real due to $4AC = B^2$. Drawing both conclusions together we find that

$I(z) > 0$ is equivalent with $4AC \geq B^2$. Now we insert our definitions for A, B, C and get the Schwarz inequality.

$$4(F \cdot F^*)(G \cdot G^*) \geq (F \cdot G^* + F^* \cdot G)^2 \tag{10.4}$$

The equality sign is applicable only if $F(x) = c\, G(x)$.

11 Sampling Theorem

On pp. 65-67 we had derived the sampling theorem. It turned out to be the perfect method for converting the discrete function $\sum A_n \delta(\nu - n\varrho)$ into a continuous function $A(\nu)$ such that $\int A(\nu) e^{2\pi i \nu x} d\nu = f(x)\mathrm{rect}\left(\frac{x}{d}\right)$. The A_n had been the Fourier-coefficients of the periodic function $f(x) = \sum A_n e^{2\pi i n \varrho x}$. Since the sampling theorem is so important for information processing we want to elaborate on it in several ways.

11.1 Properties of the SINC-Function

If $u(x) \neq 0$ only in $|x| \leq \frac{P}{2}$ then $\tilde{u}(\nu) = \sum \tilde{u}\left(\frac{n}{P}\right) \mathrm{sinc}(\nu P - n)$. This can be interpreted as: $\{\mathrm{sinc}(\nu P - n)\}$ is a complete set of basis functions for all functions $\tilde{u}(\nu)$ which are Fourier transforms of a function $u(x)$ with the property $u(x) \neq 0$ only in $|x| \leq \frac{P}{2}$. These sinc$(\nu P - n)$ functions are almost *orthonormal*. We use the Parseval theorem for demonstrating the orthogonality.

$$\int_{-\infty}^{\infty} \mathrm{sinc}(\nu P - n)\mathrm{sinc}(\nu P - m)\mathrm{d}\nu = \tag{11.1}$$

$$= \left(\frac{1}{P}\right)^2 \int_{-\infty}^{\infty} \mathrm{rect}\left(\frac{x}{P}\right) \mathrm{rect}\left(-\frac{x}{P}\right) e^{2\pi i x(n-m)\frac{1}{P}} \mathrm{d}x$$

$$= \left(\frac{1}{P}\right)^2 \int_{-\frac{P}{2}}^{\frac{P}{2}} e^{2\pi i x(n-m)\frac{1}{P}} \mathrm{d}x = \left(\frac{1}{P}\right) \delta_{nm}$$

$$\int_{-\infty}^{\infty} \mathrm{sinc}(\nu P - n)\, \mathrm{sinc}(\nu P - m)\mathrm{d}(\nu P) = \delta_{nm} \tag{11.2}$$

But this orthogonality of two sinc-functions holds only if they have the same period P and if their relative shift is an integer multiple of the period P. Otherwise we find that by applying the sampling theorem to the sinc itself $\mathrm{sinc}\{P(\nu - \nu_0)\} = \tilde{u}(\nu) = \sum \tilde{u}\left(\frac{n}{P}\right) \mathrm{sinc}(\nu P - n) = \sum$ we get:

$$\mathrm{sinc}\{P(\nu-\nu_0)\} = \sum \mathrm{sinc}(n - P\nu_0)\mathrm{sinc}(\nu P - n) \tag{11.3}$$

11.2 Sampling at Shifted Points

Usually one would sample at points $\nu_n = \frac{n}{P}$. Now suppose we have sampled at shifted positions $\nu_n = \epsilon + \frac{n}{P}$: $\{\tilde{u}\left(\frac{n}{P} - \epsilon\right)\}$. Before continuing to read, guess if this set of sampling values contains also the complete information about $\tilde{u}(\nu)$ and $u(x)$. We try it out by replacing n by $n + P\epsilon$ in the sampling formula.

$$\sum_{(n)} \tilde{u}\left(\epsilon + \frac{n}{P}\right) \mathrm{sinc}(\nu P - (n + P\epsilon)) \stackrel{?}{=} \tilde{u}(\nu) \tag{11.4}$$

As in most situations where we don't know what to do next we replace some or all functions (here $\tilde{u}$ and sinc) by their Fourier-integrals.

$$\sum_{(n)} \iint u(x) e^{-2\pi i x(\epsilon + n/P)} \frac{1}{P} \mathrm{rect}\left(\frac{x'}{P}\right) e^{-2\pi i x'(\nu - n/P - \epsilon)} \mathrm{d}x \mathrm{d}x' \tag{11.5}$$

The summation turns out to be the Fourier series of a delta-comb:

$$\sum_{(n)} e^{2\pi i n(x'-x)/P} = \sum_{(m)} \delta\left(\frac{x - x'}{P} - m\right) = P \sum_{(m)} \delta(x' - x - mP) \tag{11.6}$$

We insert the delta-comb and then perform the x'-integral, which results in $x' \longrightarrow x + mP$:

$$\begin{aligned} & \sum_{(m)} \iint u(x) \mathrm{rect}\left(\frac{x'}{P}\right) \delta(x' - xmP) e^{2\pi i(-x\epsilon - x'\nu x'\epsilon)} \mathrm{d}x' \mathrm{d}x \qquad (11.7) \\ = & \sum \int u(x) \mathrm{rect}\left(\frac{x}{P} + m\right) e^{2\pi i m P(\epsilon - \nu)} e^{-2\pi i \nu x} \mathrm{d}x \end{aligned}$$

Next we make use of the fact that $u(x) \neq 0$ only in $|x| \leq P/2$. Hence $u(x)\mathrm{rect}\left(\frac{x+mP}{P}\right) \neq 0$ for $m = 0$. Therefore the rect-function results simply in integration limits $\pm P/2$.

$$\int_{-\frac{P}{2}}^{\frac{P}{2}} u(x) e^{-2\pi i x \nu} \mathrm{d}x = \tilde{u}(\nu) \tag{11.8}$$

Hence we have proven that the set of shifted samples $\left\{\tilde{u}\left(\frac{n}{P} + \epsilon\right)\right\}$ provides full information about $u(x)$ and $\tilde{u}(\nu)$. However we assumed that the shift ϵ was known. Guess whether or not we are in trouble if ϵ is not known.

11.3 Sampling of periodic functions

Definitions: $u(x) = u(x + MP)$: M: integer;

$$u(x) = \sum C_n e^{2\pi i n \frac{x}{P}};\ C_n = \frac{1}{P} \int_{-\frac{P}{2}}^{\frac{P}{2}} u(x) e^{-2\pi i n \frac{x}{P}} \mathrm{d}x \tag{11.9}$$

The problem of finding a sampling theorem consists now of two problems in the case of a periodic function because the transform from $u(x)$ to C_n is an integral, but the transform from C_n to $u(x)$ is a series.

First let us assume a limited range Q in the x-domain, $Q < P$.

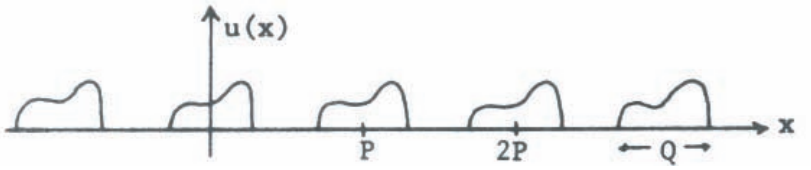

Figure 11.1: Example of a periodic function.

We expect an interpolation formula for the C_n. For example if $Q = \frac{P}{3}$ we would guess that only every third coefficient C_n is significantly new. In other words if $C_{-3}, C_0, C_{+3}, C_{+6}, \ldots$ are known we would suspect that C_1, C_2, C_4, C_5, C_7 etc. can be computed by interpolating the C_0, C_3, C_6 etc. The details can be worked out by the reader.

Now we consider the inverse problem. Assume that only $N + 1$ of the coefficients C_n are nonzero for $|n| \leq \frac{N}{2}$. The obvious guess is that $u(x)$ is completely determined by its values at the $N + 1$ discrete points $x_m = \frac{mP}{N+1}$; $m = 0, 1, \ldots N$. The reason for urging you to *always guess* beforehand what the result might be is that it helps you to develop your intuitive capabilities. Intuition is very important because it helps you to pick out the useful problems and the tractable solutions. One cannot make progress by trying out everything and selecting the few useful results. This approach would be much too slow. A case in point is the chess-playing computer. It has to go quickly through all possible moves in order to find the best move by exhausting all possibilities. Actually this would be impossible even for the fastest computer. Hence the program forbids whole classes of move sequences. Even then it is difficult for the computer to compete with a decent human chess player if more than about 20 moves occur. It is known that the human brain computer is fairly slow because the data transportation is based on slow electrochemical processes in the neurons, the data cables. But the brain can rule out whole classes of moves *at once*. This is done in a vague heuristic way, which is not quite under conscious control. Some people believe the human brain is so good simply because the human memory is so large. This is certainly a factor, but not the whole

explanation, because the search for information in that huge and slow memory would require much more time than a chess player actually needs. In my opinion it is this vague or heuristic process of making decisions about large classes of conceivable moves which accounts for the brain's skills. I believe that this skill can be developed systematically, for example by guessing before deriving or proving anything. After a while you will know when you can rely on your intuition.

Now let's start with the business of finding a sampling series for the periodic function $u(x)$ if only the C_n with $|n| \leq N$ are nonzero. For simplicity we will try to derive this sampling representation in a similar form as before with the aperiodic function. We need the equivalent to the rect-function, which is in the discrete case:

$$R_0 = \begin{cases} +1 & \text{if } |n| \leq N \\ 0 & \text{if } |n| > N \end{cases} \tag{11.10}$$

Now the identity corresponding to the one on p. 66 is:

$$C_n = R_n C_n = R_n \sum_{(m)} C_{n-m}(2N+1) \tag{11.11}$$

We will not write down R_n explicitly, but rather take it into account by identifying the summation limits properly when inserting the identity into the Fourier series for $u(x)$:

$$u(+x) = \sum_{-N}^{N} C_n e^{2\pi i n \frac{x}{P}} = \sum_{n=-N}^{N} \sum_{m=-\infty}^{\infty} C_{n-m(2N+1)} e^{2\pi i n \frac{x}{P}} \tag{11.12}$$

Herein we replace the C by its Fourier integral:

$$C_{n-m(2N+1)} = \frac{1}{P} \int_{-\frac{P}{2}}^{\frac{P}{2}} u(x') e^{-2\pi i \{n-m(2N+1)\} \frac{x'}{P}} \mathrm{d}x'; \tag{11.13}$$

Thus:

$$u(x) = \frac{1}{P} \sum_{n=-N}^{N} \sum_{m=-\infty}^{\infty} \int_{-\frac{P}{2}}^{\frac{P}{2}} u(x') e^{2\pi i \frac{[\ldots]}{P}} \mathrm{d}x' \tag{11.14}$$

where:

$$[\ldots] = nx - x'\{n - m(2N+1)\}. \tag{11.15}$$

The infinite series with index m is a delta-comb:

$$\begin{aligned}\sum(m)e^{2\pi imx'\frac{2N+1}{P}} &= \sum(m')\delta\left(x'\frac{(2N+1)}{P}-m'\right) \\ &= \frac{P}{2N+1}\sum\delta\left(x'-\frac{mP}{2N+1}\right)\end{aligned} \tag{11.16}$$

This we insert and get:

$$(2N+1)^{-1}\sum_{n=-N}^{N}\sum_{m=-\infty}^{\infty}\int_{-\frac{P}{2}}^{\frac{P}{2}}u(x')\delta\left(x'-\frac{mP}{2N+1}\right)e^{2\pi in\frac{(x-x')}{P}}\mathrm{d}x' \tag{11.17}$$

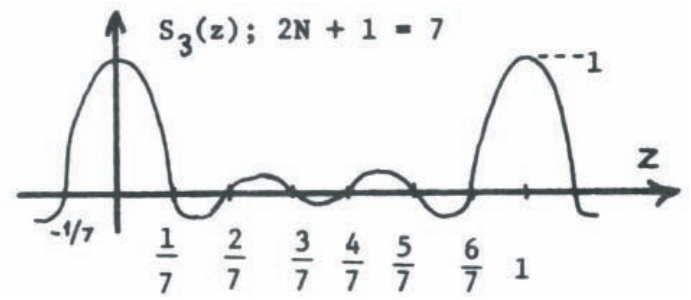

Figure 11.2: The periodic interpolation function S_N.

Because the integral extends only from $x' = -\frac{P}{2}$ to $x' = \frac{P}{2}$ only those delta functions can contribute which have singularity within that range: $|\frac{mP}{2N+1}| \leq \frac{P}{2}$; or $|m| \leq \frac{2N+1}{2}$ or $|m| \leq N$ since $\frac{(2N+1)}{2} = N + \frac{1}{2}$ is not an integer. Hence both series cover an index range from $-N$ to $+N$. The result of the integration is now:

$$\frac{1}{2N+1}\sum_{n=-N}^{N}\sum_{m=-N}^{N}u\left(\frac{mP}{2N+1}\right)e^{2\pi in\left[x-\frac{mP}{2N+1}\right]} \tag{11.18}$$

The summation over n is a two-sided geometrical series of the form:

$$\sum_{-N}^{N}e^{2\pi inx} = \frac{\sin[\pi(2N+1)z]}{\sin(\pi z)} = \frac{\mathrm{sinc}[(2N+1)z]}{\mathrm{sinc}(z)}(2N+1); \tag{11.19}$$

here: $z = \frac{x}{P} - \frac{m}{2N+1}$. We incorporate the factor $\frac{1}{2N+1}$ into the series and get:

$$u(x) = \sum_{n=-N}^{+N} u\left(\frac{mP}{2N+1}\right) S_N\left(\frac{x}{P} - \frac{m}{2N+1}\right) \tag{11.20}$$

$$S_N(z) = \frac{\mathrm{sinc}[(2N+1)z]}{\mathrm{sinc}(z)}$$

This formula is similar to the sampling formula for aperiodic functions except that the aperiodic sinc-function is now replaced by the periodic S_N function (Fig. 11.2).

11.4 Sampling at the wrong interval

Assumption: $u(x) = 0$ in $|x| > \frac{P}{2}$. Hence: $u(\tilde{\nu}) = \sum \mathrm{sinc}(\nu P - n)$.

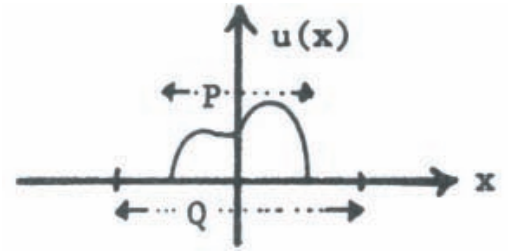

Figure 11.3: Example function.

In other words the continuous function $u(\tilde{\nu})$ is completely known already if we know it only at discrete sampling points $\nu_n = \frac{n}{P}$. Hence when measuring or computing $\tilde{u}(\nu)$ we can save a lot of work if we measure (or compute) only at points $\nu_n = \frac{n}{P}$. What happens if we misjudge the object range P? First assume we assumed a range $Q > P$. We would sample $\tilde{u}(\nu)$ at intervals $\nu_m = \frac{m}{Q}$, which is more often than at $\nu_n = \frac{n}{P}$. Hence we may guess that we probably wasted some effort but we did not lose any information about $\tilde{u}(\nu)$ and hence $u(x)$. This is indeed the case since obviously the sampling theorem must hold now too because $u(x)$ will be zero outside of $|x| < \frac{Q}{2}$ if $Q > P$ and if $u(x) = 0$ at $|x| \geq \frac{P}{2}$ as assumed. Hence it must be correct to write $\tilde{u}(\nu) = \sum \tilde{u}\left(\frac{m}{Q}\right) \mathrm{sinc}(\nu Q - m)$. One way of getting $u(x)$ back from the sampling values $\tilde{u}\left(\frac{m}{Q}\right)$ was by means a Fourier series evaluation with $C_m = \frac{1}{Q}\tilde{u}\left(\frac{m}{Q}\right)$.

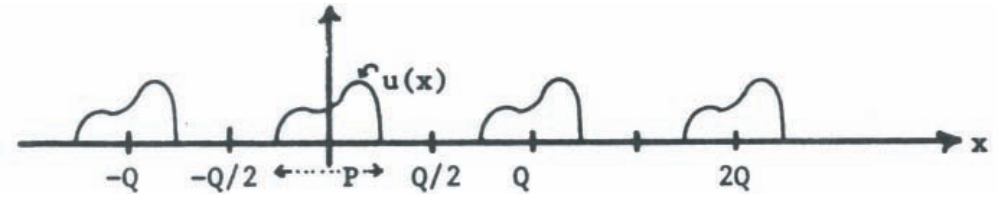

Figure 11.4: Oversampled function.

$$\begin{aligned}
\frac{1}{Q} \quad & \sum \quad \tilde{u}(\nu) e^{2\pi i m \frac{x}{Q}} = \\
\frac{1}{Q} \quad & \sum \quad u(x') e^{2\pi i m \frac{x-x'}{Q}} \mathrm{d}x' = \\
\frac{1}{Q} \quad & \sum \quad u(x') \delta\left(n - \frac{x-x'}{Q}\right) \mathrm{d}x' = \\
& \sum \quad \int u(x') \delta(x - x' - nQ) \mathrm{d}x' = \sum u(x - nQ)
\end{aligned} \tag{11.21}$$

No harm is done to the function $u(x)$, but we wasted some time by computing, in effect, many zero values between $\frac{P}{2}$ and $\frac{Q}{2}$ and between $-\frac{Q}{2}$ and $-\frac{P}{2}$.

Now let us consider the more dangerous case where we have misjudged Q as too small, $Q < P$. The sampling steps $\frac{1}{Q}$ in the ν-domain are now larger than they ought to be, namely $\frac{1}{P}$. Hence we might have lost information. This is indeed the case. The Fourier series now yields overlapping functions $u(x - nQ)$. this effect is called “aliasing”.

$$\frac{1}{Q} \sum \tilde{u}\left(\frac{m}{Q}\right) e^{2\pi i m \frac{x}{Q}} = \sum u(x - nQ) \tag{11.22}$$

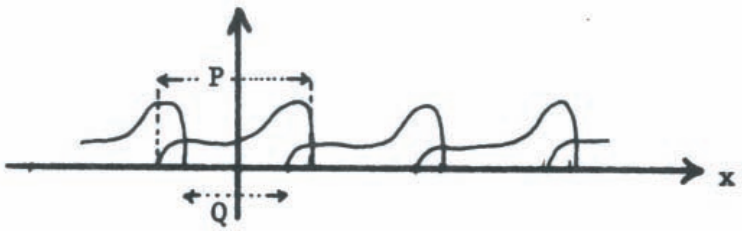

Figure 11.5: Undersampling resulting in aliasing.

This series has the same values in $\frac{Q}{2} < x < \frac{P}{2}$ as is $-\frac{P}{2} < x < \frac{Q}{2}$. Hence $u(x)$ cannot unambiguously be deduced from $\sum u(x - nQ)$ in $\frac{Q}{2} < |x| < \frac{P}{2}$. This problem is not due to the particular way we used when computing from the sampling values $\tilde{u}\left(\frac{m}{Q}\right)$ to $\sum u(x-nQ)$ by means of a Fourier series. One gets into the same kind of trouble when sing the Fourier integral transform:

$$\int \sum \tilde{u}\left(\frac{m}{Q}\right) \operatorname{sinc}(\nu Q - m) e^{2\pi i \nu x} \mathrm{d}\nu = u(x) \operatorname{rect}\left(\frac{x}{Q}\right) \tag{11.23}$$

Again the information about $u(x)$ is available only within $|x| < \frac{Q}{2}$.

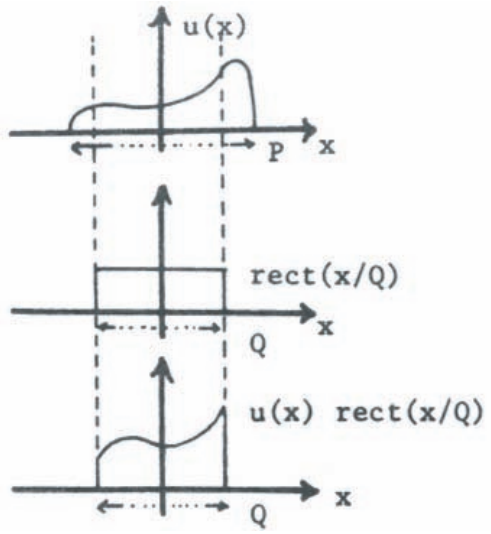

Figure 11.6: The effect of alisasing.

11.5 Sampling in two dimensions

If the function $u(x, y)$ is nonzero only in the rectangle $|x| < \frac{P}{2}$; $|y| < \frac{Q}{2}$ the Fourier transform $\tilde{u}(\nu, \mu)$ can be represented by a two-dimensional sampling series:

$$\tilde{u}(\nu, \mu) = \sum \sum \tilde{u}\left(\frac{n}{P}, \frac{m}{Q}\right) \operatorname{sinc}(\nu P - n) \operatorname{sinc}(\mu Q - m) \tag{11.24}$$

A more challenging problem occurs if $u(x, y)$ is nonzero only within a circle $x^2 + y^2 \leq R^2$. One approach would make use of a representation in polar coordinates (see Sec. 7.3; r

and φ are coordinates in Fig. 7.4). Another approach is to enclose the circle by a square with sides $2R$ long. Setting $P = Q = 2R$ reduces the problem to the previous two-dimensional cartesian sampling theorem. But since the area of square is ($\frac{4}{\pi} = 1.27$) times the area of the circle we would sample $\tilde{u}(\nu)$ more frequently by 27% than absolutely necessary. Somewhat more efficient is the enclosure of the circle by a regular hexagon. The area ratio is now $\frac{2\sqrt{3}}{\pi}$ which results in a 10% sampling waste. The product of the two sinc-functions is now to be replaced by another sampling function which is suitable for this honeycomb situation.

11.6 Fourier transform by digital computation

A digital computer is not suited for handling continuous functions. Instead it operates with a set of discrete samples. Hence integrals are to be replaced by series:

$$\begin{aligned} u(x) &= 0 \text{ in } |x| > \frac{P}{2} \qquad \tilde{u}(\nu) = \sum \tilde{u}\left(\frac{n}{P}\right) \operatorname{sinc}(\nu P - n) \\ u(x) &= \frac{1}{P} \operatorname{rect}\left(\frac{x}{P}\right) \sum \tilde{u}\left(\frac{n}{P}\right) e^{2\pi i \nu \frac{n}{P}} \end{aligned} \tag{11.25}$$

This set of equations is self-consistent, also the following set:

$$\begin{aligned} \tilde{u}(\nu) &= 0 \text{ in } |\nu| > \frac{Q}{2} \qquad u(x) = \sum u\left(\frac{m}{Q}\right) \operatorname{sinc}(xQ - m) \\ \tilde{u}(\nu) &= \frac{1}{Q} \operatorname{rect}\left(\frac{\nu}{Q}\right) \sum u\left(\frac{m}{Q}\right) e^{2\pi i m \frac{\nu}{Q}} \end{aligned} \tag{11.26}$$

However both sets together are not consistent anymore since $u(x)$ and $\tilde{u}(\nu)$ can never both stay at zero over a finite range of their coordinates x or ν.

The general proof rests on analyticity. One can make it plausible in this way:

$$u(x) \longleftrightarrow \tilde{u}(\nu); \qquad \operatorname{rect}\left(\frac{x}{P}\right) \longleftrightarrow P \operatorname{sinc}(\nu P) \tag{11.27}$$

if $u(x) = u(x)\text{rect}\left(\frac{x}{P}\right)$ then $\tilde{u}(\nu) = \int \tilde{u}(\nu')P\text{sinc}[(\nu - \nu')P]\text{d}\nu'$.

We assumed that $u(x)$ was zero at $|x| > P/2$. But now $\tilde{u}(\nu)$ can be expressed by a convolution of itself with the sinc-function. The sinc-function has infinitely long tails and no zero-stretches. Hence it is hard to imagine how this convolution could be become zero for $|\nu| > \frac{Q}{2}$. Actually not much harm is done if we forget about this mathematical problem as long as PQ is large, say 20 or more. For $PQ = N < 20$ one can improve the rigor of the mathematics by utilizing prolate sheroidal wavefunctions. However $N < 20$ is a situation which hardly occurs in physics. For $N > 20$ the relative error is of the order $\frac{1}{N} log N \approx 0$. The prolate spheroidal wavefunctions could help in principle. But their computation is a monstrous task.

What one does in practice is like this:

$$u(x) = 0 \text{ in } |x| > \frac{P}{2} \longrightarrow \tilde{u}(\nu) = \sum_{-\infty}^{\infty} \tilde{u}\left(\frac{n}{P}\right) \text{sinc}(\nu P - n). \tag{11.28}$$

If $\tilde{u}(\nu)$ appears to be very small in $|\nu| > \frac{Q}{2}$ one could replace $\tilde{u}(\nu)$ by $\tilde{u}(\nu)\text{rect}\left(\frac{\nu}{Q}\right)$ which corresponds to a "blurred" $u(x)$:

$$u(x) \longrightarrow \int u(x')\text{sinc}[(Q(x-x'))]\text{d}x' \tag{11.29}$$

However, $\text{rect}\frac{\nu}{Q} \sum_{-\infty}^{\infty} \tilde{u}\left(\frac{n}{P}\right) \text{sinc}(\nu P - n)$ is still an *infinite series*, which leads to excessive computations. Instead one limits the parameter range of the series such that only those sinc-function are considered which have their main peak within the range of the rect$\left(\frac{\nu}{Q}\right)$ function. Theses peaks are at $\nu_n = \frac{n}{P}$. Now we request $|\nu_n| \leq \frac{Q}{2}$ or $|n| \leq \frac{PQ}{2} = \frac{N}{2}$. Computing backwards to the x-domain yields:

$$\begin{aligned} &\sum_{|n| \leq \frac{PQ}{2}} \tilde{u}(\nu) \int \text{sinc}(\nu P - n) e^{2\pi i \nu x} \text{d}\nu \\ = \quad &\frac{1}{P}\text{rect}\left(\frac{x}{P}\right) \sum_{|n| \leq \frac{N}{2}} \tilde{u}\left(\frac{n}{P}\right) e^{2\pi i n \frac{x}{P}} \end{aligned} \tag{11.30}$$

The thing to remember is that the product N of the ranges P and Q indicates the number of terms in the digital Fourier transformation.

$$u(x) = 0 \text{ in } |x| > \frac{P}{2} \qquad \tilde{u}(\nu) \approx 0 \text{ in } |\nu| > \frac{Q}{2} \qquad N = PQ \tag{11.31}$$

11.7 Large digital Fourier transform

Optics is often dependent on the digital computer, for example for performing Fourier transforms. Typically a computer can h andle $64x64$ input points for a 2D Fourier transformation. This is often not large enough. The so-called "virtual memory" is supposed to alleviate this problem. But this virtual memory is quite often not optional. Furthermore it can be expensive in terms of computer time. The following trick may help then:

$$\begin{aligned}
&\text{Given :} \qquad u_n;\ -\frac{N}{2} < n \le \frac{N}{2}; \quad N \text{ terms} \\
&\text{Wanted :} \qquad \tilde{u}_m; -\frac{N}{2} < m \le \frac{N}{2} \\
&\tilde{u}_m = \sum_{n=-\frac{N}{2}+1}^{\frac{N}{2}} u_n e^{2\pi i n \frac{m}{N}} \quad N \text{ terms}
\end{aligned} \tag{11.32}$$

We split this series into two series with $\frac{N}{2}$ terms each:

$$\begin{aligned}
\tilde{u}_m &= \sum_{-\frac{N}{4}+1}^{\frac{N}{4}} \left\{ u_{2n} e^{-2\pi i 2n \frac{m}{N}} + u_{2n-1} e^{-2\pi i (2n-1) \frac{m}{N}} \right\} \\
&= \sum_{-\frac{N}{4}+1}^{\frac{N}{4}} n_{2n} e^{-2\pi i n \frac{m}{N/2}} + e^{2\pi i \frac{m}{N}} \sum_{-\frac{N}{4}+1}^{\frac{N}{4}} u_{2n-1} e^{-2\pi i n \frac{m}{N/2}}
\end{aligned} \tag{11.33}$$

Each series by itself is now periodic in m with a periodic $\frac{N}{2}$. Hence we have reduced the NxN Fourier problem into two $\frac{N}{2}$ x $\frac{N}{2}$ problems:

$$\begin{aligned}
E_m &= \sum u_{2n} e^{-2\pi i n \frac{m}{N/2}}; \qquad -\frac{N}{4} < m \le \frac{N}{4} \\
O_m &= \sum u_{2n-1} e^{-2\pi i n \frac{m}{N/2}}; \qquad -\frac{N}{4} < m \le \frac{N}{4} \\
\tilde{u}_m &= E_m + e^{2\pi i \frac{m}{N}} O_m; \qquad -\frac{N}{2} < m \le \frac{N}{2}
\end{aligned} \tag{11.34}$$

For a specific m' in the range $\frac{N}{4} < m' \le \frac{N}{2}$ we have:

$$\begin{aligned}
E_{m'} &= E_{m'-\frac{N}{2}} \qquad -\frac{N}{4} < m' - \frac{N}{2} \le \frac{N}{2} \\
O_{m'} &= O_{m'-\frac{N}{2}} \\
e^{2\pi i \frac{m'}{N}} &= e^{2\pi i \frac{(m'-N/2)}{N}} e^{2\pi i \frac{N/2}{N}} = -e^{2\pi i \frac{(m'-N/2)}{N}}
\end{aligned} \tag{11.35}$$

In other words we use the $\frac{N}{2}$ even terms u_{2n} to compute $\frac{N}{2}$ terms of E_m, and we compute the $\frac{N}{2}$ terms of O_m from the $\frac{N}{2}$ odd terms u_{2n-1}. For getting the "inner" $\tilde{u}_m$ terms ($-\frac{N}{4} < m \le \frac{N}{4}$) we multiply O_m by $e^{2\pi i \frac{m}{N}}$ and add E_m. For getting the "outer" u_m terms ($-\frac{N}{2} < m \le -\frac{N}{4}$; and $\frac{N}{4} < m \le \frac{N}{2}$) multiply O_m by $-e^{2\pi i \frac{m}{N}}$ and add E_m, which gives us $\tilde{u}_{m \pm \frac{N}{2}}$.

$$\begin{aligned}
\tilde{u}_m &= E_m + e^{2\pi i \frac{m}{N}} O_m \\
\tilde{u}_{m \pm \frac{N}{2}} &= E_m - e^{-2\pi i \frac{m}{N}} O_m \\
-\frac{N}{4} < &\quad m \quad \le \frac{N}{4}
\end{aligned} \tag{11.36}$$

For the Fourier transform on the digital computer we would use of course the “Fast Fourier Transform” subroutine, which is called “Cooley-Tukey” or FFT.

12 Fresnel-Transformation

This transform has been invented for diffraction theory by D. Gabor and also L. Mertz, who describes it in his book Transformations in Optics (J. Wiley, N. Y., 1965). The Fresnel transformation is similar to the Fourier transformation; that is, multiply with exponential and than integrate. But now the exponent is *quadratic*.

12.1 Definitions

$$\begin{aligned} \mathrm{Up-Transformation:} \qquad u(x) &\longrightarrow \hat{u}(x) = \int_{-\infty}^{\infty} u(x')e^{i\pi(x'-x)^2}\mathrm{d}x' \quad (12.1) \\ \mathrm{Down-Transformation:} \qquad u(x) &\longrightarrow \check{u}(x) = \int_{-\infty}^{\infty} u(x')e^{-i\pi(x'-x)^2}\mathrm{d}x' \end{aligned}$$

Some properties: apply $\check{}$ upon $\hat{u}$:

$$\begin{aligned} \check{\hat{u}}(x) &= \int \hat{u}(x')e^{-i\pi(x'-x)^2}\mathrm{d}x' \qquad \text{mit}: \hat{u}(x') = \int u(x'')e^{i\pi(x''-x')^2}\mathrm{d}x'' \\ \check{\hat{u}}(x) &= \iint u(x'')e^{i\pi\overbrace{[(x''-x')^2-(x'-x)^2]}^{[\ldots]=(x'')^2-x^2-2x'(x''-x)}}\mathrm{d}x'\mathrm{d}x'' = \qquad (12.2) \\ &= \int_{x''} u(x'')e^{i\pi((x'')^2-x^2)}\left\{\int_{x'} e^{-2\pi i x'(x''-x)}\mathrm{d}x'\right\}\mathrm{d}x'' = \\ &= \int_{x''} u(x'')e^{i\pi((x'')^2-x^2)}\left\{\delta(x''-x)\right\}\mathrm{d}x'' = u(x) \end{aligned}$$

Hence: $\check{\hat{u}}(x) = u(x)$; or shortly $\boxed{\check{\hat{u}}(x) = u}$; similarly: $\boxed{\hat{\check{u}}(x) = u}$.

$$\begin{aligned} \{\check{u^*}\} \neq \{\check{u}\}^* &= \left\{\int u(x')e^{-i\pi(x'-x)^2}\mathrm{d}x'\right\}^* = \qquad (12.3) \\ &= \int u^*(x')e^{i\pi(x'-x)^2}\mathrm{d}x' = \{\hat{u}\}^* \end{aligned}$$

Hence: $\boxed{\{\hat{u^*}\} = \{\check{u}\}^*}$ and $\boxed{\{\check{u^*}\} = \{\hat{u}\}^*}$

If $u(x) = v(-x)$ then $\hat{u}(x) = \hat{v}(-x)$ and $\check{u}(x) = \check{v}(-x)$.

12.2 Shift-theorem

Assume $u(x) = v(x + c)$; apply $\hat{}$ to both sides of this equation:

$$\begin{aligned} \int u(x')e^{i\pi(x'-x)^2}\mathrm{d}x' &= \int v(x+c)e^{i\pi(x'-x)^2}\mathrm{d}x' \\ = \hat{u}(x) &= \int v(x'')e^{i\pi(x''-c-x)}\mathrm{d}x'' = \hat{v}(c+x) \end{aligned} \tag{12.4}$$

$$\begin{aligned} u(x) = v(x+c) &\longrightarrow \hat{u}(x) = \hat{v}(x+c) \\ u(x) = v(x+c) &\longrightarrow \check{u}(x) = \check{v}(x+c) \end{aligned} \tag{12.5}$$

12.3 Tilt-theorem

$$\begin{aligned} u(x) &= v(x)e^{2\pi izx} \\ \hat{u}(x) &= \int v(x')e^{2\pi izx'}e^{+i\pi(x'-x)^2}\mathrm{d}x' = \\ &\quad [\ldots] = \overbrace{(x'-(x-z))^2}^{(x'-x+z)^2} + \overbrace{x^2-(x-z)^2}^{-z^2+2zx} \\ &= \int v(x')e^{i\pi\overbrace{[(x')^2-2x(x-z)+x^2]}} \mathrm{d}x' \\ &= e^{-i\pi(z^2-2zx)} \underbrace{\int v(x')e^{i\pi(x'-x+z)^2}\mathrm{d}x'}_{\hat{v}(x-z)} \end{aligned} \tag{12.6}$$

$$\begin{aligned} u(x) = v(x)e^{2\pi izx} &\longleftrightarrow \hat{u}(x) = \hat{v}(x-z)e^{-i\pi(z^2-2zx)} \\ u(x) = v(x)e^{2\pi izx} &\longleftrightarrow \check{u}(x) = \check{v}(x+z)e^{+i\pi(z^2+2zx)} \end{aligned} \tag{12.7}$$

$$u(x) = v(x)e^{i\pi x^2} \longleftrightarrow \boxed{\check{u}(x) = e^{-i\pi x^2}\tilde{v}(-x)} \tag{12.8}$$

Proof:

$$\begin{aligned}\check{v}(x) &= \int v(x')\underbrace{e^{i\pi(x')^2}e^{-i\pi(x'-x)^2}}_{e^{-i\pi(x^2-2xx')}}\mathrm{d}x' = \\ &= e^{-i\pi x^2}\int v(x')e^{2\pi i x'x}\mathrm{d}x' = e^{-i\pi x^2}\tilde{v}(-x)\end{aligned} \tag{12.9}$$

$$u(x) = v(x)e^{-i\pi x^2} \longleftrightarrow \hat{u}(x) = e^{i\pi x^2}\tilde{v}(x) \tag{12.10}$$

These connections between Fresnel transforms and Fourier transforms are quite useful because they allow us to reduce FRS to FQU for which fast computer algorithms and also many results in table form exist.

$$\begin{aligned}\hat{u}(x) &= \int u(x')e^{i\pi(x-x')^2}\mathrm{d}x' = e^{i\pi x^2}\int\{u(x')e^{i\pi x'^2}\}e^{-2\pi ixx'}\mathrm{d}x' \\ \check{u}(x) &= \int u(x')e^{-i\pi(x-x')^2}\mathrm{d}x' = e^{-i\pi x^2}\int\left\{u(x')e^{-i\pi(x')^2}\right\}e^{2\pi ixx'}\mathrm{d}x'\end{aligned} \tag{12.11}$$

Another important advantage can be derived from this Fourier-Fresnel relationship:

12.4 Sampling theorem for Fresnel transform pairs

Assume $u(x') \neq 0$ only within $|x| \leq \frac{P}{2}$ then also $u(x')e^{i\pi x'^2} \neq 0$. Call it $v(x')$ for a moment. The (Fourier-) Sampling theorem says:

$$\tilde{v}(x) = \int v(x')e^{-2\pi ixx'}\mathrm{d}x' = \sum_{(n)}\tilde{v}\left(\frac{n}{P}\right)\mathrm{sinc}(Px-n) \tag{12.12}$$

Hence the formula above is now:

$$\hat{u}(x) = e^{i\pi x^2}\sum\tilde{v}\left(\frac{n}{P}\right)\mathrm{sinc}(Px-n) \tag{12.13}$$

To find $\tilde{v}\left(\frac{n}{P}\right)$ we set $x = \frac{m}{P}$ and remember that $\mathrm{sinc}(m-n) = \delta_{mn}$.

$$\hat{u}\left(\frac{m}{P}\right) = e^{i\pi\left(\frac{m}{P}\right)^2}\sum\tilde{v}\left(\frac{n}{P}\right)\mathrm{sinc}(m-n) \tag{12.14}$$

Hence $\tilde{v}\left(\frac{m}{P}\right) = \hat{u}\left(\frac{m}{P}\right)e^{-i\pi\left(\frac{m}{P}\right)^2}$. Inserting this we get:

$$\hat{u}(x) = \sum\hat{u}\left(\frac{n}{P}\right)e^{i\pi\left\{x^2-\left(\frac{n}{P}\right)^2\right\}}\mathrm{sinc}(Px-n) \tag{12.15}$$

The Fresnel-type interpolation function $e^{-i\pi\left\{(\frac{n}{P})^2-x^2\right\}}\mathrm{sinc}(Px-n)$ has also the properties of being "l" if $x=\frac{n}{P}$, and "0" if $x=\frac{m}{P}$ ($m\neq n$, m is integer). Similarly one gets a sampling theorem for the other FRS transformation:

$$\check{u}(x)=\sum_{(n)}\check{u}\left(\frac{n}{P}\right)e^{-i\pi\left\{x^2-(\frac{n}{P})^2\right\}}\mathrm{sinc}(xP-n) \tag{12.16}$$

Another fairly general formula of the Parseval type is:

$$\underbrace{\int f_1(x)f^*(x)\mathrm{d}x}_{=\int \tilde{f}_1(\nu)(\tilde{f}_2)^*(\nu)d\nu}=\int \hat{f}_1(x)(\hat{f}_2)^*(x)\mathrm{d}x=\int \check{f}_1(x)(\check{f}_2)^*(x)\mathrm{d}x \tag{12.17}$$

From this on can derive many formulas by specializing, for example by $f_1=f_1=f$ one gets the equivalent to the Plancherel formula:

$$\int |f(x)^2|\mathrm{d}x=\int |\hat{f}(x)|^2\mathrm{d}x=\int |\check{f}(x)|^2\mathrm{d}x=\int |\tilde{f}(\nu)|^2\mathrm{d}\nu \tag{12.18}$$

The equivalent of the Wiener-Khintchine formula is obtained by substituting $f_1(x)=f_1(x+c)$

$$\int f(x+c)f^*(x)\mathrm{d}x=\int \hat{f}(x+c)(\hat{f})^*(x)\mathrm{d}x=\int \check{f}(x+c)(\check{f})^*(x)\mathrm{d}x \tag{12.19}$$

Another substitution yields

$$\begin{aligned} f_1(x) &= f_2(x)e^{2\pi izx} \\ \int |f(x)|^2e^{2\pi izx}\mathrm{d}x &= \int \hat{f}(x-z)(\hat{f}(x))^*e^{-i\pi(z^2-2zx)}\mathrm{d}x \\ &= \int \check{f}_2(x+z)(\check{f}_2(x))^*e^{i\pi(z^2-2zx)}\mathrm{d}x \end{aligned} \tag{12.20}$$

$$\begin{aligned} f_1(x) &= f_2(x)e^{i\pi x^2} \\ \int |f(x)|^2e^{i\pi x^2}\mathrm{d}x &= \int \check{f}(x)(\check{f})^*(x)e^{i\pi x^2}\mathrm{d}x \end{aligned} \tag{12.21}$$

$$\begin{aligned} f_1(x)=v(x)e^{2\pi izx} \quad ; \quad f_2(x)=v(x)e^{-2\pi izx} & \\ \int |v(x)|^2e^{4\pi ixz}\mathrm{d}x &= \int \hat{v}(x-z)(\hat{v})^*(x+z)e^{4\pi ixz}\mathrm{d}x= \\ &= \int \check{v}(x+z)(\check{v})^*(x-z)e^{4\pi ixz}\mathrm{d}x \end{aligned} \tag{12.22}$$

A special case of the last formula yields:

$$\int |v(x)|^2 \mathrm{d}x = \int \hat{v}(x-z)(\hat{v})^*(x+z)\mathrm{d}x = \int \check{v}(x+z)(\check{v})^*(x-z)\mathrm{d}x \tag{12.23}$$

Some more relations:

$$\begin{aligned} f(x) &= \delta(x-c) \longrightarrow \hat{f}(x) = e^{i\pi(x-c)}; \quad \check{f}(x) = e^{-i\pi(x-c)} \\ f(x) &= 1 \longrightarrow \hat{f}(x) = \int_{-\infty}^{\infty} e^{i\pi(x'-x)^2}\mathrm{d}x' = \int_{-\infty}^{\infty} e^{i\pi x^2}\mathrm{d}x = e^{i\frac{\pi}{4}} \\ \check{f}(x) &= [\hat{f}(x)]^* = e^{-i\frac{\pi}{4}}; \quad \text{Fresnel integral} \end{aligned} \tag{12.24}$$

$$\begin{aligned} f(x) = e^{2\pi i z x} \longrightarrow \hat{f}(x) &= \int e^{i\pi\left[2zx' + (x'-x)^2\right]}\mathrm{d}x' \\ &= \int e^{i\pi\left[x'^2 - 2x'(x-z) + x^2\right]}\mathrm{d}x' = \\ &= e^{i\pi(2xz-x^2)} \int e^{i\pi(x'+z-x)^2}\mathrm{d}x' = e^{i\pi\left(2zx - z^2 + \frac{1}{4}\right)} \end{aligned} \tag{12.25}$$

Hence:

$$\begin{aligned} f(x) &= e^{2\pi i z x} \longleftrightarrow \hat{f}(x) e^{i\pi\left(2xz - z^2 + \frac{1}{4}\right)} \\ f(x) &= e^{2\pi i z x} \longleftrightarrow \check{f}(x) e^{-i\pi\left(2xz - z^2 + \frac{1}{4}\right)} \end{aligned} \tag{12.26}$$

$$\begin{aligned} f(x) = \sum A_n e^{2\pi i n \frac{x}{P}} \longleftrightarrow \hat{f}(x) = \sum A_n e^{-i\left[\left(\frac{n}{P}\right)^2 - \frac{1}{4}\right]} e^{2\pi i n \frac{x}{P}} \\ f(x) = \sum A_n e^{2\pi i n \frac{x}{P}} \longleftrightarrow \check{f}(x) = \sum A_n e^{-i\left[\left(\frac{n}{P}\right)^2 - \frac{1}{4}\right]} e^{-2\pi i n \frac{x}{P}} \end{aligned} \tag{12.27}$$

Probably the most important formula for applications in holography is:

$$\left[\check{f}(x)\right]^* = \left[\hat{f}(x)^*\right] \tag{12.28}$$

The extension to two dimensions is straightforward:

$$\begin{aligned} \hat{f}(x,y) = \iint f(x',y') e^{i\pi\left[(x-x')^2 + (y-y')^2\right]}\mathrm{d}x'\mathrm{d}y' \\ \check{f}(x,y) = \iint f(x',y') e^{-i\pi\left[(x-x')^2 + (y-y')^2\right]}\mathrm{d}x'\mathrm{d}y' \end{aligned} \tag{12.29}$$

Again:

$$[\check{f}]^* = [\hat{f}^*] \tag{12.30}$$

Now we go over to polar coordinates:

$$\begin{aligned} x' &= r\cos\varphi; & x &= R\cos\Phi \\ y' &= r\sin\varphi; & y &= R\sin\Phi \\ \hat{F}(R,\Phi) &= \int_0^{2\pi}\int_0^{\infty} F(r,\varphi)e^{i\pi[r^2+R^2-2rR\cos(\Phi-\varphi)]}r\mathrm{d}r\mathrm{d}R \end{aligned} \tag{12.31}$$

Insert $F(r,\varphi) = \sum F_n(r)e^{in\varphi}$ and:

$$\begin{aligned} e^{-2\pi ir\cos(\varphi-\Phi)} &= e^{2\pi irR\sin\left(\Phi-\varphi-\frac{\pi}{2}\right)} = \sum J_m(2\pi rR)e^{im\left(\Phi-\varphi-\frac{\pi}{2}\right)} \\ \hat{F}(R,\Phi) &= \sum\sum\iint F_n(r)J_m(2\pi rR)e^{i\pi(r^2+R^2)}e^{i\left[n\varphi+m\left(\Phi-\varphi-\frac{\pi}{2}\right)\right]}r\mathrm{d}r\mathrm{d}\varphi \\ &= 2\pi\sum\int e^{i\pi\left(\Phi-\frac{\pi}{2}\right)}F_n(r)J_n(2\pi rR)e^{i\pi(r^2+R^2)}r\mathrm{d}r \end{aligned} \tag{12.32}$$

13 The Stationary Phase Integral

This method of computing an integral easily and in fairly good approximation is very useful in optics and other branches of physics where wave motions occur. We need two preliminary results first: the Fourier transform of the step-function, and the Fresnel integral.

13.1 Fourier transform of the step-function

$$S(x) = \begin{cases} +1 & \text{if } x \geq 0 \\ 0 & \text{if } x < 0 \end{cases} = \frac{1}{2} + \frac{1}{2} \begin{cases} +1 & \text{if } x \geq 0 \\ -1 & \text{if } x < 0 \end{cases} = \frac{1}{2} + \frac{1}{2}\text{Signum}(x) \quad (13.1)$$

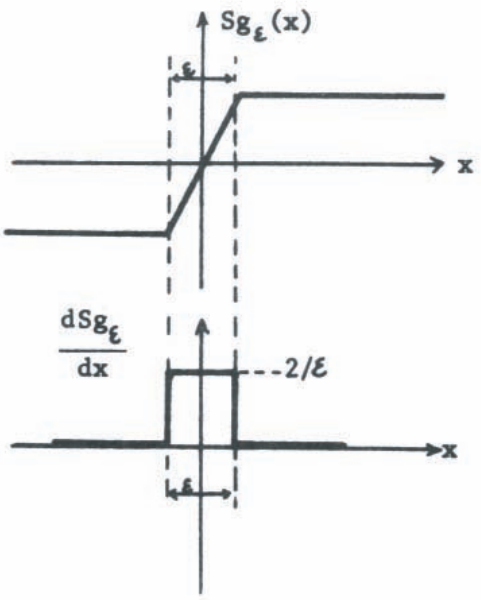

Figure 13.1: The signum function and its derivative.

where:

$$\mathrm{Signum}\{f(x)\} = \mathrm{Sg}\{f(x)\} = \begin{cases} +1 & : \text{ if } f(x) \geq 0 \\ 0 & : \text{ if } f(x) < 0 \end{cases} \tag{13.2}$$

$$\widetilde{\mathrm{Sg}}(\nu) = \int \mathrm{Sg}(x) e^{-2\pi i \nu x} \mathrm{d}x \tag{13.3}$$

$$\mathrm{Sg}(x) = \lim_{\epsilon \to 0} \mathrm{Sg}_\epsilon(x) \tag{13.4}$$

$$\widetilde{\mathrm{Sg}}(\nu) = \int \mathrm{Sg}_\epsilon(x) e^{-2\pi i \nu x} \mathrm{d}x = \int \frac{\mathrm{dSg}_\epsilon(x)}{\mathrm{d}x} \cdot \frac{e^{-2\pi i \nu x}}{2\pi i \nu} \mathrm{d}x \tag{13.5}$$

where:

$$\widetilde{\mathrm{Sg}_\epsilon}(\nu) = \frac{\mathrm{sinc}(\nu\epsilon)}{\pi i \nu} \tag{13.6}$$

now $\epsilon \longrightarrow 0$ yields $\widetilde{\mathrm{Sg}}(\nu) = \frac{1}{\pi i \nu}$;

$$\widetilde{\mathrm{Sg}}(\nu) = \frac{1}{2}\delta(\nu) + \frac{1}{2\pi i \nu} \tag{13.7}$$

13.2 The Fresnel integral

$$F = \int_{-\infty}^{\infty} e^{iax^2} \mathrm{d}x \tag{13.8}$$

The quadratic exponent is not convenient. A substitution $x^2 = z$ is not a suitable way out of this problem because the differential becomes involved: $\mathrm{d}x = \frac{1}{2}\frac{\mathrm{d}z}{\sqrt{z}}$. But we may compute the square of F and introduce polar coordinates:

$$\begin{aligned} F^2 &= \left(\int e^{iax^2} \mathrm{d}x\right)\left(\int e^{iay^2} \mathrm{d}y\right) = \int_{-\infty}^{\infty}\int_{-\infty}^{\infty} e^{ia(x^2+y^2)} \mathrm{d}x\mathrm{d}y \\ &= \int_0^{2\pi}\int_0^{\infty} e^{iar^2} r \mathrm{d}r\mathrm{d}\varphi = 2\pi \int_0^{\infty} e^{iar^2} r \mathrm{d}r \end{aligned} \tag{13.9}$$

Now it is useful to substitute such that the exponent becomes linear because now also the differential becomes simpler in the process:

$$ar^2 = 2\pi x; \quad \mathrm{d}(r^2) = 2rdr = \frac{2\pi}{a}\mathrm{d}x \tag{13.10}$$

$$\begin{aligned} F^2 &= \frac{2\pi^2}{a}\int_0^\infty e^{2\pi i x}\mathrm{d}x = \frac{2\pi^2}{a}\tilde{S}(-1) = \frac{i\pi}{a} = \frac{\pi}{a}e^{i\frac{\pi}{2}} \\ F &= \sqrt{\frac{\pi}{a}}e^{i\frac{\pi}{4}} = \int_{-\infty}^\infty e^{iax^2}\mathrm{d}x = \sqrt{\frac{\pi}{2a}}(1+i) \end{aligned} \tag{13.11}$$

13.3 The method of stationary phase

Goal: find a simple approximate solution for the integral:

$$I = \int_A^B g(x)e^{ikf(x)}\mathrm{d}x \tag{13.12}$$

Approach: reduce this integral to the Fresnel integral F.

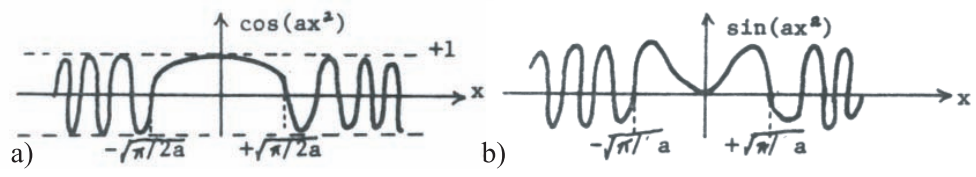

Figure 13.2: a) Real and b) imaginary part of the integrand in the Fresnel integral.

For understanding this approach let us sketch the integrand (real & imaginary) of $F = \int e^{iax^2}\mathrm{d}x = \sqrt{\frac{\pi}{2a}}(1+i)$ (Fig. 13.2).The main contribution to

$$\int_{-\infty}^\infty \cos(ax^2)\mathrm{d}x = \mathrm{Re}\{F\} = \sqrt{\frac{\pi}{2a}} \tag{13.13}$$

comes form $-\sqrt{\frac{\pi}{2a}} < x < \sqrt{\frac{\pi}{2a}}$. The rest cancels due to the oscillation of the cosine. Looking at $\sin(ax^2)$ it becomes plausible again that

$$\int_{-\infty}^{\infty} \sin(ax^2)\mathrm{d}x \tag{13.14}$$

must be something like $\sqrt{\frac{\pi}{2a}}$.

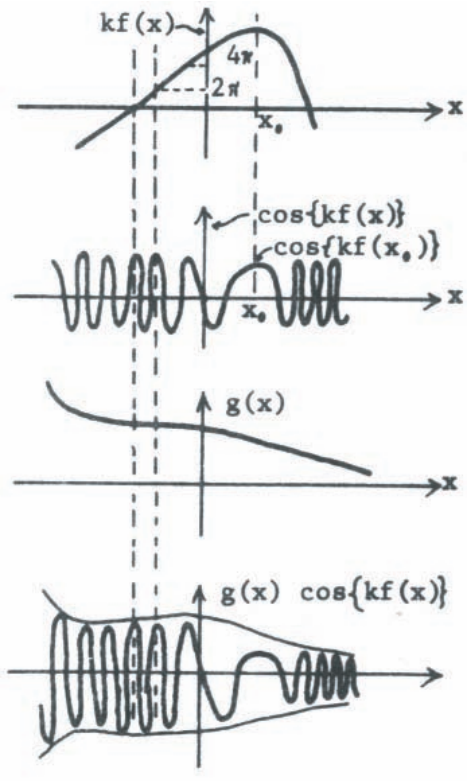

Figure 13.3: Illustration of the real part of the integrand in I (see text for detailed discussion).

Now let us see under what circumstances the integral I will assume the form of a Fresnel Integral. The exponent $kf(x)$ might vary rapidly at most x-regions, but we assume it to be "stationary" at $x = x_0$; that means $\frac{\mathrm{d}f(x)}{\mathrm{d}y} = 0$ at $x = x_0$. Hence around there we can write $f(x) \approx f(x_0) + f''(x_0)\frac{(x-x_0)^2}{2}$. The result of the integration will depend on $g(x)$ at $x = x_0$, on $\cos\{kf(x_0)\}$ and on the width of the unusually wide maximum of $\cos\{kf(x)\}$ at $x = x_0$ (Fig. 13.3). This width will be narrow, if the bend of $f(x)$ at $x = x_0$ is sharp, which depends on $\frac{\mathrm{d}^2 f}{\mathrm{d}x^2}$. The function $g(x)$ should change only little during on oscillation, which is achieved

by having k *large*. If $f(x)$ is stationary only once within $A < x < B$, then we will have a contribution only from there. If so it does not make a fifference if we extend the integration limits $A \to -\infty$ and $B \to +\infty$, as long as $kf(x)$ does not have other stationary points outside of $A < x < B$.

$$I = \int_A^B g(x) e^{ikf(x)} \mathrm{d}x \approx \int_A^B g(x) e^{ik\left[f(x_0) + f''(x_0)\frac{(x-x_0)^2}{2}\right]} \mathrm{d}x \tag{13.15}$$

$f(x_0) + f''(x_0)\frac{(x-x_0)^2}{2}$ has no stationary point besides $x = x_0$. Hence we can extend the limits of integration:

$$\int_A^B \ldots \mathrm{d}x \longrightarrow \int_{-\infty}^{\infty} \ldots \mathrm{d}x \tag{13.16}$$

The additional regions will cancel each other anyway due to oscillation.

$$I \approx e^{ikf(x_0)} \int_{-\infty}^{\infty} g(x) e^{ik\frac{f_0''(x-x_0)}{2}} \mathrm{d}x \tag{13.17}$$

To bring this into the shape of a Fresnel integral, we set $g(x) \approx g(x_0) + g'(x_0)(x - x_0)$.

$$I \approx e^{ikf_0} \left[g_0 \int_{-\infty}^{\infty} e^{ik\frac{f''(x-x_0)^2}{2}} \mathrm{d}x + g_0' \int_{-\infty}^{\infty} (x - x_0) e^{ik\frac{f_0''(x-x_0)^2}{2}} \mathrm{d}x \right] \tag{13.18}$$

The second term is zero because the exponential function is symmetrical around x_0, while the factor $(x - x_0)$ is antisymmetrical, hence also the product. The $\int$ (antisymmetrical) $\mathrm{d}x$ is zero. Now the integral I assumes the form of the Fresnel integral F.

$$I \propto g_0 e^{ikf_0} \int_{-\infty}^{\infty} e^{i\frac{kf_0''}{2}(x-x_0)^2} \mathrm{d}x \tag{13.19}$$

We change $x - x_0 = x'$ and we set $a = \frac{kf_0}{2} \to \sqrt{\frac{\pi}{a}} = \sqrt{\frac{2\pi}{kf_0''}}$. Thereby we get:

$$\boxed{I = \int_A^B g(x) e^{ikf(x)} \mathrm{d}x \approx \sqrt{\frac{2\pi}{kf''(x_0)}} g(x_0) e^{i\left[kf(x_0) + \frac{\pi}{4}\right]}} \tag{13.20}$$

If $f'(x)$ has more than one zero, say at x_n, then $I = \sum_{(n)} \sqrt{\frac{2\pi}{kf''(x_n)}} g(x_n) e^{[\dots]}$, where: $[\dots] = kf(x_n) + \frac{\pi}{4}$.

13.4 Saddle-point method

This method is in essence the same as the "method of stationary phase", only in *two* dimensions:

$$I = \int_{A_x}^{B_x} \int_{A_y}^{B_y} g(x,y) e^{ikf(x,y)} \mathrm{d}x \mathrm{d}y \tag{13.21}$$

The name of this method is "saddle-point" because $f(x,y)$ has a saddle shape at x_0, y_0, where $\frac{\partial f}{\partial x} = 0$ and $\frac{\partial f}{\partial y} = 0$. Actually three situations can occur (Fig. 13.4).

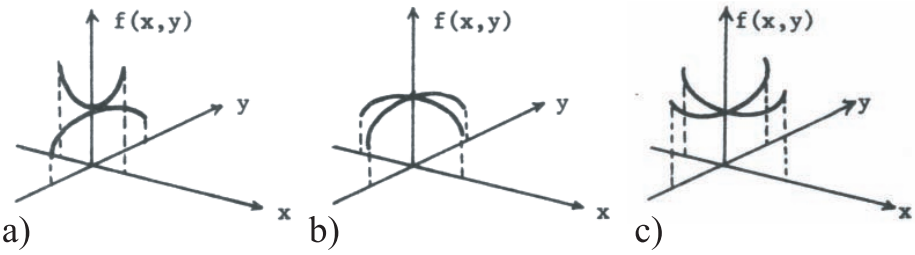

Figure 13.4: 2D functions with vanishing partial derivatives $\frac{\partial f}{\partial x} = 0$ and $\frac{\partial f}{\partial y} = 0$, resulting in a) a saddle-point for $\frac{\partial^2 f}{\partial x^2} > 0$ and $\frac{\partial^2 f}{\partial y^2} < 0$ (or vice versa), b) a total maximum for $\frac{\partial^2 f}{\partial x^2} < 0$ and $\frac{\partial^2 f}{\partial y^2} < 0$, c) a total minimum for $\frac{\partial^2 f}{\partial x^2} > 0$ and $\frac{\partial^2 f}{\partial y^2} > 0$.

All three types are called "saddle-points" by the mathematicians (non-riders). First we have to find (x_0, y_0) by solving the two equations $\frac{\partial f}{\partial x} = 0$ and $\frac{\partial f}{\partial y}$. In general there might be more than one saddle-point within $A_x < x < B_x$; $A_y < y < B_y$. Then we might subdivide the area into subareas, each containing only one saddle-point, which then is treated as follows now. Later the results from the subareas are to be added. Our approach is to approximate $f(x,y)$ around (x_0, y_0) by:

$$\begin{aligned} f(x,y) &\approx f(x_0,y_0) + \frac{\partial^2 f(x_0,y_0)}{\partial x^2} \frac{(x-x_0)^2}{2} \\ &+ \frac{\partial^2 f(x_0,y_0)}{\partial y^2} \frac{(y-y_0)^2}{2} + \frac{\partial^2 f(x_0,y_0)}{\partial x \partial y} (x-x_0)(y-y_0) \end{aligned} \tag{13.22}$$

we abbreviate:

$$f_0 + f_{xx}\frac{(x-x_0)^2}{2} + f_{yy}\frac{(y-y_0)^2}{2} + f_{xy}(x-x_0)(y-y_0) \tag{13.23}$$
$$g(x,y) \approx g(x_0,y_0) + \frac{\partial g(x_0,y_0)}{\partial x}(x-x_0) + \frac{\partial g(x_0,y_0)}{\partial y}(y-y_0)$$

We may neglect the first derivates of g because they result in asymmetric integrands.

$$\begin{aligned} I &\approx g_0 \int_{(y)} e^{ik\left[f_0 + f_{yy}\frac{(y-y_0)}{2}\right]} \cdot \\ &\cdot \left\{ \int_{(x)} e^{ik\left[f_{xx}\frac{(x-x_0)^2}{2} + f_{xy}(x-x_0)(y-y_0)\right]} \mathrm{d}x \right\} \mathrm{d}y \end{aligned} \tag{13.24}$$

The inner integral is almost a Fresnel integral. Add and subtract the quadratic supplement (or "complete the square"):

$$\begin{aligned} & f_{xx}\frac{(x-x_0)^2}{2} + f_{xy}(x-x_0)(y-y_0) = \\ = \; & \frac{f_{xx}}{2}\left[(x-x_0)^2 + 2(x-x_0)\frac{f_{xy}}{f_{xx}}(y-y_0) + \left(\frac{f_{xy}}{f_{xx}}(y-y_0)\right)^2\right] - \\ - \; & f_{xy}^2\frac{(y-y_0)^2}{2f_{xx}} \end{aligned} \tag{13.25}$$

Hence the inner integral is now:

$$\begin{aligned} & e^{-ik\left[f_{xy}^2\frac{(y-y_0)^2}{2f_{xx}}\right]} \int e^{ik\frac{f_{xx}}{2}\left[x-x_0+\frac{f_{xy}}{f_{xx}}(y-y_0)\right]^2} \mathrm{d}x = \\ = \; & e^{-ik\left[f_{xy}^2\frac{(y-y_0)^2}{2f_{xx}}\right]} \sqrt{\frac{2\pi}{kf_{xx}}} e^{\frac{i\pi}{4}} \end{aligned} \tag{13.26}$$

What remains is:

$$I \approx g_0\sqrt{\frac{2\pi}{kf_{xx}}} e^{i\left(kf_0+\frac{\pi}{4}\right)} \int_{(y)} e^{ik\frac{(y-y_0)^2}{2}\left\{f_{yy} - \frac{f_{xy}^2}{f_{xx}}\right\}} \mathrm{d}y \tag{13.27}$$

Here again we encounter a Fresnel-integral with "a$'' = \frac{k}{2}\left\{f_{yy} - \frac{f_{xy}^2}{f_{xx}}\right\} = \frac{k(f_{xx}f_{yy} - f_{xy}^2)}{2f_{xx}}$.
Hence it is $\sqrt{\frac{\pi}{a}}e^{i\frac{\pi}{4}} = e^{i\frac{\pi}{4}}\sqrt{2\pi\frac{f_{xx}}{k(f_{xx}f_{yy}-f_{xy}^2)}}$

Inserting we finally get:

$$\boxed{I \approx \frac{2\pi g(x_0, y_0)}{k\sqrt{f_{xx}f_{yy} - f_{xy}^2}} e^{i\left[kf(x_0,y_0)+\frac{\pi}{2}\right]}} \tag{13.28}$$

$$\boxed{I = \int_{A_x}^{B_x}\int_{A_y}^{B_y} g(x,y)e^{ikf(x,y)}\mathrm{d}x\mathrm{d}y}$$

14 What is Light?

14.1 History

Some of the ancient Greek thought that light *emerges* from the eye, travels to the target, and returns to the eye (Fig. 14.1). Today we would call this approach "active LIDAR" (LIDAR = RADAR with light). In the Middle Ages scientists began to believe that vision is like "passive LIDAR", which means that radiation travels only from the target to the eye, not vice verse. When observing a hypnotist one may not be so sure anymore that the old Greek were completely wrong.

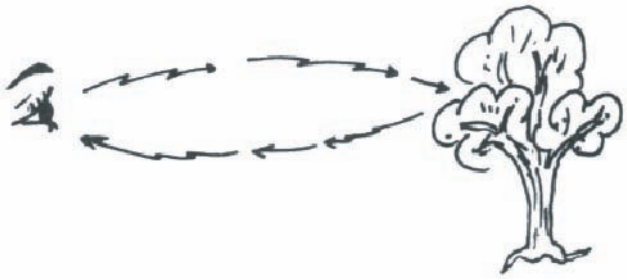

Figure 14.1: Vision according to the ancient Greek.

Galileo (1564-1642) tried to measure the speed of light, which he believed to be finite, while others before him thought it to be infinite. Newton (1642-1727) was born when Galileo died. Newton explained light as a stream of bullets, which explains very nicely the shadow. Newton also discovered the "Newton-rings", which Huygens (1629-1695) considered as one of the best proofs for the wave nature light. Römer (1644-1710) was the first one who succeeded in measuring the speed of light. Fresnel (1788-1827) formulated the first wave theory of light, which described also polarization. His equations are identical with those of Maxwell (1831-1879) except for the term D, which Maxwell added. Both thought of light as hydrodynamic ether waves. In spite of their wrong ideas their calculated predictions and descriptions of many effects ware correct. This teaches us that the quantitative truth of a system of equations is invariant to what the physicist thinks about the nature of the experiment. In a hundred years hence scientists will probably smile about our nave picture of the world, yet they might still use Maxwell's and Dirac's equations.

Michelson (1852-1931) found that the velocity of light is the same in every unaccelerated system. Based on this result Lorentz concluded that Maxwell had accidently found a set of equations which satisfied Einstein's (1879-1955) theory of special relativity. In 1900 Planck (1858-1947) deduced from the spectral distribution of the black-body radiation that light energy must consist of photons or quanta. He was not pleased with this result because it was logically unsatisfactory to think of light as waves and also as photons (like bullets). In spite of Planck's misgivings the photon theory of light progressed quickly when Einstein explained the photoelectric effect in 1905, and when Bohr (1885-1962) in 1913 showed how the atom can be understood at once if we accept the photon hypothesis. The resistance against the "wave-particle duality" diminished further when de Broglie in 1924 showed that this duality problem affects also electrons and other particles. But this duality dilemma is by no means a closed chapter. For example, P. Franken insists that it is not necessary to consider electromagnetic radiation to be quantized. Only most emitters produce this radiation in quantized parcels because that is all they can do. Also some receivers can digest radiation only in well-defined humps. If so, the radiation itself must not necessarily be quantified due to its own nature. Another theory is A. Landé's, who claims he can explain every effect with photons. Waves are not necessary. At best they are convenient mental crutch to describe the behaviour of whole bunches of photons. I wish I knew who is right. I fear however the question "what is light" is ultimately meaningless if one expects a pictorial answer like "light consists of little bullets". Einstein one answered the question in this way: Light is as paradoxial as Voltaire (a French scientist, philosopher, politician, and an international expert in intrigues; 18th century). Voltaire was born as a Catholic, he converted early to Protestantism, but returned to Catholicism shortly before dying. Light is born as a photon, it lives as a wave, but it dies as a photon again when being absorbed.

14.2 What is Observable?

The energy per volume in an electromagnetic field is proportional to $\vec{E}\vec{E} + \vec{H}\vec{H}$. This energy density can be observed by many effects, as for example photography, photoelectrons, heat, chemical reaction, radiation, pressure and torque. These effects are mainly proportional to the polarization, on the angle of incidence and on the spectral composition of the light. Usually these dependencies are only weak. Hence we will assume the probability of encountering a photon in the volume element $\mathrm{d}x\mathrm{d}y\mathrm{d}z$ around (x, y, z) during the time interval from t to $t + \mathrm{d}t$ is proportional to the square E^2 of the electrical field. The proportionality factor is very important for illumination technology. However, in all parts of optics where the information of the light beam is of interest this proportionality factor will seldom be discussed. We will refer to this proportionality factor as a "photometric aspect", which might for example determine how long a photographic plate hat to be exposed. But the structure of the photographic image is entirely determined by $E^2(x, y, z, t)$. This and similar energy- or power-quantities with unspecified proportionality factors will be called "intensities" or intensity distributions. Usually an intensity refers to a time-integrated E^2 quantity, because the receivers are too slow to resolve the time period of light, which is one to two femtoseconds in the visible region. A femtosecond is a ten to the minus fifteenth part of a second. The shortest optical effects so far

produced are laser pulses with a duration of about ten to the minus thirteen seconds.

14.3 The wave equation

We start from Maxwell's equations (1867):

$$\begin{aligned} \mathrm{curl}\vec{H} &= \frac{\partial \vec{D}}{\partial t} + \vec{I} \qquad & \mathrm{curl}\vec{E} &= -\frac{\partial \vec{B}}{\partial t} \\ \mathrm{div}\vec{B} &= 0 & \mathrm{div}\vec{D} &= \varrho \\ \vec{I} &= \sigma\vec{E} \qquad \vec{D} = \epsilon\vec{E} \qquad \vec{B}\mu\vec{H} \end{aligned} \tag{14.1}$$

If the "material's constants" ϱ, σ, ϵ, μ do not depend on E and H (which is not always true; like at very high E- and H-fields, also in certain crystals which exhibit electro-optical and magneto-optical effects) then the Maxwell equations are linear. Hence, if $\vec{E}_1$, $\vec{H}_1$ is one solution, and $\vec{E}_2$, $\vec{H}_2$ another one, then also $a_1\vec{E}_1 + a_2\vec{E}_2$, $b_1\vec{H}_1 + b_2\vec{H}_2$ is a solution. This very fortunate property of electromagnetic waves is called "undisturbed linear superposition".

Now we specialize $\varrho = 0$ (no charges around); $\sigma = 0$ (no currents); $\epsilon = \mathrm{constant}$; $\mu = \mu_0$ (constant in x and t). Then we get

$$\begin{aligned} \mathrm{curl}\vec{H} &= \epsilon\frac{\partial \vec{E}}{\partial t} \qquad & \mathrm{curl}\vec{E} &= -\mu_0\frac{\partial \vec{H}}{\partial t} \\ \mathrm{div}\vec{H} &= 0 & \mathrm{div}\vec{E} &= \varrho \end{aligned} \tag{14.2}$$

We solve this system of differential equations by applying $\mu_0\frac{\partial}{\partial t}$ to the first equation and curl to the second.

$$\mu_0\mathrm{curl}\frac{\partial \vec{H}}{\partial t} = \epsilon\mu_0\frac{\partial^2\vec{E}}{\partial t^2}; \qquad \mathrm{curl}\ \mathrm{curl}\vec{E} = -\mu_0\mathrm{curl}\frac{\partial \vec{H}}{\partial t} \tag{14.3}$$

Together, $\mathrm{curlcurl}\vec{E} + \epsilon\mu_0 = 0$. Herein we use the identity $\mathrm{curlcurl}\vec{E} = \mathrm{grad}\overbrace{\mathrm{div}\vec{E}}^{=0} - \nabla\nabla\vec{E}$. Hence we get the time-dependent wave equation. It is the same also for $\vec{H}$.

$$\boxed{\nabla^2\vec{E} - \epsilon\mu_0\frac{\partial^2\vec{E}}{\partial t^2} = 0} \tag{14.4}$$

Next we decompose the field into time frequencies.

$$\vec{E} = \vec{E}(\vec{x}, t); \qquad \vec{E}(x,t) = \int \vec{U}(\vec{x}, \nu)e^{-2\pi i\nu t}\mathrm{d}\nu \tag{14.5}$$

We insert this into the time-dependent wave equation:

$$\int \left[\nabla^2\vec{U} + (2\pi\nu)^2\epsilon\mu_0\vec{U}\right] e^{-2\pi i\nu t}\mathrm{d}\nu = 0 \tag{14.6}$$

This is formally a Fourier integral. It is zero at all times. Hence the integrand itself must be zero $[\ldots] = 0$. With the abbreviation $(2\pi\nu)\epsilon\mu_0 = k^2$ this leads to the time-independent, or stationary wave equation, which is also called "Helmholtz-equation" or simple "wave equation".

$$\boxed{\nabla^2 U + k^2 U = 0} \qquad \text{for all three components } U_x, U_y, U_z \tag{14.7}$$

14.4 Complex representation of the wavefield

You are used to the replacement $a\cos(2\pi\nu t + \varphi) \to ae^{i(2\pi\nu t+\varphi)}$. This means a "convenient ballast" $ia\ \sin(2\pi\nu t + \varphi)$ has been added. Now we want to make sure that this procedure is legal and useful. In general we add $\vec{E} \to \vec{E} + i\vec{E}_H = \text{const.}\ \vec{V}$ ($i\vec{E}_H$ is "convenient ballast", $\vec{V}$ is the "analytic signal"). Both $\vec{E}$ and $\vec{E}_H$ are real functions. Suppose we add some ballast to the starting field $\vec{E}(\vec{x}_1, t_1) \to \vec{E}_1 + i\vec{E}_{H1} = \vec{V}_1 \cdot \text{const}$ at $(\vec{x}_1, t_1)$. The "starting field" is the cause. The "effect" is $\vec{V}_2$ at $(\vec{x}_2, t_2)$ which contains effects of the ballast: $\vec{V}_2 = \frac{1}{\text{const}}\left[\vec{E}_2 + i\vec{E}_{1H}\right]$. If $\vec{V}_2$ is the result of a calculation we can recognize the ballast and subtractit, since it is imaginary. This is possible because of the linear superposition which keeps the real part and the imaginary part of $\vec{V}$ apart at all times and places. Actually the ballast removal is even simpler. Remember we measure only $\int_t^{t+T} E^2(t')\mathrm{d}t'$; $T \gg \tau = \frac{2\pi}{\omega}$. We choose E_H and const such that:

$$\int_t^{t+T} E^2\mathrm{d}t' = \int_t^{t+T} |V|^2\mathrm{d}t' \tag{14.8}$$

Hence our theory consists of the following steps:

$$E_1 \to E_1 + iE_{1H} = \text{const.}\, V_1 \to V_2 \to |V_2| \to \frac{1}{T}\int_t^{t+T} |V_2(\vec{x}, t')|^2\mathrm{d}t' = I_2(\vec{x}, t) \tag{14.9}$$

But we have to be careful if Maxwell is nonlinear, for example due to a field-dependent $\epsilon = \epsilon(E) = \epsilon^{(0)} + \epsilon^{(1)}E + \epsilon^{(2)}E^2 + \ldots$.

Now we have to find a recipe for getting E_H from E. Remember $\vec{E}(\vec{x}, t) = \vec{E}^*(\vec{x}, t)$ because the field is a physical quantity and therefore real. Hence the time-Fourier-transform

satisifes $U(\vec{x},\nu) = U^*(\vec{x},-\nu)$. This implies redundancy in $\pm\nu$ (positive and negative frequencies).

$$U(\vec{x},\nu) = \int E(\vec{x},t)e^{2\pi i\nu t}\mathrm{d}t \tag{14.10}$$

We call $U(\vec{x},r) = A(\vec{x},\nu)e^{i\varphi(\vec{x},\nu)}$ where: $A(\vec{x},\nu) = +A(\vec{x},-\nu)$; $\varphi(\vec{x},+\nu) = -\varphi(\vec{x},-\nu)$.

Now we redundancy leads us to an integral with positive-only frequencies:

$$E(\vec{x},t) = \int_{-\infty}^{\infty} U(\vec{x},\nu)e^{-2\pi i\nu t}\mathrm{d}\nu = 2\int_{0}^{\infty} A(\vec{x},\nu)\cos[2\pi\nu t - \varphi(\vec{x},\nu)]\mathrm{d}\nu \tag{14.11}$$

Now it is obvious how we get E_H from E, simply by setting $\varphi \to \varphi + \frac{\pi}{2}$;
$E_H = 2\int_0^\infty A(\vec{x},\nu)\sin[2\pi\nu t - \varphi]\mathrm{d}\nu$

$$\boxed{\{E \longleftrightarrow E_H\} \Longleftrightarrow \left\{\varphi \longleftrightarrow \varphi + \frac{\pi}{2}\right\}} \tag{14.12}$$

This procedure is called “Hilbert-Transform”:

$$E_H = \mathcal{H}\{E\}; \qquad E = \mathcal{H}^{-1}\{E_H\} \tag{14.13}$$

The backwards transformation $\mathcal{H}^{-1}$ means $\varphi \longrightarrow \varphi - \frac{\pi}{2}$. Now we arrived at the recipe for getting the complex “analytical signal” from the real field. The constant factor will turn out to be $\sqrt{2}$.

$$\boxed{V = \frac{1}{\sqrt{2}}[E + iE_H] = \sqrt{2}\int_0^\infty A(\vec{x},\nu)e^{i[2\pi\nu t - \varphi(\vec{x},\nu)]}} \tag{14.14}$$

The analytical signal has been introduced in this form by Gabor in 1948.

Now we have to justify the factor $\sqrt{2}$, which was included to achieve:

$$\int |V|^2\mathrm{d}t = \int E^2\mathrm{d}t \tag{14.15}$$

Remember now $|\tilde{V}(\nu)| = \sqrt{2}A(\nu) = \begin{cases} +1 & \text{if } \nu \geq 0 \\ 0 & \text{if}; \nu < 0 \end{cases}$

$$|\tilde{E}(\nu)| = |\tilde{E}_H(\nu)| = A(\nu) \quad \text{in} \quad \infty < \nu < \infty; \quad A(\nu) = A(-\nu) \tag{14.16}$$

We use the Plancherel theorem:

$$\begin{aligned} \int_{-\infty}^{\infty} E^2(t)\mathrm{d}t &= \int_{-\infty}^{\infty} |\tilde{E}(\nu)|^2\mathrm{d}\nu = \int_{-\infty}^{\infty} A^2(\nu)\mathrm{d}\nu = 2\int_{0}^{\infty} A^2(\nu)\mathrm{d}\nu \\ \int_{-\infty}^{\infty} |V(t)|^2\mathrm{d}t &= \int_{-\infty}^{\infty} |\tilde{V}(\nu)|\mathrm{d}\nu = 2\int_{0}^{\infty} A^2(\nu)\mathrm{d}\nu \end{aligned} \tag{14.17}$$

The infinite limits on the time-integrals are valid if we set $E(t) \longrightarrow E(t)\mathrm{rect}(\frac{t}{T})$ and do the same for $V(t)$.

Another but equivalent way of describing the Hilbert transform is as the follow:

$$\begin{aligned} E(t) &= \int_{-\infty}^{\infty} \tilde{E}(\nu)e^{-2\pi i\nu t}\mathrm{d}\nu = \int_{-\infty}^{\infty} A(\nu)e^{i[-2\pi i\nu t+\varphi(\nu)]}\mathrm{d}\nu \\ V(t) &= \sqrt{2}\int_{0}^{\infty} A(\nu)e^{-2\pi i\nu t+\varphi(\nu)}\mathrm{d}\nu \end{aligned} \tag{14.18}$$

Hence:

$$\tilde{V}(\nu) = \sqrt{2}\tilde{E}(\nu) = \begin{cases} +1 & \text{if} \quad \nu \geq 0 \\ 0 & \text{if} \quad \nu < 0 \end{cases} \tag{14.19}$$

From $V = \frac{1}{\sqrt{2}}[E + iE_H]$ follows:

$$\begin{aligned} \tilde{V} &= \frac{1}{\sqrt{2}}[\tilde{E} + i\tilde{E}_H]; \quad i\tilde{E}_H = \sqrt{2}\tilde{V} - \tilde{E} = \tilde{E} = \begin{cases} 2-1 & \text{if} \quad \nu \geq 0 \\ 0 & \text{if} \quad \nu < 0 \end{cases} \\ & \boxed{i\tilde{E}_H(\nu) = \tilde{E}(\nu) \begin{cases} +1 & \text{if} \quad \nu \geq 0 \\ 0 & \text{if} \quad \nu < 0 \end{cases}} \end{aligned} \tag{14.20}$$

Yet another representation of the Hilbert transform is obtained when this one is Fourier transformed whereby the convolution theorem is utilized:

$$iE_H(t) = \int E(t')\tilde{S}_g(t-t')\mathrm{d}t' = \frac{E(t')\mathrm{d}t'}{\pi i(t-t')} \tag{14.21}$$

14.5 Frequency averages

The analytic signal has some more advantages, for example for computing frequency averages. Assume a field at point $\vec{x}$ with a temporal power spectrum $|\tilde{E}\nu|^2 = |\tilde{E}(-\nu)|^2$. One would be inclined to talk about an average-frequency or carrier-frequency ν_c, and about a bandwidth $\delta\nu_c$. How would by compute this?

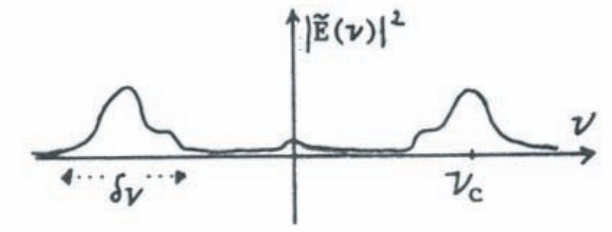

Figure 14.2: Example of the power spectrum of a typical analytic signal.

$$\int_{-\infty}^{\infty} \nu|\tilde{E}(\nu)|^2 \mathrm{d}\nu \longrightarrow \overline{\nu} = 0? \tag{14.22}$$

$$\overline{(\nu-\overline{\nu})^2} = \frac{\int(\nu-\overline{\nu})^2|\tilde{E}(\nu)|^2\mathrm{d}\nu}{\int|\tilde{E}(\nu)|^2\mathrm{d}\nu} = \frac{\int\nu^2|\tilde{E}(\nu)|^2\mathrm{d}\nu}{\int|\tilde{E}(\nu)|^2\mathrm{d}\nu} \tag{14.23}$$
$$\approx \frac{\int\nu^2\left[\delta(\nu-\nu_c)+\delta(\nu+\nu_c)\right]\mathrm{d}\nu}{\int\left[\delta(\nu-\nu_c)+m\delta(\nu+\nu_c)\right]\mathrm{d}\nu} = \nu_c^2 \longrightarrow \Delta\nu = \nu_c$$

Obviously the ordinary procedures for computing a mean value and a mean-square value don't make much sense. It rather should be $\overline{\nu} = \nu_c$, not $\overline{\nu} = 0$; and $\Delta\nu = \delta\nu$; not $\Delta\nu = \nu_c$. This trouble is avoided when computing $\overline{\nu}$ and $\Delta\nu$ with $|\overline{\nu}|^2$ as weighting function instead of $|\tilde{E}|^2$. Remember that $|\tilde{V}(\nu)|^2$ was zero for $\nu < 0$. Hence:

$$\frac{\int_{-\infty}^{\infty}\nu|\tilde{V}(\nu)|^2\mathrm{d}\nu}{\int_{-\infty}^{\infty}|\tilde{V}|^2\mathrm{d}\nu} = \frac{\int_{0}^{\infty}\nu|\tilde{V}(\nu)|^2\mathrm{d}\nu}{\int|\tilde{V}(\nu)|^2\mathrm{d}\nu} = \overline{\nu} \approx \nu_c \tag{14.24}$$

and

$$\frac{\int_{-\infty}^{\infty}(\nu-\overline{\nu})^2|\tilde{V}(\nu)|^2\mathrm{d}\nu}{\int|\tilde{V}(\nu)|^2\mathrm{d}\nu} = \frac{\int_{0}^{\infty}(\nu-\overline{\nu})^2|\tilde{V}(\nu)|^2\mathrm{d}\nu}{\int|\tilde{V}(\nu)|^2\mathrm{d}\nu} = \Delta\nu^2 \approx (\delta\nu)^2 \tag{14.25}$$

Let us consider a simple example:

Performing the above computations yields $\overline{\nu} = \nu_c;\ (\Delta\nu)^2 = \frac{(\delta\nu)^2}{12}$.

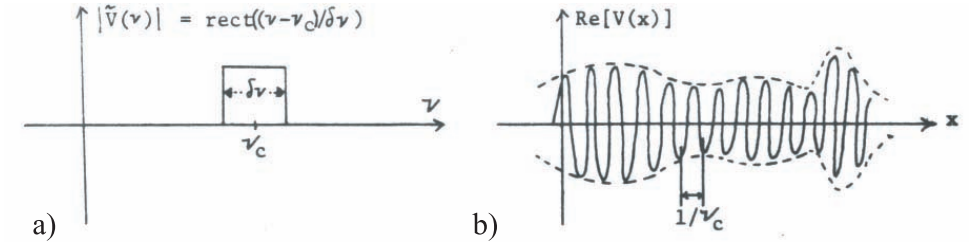

Figure 14.3: Power spectrum (a) and spatial distribution (b) of an example function.

14.6 The envelope representation of complex signals

As we have just seen, the complex notation gives us a satisfactory way to define the mean frequency $\overline{\nu}$. Using the mean frequency we can introduce the intuitively appealing "Envelope-Representation":

$$V(t) = U(t)e^{2\pi i\nu_1 t} = |U(t)|e^{i(2\pi\nu_1+\Phi(t))} \tag{14.26}$$

The choice of the "carrier frequency" ν_1 is in a sense arbitrary. With another ν_2, it would have been $V(t) = U_2(t)e^{2\pi i\nu_2 t}$ instead of $V(t) = U_1(t)e^{2\pi i\nu_1 t}$.

What is the "best carrier frequency" ν_1? Writing down the Fourier transform of $V(t) = U_1(t)e^{2\pi i\nu_1 t}$ gives us a hint. According to the shift-theorem it is: $\tilde{V}(\nu) = \tilde{U}(\nu - \nu_1)$; or just a well: $\tilde{V}(\nu + \nu_1) = \tilde{U}(\nu)$. Obviously the choice of a carrier frequency is something like the choice of a new center of a shifted coordinate system. One might suspect that $\nu_1 = \overline{\nu}$ is the "best choice" where it was:

$$\overline{\nu} = \frac{\int \nu|\tilde{V}(\nu)|^2 \mathrm{d}\nu}{\int |\tilde{V}(\nu)|^2 \mathrm{d}\nu} \tag{14.27}$$

An envelope is something which encloses something else as smoothly as possible. So we want $U(t, \nu_1)$ to be a *slowly* varying function of t. Hence we request $\int_{-\infty}^{\infty} \left|\frac{\mathrm{d}U(t,\nu_1)}{\mathrm{d}t}\right|^2 \mathrm{d}t \longrightarrow$ minimum with respect to ν_1.

$$\begin{aligned} U(t) &= V(t)e^{-2\pi i\nu_1 t} = \int \tilde{V}(\nu)e^{2\pi i(\nu-\nu_1)t}\mathrm{d}\nu \qquad (14.28)\\ \frac{dU}{dt} &= 2\pi i \int (\nu - \nu_1)\tilde{V}(\nu)e^{2\pi i(\nu-\nu_1)t}\mathrm{d}\nu \\ \int \left|\frac{dU}{dt}\right|^2 \mathrm{d}t &= \iint (2\pi i)^2(\nu-\nu_1)(\mu-\nu_1)\tilde{V}(\nu)\tilde{V}^*(\mu)e^{2\pi it[(\nu-\nu_1)-(\mu-\nu_1)]}\mathrm{d}(\nu\mu t) \end{aligned}$$

We recognize the hidden delta function: $\int e^{2\pi i t(\nu-\mu)}\mathrm{d}t = \delta(\nu-\mu);\ \int \ldots \mathrm{d}\mu \sim \mu \to \nu$.

$$\begin{aligned}\int \left|\frac{\mathrm{d}U}{\mathrm{d}t}\right|^2 \mathrm{d}t &= (2\pi i)^2 \int (\nu-\nu_1)^2 |\tilde{V}(\nu)|^2 \mathrm{d}\nu = \qquad (14.29)\\ &= \left\{(2\pi i)^2 \int |\tilde{V}(\nu)|^2 \mathrm{d}\nu\right\} \frac{\int [\nu^2 - 2\nu\nu_1 + \nu_1^2]|\tilde{V}(\nu)|^2 \mathrm{d}\nu}{\int |\tilde{V}(\nu)|^2 \mathrm{d}\nu}\\ &= C[\overline{\nu^2} - 2\nu_1\overline{\nu} + \nu_1^2]; \qquad \frac{\mathrm{d}[\ldots]}{\mathrm{d}\nu_1} = -2\overline{\nu} + 2\nu_1 = 0 \to \nu_1 = \overline{\nu}\end{aligned}$$

Now we search the *best* carrier frequency which yields the smoothest envelope. As one might have guessed the mean frequency is the best carrier frequency $\nu_1 = \overline{\nu}$. Hence the smoothest envelope representation is:

$$\begin{aligned}V(t) &= U(t)e^{2\pi i\overline{\nu}t} = |U(t)|e^{i\{2\pi\overline{\nu}t+\Phi(t)\}} \qquad (14.30)\\ &= e^{2\pi i\overline{\nu}t}\int \tilde{U}(\nu)e^{2\pi i\nu t}\mathrm{d}\nu = \int \tilde{U}(\nu)e^{2\pi i(\nu+\overline{\nu})t}\mathrm{d}t\\ &= \int \tilde{U}(\nu-\overline{\nu})e^{2\pi i\nu t}\mathrm{d}\nu = \int \tilde{V}(\nu)e^{2\pi i\nu t}\mathrm{d}\nu =\\ &= \sqrt{2}\int_0^\infty A(\nu)e^{i[2\pi\nu t+\varphi(\nu)]}\mathrm{d}\nu\end{aligned}$$

15 The Uncertainty Principle

15.1 The usual derivation

In the photon theory of light the field has a probabilistic meaning. The probability for a photon to land in the little square $(x, x + \mathrm{d}x)$, $(y, y + \mathrm{d}x)$ is proportional to the modulus square of the complex field:

$$P(x,y)\mathrm{d}x\mathrm{d}y = \frac{|V(x,y)|^2\mathrm{d}x\mathrm{d}y}{\iint |V(x,y)|^2\mathrm{d}x\mathrm{d}y} \tag{15.1}$$

The normalization $\iint P(x,y)\mathrm{d}x\mathrm{d}y = 1$ is assured by the demoninator. Physically the normalization means that we don't know at which of the many little square this photon will land, but it has to land somewhere.

The most likely place is $\overline{x}$: (now in one dimension)

$$\overline{x} = \int xP(x)\mathrm{d}x = \frac{|V(x)|^2 x\mathrm{d}x}{\int |V(x)|^2\mathrm{d}x} \tag{15.2}$$

The spread around this most likely landing place is given by Δx:

$$\begin{aligned}(\Delta x)^2 &= \int (x-\overline{x})^2 P(x)\mathrm{d}x = \int x^2 P(x)\mathrm{d}x - 2\overline{x}\int xP(x)\mathrm{d}x + \overline{x}^2\int P(x)\mathrm{d}x \\ &= \overline{x^2} - 2\overline{x}\cdot\overline{x} + \overline{x}^2 = \overline{x^2} - \overline{x}^2 \end{aligned} \tag{15.3}$$

The field $V(x)$ at the receiver plane can be decomposed into spatial frequency components:

$$V(x) = \int \tilde{V}(\nu)e^{2\pi i\nu x}\mathrm{d}\nu. \tag{15.4}$$

Instead of receiving the field itself we will use apparatus which performs a Fourier transform of the field:

$$\int V(x)e^{-2\pi i\nu x}\mathrm{d}x = \tilde{V}(\nu) \tag{15.5}$$

Actually such an "apparatus" is very simple; it consists of nothing but a lens of proper dimensions as we will learn soon. After having performed the Fourier transform, or in other words, after having produced a secondary field $V_1(x) = \tilde{V}(ax)$, we will call the spatial coordinate in this secondary plane now ν (although originally ν was a frequency), the probability for a photon to touch down between ν and $\nu + \mathrm{d}\nu$ is:

$$Q(\nu)d\nu = \frac{|\tilde{V}(\nu)|^2 \mathrm{d}\nu}{\int |\tilde{V}(\nu')|^2 \mathrm{d}\nu'} \tag{15.6}$$

The most likely spot for the photon to reach the secondary ν-plane is $\overline{\nu}$:

$$\overline{\nu} = \int \nu Q(\nu) \mathrm{d}\nu; \tag{15.7}$$

and the spread arround $\overline{\nu}$ is $\Delta\nu = \sqrt{\int (\nu - \overline{\nu})^2 Q(\nu) \mathrm{d}\nu}$.

The uncertainty principle states the Δx and $\Delta\nu$, both belonging to the same $V(x)$, are coupled, such that if Δx is small, $\Delta\nu$ cannot be small also, and vice versa. We intend to show that there is a lower limit for the product $\Delta x \Delta\nu$. In order to shorten the proof somewhat, we don't consider $V(x)$ itself, but $V(x + \overline{x})e^{-2\pi i \overline{\nu} x} = V_0(x)$. This is justified since $V_S(x) = V(x + \overline{x})$ has the same Δx as $V(x)$, and it has also the same $\overline{\nu}$ and $\Delta\nu$ as $V(x)$ since $|\tilde{V}_S(\nu)| = |\tilde{V}(\nu)|$. The next step of this justification is based on the fact that $V_S(x)$ and $V_S(x)e^{-2\pi i \overline{\nu} x} = V_0(x)$ have the same Δx, a different $\overline{\nu}$, but the same $\Delta\nu$. The field $V_0(x)$ has the convenient feature that its linear moments $\overline{x}$ and $\overline{\nu}$ are zero.

$$\int x|V(x+\overline{x})|^2 e^{-2\pi i \overline{\nu} x} \mathrm{d}x = \int_{-\infty}^{\infty} x|V(x+\overline{x})|^2 \mathrm{d}x = \tag{15.8}$$

$$= \int (x' - \overline{x})^2 |V(x')|^2 \mathrm{d}x' = \underbrace{\int x'|V(x')|^2 \mathrm{d}x'}_{\overline{x}\int |V|^2 \mathrm{d}x'} - \overline{x} \int |V(x')|^2 \mathrm{d}x' = 0$$

For computing $\overline{\nu}$, we need to know first $\tilde{V}_0(\nu)$:

$$\begin{aligned} \int V_0(x) &= e^{-2\pi i \nu x} \mathrm{d}x = \tilde{V}_0(\nu) = \int V(x+\overline{x}) e^{-2\pi i(\nu+\overline{\nu})x} \mathrm{d}x \\ &= \iint \tilde{V}(\mu) e^{2\pi i[\mu(x+x') - x(\nu-\overline{\nu})]} \mathrm{d}x \mathrm{d}\mu \end{aligned} \tag{15.9}$$

mit:

$$\int \ldots \mathrm{d}x = \delta(\mu - \nu - \overline{\nu}); \qquad \int \ldots \mathrm{d}\mu \sim \mu \to \nu + \overline{\nu}; \tag{15.10}$$

$$= \tilde{V}(\nu+\overline{\nu})e^{2\pi i\overline{x}(\nu+\overline{\nu})} = \tilde{V}_0(\nu); \qquad |\tilde{V}_0(\nu)|^2 = |\tilde{V}(\nu-\overline{\nu})|^2 \tag{15.11}$$
$$\int \nu|\tilde{V}_0(\nu)|^2\mathrm{d}\nu = \int \nu|\tilde{V}(\nu+\overline{\nu})|^2\mathrm{d}\nu = \int(\nu'-\nu)|\tilde{V}(\nu')|^2\mathrm{d}\nu' = 0$$

In other words, by shifting the origins of the x-scale and the ν-scale properly the computation of the spread reduces to the simple formulas:

$$(\Delta x)^2 = \int x^2 P(x)\mathrm{d}x; \qquad (\Delta\nu) = \int \nu^2 Q(\nu)\mathrm{d}\nu \tag{15.12}$$

What now comes is a bit of arithmetic gymnastics involving Fourier-transforms, partial integrations and the Schwarz inequality. We will use $V_0(x)$ but drop the index zero. We want to compute $\int x^2|V(x)|^2\mathrm{d}x$, multiplied by $\int \nu|\tilde{V}(\nu)|^2\mathrm{d}\nu$. The second expression can be suitably modified in the following manner.

$$\frac{\mathrm{d}V(x)}{\mathrm{d}x} = 2\pi i\int \nu\tilde{V}(\nu)e^{2\pi i\nu x}\mathrm{d}\nu \tag{15.13}$$
$$\frac{\mathrm{d}V^*(x)}{\mathrm{d}x} = -2\pi i\int \mu\tilde{V}^*(\mu)e^{-2\pi i\mu x}\mathrm{d}\mu$$

Multiplication and integration of these two terms yields:

$$\int\left|\frac{\mathrm{d}V(x)}{\mathrm{d}x}\right|^2\mathrm{d}x = \iint\!\!\!\int (2\pi)^2\nu\mu\tilde{V}(\nu)\tilde{V}^*(\mu)e^{2\pi ix(\nu-\mu)}\mathrm{d}x\mathrm{d}\nu\mathrm{d}\mu \tag{15.14}$$
$$\int\ldots\mathrm{d}x = \delta(\nu-\mu); \qquad \text{next}\int\ldots\mathrm{d}\mu \sim \mu\to\nu$$
$$= (2\pi)^2\int|\tilde{V}(\nu)|^2\nu^2\mathrm{d}\nu.$$

Now we use this in:

$$\left(\int x^2|V(x)|^2\mathrm{d}x\right)\left(\int|\tilde{V}(\nu)|^2\nu^2\mathrm{d}\nu\right) = \left(\int|xV(x)|^2\mathrm{d}x\right)\left(\int\left|\frac{\mathrm{d}V(x)}{2\pi\mathrm{d}x}\right|^2\mathrm{d}x\right) \tag{15.15}$$

call $xV(x) = F(x)$ and $\frac{\mathrm{d}V(x)}{2\pi\mathrm{d}x} = G(x)$, then the right-hand-side is $(F\cdot F^*)(G\cdot G^*)$. According to Schwarz (Chap. 10) this is $\geq \left[\frac{(F\cdot G^*)(F^*\cdot G)}{2}\right]^2$. This new expression can be evaluated further:

$$F\cdot G^* + F^*\cdot G = \int x\left\{V(x)\frac{\mathrm{d}V^*(x)}{2\pi\mathrm{d}x} + V^*(x)\frac{\mathrm{d}V(x)}{2\pi\mathrm{d}x}\right\}\mathrm{d}x = \tag{15.16}$$
$$= \frac{1}{2\pi}\int x\frac{\mathrm{d}|V(x)|^2}{\mathrm{d}x}\mathrm{d}x = \frac{1}{2\pi}\left[x|V(x)|^2\right]_{x=-\infty}^{x=\infty} - \frac{1}{2\pi}\int|V(x)|^2\mathrm{d}x$$

A physicist's field is always zero at infinity. Hence the first term vanishes. The second term is just what we need as the denominator for normalization of Δx and $\Delta\nu$:

$$F\cdot G^*+F^*\cdot G = \frac{1}{2\pi}\int |V(x)|^2\mathrm{d}x;\ \left[\frac{(F\cdot G^*+F^*\cdot G)}{2}\right]^2 = \left(\frac{1}{4\pi}\right)^2\left(\int |V(x)|^2\mathrm{d}x\right)^2 \tag{15.17}$$

Now we have:

$$\int x^2|V(x)|^2\mathrm{d}x\int \nu^2|\tilde{V}(\nu)|^2\mathrm{d}\nu \geq \left(\int |V(x)|^2\frac{\mathrm{d}x}{4\pi}\right)^2 \tag{15.18}$$

Remember now the Plancherel theorem and the probability definitions:

$$\begin{aligned} \int |V(\nu)|^2\mathrm{d}\nu &= \int |V(x)|^2\mathrm{d}x; \qquad (15.19)\\ P(x) = \frac{|V(x)|^2}{\int |V(x)|^2\mathrm{d}x}; &\qquad Q(\nu) = \frac{|\tilde{V}(\nu)|^2}{\int |\tilde{V}(\nu)|^2\mathrm{d}\nu}\\ (\Delta x)^2 = \int x^2P(x)\mathrm{d}x; &\qquad (\Delta\nu)^2 = \int \nu^2Q(\nu)\mathrm{d}\nu. \end{aligned}$$

We introduce these bother definition into the inequality, then pull the roots, and get

$$\boxed{\Delta x\Delta\nu \geq \frac{1}{4\pi}} \tag{15.20}$$

It should not bother you to find here $\frac{1}{4\pi}$, whereas sometimes you might have seen $\frac{1}{2\pi}$, $\frac{1}{2}$, 1, π and so on. The difference lies in the definition of the spread, which could have been defined instead by:

$$\Delta x_1 = \sqrt{x\overline{x^2}};\quad \Delta\nu_1 = \sqrt{a\overline{\nu^2}};\quad \Delta x_1\Delta\nu_1 = \sqrt{\overline{x^2}\cdot\overline{\nu^2}} \tag{15.21}$$

Calling the constant for example $a = 4\pi$ one gets the more pleasant form $\Delta x_1\Delta\nu_1 \geq 1$.

15.2 The uncertainty of some specific fields

Some examples may demonstrate that the lower boundary $\frac{1}{4\pi}$ is usually quite below what one can achieve:

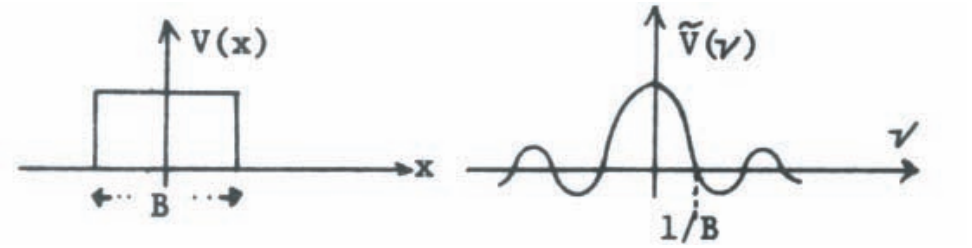

Figure 15.1: The rect-function and its Fourier transform.

- SQUARE-BOX:

$$\sqrt{\overline{x^2}} = \frac{B}{\sqrt{12}}; \qquad \sqrt{\overline{\nu^2}} = \infty; \qquad \Delta x \Delta\nu = \infty \tag{15.22}$$
$$\Delta x_Q = B \qquad \Delta\nu_Q = \frac{2}{B} \qquad \Delta x_Q \Delta\nu_Q = 2$$

The index Q refers to "qualitative". These are the spreads one would have defined intuitively by looking at the figures. This is somewhat arbitrary, but the frequency spread is now $\Delta\nu_Q \neq \infty$.

- TRIANGLE:

Figure 15.2: The trian-function and its Fourier transform.

$$V(x) = \begin{cases} +1 - \frac{|x|}{B}; & \text{if} |x| \leq B \\ 0; & \text{otherwise} \end{cases} \quad ; \quad \tilde{V}(\nu) = B\,\mathrm{sinc}^2(B\nu) \tag{15.23}$$

$$\sqrt{\overline{x^2}} = \frac{B}{\sqrt{10}}; \qquad \sqrt{\overline{\nu^2}} = \frac{\sqrt{3}}{2\pi B}; \quad \sqrt{\overline{x^2}\cdot\overline{\nu^2}} = \frac{\sqrt{3}}{2\pi\sqrt{10}} = \frac{\sqrt{\frac{6}{5}}}{4\pi}$$
$$\Delta x_Q = B; \quad \Delta\nu_Q = \frac{1}{B}; \quad \Delta x_Q \Delta\nu_Q = 1.$$

- GAUSSIAN:

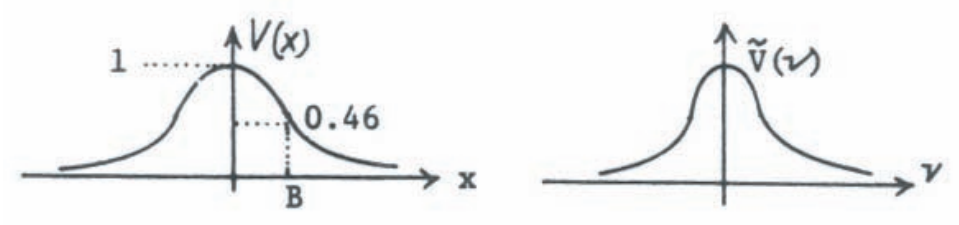

Figure 15.3: The Gaussian function and its Fouriert transform.

$$
\begin{aligned}
V(x) = e^{-\pi\left(\frac{x}{B}\right)^2}; \qquad & \qquad \tilde{V}(\nu) = Be^{-\pi(\nu B)^2}; \\
\sqrt{\overline{x^2}} = \frac{B}{\sqrt{2\pi}}; \qquad \sqrt{\overline{\nu^2}} &= \frac{1}{B\sqrt{2\pi}}; \qquad \sqrt{\overline{x^2}\cdot\overline{\nu^2}} = \frac{1}{2\pi}; \\
\Delta x_Q = 2B; \qquad \Delta\nu_Q &= \frac{2}{B}; \qquad \Delta x_Q \Delta\nu_Q = 4;
\end{aligned}
\tag{15.24}
$$

- LORENTZIAN

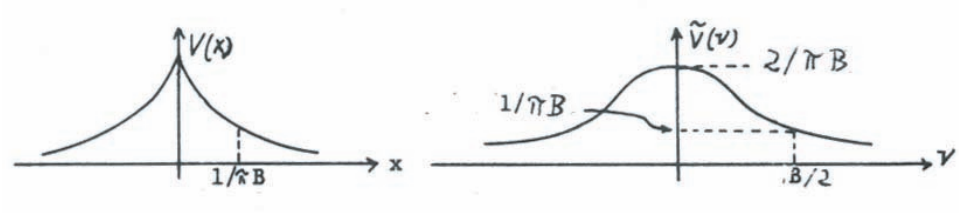

Figure 15.4: The Lorentzian profile and its Fourier transform.

$$
\begin{aligned}
V(x) = e^{-\pi B|x|}; \qquad & \qquad \tilde{V}(\nu) = \frac{\frac{2}{\pi B}}{\left[1+\left(\frac{2\nu}{B}\right)^2\right]} \\
\sqrt{\overline{x^2}} = \frac{1}{\pi B\sqrt{2}}; \qquad \sqrt{\overline{\nu^2}} &= \frac{B}{\sqrt{2\pi}}; \qquad \sqrt{\overline{x^2}\cdot\overline{\nu^2}} = \frac{1}{2\pi\sqrt{\pi}} \\
\Delta x_Q = \frac{2}{\pi B}; \qquad \Delta\nu_Q &= B; \qquad \Delta x_Q \cdot \nu_Q = \frac{2}{\pi}
\end{aligned}
\tag{15.25}
$$

These examples indicate how careful one ought to be when drawing conclusions from the uncertainty principle. It is true that for any reasonably well-behaving function it is $\sqrt{\overline{x^2}\cdot\overline{\nu^2}} \geq \frac{1}{4\pi}$. But none of our examples reaches the general lower bound $\frac{1}{4\pi}$. In the first case the root product of second moments even becomes infinite. Yet, intuitively, one would have defined the spreads so that $\Delta x_Q \Delta\nu_Q$ is only about 2. So sometimes the qualitative $\Delta x_Q \Delta\nu_Q$ is smaller than the root-product $\sqrt{\overline{x^2}\cdot\overline{\nu^2}}$, but most of the time it is considerably larger, as in the last three examples.

15.3 Other definitions of x- and $\nu-$ spreads

Matters become even more complicated when looking into the literature where the Δx and $\Delta\nu$ are defined sometimes quite differently. For example in coherence theory it makes sense to form moments with the *fourth* power of $|V|$ and $|\tilde{V}|$ employed as weighting functions, instead of the second power. One starts by defining the normalized autocorrelation function $\gamma(x)$ as:

$$\gamma(x) = \frac{\int V(x')V^*(x'-x)\mathrm{d}x'}{\int |V(x')|^2\mathrm{d}x'} \tag{15.26}$$

Its Fourier transform, which is called $\Phi(\nu)$, is:

$$\begin{aligned}\Phi(\nu) &= \int \gamma(x)e^{-2\pi i\nu x}\mathrm{d}x = \frac{\iint V(x')V^*(x'-x)\mathrm{d}x'e^{-2\pi i\nu x}\mathrm{d}x}{\int |V(x')|^2\mathrm{d}x'} \\ &= \frac{\iiiint \tilde{V}(\mu)\tilde{V}(\mu')e^{2\pi i[\mu x'-\mu'(x'-x)-\nu x]}\mathrm{d}(xx'\mu\mu')}{\int |\tilde{V}(\nu')|^2\mathrm{d}\nu'}\end{aligned} \tag{15.27}$$

with:

$$\begin{aligned}\int \ldots \mathrm{d}x' &= \delta(\mu-\mu'); \qquad \int \ldots \mathrm{d}\mu' \sim \mu' \longrightarrow \mu \\ \int \ldots \mathrm{d}x &= \delta(\mu-\nu); \qquad \int \ldots \mathrm{d}\mu \sim \mu \longrightarrow \nu\end{aligned} \tag{15.28}$$

$$\Phi(\nu) = \frac{|\tilde{V}(\nu)|^2}{\int |\tilde{V}(\nu')|^2\mathrm{d}\nu'} \tag{15.29}$$

The definitions of Δx_C and $\Delta\nu_C$ are:

$$(\Delta x_C)^2 = \frac{\int x^2|\gamma(x)|^2\mathrm{d}x}{\int |\gamma(x)|^2\mathrm{d}x}; \qquad (\Delta\nu)^2 = \frac{\int \nu^2\Phi^2(\nu)\mathrm{d}\nu}{\int \Phi^2(\nu)\mathrm{d}\nu} \tag{15.30}$$

Since $\gamma(x)$ and $\Phi(\nu)$ are a pair of Fourier transforms, we can use exactly the same mathematical treatment in showing the uncertainty relationship for this pair of spreads:

$$\Delta x_C \Delta \nu_C \geq \frac{1}{4\pi} \tag{15.31}$$

Although this law looks exactly like the first uncertainty law as derived earlier with $|V|^2$ and $|\tilde{V}|^2$ as weighting functions, it should be remembered that Δx_C means something quite different from Δx, and correspondingly $\Delta\nu$ and $\Delta\nu_C$ are to be kept apart.

Yet another definition was found to be meaningful in Quantum Electrodynamics and in Radar Theory:

$$\Delta x_R = \int |\gamma(x)|^2 \mathrm{d}x; \qquad \Delta\nu_R = \frac{1}{\int \Phi^2(\nu)\mathrm{d}\nu} \tag{15.32}$$

Since $\gamma(x)$ and $\Phi(\nu)$ are a pair of Fourier transforms, the Plancherel theorem says:

$$\int |\gamma(x)|^2 \mathrm{d}x = \int |\Phi^2(\nu)|^2 \mathrm{d}\nu \qquad (\Phi(\nu)\text{is real}) \tag{15.33}$$

Hence this version of the uncertainty relationship becomes an exact equality due to the definition of Δx_R and $\Delta\nu_R$.

$$\Delta x_R \Delta \nu_R = 1 \tag{15.34}$$

So far we have considered only one-dimensional functions. In the two-dimensional case the obvious definitions are:

$$\begin{aligned} \overline{x^2+y^2} &= \Delta^2(x,y) = \frac{\iint (x^2+y^2)|V(x,y)|^2 \mathrm{d}x\mathrm{d}y}{\iint |V(x,y)|^2 \mathrm{d}x\mathrm{d}y} \\ \overline{\nu_x^2+\nu_y^2} &= \Delta^2(\nu_x,\nu_y) = \frac{\iint (\nu_x^2+\nu_y^2)|\tilde{V}(\nu_x,\nu_y)|^2 \mathrm{d}\nu_x\mathrm{d}\nu_y}{\iint |\tilde{V}(\nu_x,\nu_y)|^2 \mathrm{d}\nu_x\mathrm{d}\nu_y} \end{aligned} \tag{15.35}$$

Here we assumed $\overline{x}$, $\overline{y}$, $\overline{\nu_x}$, $\overline{\nu_y}$ already to be zero, using the function $V_0(x,y)$ instead of $V(x,y)$ as outlined at the beginning of Chap. 15.

$$V(x+\overline{x}, y+\overline{y}) e^{-2\pi i(x\overline{\nu_x}+y\overline{\nu_y})} = V_0(x,y) \tag{15.36}$$

When computing $\Delta(x,y)\Delta(\nu_x,\nu_y)$ we use again partial integration, and we assume $|V|$ and its derivatives to go to zero sufficiently rapidly when $(x,y) \longrightarrow \infty$. The result is: $\Delta(x,y)\Delta(\nu_x,\nu_y) \geq \frac{1}{2\pi}$. Or for n-dimensional fields:

$$\Delta(x_1,x_2,\ldots,x_n)\Delta(\nu_1,\nu_2,\ldots,\nu_n) \geq \frac{n}{4\pi} \tag{15.37}$$

So far we have considered only the *spatial* dependence of $|V(x,y)|^2$, meaning that this quantity represents the probability of a photon to be absorbed in the little square $(x, x+\mathrm{d}x), (y, y+\mathrm{d}y)$. The time during which we wait for photons to arrive was infinite, or at least very large compared to the temporal period of the light wave. Now let us consider a photocathode of finite size, and ask for the probability of a photon to arrive between t and $t+\mathrm{d}t$.

$$P(t) \propto \iint |V(x,y,t)|^2 \mathrm{d}x\mathrm{d}y = |V(t)|^2 \tag{15.38}$$

Now we can go through the same uncertainty exercise with $V(t)$. We start by representing $V(t)$ as a temporal Fourier integral: $V(t) = \int \tilde{V}(\nu) e^{2\pi i \nu_t t} \mathrm{d}\nu_t$.

The final result, based on the same mathematical manipulation as before, is of course $\Delta t \Delta\nu_t \geq \frac{1}{4\pi}$, where $\Delta t = \sqrt{\overline{t^2}}$; $\Delta\nu_t = \sqrt{\overline{\nu_t^2}}$. Connecting this result with Einstein's photon formula $E = h\nu_t$, one gets with $\Delta E = h\Delta\nu$: $\Delta E \cdot \Delta T \geq \frac{h}{4\pi} = \frac{\hbar}{2}$. h is called Planck's constant, $h = 6.62 \cdot e^{-34}$ watt-sec. H-bar, $\hbar = \frac{h}{2\pi}$ is sometimes also named after Planck, but sometimes it is referred to as Dirac's constant.

Similarly, when combining de Broglie's law, which connects momentum and wavelength $|\vec{p}| = \frac{h}{\lambda}$ (or only one component of it: $p_x = h\nu_x$) with the spatial uncertainty relationship, derived earlier, one gets with $\Delta p_x = h\Delta\nu_x$:

$$\Delta p_x \Delta x \geq \frac{h}{4\pi} = \frac{\hbar}{2} \tag{15.39}$$

These two uncertainty relationships are connected with the name Heisenberg, who derived them in connection with the wave mechanics wherein $\Psi(x)$ is the wave function of an electron, with the understanding that (according to Born) the probability for the electron to be at $(x, x+\mathrm{d}x)$ is proportional to $|\Psi(x)|^2$. $\overline{x} = \int x|\Psi(x)|^2 \mathrm{d}x$ is the most likely place, and $\sqrt{\overline{(x-\overline{x})^2}}$ is the spread. Developing $\Psi(x)$ into a Fourier integral $\Psi(x) = \int \varphi(\nu) e^{2\pi i \nu x} \mathrm{d}\nu$ and realizing the connection between ν and the momentum $p_x = h\nu$, gives $\Delta x \Delta p_x \geq \frac{h}{4\pi}$, based on the same mathematics. But the physics in his case is the wave equation for electronics, in our case the Maxwell equation. The mathematics is the same. Similar uncertainty relationships for electronic signals have been derived by Nyquist and Küpfmüller shortly before the advent of quantum mechanics. The corresponding uncertainty relationship for optical images were known to Abbe and Lord Rayleigh almost one hundred years ago.

15.4 Gabor's information cells

Gabor (1946) presents a nice way for *visualizing* the contents of the uncertainty principle and of the sampling theorem. He does it in a pseudo-space, also called a "phase-domain",

which has an x-coordinate (length) and a spatial frequency coordinate ν (Actually for two-dimensional functions the phase-domain would be four-dimensional). The ν- and the x-coverage of a signal $V(x)$ are of course connected by a Fourier transform:

$$\tilde{V}(\nu) = \int V(x) e^{-2\pi i \nu x} \mathrm{d}x \tag{15.40}$$

For example rect$(\frac{x}{P})$ convers $\frac{-P}{2} \leq x \leq \frac{P}{2}$ in the x-domain; and its Fourier transform $P\mathrm{sinc}(\nu P)$ convers essentially the ν-range: $\frac{-P}{2} < \nu < \frac{P}{2}$. Hence the area covered in the (x, ν) domain $P \cdot \frac{1}{P} = 1$, of course only in approximation, since the sinc$(P\nu)$ does not have a sharp end (Fig. 15.5 a).

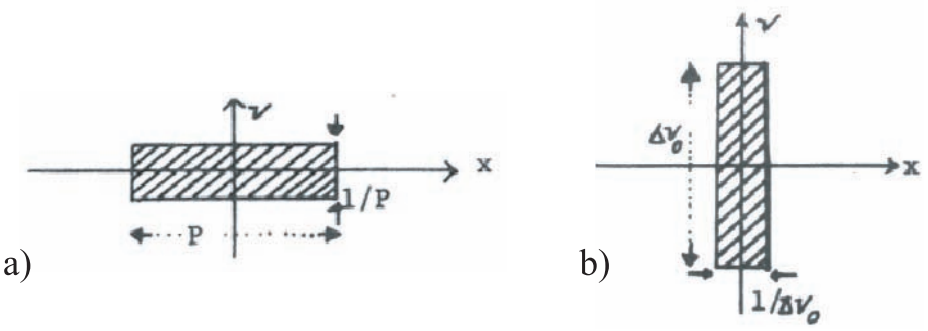

Figure 15.5: The (x, ν) space of some example functions.

Two more examples:

$$\begin{aligned} \tilde{V}(\nu) &= \mathrm{rect}\left(\frac{\nu}{\Delta\nu}\right) \\ V(x) &= \Delta\nu_0 = \mathrm{sinc}(x\Delta\nu_0) \\ e^{-\left[\frac{(x-x_0)}{a}\right]^2} \cdot e^{i\pi\left[\frac{(x-x_1)}{b}\right]^2} &= V(x) \end{aligned} \tag{15.41}$$

It is essentially $\neq 0$ in $|x - x_0| \leq a$ (Fig. 15.5 b); and the "local frequency" $\nu(x)$ is:

$$\nu(x) = \frac{\{\mathrm{d}\,\pi[\frac{(x-x_1)}{b}]^2\}/\mathrm{d}x}{2\pi} \tag{15.42}$$

This means the following: around $x = \overline{x}$ it is true that:

$$\pi\left(\frac{(x-x_1)}{b}\right)^2 \approx \pi\left(\frac{(\overline{x}-x_1)}{b}\right)^2 + \left\{\frac{\mathrm{d}\,\pi\left[\frac{(x-x_1)}{b}\right]^2}{\mathrm{d}x}\right\}_{x=\overline{x}} (x-\overline{x}) + \text{small} \tag{15.43}$$

The first term is a constant. Writing the second term as $2\pi(x-\overline{x})\cdot\nu(x)$ justifies the definition of the "local spatial frequency". It becomes more obvious when inserting the Taylor expansion into the exponential function:

$$e^{i\pi\left(\frac{x-x_1}{b}\right)^2} \approx e^{i\pi\left(\frac{\overline{x}-x_1}{b}\right)^2} e^{2\pi i\nu\overline{x}(x-\overline{x})^2} \quad \text{for } |x-\overline{x}| \text{ reasonably small} \tag{15.44}$$

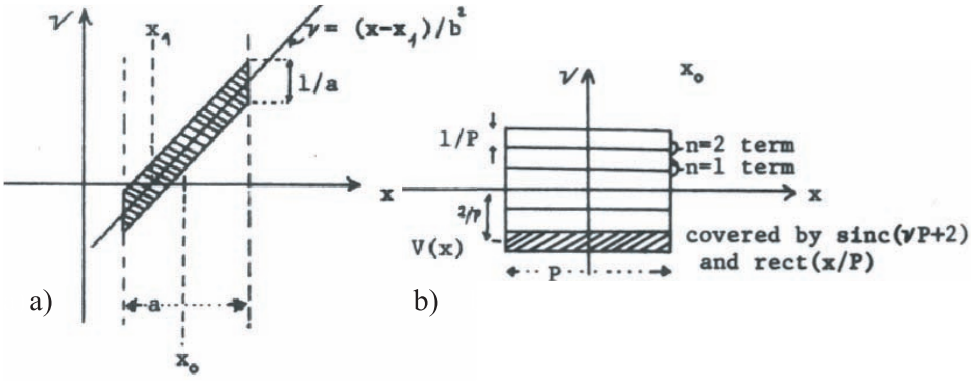

Figure 15.6: a) Local frequency in the phase domain; b) sampling in the (x,ν) domain.

Hence $\nu(\overline{x}) = \frac{\overline{x}-x_1}{b^2}$. Now let us visualize the "local frequency" in the "phase-domain", or (x,ν) domain (Fig. 15.6 a)).

$$V(x) = e^{-\left(\frac{(x-x_0)}{a}\right)^2} e^{i\pi\left(\frac{x-x_1}{b}\right)^2} \tag{15.45}$$

The choice of $\frac{1}{a}$ becomes apparent when computing:

$$\tilde{V}(\nu) = \int V(x)e^{-2\pi i\nu x}\,\mathrm{d}x \tag{15.46}$$

The (x,ν) domain visualization is also very useful for functions to which a sampling theorem can be applied (Fig. 15.6 b). It turns out that each "sample" covers a unit area in the (x,ν) domain, since $\mathrm{rect}\frac{x}{P}$ has the width P and $\mathrm{sinc}(\nu P)$ has the height $\frac{1}{P}$.

$V(x)\neq 0$ only in $|x|\leq\frac{P}{2}$:

$$\tilde{V}(\nu) = \sum \tilde{V}\left(\frac{n}{P}\right)\mathrm{sinc}(\nu P-n)(\text{Fourier sampling}) \tag{15.47}$$

Now Fresnel-sampling for the same function $V(x)$:

$$\hat{V}(x) = \sum \hat{V}\left(\frac{n}{P}\right) e^{i\pi\left[x^2-\left(\frac{n}{P}\right)^2\right]} \mathrm{sinc}(xP-n) \tag{15.48}$$

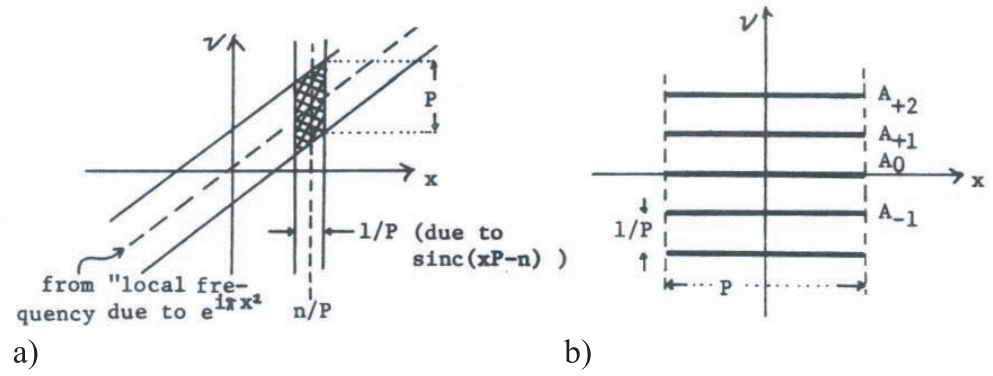

Figure 15.7: Illustration of Fresnel sampling in the phase domain.

The cross-hatched area in Fig. 15.7 c) is covered by the elementary Fresnel-sampling function $e^{i\pi x^2}\mathrm{sinc}(xP-n)$, which has a Fourier spectrum, which is essentially non-zero only in $|\nu - nP|^2 < \frac{P}{2}$ (i.e. $\int \hat{V}(x)e^{-2\pi i\nu x}\mathrm{d}x$)

A periodic function $V(x) =\sim A_n e^{2\pi i n\frac{x}{P}}$ is by definition completely known from only $|x| \leq \frac{P}{2}$, and its frequencies are apart by $\frac{1}{P}$. Hence again a unit area in (ν, x) is covered by each coefficient (Fig. 15.7 b). The general conclusion is: the amount of (x, ν) area which is covered by a family of functions $V(x)$ is equal to the number of degree of freedom, which is the same as the number of sample values, which can be significantly different from zero.

16 Fundamentals of Diffraction Theory

16.1 Terminology: diffraction and interference

In examination, and on other occasions when people want to communicate about science, it may be crucial (but not sufficient) to know the right terminology. For example the question "what is diffraction, and what is interference?" could be answered in this way:

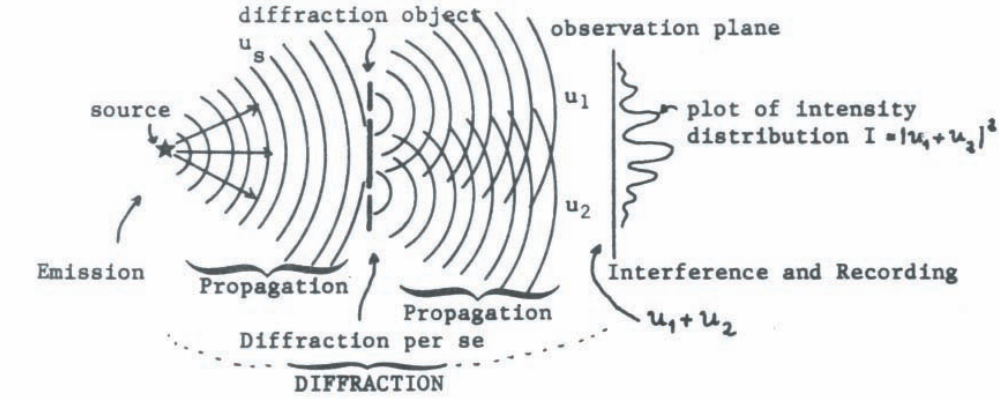

Figure 16.1: Definition of the terminology: diffraction and interference.

The term "diffraction" is sometimes used for the experiment as a whole, sometimes only for the modification of the light wave due to the diffraction-object. The later diffraction process might sometimes also be called "transmittance", or scattering, or reflection, or refraction, or partial absorption, particularly if the effect is easiest described in ray language. But since ray-optics is only a coarse approximation of wave optics, and hence a part of wave optics, these latter effects can be called also "diffraction" (which not every examiner might like). The term "interference" can be best illustrated by the following Gedanken-experiment (Fig. 16.1). At first only slit $\#1$ is open, hence only the wave u_1 travels to the plane of observation, where the intensity $|u_1|^2$ will cause an effect, as for example exposing a photographic plate. Next we open only slit $\#2$, yielding intensity $|u_2|^2$. Now we open both slits, from which $u_1 + u_2$ will emerge and propagate to the observation plane, where an effect is caused by:

$$|u_1+u_2|^2 = |u_1|^2 + |u_2|^2 + u_1u_2^* + u_1^*u_2 = I_1 + I_2 + \underbrace{2\mathrm{Real}(u_1u_2^*)}_{\text{interference term}} \tag{16.1}$$

This term "interferes" with the simple-mined prediction based on the two single-slit experiments. Occasionally this term is called "mutual intensity", while the nomenclature is slightly modified:

$$\begin{aligned} u_1 = |u_1|e^{i\alpha_1} &= \sqrt{I_1}e^{i\alpha_1}; \qquad u_2 = \sqrt{I_2}e^{i\alpha_2} \\ u_1u_2^* &= \sqrt{I_1I_2}e^{i(\alpha_1-\alpha_2)}; \qquad 2\mathrm{Real}(u_1u_2^*) = \sqrt{I_1I_2}\cos(\alpha_1-\alpha_2) \end{aligned} \tag{16.2}$$

This terminology is favoured in the theory of partial coherence.

16.2 History and classification of diffraction theories

Huygens' well-known principle states that every point which is reached by a wave will act a point source for a secondary *spherical wave*. In other words, every wavefield can be subdivided into or composed by spherical waves. Huygens himself used his principle for explaining diffraction effects by means of a graphic construction. Fresnel and later Kirchhoff put Huygens' principle on a sound basis by showing that spherical waves are indeed solutions of the wave equation. Furthermore a spherical wave is the "Green's function" of the wave equation, which means that it is the consequence of a point source. Finally the set of spherical waves forms a complete set of elementary functions which may serve as a basis for constructing all other functions which satisfy the wave equation.

A British physician, Thomas Young, disagreed with Huygens and his disciples. Young claimed that diffracted waves originate from the *edges* of slits and other diffraction objects, not from immaterial points within the slit as Huygens claimed. Young's way of explaining was quite convenient in many instances, but it did not become too popular since he could not back up this hypothesis by integrals as could the Huygens school. Long after Young's death, Maggi, Rabinowicz, and Sommerfeld proved that Young's hypothesis is actually equivalent and not contradictory to Huygens' principle. In more mathematical terms their proof stated that *cylindrical waves* (which are often created on edges) are also a complete set of elementary waves.

A third set of complete waves are the *plane waves*, which were probably recognized as very useful elementary waves at first by Lord Rayleigh, later also by Sommerfeld, Debye and Picht.

If these three sets of elementary waves are all complete then it must be possible to decompose for example a spherical wave into plane waves, or a cylindrical wave into spherical waves, and so on. We will later demonstrate some of the six equivalences. In symbolic form the three diffraction theories are indicated in Fig. 16.2:

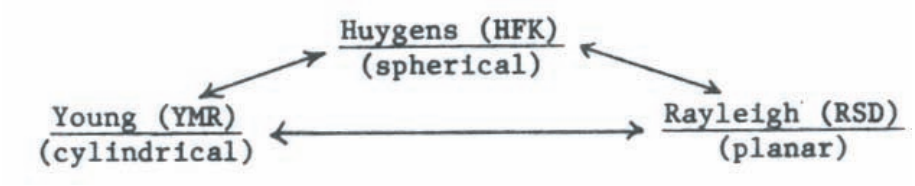

Figure 16.2: The three approaches to diffraction theory.

Another approach to the classification of diffraction phenomena has to do with the distance from the diffraction object to the observer, which might be a photographic plate or a photomultiplier. An infinite distance relates to the so-called *Fraunhofer diffraction*. If the distance is only a few wavelength we will talk about "near-field diffraction". Everything in between is called *Fresnel diffraction*. Obviously, Fresnel diffraction theory is the most general branch, since it contains the two other branches as extreme cases. Therefore we will start with Fresnel diffraction. The distinction of these three branches is meaningful since the effects are quite different, and the useful mathematical approximations are also quite different. Hence all three branches deserve our attention. Also the three diffraction theories based on different elementary waves (HFK: spherical, YMR: cylindrical; RSD: planar) are worth considering, since no single one among them is always good for visualizing or computing what happens with light.

One more comment on nomenclature is desirable to avoid confusion later. Kirchhoff made two independent contributions which are often not seen clearly apart. He justified the usefulness of spherical waves. Furthermore he developed a simple recipe for getting boundary values of the wavefield if the structure of the object (such as a double slit) is known. This second contribution will be referred to as "Kirchhoff-approximation". It is used equally often for spherical, for cylindrical, and for planar waves.

16.3 Kirchhoff-approximation

Our problem is: given the boundary value $(x, y, 0)$ of the complex amplitude u in plane $z = 0$, what is the complex amplitude in the half space $z \geq 0$ to the right of the boundary plane $z = 0$? If the half-space $z \geq 0$ is homogeneous the wave equation $\nabla^2 u + k^2 u = 0$ applies. We assume monochromatic light at the boundary and $k = \frac{2\pi\nu_t n}{c}$. Before we solve the wave equation we have to know what the field $u(x, y, 0)$ at the boundary is. Assume we illuminate from the left $(z < 0)$ with a plane wave of normal incidence. $u_{\mathrm{LEFT}}(x, y, z) = e^{ikz}$. At $z = -0$, it becomes $u_{\mathrm{LEFT}}(x, y, -0) = 1$. Herein $z = -0$ means immediately to the left from the plane $z = 0$, which is the boundary plane itself, containing the double lit or any other "diffraction-object" (Fig. 16.3). Later, $z = +0$ will refer to the plane immediately to the right from the boundary plane $z = 0$. Now let us assume that the diffraction object is opaque in some parts and has holes in other parts. This can be described as an amplitude transmittance:

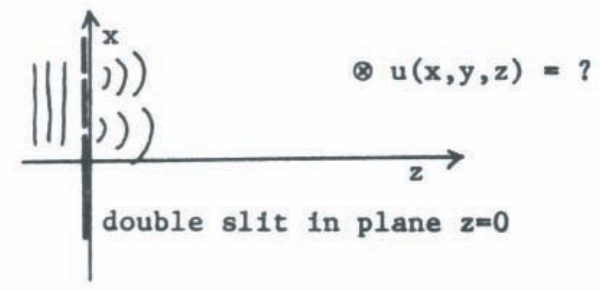

Figure 16.3: The problem in diffraction theory.

$$u_0(x,y)\begin{cases} +1 & \text{if hole} \\ 0 & \text{otherwise;} \end{cases} \tag{16.3}$$

or in more general form:

$$\boxed{u_0(x,y) = \frac{u(x,y,+0)}{u(x,y,-0)}} \tag{16.4}$$

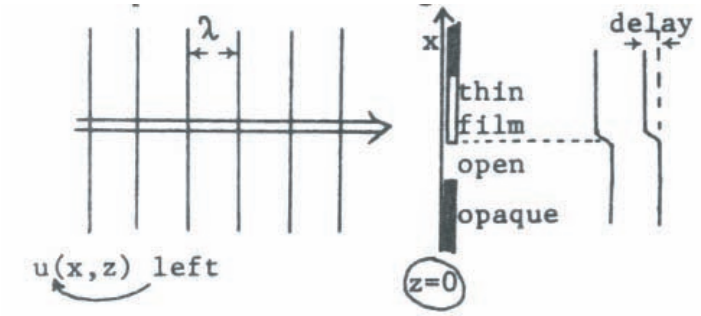

Figure 16.4: A general diffraction element.

In general the diffraction object might contain not only transparent and opaque parts. It might be partially transparent: $0 < |u_0| < 1$; Or some parts might shift the phase: $\arg(u_0) \neq 0$, which physically might happen due a thin transparent film, the phase velocity was $v = \frac{c}{n}$, which means that any film with $n > 1$ will delay the wave front, for example as in Fig. 16.4.

Now let us compute the phase shift. The time needed to go through the thin film is $t_F = \frac{D}{\frac{c}{n}}$. The time it takes to travel over the same distance D in air beside the film $t_A = \frac{D}{c}$. The time

difference is $\Delta t = t_F - t_A = (n-1)\frac{D}{c}$, and the phase difference $\Delta\varphi = 2\pi\nu_t\Delta t = 2\pi(n-1)D\frac{\nu_t}{c}$, which becomes with $\lambda\nu_t = c$:

$$\boxed{\Delta\varphi = \frac{2\pi}{\lambda}(n-1)D} \qquad \text{phase shift} \tag{16.5}$$

This $\Delta\varphi$ is the argument of the complex amplitude transmittance $u_0(x)$.

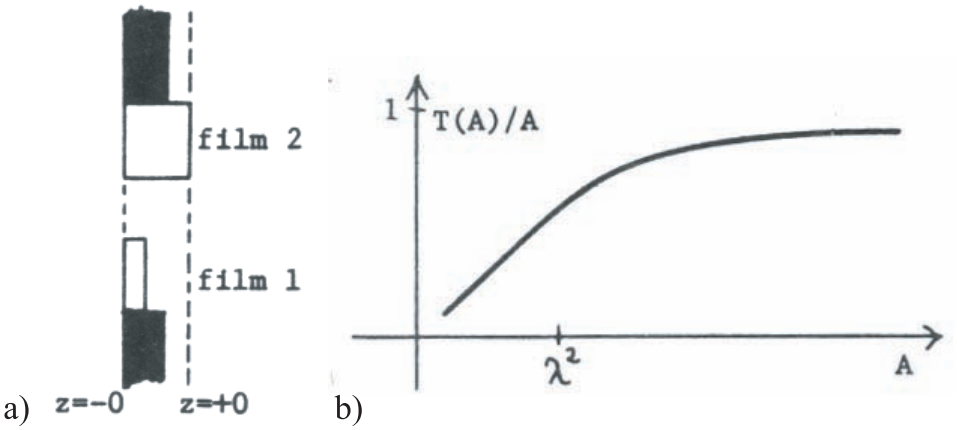

Figure 16.5: a) a phase shifting diffractive object; b) transmittance vs. size of the opening of a pinhole.

Several things were presented rather crudely when introducing the concept of the "amplitude transmittance". For example we talked about $z = -0$ as the planes where the "diffraction-object" begins, and where it ends. This implies an infinitely thin object, which certainly is nonsense, even more so since we talked about a film of finite thickness D, which might be a part of the object (Fig. 16.5 a). We mean by $z = -0$ the most-left plane containing physical parts of the object, while $z = +0$ refers to the most-right part of the object. If the lateral dimensions of the object are large compared to the wavelength (say $> 5\lambda$) this approximation is not very harmful, as experience has shown. - The following experiment illustrates the risk. We shine light through a hole of size A and measure how much intensity arrives on the other side. One would expect a total intensity transmittance which is proportional to the area A as $T(A) = (\text{const.})A$ or $\frac{T(A)}{A}$ =const. Instead this is not true if the dimension of the hole become comparable with the wavelength. Hence the simple multiplication rule: — outgoing amplitude = incoming amplitude times amplitude transmittance — does not hold in regions of a size comparable with the wavelength (Fig. 16.5 b). Nevertheless, this wrong multiplication rule, which is called the "Kirchhoff-Approximation" is used widely. Usually it is justified, because the typical dimensions of most man-made objects are larger than the wavelength. Counter-examples are very fine diffraction gratings, narrow slits, and holes. Problems of this

sort are often called “rigorous diffraction theory”. However, in practical optical applications we can use the Kirchhoff approximation almost always.

In most cases we will assume $u(x, y, z)$ for $z < 0$, which is the illuminating wave, coming from the left, to be e^{ikz}, hence $u(x, y, -0) = 1$, and consequently the Kirchhoff approximation reduces to $u(x, y, +0) = u_0(x, y)$. So far we have classified different approaches to diffraction theory in which the diffraction object was composed of points (Huygens-Fresnel-Kirchhoff), or out of edges (Young-Maggi-Sommerfeld-Rubiniwicz). Now let us proceed to the *Rayleigh-Sommerfeld* approach. Now a prism is a very useful elementary object. It may have an index n and wedge angle α. The thickness of this prism is $D(x) = x \tan \alpha$ (Fig. 16.6), hence the phase:

$$\arg\{u_0(x, y)\} = \varphi_0(x, y) = \frac{2\pi}{\lambda}(n-1)D(x) = 2\pi\left[(n-1)\frac{\alpha}{\lambda}\right]x \tag{16.6}$$

$|u_0| = 1$ (no absorption assumed);

$$u_0 = e^{i\varphi_0} = e^{2\pi i(n-1)\frac{\alpha x}{\lambda}} \tag{16.7}$$

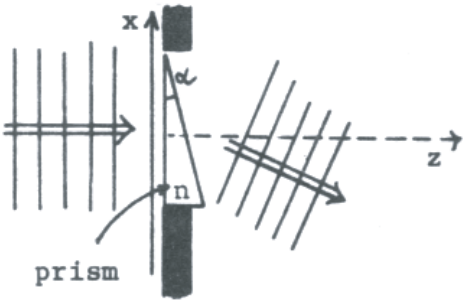

Figure 16.6: The prism as a phase element.

This looks like a Fourier element $e^{2\pi i(\nu x+\mu y)}$. With $\nu = (n-1)\frac{\alpha}{\lambda}$ and $\mu = 0$. This particular prism had its wedge oriented parallel to the y-axis. A slightly more general object would be a prism with its wedge still in the (x, y) plane, but not necessarily parallel to the y-axis. Furthermore the prism might be coated with an amplitude-reducing thin film. Such an object would be described by the complex amplitude transmittance

$$u_0(x, y) = a\, e^{2\pi i\frac{(n-1)\alpha}{\lambda}(x\cos\theta + y\sin\theta)} = |u_0|e^{i\varphi_0} \tag{16.8}$$

Sometimes it is convenient to use polar coordinates.

$$\varphi_0 = 2\pi(x\nu + y\mu) = 2\pi r\varrho\cos(\varphi - \theta) \tag{16.9}$$

$$\nu = \left[(n-1)\frac{\tan(\alpha)}{\lambda}\right]\cos\theta \qquad | \qquad \mu = \left[(n-1)\frac{\tan(\alpha)}{\lambda}\right]\sin\theta \tag{16.10}$$

$$\varrho^2 = \nu^2 + \mu^2;\ \tan\theta = \frac{\mu}{\nu} \qquad | \qquad \nu = \varrho\cos\theta;\ \mu = \varrho\sin\theta$$

$$r^2 = x^2 + y^2;\ \tan\varphi = \frac{y}{x} \qquad | \qquad x = \vec{r}\cos\varphi;\ y = \vec{r}\sin\theta$$

Hence $x\nu + y\mu = \vec{r}\varrho[\cos\varphi\cos\theta + \sin\varphi\sin\theta] = \vec{r}\varrho\cos\varphi - \theta$; $\varrho = (n-1)\frac{\alpha}{\lambda}$.

The most general object $u_0(x,y)$ can be thought of as consisting of many such prisms, with different orientations θ and different prism angles α, each prism having its own specific amplitude a, and also a "typical phase" for $(x=0,\ y=0)$, which be called γ (gamma).

$$u_0(x,y) = a\ e^{i\gamma}e^{2\pi i(x\nu+y\mu)} \tag{16.11}$$

If you now believe in the mathematical statement that a Fourier integral of the type $\iint \tilde{u}_0(\nu,\mu)e^{2\pi i(x\nu+y\mu)}\mathrm{d}\nu\ \mathrm{d}\mu$ is suitable as a representation for every healthy function $u_0(x,y)$, provided $\tilde{u}(\nu,\mu)$ is chosen properly, then you also must believe that the most general diffraction object $u_0(x,y)$ can be thought of as a superposition of many prisms. Now, you might think, this is nonsense, because these many prisms would penetrate each other since they occupy the same (x,y) region. Certainly this involved penetration is somewhat hard to visualize, but I hope you will get used to it, and learn to visualize it some day.

It ought to be clear what we think when writing down a Fourier integral for the object transmittance u_0:

$$u_0(x,y) = \iint \tilde{u}(\nu,\mu)e^{2\pi i(\nu x+\mu y)}\mathrm{d}\nu\mathrm{d}\mu \tag{16.12}$$

If you don't like to consider this as a physical superposition of prisms, you might restrict yourselves to thinking of this as a mathematical superposition of Fourier elements. Even so, you will arrive at the same end result, because you can do theory like grinding coffee beans, which are the input (= boundary conditions) into your black box (differential equations). You just do the mathematics without thinking, and collect the coffee powder in the output box. To compute without visualizing for example little prisms is usually quicker and cleaner. But in the end it is better to be able to visualize what you compute. Otherwise you will rarely invent something.

16.4 The RSD theory of Fresnel diffraction

Personally I like the plane wave approach best, because it is mathematically the most simple one. Our problem is now: Given $u(x,y,z_0)$, wanted $u(x,y,z)$ for $z \geq z_0$. $u(x,y,z)$ has to satisfy

A : the wave equation: $\nabla^2 u + k^2 u = 0$;

B : the boundary condition: $\lim_{z\to 0}\{u(x,y,z)\} \Longrightarrow u(x,y,z_0)$

C_1 : the irradiation condition

C_2 : the damping condition

C_1 and C_2 will be explained shortly.

It is not forbidden (and it will turn out to be very convenient) to represent the complex amplitude $u(x,y,z)$ in the arbitrary plane z by a Fourier integral in two dimensions (x,y) and (ν,μ):

$$u(x,y,z) = \iint \tilde{u}(\nu,\mu;z) e^{2\pi i(\nu x+\mu y)} \mathrm{d}\nu \mathrm{d}\mu \tag{16.13}$$
$$\tilde{u}(\nu,\mu,z) = \iint u(x,y,z) e^{-2\pi i(\nu x+\mu y)} \mathrm{d}x \mathrm{d}y$$

Let's go with this Fourier representation into the wave equation:

$$\left\{\frac{\partial^2}{\partial x^2} + \frac{\partial^2}{\partial y^2} + \frac{\partial^2}{\partial z^2} + k^2\right\} u(x,y,z) = 0 = \tag{16.14}$$
$$= \iint \left\{(2\pi i\nu)^2 \tilde{u} + (2\pi i\mu)^2 \tilde{u} + \frac{\partial^2 \tilde{u}}{\partial z^2} + k^2 \tilde{u}\right\} e^{2\pi i(\nu x+\mu y)} \mathrm{d}x \mathrm{d}y$$

If this integral (which is nothing but the wave equation) is to be zero for every x, y, then the Fourier kernel $\{\ldots\}$ must be zero itself for every Fourier coordinate ν, μ:

$$\{\ldots\} = \tilde{u}(\nu,\mu,z) = \left[k^2 - (2\pi)^2(\nu^2+\mu^2)\right] + \frac{\partial^2 \tilde{u}(\nu,\mu,z)}{\partial z^2} = 0 \tag{16.15}$$

Hence we have reduced the 3D differential equation $\nabla^2 u + k^2 u = 0$ into a one- dimensional differential equation with z as variable (and ν, μ as parameters).

$$\boxed{\frac{\partial^2 \tilde{u}}{\partial z^2} + k^2 \tilde{u}\left[1 - \lambda^2(\nu^2+\mu^2)\right] = 0} \tag{16.16}$$

The solution is $\tilde{u}(\nu,\mu,z) = A(\nu,\mu)e^{ikz\sqrt{[\ldots]}} + B(\nu,\mu)e^{-ikz\sqrt{[\ldots]}}$. A and B have to be found from the boundary value condition

$$\lim_{z\to z_0}\{u(x,y,z)\} \Longrightarrow u(x,y,z_0) = \tag{16.17}$$
$$= \iint \tilde{u}(\nu,\mu,z_0) e^{2\pi i(\nu x+\mu y)} \mathrm{d}\nu \mathrm{d}\mu =$$
$$= \iint \left[A e^{ikz_0\sqrt{[\ldots]}} + B e^{-ikz_0\sqrt{[\ldots]}}\right] e^{2\pi i(\nu x+\mu y)} \mathrm{d}\nu \mathrm{d}\mu$$

By comparison we conclude:

$$\tilde{u}(\nu,\mu,z_0) = Ae^{ikz_0\sqrt{\cdots}} + Be^{-ikz_0\sqrt{\cdots}} \tag{16.18}$$

This is only *one* equation for two unknowns, A and B. Ordinarily in mathematics one would require $\left\{\frac{\partial u}{\partial z}\right\}_{z=z_0}$ as additional boundary condition value to be known. We will do something equivalent, but indirectly. This way of finding the second boundary condition depends on considerations of physics.

What does a typical term in our unfinished solution mean?

$$u(x,y,z) = \iint \left[A(\nu,\mu)e^{+ikz\sqrt{1-\lambda^2(\nu^2+\mu^2)}} + Be^{-ikz\sqrt{1-\lambda^2(\nu^2+\mu^2)}}\right] e^{2\pi i(\nu x+\mu y)}\mathrm{d}\nu\mathrm{d}\mu \tag{16.19}$$

The typical term is the static part of a plane wave

$$\begin{aligned} & e^{ik\sqrt{\cdots}}e^{2\pi i(x\nu+y\mu)} = \\ = \quad & e^{i\frac{2\pi}{\lambda}\left[x\lambda\nu+y\lambda\mu+z\sqrt{1-(\lambda\nu)^2-(\lambda\mu)^2}\right]} = e^{i\vec{k}\vec{x}} \end{aligned} \tag{16.20}$$

The exponent is a vector product of $\vec{x} = (x,y,z)$ and of $\vec{k} \hat{=} \frac{2\pi}{\lambda}(\lambda\nu, \lambda\mu, \sqrt{\cdots})$; $|\vec{k}| = \frac{2\pi}{\lambda}$. Together with the temporal factor $e^{-i\omega t}$ in $V(\vec{x},t) = u(\vec{x})e^{-i\omega t}$, we get $e^{i(\vec{k}\vec{x}-\omega t)}$, which is a *plane wave*. A hypothetical observer, moving in k direction with velocity $\frac{\omega}{k}$, will always stay on the same wave crest at any time:

$$(\vec{x_1},t) \longrightarrow \left(\vec{x_1} + \frac{\vec{k}}{k}\frac{\omega}{k}(t_2-t_1), t_1+(t_2-t_1)\right) = (\vec{x_2},t_2) \tag{16.21}$$

Proof:

$$\vec{k}\vec{x_2} - \omega t_2 = \vec{k}\vec{x_1} + \frac{\vec{k}\vec{k}}{k^2}\omega(t_2-t_1) - \omega_2 t_2 = \vec{k}\vec{x_1} - \omega t_1 \tag{16.22}$$

In other words, $\frac{\vec{k}}{k^2}$ is the velocity vector of the "wave rider".

So far we have considered only the first term $Ae^{ikz\sqrt{\cdots}}e^{2\pi i(\nu x+\mu y)}$. Now we discuss the second term with the minus sign in the exponent:

$$Be^{-ikz\sqrt{\cdots}}e^{2\pi i(\nu x+\mu y)} \tag{16.23}$$

The two $\vec{k}$-vectors belonging to the A term and to the B term, respectively, have identical x- and y-components $(k\lambda\nu, k\lambda\mu)$, but opposite z-components $\pm k\sqrt{1-\lambda^2(\nu^2+\mu^2)}$ (Fig. 16.7). Only $\vec{k}_A$ makes sense for the physicist, since we assumed that the object was illuminated from the left, that is, from negative z-direction. Hence for physical reasons we set $B(\nu,\mu)$. In doing so we satisfy the so-called *Irradiation Condition* (C_1).

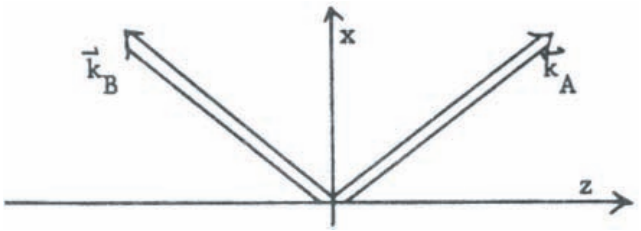

Figure 16.7: Physical interpretation of the solutions of the wave equation (irradiation condition).

Without saying it we had assumed $\sqrt{1-\lambda^2(\nu^2+\mu^2)}$ to be real; that means $\nu^2+\mu^2 \leq \frac{1}{\lambda^2}$. However the Fourier integral $\int \ldots \mathrm{d}\nu\mathrm{d}\mu$ covers the whole (ν,μ) domain $(-\infty,\infty)$. Hence we have to consider now those ν,μ which are outside of the circle $\nu^2+\mu^2=\frac{1}{\lambda^2}$. In that case the root becomes imaginary, $\sqrt{1-\lambda^2(\nu^2+\mu^2)} = i\sqrt{\lambda^2(\nu^2+\mu^2)-1}$. Again let us discuss the physical meaning of:

$$\begin{aligned} Ae^{ikz\sqrt{1-\lambda^2(\nu^2+\mu^2)}}e^{2\pi i(\nu x+\mu y)} &= Ae^{-kz\sqrt{\lambda^2(\nu^2+\mu^2)-1}}e^{2\pi i(\nu x+\mu y)} \\ Be^{-ikz\sqrt{1-\lambda^2(\nu^2+\mu^2)}}e^{2\pi i(\nu x+\mu y)} &= Be^{+kz\sqrt{\lambda^2(\nu^2+\mu^2)-1}}e^{2\pi i(\nu x+\mu y)} \end{aligned} \tag{16.24}$$

Both the A-wave and the B-wave propagate now in a direction which has no z-component, as can be seen from $e^{2\pi i(\nu x+\mu y)}$. The amplitude of the A-wave decreases exponentially as a function of the distance z. Therefore this wave is called "evanescent" or surface wave or sub wave. The B-wave has a very large amplitude at large z-value. That does not make sense. Hence we set $B=0$ (C_2). This result is very important. Hence we will write it down again, together with the Fourier relation for the boundary:

$$\tilde{u}(\nu,\mu,z_0) \hat{=} \iint u(x',y',z_0)e^{-2\pi i(\nu x'+\mu y')}\mathrm{d}x'\mathrm{d}y' \tag{16.25}$$

We will call this result the RSD formula for Rayleigh-Sommerfeld-Debye. Four equivalent versions will turn out to be convenient at various instances:

$$\begin{aligned} u(x,y,z) &= \iint \tilde{u}(\nu,\mu,z)e^{2\pi i[\nu x+\mu y+\sqrt{1-\lambda^2(\nu^2+\mu^2)}\frac{z-z_0}{\lambda}]}\mathrm{d}\nu\mathrm{d}\mu \\ &= \iiiint u(x',y',z_0)e^{2\pi i[\nu(x-x')+\mu(y-y')+\sqrt{1-\lambda^2(\nu^2+\mu^2)}\frac{z-z_0}{\lambda}]}\mathrm{d}\nu\mathrm{d}\mu\mathrm{d}x'\mathrm{d}y' \\ \tilde{u}(\nu,\mu,z) &= \tilde{u}(\nu,\mu,z_0)e^{2\pi i\sqrt{1-\lambda^2(\nu^2+\mu^2)}\frac{z-z_0}{\lambda}} \\ &= \iint u(x',y',z_0)e^{2\pi i[-\nu x'-\mu y'+\sqrt{1-\lambda^2(\nu^2+\mu^2)}\frac{z-z_0}{\lambda}]}\mathrm{d}x'\mathrm{d}y' \end{aligned} \tag{16.26}$$

The range of ν, μ covers both the plane waves $\nu^2+\mu^2 \le \frac{1}{\lambda^2}$ and the evanescent waves $\nu^2+\mu^2 > \frac{1}{\lambda^2}$. The most important feature of the evanescent waves is their absence at a distance $z-z_0 \gg \lambda$ due to the damping factor $e^{-2\pi\sqrt{\lambda^2(\nu^2+\mu^2)-1}\frac{z-z_0}{\lambda}}$. Hence the spatial frequency spectrum $\tilde{u}(\nu,\mu,z)$ of $u(x,y,z)$ does not know anything about the superhigh spatial frequencies $\nu^2+\mu^2 > \frac{1}{\lambda^2}$ of the object spectrum $\tilde{u}(\nu,\mu,z_0)$. In other words, optical waves cannot reveal object details smaller than a fraction of λ, if the observer is many wavelength away from the object. This is true no matter what lens, mirror or other long distance gadget you use. To break this barrier of the "fundamental resolution limit" is one of the most prestigious problems of today. To solve it one has to learn to handle evanescent waves. Another interesting aspect of evanescent waves is that they have a phase velocity smaller than c, and they can have a vector-component of the electric field parallel to the direction of wave propagation. Using these two properties it should be possible to use evanescent waves for a particle accelerator. To get a feel for the damping of evanescent waves we assume $\sqrt{\nu^2+\mu^2} = \frac{\sqrt{2}}{\lambda}$. Then:

$$e^{-2\pi\sqrt{\lambda^2(\nu^2+\mu^2)-1}\frac{z}{\lambda}} = e^{-2\pi\frac{z}{\lambda}} \tag{16.27}$$

Already at a distance of $\frac{\lambda}{2\pi}$ the amplitude is reduced by a factor $\frac{1}{e} = 0.37$.

Or we may look at the damping problem in another way. How much percentage-wise can we increase the range of observable frequencies if we are able to measure amplitudes $\frac{1}{e}$ at a distance of one wavelength? The intensity at that distance would be down to $\left(\frac{1}{e}\right)^2 = 0.14$.

$$\sqrt{\nu^2+\mu^2} = \frac{1+p}{\lambda}; \qquad 2\pi\sqrt{\lambda(\nu^2+\mu^2)-1}\,\frac{z}{\lambda} = 2\pi\sqrt{(1+p)^2-1}\,\frac{z}{\lambda} \approx 2\pi\sqrt{2}\frac{z}{\lambda} \tag{16.28}$$

For $z=\lambda$ the damping factor is now $e^{-2\pi\sqrt{2p}}$. The specific percentage p which leads to a damping factor $\frac{1}{e}$ is given by $2\pi\sqrt{2p} = 1 = 4\pi^2 2p$; $p = \frac{1}{8\pi^2} \approx \frac{1}{80} = \frac{1.25}{100}$. In other words, to improve the resolution or spatial bandwidth by 1.25% we need to go as close as one wavelength to the object, and measure there intensities which are reduced to 14% of their original values. Bleak prospects!

16.5 Derivation of the HFK-integral from the RSD-intgral

The configuration of our diffraction problem is shown in Fig. 16.8.

We know that according to H., F & K. a spherical wave starts from each luminous point (x', y') in z_0 and reaches the various points (x, y) in the observation plane. Let us call this spherical wave $S(x, y; x', y')$ for the moment. Hence the HFK theory must yield a result in the form of:

$$u(x, y, z) = \iint u(x', y', z_0) S(x, y, x', y') f(x, y, x', y') \mathrm{d}x' \mathrm{d}y' \tag{16.29}$$

The function f will turn out to be almost constant for small angles, like the cosine. I wrote this down in order to see which of the four forms of the RSD formulas is most appropriate. The third one is surely the simplest (only multiplication), but it is the second one which we can bring into the desired form:

$$u(x, y, z) = \iint_{x'y'} u(x', y', z_0) \left\{ \iint_{\nu\,\mu} e^{\cdots} e^{2\pi i \left[\nu(x-x')+\mu(y-y')+\sqrt{1-\lambda^2(\nu^2+\mu^2)}\frac{z-z_0}{\lambda}\right]} \mathrm{d}\nu \mathrm{d}\mu \right\} \mathrm{d}x' \mathrm{d}y' \tag{16.30}$$

If we really can derive HFK from RSD, then this $\{\ldots\}$ must represent a spherical wave, possibly modified by a smooth function f.

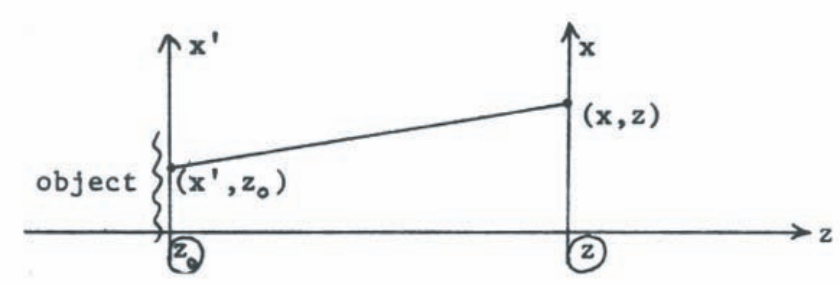

Figure 16.8: The diffraction problem.

Let's see what $\{\ldots\}$ really is by solving the $\int_\nu \int_\mu \ldots$ with the saddle-point method:

$$\iint e^{ikf(\nu,\mu)} \mathrm{d}\nu \mathrm{d}\mu \approx \frac{2\pi e^{ikf(\nu_0,\mu_0)+\frac{\pi}{2}}}{k\sqrt{f_{\nu\nu} f_{\mu\mu} - f_{\nu\mu}^2}} \tag{16.31}$$

Here:

$$kf(\nu,\mu) = \frac{2\pi}{\lambda}\left[\lambda\nu(x-x') + \lambda\mu(y-y') + \sqrt{1-\lambda^2(\nu^2+\mu^2)}(z-z_0)\right] \quad (16.32)$$

$$\frac{\partial f}{\partial \nu} = 0 = \lambda(x-x') - \frac{\lambda^2\nu_0(z-z_0)}{\sqrt{1-\lambda^2(\nu^2+\mu^2)}};\ \frac{\partial f}{\partial \mu} = 0 = \lambda(y-y') - \frac{\lambda\mu_0(z-z_0)}{\sqrt{1-\lambda^2(\nu^2+\mu^2)}} \quad (16.33)$$

We want to solve this for ν_0 and μ_0, for different values of (x,y) and (x',y'). From $\frac{\partial f}{\partial \nu} = 0$ we get:

$$\frac{\lambda\nu_0}{\sqrt{1-\lambda^2(\nu_0^2+\mu_0^2)}} = \frac{x-x'}{z-z_0}; \qquad \frac{\lambda\mu_0}{\sqrt{1-\lambda^2(\nu_0^2+\mu_0^2)}} = \frac{y-y'}{z-z_0} \text{ from } : \frac{\partial f}{\partial \mu} = 0 \quad (16.34)$$

Hence:

$$f(\nu_0,\mu_0) = \sqrt{1-\lambda^2(\nu_0^2+\mu_0^2)}\left[\frac{(x-x')^2}{z-z_0} + \frac{(y-y')^2}{z-z_0} + z - z_0\right] \quad (16.35)$$

The square bracket can be simplified:

$$\frac{(x-x')^2+(y-y')^2+(z-z_0)^2}{z-z_0} = \frac{r^2}{z-z_0} \quad (16.36)$$

We get the $\sqrt{1-\lambda^2(\nu_0^2+\mu_0^2)}$ as a function of (x',y',z_0) and (x,y,z) by computing the follow expression in two ways:

$$\begin{aligned}
\left(\frac{\lambda\nu_0}{\sqrt{\cdots}}\right)^2 + \left(\frac{\lambda\mu_0}{\sqrt{\cdots}}\right)^2 + 1 &= \frac{\lambda^2(\nu_0^2+\mu_0^2)}{1-\lambda^2(\nu_0^2+\mu_0^2)} + \frac{1-\lambda^2(\nu_0^2+\mu_0^2)}{1-\lambda^2(\nu_0^2+\mu_0^2)} = \left(\frac{1}{(\sqrt{\cdots})^2}\right) \\
\left(\frac{\lambda\nu_0}{\sqrt{\cdots}}\right)^2 + \left(\frac{\lambda\mu_0}{\sqrt{\cdots}}\right)^2 + 1 &= \frac{(x-x')^2}{(z-z_0)^2} + \frac{(y-y')^2}{(z-z_0)^2} + \frac{(z-z_0)^2}{(z-z_0)^2} = \left(\frac{r}{z-z_0}\right)^2
\end{aligned} \quad (16.37)$$

Hence by comparison we find $\frac{r}{z-z_0} = \frac{1}{\sqrt{1-\lambda^2(\nu_0^2+\mu_0^2)}}$. This inserted into $f(\nu_0,\mu_0)$ gives simply $f(\nu_0,\mu_0) = r = \sqrt{(x-x')^2+(y-y')^2+(z-z_0)^2}$. This looks already fine since the saddle-point integral gives now so far:

$$\frac{2\pi e^{\left[ikr+\frac{\pi}{2}\right]}}{k\sqrt{f_{\nu\nu}f_{\mu\mu}-f_{\nu\mu}^2}} \tag{16.38}$$

Now we have to compute the denominator of the saddle-point integral:

$$\begin{aligned}
\frac{\partial^2 f}{\partial\nu^2} &= -\lambda^2(z-z_0)\frac{\partial\left[\nu\left\{1-\lambda^2(\nu^2+\mu^2)\right\}^{\frac{1}{2}}\right]}{\partial\nu} = \qquad (16.39)\\
&= -\lambda^2(z-z_0)\frac{1-\lambda^2\mu^2}{(\sqrt{\ldots})^3};\quad \frac{\partial^2 f}{\partial\mu^2} = -\lambda^2(z-z_0)\frac{1-\lambda^2\nu^2}{(\sqrt{\ldots})^3};\\
\frac{\partial^2 f}{\partial\nu^2}\frac{\partial^2 f}{\partial\mu^2} &= \frac{\lambda^4(z-z_0)^2}{(\sqrt{\ldots})^6}(1-\lambda^2\nu^2)(1-\lambda^2\mu^2);\quad \frac{\partial f^2}{\partial\nu\partial\mu} = \frac{\lambda^4(z-z_0)\nu\mu}{(\sqrt{\ldots})^3}\\
\frac{\partial^2 f}{\partial\nu^2}\frac{\partial^2 f}{\partial\mu^2} - \left(\frac{\partial f^2}{\partial\nu\partial\mu}\right)^2 &= \frac{\lambda^4(z-z_0)^2}{(\sqrt{\ldots})^6}\left[(1-\lambda^2\nu^2)(1-\lambda^2\mu^2)-\lambda^4\nu^2\mu^2\right]
\end{aligned}$$

The square bracket is simply $(\sqrt{\ldots})^2$. Hence the content of the denominator root reduces to $\frac{\lambda^4(z-z_0)^2}{(\sqrt{\ldots})^4}$. This can be further simplified to $\frac{\lambda^4 r^4}{(z-z_0)^2}$ by using $\frac{1}{\sqrt{\ldots}} = \frac{r}{(z-z_0)}$. Now let us interpret the denominator geometrically:

$$\frac{1}{\sqrt{f_{\nu\nu}f_{\mu\mu}-f_{\nu\mu}^2}} = \frac{z-z_0}{\lambda^2 r^2} = \frac{1}{\lambda^2}\frac{z-z_0}{r}\frac{1}{r} \tag{16.40}$$

From the Fig. 16.9 we conclude $\frac{z-z_0}{r} = \cos\epsilon = \sqrt{\ldots}$. Now all parts of the saddle-point integral are ready:

$$\frac{2\pi e^{ikf(\nu_0,\mu_0)+\frac{\pi}{2}}}{k\sqrt{f_{\nu\nu}f_{\mu\mu}-f_{\nu\mu}^2}} = \cos\epsilon\,\frac{e^{i(kr+\frac{\pi}{2})}}{\lambda r} \approx \iint\limits_{\nu\,\mu} e^{2\pi i[\nu(x-x')+\mu(y-y')+\sqrt{1+\lambda^2(\nu^2+\mu^2)}\frac{(z-z_0)}{\lambda}]}\mathrm{d}\nu\mathrm{d}\mu \tag{16.41}$$

This inserted into the RSD formula (Eq. 16.26) gives:

$$\boxed{u(x,y,z) \approx \frac{1}{\lambda}\underbrace{\iint u(x',y',z_0)\frac{\cos\epsilon}{r}e^{i\left(kr+\frac{\pi}{2}\right)}\mathrm{d}x'\mathrm{d}y'}_{\mathrm{Kirchhoff-Integral}}} \tag{16.42}$$

This took us about two pages. With a little bit less rigor it would have been much faster. Assume $\sqrt{1-\lambda^2(\nu^2+\mu^2)} \approx 1-\frac{\lambda^2(\nu^2+\mu^2)}{2}$ This means that we concentrate on not-too-large

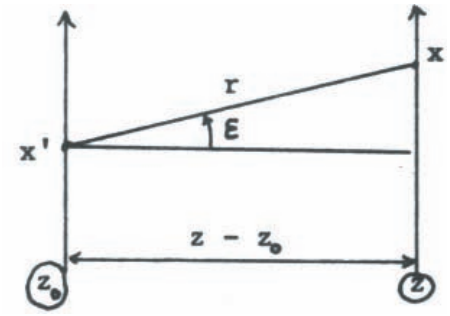

Figure 16.9: Graphical interpretation of Eq. 16.40

spatial frequencies. A more geometrical interpretation of this approximation means that we assume:

$$\cos\epsilon = \sqrt{1-\sin^2\epsilon} \approx 1 - \frac{1}{2}\sin^2\epsilon; \quad \cos\epsilon = \sqrt{1-\lambda^2(\nu^2+\mu^2)} \tag{16.43}$$

We apply again the saddle point method for $\left\{ \iint e^{\left[2\pi i[\nu(x-x')+\mu(y-y')+\frac{(z-z_0)}{\lambda}-\frac{\lambda}{2}(\nu^2+\mu^2)]\right]} \mathrm{d}\nu\mathrm{d}\mu \right\}$. Now we have:

$$\begin{aligned}
f(\nu,\mu) &= \lambda\nu(x-x') + \lambda\mu(y-y') + (z-z_0) - \lambda^2(\nu^2+\mu^2)\frac{(z-z_0)}{2} \\
\frac{\partial f}{\partial \nu} &= 0 = \lambda(x-x') - \lambda(z-z_0)\nu \rightarrow \nu_0 = \frac{(x-x')}{\lambda(z-z_0)}; \quad \mu_0 = \frac{y-y'}{\lambda(z-z_0)} \\
\frac{\partial^2 f}{\partial \nu^2} &= -\lambda^2(z-z_0) = \frac{\partial^2 f}{\partial \mu^2}; \quad \frac{\partial^2 f}{\partial \nu \partial \mu} = 0; \quad \sqrt{f_{\nu\nu}f_{\mu\mu} - f_{\nu\mu}^2} = \lambda^2(z-z_0) \\
f(\nu_0,\mu_0) &= \frac{(x-x')^2}{z-z_0} + \frac{(y-y')^2}{z-z_0} + (z-z_0) - \frac{1}{2}\frac{(x-x')^2+(y-y')^2}{z-z_0} \\
&= (z-z_0) + \frac{(x-x')^2+(y-y')^2}{2(z-z_0)}
\end{aligned} \tag{16.44}$$

Hence:

$$\left\{ \iint e^{2\pi i\left[\nu(x-x')+\mu(y-y')+\left[1-\frac{\lambda^2}{2}(\nu^2+\mu^2)\right]\frac{z-z_0}{\lambda}\right]} \mathrm{d}\nu\mathrm{d}\mu \right\} \approx \tag{16.45}$$

$$= \frac{e^{i\left[k(z-z_0)+\frac{\pi}{2}\right]}}{\lambda(z-z_0)} e^{i\pi\frac{\left[(x-x')^2+(y-y')^2\right]}{\lambda(z-z_0)}}$$

Inserted into the second form of RSD we get:

$$\boxed{u(x,y,z) \approx \frac{e^{i\left[k(z-z_0)+\frac{\pi}{2}\right]}}{(z-z_0)} \iint u(x',y',z_0) e^{i\pi \frac{\left[(x-x')^2+(y-y')^2\right]}{\lambda(z-z_0)}} \mathrm{d}x'\mathrm{d}y'} \tag{16.46}$$

This is called the quadratic or parabolic approximation of HFK. In essence the process of Fresnel diffraction is described in this approximation by a Fresnel transformation. That is why Mertz gave this name to this transform. Hence we can use the FRS-TRAFO tools as developed earlier. However there are some minor differences: a constant factor; two-dimensional; scale change $(\lambda(z-z_0))$.

16.6 The sampling theorem for FRS-diffraction

The "parabolic HFK" can be written briefly as:

$$\begin{aligned} u(x,y,z) &= c \iint u(x',y',z_0) e^{i\pi \frac{\left[(x-x')^2+(y-y')^2\right]}{\lambda(z-z_0)}} \mathrm{d}x'\mathrm{d}y' = \\ &= c\, e^{i\pi \frac{(x^2+y^2)}{\lambda(z-z_0)}} \iint \left\{ u(x',y',z_0) e^{i\pi \frac{(x'^2+y'^2)}{\lambda(z-z_0)}} \right\} e^{-2\pi \frac{(x'xy'y)}{\lambda(z-z_0)}} \mathrm{d}x'\mathrm{d}y' \end{aligned} \tag{16.47}$$

Let us call the $\{\ldots\}$ temporarily $v(x',y')$. Now assume that $u(x',y',z_0)$ is only $\neq 0$ in $|x'| \leq \frac{P}{2}$ and $|y'| \leq \frac{Q}{2}$. Hence the same is true for $v(x',y')$. The integral is a *Fourier* integral:

$$\iint v(x',y') e^{-2\pi i\left[\frac{x'x}{\lambda(z-z_0)}+\frac{yy'}{\lambda(z-z_0)}\right]} \mathrm{d}x'\mathrm{d}y' = \tilde{v}\left(\frac{x}{\lambda(z-z_0)}, \frac{y}{\lambda(z-z_0)}\right) \tag{16.48}$$

Due to the sampling theorem we can write:

$$\tilde{v}(\nu,\mu) = \sum_n \sum_m \tilde{v}\left(\frac{n}{P}, \frac{m}{Q}\right) \mathrm{sinc}(\nu P - n)\, \mathrm{sinc}(\mu Q - m) \tag{16.49}$$

Now we insert $\lambda\nu = \frac{x}{z-z_0}$ and $\lambda\mu = \frac{y}{z-z_0}$:

$$\begin{aligned} \tilde{v}\left(\frac{x}{\lambda(z-z_0)}, \frac{y}{\lambda(z-z_0)}\right) = \sum_n \sum_m \tilde{v}\left(\frac{n}{P}, \frac{m}{Q}\right) \mathrm{sinc}\left(\frac{xP}{\lambda(z-z_0)} - n\right) \cdot \\ \cdot \mathrm{sinc}\left(\frac{yQ}{\lambda(z-z_0)} - m\right) \end{aligned} \tag{16.50}$$

This inserted into $u(x,y,z) = c\, e^{i\pi \frac{x^2+y^2}{\lambda(z-z_0)}}\, \tilde{v}\left(\frac{x}{\lambda(z-z_0)}, \frac{y}{\lambda(z-z_0)}\right)$ give a sampling representation for $u(x,y,z)$, and we know already the sampling step width: $\delta x = \frac{\lambda(z-z_0)}{P}$; $\delta y = \frac{\lambda(z-z_0)}{Q}$. But it is not quite satisfactory still to have $\tilde{v}$ appear in our formula. What is

$\tilde{v}\left(\frac{n}{P},\frac{m}{Q}\right)$? To find out we take the special coordinate values $x = \frac{N\lambda(z-z_0)}{P}$ and $y = \frac{M\lambda(z-z_0)}{Q}$; ($n, M$ integers). Then, in the sampling series only the term $(n = N, m = M)$ will survive, since all other sinc-terms are zero. This leaves us with:

$$u\left(\frac{N\lambda(z-z_0)}{P},\frac{M\lambda(z-z_0)}{Q},z\right) = c\, e^{i\pi\left[\left(\frac{N}{P}\right)^2+\left(\frac{M}{Q}\right)^2\right]\lambda(z-z_0)}\tilde{v}\left(\frac{N}{P},\frac{M}{Q}\right) \quad (16.51)$$

We use this for replacing $\tilde{v}\left(\frac{n}{P},\frac{m}{Q}\right)$ in the sampling:

$$\boxed{\begin{array}{c} u(x,y,z) = \sum_n \sum_m u\left(\frac{n\lambda(z-z_0)}{P},\frac{m\lambda(z-z_0)}{Q},z\right) e^{i\pi[\ldots]} \\ \operatorname{sinc}\left(\frac{xP}{\lambda(z-z_0)}-n\right)\operatorname{sinc}\left(\frac{yQ}{\lambda(z-z_0)}-m\right) \\ [\ldots] = \frac{x^2+y^2}{\lambda(z-z_0)} - \lambda(z-z_0)\left\{\left(\frac{n}{P}\right)^2+\left(\frac{m}{Q}\right)^2\right\} \end{array}} \quad (16.52)$$

16.7 Justification of Young's Diffraction Theory (YMR)

As stated on page 142 Thomas Young said that diffraction takes place at the edge of a slit (for example), and not *within* the slit as Huygens had claimed. We want now to show that both points of view are right. More specifically we want to show that not only the HFK spherical wave theory can be derived from the RSD plane wave theory but also the YMR edge wave theory. By "edge wave" we mean a cylinder wave, but multiplied by an angle-dependent amplitude factor. We consider now diffraction on a slit of width B.

$$\begin{aligned} z<0 \quad &: \quad u(x,z) = e^{ikz} \\ z=-0 \quad &: \quad u(x,-0) = 1 \\ z=+0 \quad &: \quad u(x,+0) = \operatorname{rect}\left(\frac{x}{B}\right) \end{aligned} \quad (16.53)$$

For computing $u(x,z)$ for $z>0$ we use the second form of the RSD integral (Eq. 16.26), here for two dimensions only:

$$u(x,y) = \iint u(x',+0)e^{2\pi i\left[\nu(x-x')+\sqrt{1-\lambda^2\nu^2}\frac{z}{\lambda}\right]}\mathrm{d}x'\mathrm{d}\nu \quad (16.54)$$

Now we insert $u(x',+0) = \operatorname{rect}\left(\frac{x'}{B}\right)$ and get

$$\begin{aligned} u(x,z) &= \int \frac{e^{-i\pi\nu B} - e^{+i\pi\nu B}}{-2\pi i\nu} e^{2\pi i\left(\nu x + \sqrt{\cdots}\frac{z}{\lambda}\right)} \mathrm{d}\nu \\ &= Y\left(x - \frac{B}{2}, z\right) - Y\left(x + \frac{B}{2}, z\right); \\ Y(x,z) &= \frac{i}{2\pi} \int \frac{1}{\nu} e^{2\pi i\left(\nu x + \sqrt{\cdots}\frac{z}{\lambda}\right)} \mathrm{d}\nu \end{aligned} \tag{16.55}$$

We will now show that $Y(x,z)$ is something like a cylinder wave emerging from $x = 0$ and $z = 0$. If that is so then $Y(x - B/2, z) - Y(x + B/2, z)$ consists of two cylinder waves emerging from the edges of the slit at $z = 0$ at $x = \frac{+B}{2}$ and $x = \frac{-B}{2}$, just as stipulated by Young.

The disagreeable feature about the $Y(x,z)$ integral is the singularity at $\nu = 0$. Therefore we attack the problem at a slow pace, first looking at some general features like symmetries. One is $Y(0,z) = 0$ since for $x = 0$ the integrand is antisymmetric. Another feature is $Y(+x,z) = +Y(-x,z) = 0$ or $Y(-x,z) = -Y(+x,z)$. This becomes obvious if we write $Y(+) + Y(-)$ as a single integral, which has an antisymmetric integrand. Therefore the integral vanishes.

Now we do something which is shaky. We apply the method of stationary phase to the Y-integral. This would be all right if $\nu = 0$ would not be within the range of integration. So let's exclude the singularity for a moment. The phase is:

$$\begin{aligned} \varphi &= 2\pi(\nu x + \sqrt{1 - \lambda^2\nu^2}\frac{z}{\lambda}); \qquad \frac{1}{2\pi}\frac{\mathrm{d}\varphi}{\mathrm{d}\nu} \ldots = x - z\frac{\lambda\nu}{\sqrt{\cdots}}; \\ \frac{\mathrm{d}\varphi}{\mathrm{d}\nu} &= 0 \to \frac{\lambda\nu_0}{\sqrt{\cdots}} = \frac{x}{z} = \tan\epsilon; \\ \lambda\nu_0 &= \sin\epsilon; \quad \sqrt{1 - \lambda^2\nu_0^2} = \cos\epsilon; \quad x = r\sin\epsilon; \quad z = r\cos\epsilon \end{aligned} \tag{16.56}$$

Hence the phase becomes $\frac{2\pi r}{\lambda} = kr$ for the stationary point ν_0. Let us not worry about the root-denominator since we don't intend to be quantitative in all details anyway. But we can see already the most important features of the edge wave $Y(x,z)$ which are expressed in this Fig. 16.10.

To prove that the singularity $\frac{1}{\nu}$ is harmless it is convenient to introduce new variables $\lambda\nu = \sin\epsilon$; $\sqrt{\cdots} = \cos\epsilon$; $x = r\sin\epsilon$; $z = r\cos\epsilon$; $\lambda\mathrm{d}\nu = \cos\epsilon\ \mathrm{d}\epsilon$. Now the exponential of the Y-integral can be written as:

$$e^{ikr\cos(\epsilon - \varphi)} = \sum_{-\infty}^{+\infty} J_n(kr) e^{in\left(\epsilon - \varphi + \frac{\pi}{2}\right)} \tag{16.57}$$

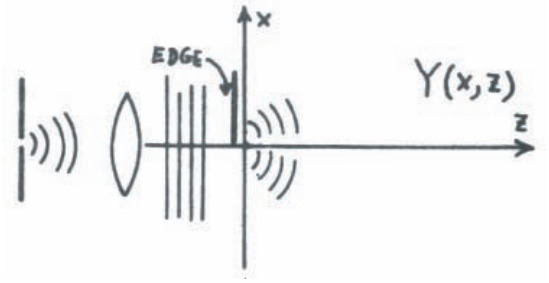

Figure 16.10: The most important features of the edge waves.

Furthermore we combine the $(+n)$ and $(-n)$ terms, considering that $J_{-n} = (-1)^n J_{+n}$. Thereby many terms drop out because that particular integrand is antisymmetric. The terms with symmetric integrands do not blow up since the zero-values of the denominator are fully compensated as in this expressions:

$$\frac{\sin(n\epsilon)}{\sin\epsilon};\ \text{which has}\ |\ldots| \leq |n| \tag{16.58}$$

Most of the terms are small for other reasons since $J_n(kr)$ is significant only if $|kr|$ equals roughly the index $|n|$ of the Bessel function.

All these considerations together don't clearly define the edge wave $Y(x,z)$. But it is obvious that Y has the main features of a cylinder wave emerging from a slit edge. This is enough to know since we don't intend to apply the YMR theory for any specific purpose. However, we want to show that this edge wave $Y(x,z)$ is relevant (not only) for all piece-wise constant objects (Fig. 16.11).

$$u(x,0) = \sum u_n \text{rect}\left[\frac{x - \frac{(x_n + x_{n+1})}{2}}{x_{n+1} - x_n}\right] \tag{16.59}$$

This representation of the piece-wise constant object can be interpreted as many slits of width $n_{n+1} - x_n$ side-by-side, closely packed, with amplitudes u_n. Hence we can generalize the earlier result from the single-slit case to this many-slit case:

$$u(x,z) = \sum u_n \left[Y(x - x_{n+1}, z) - Y(x - x_n, z)\right] \tag{16.60}$$

In this expression a specific edge x_m will occur twice, once as $-u_m Y(x - x_m, z)$ and once more as $u_{m-1} Y(x - x_m, z)$. We rearrange the two sums accordingly, which implies the arithmetic step $n + 1 = m$ in the first sum, and get

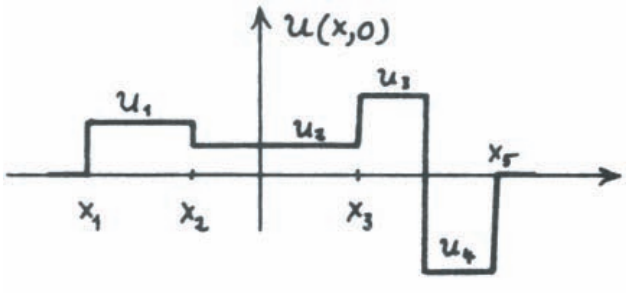

Figure 16.11: The piecewise constant function $u(x,0)$.

$$u(x,z) = \sum (u_{m-1} - u_m) Y(x - x_m, z) = \sum \Delta u_m Y(x - x_m, z) \tag{16.61}$$

This means that edge waves emerge from every step of the object at x_m. The amplitudes of these edge waves are determined by the step height Δu_m.

A slightly different approach would have yielded the same result. Instead of subdividing the objects into edges like shown in Fig. 16.11 we may subdivide it into Heavyside stepfunctions (Fig. 16.13).

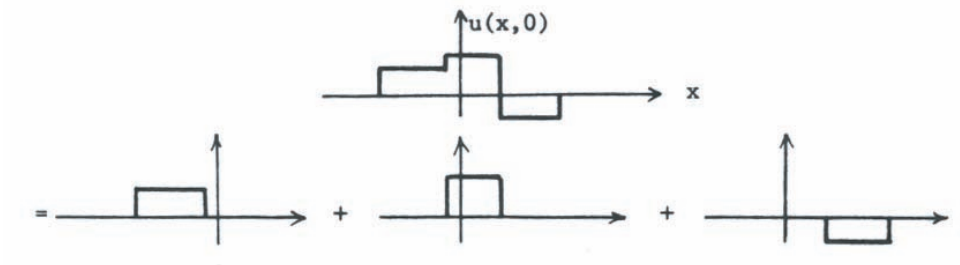

Figure 16.12: Subdivision of $u(x,0)$.

In formulas this means:

$$\begin{aligned} u(x,0) &= \sum u_n \mathrm{rect}\left[\frac{x - \frac{x_n + x_{n+1}}{2}}{(x_{n+1} - x_n)}\right] \\ &= \sum \Delta u_n H(x - x_n) \\ H(x - x_n) &= \begin{cases} +1: & \text{if } x - x_n \geq 0; \text{ or } x \geq x_n \\ 0: & \text{if } x - x_n < 0; \text{ or } x < x_n \end{cases} \end{aligned} \tag{16.62}$$

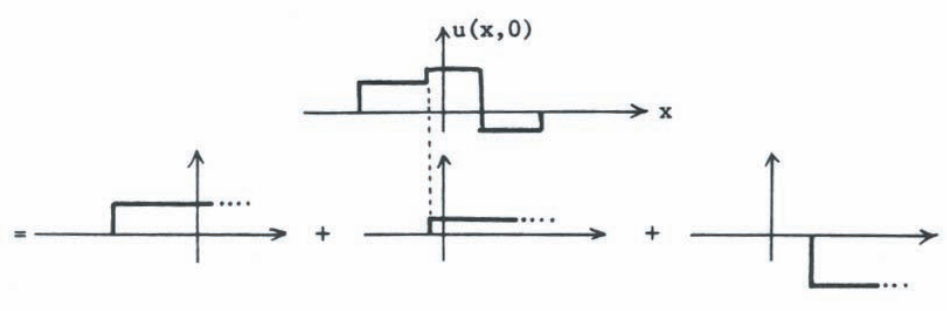

Figure 16.13: Subdivision of u(x,0) into Heavyside stepfunctions.

With the latter form of our object inserted into the RSD formula we find that the edge wave $Y(x - x_n, z)$ is obviously the "response" to the "Heavyside-object" $H(x - x_n)$.

We can generalize our YMR theory one step further by allowing now continuous objects. As always in calculus we think of the truly continuous function as a multi-step function with infinitesimally fine steps. As the Fig. 16.14 below indicate this may lead to a "Dirac-decomposition" or to a "Heavyside decomposition" of the object $u(x, 0)$.

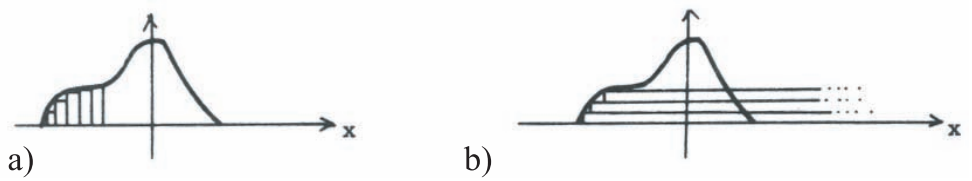

Figure 16.14: Decomposition of a continuous function into a) dirac-distributions; b) Heavyside-functions.

$$u(x,0) = \int u(x',0)\delta(x-x')\mathrm{d}x'; \qquad u(x,0) = \int u'(x',0)H(x-x')\mathrm{d}x' \quad (16.63)$$

The last form or "Heavyside form" needs some more support:

$$\int_{-\infty}^{\infty} u'(x',0)H(x-x')\mathrm{d}x' = \int_{-\infty}^{\infty} \left[\frac{\mathrm{d}u(x',0)}{\mathrm{d}x'}\right] H(x-x')\mathrm{d}x' \quad (16.64)$$

$$H(x-x') = \begin{cases} +1: & \text{if } x-x' \geq 0; \text{ or } x' \geq x \\ 0: & \text{if } x-x' < 0; \text{ or } x' < x \end{cases}$$

Hence we can express the effect of $H(x - x')$ by the limits of integration:

$$\int_{-\infty}^{\infty} \left[\frac{\mathrm{d}u(x', 0)}{\mathrm{d}x'} \right] \mathrm{d}x' = u(x, 0) - u(-\infty, 0) = u(x, 0) \tag{16.65}$$

Before closing these YMR considerations be reminded again how important it was that the wave equation is a *linear* differential equation. That is why it is allowed to split up an arbitrary object into many little slits or into many Heavyside steps, whichever we may find convenient. Knowing then the wavefield behind a slit or behind an edge or behind any other conceivable "elementary object" allows us to put together the wavefield behind an arbitrary object, if we know how this arbitrary object is built together from many elementary objects. How convenient! But how tempting to believe the world is always governed by linear laws. The consequences are very far-reaching. For example, as long as we describe quantum theory by the *linear* Schrödinger equation we will have to live with the Uncertainty Principle, which was the outcome of linear Fourier mathematics. The Uncertainty Principle would not necessarily occur in a nonlinear theory and hence one might overcome the ugly wave-particle duality. This is indeed the goal of some elementary-particle theoreticians like Heisenberg and de Broglie. But the math becomes a real mess. It seems as if the limitations of the human brain prevent us from understanding nature better than we do now. Can digital computers help? I doubt it. As I see it a scientist can let a computer solve only those problems that he has understood already in principle.

17 More About Evanescent Waves

On p. 151 we discussed the significance of the evanescent waves for the fundamental limit of resolution. In that case the evanescent waves played a negative role, in that *their* absence meant something. However, evanescent waves are also useful directly. For example a light wave travelling in a thin light fiber or a thin film (thickness of the order of one or a few wavelights), parts of the light will travel *outside* of the thin film in the form of evanescent waves. Even if the film itself is "lossy" (absorption, scattering) this does not reduce the amplitude propagation of the evanescent wave. Hence light fibers have much losses than one would expect when considering only the absorption coefficient of glass bulk material. Investigations of this type belong into the field of "Integrated Optics", which tries to solve data communications and processing problems, for example for light wave telephones in urban centers. Integrated Optics is booming now like the laser field did in the early sixties, and holography in the late sixties. Ultimately contributions to the solution of important problems might arise which utilize all three fields in combination.

Another speculated application of evanescent waves was mentioned briefly already on p. 151: Particle Acceleration by Light Waves. At the time the attached IBM Note TN-5 was written, only very unstable Ruby lasers were available. Now powerful CO_2 lasers are relatively cheap. Their long wavelength $(10.6\mu m)$ makes all tolerances much easier to satisfy. So if anyone still wants to accelerate particles he probably could do it quite well with lasers. For understanding the proposed system one has to know how light waves behave at boundaries. Since this behaviour is important in many other instances as well we, will study it now.

17.1 Boundary conditions for $\vec{E}$ and $\vec{H}$; Fresnel coefficients

Integration of the first Maxwell equation, and use of Stoke's lemma yields:

$$\begin{aligned} \operatorname{curl} \vec{E} &= -\dot{\vec{B}} \\ \int_{(O)} \operatorname{curl} \vec{E}\, \mathrm{d}\vec{o} &= -\int_{(O)} \dot{\vec{B}}\, \underbrace{\mathrm{d}\vec{o}}_{\substack{\text{surface differential on the surface (O)}}} = \underbrace{\oint}_{\substack{\text{integration path around (O)}}} \vec{E}\, \underbrace{\mathrm{d}\vec{s}}_{\substack{\text{path element at periphery of (O)}}} \end{aligned} \tag{17.1}$$

This integral-version of the first Maxwell equation will now be applied to the scene shown in Fig. 17.1:

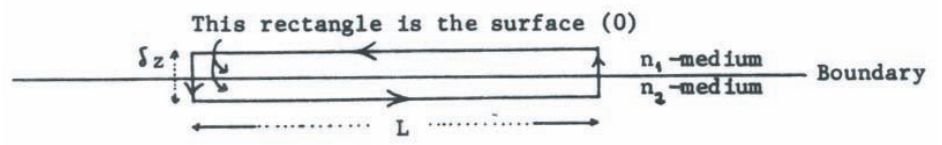

Figure 17.1: The situation at the boundary between media with different refractive indices.

$$\oint \vec{E}\,\mathrm{d}\vec{s} \approx L\,E_{2\mathrm{tangential}} + \delta z E_{\mathrm{normal}} - L E_{1\mathrm{tangential}} - \delta z E_{\mathrm{normal}} \tag{17.2}$$

L is assumed to be small, and δz *very* small. Even if the E_{normal} at the two boundary crossings are not exactly alike, yet these terms are $\ll L E_{\mathrm{tangential}}$ because $\delta z \ll L$. Hence:

$$\oint \vec{E}\,\mathrm{d}\vec{s} \approx L(E_{2\mathrm{tangential}} - E_{1\mathrm{tangential}}) \tag{17.3}$$

The other part of the first Maxwell equation is:

$$-\oint \dot{\vec{B}}\,\mathrm{d}\vec{o} \approx L\,\delta z \dot{B}_{\mathrm{average}} \ll L\,E_{\mathrm{tangential}} \tag{17.4}$$

because δz is so small.

Hence $\oint \vec{E}\,\mathrm{d}\vec{s} = -\int \dot{\vec{B}}\mathrm{d}\vec{o}$ yields:

$$\boxed{E_{2\ \mathrm{tangential}} = E_{1\ \mathrm{tangential}}} \tag{17.5}$$

Similarly $\mathrm{curl}\vec{H} = \dot{\vec{D}} + \vec{I}$ yields:

$$\boxed{H_{2\ \mathrm{tangential}} = H_{1\ \mathrm{tangential}}} \tag{17.6}$$

Personally, I would not trust this derivation of continuity of the tangential components of $\vec{E}$ and $\vec{H}$, if the consequences of these boundary conditions were not so well confirmed experimentally, as they actually are. A sizable industry, "Thin Films", is based on the correctness of these consequences, called *"Fresnel's Reflection and Transmittance Coefficients"*. They are the amplitude ratios and phase shifts of the following three electromagnetic plane

waves: incident wave with $\vec{k_1} = n_1 k_0[\hat{x}\sin\alpha_1 + \hat{z}\cos\alpha_1]$; reflected wave with $\vec{k_R} = n_1 k_0[\hat{x}\sin\alpha_1 - \hat{z}\cos\alpha_1]$ and transmitted wave with $\vec{k_2} = n_2 k_0[\hat{x}\sin\alpha_2 + \hat{z}\cos\alpha_2]$ (Fig. 17.2). These three wave vectors are all in the same plane. Hence we could choose a coordinate system so that all y-components are zero. However the E-fields themselves might very well have a y-component, which is usually called the σ-component ($\sigma \approx S$ = "senkrecht" = perpendicular to the plane of incidence, containing $\vec{k_1}$ and the surface normal). The σ-wave has its own story, independent of the π-wave (π = parallel to plane of incidence), which has $\vec{E}$-fields with x- and z-components. An H_π is tied to E_σ, and an H_σ to E_π.

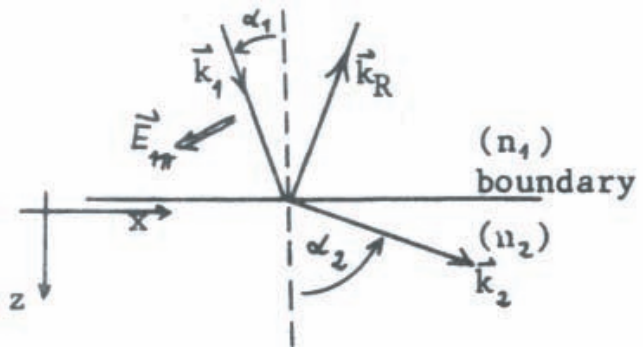

Figure 17.2: Reflection at a boundary: notation of the $\vec{k}$-vectors.

What Fresnel derived from the boundary conditions were the following ratios of complex amplitudes:

$$\frac{A_{R\pi}}{A_{1\pi}}; \quad \frac{A_{2\pi}}{A_{1\pi}}; \quad \frac{A_{R\sigma}}{A_{1\sigma}}; \quad \frac{A_{2\sigma}}{A_{1\sigma}} \tag{17.7}$$

These terms are defined in the following way:

$$\begin{aligned} \text{incident wave}: &\quad [\hat{y}A_{1\sigma} + (\hat{x}\cos\alpha_1 - \hat{z}\sin\alpha_1)A_{1\pi}]e^{i\vec{k_1}\vec{x}} = E_1 \\ \text{reflected wave}: &\quad [\hat{y}A_{R\sigma} + (\hat{x}\cos\alpha_1 + \hat{z}\sin\alpha_1)A_{R\pi}]e^{i\vec{k_R}\vec{x}} = E_R \\ \text{transmitted wave}: &\quad [\hat{y}A_{2\sigma} + (\hat{x}\cos\alpha_2 - \hat{z}\sin\alpha_2)A_{2\pi}]e^{i\vec{k_2}\vec{x}} = E_2 \end{aligned} \tag{17.8}$$

The cos and sin are such that $\vec{E_1}\vec{k_1} = 0$ etc., as you know from E&M theory; similarly for $\vec{H}$. Now form the tangential components (omit z-components) and fix $\vec{x}$ to the boundary plane $z = 0$. In medium (n_1) we have $\vec{E_1} + \vec{E_R}$, in (n_2), $\vec{E_2}$.

$$\begin{aligned} & \hat{y}[A_{1\sigma}e^{in_1k_0x\sin\alpha_1} + A_{R\sigma}e^{in_1k_0x\sin\alpha_1}] + \hat{x}\cos\alpha_1(A_{1\,\pi} + A_{R\pi})e^{in_1k_0x\sin\alpha_1} \\ = \quad & \hat{y}A_{2\sigma}e^{ik_0n_2x\sin\alpha_2} + \hat{x}\cos\alpha_2 A_{2\pi}e^{ik_0n_2x\sin\alpha_2} \end{aligned} \tag{17.9}$$

Equality of these $E_{\text{tangential}}$ vectors in $z = 0$ reduces to two separate equation for the $\hat{y}$- and the $\hat{x}$-components:

$$(A_{1\sigma} + A_{R\sigma})e^{ik_0 x n_1 \sin\alpha_1} = A_{2\sigma} e^{ik_0 x n_2 \sin\alpha_2} \tag{17.10}$$

If there is any σ-wave in the (n_2)-medium, then $A_{2\sigma}$ must be $\neq 0$. If $A_2 \neq 0$, then we can remodel that equation into:

$$\frac{A_{1\sigma} + A_{R\sigma}}{A_{2\sigma}} = e^{ik_0 x(n_2 \sin\alpha_2 - n_1 \sin\alpha_1)} \tag{17.11}$$

The left-hand term is a constant as far as x is concerned. Hence the other side of the equation must be constant too. That requires $n_2 \sin\alpha_2 - n_1 \sin\alpha_1 = 0$, which is Snell's law. Then $A_{1\sigma} + A_{R\sigma} = A_{2\sigma}$; similarly $(A_{1\pi} + A_{R\pi})\cos\alpha_1 = A_{2\pi}\cos\alpha_2$. Similar results follow from the continuity of the H-waves $\vec{H} = Ce^{i\vec{k}\vec{x}}$ for the coefficients $C_{1\pi}$, $C_{R\pi}$, $C_{2\pi}$, $C_{1\sigma}$, $C_{R\sigma}$, $C_{2\sigma}$. Finally, Maxwell is used once more for connecting the $A\ldots$ and the $C\ldots$, so that we have enough equations for solving them all, with $A_{1\sigma}$ and $A_{1\pi}$ being the supposedly known coefficients of the wave coming from the source.

Anyway, what matters here for our study of evanescent waves is $k_{1x} = k_{2x}$ (or $k_0 n_1 \sin\alpha_1 = k_0 n_2 \sin\alpha_2$). k_{1x} and k_{2x} on the other hand are tied with k_{1z} and k_{2z}, respectively, due to the wave equations in those two media:

$$\begin{array}{lll} \left\{\nabla^2 + (n_1 k_0)^2)\right\} u = 0 & \left\{\nabla^2 + (n_2 k_0)^2\right\} u = 0 & \\ k_{1x}^2 + k_{1z}^2 = k_1^2 = n_1^2 k_0^2 & k_{2x}^2 + k_{2z}^2 = k_2^2 = n_2^2 k_0^2 & (k_{iy} \text{ was zero}) \end{array} \tag{17.12}$$

Now we can deduce that k_{2z} may get imaginary, which is what causes $\vec{E}$ to be an evanescent wave:

$$k_{2z}^2 = k_2^2 - k_{2x}^2 = k_0^2 n_2^2 - k_{2x}^2 = k_0^2 n_2^2 - k_{1x}^2 = k_0^2 n_2^2 - k_0^2 n_1^2 \sin^2\alpha_1 \tag{17.13}$$

due to $k_{1x} = k_{2x}$ from boundary condition:

$$k_{2z}^2 = k_0^2(n_2^2 - n_1^2 \sin^2\alpha_1) \rightarrow k_{2z}^2 \text{ negative and } k_{2z} \text{ imaginary} \tag{17.14}$$

if $n_1^2 \sin\alpha_1 > n_2^2$, or $|\sin\alpha_1| > \frac{n_2}{n_1}$. In that case we will call $k_{2x} = k'$ and $k_{2z} = ik''$, in order to get the old form:

$$\vec{E_2} \propto e^{ik'x} e^{-k''z} \tag{17.15}$$

17.2 A more abstract look at evanescent waves

Put $v(\vec{x},t) = e^{i(\vec{k}\vec{x}-\omega t)}$ into $\nabla^2 v - \frac{\ddot{v}}{c^2} = 0$:

$$\left\{-\vec{k}\vec{k} + \frac{\omega^2}{c^2}\right\} v(\vec{x},t) = 0 \tag{17.16}$$

$\vec{k}\vec{k} = \frac{\omega^2}{c^2}$; ω and c are real, also $\vec{k}\vec{k}$ has to be real, but this does not force $\vec{k}$ to be real. $\vec{k}$ can be $\vec{k} = \vec{k'} + i\vec{k''}$ ($\vec{k'}$ is the real part, $i\vec{k''}$ is the imaginary part).

$$(\vec{k'} + i\vec{k''}) \cdot (\vec{k'} + i\vec{k''}) = k'^2 + \underbrace{2i\vec{k'}\vec{k''}}_{\text{this must be zero}} + k''^2 = k^2 \tag{17.17}$$

hence $\vec{k'} \perp \vec{k''}$ (orthogonal); $k'^2 = k^2 + k''^2 \rightarrow k'^2 \geq k^2$.

$$v(\vec{x},t) = \underbrace{e^{i(\vec{k'}\vec{x}-\omega t)}}_{\text{propagation}} \quad \underbrace{e^{-\vec{k''}\vec{x}}}_{\text{damping}}; \qquad \underbrace{v' = \frac{\omega}{k'} < \frac{\omega}{k} = c}_{\text{phase velocity}} \tag{17.18}$$

The phase velocity of the evanescent wave is $< c$. Since $\omega' = \omega$ and $\lambda' = \frac{2\pi}{k'}$, $\lambda' = \lambda$. From $k' = k^2 + k''^2$ follows:

$$\left(\frac{1}{\lambda'}\right)^2 = \left(\frac{1}{\lambda}\right)^2 + \left(\frac{1}{\lambda''}\right)^2; \qquad \frac{\lambda'}{\lambda''} = \sqrt{1 - \left(\frac{\lambda'}{\lambda}\right)^2} = \frac{1}{\sqrt{1 + \left(\frac{\lambda''}{\lambda}\right)^2}} \tag{17.19}$$

Interesting also are the *vectorial* properties of evanescent waves. Set $\vec{V}(\vec{x},t) = \{\hat{x}a + \hat{y}b + \hat{z}c\}\, v(\vec{x},t)$, where $\hat{x},\ \hat{y}$ and $\hat{z}$ are unit vectors and a, b, and c are constants.

$$v(\vec{x},t) = e^{i(\vec{k'}\vec{x}-\omega t)} e^{-\vec{k''}\vec{x}} \tag{17.20}$$

Since $\vec{k'}$ and $\vec{k''}$ are known to be orthogonal we might choose the coordinate system such that $\vec{k'} \| \hat{x}$ and $\vec{k''} \| \hat{y}$.

$$\Longrightarrow v(\vec{x},t) = e^{2\pi i\left[\frac{x}{\lambda'} - \nu t\right]} e^{-2\pi \frac{y}{\lambda''}} \tag{17.21}$$

$\left(\omega = 2\pi\nu;\ k' = \frac{2\pi}{\lambda};\ k'' = \frac{2\pi}{\lambda''}\right)$. Since $v(\vec{x},t)$ satisfies the wave equation, also $\vec{V}(\vec{x},t)$ will. More knowledge about the vector character of $\vec{V}$ can be derived from the third Maxwell equation $\mathrm{div}\vec{V} = 0$ ($\vec{V} \sim \vec{E}$; $\epsilon =$ const. assumed).

$$\mathrm{div}\vec{V} = a\frac{\partial v}{\partial x} + b\frac{\partial v}{y} + c\frac{\partial v}{\partial z} = 0 \tag{17.22}$$

Since $\frac{\partial v}{\partial z} = 0$, c may be anything. That c is one of the two polarization components. $\mathrm{div}\vec{V} = 2\pi v\left[i\frac{a}{\lambda'} - \frac{b}{\lambda''}\right] = 0 \rightarrow b = ia\frac{\lambda''}{\lambda'}$; $\quad \frac{\lambda''}{\lambda'} = \frac{1}{\sqrt{1-\left(\frac{\lambda'}{\lambda}\right)^2}} \geq 1.$

$$\underbrace{V_z}_{\text{transverse}} = c\, v(\vec{x},t); \qquad \vec{V}_{xy} = a\, v(x,t)\{\overbrace{\hat{x}}^{\text{long.}} + \underbrace{i\frac{\lambda''}{\lambda'}\hat{y}}_{\text{trans.}}\}; \qquad i = e^{i\frac{\pi}{2}} \tag{17.23}$$

$$\mathrm{Real}\{\vec{V}_{xy}\} = a\left\{\hat{x}\cos\left[2\pi\left(\frac{x}{\lambda'} - \nu t\right)\right] - \frac{\lambda''}{\lambda'}\hat{y}\sin\left[2\pi\left(\frac{x}{\lambda'} - \nu t\right)\right]\right\} e^{-2\pi\frac{y}{\lambda''}} \tag{17.24}$$

(Later we will see that these evanescent waves are good for an accelerator).

IBM TN-5

Electron Acceleration by Light Waves

October 3, 1962

A. Lohmann*

TECHNICAL

NOTE

Summary

Light, particularly in the form of evanescent waves, can be employed to accelerate charged particles. Since the field strength in LASER radiation is expected to be of the order of 10^9 V/m, an accelerator of significantly reduced dimensions based upon this concept appears feasible. The proposed accelerator works on what may be defined as the time-reversed Smith-Purcell effect.

Department 522
Photo-Optics
Technology

GPD Development
Laboratory
San Jose

*Resident Consultant 1961-62.
On leave of absence from Technische Hochschule, Braunschweig.

ELECTRON ACCELERATION BY LIGHT WAVES

I. Introduction

Increased physical size, providing longer accelerating paths, has been the trend of modern acceleration design aimed at higher particle energies. An alternative to this approach would be the utilization of greater field strength, if this were feasible.

It is our aim to set forth some ideas which may lead to the realization of this alternative through utilization of the high field strength attainable in optical MASER radiation.

The mechanism through which charged particles may be accelerated by light waves is related to an effect reported by Smith & Purcell.[1] This effect has been demonstrated to produce radiation in the visible and infrared region as a result of an electron traveling near the surface of a diffraction grating. The structure of the grating causes periodic motion of the charge induced on the surface by the moving electrons which in turn gives rise to radiation of frequency ν . This frequency is related to the electron velocity v and the grating pitch θ . According to grating manufacturers intense radiation sources based on this effect are now feasible. This implies the existence of gratings of sufficient flatness, controlled grating spacing and groove geometry to permit an electron beam to pass within maybe 1/2

the grating pitch over a reasonably extended grating comprising 50,000 grooves or more as reported by Smith & Purcell.

Now imagine the process reported by Smith & Purcell to occur in reverse. Light is incident upon the grating surface, and the electric field of the light wave will accelerate the electron. Since an electric field strength of 10^9 V/m in the radiation from an optical MASER is feasible, the reverse of the Smith-Purcell effect could be the basis for an unusually short accelerator.

To complete this introduction, attention is drawn to further considerations based on Toraldo di Francias'[2] explanation of the Smith-Purcell effect. His theory shows that the grating may consist equally well of a dielectric material and explains the role played by evanescent waves in the Smith-Purcell effect. Both of these concepts are more fully treated in what is to follow.

II. Acceleration by Generalized Plane Waves

The acceleration of electrons by light waves can best be described by considering two conditions which must be fulfilled: (1) the phase velocity V of the accelerating field must match the particle speed v where $v < c$ always holds; and (2) the electric field must have a component in the direction in which the particles travel.

Without loss of generality, we consider only plane waves moving parallel to the particle.

A monochromatic plane wave, moving in the z direction with phase velocity V, not dependent on the Y coordinate has the form:

-3-

$$U(x,z,t) = f(x) \cdot \exp\left[-i\omega\left(t - z/v\right)\right] \tag{1}$$

In a charge-free dielectric and homogeneous space, the wave equation

$$(\nabla)^2 U - (n/c)^2 \cdot \partial^2 U/\partial t^2 = 0 \tag{2}$$

then reduces to

$$d^2f/dx^2 + f \cdot (n\omega/c)^2 \cdot \left\{1 - (c/nV)^2\right\} = 0 \tag{3}$$

For convenience of notation let the term in brackets

$$\left\{1 - (c/nV)^2\right\} = \alpha \tag{4}$$

If $\alpha = 0$ one obtains the usual plane wave, $f =$ constant and $V = c/n$ but without a longitudinal component of the electric field.

If $\alpha > 0$ one obtains a plane wave with a transverse modulated amplitude $f(x) = \cos\left[(n\omega/c) \cdot \alpha^{1/2} \cdot x\right]$. Matching of the phase velocity V and the particle speed v is possible, since $\alpha > 0$ satisfies the condition for a phase velocity lower than the vacuum velocity of light, i.e. $c > V > c/n$. Moreover, this requires the particle beam to exist in the presence of matter in order to have a refractive index $n > 1$.

From Maxwell's divergency equation follows the existence of a longitudinal component in the electric field. These transverse modulated

plane waves should thus be able to accelerate electrons.

This was pointed out already by K. Shimoda[8] who proposed a gas filled cavity surrounded by a cylindrical MASER as an accelerator. He noted also, that his idea predicts the reverse process of the Cerenkov effect. This is indicated by the velocity condition $v = V > c/n$ and it follows immediately if one composes the transverse modulated plane wave by two symmetrically inclined ordinary plane waves:

$$2\cos[(n\omega/c)\,\alpha^{1/2}\cdot x]\,\exp[-i\omega(t-z/v)] =$$

$$\exp[ik(\alpha x+\gamma z)-\omega t]+\exp[ik(-\alpha x+\gamma z)-\omega t];\quad k=n\omega/c,\quad \alpha^2+\gamma^2=1$$

$$k_z = \omega/v = k\gamma = k\cos\varepsilon\,;\quad \cos\varepsilon = c/nv$$

The connection with the Cerenkov effect is evident, since the inclination ε of these two ordinary plane waves is given by the MACH formula.

III. Acceleration by Evanescent Plane Waves

If $\alpha < 0$ or $V < c/n$ the differential equation for the wave amplitude f(x) (eq. 3) has an exponential solution.

This leads to an evanescent wave of the form

$$U(x,z,t) = \exp[-k''x]\cdot\exp[i(k'z-\omega t)]$$

-5-

This is the only kind of a plane wave with a phase velocity v smaller than c even in vacuum ($n = 1$). In other words, this seems to be the only way to match the speed of the light phase with that of the particle when the process is to take place in vacuum.

IV. Means for Producing Evanescent Waves

Before proceeding with the discussion of the properties of evanescent waves, let us consider means for their production.

The existence of these waves has been predicted already by Lord Rayleigh in connection with Woods anomalies in grating diffraction. Under certain conditions the diffraction grating converts ordinary plane waves into evanescent waves. For their existence, it is necessary to have a wave vector k smaller than one of its components: $k < k_z$. The law of diffraction and refraction, which governs the tangential components of the wave vector at a boundary, as in Fig. 1, tells us when this will happen: $\sin\varphi' = n \cdot \sin\varphi + m\lambda/a$

(m = diffraction order)

$k_z = k \sin\varphi'$; $|k_z| > k \rightarrow |\sin\varphi'| > 1$

if $m = 0$, $n > 1/\sin\varphi$ (total reflection)

if $m \neq 0$ and $\varphi = 0$, $a < |m| \cdot \lambda$ (fine grating).

This indicates that total reflection and diffraction (not only at periodic objects and not only at normal incidence ($\varphi = 0$) can convert ordinary plane waves into evanescent waves. The dimension of the zone near the boundary, where the amplitude assumes large values, is given by the damping

length $\lambda'' = \lambda/(\sin^2\varphi' - 1)^{1/2}$. The phase velocity is $V = c/\sin\varphi'$. Here again one sees that the damping length goes to infinity, if the phase velocity and with it the speed of the particle approaches the speed of light in vacuum. This is of practical importance since the electron must travel in close proximity of the grating where the amplitude of the electric field is not seriously damped. Hence, the difficulty of guiding the electron becomes less critical already when the energy is several times higher than the rest energy.

V. Vectorial Properties of Evanescent Waves

One can consider evanescent waves as plane waves, having a complex wave vector:

$$k = k' + ik''; \quad k^2 = (n\omega/c)^2 = k'^2 - k''^2; \quad k' \perp k''$$

The wave equation tells us that the real and imaginary parts are normal to each other, e.g. in the z and x direction, respectively. The real part is longer than the wave vector $k' > k = n\omega/c$ of an ordinary plane wave. From that follows the inequality for the phase velocity

$$V = \omega/k' = \omega/k \cdot k/k' = c/n \cdot k/k' < c/n$$

One can define a damping length $\lambda'' = 2\pi/k''$ describing the attenuation of the amplitude along the x axis. This damping length λ'' is connected with the wavelength $\lambda' = 2\pi/k'$ and with the velocity $V = v = c \cdot \beta$

$$\lambda''/\lambda' = 1/(1-\beta^2)^{1/2}; \quad \lambda' = \beta\cdot\lambda; \quad (n=1)$$

This indicates that there will be essentially no damping if one approaches the speed of light in vacuum $\beta \to 1$

The vectorial properties of the evanescent waves follow from Maxwell's divergency equation; that is, the longitudinal component E_z is associated with the transverse component E_x as $ik' E_z = k'' E_x$ or

$$|E_z| = |E_x| (k''/k') = |E_x| (1-\beta^2)^{1/2}$$

$$E_{\frac{x}{z}} = A_{\frac{x}{z}} \exp[-k''x] \cdot \exp[i(k'z - \omega t)]$$

Hence, the longitudinal component E_z which produces the acceleration of the electrons will decrease when one approaches the vacuum speed of light.

The significance of this problem was pointed out by W. Panofsky;[4] possible means of its avoidance will be the subject of a future communication.

VI. Focussing and Phase Stability of the Particle Beam

The associated transverse component E_x will cause the electron to deviate from the desired path or cause defocussing of the electron beam. This is true also if one superposes two evanescent waves with opposite directions of damping. This means a replacement of the exponential amplitude function $f(x) = \exp[-k''x]$ by the hyperbolic cosine $\cosh[k''x]$. For this case the field lines are shown in Fig. 2. There, at $z - vt = \lambda'/2$ is a longitudinal saddle which can hold the electron at the phase velocity of the wave and thus provide acceleration. Since Maxwell's divergency equation forbids a crater but allows only saddles, one cannot provide phase stability and focus at the same time. If after a period of acceleration, the electron

is deviated too much towards the grating, we let it change into a transverse saddle (at $z - vt = \lambda'$). Indeed the field will have such a jump of $\lambda'/2$ if it arrives at a point above the grating where the spacing changes by half a period (see Fig. 2, far right). This phase jump has been demonstrated experimentally in the case when ordinary plane waves emerge from the grating. [5]

The transverse component is always greater than the longitudinal component of the electric field. Therefore, the distance required to refocuss the electron, i.e. the path length over which the electron rides in the transverse saddle, is a relatively small fraction of the grating length.

After a short distance, another jump in the grating will transfer the electron again to an accelerating saddle. Actually this proposal is nothing more than the implementation of Courant, Livingston, and Snyder's idea of the alternating gradient in this type of accelerator.

VII. Realization of Particle Acceleration by Light Waves

It may be somewhat premature to consider the problems of practical realization of an accelerator based upon the ideas here set forth. However, their early statement may lead to timely solutions.

The problem of guiding the electrons properly is certainly a delicate one. Since these difficulties seem to have been resolved in the case of Smith-Purcell radiation sources, they should not be an obstacle in the case of an accelerator based upon the inverse process.

Especially for high speed electrons the alignment may become easier, since the transverse damping length λ'' of the accelerating field increases by a factor of $\beta(1-\beta^2)^{1/2}$.

The phase of the accelerating field has to be stable for the time of interaction, which may be about 10^{-9} sec. for a 30 cm grating. This is feasible for light generated by an optical MASER.

Repetitive interaction with a grating by virtue of a circular path appears difficult to realize in terms of phase stability at optical wave length over many revolutions. This possibility should not be ruled out for longer wave length.

Selection of a suitable mode for the optical MASER is a problem which seems to be on the way to a solution.

The amount of power within the illuminating beam has to be large enough to overcome the energy losses of the electrons due to Smith-Purcell radiation. Therefore, the power output of the LASER limits the possible electron current.

The amount of current is also related to the question, how effectively the grating may convert incident ordinary plane waves into evanescent waves. This question has some similarities with frustrated total reflection and is analogue to the problem of the blaze of a grating, where it is intended to convert all of the incident light into a single diffraction order. It is likely that a very low angle of incidence will be most favorable, since the Smith-Purcell radiation of very fast electrons emerges for the most part along and nearly parallel to the direction of electron acceleration (see Toraldo, Ref. 2). This also appears reasonable if one thinks in terms of transitions of momentum.

The possible monochromaticity in speed $\Delta V/V$ can be deduced from the uncertainty principle: $\Delta z \cdot \Delta k_z \sim 2\pi ; k_z = 2\pi/\lambda' ;$

$$V = \lambda' \cdot \nu = \beta \cdot c \quad ; \quad \Delta V/V \sim \lambda'/\Delta z = \beta \cdot \lambda/\Delta z$$

where Δz denotes the path length along the grating. It is clear that the length of the accelerator is inversely proportional to the field strength to attain a given acceleration. The feasible field strength depends not only upon the output of the source and geometrical configuration, but may be limited by breakdown effects. Little is known about breakdown effects at optical frequencies, and as A. L. Schawlow pointed out, this problem may here be of significance.

Addendum

Relating to the question of the vanishing field E_z when $\beta \to 1$ it can be stated that this is true in the case of "one-side-interaction" like in Fig. 3, but not in the case of "both-side-interaction" (Fig. 4). Hence the accelerators feasibility extends to $\beta \to 1$.

-11-

FIGURES

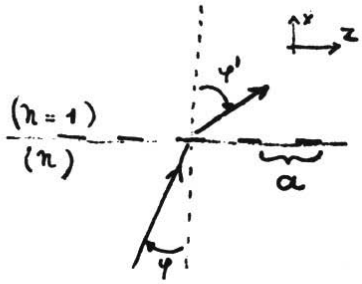

Figure 1: Diffraction and refraction of light at a plane surface, containing a grating.

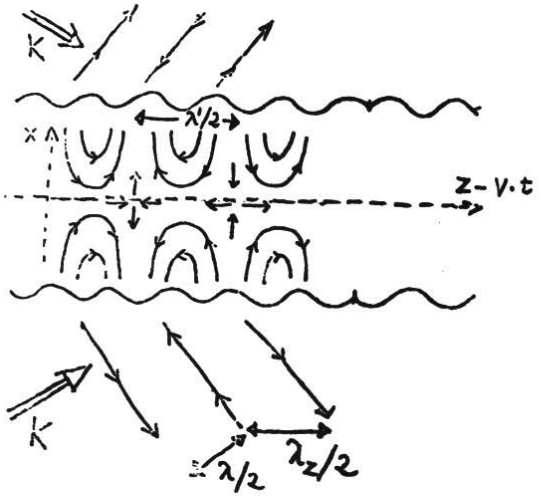

Figure 2: The wavy lines represent the surfaces of two transparent gratings. The electron is traveling along the Z-axis. From the outside arrive two ordinary plane waves, assumed to be emitted by the same source. They are (partially) converted into a pair of evanescent waves. Straight lines with arrows represent the electric field of the waves. There is a longitudinal saddle at $Z - vt = \lambda/2$ which is suitable for acceleration, since it forces the electron to stay on this traveling saddle. But this saddle has transverse gaps. Hence at $Z - vt - \lambda'$ it is suitable for transverse focussing. At the far right both gratings have a phase jump by half a period. This shall force the electron to change from a longitudinal to a transverse saddle or vice versa. Note that the following inequalities will hold:

$$\lambda_z \geq \lambda \geq \lambda'; \quad a \geq \lambda'$$

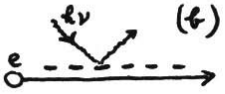

Figure 3:
"One-side-interaction"
(a) one prism for producing the evanescent waves.
(b) one grating.

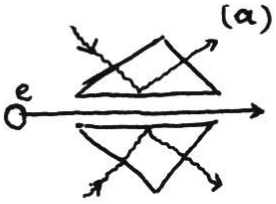

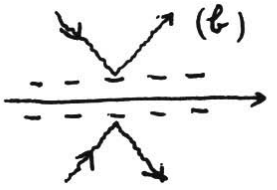

Figure 4:
"Two-side-interaction"
(a) the particle passes between two prism
(b) between two gratings. Now E_z does not tend to zero if β approaches 1.

REFERENCES

1. S. J. Smith and E. N. Purcell: Physics Rev. 92, 1069 (1953).
2. G. Toraldo di Francia: Nuovo Cimento X 16, 61 (1960).
3. K. Shimoda: Appl. Optics 1, 37 (1962).
4. W. Panofsky: Private Communication.
5. D. Hauk and A. Lohmann: Optik 15, 275 (1958).

18 Fresnel Diffraction on Periodic Objects — The Talbot-Effect (1836)

In 1836 Fox Talbot discovered that the wavefield behind a grating is periodic along the axis of propagation. In other words the grating is "imaged" without any lens or mirror at distances $\frac{2d^2}{\lambda}$, $\frac{4d^2}{\lambda}$, etc. By "d" we mean the grating constant or period. It is assumed that the grating is illuminated by a monochromatic plane wave.

This effect is sometimes called "Fourier-imaging", or "Fresnel-imaging", or "self-imaging". The observation of this effect is puzzling and even beautiful, particularly in white light. But this effect is also useful, for example for a spectroscopic instrument, which will be described later in this paragraph. An article in the Proc. ICO Conference on Optical Instruments, London 1961, concerns the effect. It describes that spectroscopic instrument, but in a much more condensed form. This gives you a taste of the usually rather concentrated style of scientific publications. Also another reprint about the "Talbot Interferometer" from "Optics Communications", Vol. 2, 1971, is quite short. The Talbot effect is probably used also in the Schwarz-Hora experiment where a laser beam modulates an electron wave at light frequencies (Applied Physics Letters, **15**, 349, 1969, and Physics Today, June 1971).

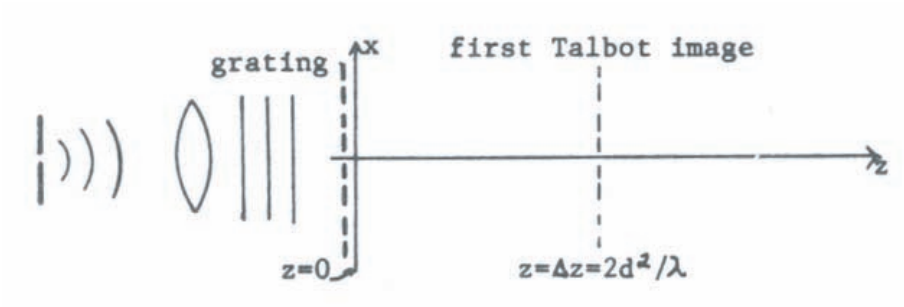

Figure 18.1: Setup for the experimental demonstration of the Talbot effect.

We will present the theory of the Talbot effect in three ways, each of them being best in its own right. The third method is particularly tuned to the spectrometer. At the end of this section we will show how the Talbot effect could have been invented by a theoretician.

18.1 HFK-theory of the Talbot effect

We use the quadratic approximation of the HFK theory, and we omit constant factors.

$$\begin{aligned}
\text{In}: \ z &< 0: \ u(x,z) = e^{ikz}; \quad \text{in } z = 0: \ u(x,-0) = 1 \\
\text{in}: \ z &= 0: \ u(x,+0) = \sum A_n e^{2\pi i n\nu x}; \quad \nu = \frac{1}{d}; \\
\text{in}: \ z &\geq 0: \ u(x,z) \approx \int u(x',0) e^{i\frac{\pi}{\lambda z}(x-x')^2} \mathrm{d}x' \\
&= \sum A_n \int e^{i\pi\left[\frac{(x-x')^2}{\lambda z} + 2n\nu x'\right]} \mathrm{d}x' \\
&= \sum A_n \int e^{i\frac{\pi}{\lambda z}\left[(x-x')^2 + 2x' n\lambda\nu z\right]} \mathrm{d}x'; \\
&[\ldots] = x^2 + x'^2 - 2x'(x - n\lambda\nu z) + (\ldots)^2 - (\ldots)^2; \\
&u(x,z) = \sum A_n e^{i\frac{\pi}{\lambda z}\left[x^2 - (x - n\lambda\nu z)^2\right]} \int e^{i\frac{\pi}{\lambda z}(x' - x + n\lambda\nu z)^2} \mathrm{d}x'
\end{aligned} \tag{18.1}$$

The integral with its limits at $\pm\infty$ is the "Fresnel integral", which yields an uninteresting constant factor, which we neglect from now on. What remains is:

$$u(x,z) = \sum A_n e^{-i\pi(n\nu)^2 \lambda z} e^{2\pi i n\nu x} \tag{18.2}$$

This wavefield in the plane z is the same as $u(x,+0)$ immediately behind the object if $\pi(n\nu)^2\lambda z = 2\pi$, or $\nu^2\lambda z = 2$, or $z = \frac{2}{\nu^2\lambda}$, or $z = 2\frac{d^2}{\lambda}$. We will call $2\frac{d^2}{\lambda}$ the "Talbot length". Obviously the wavefield $u(x,z)$ equals the object field $u(x,+0)$ not only at a single Talbot length Δz away from the object, but also at integer multiples of the Talbot length. A typical example: $d = 0.1$ mm; $\lambda = \frac{2}{3} \cdot 10^{-3}$ mm; $\Delta z = 30$ mm.

18.2 RSD-Theory of the Talbot effect

We start from the RSD formulas Eq. 16.26. In principle we can use any one of the four forms. However, the third form will turn out to lead very quickly to our goal. In two dimensions (x,z) this second form gives:

$$\tilde{u}(\nu,z) = \tilde{u}(\nu,0) e^{2\pi i\sqrt{1-(\lambda\nu)^2}\,\frac{z}{\lambda}} \tag{18.3}$$

Now we specialize on periodic objects in plane $z = 0$:

$$\begin{aligned}
u(x,0) &= \sum A_n e^{2\pi i n\nu_0 x} \\
\tilde{u}(\nu,0) &= \int u(x,0) e^{-2\pi i\nu x} = \sum A_n \delta(\nu - n\nu)
\end{aligned} \tag{18.4}$$

This inserted into the third RSD formula yields:

$$\tilde{u}(\nu, z) = \sum A_n \delta(\nu - n\nu_0) e^{2\pi i \sqrt{1-(\lambda\nu)^2}\frac{z}{\lambda}} \tag{18.5}$$

Due to the delta function $\tilde{u}(\nu, z)$ will be non-zero only at $\nu = n\nu_0$. Hence we insert this into the root at the exponent:

$$\tilde{u}(\nu, z) = \sum A_n \delta(\nu - n\nu_0) e^{2\pi i \sqrt{1-(n\lambda\nu_0)^2}\frac{z}{\lambda}} \tag{18.6}$$

Now we assume that our grating object is not extremely fine. In other words the grating constant d is $d \gg \lambda$. Even $d \gg n\lambda$ shall hold for all indices n for which A_n is substantially non-zero. In that case we may develop the root of the exponent:

$$\sqrt{1-(n\lambda\nu_0)^2} \approx 1 - \frac{(n\lambda\nu_0)^2}{2} \tag{18.7}$$

Actually, since this root occurs in the argument of a trigonometric function we have to be a little careful with our approximations. It is not enough to say $\sqrt{1-\epsilon^2} \approx 1 - \frac{\epsilon^2}{2}$ if $\frac{\epsilon^4}{8} \ll 1$ ($-\frac{\epsilon^4}{8}$ is the next term of the Taylor series for the root.) Instead we must require $2\pi\frac{\epsilon^4}{8}\frac{z}{\lambda} = \frac{\pi}{4} z (n\nu_0)^4 \lambda^3 \leq \frac{\pi}{4} \ll 2\pi$. Since the distance z is now involved, our approximation will deteriorate as we go farther away from the object.

Now we have:

$$\tilde{u}(\nu, z) \approx e^{2\pi i \frac{z}{\lambda}} \sum A_n \delta(\nu - n\nu_0) e^{-i\pi(n\nu_0)^2 z\lambda} \tag{18.8}$$

We may interpret this result in the following way: The Fourier series coefficients are different for different planes $z =$ constant like $A_n(z) = A_n e^{-i\pi(n\nu_0)^2\lambda z}$. However, this variation is periodical with a period $\Delta z = \frac{2d^2}{\lambda}$. Now, if the Fourier series coefficients $A_n(M\Delta z)$ are alike for all planes $z = M\Delta z$ (M integer) then also the wavefields in those planes must be alike, since they can be computed as a Fourier series with those identical Fourier coefficients.

18.3 Plane wave theory of the Talbot effect

This form of the Talbot theory is again of the RSD variety. But it is particularly modified in view of the Fourier spectrometer, which we want to explain immediately after this section.

The plane wave interpretation of the Talbot effect is based upon the setup shown in Fig. 18.2. The so-called collimating lens in Fig. 18.2 makes a plane wave. “Talbot-images” of the grating are formed without a lens.

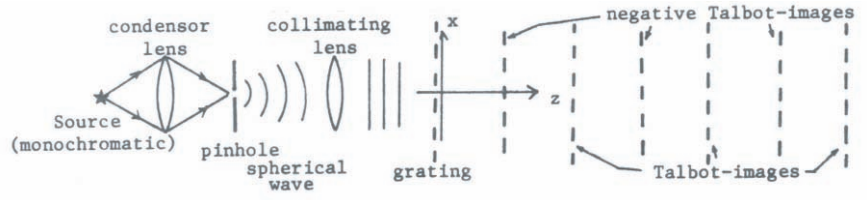

Figure 18.2: The configuration which forms the basis for the plane wave interpretation of the Talbot effect.

Theory:

$$\begin{aligned} \text{In } z &< 0: \text{ (in front of the grating) } u(x,z) = e^{ikz}; \quad \text{(plane wave } \vec{k} \| z-\text{axis)} \\ \text{in } z &= -0: \; u(x,-0) = 1 \\ \text{in } z &= +0: \; u(x,+0) = \frac{[1+\cos(2\pi\nu_0 x)]}{2} \end{aligned} \tag{18.9}$$

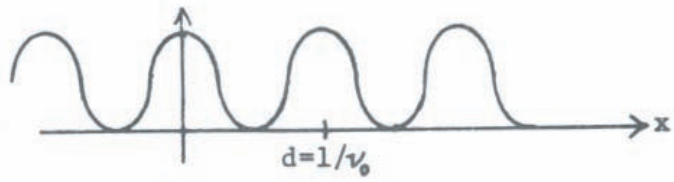

Figure 18.3: The amplitude distribution of the cosine grating.

$u(x,+0)$ is a cosine-grating, which is a pure-amplitude grating (Fig. 18.3). This restriction is not necessary but it makes the theory easier. In $z > 0$: $u(x,z)$ will be periodic also as a function of x in every z-plane, because $u(x,z)$ is the "effect" of the periodic "cause" $u(x,+0)$. Hence we try to solve the wave equation for $u(x,z) = A_0(z) + A_1(z)\cos(2\pi\nu_0 x)$. We must find suitable functions A_0 and A_1 such that $\left\{\nabla^2 + k^2\right\} u = 0$, and such that the boundary condition for $z \to 0$ is satisfied:

$$\begin{aligned} \nabla^2 u + k^2 u = & \overbrace{-A_1(z)(2\pi\nu_0)^2\cos(2\pi\nu_0 x)}^{\frac{\partial^2 u}{\partial u^2}} + \overbrace{A_0'' + A_1''\cos(2\pi\nu_0 x)}^{\frac{\partial^2 u}{\partial z^2}} + \\ & + k^2(A_0 + A_1\cos(2\pi\nu_0 x)) = \\ = & \, k^2 A_0(z) + A_0''(z) + \left\{(-2\pi\nu_0)^2 A_1(z) + k^2 A_1(z) + A_1''(z)\right\}\cos(2\pi\nu_0 x) = 0 = \\ = & \, C_0 + C_1\cos(2\pi\nu_0 x) \end{aligned} \tag{18.10}$$

We may interpret this expression as a Fourier series which happens to be zero for every x. Then it follows $A_0 = 0$ and $A_1 = 0$. Hence we get separate differential equations for A_0 and

A_1.

$$A_0''(z) + k^2 A_0(z) = 0 \rightarrow A_0(z) = a_0 e^{\pm ikz} \tag{18.11}$$

Only the plus sign is meaningful, since it refers to a forward wave.

$$A_1''(z) + k^2 \left\{1 - \lambda^2 \nu_0^2\right\} A_1(z) = 0 \rightarrow A_1(z) = a_1 e^{\pm ikz\sqrt{1-\lambda^2\nu_0^2}z} \tag{18.12}$$

Again, only the plus sign makes sense. Now let us find the constants $a_0,\ a_1$ from the boundary condition.

$$u(x,z) = a_0 e^{ikz} + a_1 \cos(2\pi\nu_0 x) e^{ik\sqrt{1-\lambda^2\nu_0^2}z} \tag{18.13}$$

Letting $z \rightarrow 0$ and comparing it with $u(x,0) = [1 + \cos(2\pi\nu_0 x)]$ we conclude:

$$a_0 = \frac{1}{2}: \qquad u(x,z) = \frac{1}{2}\left[e^{ikz} + \cos(2\pi\nu_0 x) e^{ik\sqrt{1-\lambda^2\nu_0^2}z}\right] \tag{18.14}$$

part of Eq. 18.14	e^{ikz}	$\cos(2\pi\nu_0 x)e^{ik\sqrt{1-\lambda^2\nu_0^2}z}$
wave type	ordinary plane wave	modulated plane wave
amplitude	1	$\cos(2\pi\nu_0 x)$
propagation direction	z-axis	also z-axis since only a z in the exponent
wavelength	$\frac{2\pi}{k} = \lambda$	$\frac{2\pi}{k\sqrt{\cdots}} = \frac{\lambda}{\sqrt{1-\lambda^2\nu_0^2}} > \lambda$!
phase velocity	V= $\lambda\frac{c}{\lambda} = c$	$V = \frac{\lambda}{\sqrt{\cdots}}\frac{c}{\lambda} = \frac{c}{\sqrt{1-\lambda^2\nu_0^2}} > c$!

Table 18.1: Interpretation of the different terms in Eq. 18.14.

A "wavelength" is defined as that z-step which increases the argument by 2π, because that is obviously the z-period. The phase velocity is wavelength times temporal frequency $\frac{c}{\lambda}$.

Notice: a *phase* velocity $> c$ is not in contradiction with relativity theory, because signals do not travel with the phase velocity, which refers to an absolutely periodic wave, which cannot transmit a single bit/sec. Instead signals travel with the "signal velocity", which can be (but does not have to be) equal to the "group velocity", describing the speed of a finite wave train.

18.4 What are these modulated plane waves, really?

One might answer: they are composed of two ordinary plane waves:

$$\cos(2\pi\nu_0 x)e^{ik\sqrt{1-\lambda^2\nu_0^2}z} = \tag{18.15}$$
$$= \frac{1}{2}e^{ik(\lambda\nu_0 x+\sqrt{\dots}z)} + \frac{1}{2}e^{ik(-\lambda\nu_0 x+\sqrt{\dots}z)} =$$
$$= \frac{e^{i\vec{k}_+\vec{x}} + e^{i\vec{k}_-\vec{x}}}{2}; \qquad \vec{k}_\pm = k\left\{\pm\lambda\nu_0, \sqrt{1-\lambda^2\nu_0^2}\right\}$$

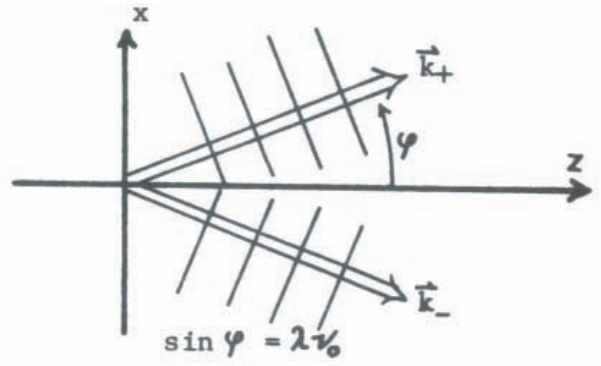

Figure 18.4: Interpretation of the plane waves.

Hence these new strange waves look rather artificial, because they consist of two simple plane waves, which are "elementary waves". However, these modulated plane waves are as much "elementary" as the ordinary plane waves, since in turn each ordinary plane wave consists of two modulated plane waves:

$$e^{ik(\lambda\nu_0+\sqrt{\dots}z)} = e^{2\pi i\nu_0 x}e^{ik\sqrt{\dots}z} = \cos(2\pi\nu_0 x)e^{ik\sqrt{\dots}z} + i\sin(2\pi\nu_0 x)e^{ik\sqrt{\dots}z} \tag{18.16}$$

The second modulated plane wave is $\frac{\pi}{2}$-phase shifted (i), and it is also laterally shifted in x by $\frac{d}{4}$, since the $\cos$ is replaced $\sin$.

These modulated plane waves are quite useful for explaining the Talbot-effect. Let us write down the wavefield both in terms of modulated plane waves and in terms of ordinary plane waves:

$$2u(x,z) = e^{ikz} + \cos(2\pi\nu_0 x)e^{ik\sqrt{\dots}z} = e^{ikz} + \frac{1}{2}e^{ik(+\lambda\nu_0 x+\sqrt{\dots}z)} + \frac{1}{2}e^{ik(-\lambda\nu_0 x+\sqrt{\dots}z)} \tag{18.17}$$

Although both pictures are valid, it is easier to consider only <u>two</u> plane waves, which have the <u>same</u> propagation direction, rather than three plane waves of different propagation

directions. We can understand the Talbot-images simply as an interference effect between one ordinary and one modulated plane wave. Since the phase velocities are different, it will require some travel distance Δz, till both waves are again in phase (exept for a full 2π, which does not have any effect). This comes out best by re-writing $u(x,z)$ slightly differently:

$$2u(x,z) = e^{ikz} + \cos(2\pi\nu_0 x)e^{ik\sqrt{\cdots}z} = e^{ikz}\left[1 + \cos(2\pi\nu_0 x)e^{ikz(\sqrt{\cdots}-1)}\right] \quad (18.18)$$

The factor e^{ikz} is an "overall phase factor", which is not observable as intensity: $|2u(x,z)|^2 = |[\ldots]|^2$. Hence, Talbot-images will occur whenever $kz(\sqrt{\ldots}-1) = 0,\ 2\pi,\ 4\pi\ldots$. The longitudinal period Δz, or the distance between Talbot images, follows from $|k\Delta z(\sqrt{\ldots}-1)| = 2\pi$.

$$\boxed{\Delta z = \frac{\lambda}{1-\sqrt{1-\lambda^2\nu_0^2}}} \quad (18.19)$$

If $\lambda^2\nu_0^2 << 1$ we get in approximation:

$$\boxed{\Delta z \approx \frac{2}{\lambda\nu_0^2} = \frac{2d^2}{\lambda}} \quad (18.20)$$

Notice that this distance is λ-dependent, which is a good reason for trying to invent some kind of spectrometer. — "Negative Talbot-images" occur at $z = \frac{\Delta z}{2},\ \frac{3\Delta z}{2},\ \ldots$, where $kz(1-\sqrt{\ldots}) = \pi,\ 3\pi,\ \ldots$.

$$2u\left(x, \frac{\Delta z}{2}\right) = e^{ik\frac{\Delta z}{2}}\left[1 + \cos(2\pi\nu_0 x)e^{-i\pi}\right] = e^{ik\frac{\Delta z}{2}}\left[1 - \cos(2\pi\nu_0 x)\right] \quad (18.21)$$

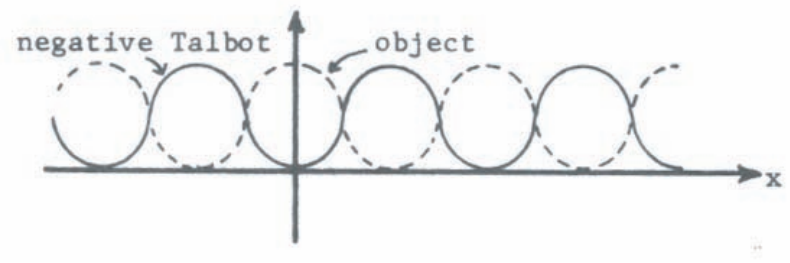

Figure 18.5: Positive and negative Talbot images.

18.5 A Fourier spectrometer based on the Talbot effect

First some terminology. A spectrograph records light on a photographic plate, while in a spectrometer the light is detected by a photon detector such as a photomultiplier, which usually travels together with a slit across the exit plane of the spectrometer. The attribute "Fourier" means that the measured data have to be Fourier-transformed mathematically before being ready for interpretation.

Now we have all the facts together for our spectrometer. Remember, the essential feature was that the Talbot-images did appear at intervals $\Delta z = \frac{2d^2}{\lambda}$, which depend on the wavelength λ. So we can expect that the elementary (= single-λ) Talbot-images will build up to λ-integrated Talbot-images *best* if the range $\Delta\lambda$ of existing wavelengths is only small. On the other hand, if for example the source sends out a "doublet" λ_1 and λ_2, then it might happen that in a particular plane z_0, λ_1 has a Talbot-image ($z_0 = N\Delta z(\lambda_1) = 2N\frac{d^2}{\lambda_1}$), while λ_2 has there a *negative* of a Talbot-image ($z_0 = (N+\frac{1}{2})\Delta z(\lambda_2) = 2(N+\frac{1}{2})\frac{d^2}{\lambda_2}$). This will occur at the N-th Talbot image if:

$$\begin{aligned} \frac{2Nd^2}{\lambda_1} \quad &= \quad z_0 = \frac{2(N+\frac{1}{2})d^2}{\lambda_2} \rightarrow \frac{N}{\lambda_1} = \frac{N+\frac{1}{2}}{\lambda_2} = \frac{N+\frac{1}{2}}{\lambda_1+\delta\lambda} = \frac{N}{\lambda_1}\cdot\frac{1+\frac{1}{2N}}{1+\frac{\delta\lambda}{\lambda_1}} \\ \Longrightarrow \quad &\frac{1}{2N} = \frac{\delta\lambda}{\lambda_1} \quad \text{or} \quad \boxed{\frac{\lambda_1}{\delta\lambda} = 2N} \end{aligned} \tag{18.22}$$

For example, the yellow solium line is actually a doublet with data about like $\lambda_1 \sim 6000$ Å and $\delta\lambda = 10$ Å. Hence $600 = 2N$; $N = 300 \rightarrow z_0 = \frac{2Nd^2}{\lambda_1} = 600\frac{d^2}{6\cdot 10^{-4}\mathrm{mm}} = 10^6\cdot d^2[\mathrm{mm}]$. For $d = 10^{-2}$ mm $\rightarrow z_0 = 100$ mm; for $d = 10^{-1}$ mm $\rightarrow z_0 = 10^4$ mm $= 10$ m.

We hope, of course, that our instrument will be able to handle more general spectra, not only doublets. For doing this we need first of all a setup by which we can measure conveniently and automatically the presence or absence of Talbot-images. Since we know the grating constant d of the object grating, we know also the period d of the suspected Talbot images. Hence, a simple way to measure the Talbot image is to take a second identical grating, putting it into plane z, where we want to measure, orient its grating bars parallel to those of the object grating, and move the second grating laterally. If there was a Talbot-image in plane z, then the light flux through the second grating will vary while we move it. If there is no Talbot-image, only a uniform light distribution, then this flux will remain constant. Hence let us take a photo-receiver, which collects all the light behind the second grating. Of the resulting photocurrent, only the a.c. portion will be of interest.

The actual receiver might be much smaller than indicated here. In that case a collecting lens is placed between the second grating and the receiver.

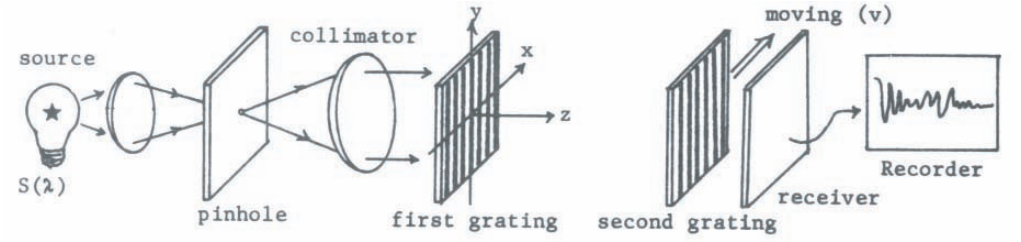

Figure 18.6: The configuration of a Fourier spectrometer based on the Talbot effect.

Theory: for a single wavelength λ, the intensity at plane z will be

$$\begin{aligned} |u(x,z)|^2 &= |e^{ikz} + \cos(2\pi\nu_0 x)e^{ikz\sqrt{1-\lambda^2\nu_0^2}}|^2 \\ &= 1 + \cos^2(2\pi\nu_0 x) + 2\cos(2\pi\nu_0 x)\cos\left\{kz(1-\sqrt{1-\lambda^2\nu_0^2})\right\} \\ &= \frac{3}{2} + \frac{1}{2}\cos(4\pi\nu_0 x) + 2\cos(2\pi\nu_0 x)\cos(\pi z\lambda\nu_0^2) \;\; (\text{if } \sqrt{\ldots} \approx 1 - \frac{\lambda^2\nu_0^2}{2}) \end{aligned} \tag{18.23}$$

The amplitude transmittance of the second grating (which is moving, velocity v) will be at the moment t:

$$1 + \cos\{2\pi\nu_0(x+vt)\} \tag{18.24}$$

and the intensity transmittance:

$$(1+\cos\{\ldots\})^2 = 1+\cos^2+2\cos = \frac{3}{2}+\frac{1}{2}\cos\{4\pi\nu_0(x-vt)\}+2\cos\{2\pi\nu_0(x-vt)\} \tag{18.25}$$

The intensity behind the second grating is the product of incoming intensity times intensity transmittance:

$$\begin{aligned} B(x,z,t,\lambda) &= \left[\frac{3}{2} + \frac{1}{2}\cos(4\pi\nu_0 x) + 2\cos(2\pi\nu_0 x)\right]\cdot \\ &\cdot \left[\frac{3}{2} + \frac{1}{2}\cos\{4\pi\nu_0(x-vt)\} + 2\cos\{2\pi\nu_0(x-vt)\}\right] \end{aligned} \tag{18.26}$$

This expression has to be x-integrated since we use a large area receiver: $\int B(x,z,t,\lambda)\mathrm{d}x$. The math would become now very clumsy if we would treat all terms. Fortunately only one term is relevant for the operation of the Fourier spectrometer. This term is part of the a.c. component. Actually B contains two a.c.-components with time-frequencies $2\nu_0 v$ and $\nu_0 v$.

Which one do we want? When integrating over many x-periods, only those terms of $[\ldots]\,[\ldots]$ will survive which are constant in x. Of those, the term with $\cos(\pi z\lambda\nu_0^2)$, which is germane to the Talbot-effect, is of course the one we want to keep:

$$\begin{aligned} & 2\cos(2\pi\nu_0^2 x)\cos(\pi z\lambda\nu_0^2)2\cos\{2\pi\nu_0(x-vt)\} = \\ = \;& 2\cos(\pi z\lambda\nu_0^2)\left[\cos\{2\pi\nu_0(2x-vt)\}+\cos(2\pi\nu_0 vt)\right] \end{aligned} \tag{18.27}$$

Of these two terms $2\cos(\pi z\lambda\nu_0^2)\cos(2\pi\nu_0 vt)$ will survive the x-integration. There are of course other terms of $\int B\mathrm{d}x$, which survive the x-integration as well; they will be $\left(\frac{3}{2}\right)^2$ and $\frac{1}{2}\left(\frac{1}{2}\right)^2\cos(4\pi\nu_0 Vt)$ with a time-frequency zero or $2\nu_0 v$. But the $\nu_0 v$-time-frequency is what we want. We get it by means of an electronic narrow-band filter behind the photomultiplier. The selection of the $\nu_0\nu$-frequency can be mathematically represented by a Fourier-time-integral:

$$\begin{aligned} & \iint B(x,z,t,\lambda)e^{-2\pi i\nu_0 Vt}\mathrm{d}t\mathrm{d}x = \\ = \;& 2\cos(\pi z\lambda\nu_0^2)\int\cos(2\pi\nu_0 vt)e^{-2\pi i\nu_0 vt}\mathrm{d}t = \cos(\pi z\lambda\nu_0^2) \end{aligned} \tag{18.28}$$

So this expression is the "monochromatic response" of our apparatus. Now comes the <u>total</u> response, that is the joint contribution of all wavelengths of the source, which had the distribution $S(\lambda)$.

$$\int S(\lambda)\cos(\pi z\lambda\nu_0^2)\mathrm{d}\lambda \tag{18.29}$$

In a more general situation there might be spectral filters in the apparatus. Or the spectral response of the receiver might be wavelength- dependent. Let us assume that these effects are included in the spectral distribution $S(\lambda)$. Now we compute the output signal as a function of z, which was the longitudinal position of the second grating.

$$\begin{aligned} & \int S(\lambda)\cos(\pi\lambda z\nu_0^2)\mathrm{d}\lambda = \frac{1}{2}\int S(\lambda)e^{2\pi i\lambda\varrho}\mathrm{d}\lambda + \frac{1}{2}\int S(\lambda)e^{-2\pi i\lambda\varrho}\mathrm{d}\lambda \\ = \;& \frac{1}{2}\int\left[S(\lambda)+S(-\lambda)\right]e^{-2\pi i\lambda\varrho}\mathrm{d}\lambda = \frac{1}{2}\int\left[S(\lambda)+S^*(\lambda)\right]e^{-2\pi i\lambda\varrho}\mathrm{d}\lambda = \\ = \;& \frac{1}{2}\int\left[\tilde{S}(\varrho)+\tilde{S}^*(\varrho)\right] = \mathrm{Real}\left\{\tilde{S}(\varrho)\right\}; \qquad (\varrho=\frac{z\nu_0^2}{2}) \end{aligned} \tag{18.30}$$

So we measure in essence the Fourier transform $\tilde{S}$ of what we actually want to measure, S. If we know $\tilde{S}$, we can compute S by means of a Fourier transform-computer, either digital or analog (Moiré, see Chap. 3): $S(\lambda)=\int\tilde{S}(\varrho)e^{2\pi i\varrho\lambda}\mathrm{d}\varrho$. But do we really know $\tilde{S}(\varrho)$? Only Real$\{\tilde{S}(\varrho)\}$ comes out of the measurements. As we see from the above formulas, if we apply a Fourier transform to Real$\{\tilde{S}(\varrho)\}$ instead of $\tilde{S}(\varrho)$ itself, we get $\frac{1}{2}(S(\lambda)+S(-\lambda))$ instead of

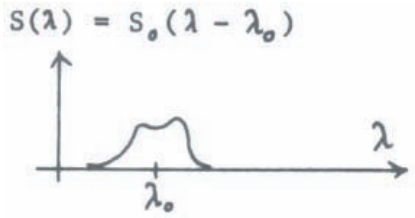

Figure 18.7: Example of the spectral source distribution.

$S(\lambda)$. But that is good enough since $S(\lambda)$ is non-zero only for positive wavelengths. Hence, the computer output $S(\lambda) + S(-\lambda)$ is unambiguous.

One may look at the same problem also from another point of view. We need for $S(\varrho)$ the modulus $|\tilde{S}(\varrho)|$ and $\arg\{\tilde{S}(\varrho)\} = \sigma(\varrho)$. But measured, it is only $|\tilde{S}(\varrho)| \cos\sigma(\varrho) = \mathrm{Real}\{\tilde{S}(\varrho)\}$. Considering that $S(\lambda)$ is non-zero only for $\lambda > 0$, we can write $S(\lambda) = S_0(\lambda - \lambda_0)$ (Fig. 18.7), where λ_0 could be (but does not have to be) the mean-wavelength:

$$\lambda_0 \frac{\int \lambda S(\lambda) \mathrm{d}\lambda}{\int S(\lambda) \mathrm{d}\lambda} \tag{18.31}$$

From the shift-theorem follows: $S(\lambda) = S_0(\lambda - \lambda_0) \Leftrightarrow \tilde{S}(\varrho) = \tilde{S}_0(\varrho) e^{-2\pi i \varrho \lambda_0}$. The right hand side can be also expressed in terms of modulus and phase:

$$|\tilde{S}(\varrho)| = |\tilde{S}_0(\varrho)|; \qquad \sigma(\varrho) = \sigma_0(\varrho) - 2\pi\varrho\lambda_0 \tag{18.32}$$

Hence we get:

$$\mathrm{Real}\left\{\tilde{S}(\varrho)\right\} = \overbrace{|\tilde{S}_0(\varrho)|}^{\substack{\text{like}\\ \text{amplitude}\\ \text{modulation}}} \cos(\underbrace{2\pi\varrho\lambda_0}_{\substack{\text{like}\\ \text{carrier}\\ \text{frequency}}} - \overbrace{\sigma_0(\varrho)}^{\substack{\text{like}\\ \text{phase}\\ \text{modulation}}}) \tag{18.33}$$

The example of the doublet might help to clarify the situation:

$$\begin{aligned} S(\lambda) &= \delta(\lambda - \lambda_0 - \frac{\delta\lambda}{2}) + \delta(\lambda - \lambda_0 + \frac{\delta\lambda}{2}) \\ \tilde{S}(\varrho) &= 2e^{-2\pi i \varrho \lambda_0} \cos(\pi\varrho\delta\lambda) \\ \mathrm{Real}\left\{\tilde{S}(\varrho)\right\} &= 2\cos(2\pi\varrho\lambda_0)\cos(\pi\varrho\delta\lambda) \end{aligned} \tag{18.34}$$

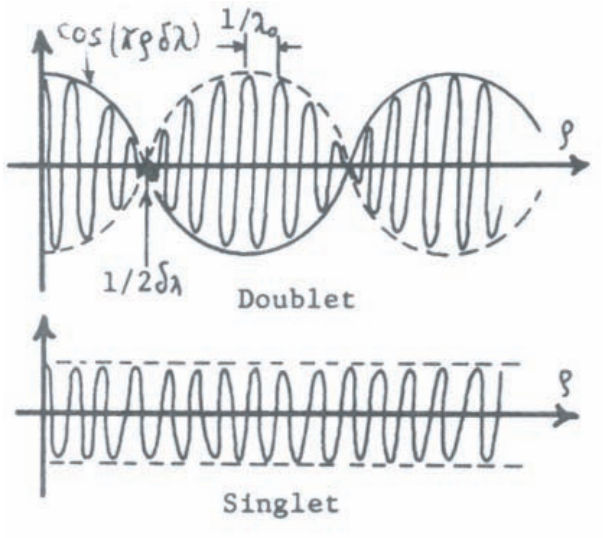

Figure 18.8: Interference pattern of a source with a spectral distribution described by Eq. 18.34.

"Resolution" means that we can decide reliably if the source $S(\lambda)$ was a doublet $(\delta\lambda)$ or a singlet $(\delta\lambda = 0)$. If we go along the doublet curve, where it drops down to $\cos\left(\frac{\pi}{4}\right) \approx 0.7$ of its maximum, we can clearly identify the doublet (Fig. 18.8). So for detecting the doublet line separation $\delta\lambda$ a $\varrho_{\max}$ is needed, for which:

$$\cos(\pi\varrho_{\max}\delta\lambda) = \cos\left(\frac{\pi}{4}\right) \longrightarrow \varrho_{\max} = \frac{1}{4}\delta\lambda. \qquad \varrho_{\max} = \frac{\nu^2}{2} z_{\max} \tag{18.35}$$

For practical reasons $z_{\max}$ is of course dictated by the length of the room. As we will see next the achieveable $z_{\max}$ is also dependent on the finite width of the 1-st grating, or in similar terms: by the number M of periods of the grating. This number M is roughly in proportion to the price of the grating.

18.6 The walk-off effect

The following arguments are hoped to be plausible. They will be legalized later when we will have studied "parageometrical optics". At first the plane wave hits the grating $1 + \cos(2\pi\nu_0 x) = 1 + [e^{2\pi i\nu_0 x} + e^{-2\pi i\nu_0 x}]$. Behind it there will be three plane waves, which hit then the "slit", which in this case is simply the frame of the grating with a width Md. Parageometrical optics tells us that in essence these three plane waves will continue to propagate, but with *finite* lateral width, due to the slit. The lateral edges of these finite plane waves get fuzzier with increasing distance z. This is a diffraction effect due to the slit with width Md.

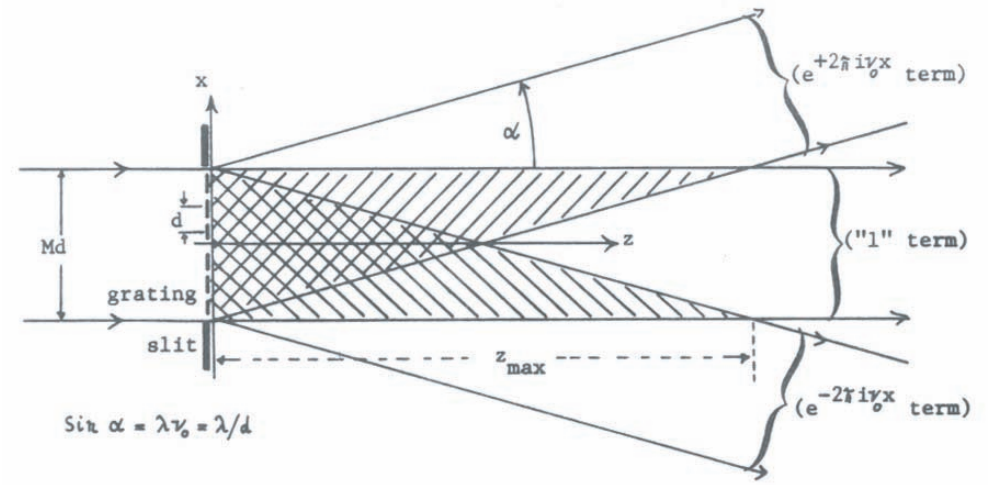

Figure 18.9: Explanation of the walk-off effect.

As we will see later in the section on "parageometrical optics" the fuzzy edges are harmless if $z < \frac{M^2 d^2}{\lambda}$. After a distance $z_{\max}$ these three limited plane waves will not overlap anymore. Hence there will be no interference fringes (and no Talbot-images) at $z > z_{\max}$, which is determined by:

$$\begin{aligned} \tan\alpha &= \frac{Md}{z_{\max}} \approx \sin\alpha \frac{\lambda}{d} = \lambda\nu_0 \qquad \text{diffraction grating} \\ z_{\max} &\approx \frac{Md^2}{\lambda} \rightarrow \varrho_{\max} = z_{\max}\frac{\nu_0^2}{2} = \frac{M}{2\lambda} \end{aligned} \tag{18.36}$$

On the other hand, for resolving $\delta\lambda$ we need $\varrho_{\max} = \frac{1}{4}\delta\lambda$. Both together tell us that the spectral resolution depends on the number M of grating periods.

$$\boxed{\frac{\lambda}{\Delta\lambda} = 2M} \tag{18.37}$$

Notice that $z_{\max} = \frac{Md^2}{\lambda} \ll \frac{M^2 d^2}{\lambda}$ if $M \gg 1$. In other words we are well within the boundaries of parageometrical optics. Hence we don't have to worry about the fuzzy edges of the finite plane waves.

Earlier we encountered a formula $2N = \frac{\lambda_1}{\delta\lambda}$, where N meant the number of Talbot-images one has to go through from $z = 0$ till $z_{\max}$, if $z_{\max}$ is just large enough to resolve the $\delta\lambda$ of a doublet. This last figure tells us now that the number N of Talbot-images one can observe is limited due to walk-off. Hence in purely monochromatic light the number of observable Talbot

images equals the number of periods M within the grating of finite width Md. - If you were somehow disturbed during these resolution considerations, and you felt that a factor 2 or $\frac{1}{2}$ was not proper, don't worry, because the definition of resolution is a little bit arbitrary, by a factor of the order $\frac{1}{2} \ldots 2$ anyway.

18.7 Yet another look at Talbot images

Whenever you come up with a new result, it is worthwhile (although sometimes strenuous) to find out whether the assumptions from which you started were *necessary or sufficient* for getting that result. Maybe you will find that your assumptions were more restrictive than needed. This may give you a hint for further discoveries or inventions. Here is such an example (due to W. D. Montgomery, JOSA 58, 1112, 1968). So far we have seen that lateral periodicity of the object is *sufficient* for getting Talbot-images. But this lateral periodicity is *not necessary*. The lateral periodicity of the object is more restrictive than it could be. The total set of objects which will produce Talbot images contains the periodic objects as a subset (and even that is true only in approximation).

The whole history of Talbot-images consists roughly of three steps: (1) accidental observation by an alert experimentalist (1836); (2) theoretical explanations (various forms since 100 years ago, the latest with "modulated plane waves"); (3) establishment of *all* Talbot-images, not just for periodic objects. This third step is due to Montgomery. He asked himself the question: If a wavefield has a longitudinal period Δz, what are its properties? The first step is (as always) to formulate the question in quantitative terms. If $u(x, y, z)$ is z-periodic, then it must be representable by a Fourier series with z as variable.

$$u(x, y, z) = \sum_{(m)} v_m(x, y) e^{2\pi i m \frac{z}{\Delta z}} \tag{18.38}$$

This wavefield is subject to two minor constraints. The index m should not be negative since $m < 0$ would refer to a backwards wave, if the time dependence is written as $e^{-i\omega t}$. The boundary condition at $z = 0$ requires $u(x, y, 0) = \sum v_m(x, y)$. The crucial question is whether this hypothetical wavefield fits into the wave equation. Let's try it.

$$\nabla^2 u + k^2 u = \sum e^{2\pi i m \frac{z}{\Delta z}} \left[\frac{\partial^2 v_m}{\partial x^2} + \frac{\partial^2 v_m}{\partial y^2} - \left(\frac{2\pi m}{\Delta z} \right)^2 v_m + k^2 v_m \right] = 0 \tag{18.39}$$

We may consider this as a Fourier series for a function of z, which happens to be zero for all z. We must have $[\ldots] = 0$ for every m, since $[_{(m)}]$ is the m-th Fourier-coefficient of this Fourier series. $[\ldots] = 0$ is a 2D-differential equation:

$$\frac{\partial^2 v_m}{\partial x^2} + \frac{\partial^2 v_m}{\partial y^2} + k^2 \left\{ 1 - \left(\frac{m\lambda}{\Delta z} \right)^2 \right\} = 0 \tag{18.40}$$

It has essentially three types of solutions, depending on $\{\ldots\} \overset{<}{>} 0$.

$$\{\ldots\} < 0 \rightarrow v_m = e^{\pm ax} e^{\pm by} \text{ with } a^2 + b^2 + k^2 \left\{ 1 - \left(\frac{m\lambda}{\Delta z} \right)^2 \right\} = 0 \tag{18.41}$$

This damped or exploding wave-type is physically meaningless here, since we assumed no lateral restrictions of $u(x, y, z)$, hence $e^{\pm ax}$ would blow up at $x, y = \pm\infty$. In other words, we should exclude all those v_m from our hypothesis $u = \sum v_m e^{2\pi i m \frac{z}{\Delta z}}$ which would make $\left\{ 1 - \left(\frac{m\lambda}{\Delta z} \right)^2 \right\}$ negative. This is the same as requesting $|m| \leq m_{\max} < \frac{\Delta z}{\lambda}$. Since m and $m_{\max}$ are integers, it follows also that Δz has to be $\geq \lambda$. Otherwise only $m = 0$ would be allowed to be part of the series over m. The case $m = 0$ means: $u(x, y, z) \Rightarrow v_0(x, y)$, which will propagate perpendicular to the z-axis. This special case is as trivial as saying that a constant number is periodic in z. So, really, we should restrict the series to $1 \leq m \leq \frac{\Delta z}{\lambda}$. The case where $\{\ldots\} = 0$, or $\Delta z = m\lambda$, is trivial too:

$$\frac{\partial^2 v_m}{\partial x^2} + \frac{\partial^2 v_m}{\partial y^2} = 0 \tag{18.42}$$

This leads to:

$$v_m = a + bx + cy \tag{18.43}$$

and

$$v_m e^{2\pi i m \frac{z}{\Delta z}} = v_m e^{2\pi i \frac{z}{\lambda}} = (a + bx + cy) e^{ikz} \tag{18.44}$$

Again, $b \neq 0$ and $c \neq 0$ would blow up. What is left is the ordinary plane wave, travelling in z-direction.

Now comes the important case: $\{\ldots\} > 0$, or $\frac{\Delta z}{\lambda}$. What is the set of function V_m which fits into:

$$\frac{\partial^2 v_m}{\partial x^2} + \frac{\partial^2 v_m}{\partial y^2} + k^2 \left\{ 1 - \left(\frac{m\lambda}{\Delta z} \right)^2 \right\} v_m(x, y) = 0 \quad \text{with} \quad 0 < \frac{m\lambda}{\Delta z} < 1? \tag{18.45}$$

As so often happens, the question becomes clearer when translated into the other Fourier domain. So let us write:

$$v_m(x, y) = \iint \tilde{v}(\nu, \mu) e^{2\pi i(\nu x + \mu y)} \mathrm{d}\nu \mathrm{d}\mu \tag{18.46}$$

and go with this into the differential equation for $v_m(x,y)$:

$$\iint \tilde{v}_m(\nu,\mu)e^{2\pi i(\nu x+\mu y)}\left[-(2\pi)^2(\nu^2+\mu^2)+k^2\left\{1-\left(\frac{m\lambda}{\Delta z}\right)^2\right\}\right]\mathrm{d}\mu\mathrm{d}\nu = 0 \quad (18.47)$$

This "Fourier-integral" will be zero for every $x,\ y$, if $\tilde{v}_m = 0$, or if $[\ldots] = 0$, or both. $[\ldots] = 0$ occurs when $\nu^2+\mu^2 = \frac{1}{\lambda^2} - \frac{m^2}{\Delta z^2} = \varrho_m^2$. This equation refers to rings of radii ϱ_m in the frequency domain (ν,μ). Hence $\tilde{v}_m(\nu,\mu)$ has to be zero, except on these rings:

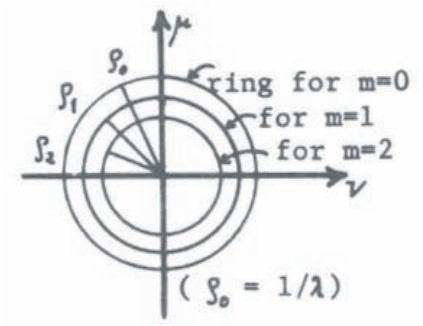

Figure 18.10: Graphical illustrations of the solutions of Eq. 18.47.

Each $\tilde{v}_m$ has its own ring.

$$\begin{aligned} \tilde{v}_m(\nu,\mu) &= \delta(\varrho-\varrho_m)\Phi_m(\theta)C_m \quad (18.48)\\ \nu^2+\mu^2 &= \varrho^2; \quad \nu = \varrho\cos\theta; \quad \mu = \varrho\sin\theta \end{aligned}$$

With also $x,\ y$ in polar form $x = \vec{r}\cos\varphi$; $y = r\sin\varphi$, we get:

$$u(x,y,z) = \sum_{m=0}^{m_{\max}} C_m \int_{-\pi}^{\pi}\int_{0}^{\infty} \Phi_m(\theta)\delta(\varrho-\varrho_m)e^{2\pi i[r\varrho\cos(\varphi-\theta)+m\frac{z}{\Delta z}]}\varrho\mathrm{d}\varrho\mathrm{d}\theta \quad (18.49)$$

where $(r\varrho\cos(\varphi-\theta) = \nu x+\mu y)$

$$\boxed{u(x,y,z) = \sum C_m\varrho_m\int \Phi_m(\theta)e^{2\pi i[r\varrho\cos(\varphi-\theta)+\frac{mz}{\Delta z}]}\mathrm{d}\theta} \quad \text{(Montgomery)} \quad (18.50)$$

$$\begin{aligned} \varrho_m^2 &= \left(\frac{1}{\lambda}\right)^2 - \left(\frac{m}{\Delta z}\right)^2; \quad (18.51)\\ m_{\max} &\le \frac{\Delta z}{\lambda}; \ \ u(x,y,z) = u(x,y,z+N\Delta z), \ \ (N \text{ integer}) \end{aligned}$$

So this result contains all $u(x,y,z)$ wavefields which are periodic in z. At a first glance, it really does not look as if it contains the historical Talbot-case, which said: if $u(x,0) = u(x+Nd,0)$ is a laterally periodic object (N integer, $d = \frac{1}{\nu_0}$ the grating constant), then the wavefield $u(x,z)$ behind it will be longitudinally periodic with $\Delta z \approx \frac{2d^2}{\lambda}$:

$$u(x,z) = \sum A_n e^{2\pi i[\frac{nx}{d} + \sqrt{1-\left(\frac{n\lambda}{d}\right)^2}\frac{z}{\lambda}]} \approx e^{ikz}\sum A_n \ldots e^{2\pi i n\frac{x}{d}} e^{-i\pi\lambda z\left(\frac{n}{d}\right)^2} \quad (18.52)$$

Let us extract this special case from Montgomery's formula, above. First we see that our special case does not depend on y. This is equivalent to saying: $\Phi(\theta) = \delta(\theta)$, because for a function $f(x,y) = \iint \tilde{f}(\nu,\mu)e^{2\pi i(\nu x+\mu y)}\mathrm{d}\nu\mathrm{d}\mu$, which in reality is simply $f(x)$, $\tilde{f}(\nu,\mu)$ reduces to $\tilde{f}(\nu.\mu)\delta(\mu)$. Since $\delta(\mu)$ means $\mu = 0$, and since $\mu = \varrho\sin\theta$, we conclude $\theta = 0$ or π, hence $\cos\theta \to 1$ and $\varrho = \frac{\nu}{\cos\theta} \to \nu$. The last step can be done somewhat more slowly; with $\Phi(\theta) = \delta(\theta)$ we get:

$$\begin{aligned} u(x,z) &= \sum C_m \int \delta(\varrho-\varrho_m)e^{2\pi i[r\varrho\cos\varphi + m\frac{z}{\Delta z}]}\varrho\mathrm{d}\varrho = \quad (18.53)\\ &= \sum C_m\delta_m e^{2\pi i[r\varrho_m\cos\varphi + m\frac{z}{\Delta z}]}; \qquad \text{remember}: r\cos\varphi = x \end{aligned}$$

In order to get a form which looks more like what we hope to find we call $C_m\varrho_m = B_m$.

$$u(x,z) = \sum B_m e^{2\pi i(x\varrho_m + m\frac{z}{\Delta z})}; \qquad 1 \le m \le M \le \frac{\Delta z}{\lambda} \quad (18.54)$$

Herein $\varrho_m^2 = \left(\frac{1}{\lambda}\right)^2 + \left(\frac{m}{\Delta z}\right)^2$, as we found earlier. Now let us make a simplification which turns out not to be absolutely necessary but very helpful. We assume that the longitudinal period is an integer multiple of the wavelength $\Delta z = M\lambda$. This integer M may be a fairly large number. Inserting this into the equation for the allowed rings in the frequency domain we get:

$$\varrho_m^2 = \left(\frac{1}{\lambda}\right)^2\left[1 - \left(\frac{m}{M}\right)^2\right] = \frac{M^2-m^2}{M^2\lambda^2} = \frac{(M-m)(M+m)}{M^2\lambda^2} \quad (18.55)$$

As with most Fourier series we expect the coefficients B_m with the lowest indices to be most significant ones. That makes sense usually since it means that the fundamental period is very clearly apparent while the higher harmonics only modify the shape of the period, for example from a sine-wave into a square wave. Hence we will try naturally at first how the wavefield $u(x,y)$ will look like if only B_{+1} and B_{-1} are non-zero. Next we will add B_{+2} and B_{-2} contributions. This approach leads to undesirable results, which don't satisfy our hopes for finding the old Talbot case as a special case of the Montgomery theory. This becomes apparent in Fig. 18.11 where some of the Montgomery circles are plotted in the frequency domain. The trouble is that the (ν,μ) circles, which represent the spatial frequencies for *lateral* periodicities are very large when the *longitudinal* frequencies $\frac{m}{\Delta z}$ are very small and vice versa.

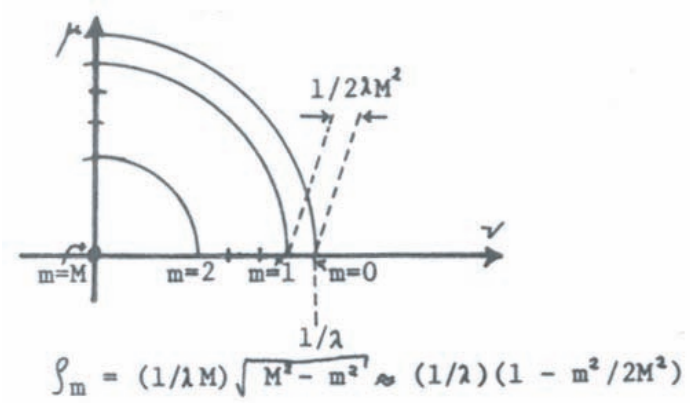

Figure 18.11: Montgomery circles in the frequency plane.

This situation is incompatible with our belief that the big Fourier coefficients always go with the low-frequency components. We have to make a choice: either the big coefficients are attached to the *low longitudinal* frequencies, but also with *high lateral* frequencies. Or should the big coefficients be attached to the *low lateral* and *high longitudinal* frequencies?

The second choice makes more sense since the lateral frequencies are due to the lateral structures of a man-made object while the longitudinal frequencies are immaterial wave structures, made by Mother Nature. Mother Nature is certainly better in making fine details than we are. Hence we may guess that of all frequencies with index m in the range $1 \leq m \leq M = \frac{\Delta z}{\lambda}$ those frequencies will be strongest (biggest B_m) which lead to coarse lateral structures. Looking at the formula for the Montgomery circles we conclude that the large values of m and hence the small values of $M - m$ should be predominant. We will call now $M - m = n$:

$$\begin{aligned} \varrho_m^2 &= \frac{(M-m)(M+m)}{M^2\lambda^2} = \frac{n(2M-n)}{M^2\lambda^2} \approx \frac{2n}{M\lambda^2}; \\ \varrho_m &= \varrho_{M-n} \approx \sqrt{\frac{2n}{M\lambda^2}} = \sqrt{n}\varrho_{M-1} \end{aligned} \tag{18.56}$$

This approximation is now inserted into the general formula for logitudinally periodic wavefields:

$$\begin{aligned} &u(x,z) = \sum B_{M-n} e^{2\pi i[x\varrho_{M-1}\sqrt{n} + z\frac{M-n}{\Delta z}]} = e^{2\pi i\frac{z}{\lambda}} \sum B_{M-n} e^{2\pi i[x\varrho_{M-1}\sqrt{n} - \frac{nz}{\Delta z}]}; \\ &\text{mit}: \quad n = 0, 1, 2, \ldots, M \end{aligned} \tag{18.57}$$

Let us check if the result encompasses the ordinary grating as possible objects. For this purpose we go to the object plane $z = 0$.

$$u(x,0) = \sum B_{M-n} e^{2\pi i x \varrho_{M-n} \sqrt{n}} \tag{18.58}$$

This "Montgomery-object set" contains gratings as a special case if only $B_M,\ B_{M-1},\ B_{M-4},\ B_{M-9}$, etc. are non-zero. Hence Montgomery really discovered something new on the basis of an abstract theoretical approach. So far no one has found any use for Montgomery's discovery. Not even the structure of non-trivial Montgomery objects has been explored. By "trivial" I mean gratings in this case. My guess is that Montgomery's theory might become useful for optical waveguides in connection with data transmission.

Proc. ICO Conf. on Optical Instruments,
K.J. Habbell Ed., London 1961, Butterworth
p.58-61

A NEW FOURIER-SPECTROMETER CONSISTING OF A TWO-GRATINGS-INTERFEROMETER

A. Lohmann
Technische Hochschule Braunschweig, Germany

Summary: Gratings as beam splitters are well known in interferometry. Here the interferometer consists of two gratings in series. The action of this interferometer can be understood as an interference effect between a usual plane wave and one (or more) transversely modulated plane wave. The total output flux behind the second grating gives essentially the Fourier transform of the spectral input $S(\lambda)$. For varying the Fourier coordinate, one has to increase the distance of the two gratings. The resolution of this Fourier spectrometer depends on the number of grating periods. But the luminosity can be improved very much with respect to the ordinary grating spectrometer, when replacing the entrance slit by a variable grid (moiré). On the same basic idea one can develop spectral filters. For this more than two gratings are built up either equidistant or multiple-distant. Unusual is the fact, that these filters let pass, beside the basic wavelength λ the harmonic wavelength $2\lambda, 3\lambda..$ rather than the subharmonics $\lambda/2, \lambda/3..$ as in usual interference filters.

When illuminating a transmitting grating by a monochromatic plane wave, the wave field behind the grating is periodic transversely as well as longitudinally. The longitudinal periodicity has been known for 125 years (Talbot,[1]). In equidistant planes appear images of the grating, called "Fourier Images" by Cowley and Moodie[2]. The distance $2d^2/\lambda$ of these planes depends on the wavelength λ and on the grating constant d. One observes the more "Fourier Images", the finer the illuminating spectral line

is. The contrast in the Fourier images as a function of the distance Z from the grating is essentially the Fourier transform of the spectral distribution $S(\lambda)$:

$$\text{contrast} \propto \int S(\lambda) \cos(\pi Z \lambda / d^2)\, d\lambda$$

We measure the contrast with the help of a second identical grating, placed at the distance Z and slowly shifted in a transversed direction. So the a.c. component in the photoelectrically integrated light flux delivers the Fourier-encoded spectral distribution. Historically, the work of E. Lau[3] is of interest. He, mainly, illuminated two and more gratings in series and observed colour strips at infinity. Since Lau illuminated incoherently, but we coherently, his explanation is of a different form.
For the explanation of the longitudinal period of the wave field we assume a cosine-grating for sake of simplicity. It means a complex amplitude $u(x,0)$ directly behind the grating:

$$u(x,0) = 1 + \cos(2\pi x/d)$$

The light distribution $u(x,z)$ at the finite distance Z has to fullfill the wave equation and to fit $u(x,0)$, when $Z \to 0$. We will write down $u(x,Z)$ and also the typical features of the two parts contained in it. $(K = 2\pi/\lambda)$

$$u(x,Z) = \exp(iKZ) + \cos(2\pi x/d)\exp\left[ikz\sqrt{1-(\lambda/d)^2}\right]$$

direction	+Z	+Z
frequency	$\omega/2\pi$	$\omega/2\pi$
wavelength	λ	$\tilde{\lambda} = \lambda / \sqrt{1-(\lambda/d)^2} > \lambda$
phase speed	c	$V = c / \sqrt{1-(\lambda/d)^2} > c$
amplitude	1	$\cos(2\pi x/d)$
type	usual plane wave	transversely-modulated plane wave

A short stop only is necessary to consider the properties of the transversely modulated waves. The amount of the completeness as a set of orthogonal elements for the composition of any arbitrary wave field is the same both for the usual plane waves as well as for the transversely modulated plane waves.
It is easily seen by the connection between the two wave types:

$$2\cos(2\tilde{\pi}x/d)\exp\left[ikz\sqrt{1-(\lambda/d)^2}\right] =$$

$$= \exp\left[ik\left(+x\,\lambda/d + z\sqrt{\ldots}\right)\right] + \exp\left[ik\left(-x\,\lambda/d + z\sqrt{\ldots}\right)\right]$$

$$\exp\left[ik\left(+x\,\lambda/d + z\sqrt{\ldots}\right)\right] =$$

$$= \cos(2\tilde{\pi}x/d)\exp\left(ikz\sqrt{\ldots}\right) + i\sin(2\tilde{\pi}x/d)\exp\left(ikz\sqrt{\ldots}\right)$$

But for full completeness, one has to add a set of evanescent waves, either standing or moving. These waves correspond to $d < \lambda$.

Since the modulated wave has a higher speed than the usual plane wave, it will happen that after some distance Δz the one wave overtakes the other. This occurs when the phase difference becomes just $2\tilde{\pi}$. From this follows the longitudinal period Δz:

$$\left(\frac{2\tilde{\pi}}{\lambda} - \frac{2\tilde{\pi}}{\tilde{\lambda}}\right)\Delta z = 2\tilde{\pi} \longrightarrow \Delta z = \frac{\lambda}{1-\sqrt{1-(\lambda/d)^2}} \approx \frac{2d^2}{\lambda}$$

Once understanding the longitudinal period, the rest of the theory of our new spectrometer is only usual Fourier mathematics.

For discussing the resolution of a spectral doublet $\Delta\lambda$, one has to bring together two facts. Firstly, if the lines of the doublet are close, one needs a big grating distance Z for detecting any loss of contrast. It is convenient to define a contrast reduction of $0.71\ \left(=\cos\frac{\tilde{\pi}}{4}\right)$ as detectable. Secondly one has to consider whether there is any limit to big grating distances Z. This limit is due to the finite width of the grating and hence due to the Number N of the grating periods. If the grating is small, it will diverge the transversely-modulated plane wave into the two usual

oblique plane waves (symmetrical diffraction orders). Putting together these two facts on gets as the limit of resolution in the above defined sense: $\lambda/\Delta\lambda = 2N$

As has been pointed out by several authors[4], especially in the infrared region the question of luminosity is a very important one. In this respect the Fourier spectrometers generally can have some advantages. Here we improve the luminosity when replacing the entrance slit by a grid. Every slit of the grid will produce its own Fourier image from the first grating in the plane of the second grating. Of course, these Fourier images have to lie in coincidence, shifted only by integers of the grating constant. For this the grid constant has to decrease, when the grating distance Z increases. Such a variable grid is realized by Moiré fringes from two inversely rotating grids[5], or by Moiré fringes from two opposite moving Fresnel zone plates[7].

Our two-gratings-interferometer is possible also in reflection. Actually one needs only one grating, if the light can interact two times with the one grating. The basic idea is also applicable to spectral filters, when putting some gratings equidistant in series. Since the theory is then the same as in the case of X-ray diffraction in a crystal lattice, we call this type "Laue-Bragg". With the same number of gratings, arranged not equidistant but multiple-distant, one gets the "Lyot-Öhman" type. Then the spectral band width is somewhat improved, but the spectral purity has somewhat deteriorated.

Both types of spectral filters let pass the wavelength $\lambda_m = m\, 2d^2/Z$. It is a remarkable fact, that here the harmonics are treated like the basic wave λ_1. In usual interference filters the subharmonics $\lambda_1/2$, $\lambda_1/3$, ... would have the same fate. Already E. Lau[3] has mentioned this curiosity. L. Genzel[6] has suggested that a combination of a grating filter and an interference filter would be good for eliminating both the harmonics and the subharmonics, thus isolating the basic wave.

A more detailed description will follow in the "Zeitschrift f.Physik"

REFERENCES:

1.Talbot F., Phil. Mag. 9, 401 (1836)
2.Cowley J.M. and Moodie A.F.,Proc.Phys.Soc.B70,486,497,505 (1957); 76,378 (1960).
3.Lau E., Ann. der Phys.(6)2,417(1948); Wiss.Ann.1,43(1952).
4.Spectroscopie interferentiel, in J.Phys.Rad.19,nr 3(1958)
5.Lohmann A., Optik 14,510(1957); Optica Acta 6,37(1959)
6.Genzel L., private communication
7.Lohmann A., Optik 18,514(1961)

19 Fresnel Diffraction on Zone Plates and Lenses

19.1 About inventing

The content of this chapter is somewhat unconventional. You might not like it unless you are told beforehand *why* these items are treated in this particular way. Briefly we will study Fresnel diffraction with a Fresnel zone plate as diffraction object. As is customary in all textbooks we will find that the light behind a FZP will be concentrated into a few focal points.

Next we conclude the FZP is not really ideal as a focal glass, for example to light a match. We will systematically improve the FZP and thereby invent the lens. Why such an anachronistic approach to introduce the lens as an extreme special case of the FZP? In the first place, in presenting it this way you will see how the lens could have been invented. I believe that "inventing" can be taught. Here I want to show you how it could have happened. The fact that historically the lens was invented independently of the FZP does not diminish the usefulness of our approach, which in its style is representative for inventing in general. True, some inventions come like a flash from heaven, others by trial and error. But many inventions are the straightforward result of hard work and logical analysis.

Another reason for our approach is symbolically expressed in these two equations:

$$\begin{aligned} \text{Grating} &= \sum C_m \text{Prisms}(m) \\ \text{Zone Plate} &= \sum C_m \text{Lenses}(m) \end{aligned} \tag{19.1}$$

(in contrast to the Fourier transformation). Based on theses three facts:

$$\begin{aligned} &\text{lens transmittance :} && e^{i\pi\frac{(x^2+y^2)}{\lambda f}}; \qquad (\text{f positive or negative}) \\ &\text{FZP transmittance :} && \sum C_m e^{2\pi i m\frac{(x^2+y^2)}{R}}; \\ &\text{general transmittance :} && u_0(x,y) = \iint \breve{u}(x',y') e^{i\pi\frac{((x-x')^2+(y-y')^2)}{\lambda z}} \mathrm{d}x'\mathrm{d}y' \end{aligned} \tag{19.2}$$

we will arrive at the following conclusions:

A FZP can be thought of as a superposition of concentric lenses with focal powers $\frac{1}{f_m} = \frac{-2m\lambda}{R^2}$; $m = 0,\ \pm1,\ \pm2,\ \ldots$. The term "concentric" means that all lens centers coincide. Furthermore, since the Fresnel transformation is a complete representation we can think of

the general object $u(x, y)$, as being built together by many lenses with equal focal powers $\frac{1}{f} = -\frac{1}{z}$ (z arbitrary but fixed) and with shifted center locations (x', y') and corresponding "strengths" $\breve{u}(x'y')$.

Finally we will derive the so-called lens equation based on waveoptical considerations. This might be clumsier than the usual geometrical optics derivation, which however is not quite so true since waves are truer than rays.

19.2 Diffraction on the Fresnel Zone Plate

The transmittance of the Fresnel zone plate is:

$$\mathrm{FZP}(x) = \sum A_m e^{2\pi i m\left(\frac{x}{R}\right)^2} \tag{19.3}$$

Let us assume the FZP to be in $z = 0$, and illuminated with a plane wave $u(x, y, z) = e^{ikz}$ in $z < 0$. Hence $u(x, y, +0) = u_0(x, y) = \mathrm{FZP}(x)$. We use now the parabolic HFK formula (Eq. 16.46), and we omit constant factors.

$$u(x, z) = \int \sum A_m e^{i[2\pi m\left(\frac{x'}{R}\right)^2 + \frac{\pi(x-x')^2}{\lambda z}]} \mathrm{d}x' \tag{19.4}$$

The exponent has the form:

$$x'^2\pi(\frac{2m}{R^2} + \frac{1}{\lambda z}) + \frac{\pi x^2}{\lambda z} - \frac{2\pi x x'}{\lambda z} \tag{19.5}$$

There are some very interesting solutions to this integral, i.e. if the factor attached to x'^2 becomes zero:

$$\frac{2m}{R^2} + \frac{1}{\lambda z} = 0 \qquad \boxed{z_m = -\frac{R^2}{2m\lambda}} \tag{19.6}$$

In these particular planes the m-th term of $\sum(m)$ becomes a δ-function:

$$A_m \int e^{i\pi\frac{(x^2 - 2xx')}{\lambda z_m}} \mathrm{d}x' = A_m \delta\left(\frac{x}{\lambda z_m}\right) e^{i\pi\frac{x^2}{\lambda z_m}} \tag{19.7}$$

If the FZP has only a finite width, the object function has to be modified by a rect-function:

$$\begin{aligned} u_0(x') &= \mathrm{FZP}(x')\mathrm{rect}\left(\frac{x'}{\Delta x}\right) \\ A_m \int_{\frac{-\Delta x}{2}}^{\frac{\Delta x}{2}} e^{i\pi\frac{(x^2 - xx')}{\lambda z_m}} \mathrm{d}x' &= \Delta x A_m e^{i\pi\left(\frac{x^2}{\lambda z_m}\right)} \mathrm{sinc}\left(\frac{x\Delta x}{\lambda z_m}\right) \end{aligned} \tag{19.8}$$

This light spot has a width of about $\frac{\lambda z_m}{\Delta x}$, and it is situated at a distance $z_m = \frac{-R^2}{2m\lambda}$ away from the FZP. The width can be expressed also in some other ways, whereby Δx refers to the diameter of the FZP, and N to the number of rings, which is given by $\frac{\Delta x}{2} = \sqrt{N}R$.

$$\delta x_m = \frac{|\lambda z_m|}{\Delta x} = \frac{R^2}{2\Delta x|m|} = \frac{R}{4\sqrt{N}|m|} = \frac{\Delta x}{8N|m|} \tag{19.9}$$

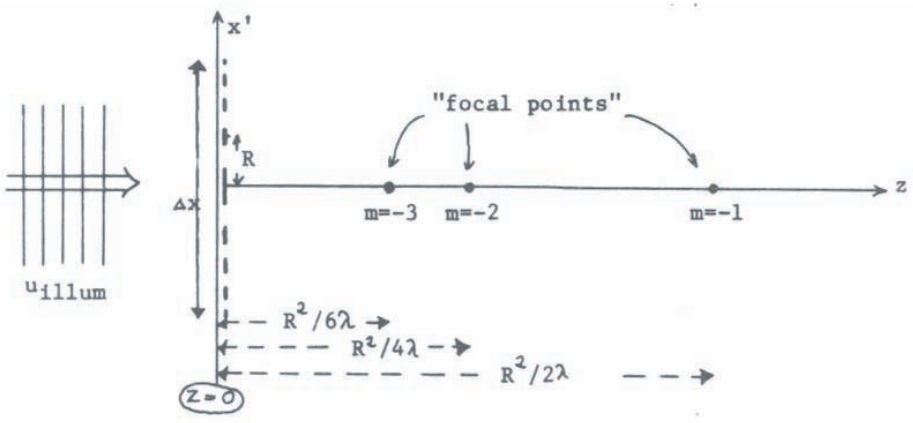

Figure 19.1: Focus spots generated by a Fresnel Zone Plate.

Hence the FZP can be used as a focal glass, or rather as a superposition of many focal glasses, with focal lengths $f_m = \frac{R^2}{2\lambda|m|}$.

These Fresnel Zone Plates are not very useful as focal-glasses or lenses because the multiplicity of focal lengths confuses. But an understanding of this diffraction effect is worthwhile in view of holography. Furthermore, if nobody had invented a lens yet, our new knowledge about the FZP would strongly suggest how to invent a lens. So far we used the FZP only as a "focal glass", which is what one does (but should not) when holding a lens in bright sunlight a few centimetres above some dry paper or grass. The distance is chosen such that the focal spot is as sharp and bright as possible. Anyway, a term of the form $e^{2\pi i m\left(\frac{x}{R}\right)^2}$ as part of our object function $u_0(x) = \sum A_m e^{2\pi i m\left(\frac{x}{R}\right)^2}$ created a focal spot at $z_m = -\frac{R^2}{2m\lambda}$. Calling $|z_m|$ the focal length, one obviously would prefer an object function like this: (the complex transmittance of a one-dimensional lens, a so-called cylinder lens)

$$u_0(x) = e^{i\pi\frac{x^2}{\lambda f}} \tag{19.10}$$

This "lens" is a better focal glass since it concentrates all the light into one single focal spot. The same in two dimensions is (spherical lens, Fig. 19.2):

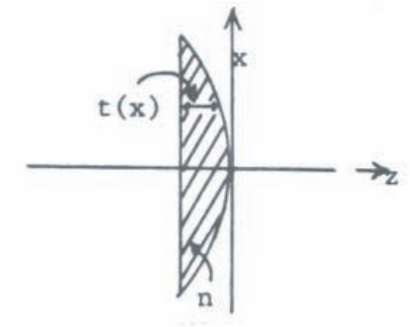

Figure 19.2: The physical shape of a lens.

$$
\begin{aligned}
u_0(x,y) &= e^{-i\pi\frac{(x^2+y^2)}{\lambda f}} \qquad (19.11)\\
t(x) = t_0 - t_2x^2 &= t_0 - \frac{x^2}{2R'} \qquad \text{(Radius of curvature)}\\
\varphi(x) &= \frac{2\pi}{\lambda}(n-1)t(x) = \underbrace{\frac{2\pi}{\lambda}(n-1)t_0}_{\text{just a constant}} - \frac{\pi(n-1)}{\lambda R^2}x^2
\end{aligned}
$$

By comparison we see:

$$\boxed{f = \frac{R'}{n-1}} \qquad (19.12)$$

So far we have considered only the focal-glass action of a lens. More important are two other functions: image formation and Fraunhofer diffraction. We want now to show that our lens, which so far we had conceived on the basis of a somewhat shaky analogy, really is a lens in the sense of being able to perform two actions.

19.3 Image formation in terms of Fresnel diffraction

We will use the parabolic HFK (Eq. 16.46) twice for computing wave propagations. The lens will be taken into account by a multiplication.

We start with $u_0(x')$ in $z = 0$ (Fig. 19.3):

$$
\begin{aligned}
u_0(x') &\longrightarrow u(x'',z) = u_1(x'') = \int u_0(x')e^{i\pi[\frac{(x'-x'')^2}{\lambda z_1}]}\mathrm{d}x' \qquad (19.13)\\
u_1(x'') &\longrightarrow v_1(x'') = u_1(x'')e^{-i\pi\frac{x''^2}{\lambda f}}\\
v_1(x'') &\longrightarrow v(x) = \int v_1(x'')e^{i\pi\frac{(x-x'')^2}{\lambda z_1}}\mathrm{d}x''
\end{aligned}
$$

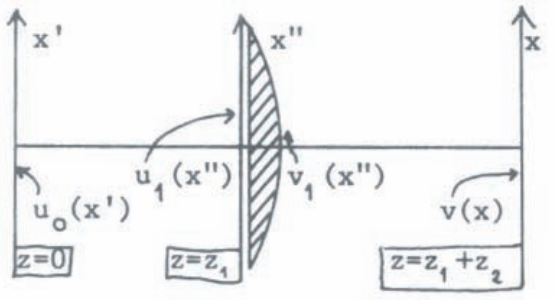

Figure 19.3: Image formation in the Fresnel approximation.

These were the steps, now let us compute $v(x)$, where we will look for values of z_2 which will lead to the formation of an image.

$$\begin{aligned} v(x) &= \int v_1(x'')e^{\frac{i\pi}{\lambda}\frac{(x-x'')^2}{z_2}}\mathrm{d}x'' = \int u_1(x'')e^{\frac{i\pi}{\lambda}\left[\frac{(x-x'')^2}{z_2}-\frac{x''^2}{f}\right]}\mathrm{d}x'' = \\ &= \iint u_0(x')e^{\frac{i\pi}{\lambda}\left[\frac{(x-x'')^2}{z_2}-\frac{x''^2}{f}+\frac{(x'-x'')^2}{z_1}\right]}\mathrm{d}x'\mathrm{d}x'' \end{aligned} \tag{19.14}$$

Since we hope that $v(x)$ is an image of $u(x')$, we are eagerly looking for something like a delta-function, which changes the x' of $u(x')$ into the x of $v(x)$. To this end we sort the $[\ldots]$ of the exponent.

$$\left[\frac{(x-x'')^2}{z_2}-\frac{x''^2}{f}+\frac{(x'-x'')^2}{z_1}\right] = x''^2\left\{\frac{1}{z_2}-\frac{1}{f}+\frac{1}{z_1}\right\}-2x''\left(\frac{x}{z_2}+\frac{x'}{z_1}\right)+\frac{x^2}{z_2}+\frac{x'^2}{z_1} \tag{19.15}$$

If in Eq. 19.14 any one of the two integrations over (x') and (x'') yields a delta function then it must be the (x'') integral because (x'') does not occur in the lower part of the integrand. The (x'') integral has the form:

$$\int e^{\frac{i\pi}{\lambda}\left[x''^2\left(\frac{1}{z_2}-\frac{1}{f}+\frac{1}{z_1}\right)-2x''\left(\frac{x}{z_1}+\frac{x'}{z_1}\right)\right]}\mathrm{d}x'' \tag{19.16}$$

For our purposes the x''^2 term is a nuisance. Hence we chose a plane z_2, such that the x''^2 coefficient vanishes.

$$\boxed{\frac{1}{f}=\frac{1}{z_1}+\frac{1}{z_2}} \tag{19.17}$$

This is actually the lens formula, connecting focal length f, object distance z_1, and image distance z_2. Now the x'' integral is only:

$$\int e^{-\frac{2i\pi x''}{\lambda}\left(\frac{x}{z_1}+\frac{x'}{z_1}\right)}\mathrm{d}x'' = \delta\left(\frac{x}{z}+\frac{x'}{z}\right) = \lambda z_1 \delta\left(x'+x\frac{z_1}{z_2}\right) \tag{19.18}$$

We neglect the factor λz_1, and we insert the delta-function

$$\begin{aligned} v(x) &= e^{i\pi\frac{x^2}{\lambda z_2}}\int u_0(x')e^{i\pi\frac{x'^2}{\lambda z_1}}\delta\left(x\frac{z_1}{z_2}+x'\right)\mathrm{d}x' \\ &= u_0\left(x\frac{z_1}{z_2}\right)e^{i\frac{\pi x^2}{\lambda}\left(\frac{1}{z_2}+\frac{z_1}{z_2^2}\right)} \end{aligned} \tag{19.19}$$

The corresponding intensities are:

$$|v(x)|^2 = \left|u_0\left(-x\frac{z_1}{z_2}\right)\right|^2; \quad |v(x,y)|^2 = \left|u_0\left(-\frac{x}{M},-\frac{y}{M}\right)\right|^2 \tag{19.20}$$

The factor $\frac{z_2}{z_1}$ signifies the magnification M. The minus sign means an inversion. The phase factor of $v(x)$ is normally not observable.

This theory can be easily expanded so as to predict also the limit of resolution. For this purpose we carry out the (x'') integration only over the finite diameter of the lens. This yields a sinc-function. Hence the image amplitude $v(x)$ is a convolution of the object amplitude $u_0(x)$ and a sinc-function. The blurring due to the sinc-convolution limits the resolution of the image. *More later*.

20 What is a Light Ray?

20.1 Motivation of our approach

Geometrical optics or ray optics is only a coarse approximation of the more rigorous wave optics. Why then is anyone interested in ray optics? Because it is usually much simpler, wherever it is applicable. The big question is: *When* is ray optics applicable and when not? A good understanding of this question is very important. It may help you considerably to shorten the theory of a new optical experiment if you know when a ray-optical shortcut is permissible. Often in the theory of a single experiment some aspects will be treated wave-optically, others ray-optically. No doubt, this saves time in comparison to an all-wave-optical theory. Maybe you don't like such a hybrid or schizophrenic approach. Personally, I like it very much, since this mixed treatment is as challenging as dancing on a rope. And aren't all interesting persons a bit schizophrenic anyway?

There are at least four different approaches to ray-optics to choose from. They are:

1. Axiomatic (starting from Snellius and reflection laws);
2. Limit ($\lambda \to 0$) of wave optics is "ray optics";
3. Energy conservation a axiom (see H. G. Zimmer's book Geometrical Optics, Springer, 1970);
4. Approximation of wave optics by the method of stationary phase.

I prefer the fourth approach, which was well presented by A. Walther in the American Journal of Physics 35, 808 (1967). It is almost the same as "Parageometrical Optics", developed by G. Toraldo di Francia.

Briefly, the result of our treatment will be: A "ray" is the wave vector of that particular plane wave component which is singled out by the method of stationary phase. That particular wave is found by minimizing the optical path $\int n\mathrm{d}s = \mathrm{OPD}$. Remember the phase is $\frac{2\pi}{\lambda} \cdot \mathrm{OPD} = k{\cdot}\mathrm{OPD}$. The minimum value of this phase represent the stationary phase. The minimization of the OPD is what Fermat used as the single axiom for deriving all laws of geometrical optics. All the statements of this short paragraph will be explained later in this Chapter 20.

We already got a taste of ray optics on pp. 152-156, where we derived the HFK integral from the RSD integral. We made use of the method of stationary phase, which in two dimensions is often called "saddle-point method". The derivation was briefly like this:

$$\begin{aligned}
\text{R.S.D.} \quad u(x,y,z) &= \iint u(x',y',z') \left\{ \iint e^{i\vec{k}(\nu,\mu)\cdot(\vec{x}-\vec{x'})} \mathrm{d}\nu \mathrm{d}\mu \right\} \mathrm{d}x' \mathrm{d}y' \\
\text{where :} \quad \vec{k}(\nu,\mu) &= \frac{2\pi}{\lambda} \left\{ \lambda\nu, \lambda\mu, \sqrt{1-\lambda^2(\nu^2+\mu^2)} \right\}; \quad \vec{x} = (x,y) \qquad (20.1) \\
\text{H.F.K.} \quad u(x,y,z) &= \iint u(x',y',z') \cos\epsilon \frac{e^{i\vec{k}(\nu_0,\mu_0)\cdot(\vec{x}-\vec{x'})}}{\lambda|\vec{x}-\vec{x'}|} \mathrm{d}x' \mathrm{d}y' \\
\text{where :} \quad \cos\epsilon &= \frac{z_0(\vec{x}-\vec{x'})}{|\vec{x}-\vec{x'}|}; \quad r = |\vec{x}-\vec{x'}|; \quad \vec{x} = \{x,y,z\}; \\
\nu_0 \text{ and } \mu_0 \text{ from :} \quad & \frac{\partial[\vec{k}(\nu,\mu)\cdot(\vec{x}-\vec{x'})]}{\partial\nu} = 0 \quad \text{and} \quad \frac{\partial[\ldots]}{\partial\mu} = 0
\end{aligned}$$

There is one particular plane wave with $\vec{k} = \vec{k}(\nu_0, \mu_0)$, which dominates the $\{\int \ldots \mathrm{d}\nu, \mathrm{d}\mu\}$ in the RSD-integral, because the rest cancel each other. This particular plane wave has just the direction from $\vec{x}$ to $\vec{x'}$. Hence $\vec{k}(\nu_0,\mu_0) \parallel (\vec{x}-\vec{x'})$ (parallel) $\rightarrow \vec{k}(\nu_0,\mu_0)\cdot(\vec{x}-\vec{x'}) = k(|\vec{x}-\vec{x'}|) = kr$. This parallelism of $\vec{k}(\nu_0,\mu_0)$ and $\vec{x}-\vec{x'}$ suggests, or is at least compatible with the statement, that the contribution from the object amplitude $u(x',y',z')$ at $\vec{x'}$ to the diffraction amplitude $u(x,y,z)$ at $\vec{x}$ *goes along a straight line* from $\vec{x}$ *to* $\vec{x'}$. This "straight path of contribution" may be called a "ray".

20.2 The Fermat Principle as a consequence of wave optics

We want to understand in more detail how the "rays" emerge as approximations, so that we know when we can without danger consider light simply as rays, and when we have to take the wave character into account.

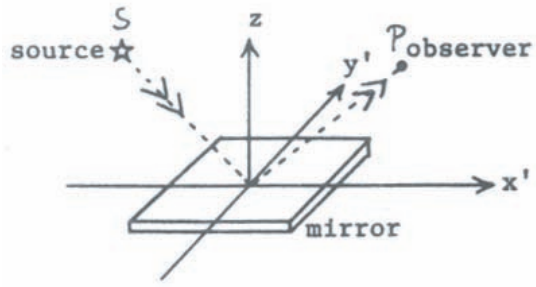

Figure 20.1: Fermat's principle and the law of reflection.

Reflection:

Since we know of course the law of reflection, we may as well position our coordinate system so that the analysis comes out easily. This is always wise to do, and never excludes the truth, even if the choice of the coordinate system was done based on a wrong anticipation. From source S a spherical wave emerges. $S(-x, 0.z)$; $P(+x, 0, z)$. In plane z it is $u_S = \delta(x'+x)\delta(y')$. From there in the negative z-direction towards the mirror in $z = 0$ we get with HFK:

$$\begin{aligned} u(x'', y'', 0) &= \iint \delta(x'+x)\delta(y')\cos\epsilon \frac{e^{ikr}}{\lambda r}\mathrm{d}x'\mathrm{d}y'; \\ r &= \sqrt{z^2+(x''+x')^2+(y''-y')^2}; \quad \cos\epsilon = \frac{z}{r} \end{aligned} \tag{20.2}$$

$(x'', y'', 0)$ ∼arbitrary point on M; (x', y', z) ∼ arbitrary point in S-plane z. Executing this integral gives $u(x'', y'', 0) = \cos\epsilon \frac{e^{ikr}}{\lambda r}$, where now r means $r = \sqrt{z^2+(x''+x)^2+y''^2}$; $\cos\epsilon = \frac{z}{r}$. Now we assume $u(x'', y'', 0)$ our "secondary object", from which light will propagate in the positive-z direction. Again HFK; particularly for point $P(+x, 0, z)$:

$$\begin{aligned} u(x, 0, z) &= \iint u(x'', y'', 0)\cos\epsilon' \frac{e^{ikr'}}{\lambda r'}\mathrm{d}x''\mathrm{d}y'' \\ &= \iint \cos\epsilon\cos\epsilon' \frac{e^{ik(r+r')}}{\lambda^2 r r'}\mathrm{d}x''\mathrm{d}y'' \\ r' &= \sqrt{(x-x'')^2+y''^2+z^2}, \qquad \cos\epsilon' = \frac{z}{r'} \end{aligned} \tag{20.3}$$

This integral just begs be handles by the saddle-point method, whereby $g(x'', y'') = \frac{\cos\epsilon\cos\epsilon'}{rr'}$ and $f(x'', y'') = r + r'$. Let's find the saddle-point:

$$\begin{aligned} \frac{\partial f}{\partial x''} &= \frac{x''+x}{r} + \frac{x''-x}{r}; \qquad \frac{\partial f}{\partial y''} = \frac{y''}{r} + \frac{y''}{r'}; \quad \frac{\partial f}{\partial y''} = 0 \quad \text{for} \quad y'' = 0; \\ \frac{\partial f}{\partial x''} &= 0; \quad \text{if} \quad \frac{x-x''}{r'} = \frac{x+x''}{r} \end{aligned} \tag{20.4}$$

Since $\frac{\partial f}{\partial y''} = 0$ gave $y_0'' = 0$, the $\frac{\partial f}{\partial x''} = 0$ condition is easy to draw in the $(x-z)$-plane. $\frac{x-x''}{r'} = \cos\epsilon''$; $\frac{x+x''}{r} = \cos\epsilon$; hence $\epsilon = \epsilon'$. So we have got both features of the reflection law (Fig. 20.2):

1. $\epsilon = \epsilon'$;
2. reflection point with P and S in a plane perpendicular to mirror.

However, without really performing the saddle-point method, we can interpret it in a nice and general way. It was $f = r + r'$. Now $\frac{\partial f}{\partial x''} = 0$ and $\frac{f}{y''} = 0$ mean, that *the smallest* $r + r'$ (or the longest) of all paths from S to any mirror point to P will be the one which *really counts*. All other paths are not blocked, but they account for the oscillating contributions of

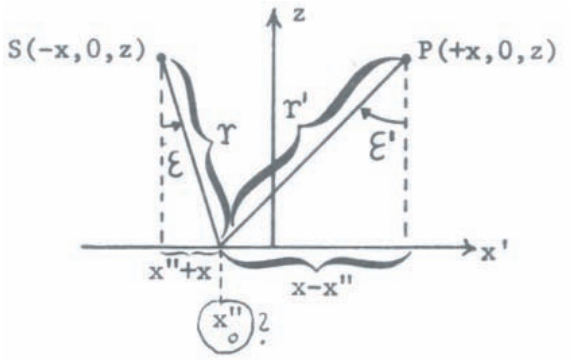

Figure 20.2: The law of reflection: definition of the parameters used in the derivation.

the HFK integral. The integrand (essentially) is $\cos[k(r+r')]$. In this sense we can say that in the process of reflection the essential amount of u_P comes from U_S along the shortest $r - r'$. This is one part of the so-called Fermat-principle, which Fermat (1601—1665) deduced as the one principle underlying all known ray-optical effects.

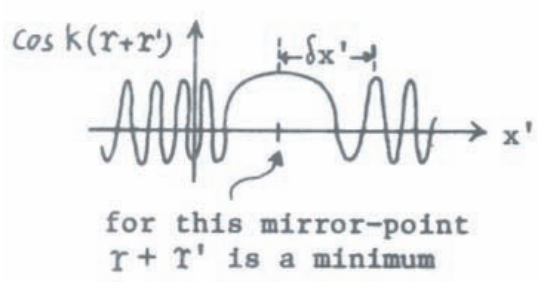

Figure 20.3: The cosine factor illustrating the principle of the saddle-point method.

To get an idea of how well this works, let us compute $\delta x'$ (see Fig. 20.3) $\cos kf \approx \cos\left\{k(f_0 + f_0''\frac{(x'-x_0')^2}{2} + \ldots)\right\}$, $kf_0''\frac{(\delta x')^2}{2} = 2\pi\delta x' = \frac{\sqrt{\lambda r}}{\cos\epsilon}$. Except for the factor $\frac{1}{\cos\epsilon}$ this is the same "beam unsharpness", as we will encounter later in parageometrical optics. Even the cosine-factor is justified, considering that the mirror plane is tilted by $\frac{\pi}{2} - \epsilon$ with respect to the "ray". The important consequence is that the mirror does not have to be infinitely large; if it is only $2\delta x'$ wide, that is enough. The rest of the mirror transmits anyway only oscillating contributions.

Now let us derive similarly the *law of refraction*, which could be done more simply and

more rigorously by using the RSD-plane wave presentation. But HFK is nicer for getting the ray-picture out of it. We have to remember here that the wave equations for a medium with (homogeneous) refractive index $n \neq 1$ the k^2 goes into $k^2 n^2$. Hence also in the HFK integral: $k \to nk$. Object in $(-z)$: $\delta x' \delta y'$; from there to $z = 0$ in medium n_1

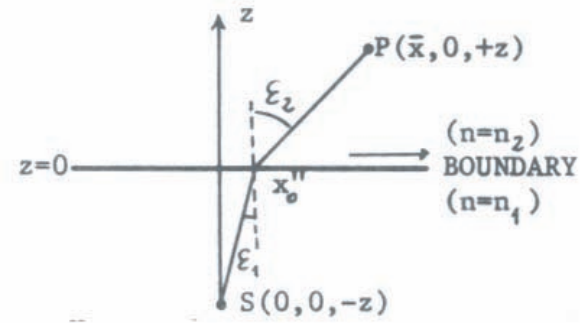

Figure 20.4: The law of refraction: definition of the parameters used in the derivation.

$$\begin{aligned} u(x'',y'',0) &= \iint \delta x'\delta y' \cos\epsilon'' \frac{e^{in_1 k r''}}{\frac{\lambda r''}{n_1}} \mathrm{d}x'\mathrm{d}y' = \cos\epsilon_1' \frac{e^{in_1 k r_1'}}{\frac{\lambda r'}{n_1}} \\ r_1 &= \sqrt{z^2 + x''^2 + y''^2}; \qquad \cos\epsilon_1 = \frac{z}{r_1} \end{aligned} \tag{20.5}$$

Now from $z = 0$ to $+z$ in medium n_2, particularly $y = 0$ and $x = \overline{x}$:

$$\begin{aligned} u(\overline{x},0,z) &= \iint \cos\epsilon_1 \cos\epsilon_2 \frac{e^{ik(n_1 r_1 + n_2 r_2)}}{\lambda_1 r_1 \lambda_2 r_2} \mathrm{d}x''\mathrm{d}y''; \quad \lambda_1 = \frac{\lambda}{n_1}; \quad \lambda_2 = \frac{\lambda}{n_2} \\ r_2 &= \sqrt{z^2 + (\overline{x} - x'')^2 + y''^2}; \quad \cos\epsilon_2 = \frac{z}{r_2} \end{aligned} \tag{20.6}$$

Again we use the saddle point method: $\frac{g=(\cos\epsilon_1, \cos\epsilon_2)}{r_1 r_2}$; $f = n_1 r_1 + n_2 r_2$; $\frac{\partial f}{\partial x''} = 0$ and $\frac{\partial f}{\partial y''} = 0$. Select the saddle point (x_0, y_0) such that the *optical path* $n_1 r_1 + n_2 r_2$ *will be a minimum* (Fermat).

$$\begin{aligned} \frac{\partial f}{\partial y''} &= 0 = y'' \left(\frac{n_1}{r_1} + \frac{n_2}{r_2} \right) \to y_0'' = 0 \\ \frac{\partial f}{\partial x''} &= 0 = \frac{n_1 x_0''}{\sqrt{z^2 + x_0''}} + \frac{n_2 (x_0'' - \overline{x})}{\sqrt{z^2 + (\overline{x} - x_0'')^2}} \end{aligned} \tag{20.7}$$

This equivalent with $\boxed{n_1 \sin\epsilon_1 = n_2 \sin\epsilon_2}$. It is due to Snell (1581 - 1626). A δx-consideration would come out just as it did for reflection.

20.3 What are Shadows or "Non-Rays"?

The way we have so far introduced "rays" is not yet quite satisfactory, because we would like to be sure, that what is called a "ray" during this lecture is the same as the "ray" we know from daily life. What do we know about daily-life rays? If your eye perceives a candle light, and you move a finger along a straight line from your eye to the candle light, your finger will move right into the source which causes the light sensation in your eye. You will feel it, to be convinced. If you move your finger in another direction, where your finger will not feel that hot sensation, then you may conclude that there is no candle-light; or if your finger hits a cold obstacle, you may conclude that some cold obstacles will stop the rays. Based on these simple experiences you will conclude that rays go straight, and can be blocked. (Let us assume that the medium is air, so that you are not fooled by such light-ray deviating effects as reflection and refraction).

All this suggests that we should investigate an experiment as show in Fig. refshadow. We want to find out if a wave-optical investigation gives (at least in approximation) the same result as we expect from our "daily-life rays".

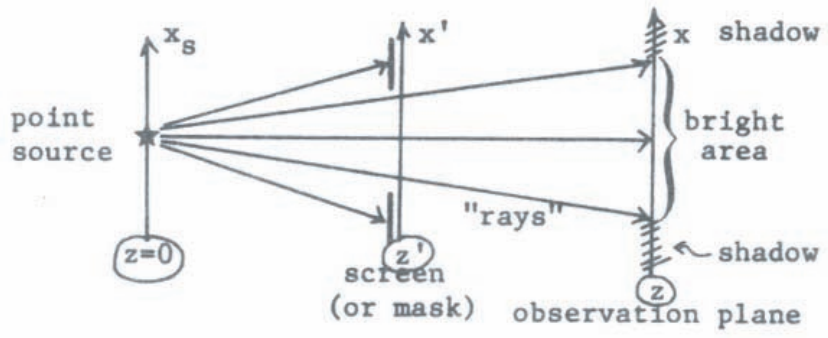

Figure 20.5: Experimental investigation of shadow effects based on ray-optics.

First step from $z = 0$ to $z = z'$:

$$u(x', y', z') = \iint u(x_s, y_s, 0) \cos\epsilon' \frac{e^{ikr'}}{\lambda r'} \mathrm{d}x_s \mathrm{d}y_s \tag{20.8}$$

$$\text{where :} \qquad r' = \sqrt{(x' - x_s)^2 + (y' - y_s)^2 + z'^2}; \qquad \cos\epsilon' = \frac{z'}{r'}$$

Point source:

$$u(x_s, y_s, 0) = \delta(x_s, y_s) \rightarrow u(x', y', z') = \cos\epsilon' \frac{e^{ikr'}}{\lambda r'} \tag{20.9}$$

$$\text{now :} \qquad r' = \sqrt{x'^2 + y'^2 + z'^2}$$

Second step from $z = z' - 0$ to $z = z' + 0$

$$u(x', y', z' - 0) \to u(x', y', z' + 0) = \underbrace{S(x', y')}_{\substack{\text{screen,} \\ \text{either 1 or 0}}} \cdot u(x', y', z' - 0) \tag{20.10}$$

The second step is what we called "Kirchhoff-approximation".
Third step from $z' + 0$ to z:

$$u(x, y, z) = \iint u(x', y', z' + 0) \cos\epsilon \frac{\exp ikr}{\lambda r} \mathrm{d}x' \mathrm{d}y' \tag{20.11}$$

$$r = \sqrt{(x - x')^2 + (y - y')^2 + (z - z')^2}; \quad \cos\epsilon = \frac{z - z'}{r}$$

Inserting $u(x', y', z' + 0)$ as we know it already yields:

$$u(x, y, z) = \iint \cos\epsilon \cos\epsilon' \frac{e^{ik(r'+r)}}{\lambda r r'} \mathrm{d}x' \mathrm{d}y' \tag{20.12}$$

This integral would be interpreted by Huygens like this: first the point sources created a spherical wave, from which the screen cuts out a portion. Each point x' in the screen (with proper phase kr' and amplitude) creates another spherical wave, with an additional phase kr, where r is the distance from this secondary point source at x' to the point of observation at x.

In order to understand this integral better we use again the method of stationary phase. The integral has the form

$$\iint g(x', y') e^{ikf(x', y')} \mathrm{d}x' \mathrm{d}y' \approx g(x_0, y_0) A(x_0, y_0) e^{ikf(x_0, y_0)} \tag{20.13}$$

whereby x_0 and y_0 are to be determined according to the stationary phase recipe:

$$\frac{\partial f}{\partial x'} = 0 = \frac{\partial r' + r}{\partial x'} = \frac{x' - x}{r'} + \frac{x' - x}{r} \to \frac{x'_0}{r'} = \frac{x - x'_0}{r} \tag{20.14}$$

$$\frac{\partial f}{\partial y'} = 0 \to \frac{y'_0}{r'} = \frac{y - y'_0}{r}$$

(with $r' = \sqrt{x'^2 + y'^2 + z'^2}$ and $r = \sqrt{(x - x')^2 + (y - y')^2 + (z - z')^2}$)
This result from $\frac{\partial f}{\partial x'}$ can be interpreted very easily in terms of "rays":

$$\frac{x'}{r'} = \sin\epsilon'; \quad \frac{x - x'}{r} = \sin\epsilon \tag{20.15}$$

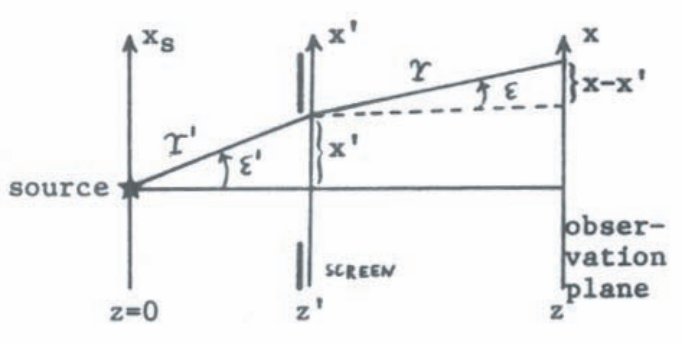

Figure 20.6: Illustration of the ray-optical shadow obtained form the solution of Eq. **??**.

hence $\frac{x_0'}{r_0'} = \frac{x-x_0'}{r_0}$ means $\epsilon_0' = \epsilon_0$ or a straight line. We don't need to calculate explicitly the $g(x_0, y_0)$ and $A(x_0, y_0)$, we know already enough for our present purpose.

What we found is: the point $\vec{x}$ in the observation plane gets essentially all its light from that particular point $\vec{x_0'}$ which lies in planes z' (screen plane) on a *straight line between the source point and the observation point*. Of course, the stationary phase method does not say that there is no other wave contribution besides the straight-line contribution. All the many other contributions, however, cancel each other, because the phases $k(r' + r)$ vary rapidly, depending on the point x', y', in the z' plane where these other wave contributions intercept the z'-plane.

What happens if the "straight-line-point" (x_0', y_0', z') falls onto the screen where $S(x_0', y_0') = 0$? In that case only oscillating contributions reach $\vec{x}$. Hence $u(x, y, z)$ will be approximately zero for those points in the observation plane from where one cannot see the source. In other words our diffraction theory confirms that there will be shadows.

20.4 Two examples of parageometrical optics

The term "parageometrical optics", coined by Toraldo di Francia, means that it is an approximation of wave-optics, which has some typical features of geometrical optics or ray optics. In terms of accuracy it stands in the middle. We will see that it is often useful, because it is much simpler than the more rigorous wave optics, yet it does not neglect completely the wave nature of light, as geometrical optics does. We will study two particular cases, and later an application relating to Talbot images.

20.4.1 Tilted plane wave falling onto wide screen

We will use the parabolic approximation of the HFK theory (Fig. 20.7):

$$
\begin{aligned}
&\text{in } z<0: && u(x,z)=e^{2\pi i[\nu_0 x+\sqrt{1-\lambda^2\nu_0^2}\frac{z}{\lambda}]} \qquad (20.16)\\
& && \lambda\nu_0=\sin\alpha_0;\quad \sqrt{1-\lambda^2\nu_0^2}=\cos\alpha_0\\
&\text{in } z=-0: && u(x,-0)=e^{2\pi i\nu_0 x}\\
&\text{in } z=+0: && u(x,+0)=e^{2\pi i\nu_0 x}\mathrm{rect}\left(\frac{x}{\Delta x}\right)\\
&\text{in } z\geq 0: && u(x,z)\approx u(x',0)e^{i\pi\frac{(x-x')^2}{\lambda z}}\mathrm{d}x'\\
& && =\int\limits_{-\frac{\Delta x}{2}}^{\frac{\Delta x}{2}} e^{2\pi i\nu_0 x'}e^{i\pi\frac{(x-x')^2}{\lambda z}}\mathrm{d}x'=\int\limits_{-\frac{\Delta x}{2}}^{\frac{\Delta x}{2}} e^{i\pi\left[\frac{(x-x')^2}{\lambda z}+2\pi\nu_0 x'\right]}\mathrm{d}x'
\end{aligned}
$$

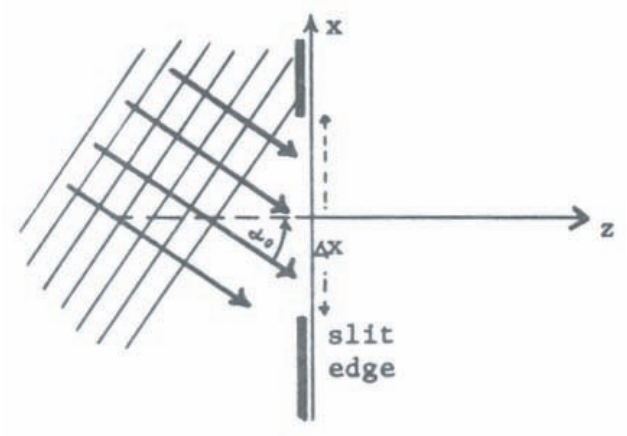

Figure 20.7: Propagation of a tilted plane wave through an aperture.

$$
\begin{aligned}
[\ldots] &= \frac{x'^2-2x'(x-\lambda\nu_0 z)+(x-\lambda\nu_0 z)^2}{\lambda z}+\frac{x^2-(x-\lambda\nu_0 z)}{\lambda z}= \qquad (20.17)\\
&= \frac{(x'-x+\lambda\nu_0 z)^2}{\lambda z}+2\nu_0 x-\lambda z\nu_0^2
\end{aligned}
$$

$$
u(x,z)=e^{i\pi(2\nu_0 x-\lambda z\nu_0^2)}\int\limits_{-\frac{\Delta x}{2}}^{\frac{\Delta x}{2}} e^{i\pi\frac{(x'-x+\lambda\nu_0 z)^2}{\lambda z}}\mathrm{d}x' \qquad (20.18)
$$

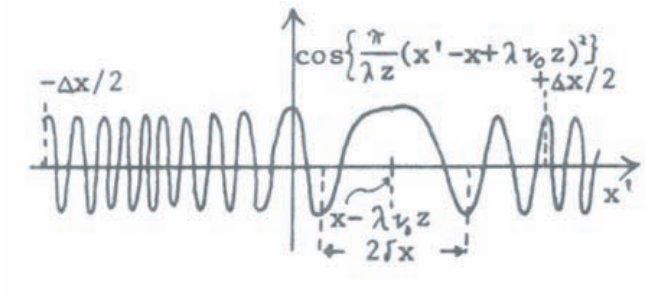

Figure 20.8: Real part of the integrand in Eq. 20.18.

To evaluate the integral, let's plot the real part of the integrand (Fig. 20.8). There will be three significantly different cases, depending on whether the stationary phase point $x'_0 = x - \lambda\nu_0 z$ is either well inside of the slit range $-\frac{\Delta x}{2} \le x' \le \frac{\Delta x}{2}$ (case 1), or close to the slit edges $x' = \pm\frac{\Delta x}{2}$ (case 2), or far outside: $|x'| > \frac{\Delta x}{2}$ (case 3). More specifically the three cases are defined as follows:

$$\int_{-\frac{\Delta x}{2}}^{\frac{\Delta x}{2}} e^{i\pi\frac{(x'-x+\lambda\nu_0 z)^2}{\lambda z}}\,\mathrm{d}x' = \begin{cases} \text{case 1} & \text{if } |x-\lambda\nu_0 z| + \delta x < \frac{\Delta x}{2} \\ \text{case 2} & \text{if } |x-\lambda\nu_0 z| - \frac{\Delta x}{2} < \delta x \\ \text{case 3} & \text{if } |x-\lambda\nu_0 z| - \delta x > \frac{\Delta x}{2}; \end{cases} \tag{20.19}$$

In case (1) we add only negligible oscillating contributions, if we extend the range of integration from $[-\frac{\Delta x}{2}, +\frac{\Delta x}{2}]$ to $[-\infty, \infty]$:

$$\text{case 1:} \qquad = \int_{-\infty}^{\infty} e^{i\pi\frac{(x'-x+\lambda\nu_0 z)^2}{\lambda z}}\,\mathrm{d}x' = \int_{-\infty}^{\infty} e^{i\pi\frac{x'^2}{\lambda z}}\,\mathrm{d}x' = \sqrt{i\lambda z} \tag{20.20}$$

The case (2) is somewhere between (1) and (3). It is the philosophy of parageometrical optics to forget about this (2)-part, and pretend as if only (1) and (3) existed. In a minute we will see if and how this makes sense in the experimental situation we are considering now. In case (3) the integral is practically zero because only the oscillating parts of $\cos(\ldots x'^2)$ contribute.

The width δx of the stationary phase center region is defined by an increase of the cos-argument by π from x'_0 to $x'_0 + \delta x$. At x'_0 itself the cos-argument is zero. We conclude:

$$\pi\frac{(\delta x)^2}{\lambda z} = \pi \quad \text{or} \quad \delta x = \sqrt{\lambda z} \tag{20.21}$$

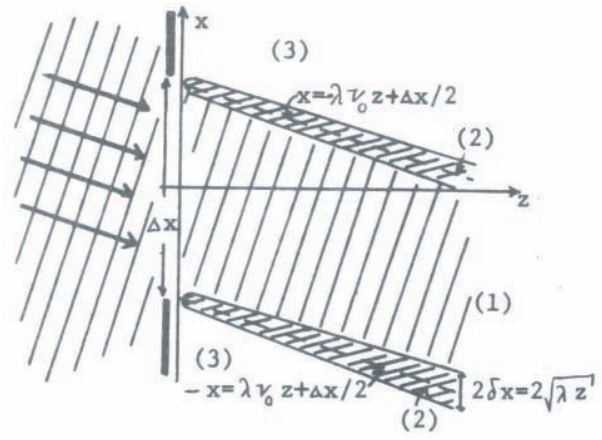

Figure 20.9: Illustration of the parageometrical region on the example of a plane wave.

In Fig. 20.9 the various case (1), (2), and (3) are indicated in the (x, z) space. Obviously the region (2) is negligible as long as $\delta x \ll \Delta x$. In other words the parageometrical approximation makes sense if $\delta x \ll \Delta x$. Together with $\delta x = \sqrt{\lambda z}$ this leads to condition for the validity of parageometrical optics:

$$\boxed{z \ll \frac{(\Delta x)^2}{\lambda}} \tag{20.22}$$

The actual solution for the region (1) is:

$$u(x,z) \approx C' e^{i\pi(2\nu_0 x - \lambda z \nu_0^2)\sqrt{i\lambda z}} \tag{20.23}$$

The factor C', which is usually dismissed as uninteresting, contains a factor e^{ikz}. When not neglecting this factor e^{ikz} we get:

$$u(x,z) = e^{i(kz + 2\pi\nu_0 x - \pi\lambda z\nu_0^2)} = e^{2\pi i\left[\nu_0 x + z\frac{(1-0.5\lambda^2\nu_0^2)}{\lambda}\right]} \approx e^{2\pi i\left[\nu_0 x + \sqrt{1-\lambda^2\nu_0^2}\frac{z}{\lambda}\right]} \tag{20.24}$$

which is the same plane wave which illuminated the slit. In summary we have:

$$u(x,z) \approx \begin{cases} e^{2\pi i\left[\nu_0 x + \sqrt{1-\lambda^2\nu_0^2}\frac{z}{\lambda}\right]} & : \text{ in region (1);} \\ 0 & : \text{ in region (3).} \end{cases} \qquad (z > 0) \tag{20.25}$$

Terminology

Before we continue let's comment briefly on terminology. The rigorous RSD-formula holds for every distance $z \geq 0$ behind the diffraction object in $z = 0$. Evanescent waves are significant mainly in $0 \leq z \leq 4\lambda$, wherby 4λ is of course not a sharp limit. The parageometrical-optics approximation is reasonably good in $4\lambda < z \leq \frac{(\Delta x)^2}{\lambda}$. In the z-region of Fresnel-diffraction it is meaningful to approximate like: $\exp ikr = \exp ik\sqrt{z^2 + x^2}$. That will be the case, if the next higher term in the exponent's expansion is $< \frac{\pi}{4}$; in other words $kz\left(\frac{x}{z}\right)^4 < \frac{\pi}{4} \rightarrow \left|\frac{x}{z}\right|^2 < \frac{\lambda}{z}$ or $|x| < (z\lambda)^{\frac{1}{2}}\left(\frac{z}{\lambda}\right)^{\frac{1}{4}}$. Finally, Fraunhofer diffraction will occur in $z > \frac{(\Delta x)^2}{\lambda}$. These statements will be verified in detail.

20.4.2 A spherical wave falling onto a wide slit

Now the second example of parageometrical optics: A (convergent) spherical wave falls upon a slit of width Δx. At $z < 0$: $u = \frac{e^{-ikr}}{r}$, $r = \sqrt{(z - z_1)^2 + (x - x_1)^2 + (y - y_1)^2}$. The minus sign indicates *convergence* rather than divergence. At plane $z = -0$:

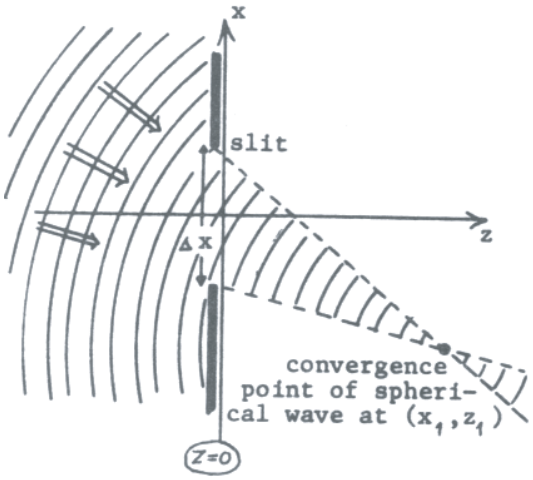

Figure 20.10: Illustration of the parageometrical region on the example of a spherical wave.

$$u(x, -0) = \frac{e^{-ikr_0}}{r_0} \approx \frac{1}{z_1} e^{-ikz_1\left[1 + \frac{(x - x_1)^2}{2z_1^2}\right]} \tag{20.26}$$

At plane $z = +0 : u(x, +0) = u(x, -0)\text{rect}\left(\frac{x}{\Delta x}\right)$.
At plane $z > 0$:

$$u(x,z) \approx \int u(x',+0) e^{i\pi \frac{(x'-x)^2}{\lambda z}} \mathrm{d}x' = \int\limits_{-\frac{\Delta x}{2}}^{\frac{\Delta x}{2}} e^{\frac{i\pi}{\lambda}\left[-\frac{(x'-x_1)^2}{z_1}+\frac{(x'-x)^2}{z}\right]} \mathrm{d}x' \qquad (20.27)$$

We investigate now the square bracket:

$$\begin{aligned}
[\ldots] &= x'^2\left(\frac{1}{z}-\frac{1}{z_1}\right)+2x'\left(\frac{x_1}{z_1}-\frac{x}{z}\right)+\frac{x^2}{z}+\frac{x_1^2}{z_1}= \qquad (20.28)\\
&= \frac{z_1-z}{zz_1}\left\{x'^2+2x'\left(\frac{x_1}{z_1}-\frac{x}{z}\right)\frac{zz_1}{z_1-z}+\left(\frac{x_1}{z_1}-\frac{x}{z}\right)^2\left(\frac{zz_1}{z_1-z}\right)^2\right\}\\
&+ \frac{x^2}{z}+\frac{x_1}{z_1}-\left(\frac{x_1}{z_1}-\frac{x}{z}\right)^2\frac{zz_1}{z_1-z}
\end{aligned}$$

where: $\{\ldots\} = \left[x'+\left(\frac{x_1}{z_1}-\frac{x}{z}\frac{zz_1}{z_1-z}\right)^2\right]$.

The position of the stationary phase point is $x_0' = -\left(\frac{x_1}{z_1}-\frac{x}{z}\right)\frac{zz_1}{z_1-z}$. We distinguish three cases:

1. if x_0' is well inside of the integration range $-\frac{\Delta x}{2} \le x' \le \frac{\Delta x}{2}$;
2. if x_0' is close to $+\frac{\Delta x}{2}$ or $-\frac{\Delta x}{2}$;
3. if x_0' is well outside of the integration region.

The width δx of the stationary phase region around x_0' is given by $\frac{\pi}{\lambda}\frac{z_1-z}{z_1 z}(\delta x)^2 = \pi \rightarrow \delta x = \sqrt{|\frac{\lambda z z_1}{(z_1-z)}|}$; or $\frac{\delta x}{\sqrt{\lambda}}\frac{1}{\sqrt{|\frac{1}{z}-\frac{1}{z_1}|}}$.

We notice that $z = z_1$ is a special case which we will have to treat separately. If we are still relatively close to the object, say $z < \frac{z_1}{2}$, then $\delta x = \sqrt{\frac{\lambda z z_1}{z_1-z}} = \sqrt{\lambda z}\sqrt{\frac{z_1}{z_1-z}} \approx \sqrt{\lambda z}$. So the case (2) zones are again fairly small, if $\sqrt{\lambda z}\sqrt{\frac{z_1}{z_1-z}}$ is small compared to the cone-width $\Delta x\frac{z_1-z}{z_1}$ at plane z (compare Fig. 20.10). From $\Delta x\frac{(z_1-z)}{z_1} \gg \delta x$ it follows that $z \ll \frac{(\Delta x)^2}{\lambda}\left(\frac{z_1-z}{z_1}\right)^3$. The centers of the (2)-zones occur when one of the integration limits $\frac{\Delta x}{2}$ coincides with the stationary phase point at $x_0'(z)$. This happens right on the edge of the ray-optical cone, which converges at (x_1, z_1) and which touches the edges of the slit.

Now let us see if the case (1) solution inside of the cone is really a spherical wave. Hence we compute $u(x,z)$ for case (1). Since x_0' is supposed to be well inside of $-\frac{\Delta x}{2} \ll x' \ll +\frac{\Delta x}{2}$, we can expand the integration limits:

$$\int_{-\frac{\Delta x}{2}}^{+\frac{\Delta x}{2}} \dots \mathrm{d}x' = \int_{-\infty}^{+\infty} \dots \mathrm{d}x' \tag{20.29}$$

because only oscillating parts are added that way. After shifting coordinates ($x' - x'_0 = x''$) we get:

$$\int_{-\infty}^{+\infty} e^{i\pi\left[\frac{(z_1-z)}{\lambda z z_1}\right]x''^2} \mathrm{d}x'' = \sqrt{\frac{i\lambda z z_1}{(z_1-z)}} = e^{\pm i\frac{\pi}{4}}\sqrt{\frac{\lambda z z_1}{|z_1-z|}} \tag{20.30}$$

The sign-ambiguity of the phase factor $e^{\pm\frac{i\pi}{4}} = \sqrt{\frac{i}{\pm 1}}$ refers to the two depth ranges $z_1 - z > 0$ or ¡ 0. The case $z = z_1$ will be treated separately. Hence there is a *phase jump* of the wavefield along the z-direction at $z = z_1$ This phase jump ($\frac{\pi}{2}$ in the x, z case and π in x, y, z) has been known for about 100 years, due to Gouy. The other phase factors outside of the $\int \dots \mathrm{d}x'$ were (see Eq. 20.28 on page 225):

$$e^{\frac{i\pi}{\lambda}\left[\frac{x^2}{z} - \frac{x_1^2}{z_1} - \left(\frac{x_1}{z_1} - \frac{x}{z}\right)^2 \frac{z z_1}{z_1 - z}\right]} = e^{i\pi\frac{x^2 - x_1^2 - 2x x_1}{\lambda(z_1 - z)}} \tag{20.31}$$

The waves crest are where the exponent is $2\pi N$ (N is integer). From this it follows $z - z_1 = \frac{(x-x_1)^2 - 2x_1^2}{2N\lambda}$. This is the parabolic approximation of a set of concentric circles around (x_1, z_1). Adjacent circles are separated by one wavelength λ. Hence these circles are the spherical wavefronts we hoped to find.

We have seen at least twice in this parageometrical analysis that $z = z_1$ would be a bad case, where some formulas blew up. For example on page 225 we had the formula (Eq. 20.28):

$$u(x,z) = e^{\frac{i\pi}{\lambda}\left[x'^2\left(\frac{1}{z} - \frac{1}{z'}\right) + 2x'\left(\frac{x_1}{z_1} - \frac{x}{z}\right) + \frac{x^2}{z} + \frac{x_1^2}{z_1}\right]} \mathrm{d}x' \tag{20.32}$$

Now let us specialize and set $z = z_1$. If we would expand the integration limits to $\pm\infty$ we would get a delta function:

$$u(x,z_1) = \int_{\frac{\Delta x}{2}}^{\frac{\Delta x}{2}} e^{2\pi i x' \frac{x_1 - x}{\lambda z_1}} \mathrm{d}x' e^{i\pi\frac{(x^2 - x_1^2)}{\lambda z_1}} \approx \int_{-\infty}^{\infty} e^{2\pi i x' \frac{x_1 - x}{\lambda z_1}} \mathrm{d}x' e^{i\pi\frac{(x^2 - x_1^2)}{\lambda z_1}} \tag{20.33}$$

and

$$\int_{-\infty}^{\infty} e^{2\pi i x' \frac{x_1 - x}{\lambda z_1}} \mathrm{d}x' = \delta\left(\frac{x_1 - x}{\lambda z_1}\right) = \lambda z_1 \delta(x - x_1) \tag{20.34}$$

This result describes a sharp point in plane $z = z_1$, at $x = x_1$. However, it is more realistic to maintain the finite integration limits. Thereby we arrive for the focal plane $z = z_1$ at the following solution:

$$u(x, z_1) = C' e^{i\pi \frac{(x^2 - x_1^2)}{\lambda z_1}} \Delta x \, \mathrm{sinc} \left\{ \frac{\Delta x}{\lambda z_1} (x_1 - x) \right\} \tag{20.35}$$

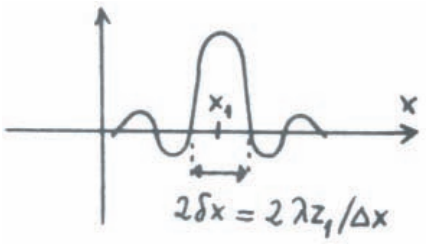

Figure 20.11: The shape of the sinc-function.

$|u(x, z_1)|^2 \sim \mathrm{sinc}^2 \{\ldots\}$ is a "diffraction point" of width $\frac{\lambda z_1}{\Delta x}$. The finite width of this point is the cause of the limit of resolution.

Summary of parageometrical optics:
Waves impinging on a relatively *wide* opening Δx, continue to propagate undisturbed within a cone, which is determined by the opening and the convergence point. Outside of that cone the amplitude is zero (shadow). Hence in a situation like this one, waves propagate almost like rays. But the phase is remembered in the theory of parageometric optics.

20.4.3 An application of parageometric optics:

The walk-off effect in Talbot imaging

On page 195 we had studied the walk-off effect which limits the spectral resolution of the Talbot-Fourier spectrometer. We concluded from the geometry of the setup as shown in the Fig. 18.9 on page 195 that the various diffraction orders will be completely separated at a distance $z_{\max} = \frac{Md^2}{\lambda}$, where M is the number of periods within the finite width of the grating. We assumed tacitly that the various grating diffraction orders can be described as plane waves of finite width. With the help of parageometrical optics we will show that this description is indeed justified for $z \leq z_{\max}$

The trick which we use is the following concept:
FINITE GRATING = INFINITE GRATING, FOLLOWED BY FINITE SLIT.

In other words we assume that the following two objects will create identical diffraction effects:

Object (1): a grating of finite width $B = Md$, surrounded by an opaque frame.
Object (2): an infinitely large grating, with an opaque frame of inner width $B = Md$ immediately behind that grating.

The second object is infinitely expensive, but it allows us to split the interaction between light and object into two steps, at least in concept. We assume that an infinitely extended monochromatic plane wave hits the infinite grating. In this pure case many infinitely extended plane waves will be created immediately behind the grating. Each plane wave is a diffraction order with its specific direction of propagation. Now each of these tilted plane waves with infinite width hits the frame of finite width. The resulting effect was treated in detail as the first example of parageometrical optics. We have now many tilted plane waves of finite widths. The edges of these finite plane waves are blurred over a lateral region $\delta x = \sqrt{\lambda z}$! It is meaningful to talk about finite plane waves as long as the blur width δx is small compared to the wave width $B = Md$:

$$\delta x \ll Md; \qquad \sqrt{\lambda z} \ll Md; \qquad z \ll \frac{(Md)^2}{\lambda} \tag{20.36}$$

This distance z however is much larger than $z_{\max} = \frac{Md^2}{\lambda}$ (if $M \gg 1$). The $z_{\max}$ distance is the longest length over which it makes sense to operate the Talbot-Fourier spectrometer. Beyond $z_{\max}$ no Talbot images appear anymore due to the walk-off effect. In other words long before the edges of the finite plane waves are significantly blurred will the grating diffraction orders be completely separated.

21 Application of Fresnel Diffraction to Signal Detection

In this chapter we want to demonstrate again that Fresnel diffraction experiments can be useful, contrary to some widespread opinions. In particular we want to present a method of "key word detection" which might be useful in a library or in any large filing system as is used in government agencies and big companies. Suppose you are interested in optics, and you got a big book with many miscellaneous topics in it, most of them not "optics". If neither the table of contents nor the subject index is useful you would have to take a glance at every page and see if the word "optics" is present. If so a more detailed study would follow.

There are several methods which could do such a job. These methods have all their specific advantages and disadvantages, which are related to speed of operation, speed of preparation, price, reliability and so on. The "speed of preparation" is an important feature, which sometimes is not sufficiently appreciated. For example in our case the "input" has to exist in the form of a transparency. In other words we have to assume that the library or file is photographed on microfilm. This requirement is somewhat limiting, but probably not much of handicap in the future. Books and files at normal size (ready or reading and copying without magnification) are just too bulky. Another requirement is that the "target" or "keyword" (in our example, "optics") exists also in the form of a transparency. This latter requirement is comparatively easy to satisfy. In other methods one has to make a hologram of the "keyword", which is more difficult.

The theory and the experiments are described in a paper on "Signal Detection by Correlation of Fresnel Diffraction Patterns". It appeared in Applied Optics, vol. 6, pages 2171 - 2175, in 1967. The standard abbreviation of such a reference is: Appl. Opt. 6, 2171 (1967).

22 Fraunhofer Diffraction

Fraunhofer-Diffraction is usually defined as “observer very far away from diffraction object”. But we will see that this definition is too narrow when we study several configurations which give the “Fraunhofer diffraction pattern”.

22.1 Observer at distance R—no lens is involved

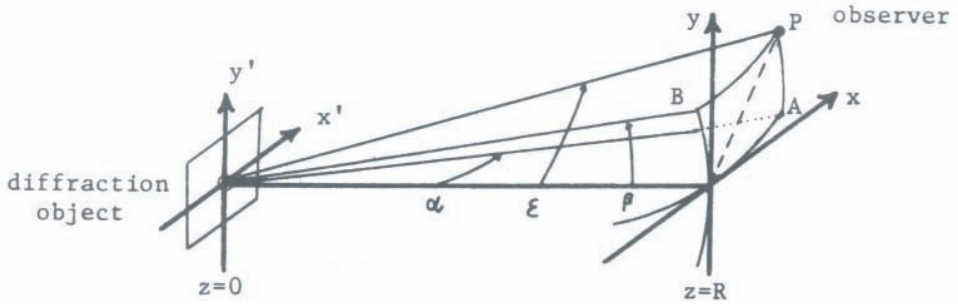

Figure 22.1: Schematic of the configuration for Fraunhofer diffraction.

Observer P is at distance R from the object center $(0,0,0)$.

$$P(\underbrace{R\sin\alpha}_{x_P},\underbrace{R\sin\beta}_{y_P},\underbrace{R\cos\epsilon}_{z_P}) \qquad \cos\epsilon=\sqrt{1-\sin^2\alpha+\sin^2\beta} \tag{22.1}$$

Start from $z=0$, where $u(x,y,0)=u_0(x,y)$, and $\tilde{u}_0(\nu,\mu)=\int u_0(x,y)e^{-2\pi i(\,nux+\mu y)}\,\mathrm{d}x\mathrm{d}y$. Now use RSD for propagation from $z=0$ to observer in P.

$$\begin{aligned} u_P &= u(x_P,y_P,z_P)=u(R\sin\alpha,R\sin\beta,R\cos\epsilon)= \\ &= \iint \tilde{u}_0(\nu,\mu)e^{2\pi iR(\nu\sin\alpha+\mu\sin\beta+\sqrt{1-\lambda^2(\nu^2+\mu^2)}\frac{\cos\epsilon}{\lambda})}\mathrm{d}\nu\mathrm{d}\mu \end{aligned} \tag{22.2}$$

This integral is built up of many plane waves (and also evanescent waves, which however are negligible at $R\ll\lambda$), but only one of them really contributes significantly in point P.

It is the one with a $\vec{k}$-vector going from $(0,0,0)$ to P, as we will see by making use of the saddle-point method for solving the u_P-integral.

$$\begin{aligned} u_P &= \iint \tilde{u}(\nu,\mu) e^{2\pi i R f(\nu,\mu)} \mathrm{d}\nu \mathrm{d}\mu; \\ f(\nu,\mu) &= \nu \sin\alpha + \mu \sin\beta + \cos\epsilon \frac{\sqrt{1-\lambda^2(\nu^2+\mu^2)}}{\lambda} \end{aligned} \tag{22.3}$$

$2\pi R$ stands for the "large constant" in the exponent, which in most earlier cases was k. The saddle-point follows from:

$$\begin{aligned} &\frac{\partial f}{\partial \nu} = 0; \qquad \frac{\partial f}{\partial \mu} = 0; \qquad \sin\beta - \frac{\cos\epsilon}{\lambda}\frac{\lambda^2\mu}{\sqrt{\dots}} = 0 \\ 0 = \sin\alpha - \frac{\cos\epsilon}{\lambda}\frac{\lambda^2\nu}{\sqrt{\dots}}; &\qquad \frac{\lambda\nu_0}{\sqrt{\dots}} = \frac{\sin\alpha}{\cos\epsilon}, \qquad \frac{\lambda\mu_0}{\sqrt{\dots}} = \frac{\sin\beta}{\cos\epsilon} \end{aligned} \tag{22.4}$$

Now we try to compute $\cos\epsilon$. Since $\cos^2\epsilon = 1 - \sin^2\alpha - \sin^2\beta$, it is given by $\frac{\sin^2\alpha}{\cos^2\epsilon} + \frac{\sin^2\beta}{\cos^2\epsilon} + 1 = \frac{1}{\cos\epsilon}$; we insert earlier results:

$$\frac{(\lambda\nu_0)^2 + (\lambda\mu_0)^2 + (\sqrt{\dots})^2}{\sqrt{\dots}} = \frac{\lambda^2\nu_0^2 + \lambda^2\mu_0^2 + 1 - \lambda^2(\nu_0^2+\mu_0^2)}{1-\lambda^2(\nu_0^2+\mu_0^2)} = \frac{1}{1-\lambda^2(\nu_0^2+\mu_0^2)} \tag{22.5}$$

hence:

$$\cos\epsilon = \sqrt{1-\lambda^2(\nu_0^2+\mu_0^2)} \rightarrow \lambda\nu_0 = \sin\epsilon; \qquad \lambda\mu_0 = \sin\beta \tag{22.6}$$

We need also:

$$\begin{aligned} \frac{\partial^2 f}{\partial \nu^2} &= -\lambda\cos\epsilon \frac{\partial \frac{\nu}{\sqrt{\dots}}}{\partial \nu} = -\lambda\cos\epsilon \frac{1-\lambda^2\mu_0^2}{(\sqrt{\dots})^2} = -\lambda\frac{1-\lambda^2\mu_0^2}{\cos^2\epsilon} \\ \frac{\partial^2 f}{\partial \mu^2} &= -\frac{\lambda(1-\lambda^2\nu_0^2)}{\cos^2\epsilon} \\ \frac{\partial^2 f}{\partial \nu \partial \mu} &= -\cos\epsilon\ \lambda\nu_0 \frac{\partial \frac{1}{\sqrt{\dots}}}{\partial \mu} = -\lambda\nu_0\cos\epsilon \frac{\lambda^2\mu_0}{(\sqrt{\dots})^2} = -\frac{\lambda^3\nu_0\mu_0}{\cos^2\epsilon} \\ \frac{\partial^2 f}{\partial \nu^2}\cdot\frac{\partial^2 f}{\partial \mu^2} - \frac{\partial^2 f}{\partial \nu \partial \mu} &= \frac{\lambda^2}{\cos^4\epsilon}\left\{(1-\lambda^2\mu_0^2)(1-\lambda^2\nu_0^2) - \lambda^4\nu_0^2\mu_0^2\right\} = \frac{\lambda^2}{\cos^2\epsilon} \\ \text{since}: \quad \{\dots\} &= 1-\lambda^2(\nu_0^2+\mu_0^2) = \cos^2\epsilon \end{aligned} \tag{22.7}$$

Now we have everything together for the saddle-point integral (see page 116):

$$\boxed{u_P(R\sin\alpha, R\sin\beta, R\cos\epsilon) \approx \frac{\cos\epsilon}{\lambda R} e^{i\left[2\pi\frac{R}{\lambda}+\frac{\pi}{2}\right]} \tilde{u}_0\left(\frac{\sin\alpha}{\lambda}, \frac{\sin\beta}{\lambda}\right)} \tag{22.8}$$

The configuration (Fig. 22.1) which gives this nice result is particularly well justified in X-ray diffraction, where $\frac{R}{\lambda}$ is very, very large, say 10^9 for $R = 1\text{m}$ and $\lambda = 10^{-9}\ \text{m} = 10\ \text{Å}$.

22.2 Plane wave illumination—single lens

"Infinity" is something defined as the place where parallel rays meet. This is what actually happens in the rear focal plane of a lens. Hence, to observe the Fraunhofer diffraction at infinity, we might introduce a lens, which permits a reasonably short setup compared to the previous one.

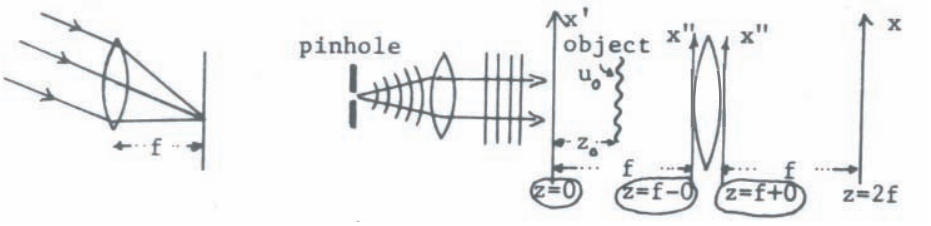

Figure 22.2: Fraunhofer diffraction setup with a single lens.

$$\begin{aligned} z<0: \qquad & u = e^{ikz} \quad \text{monochromatic plane wave;} \quad z = z_0 - 0: \ e^{ikz_0} \\ z = z_0 + 0: \qquad & e^{ikz_0} u_0(x,y) = e^{ikz_0} \iint \tilde{u}(\nu,\mu) e^{2\pi i[\nu x + \mu\nu]} \mathrm{d}\mu \mathrm{d}\nu \end{aligned} \tag{22.9}$$

From now on we will use the approximated HFK-formula, whereby factors such as e^{ikz_0} are omitted. From $z = z_0 + 0$ to $z = f - 0$:

$$u(x'', y'', f-0) = \iint u(x', y', z_0+0) e^{i\pi\frac{[(x''-x')^2+(y''-y')^2]}{\lambda(f-z_0)}} \mathrm{d}x' \mathrm{d}y' \tag{22.10}$$

Now through the lens, from $z = f - 0$ to $z = f + 0$:

$$u(x'', y'', f+0) = u(x'', y'', f-0) \underbrace{e^{-i\pi\frac{x''^2+y''^2}{\lambda f}}}_{\substack{\text{phase factor describing the} \\ \text{lens action}}} \tag{22.11}$$

Finally propagation from $z = f + 0$ to $z = 2f$, which is the rear focal plane of the lens:

$$u(x, y, 2f) = \iint u(x'', y'', f + 0) e^{i\pi \frac{[(x-x'')^2 + (y-y'')^2]}{\lambda f}} \, \mathrm{d}x'' \mathrm{d}y'' \tag{22.12}$$

Now we put all these steps together into one final formula:

$$\begin{aligned} u(x, y, 2f) &= \iiiint u(x', y', z_0 + 0) e^{i\frac{\pi}{\lambda}[\ldots]} \, \mathrm{d}x' \mathrm{d}y' \mathrm{d}x'' \mathrm{d}y'' \qquad (22.13) \\ [\ldots] &= \frac{(x'' - x)^2 + (y'' - y)^2}{f - z_0} + \frac{(x - x'')^2 + (y - y'')^2}{f} - \frac{x''^2 + y''^2}{f} \end{aligned}$$

For $u(x', y', z_0 + 0)$ we set the object $u_0(x', y') = \iint \tilde{u}_0(\nu, \mu) e^{2\pi i(\nu x + \mu y)} \, \mathrm{d}\nu, \mathrm{d}\mu$:

$$\begin{aligned} u(x, y, 2f) &= \iiiiii \tilde{u}_0(\nu, \mu) e^{i\frac{\pi}{\lambda}\{\ldots\}} \, \mathrm{d}(\nu \; \mu \; x' \; y' \; x'' \; y''); \qquad (22.14) \\ \{\ldots\} &= [\ldots] + 2\lambda(\nu x' + \mu y') = \left\{ \frac{x''^2}{(\sqrt{f - z_0})^2} + 2x'' \left(\frac{x'}{f - z_0} + \frac{x}{f} \right) \right\} \\ &+ \frac{x'^2}{f - z_0} + \frac{x^2}{f} + 2\lambda\nu x' + (\text{etc in } y'', y', y, \mu) \end{aligned}$$

(i.e., for convenience we write only the x-terms, the y-terms being similar).

$$\{\ldots\} = \left\{ \frac{x''}{\sqrt{f - z_0}} - \sqrt{f - z_0} \left(\frac{x'}{f - z_0} + \frac{x}{f} \right) \right\}^2 - (f - z_0) \left(\frac{x'}{f - z_0} + \frac{x}{f} \right)^2 \tag{22.15}$$

the x''integral is:

$$\int e^{i\frac{\pi}{\lambda}\{\ldots\}} \mathrm{d}x'' \underbrace{=}_{\substack{\text{variable} \\ \text{shifted}}} \int e^{i\frac{\pi}{\lambda}x''^2} \mathrm{d}x'' = \text{const.}; \qquad \text{similarly}: \quad \int \ldots \mathrm{d}y'' \tag{22.16}$$

Now $u(x, y, 2f)$ is a four-fold integral:

$$\begin{aligned} u(x, y, 2f) &= \iiiint \tilde{u}(\nu, \mu) e^{i\frac{\pi}{\lambda}[\ldots]} \mathrm{d}(x' \; y' \; \nu \; \mu) \qquad (22.17) \\ \text{with}: [\ldots] &= -(f - z_0) \left(\frac{x'}{f - z_0} + \frac{x}{f} \right)^2 + \frac{x'^2}{f - z_0} + \frac{x^2}{f} + 2\lambda\nu x' + \text{etc. (in } \mu \text{ y y}') \\ &= \frac{z x^2}{f^2} + 2x' \left[\lambda\nu - \frac{x}{f} \right] + \text{etc.} \end{aligned}$$

$$u(x,y,2f) = e^{i\pi z_0 \frac{(x^2+y^2)}{\lambda f}} \iint \tilde{u}(\nu,\mu) e^{2\pi i\left[x'\left(\nu-\frac{x}{\lambda f}\right)+y'\left(\mu-\frac{y}{\lambda f}\right)\right]} \mathrm{d}(x'\ y'\ \nu\ \mu) \quad (22.18)$$

Herin $\int e^{2\pi i x'\left(\nu-\frac{x}{\lambda f}\right)} \mathrm{d}x' = \delta\left(\nu - \frac{x}{\lambda f}\right)$; hence $\int \ldots \mathrm{d}\nu$ means $\nu \rightarrow \frac{x}{\lambda f}$. Similarly $\int \ldots \mathrm{d}y' \mathrm{d}\mu \sim \mu \rightarrow \frac{y}{\lambda f}$

$$\boxed{u(x,y,2f) = e^{i\pi \frac{x^2+y^2}{\lambda f}} \tilde{u}\left(\frac{x}{\lambda f}, \frac{y}{\lambda f}\right)} \quad (22.19)$$

Again, the Fraunhofer diffraction experiment accomplishes a two-dimensional Fourier transformation of the complex light amplitude. If the quadratic phase factor disturbs, one may set $z_0 = 0$, meaning that the object is in the front focal plane of the lens. Most of the time, however, this factor does not matter, since what we see is only $|u(x,y,2f)|^2 = |\tilde{u}\left(\frac{x}{\lambda f}, \frac{y}{\lambda f}\right)|^2$. If, however, the light continues to travel beyond the rear focal plane $2f$, then this quadratic phase is important, for it is the only thing which "remembers" where (at z_0) the object $u_0(x,y)$ was.

22.3 About the lens used for creating "infinity"

A lens may have defects, called "aberrations", which create wrong phases (details later); the lens may also have amplitude defects (dust, dirty fingerprints), and a lens is imperfect because its diameter is finite. The influence of the lens diameter in connection with Fraunhofer diffraction is usually neglected in the literature. We will see that the allowable object diameter a, the lens diameter h, and the frequency range $\Delta\nu$ of the object are interrelated. For simplicity we assume a one-dimensional object $u_0(x) = u_{00}(x)\mathrm{rect}\left(\frac{x}{a}\right)$;

$$\mathrm{rect}\left(\frac{x}{a}\right) = \begin{cases} +1 & \text{in } -\frac{a}{2} \leq x \frac{a}{2} \\ 0 & \text{elsewhere} \end{cases} \quad (22.20)$$

$u_{00}(x)$ is the "object per se", and "rect" describes the "field limits". $u_{00}(x)$ may have a Fourier spectrum or spatial frequency spectrum $\tilde{u}_{00}(\nu)$ which is non-zero only in $-\frac{\Delta\nu}{2} \leq \nu \leq \frac{\Delta\nu}{2}$. When the illuminating plane wave hits the object per se $u_{00}(x)$ at $z = 0$ a particular frequency component $e^{2\pi i x \nu_0}$ of $u_{00}(x)$ (hence $|\nu_0| \leq \frac{\Delta\nu}{2}$) will produce a tilted plane wave: $e^{2\pi i\left(\nu_0 x + \sqrt{1-\lambda^2\nu_0^2}\frac{z}{\lambda}\right)}$, which then hits immediately the field limitaction $\mathrm{rect}\left(\frac{x}{a}\right)$. According to parageometrical optics, what this $\mathrm{rect}\left(\frac{x}{a}\right)$ does is essentially only to limit the plane wave laterally. While being confined to within $-\frac{a}{2} \leq x \leq +\frac{a}{2}$ at $z = 0$, it will be shifted upwards by an amount $f\tan\varphi$ when reaching the lens, where φ is the diffraction angle, given by $\lambda\nu_0 = \sin\varphi$, which is the same as $\lambda/d = \sin\varphi$. Hence the upper end of the limited plane wave is at $\frac{a}{2} + f\tan\varphi \approx \frac{a}{2} + f\sin\varphi = \frac{a}{2} + f\lambda\nu_0$. For the largest possible frequency $\nu_{\max} = \frac{\Delta\nu}{2}$, this is at $x = \frac{a+\lambda\Delta\nu f}{2}$. This "ray" should still be caught by the lens. Otherwise

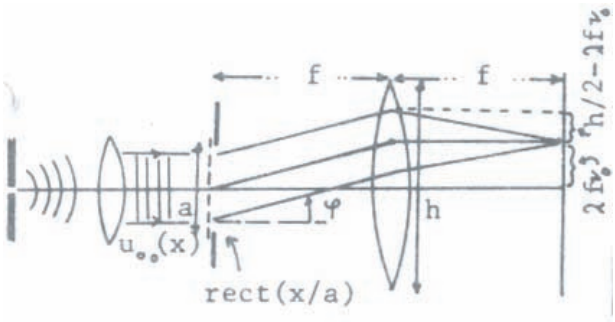

Figure 22.3: Fourier transforming properties of a single lens ("creating infinity").

the finite diameter h of the lens would degrade the Fourier-transform action of the lens. Hence we require $\frac{a+\lambda f \Delta\nu}{2} \leq \frac{h}{2}$, or

$$\boxed{a + \lambda f \Delta\nu \leq h} \tag{22.21}$$

Looking at Fig. 22.3, it becomes obvious that $\lambda f \Delta\nu$ is also the area of the rear focal plane, which really contains $\tilde{u}_0(\nu)$. Calling the useful diameter of the rear focal plane b, we can write:

$$\boxed{a + b \leq h} \tag{22.22}$$

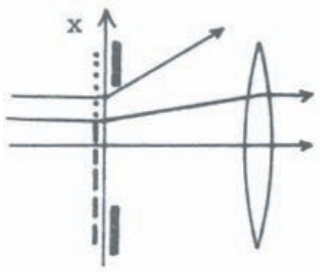

Figure 22.4: Loss of high frequencies due to the limited aperture of a single lens.

As a counter-example let us see what happens if the object $u_{00}(x)$ has a coarse grating on-axis, and a fine grating (higher frequency) off-axis. The high frequencies are not caught by the lens. Hence, the observation at $2f$ is misleading. The above condition can also be interpreted in this way: given a lens of diameter h, and an object of diameter a. We can be sure to analyze all frequencies $|\nu| \leq \frac{h-a}{\lambda f}$. But our analysis at higher frequencies will be inaccurate.

22.4 The "light tube"

This is yet another way to accomplish Fraunhofer diffraction. It is not too well known, although it is simple and practical. It consists of two equal lenses separated by one focal length f. Assume $u(x, y, -0)$ is known, possibly because a plane wave e^{ikz} fell onto an object $u(x, y)$ in that plane. The first lens with focal length f acts like this:

$$\underbrace{u(x,y,-0)}_{z=-0} \rightarrow \underbrace{u(x,y,+0)}_{z=+0} = u(x,y,-0)e^{i\pi\frac{x^2+y^2}{\lambda f}} \tag{22.23}$$

Figure 22.5: The configuration of the "light tube" for generating Fraunhofer diffraction.

Next we have a propagation process over the distance f:

$$u(x,y,f-0) = \int u(x',y',+0)e^{i\pi\frac{(x-x')^2+(y-y')^2}{\lambda f}}\,\mathrm{d}x'\,\mathrm{d}y' \tag{22.24}$$

Thereafter comes the second lens:

$$u(x,y,f-0) \rightarrow u(x,y,f+0) = u(x,y,f-0)e^{i\pi\frac{(x^2+y^2)}{\lambda f}} \tag{22.25}$$

Altogether we get:

$$u(x,y,f+0) = e^{-i\pi\frac{x^2+y^2}{\lambda f}} \iint u(x',y',-0)e^{-i\pi\frac{x'^2+y'^2}{\lambda f}} e^{i\pi\frac{(x-x')^2+(y-y')^2}{\lambda f}}\,\mathrm{d}x'\,\mathrm{d}y' \tag{22.26}$$

All square-terms in the exponents cancel. A Fourier transform remains:

$$\boxed{u(x,y,f+0) = \iint u(x',y',-0)e^{-2\pi i\frac{xx'+yy'}{\lambda f}}\mathrm{d}x'\mathrm{d}y' = \tilde{u}\left(\frac{x}{\lambda f},\frac{y}{\lambda f},-0\right)} \tag{22.27}$$

An attractive feature of this type of "Fourier transformer" is the simple fashion in which the lens diameters influence the operation.

22.5 Convergent illumination

The most obvious approach would be to start from the source, propagate to the lens, traverse through the lens etc.; in other words, compute always in the same direction as the light actually propagates. However it is much simpler to compute the way I have sketched as "symbolic path" in Fig. 22.6. This includes computation-wise also a backwards-propagation, or "virtual propagation". Physically, a virtual propagation means this: assume we know $u(x, z_2)$, and we know the light propagates in the positive z-direction. If we now compute $u(x, z_1)$ with $z_1 < z_2$ it means: what must u have been like in plane z_1, in order to come up with $u(x, z_2)$ in plane z_2 after propagation over $z_2 - z_1$? Nothing forbids us to compute $u(x, z_1)$ from $u(x, z_2)$ even if there were maybe some obstacles ("objects") between z_1 and z_2. In that case we cannot know that the simple $u(x, z_1)$ did *not* exist in z_1 which was computed by virtual propagation through free space. Nevertheless, it is sometimes quite useful to compute the *virtual* wave amplitude $u(x, z_1)$, both to make the computations simple, and also because to any observer at $z \geq z_1$ the field looks exactly *as if* it had been $u(x, z_1)$ in z_1. The term "as if" means the same a "virtually".

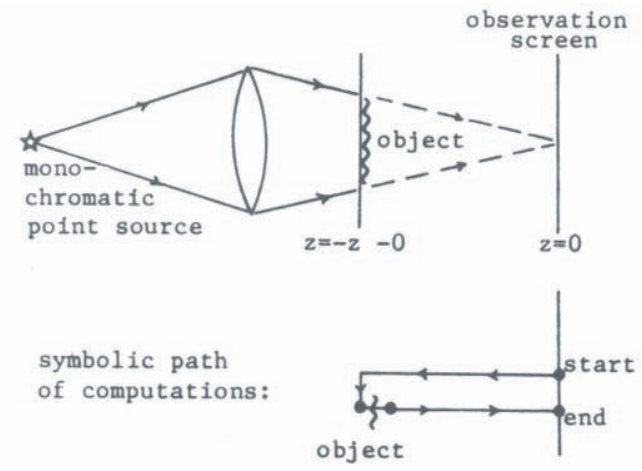

Figure 22.6: Fraunhofer diffraction in convergent illumination and symbolic path of computation.

Now let's compute along the symbolic path. If we have set up the point source and the lens (as in Fig. 22.6), we will move the screen along the axis, till the image point is sharp. We will call that plane $z = 0$. Since the light is concentrated there into a point, it must have been a spherical wave previously. For example in $z = -z_0 - 0$, it must have been:

$$u(x, y, -z_0 + 0) \approx e^{-i\pi \frac{x^2+y^2}{\lambda z_0}} \tag{22.28}$$

This was the first step of our symbolic path. Only now do we take the object into account. From $-z_0 - 0$ to $-z_0 + 0$:

$$u(x,y,-z_0+0) = u(x,y,-z_0-0) \quad \underbrace{u_0(x,y)}_{\substack{\text{complex}\\ \text{object}\\ \text{transmittance}}} \tag{22.29}$$

Now a "real" propagation from $z = -z_0 + 0$ to $z = 0$: (The word "real" is used here in contrast to "virtual", which is a somewhat unfortunate but common convention).

$$\begin{aligned} u(x,y,0) &= \iint u(x',y',-z_0+0) e^{i\pi \frac{(x-x')^2+(y-y')^2}{\lambda z_0}} \mathrm{d}x'\ \mathrm{d}y' = \\ &= \iint e^{-i\pi \frac{x'^2+y'^2}{\lambda z_0}} u_0(x',y') e^{i\pi \frac{(x-x')^2+(y-y')^2}{\lambda z_0}} \mathrm{d}x'\ \mathrm{d}y' \\ &= e^{i\pi \frac{x^2+y^2}{\lambda z_0}} \iint u_0(x',y') e^{-2\pi i \frac{xx'+yy'}{\lambda z_0}} \mathrm{d}x'\ \mathrm{d}y' \\ &= e^{i\pi \frac{x^2+y^2}{\lambda z_0}} \tilde{u}\left(\frac{x}{\lambda z_0}, \frac{y}{\lambda z_0}\right) \end{aligned} \tag{22.30}$$

$$\boxed{u(x,y,0) = e^{i\pi \frac{x^2+y^2}{\lambda z_0}} \tilde{u}\left(\frac{x}{\lambda z_0}, \frac{y}{\lambda z_0}\right)} \tag{22.31}$$

A practical convenience: by shifting the object along the axis, one can vary z_0, and hence the scale of $\tilde{u}_0$.

22.6 Divergent illumination

$$\begin{aligned} z = 0: &\qquad \delta(x)\delta(y) \\ z = z_0 - 0: &\qquad e^{i\pi \frac{x^2+y^2}{\lambda z_0}} \\ z = z_0 + 0: &\qquad u(x,y,z+0) = e^{i\pi \frac{x^2+y^2}{\lambda z_0}} u_0(x,y) \end{aligned} \tag{22.32}$$

Actually the light will continue to travel forward, but let us assume that the observer does not focus onto the object (e.g. umbrella) but on the source (far away street light). To him it will seem as if $u(x,y,0)$ had been there.

$$\begin{aligned} u(x,y,0) &= \iint u(x',y',z_0+0) e^{-i\pi \frac{(x-x')^2+(y-y')^2}{\lambda z_0}} \mathrm{d}x'\ \mathrm{d}y' \\ &= \iint e^{i\pi \frac{x'^2+y'^2}{\lambda z_0}} u_0(x'y') e^{-i\pi \frac{(x-x')^2+(y-y')^2}{\lambda z_0}} \mathrm{d}x'\ \mathrm{d}y' \\ &= e^{-i\pi \frac{x^2+y^2}{\lambda z_0}} \iint u_0(x',y') e^{2\pi i \frac{xx'+yy'}{\lambda z_0}} \mathrm{d}x'\ \mathrm{d}y' \end{aligned} \tag{22.33}$$

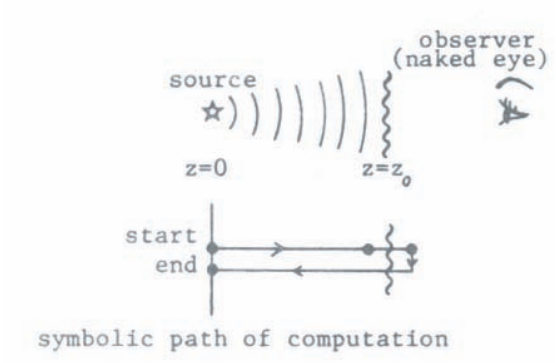

Figure 22.7: Fraunhofer diffraction in divergent illumination.

$$\boxed{u(x,y,0) = e^{-i\pi\frac{x^2+y^2}{\lambda z_0}}\tilde{u}_0\left(-\frac{x}{\lambda z_0}, -\frac{y}{\lambda z_0}\right)} \tag{22.34}$$

Hence to the observer there seems to be the intensity $|\tilde{u}_0\left(-\frac{x}{\lambda z_0}, -\frac{y}{\lambda z_0}\right)|^2$ located in plane $z = 0$.

Here, as well as in the previous section on convergent illumination, we saw that "observation at infinity" is really not the necessary and sufficient feature for getting a Fourier transform from the object. Instead it is the plane where the illuminating point source would have been observable as a sharp point if the object were out of the beam. Hence, if Fraunhofer diffraction shall imply a Fourier transform (as it does in fact to most people) than the term "Fraunhofer diffraction" ought to be re-defined as being observed in the image plane of a point source.

22.7 Fraunhofer diffraction by an array of equal objects

We assume that the object consists of many equal objects which might be arranged irregularly as in this figure or periodically as in a grating.

$$\begin{aligned} u(x,y) &= \sum_{(m)} u_0(x-m, y-y_m); \\ \tilde{u}(\nu,\mu) &= \tilde{u}_0(\nu,\mu)\sum e^{-2\pi i(\nu x_m, \mu y_m)}; \end{aligned} \tag{22.35}$$

$$|\tilde{u}(\nu,\mu)|^2 = |\tilde{u}_0(\nu,\mu)|^2|\sum e^{-2\pi i(\nu x_m + \mu y_m)}|^2 = F(\nu,\mu)A(\nu,\mu) \tag{22.36}$$

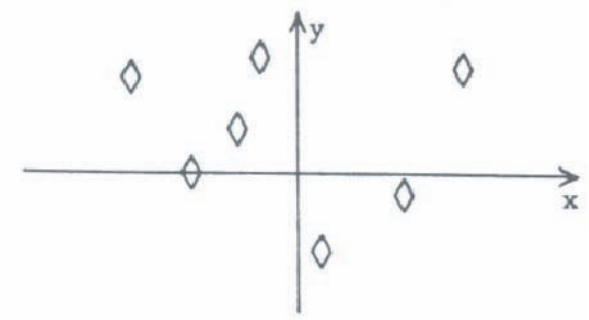

Figure 22.8: An array of diffracting objects.

The first term $|\tilde{u}_0(\nu,\mu)|^2$ is often called the "form factor" $F(\nu,\mu)$ because it is entirely determined by the shape of the individual object u_0. The second term $|\sum \ldots|^2$ is often called the "array factor" $A(\nu,\mu)$ because it depends only on the arrangement of the objects, not on their form.

If the positions (x_m, y_m) are distributed at random the problem of computing the array factor is the "random walk problem". Its main features are as follows:

$$\text{For } \nu=0,\ \mu=0: \qquad A(0,0) = |\sum_{m=1}^{M} 1|^2 = M^2 \tag{22.37}$$

$$\text{for } \nu\neq 0,\ \mu\neq 0: \qquad A(\nu,\mu) = |\sum \ldots|^2 = \sum\sum e^{-2\pi i[\nu(x_m-x_n)+\mu(y_m-y_n)]}$$

$$= \sum \sum_{n=m} \ldots + \sum \sum_{n\neq m} \ldots$$

$$\text{where: } \qquad \sum\sum \ldots = M$$

Now let us discuss the summation of the cross terms $\sum \sum_{n\neq m}$. We assume that the object locations are uniformly (but nevertheless randomly) distributed within a circle of radius R in the (x,y) object domain: $x_m^2 + y_m^2 = R^2$. If now $\nu^2+\mu^2 = \varrho^2$ is $\geq \frac{1}{R^2}$ then the phase $2\pi(\nu x_m + \mu y_m) = 2\pi\varrho r_m \cos(\Theta - \varphi_m)$ of the series $\sum_{(m)}$ will occupy with uniform probability the range $(-2\pi, 2\pi)$. Hence this series will have a very small result. The expectation value of this series is zero. This is still true if we leave out one specific term, the n-th (assuming that $M \ll 1$). This particular series $\sum_{\substack{m\ =\ 1,2,\ldots M;\\ \text{but } n\neq m}} = \sum_{(m)}^{(n)} = C_n$ is a part of the double series of cross terms

$$\sum\sum_{n\neq m} e^{-2\pi i[\nu(x_m-x_n)+\mu(y_m-y_n)]} \quad = \quad \sum_{n=1}^{M} e^{2\pi i(\nu x_n+\mu y_n)} C_n; \tag{22.38}$$

$$C_n(\nu,\mu) = \sum_{(m)}^{(n)} e^{-2\pi i(\nu x_m+\mu y_m)}; \qquad \langle C_n(\nu,\mu)\rangle = 0 \quad \text{if} \quad \nu^2+\mu^2 \geq \frac{1}{R^2}$$

If $\langle C_n(\nu,\mu)\rangle = 0$ then also $\langle e^{2\pi i(\nu x_n+\mu y_n)} C_n(\nu,\mu)\rangle$ and also $\langle \sum_{(n)} e^{\cdots} C_n\rangle$. In summary we found these feature of the array factor for a random distribution within an (x,y) circle of radius R:

$$A(0,0) = M^2; \qquad A(\nu,\mu) \approx M \quad \text{if} \quad \nu^2+\mu^2 \geq \frac{1}{R^2}; \quad M = \text{number of elements} \tag{22.39}$$

Now let us consider the case of a periodic one dimensional array, which is a grating: $x_m = md$; $|m| \leq \frac{M}{2}$ (M even):

$$A(\nu) = |\sum_{-\frac{M}{2}}^{\frac{M}{2}} e^{-2\pi i\nu md}|^2 = \left[\frac{\sin(\pi\nu d(M+1))}{\sin(\pi\nu d)}\right]^2 = (M+1)^2 \frac{\text{sinc}^2[\nu d(M+1)]}{\text{sinc}(\nu d)} \tag{22.40}$$

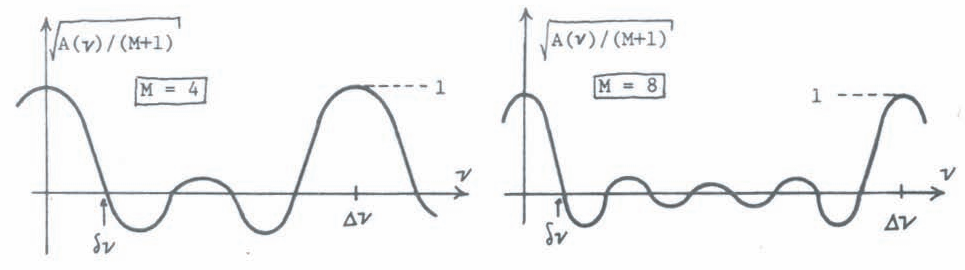

Figure 22.9: The array factor for a periodic array (grating) with an increasing number M of periods.

This function does not blow up when the denominator becomes zero because the numerator will be zero too at those coordinates. But the function will have a maximum of height $(M+1)^2$ whenever $\pi\nu d = n\pi$. At a distance $\delta\nu$ with $\pi\delta\nu d(M+1) = \pi$ or $\delta\nu = \frac{1}{(M+1)d}$ on both sides of the maximum will $A(\nu,\mu)$ be zero. $A(\nu,\mu)$ is periodic with $\Delta\nu = \frac{1}{d}$ if M is

even. M odd does not make sense since the limits of summation $\pm\frac{M}{2}$ ought to be integers.

Since the individual object element $u_0(x)$ is always smaller or at least not bigger than the period d, the form factor $F(\nu,\mu) = |\tilde{u}_0(\nu,\mu)|^2$ will be wider than one period $\Delta\nu = \frac{1}{d}$ of the array factor $A(\nu,\mu)$. For example in the case of a Ronchi ruling it is $u_0(x) = \mathrm{rect}\left(\frac{x}{\frac{d}{2}}\right)$ and $\tilde{u}_0(\nu) = \frac{d}{2}\mathrm{sinc}\left(\frac{\nu d}{2}\right)$, and $F(\nu) = \left(\frac{d}{2}\right)^2 \mathrm{sinc}^2\left(\frac{\nu d}{2}\right)$. As a general statement we can say that the Fraunhofer diffraction pattern $|\tilde{u}(\nu)|^2 = F(\nu)A(\nu)$ of a grating consists of spikes (due to the array factor) which are separated by $\Delta\nu = \frac{1}{d}$. The strength of these spikes is determined by the form factor $F(\nu)$ which lies like an envelope over the grating diffraction pattern.

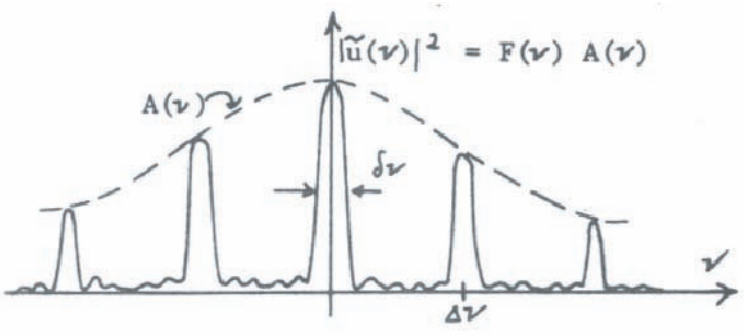

Figure 22.10: Diffraction amplitude of a finite diffraction grating.

Another distribution of elements occurs when the grating lines have a periodic position error $E_m = B\sin\left(\frac{2\pi md}{D}\right)$; $x_m = md + E_m$. The theory for this type of array factor makes use of the Jacobi-Bessel series $e^{iB\sin(z)} = \sum J_n(B)e^{inz}$. The significant feature of this array factor are the "ghosts". These are some extra peaks in unexpected places. Their name expresses the despair of early spectroscopists who sometimes thought they had discovered a new chemical element. But in reality the "ghosts" had fooled them.

22.8 Babinet's principle

Suppose you have two complimentary diffraction objects $u_O(x)$ and $u_C(x)$ such that $u_O + u_C = 1$. The u_C object is the "negative" of the u_O-object. The common but sloppy way of stating Babinet's principle is to say that u_O and u_C create the same diffraction patterns. Let's see in what sense this is true. We use RSD theory (which is exact). The object in $z = 0$ is illuminated by a monochromatic plane wave e^{ikz}. The RSD says:

$$u(x,z) = \int \tilde{u}(\nu,0)e^{2\pi i\left[\nu x+\sqrt{1-\lambda^2\nu^2}\frac{z}{\lambda}\right]}\mathrm{d}\nu \tag{22.41}$$
$$\tilde{u}(\nu,0) = \int u(x,+0)e^{-2\pi i\nu x}\mathrm{d}x$$

In our case it is due to $u_C = 1 - u_O(x)$:

$$\tilde{u}(\nu,0) = \tilde{u}_O(\nu) \quad \text{or} \quad \tilde{u}_C(\nu) = \delta(\nu) + \tilde{u}_O(\nu) \tag{22.42}$$
$$u(x,z) = \int \tilde{u}_O(\nu)e^{2\pi i\left(\nu x+\sqrt{\frac{\lambda}{z}}\right)}\mathrm{d}\nu = u_O(\nu,z) \quad \text{or} \quad u_C(x,z) = e^{ikz} - u_O(x,z)$$
$$|u(x,z)|^2 = |u_O(x,z)|^2 \text{ or } |u_C(x,z)|^2 = |u_O(x,z)|^2 + 1 - 2\mathrm{Real}[u_O(x,z)e^{-ikz}]$$

This result is not quite expected. We get closer to what we want when specializing on Fraunhofer diffraction because then the '1' term of $u_C = 1 - u_O$ is concentrated into one point at $\nu = 0$. Everywhere else we have $\tilde{u}_C = -\tilde{u}_O$ and $|\tilde{u}_C|^2 = |\tilde{u}_O|^2$. Actually the pure concept of two complimentary objects is not realistic since at least one of the two would stretch out to $x = \pm\infty$. Instead we may compare $v_O(x) = u_0\mathrm{rect}\left(\frac{x}{B}\right)$ and $v_C(x) = u_C(x)\mathrm{rect}\left(\frac{x}{B}\right)$ with $u_O(x) + u_C(x) = 1$. $|\tilde{v}_C(\nu)|^2 = |\tilde{v}_O(\nu)|^2 + \mathrm{sinc}(\nu B)[\mathrm{sinc}(\nu B) - 2\mathrm{Real}\{\tilde{v}_O(\nu)\}]$.

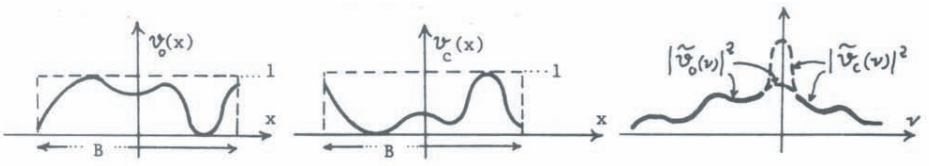

Figure 22.11: Diffraction at complementary screens (Babinet's principle).

23 Application of Fraunhofer Diffraction to Optical Character Recognition

By “character” we mean in this context letters, numbers, and other information-carrying symbols. It is desirable to read letters automatically at a high speed for example at the input-end of a computer, which shall translate Chinese text into English text. Also the U.S. Post Office employs “automatic readers” for identifying ZIP codes. All existing optical character readers use optical components such as lenses merely for “transporting” signals. The intelligent operations are all done by electric components. This must not necessarily be so as the experiment in Appl. Opt. 4, 461 (1965) indicates. In that project the special feature is the “shift-invariance” of the object. That means the lateral position of the input letter is uncritical. Hence one saves the time and complexity needed for careful adjustments at high speeds like 10,000 characters per minute.

24 Coherent Image Formation

Coherent image formation has been treated already as an application of Fresnel diffraction. "Coherent" means that the illuminating light wave comes from a monochromatic point source. The other types of image formation, "partially coherent" and "incoherent", will be treated in later chapters. Here we want to discuss typical setups for coherent image formation. Next the theory will be presented in the form of a convolution integral. When deriving the integral which described the process of coherent image formation, we encounter the important attributes "linear" and "space-invariant". Their significance will be illustrated by citing also some counterexamples. Finally, the image formation integral will be re-formulated, which leads us to "spatial filtering". Some spatial filtering systems will be discussed in Chap. 25, others in a summarizing paper by A. Vander Lugt, "Summary of Optical Data Processing", Optica Acta 15, 1 - 33 (1968), and in a paper on "Theta Modulation", Appl. Opt. 4, 399 (1965).

24.1 Two setups

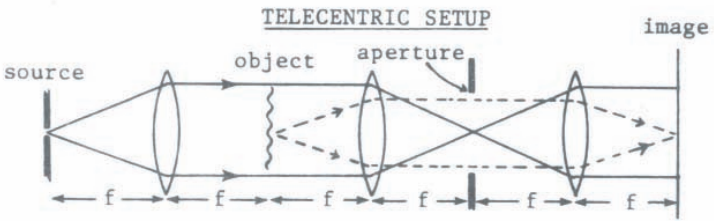

Figure 24.1: The telecentric setup for coherent imaging.

In textbooks and publications one finds most often a drawing of the "telecentric setup". It is pedagogically appealing since one recognizes immediately the various Fourier transform steps. The aperture diameter b has to be $b \leq h - a$, where h refers to the lens diameter and a to the object diameter. This was necessary (see Chap. 22) in order to assure cleancut Fourier transforms. The name "telecentric" implies that the two lenses between object and image are apart from each by the sum of their focal lengths (which happen to be equal in our figure 24.1). A telecentric system has the appealing feature that a plane wave in the object domain

creates another plane wave in the image domain. All other image forming setups convert plane waves into spherical waves and vice versa. That does not cause any serious harm, but it makes the theory a bit clumsier. You will notice two types of rays in the figure. The full-line rays are confined to points in the source plane and in the aperture or Fourier plane, while these same rays are parallel in the object and image domain. The dotted rays have just the reverse properties. We will call the dotted rays the "imaging rays" since they connect object points with image points. The full-line rays are the "illuminating rays".

Maybe not quite so esthetically pleasing but more useful and common in practice is the "single-lens system" (Fig. 24.2). The image-forming lens acts also as the aperture, where the Fourier transform of the object is displayed. The main virtue of this setup is the lower number of glass-air boundaries. That means less reflected light and less dust from which scattered light will emerge and soften up the image.

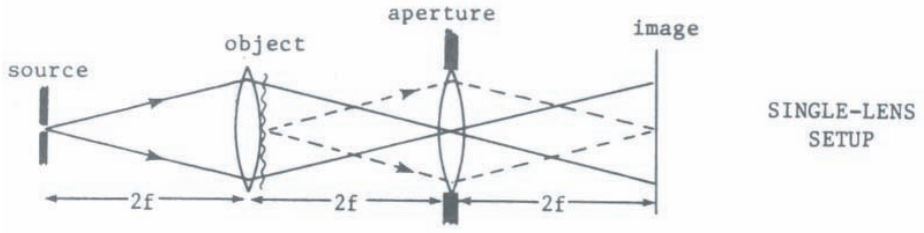

Figure 24.2: The single lens setup for image formation.

24.2 Convolution theory of image formation

The idea is to start with a single object point which results in a point-image or point-spread function or impulse response called $F(x)$. This $F(x)$ will not be quite as sharp as the delta-object for a number of reasons. For the moment let us look at the process of image formation in a somewhat formalistic way as illustrated in the following figures.

Some people also include the feature "space-invariance" in "linearity", which I consider to be a bad practice, because it blurs the issues. A system may very well be:

- linear and space-invariant
- linear and space variant
- nonlinear and space-invariant
- nonlinear and space variant

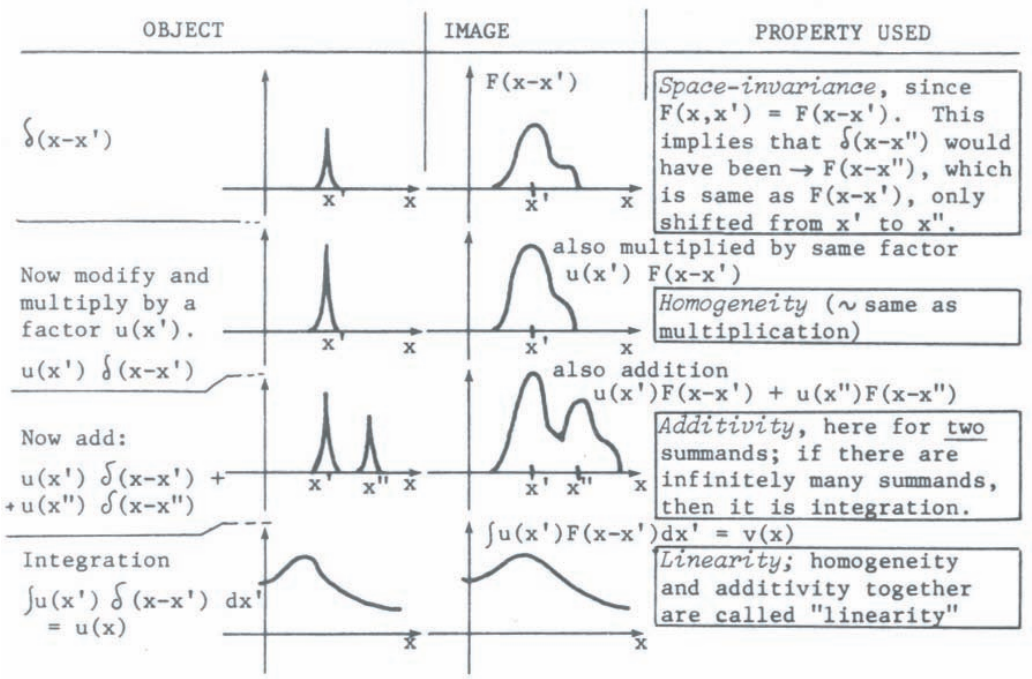

Figure 24.3: Image formation as convolution with a point spread function.

The first variety is most desirable, but never quite realizable. For example receivers (eye, photo-plate, photo-detector) are never quite linear. Even such a harmless dielectric transparent medium as glass is not entirely linear, since, at very high light power, it might create second-harmonic light, or it will be damaged; or even heating is a non-linear effect in the sense that at low light level the transmission properties of glass are different from those at higher intensities. Also ideal space-invariance is only a fiction. The eye, the camera, the telescope. they all produce different image quality off-axis. However, when restricting our attention only to the center part of the image plane, sometimes called the “isoplanatic patch”, then space-invariance is fairly well fulfilled in most practical situations.

Why are space-invariance and linearity so desirable? These two properties make it considerably simpler to interpret an image. As a counter-example, consider a sketch of a space-variant system, where three quite different object details lead to three identical image details (Fig. 24.4). Here, one cannot conclude from the equality of the three images that the three objects were alike. Since image evaluation means usually to conclude from observed image details what the original object details were by comparing known and unknown image details, space-invariance obviously clouds the task.

Now a few comments about non-linearity, which you probably have encountered in elec-

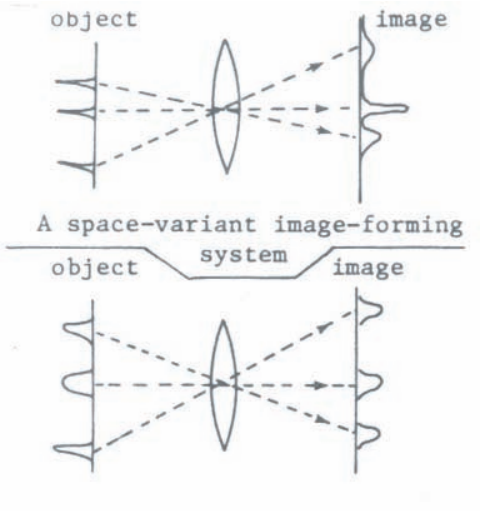

Figure 24.4: A space-variant imaging system.

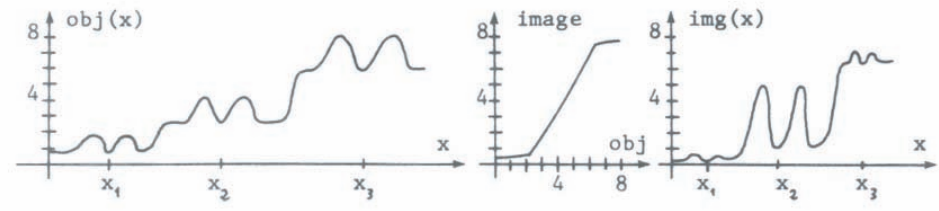

Figure 24.5: An example of a nonlinear imaging system.

tronics. To the left in Fig. 24.5 is the object structure, in the middle the "nonlinear characteristic curve", and to the right the image structure. A nonlinearity can also create difficulties when concluding from the observed image back to the object. As can be seen in Fig. 24.5, the object details around x_1 and x_3 did suffer quite a bit from the "threshold" and "saturation" effects of this particular nonlinearity, which is about typical for photography (except for the sharp edges). By the way, this non-linear effect belongs to the simplest class of nonlinearities, the so-called "point-to-point nonlinearities", because each image point depends only on one object point. For time-signals the corresponding class of nonlinearities is called "memoryless" or "amnesiac".

To make the picture complete, we must also mention why it is sometimes very desirable to have a *nonlinear* and/or *space-variant* system. In general such systems will be advantageous if the set of objects is somehow restricted in its generality. For example, if we know beforehand

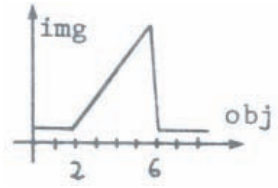

Figure 24.6: A specific type of nonlinearity.

that all possible objects obj(x) (see Fig. 24.6) occupy only amplitude levels between 2 and 6, and amplitude levels ≥ 6 or ≤ 2 mean "noise", then the specific nonlinear characteristic curve would cut out all the noise, but leave the object signal untouched.

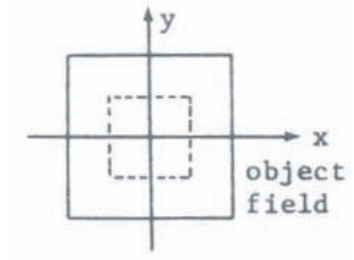

Figure 24.7: Different areas of the object field.

Or considers this example: the class of objects might have high-resolution details (spatial frequencies up to 100 lines per mm) only in the inner portion of the object field, while the object details in the outer portions are always coarser (spatial frequencies up to 25 mm^{-1}). In that case one can afford to use a lens which is considerably worse of the outer parts of the object field as compared to the field center. If a lens-designer knows this feature of the object set for which the lens is going to be used, he can make a lens cheaper than another one, which would be about equally good over the whole field. This approach is actually used more or less in designing cheaper camera lenses. Many customers will never be aware of this compromise of highly space-variant image quality, because they tend to arrange the most important object details close to the field center. Hence, while focusing and while later admiring the print or the projected slide, these customers don't notice the poor image quality at the field corners. They don't miss anything, because these outer image details will be unsharp anyway, because they might be at different depths, hence defocused anyway.

These two examples, where nonlinearity or space-variance were *desirable* features, have in common that the set of expected objects was restricted. In other words, we had some *a priori* information about the objects. As we will see later when discussing superresolution, such situations occur quite often, where the set of objects is somehow restricted. For the in-

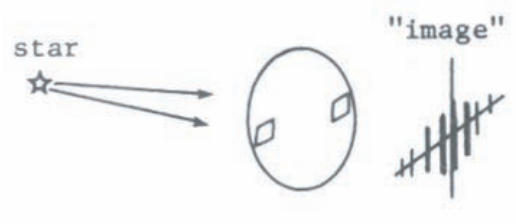

Figure 24.8: Michelsons stardiameter interferometer.

ventor this means two things: (1) recognize that the set of objects is restricted: (2) devise a special-purpose system which covers all the free parameters of the specific object set, but not more. There exist already many cases where such an approach has simplified the instrumentation considerably in comparison to the general-purpose system. Often, it is even impossible to advance the general-purpose instrument so far that it will handle the task. An important classical case of this variety is Michelon's Star-Diameter interferometer (Fig. 26.20). Set of objects: single stars of circular shape, but unknown (angular) diameter. A general-purpose telescope would need a diameter of 20 meters, which is impossible, so far. But for this highly restricted object set it is not necessary to have a full lens aperture of 20 m diameter. Two aperture pieces, 20 m apart, are enough. This special purpose instrument would be confused if confronted with an object which does not belong to the set for which it is designed.

24.3 Spatial Filter theory of coherent image formation

We saw earlier in this chapter that the complex image amplitude $v(x)$ is the result of convolving the object amplitude $u(x)$ with the point-spread function $F(x)$.

$$v(x) = \int u(x')F(x-x')\mathrm{d}x' \tag{24.1}$$

If we replace $u(x)$ and $F(x)$ by their Fourier transforms we arrive at the filter theory of coherent image formation, which was formulated about 100 years ago by Ernst Abbe:

$$u(x) = \int \tilde{u}(\nu)e^{2\pi i\nu x}\mathrm{d}\nu; \qquad F(x) = \int \tilde{F}(\nu)e^{2\pi i\nu x}\mathrm{d}\nu \tag{24.2}$$

$$\boxed{v(x) = \int \tilde{u}(\nu)\tilde{F}(\nu)e^{2\pi i\nu x}\mathrm{d}\nu; \qquad \tilde{v}(\nu) = \tilde{u}(\nu)\ \tilde{F}(\nu)}$$

The function $\tilde{F}$ is called the spatial filter function or sometimes the "pupil function". We can interpret it best by referring to the first figure of this chapter 24, where the image was formed by a telecentric system. Since $v(x)$ arrives in the image plane, and since a Fourier transform takes place when the light travels from the aperture plane to the image plane, there

must have been the Fourier transform $\tilde{v}(\nu)$ at the front side of the last Fourier transform lens. What arrives in the aperture plane from the object $u(x)$ is its Fourier transform $\tilde{u}(\nu)$. In other words it is:

$$\text{in } z = z_{\text{aper}} - 0: \quad \tilde{u}\left(\frac{x}{\lambda f}\right) \qquad \text{in } z = z_{\text{aper}} + 0: \; \tilde{v}\left(\frac{x}{\lambda f}\right) = \tilde{u}\left(\frac{x}{\lambda f}\right)\tilde{F}\left(\frac{x}{\lambda f}\right) \tag{24.3}$$

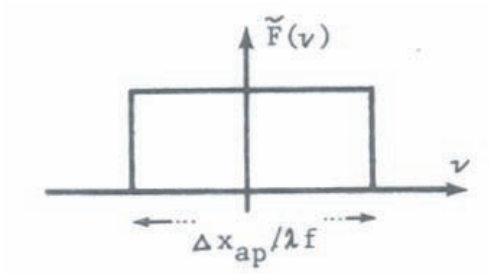

Figure 24.9: Pupil function as low pass filter in an imaging system.

Hence we conclude that in this case the filter function $\tilde{F}(\nu)$ is materialized by the aperture frame. This particular filter function is a so-called "low-pass filter". Notice: it has sharp edges, a feature which is impossible to achieve with time-frequencies, because that would contradict the causality axiom. This low-pass filter is responsible for the limit of resolution. One may even say the high-frequency cutoff *is* the limit of resolution. However, this wordage is not accepted everywhere, since in the past resolution meant the ability to distinguish two close image points. But the question of how to define resolution is more a problem of semantics. What is important here is the fact that coherent image formation can be described as a linear filter with spatial frequency transmittance properties which are characterized by the filter function $\tilde{F}(\nu)$. The low-pass filter is only the most simple example of a large variety of more interesting filter functions, which will be discussed in the following chapter.

25 Some Applications of Spatial Filtering

25.1 Historical remarks about Ernst Abbe (1840 - 1905)

Ernst Abbe, the inventor of spatial filtering, was the son of a foreman in a weaving factory. His father had to work 90 hours per week, which was typical at that time. Typical also was that a man was a wreck at about age 40. Abbe's father lasted till he was 48. When in 1848/49 the students in Germany, France and Russia staged a bloody but unsuccessful revolution against the feudalistic and capitalistic exploitation and for a socialized united country (Germany was then split into more then 300 independent small states), Father Abbe sympathized. He helped some persecuted students to escape from the police. Young Ernst, being a small unsuspicious boy, was actively involved. Later Abbe read and discussed the writings of Marx, Engels, Feuerbach and other theoreticians of social reform. One must know this background to appreciate fully Abbe's actions in his later life.

A fair report about Abbe must mention also that the owner of the factory where Father Abbe worked paid for Ernst's secondary education, assuming that Ernst might become an accountant in his service. When Ernst graduated he had an argument with the factory owner about basic human rights. He must have been very good at it, since the employer not only released him but also paid a small stipend for two years while Abbe studied physics and mathematics at the University of Göttingen. He got his Ph.D. after two years. His examiners were Gauss, Riemann and Weber.

The job market for Ph.D.'s was not very good then. After two hungry years as a private tutor Abbe became Assistant Professor of Theoretical Physics at the University of Jena. Only full professors received a regular salary, assistant professors got parts of the fees paid by the students in their class. In average he had seven students. Therefore he worked also part time in industry from 6 am till noon, when the (mostly rich) students were still asleep or had a hangover from their beer drinking contests. Abbe worked for Carl Zeiss, a craftsman who fabricated microscopes together with his five apprentices. This was done by arranging a few lenses behind each and trying to get a reasonably good image to emerge. Zeiss asked Abbe to develop a quantitative systematic approach for the design of microscope objectives. Abbe devised a ray-optical theory, but the resulting lenses were still poor because the image quality was good only in the center of the field. This problem was overcome when Abbe discovered the "sine-condition". Now the image quality was *uniformly* mediocre across the field.

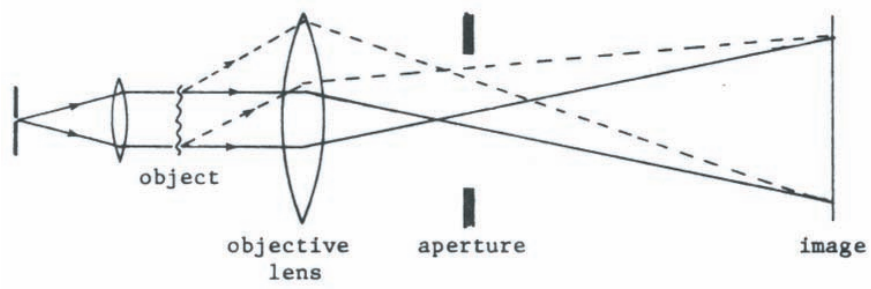

Figure 25.1: Abbe's ray optical theory of imaging.

The problem was that Abbe had designed the diameter h of the objective lens just as wide as the object diameter a. As we understand now very well this prevents the diffracted (dotted) rays from contributing to the image. Since the bandwidth for spatial frequencies is $\Delta\nu \leq \frac{(h-a)}{\lambda f}$ (as we have learned in Chap. 22 in the context of Fraunhofer diffraction) Abbe's lenses would transmit only very low frequencies. His reason for making the lens diameter so small was that in terms of ray optics a lens is the better the smaller it is, because it is much easier to correct the ray paths for the on-axis region. About 100 years ago Abbe recognized the significance of diffraction for the process of coherent image formation. At first he was ridiculed by the scientific establishment. The diffraction (dotted) rays were called "Abbe's black rays". To prove his point he devised a set of experiments, which he published in 1873. The introductory page 413 and one of the later pages (447) are reproduced on page 257 of these notes. He used for example as an object what we would call now a Ronchi-ruling. As you know in the aperture plane there will be a zeroth diffraction order light spot, and more spots from the plus- and minus-first order, from the plus- and minus-third order and so on. The even orders happen to be dark for a Ronchi grating. First Abbe let pass only one order through a small hole in the aperture plane. This resulted of course in uniform brightness. If only the zeroth, plus-first and minus-first order were to pass together through the aperture the grating image had a soft sinusoidal intensity profile. Blocking out the zeroth order decreased the image periodicity by a factor $\frac{1}{2}$. With only zeroth, plus-third and minus-third order passing through the aperture the image period became three times finer.

With these and similar experiments Ernst Abbe proved his theory to be correct. Based on his superior fundamental understanding he was now able to make significant progress in practical optics as well. The Zeiss microscopes were soon leading all over the world. This was attested for example by an American customer who insisted on playing more for the microscope after he received it and appreciated it. But the Zeiss company refused to accept the voluntary overpayment. Another proof of the high quality of Zeiss microscopes was the discovery of bacteria by the country doctor Robert Koch. Until then it was generally believed that illnesses such as TB and cholera are caused by something like a philosophical affliction.

Beiträge zur Theorie des Mikroskops und der mikroskopischen Wahrnehmung.

I. Die Construction von Mikroskopen auf Grund der Theorie. II. Die dioptrischen Bedingungen der Leistung des Mikroskops. III. Die physikalischen Bedingungen für die Abbildung feiner Structuren. IV. Das optische Vermögen des Mikroskops.

Von

Dr. E. Abbe,

ao. Professor in Jena.

I. Die Construction von Mikroskopen auf Grund der Theorie.

1. In den Handbüchern der Mikrographie findet man gelegentlich die Thatsache berührt, dass die Construction der Miksroskope und ihre fortschreitende Verbesserung bisher fast ausschliesslich Sache der Empirie, geschickten und ausdauernden Probirens von Seiten erfahrener Praktiker, geblieben ist. Hin und wieder wird auch wohl die Frage aufgeworfen: warum die Theorie, nach welcher man von der Wirkungsweise des fertigen Mikroskops genügend Rechenschaft geben kann, nicht zugleich die Grundlage für seine Herstellung geworden sei, warum man also nicht auch diese Art von optischen Instrumenten nach theoretisch entwickelten Rechnungsvorschriften construire, wie solches seit Fraunhofer mit dem Fernrohr und in neuerer Zeit mit den optischen Theilen der photographischen Camera so erfolgreich geschieht. Der Grund für das Fortbestehen des empirischen Verfahrens wird allgemein in technischen Schwierigkeiten gesucht — in der vermeintlichen Unmöglichkeit, bei der Ausführung der Mikroskopobjective vorgeschriebene

Schultze, Archiv f. mikrosk. Anatomie. Bd. 9. p. 413–459, 1873

3) Wenn dagegen mindestens drei getrennte Lichtbüschel in das Mikroskop eingelassen werden, so zeigt das Bild stets ein scharf markirtes Detail, sei es in Form eines oder mehrerer Liniensysteme oder in Form isolirter Felder. Dabei ist es gleichgiltig, ob unter den eintretenden Strahlenkegeln das ungebeugte Licht enthalten ist oder nicht, d. h. ob das Bild in hellem oder in dunklem Gesichtsfeld erscheint. Andere Lichtbüschel in Wirksamkeit gesetzt, entsteht aber immer anderes Detail — verschieden, entweder nach dem Grade der Feinheit oder nach der Art der Zeichnung —; und dieses Detail braucht weder dem Inhalte des mikroskopischen Bildes bei normaler Beleuchtung noch auch der anderweit bekannten wirklichen Structur des Objects conform zu sein. Einige nähere Bestimmungen in Betreff des letzten Punktes enthalten die beiden folgenden Sätze.

4) Ein einfaches Streifensystem wird zwar stets auch als solches abgebildet, wenn zwei oder mehrere Lichtbüschel zur Wirkung gelangen, aber in doppelter, dreifacher . . . Feinheit, sobald unter jenen nicht zwei consecutive Büschel enthalten sind, sondern ein, zwei, ... zwischenliegende übersprungen werden; eine Gruppe von nur zwei Linien im Object z. B. erscheint dabei als aus drei, vier . . . getrennten Strichen zusammengesetzt. Die so erzeugten Scheinbilder sind aber in Hinsicht auf ihre Schärfe und die Constanz ihres Auftretens bei keiner Vergrösserung von dem normalen Bilde einer wirklich doppelt, dreifach, . . . so feinen Streifung gleicher Art zu unterscheiden, wie sich durch ein eclatantes Experiment, bei welchem eine solche verdoppelte Theilung unmittelbar neben dem Bilde einer wirklich doppelt so feinen im Gesichtsfeld erscheint, darthun lässt.

5) Wenn zwei einfache Gitter in demselben Niveau unter beliebigem Winkel sich kreuzen, so kann man nicht nur durch geeignete Regulirung des Lichtzutritts nach Belieben beide Liniensysteme einzeln oder gleichzeitig sichtbar machen, sondern man kann auch durch andere Formen der Abblendung in gleicher Schärfe und Markirtheit zahlreiche neue Liniensysteme, welche als solche im Object gar nicht vorhanden sind, und mannigfach geformte Felder, zur Erscheinung bringen. Die neu auftretenden Liniengruppen entsprechen dabei, nach ihrer Lage und der Liniendistanz in

Figure 25.2: Two pages from the original publication by E. Abbe

Success meant growth of the Zeiss company and also personal wealth for Ernst Abbe, who had become a co-owner with Carl Zeiss. Besides inventing, managing, taking care without secretary or typewriter of the English correspondence, Abbe devoted more and more time to the social aspects of a large company. A conflict on such issues arose between Abbe and Zeiss Jr., who had taken over his father's position. Abbe took all his money, and borrowed some more in order to buy out Zeiss Jr. Being then the sole owner he gave almost all his property to a foundation named after his old companion Carl Zeiss. This foundation has since then been the owner of the Zeiss Company and of the Schott glass works. Abbe himself devised the statutes, which said that hiring, firing and promoting should be done without regard to race, creed or political party. These were not empty statements since Jews, atheists and socialists or Marxists were often discriminated against. Abbe also introduced job security, the right to paid vacation and 75% retirement income, 8-hour days (6 per week), and worker representation on some corporation committees. The highest salary (his own) was not so exceed tenfold the amount of a 24-year old skilled laborer. So Abbe divested himself of several million dollars and allowed his salary to be about US$ 10,000/year. He also decided that no patents should be applied for when an invention could lead to medical instruments. A patent is a monopoly. It is immoral to exploit a monopoly at the expense of ill people. To my knowledge this is the rule which Abbe's successors abolished under competitive pressure. Otherwise the Zeiss Foundation is still active. It was in danger of being lost when the Russians occupied Jena as part of East Germany and declared all property to be owned by the people. However, many Zeiss employees fled to West Germany, where they set up a new company, which installed the Foundation rules after a few years.

When reading any book on the theory of optical instruments the name Abbe appears quite often. But Abbe himself was prouder of his social achievements. He held that social progress by evolution, not by revolution, is the way to go for a rational people. His example inspired other employers and even the parliament of Prussia, which conceived about 90 years ago the first social laws anywhere installed, to my knowledge.

25.2 Phase contrast microscopy

Another optical physicist who contributed greatly to medical instrumentation was the Dutchman Fritz Zernicke, who invented around 1930 the phase contrast microscope. Its virtue is to make small phase objects visible. Before that phase objects (like bacteria) had to be stained as introduced by Robert Koch. Some bacteria rejected every stain, and most of them died in the process, which is undesirable from the scientific research point of view.

We can treat phase contrast as a special case of spatial filtering. For convenience we assume the object to be periodic (Fig. 25.3).

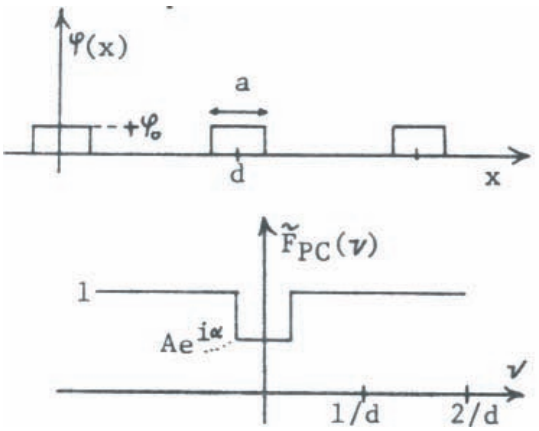

Figure 25.3: The phase object an the phase contrast filter.

$$\begin{aligned} u(x) &= e^{i\varphi(x)} = \sum C_n e^{2\pi i n \frac{n}{d}} \\ C_0 &= \left(1 - \frac{a}{d}\right) + \frac{a}{d} e^{i\varphi(x)} \\ C_n &= \frac{a}{d} \operatorname{sinc}\left(\frac{na}{d}\right)\left(e^{i\varphi_0} - 1\right) \end{aligned} \tag{25.1}$$

The zeroth order coefficient C_0 hits the center part of the phase contrast filter where the light is reduced in amplitude by a factor A and phase-shifted by α. All other diffraction orders $(n \neq 0)$ pass through the filter without modification (except for high frequency cutoff). Hence we get as the image amplitude:

$$\begin{aligned} v(x) &= C_0 A e^{i\alpha} + \sum_{n\neq 0} C_n e^{2\pi i n \frac{n}{d}} \\ &= C_0\left(Ae^{i\alpha} - 1\right) + \sum_{-\infty}^{+\infty} C_n e^{2\pi i n \frac{n}{d}} = C_0\left(Ae^{i\alpha} - 1\right) + u(x) \end{aligned} \tag{25.2}$$

The object $u(x)$ was either $e^{i\varphi_0}$ around $x = 0$ or $u\left(\frac{d}{2}\right) = 1$.

$$v(0) = C_0(Ae^{i\varphi_0} - 1) + e^{i\varphi_0}; \qquad v\left(\frac{d}{2}\right) = C_0\left(Ae^{i\alpha} - 1\right) + 1 \tag{25.3}$$

The case of a small and weak biological object is best described by $\frac{a}{d} \ll 1$ and $\varphi_0 \ll \pi$. Under these conditions a phase shift $\alpha = \frac{\pi}{2}$ of the filter turns out to be desirable. We neglect all second order terms like φ_0^2, $\left(\frac{a}{d}\right)^2$ and $\varphi_0\left(\frac{a}{d}\right)$. Hence it is $C_0 \approx 0$.

$$v(0) \approx \pm iA - 1 + 1 + i\varphi_0 = i(\varphi_0 \pm A); \quad v\left(\frac{d}{2}\right) \approx \pm iA - 1 + 1 = \pm iA$$

$$|v(0)|^2 = (\varphi_0 \pm A)^2; \qquad \left|v\left(\frac{d}{2}\right)\right|^2 = A^2 \tag{25.4}$$

contrast:

$$\frac{|v(0)|^2 - |v\left(\frac{d}{2}\right)|^2}{|v(0)|^2 + |v\left(\frac{d}{2}\right)|^2} = \frac{\varphi_0^2 \pm 2\varphi_0 A}{\varphi_0^2 \pm 2\varphi_0 A + 2A^2} \approx \pm\frac{\varphi_0}{A}; \quad \text{if} \quad A^2 \gg \varphi_0^2 \tag{25.5}$$

25.3 Differential interference contrast

This method has recently replaced phase contrast in many situations. It is sometimes called the "Nomarski method". The image is the first partial derivative of the object. Writing down both the object $u(x, y)$ and the image as Fourier integrals tells us immediately which filter function $\tilde{F}$ is required.

$$u(x,y) = \iint \tilde{u}(\nu,\mu) e^{2\pi i(x\nu + y\mu)} \mathrm{d}\nu \mathrm{d}\mu \tag{25.6}$$

$$v(x,y) = \frac{\partial u(x,y)}{\partial x} = \iint 2\pi i\nu \tilde{u}(\nu,\mu) e^{2\pi i(x\nu+y\mu)} \mathrm{d}\nu \mathrm{d}\mu$$

$$\tilde{F}(\nu,\mu) = 2\pi i\nu; \quad |\tilde{F}| = 2\pi|\nu|; \quad \arg\{\tilde{F}\} = \pm\frac{\pi}{2}$$

$$\text{If } u = e^{i\varphi} \text{ then } |v(x,y)|^2 = \left(\frac{\partial\varphi(x,y)}{\partial x}\right)^2$$

25.4 Several image enhancement methods

Summarizing articles on this subject have been written by J. Tsujiuchi, Prog. Opt. 2, 133 (1963), and by A. Vander Lugt, Optica Acta 15, 1 (1968). This field is still in flux.

About 20 years ago Maréchal used amplitude filters to sharpen a washed-out image. In that case the filter function ($\tilde{F}_M$) was real and positive (Fig. 25.4). It was produced by photographic means. Tsujiuchi extended the art to filters with real values, which could be positive or negative. He wanted to compensate the blurring encountered by defocusing, and described by a filter function $\tilde{F}_B$. That is not quite possible where the blur filter becomes zero. His filter $\tilde{F}_T$ consisted of two layers. The amplitude layer was a photographic emulsion. On top of it were pieces of thin transparent film ($\tilde{F}_P$) which shifted the phase by π where $\tilde{F}_T$ had to be negative. A quick but approximated theory assumes that each object point $\delta(x - x', y - y')$ is converted into rect $\left[\frac{\sqrt{(x-x')^2+(y-y')^2}}{2R}\right]$. In other words according to geometrical optics the

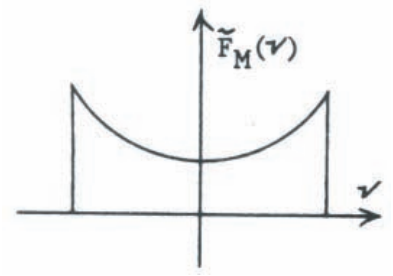

Figure 25.4: Spatial filter for image deblurring introduced by Maréchal.

point spread function of a defocussed system is a disc of radius R (Fig. 25.5).

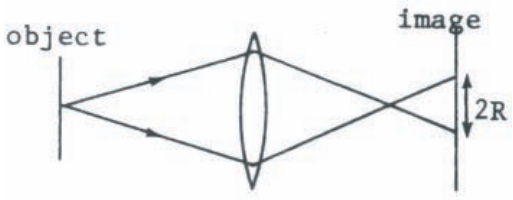

Figure 25.5: The effect of defocussing based on geometrical optics.

The Fourier transform of the disc is the filter function $\tilde{F}_B$ of the blur process, in this case the first Bessel function divided by the argument of that function. As stated before where $\tilde{F}_B$ is very small or even zero a perfect compensation is not possible. But a final image which has been subjected to $\tilde{F}_B\tilde{F}_T$ is certainly better than the blurred image (Fig. 25.6). One of the limitations of this method is the spatial noise due to the grains and dust in the blurred photograph. By enhancing the higher frequencies one also enhances the noise, which usually has a fairly flat spatial power spectrum.

If the object is known to occupy only a small frequency band while the noise is "broadband" it is possible to improve the signal-to-noise by filtering out all those frequencies which contain only noise. O'Neill performed such an experiment, which is reported in Vander Lugt's paper. Sometimes the object covers the frequency spectrum continuously while the noise occupies only a few small spatial frequency sections. This is the case with "half-tone" prints which contain a fine cross-grating superposed on the object. Sayanagi demonstrated that the image can be improved if those grating frequencies are removed by appropriate black dots in the filter function. If the structure of the cross-grating is much finer than the finest object details the spatial frequency spectrum of this half-tone print will consist of several frequency islands. Madame Marquet and J. Tsujiuchi performed spatial filtering experiments wherby only one such frequency island at a time could pass through the filter. The images should have

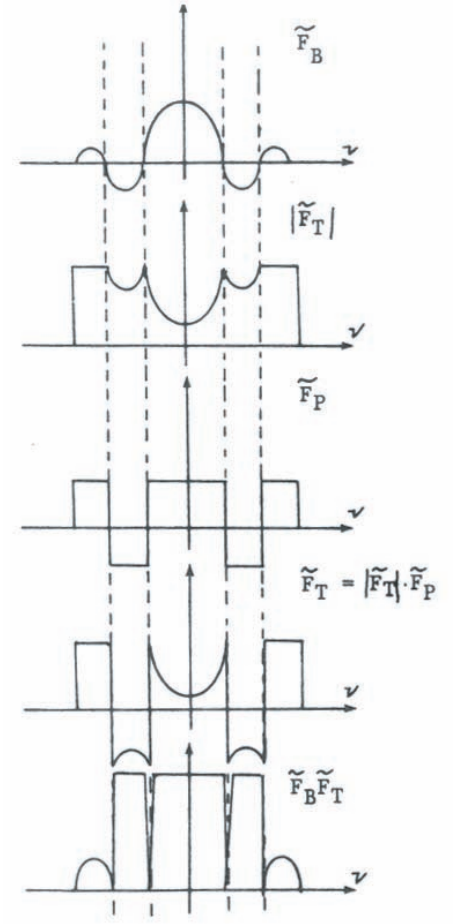

Figure 25.6: Image deblurring by a filter consisting of an amplitude filter $|\tilde{F}_T|$ and a phase shifting filter $\tilde{F}_P$.

contrast reversal and sometimes non-monotonic grey-tone modifications as shown in Optica Acta 8, 267 (1961).

These examples represent only a small portion of the field of spatial filtering. We will return to this area after we are familiar with holography. We will then be in a position of producing arbitrary complex spatial filters.

26 Incoherent Image Formation

26.1 Definition of "coherent" and "incoherent" light

Coherent light is orderly in its phase distributions, while incoherent light is completely disorderly. Laser light is almost completely coherent, while light from thermal sources (the sun, bulbs, etc.) is almost completely incoherent. Also in-between situations exist if laser light or thermal light is properly manipulated by moving diffusers, pinholes, spectral filters and the like. However this in-between situation, which is called "partial coherence", occurs mainly in connection with interference (Chap. 30). It does not have much signification for image formation, except in some microscopes. Hence we concentrate now on incoherent image formation.

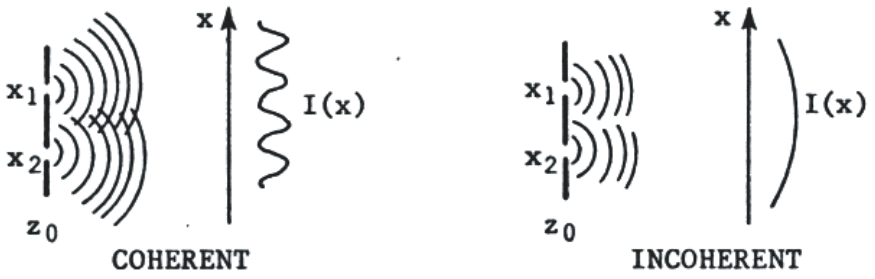

Figure 26.1: Coherent and incoherent light sources.

The empirical test of coherence is to see if interference fringes occur. More specifically, if we want to know whether light at (x_1, z_0) is coherent in relation to light at (x_2, z_0) we place an opaque screen in plane z_0, but with two pinholes at x_1 and x_2. Next we see if interference fringes occur far away where the two spherical waves overlap. If the phase difference between the two point sources jumps in time also the interference fringes will jump around. All receivers are time-integrators, for example the photographic plate integrates over the exposure time, and the eye has a response time of about $1/30$ sec. Hence the fringes will be wiped out in time average if the integration time is longer than the typical interval between phase jumps. Why such phase jumps might occur is a problem of atomic physics which will be discussed in Chap. 30. For now it may suffice to say that self-luminous sources such as hot filaments are incoherent. Later in this chapter we consider also other situations of incoherence. For the time being we may think of incoherent objects as hot filaments, or the stars, or the phosphor

grains on a CRT surface.

The theory of incoherent image formation is of course old, since the problem has existed for a long time. But the topic became hot only around 1955. At that time I worked on interference experiments at a university. One day some TV development engineers visited us and asked "how many dB has a lens"? After a while we concluded they wanted to know something about the quality of the lens used in the TV camera. We told them that lens quality is determined by aberrations and diffraction. They did not know what aberrations are, and we had never heard anything about dB. Since they came to us for advice we suggest that they should learn what aberrations are. But after a while we recognized that we ought to learn about the dB's of the transfer function of a lens, as it was called later. At that time we re-discovered what Duffieux in France, Schade in the U.S.A. and Hopkins in England had done already, the linear filter theory of incoherent image formation. I like to tell this story because it indicates that progress often arises when concepts of communications technology and optics merge. This happened again around 1960 when the Laser emerged from the Maser and Fabry-Pérot interferometry. Also holography can be considered as a union of heterodyne receiver philosophy and interferometry. And the latest fad, "Integrated Optics", is again based on mixed concepts such as integrated electronic circuit technology, thin film optics and fiber optics. Since fads in optics come in fairly regular 5-year intervals we may expect another one in 1975. The big question is "what will it be"? Since all fads had their early forerunners it is very likely that some papers exist already which are neglected by most, but will be cited often and celebrated in 1975.

26.2 Convolution theory of incoherent image formation

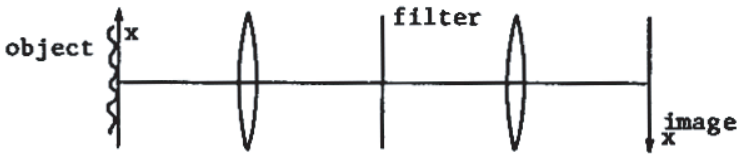

Figure 26.2: Incoherent image formation.

The object may be self-luminous, emitting an amplitude $A(x)$ with a time-varying phase $\varphi(x,t)$.

$$u_0(x,t) = A(x)e^{i\varphi(x,t)}; \qquad \langle u_0 \rangle = 0; \qquad \langle |u_0|^2 \rangle = A^2 = I_0(x) \tag{26.1}$$

The symbol $\langle \ldots \rangle$ means time-averaging, or better, "time-integrating". Now we start on the basis of what we know from the theory of *coherent* image formation. An object point at x' with amplitude $\delta(x-x')$ produces $F(x-x')$ in the image plane. $F(x)$ is Fourier-related to the filter function $\tilde{F}(\nu)$ in the plane FILT. Symbolically:

$$\begin{aligned} \delta(x-x') &\longrightarrow F(x-x') \\ u_0(x',t)\delta(x-x') &\longrightarrow u_(x',t)F(x-x') \\ \int u_0(x',t)\delta(x-x')\mathrm{d}x' = u_0 &\longrightarrow \int u_0(x',t)F(x-x')\mathrm{d}x' = v(x,t) \end{aligned} \tag{26.2}$$

The complex image amplitude $v(x,t)$ has a zero-time-average if the phase $\varphi(x,t)$ varies wildly during the exposure time T.

$$\langle v(x,t)\rangle = \int \langle e^{i\varphi(x',t)}\rangle A(x')F(x-x')\mathrm{d}x' = 0 \tag{26.3}$$

due to

$$\langle e^{i\varphi(x',t)}\rangle = 0 \tag{26.4}$$

That is not tragic since receivers do not respond to v but to $|v|^2$.

$$\langle |v|^2\rangle = \iint \langle e^{i[\varphi(x',t)-\varphi(x'',t)]}\rangle A(x')A(x'')F(x-x')F^*(x-x'')\mathrm{d}x'\,\mathrm{d}x'' \tag{26.5}$$

We assume that the space-and-time fluctuations of the phase factor follow a delta law:

$$\langle e^{i[\varphi'-\varphi'']}\rangle = \delta(x'-x''); \qquad \left(\langle\ldots\rangle = \lim_{T\to\text{big}} \int_{-\frac{T}{2}}^{\frac{T}{2}} \ldots \mathrm{d}t\right) \tag{26.6}$$

I hope this is intuitively appealing, since I don't have completely convincing arguments in support of this delta law. My guess is that the mathematical tools used by O'Neill in "Statistical Optics" when discussing the random walk problem of complex numbers would be adequate to develop support for the delta-law. By the way it has been used without derivation in several journal articles by respectable authors. Using the delta law we get now

$$\begin{aligned} \langle |v|^2\rangle &= \int A^2(x')|F(x-x')|^2\mathrm{d}x'; \quad \langle |v|^2\rangle = I_B; \quad A^2 = I_0; \quad |F|^2 = D \\ &\boxed{I_B(x) = \int I_0(x')D(x-x')\mathrm{d}x'} \end{aligned} \tag{26.7}$$

The recorded image intensity I_B is the convolution of object intensity I_0 and (incoherent) point spread function $D(x)$. The name "psf" indicates that D is the image of a point object.

26.3 Linear filter theory of incoherent image formation

If all intensities in the previous convolution formula are expressed as Fourier integrals we find:

$$\boxed{\tilde{I}_B(\nu) = \tilde{I}_0(\nu)\tilde{D}(\nu) = \int I_B(x) e^{-2\pi i \nu x} \mathrm{d}x} \tag{26.8}$$

The term $\tilde{D}$ is mostly called "optical transfer function OTF", and its modulus $|\tilde{D}|$ the "modulation transfer function MTF". Since $D(x)$ and $D(x, y)$ (in two dimensions) are real the OTF obeys the reality symmetry:

$$\tilde{D}(\nu) = \tilde{D}^*(-\nu); \qquad |\tilde{D}(\nu)| = +|\tilde{D}(-\nu)|; \qquad \theta(\nu) = -\theta(-\nu) \tag{26.9}$$

Often $D(x)$ is symmetrical, $D(x) = D(-x)$ or nearly so. Then it follows also that $\tilde{D}(\nu) = \tilde{D}(-\nu)$. In that case the transfer phase can be only 0 or π.

The meaning oft the OTF is best understood if we consider a special object:

$$I_0(x) = 1 + A_0 \cos(2\pi\nu_0 x) \tag{26.10}$$

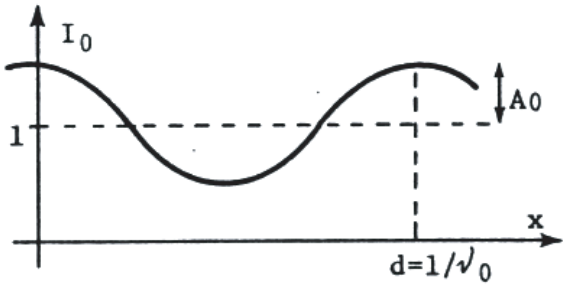

Figure 26.3: Example of an object for incoherent imaging.

$$\begin{aligned} I_B(x) &= 1 + A_B \cos(2\pi\nu_0 x + \theta) \\ \delta x &= -\frac{\theta(\nu_0)}{2\pi\nu_0} \\ A_B &= A_0 |\tilde{D}(\nu_0)| \end{aligned} \tag{26.11}$$

The formulas (Eqs 26.10 and 26.11) can easily be verified by computing the Fourier spectra such as:

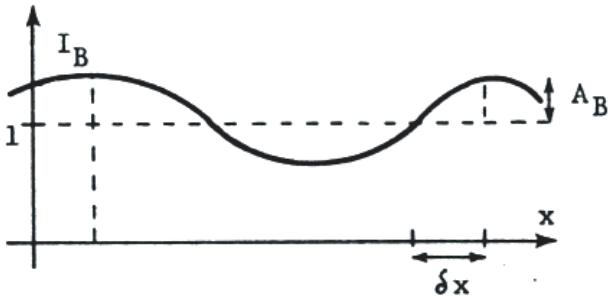

Figure 26.4: The intensity distribution of the incoherent image of I_0.

$$\tilde{I}_0(\nu) = \delta(\nu) + \frac{A_0}{2}\left[\delta(\nu - \nu_0) + \delta(\nu + \nu_0)\right] \tag{26.12}$$

It is customary to normalize the OTF at zero frequency:

$$\tilde{D}(\nu) = 1;\ \text{hence}\ \int I_0(x)\mathrm{d}x = \tilde{I}_0(0) = \tilde{I}_B(0) = \int I_B(x)\mathrm{d}x \tag{26.13}$$

This implies something about energy conservation. Actually not all of the object energy per time $\int I_0(x)\mathrm{d}x$ will arrive at the image plane since the object radiates into a much wider angle than any lens can accept. Hence the normalization convention $\tilde{D}(0) = 1$ implies that we forget for the moment any questions of *absolute* brightness. Only the geometrical structure of relative brightness is of interest now. The unanswered questions belong to the area of photometry.

Sometimes the OTF is also called "contrast transfer function" (CTF or KTF). this is related to contrast as it perceived by the almost-logarithmic eye:

$$C = \frac{I_{\max} - I_{\min}}{I_{\max} + I_{\min}} \tag{26.14}$$

In relation to the figure on the previous page we find

$$C_{\mathrm{obj}} = A_0; \quad C_{\mathrm{im}} = A_B = A_0|\tilde{D}|; \quad \frac{C_{\mathrm{im}}}{C_{\mathrm{obj}}} = |\tilde{D}| \tag{26.15}$$

In other words the MTF describes the contrast reduction.

26.4 The Duffieux formula

We found that the incoherent psf $D(x)$ is the modulus square of the coherent psf $F(x)$, and the OTF is the (normalized) Fourier transform of the incoherent psf $D(x)$. The coherent psf is the Fourier transform of the coherent filter fct. or "pupil fct. $\tilde{F}(\nu)$".

$$\begin{aligned} D(x) &= |F(x)|^2 \\ \tilde{D}(\nu) &= \frac{\int D(x)e^{-2\pi i\nu x}\mathrm{d}x}{\int D(x)\mathrm{d}x} \\ F(x) &= \int \tilde{F}(\nu)e^{2\pi i\nu x}\mathrm{d}\nu \\ \int D(x)e^{-2\pi i\nu x}\mathrm{d}x &= \int |F(x)|^2 e^{-2\pi i\nu x}\mathrm{d}x \\ &= \iiint \tilde{F}(\nu')\tilde{F}^*(\nu'')e^{2\pi ix(-\nu+\nu'-\nu'')}\mathrm{d}x\,\mathrm{d}\nu'\,\mathrm{d}\nu'' \\ &= \int \tilde{F}(\nu')F^*(\nu'-\nu)\mathrm{d}\nu' = \int \tilde{F}\left(\nu'+\frac{\nu}{2}\right)\mathrm{d}\nu' \end{aligned} \tag{26.16}$$

Duffieux:

$$\boxed{\tilde{D}(\nu) = \frac{\int \tilde{F}\left(\nu'+\frac{\nu}{2}\right)\tilde{F}^*\left(\nu'-\frac{\nu}{2}\right)\mathrm{d}\nu'}{\int |\tilde{F}(\nu')|^2\mathrm{d}\nu'}} \tag{26.17}$$

or in two dimensions:

$$\tilde{D}(\nu) = \frac{\iint \tilde{F}\left(\nu'+\frac{\nu}{2},\mu'+\frac{\mu}{2}\right)\tilde{F}^*\left(\nu'-\frac{\nu}{2},\mu'-\frac{\mu}{2}\right)\mathrm{d}\nu'\mathrm{d}\mu'}{\iint |\tilde{F}(\nu',\mu')|^2\mathrm{d}\nu'\mathrm{d}\mu'} \tag{26.18}$$

Often the Duffieux-formula is written in terms of the genuine coordinates (x, y) in the pupil domain with $\tilde{F}(x, y)$ and:

$$D(x,y) = \left|\iint \tilde{F}(x',y')e^{-2\pi i\frac{xx'+yy'}{\lambda f}}\mathrm{d}x'\mathrm{d}y'\right|^2 \tag{26.19}$$

$$\boxed{\tilde{D}(\nu,\mu) = \frac{\iint \tilde{F}\left(x+\frac{\lambda f\nu}{2},y+\frac{\lambda f\mu}{2}\right)\tilde{F}^*\left(x-\frac{\lambda f\nu}{2},y-\frac{\lambda f\mu}{2}\right)\mathrm{d}\nu'\mathrm{d}\mu'}{\iint |\tilde{F}(x,y)|^2\mathrm{d}x\mathrm{d}y}} \tag{26.20}$$

Before going deeper into the theory of the OTF we will discuss now ways to measure the transfer function.

26.5 Measurement of the OTF

Figs 26.3 and 26.4 indicate the most obvious way to measure the OTF. We need an object $I_0(x,y) = 1 + A_0 \cos\{2\pi(\nu_0 x + \mu_0 y)\}$, which will cause an image $I_B(x,y) = 1 + A_0|\tilde{D}(\nu_0,\mu_0)|\cos\{2\pi(\nu_0 x + \mu_0 y) + \theta(\nu_0,\mu_0)\}$. Comparing the contrasts A_0 and $A_0|\tilde{D}|$ yields the MTF, while the fringe shift $\delta x = -\frac{\theta}{2\pi\varrho_0}$ reveals the transfer phase ($\varrho_0^2 = \nu_0^2 + \mu_0^2$). We want to know the OTF for *all* frequencies (ν_0, μ_0). Hence a test object with variable spatial frequency is desirable. The Moiré grating is ideal for this purpose.

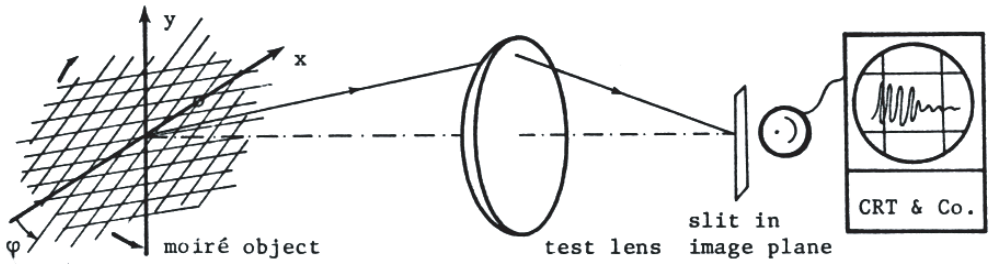

Figure 26.5: Measurement setup for OTF measurements.

$$\text{object}: \quad 1 + A_0 \cos\{2\pi\nu(t)(x - x_0)\} \tag{26.21}$$

Assuming constant angular velocity of the two Moiré gratings $\varphi = \omega t$ we get:

$$\nu(t) = 2\sin\frac{\varphi(t)}{d} \approx \frac{2\omega t}{d} = at \quad (|\varphi| < 15^\circ) \tag{26.22}$$
$$\text{image}: \quad 1 + A_0|\tilde{D}(a,t)|\cos\{2\pi at(x - x_0) + \theta(a,t)\}$$

PMT-signal, recorded at slit position $x = 0$:

$$S(t) = 1 + A_0|\tilde{D}(a,t)|\cos\{2\pi a x_0 t - \theta(a,t)\} \tag{26.23}$$

The MFT appears as amplitude modulation, θ as phase modulation, while $ax_0 = \frac{2\omega x_0}{d}$ is the temporal carrier frequency. Another popular test object is a rotating drum with a bar pattern of increasing spatial frequency on it.

The first method has the advantage that higher spatial harmonies (if the moiré patterns are not truly sinusoidal) can be eliminated electronically. Hence the CRT displays only the response to a true sine wave. Such an operation is not possible in the second setup where the spatial frequencies on the drum are converted directly into temporal frequencies, which vary also. This could be alleviated by spinning the drum faster while the low frequencies are

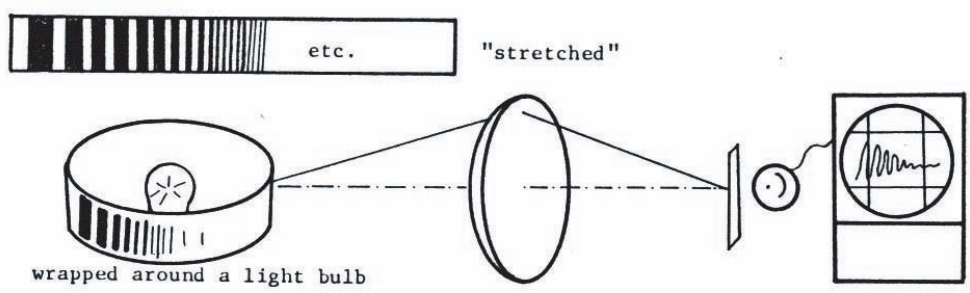

Figure 26.6: OTF measurement setup 2.

imaged onto the slit.

Both methods can be inverted, which means that a slit source is imaged onto variable sine-wave targets:

$$\delta(x) \longrightarrow D(x) \longrightarrow D(x)[1 + A_0 \cos\{2\pi a t(x - x_0)\}] \longrightarrow \tag{26.24}$$
$$\longrightarrow \int D(x)[1 + A_0 \cos \ldots]\mathrm{d}x = \text{same as before}$$

Which way to go depends largely on whether a magnifying or a minifying lens is tested.

There exist also a few indirect methods. For example a moving slit $\delta(x - vt)$ may be imaged onto a receiver slit at $x = 0$, which allows the display of the line spread function $D(-vt)$. An electronic or digital Fourier transform of the line spread function yields the OTF. Yet another indirect method employs an edge object $H(x - vt)$, imaged onto a receiver slit.

$$H(x) \begin{cases} +1 & \text{if } x \geq 0 \\ 0 & \text{if } x < 0 \end{cases} \tag{26.25}$$

$$H(x - vt) \longrightarrow \int H(x' - vt)D(x - x')\mathrm{d}x' \longrightarrow \int H(x' - vt)D(-x')\mathrm{d}x' = S(vt)$$

$$S(vt) = \int_{vt}^{+\infty} D(-x')\mathrm{d}x' = \tag{26.26}$$

$$= \int_{vt}^{v(t+\mathrm{d}t)} D(-x')\mathrm{d}x' + \int_{v(t+dt)}^{+\infty} D(-x')\mathrm{d}x' \approx D(-vt)v\mathrm{d}t + S(v(t + \mathrm{d}t))$$

Hence: $\frac{\mathrm{d}S(vt)}{\mathrm{d}(vt)} = -D(-vt)$.

In other words, the derivative of the edge image is the line image. Electronic differentiation is a simple process for getting D from S. For sake of brevity we have utilized often a one-dimensional form. However we should clearly understand how the point-spread function $D(x, y)$, the line spread function and the OTF $\tilde{D}(\nu, \mu)$ or $\tilde{D}(\nu, 0)$ are related to each other.

The Fourier transform of the line image $L(x)$ is the OTF along a perpendicular line in the Fourier domain.

$$\tilde{D}(\nu,0) = \iint D(x,y)e^{2\pi i[\nu x+0]}\mathrm{d}x\mathrm{d}y = \int_{(x)} \underbrace{\left[\int_{(y)} D(x,y)\mathrm{d}y\right]}_{L(x)} e^{-2\pi i\nu x}\mathrm{d}x \tag{26.27}$$

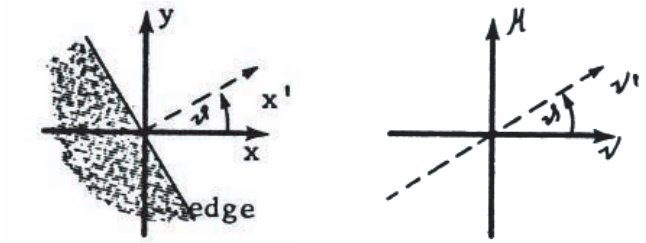

Figure 26.7: The relation between edge object and the resulting OTF.

26.6 Incoherent image formation with transparent objects

A slide protector is an example of an incoherent image forming system which does not employ self-luminous objects but transparent objects. We will call the image forming system incoherent if the object intensity $I_0(x)$, the image intensity $I_B(x)$ and the incoherent psf $D(x)$ (i.e., the intensity distribution in the image of a point object) are related by a convolution:

$$I_B(x) = \int I_0(x')D(x-x')\mathrm{d}x' \tag{26.28}$$

We will show that this formula applies if the image of the extended source fills the whole aperture.

For mathematical convenience we replace the actual projection system by a telecentric system with $1:1$ magnification. At first we pick only one source point x_S, which allows us to use the theory of coherent image formation. Later on we integrate $\ldots\,\mathrm{d}x_S$ over the source.

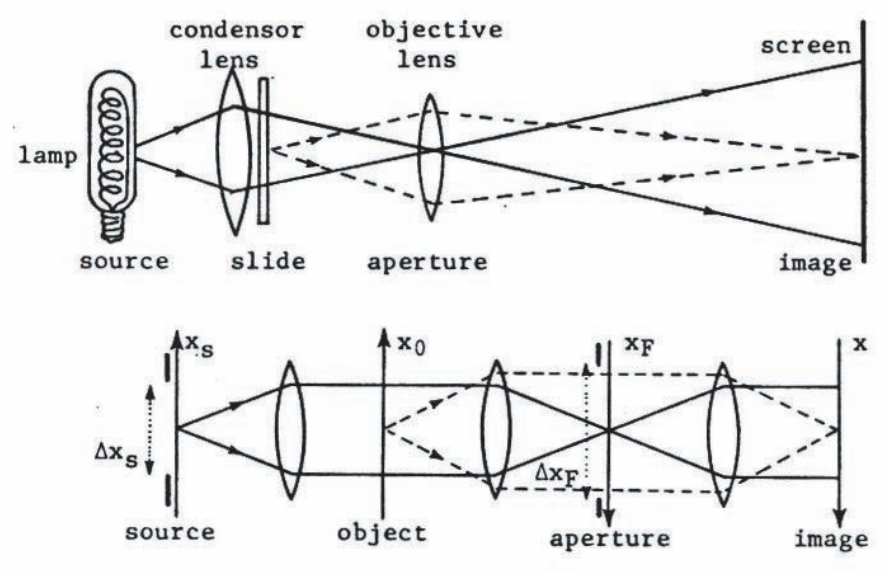

Figure 26.8: A slide projector as an incoherent imaging system.

$$\underbrace{\delta(x-x_S)}_{\text{in } z_{\text{sou}}} \longrightarrow \underbrace{e^{2\pi i \frac{x_0 x_S}{\lambda f}} \longrightarrow e^{2\pi i \frac{x_0 x_S}{\lambda f}} u_0(x_0)}_{\text{in } z_{\text{obj}}} \longrightarrow \tag{26.29}$$

$$\longrightarrow \underbrace{\int u_0(x_0) e^{2\pi i \frac{x_0 x_S}{\lambda f}} F(x-x_0)\mathrm{d}x_0 = v(x;x_S)}_{\text{in } z_{\text{im}}}$$

where:

$$\text{in } z_{\text{ap}}: \quad F(x) = \int \tilde{F}\left(\frac{x_F}{\lambda f}\right) e^{2\pi i \frac{x\, x_F}{\lambda f}} \mathrm{d}x_F \tag{26.30}$$

The complex amplitude in z_{sou} has a fluctuating phase $\varphi(x_S,t)$ but a time-independent modulus $\sqrt{I_S(x_S)}$.

$$\delta(x-x_S) \longrightarrow \sqrt{I_S(x_S)} e^{i\varphi(x_S,t)} \delta(x-x_S) \sim v(x,x_S) \longrightarrow v(x,x_S)\sqrt{I_S(x_S)} e^{i\varphi(x_S,t)} \tag{26.31}$$

Instantaneous complex amplitude in the image from all source points is:

$$\int v(x,x_S)\sqrt{I_S(x_S)}e^{i\varphi(x_S,t)}\mathrm{d}x_S \tag{26.32}$$

Instantaneous intensity:

$$|\int v\sqrt{I_S}e^{i\varphi}\mathrm{d}x_S|^2 \tag{26.33}$$

The observed time-integrated intensity $I_B(x)$ is:

$$\begin{aligned} I_B(x) &= \int_0^T |\int v\sqrt{I_S}e^{i\varphi}\mathrm{d}x_S|^2 dt = \qquad (26.34)\\ &= \iint\int v(x,x_S)v^*(x,x'_S)\sqrt{I_S(x_S)}\sqrt{I_S(x'_S)}e^{i[\varphi(x_S,t)-\varphi(x'_S,t)]}\mathrm{d}x_S\,\mathrm{d}x'_S\,\mathrm{d}t \\ \text{where :}\quad &\int_0^T e^{i[\varphi(x_S,t)-\varphi(x'_S,t)]}\mathrm{d}t \approx \delta(x_S-x'_S) \end{aligned}$$

This implies that the phase fluctuations at source point x_S have nothing to do with the fluctuations in x'_S (unless $x_S = x'_S$). Hence $\int \ldots \mathrm{d}x'_S \sim x'_S \longrightarrow x_S$.

$$I_B(x) = \int |v(x,x_S)|^2 I_S(x_S)\mathrm{d}x_S \tag{26.35}$$

Now we insert $v(x,x_S) = \int u_0(x')e^{2\pi i\frac{x'x_S}{\lambda f}}F(x-x')\mathrm{d}x'$

$$I_B(x) = \iint\int u_0(x')u_0^*(x'')e^{2\pi i\frac{x_S(x'-x'')}{\lambda f}}F(x-x')F^*(x-x'')I_S(x_S)\mathrm{d}x'\,\mathrm{d}x''\,\mathrm{d}x_S \tag{26.36}$$

If the source is uniformly bright within $|x_S| \le \frac{\Delta x_S}{2}$ we describe it by $I_S(x_S) = \mathrm{rect}\left(\frac{x_S}{\Delta x_S}\right)$. Now the x_S integral can be executed.

$$\int I_S(x_S)e^{2\pi i x_S\frac{(x'-x'')}{\lambda f}}\mathrm{d}x_S = \Delta x_S \mathrm{sinc}\left(\frac{\Delta x_S(x'-x'')}{\lambda f}\right) \tag{26.37}$$

This sinc-function has a peak width of $\delta x_S = \frac{\lambda f}{\Delta x_S}$. Can we treat this sinc-function like a delta function? This depends on whether δx_S is smaller than the fine image details. The coherent image amplitude would have been:

$$\int u_0(x')F(x-x')\mathrm{d}x' = \Delta x_F \int u_0(x')\mathrm{sinc}\left(\frac{\Delta x_F(x-x')}{\lambda f}\right)\mathrm{d}x' \tag{26.38}$$

if the aperture is described by $\tilde{F}(x_F) = \mathrm{rect}\left(\frac{x_F}{\Delta x_F}\right)$. Since $I_B(x)$ actually consists of integrals of this type we conclude the image resolution is determined by the peak width $\delta x_F = \frac{\lambda f}{\Delta x_F}$ of $F(x) = \Delta x_F \ \mathrm{sinc}\left(\frac{\Delta x_F x}{\lambda f}\right)$. Hence we require for $\Delta x_S \ \mathrm{sinc}\left(\frac{x'-x''}{\delta x_S}\right)$ that $\delta x_S \leq \frac{1}{2}\delta x_F$. Using $\delta x_S = \frac{\lambda f}{\Delta x_S}$ and $\delta x_F = \frac{\lambda f}{\Delta x_F}$ we get:

$$\boxed{\Delta x_S \geq 2\Delta x_F} \tag{26.39}$$

This means that the image of the source should be twice as big as the aperture diameter Δx_F. Several authors are satisfied with $\Delta x_S \geq \Delta x_F$ as a condition for achieving incoherent illumination.

Under those circumstances it is justified to set

$$\int I_S(x_S)e^{2\pi i x_S \frac{x'-x''}{\lambda f}}\mathrm{d}x_S \approx \delta(x'-x'') \tag{26.40}$$

Hence $\int \ldots dx''$ in $I_B(x)$ has $x'' \longrightarrow x'$ as consequence:

$$I_B(x) = \int |u_0(x')|^2 |F(x-x')|^2 \mathrm{d}x' \tag{26.41}$$

or with $|u_0(x)|^2 = I_0(x)$ and $|F(x)|^2 = D(x)$

$$\boxed{I_B(x) = \int I_0(x')D(x-x')\mathrm{d}x'} \tag{26.42}$$

26.7 Lens aberrations

Soon we want to compute the OTF of a lens if the aberrations of that lens are known from the design or from aberration measurements. But first we must clarify what aberrations really are. There are (at least) four ways to describe the aberrations (Fig.26.9), called "longitudinal", "lateral", "angular", or "wave aberrations". For the time being we will think mainly of photographic lenses. For them the object is usually at infinity, while the image is in the rear focal plane. Hence a perfect lens will combine a bunch of incoming parallel rays into a point in the real focal plane. $\Delta s(h)$ is called the "longitudinal aberration" and $\xi(h)$ the "lateral aberration". $\xi(h) = -s(h)\frac{h}{f}$.

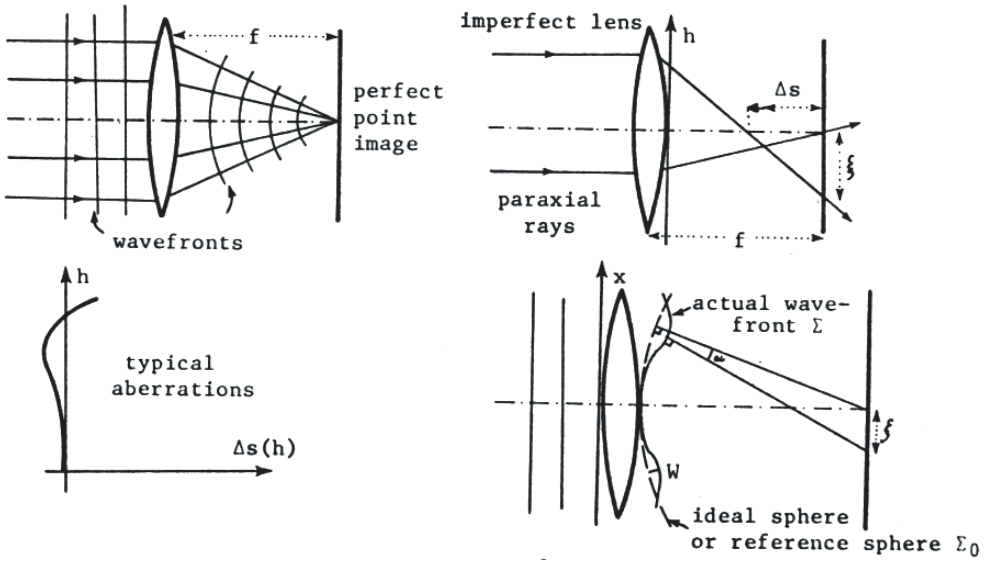

Figure 26.9: Representation of aberrations, as longitudinal, transversal, angular deviation of the rays from their ideal path and as wavefront deviations.

The deviation between the ideal wavefront Σ_0 ant the actual wavefront Σ is called the wave aberration $W(x, y)$. (The notations on this page are perhaps not consistent, but are according to common practice.) Hence the complex amplitude on Σ is e^{ikW} with $k = \frac{2\pi}{\lambda}$. Since rays are perpendicular to wavefronts the "angular aberration α" of the actual versus ideal ray is $\alpha = \frac{\partial W}{\partial x}$. The angular aberration α is tied to the lateral aberration ξ by $\xi = -\frac{f}{\alpha} = -f\frac{\partial W(x,y)}{\partial dx}$. All theses equations are correct only for reasonably small angles since we assumed angles to be approximately equal to the tangents of those angles. For $F/2$ lens these approximations are considered to be good enough by most lens designers, though not for $F/1.4$.

An alternative way of presenting lens aberrations is the "spot diagram" (Herzberg, Linfoot).

One divides the lens aperture or "pupil" into small areas of equal size. The lateral aberrations $\xi(x_n, y_n)$ and $\eta(x_n, y_n)$ for the ray from the center (x_n, y_n) of the n-th small area are computed for $n = 1, 2 \ldots N$ and plotted in the image plane. A high concentration of spots indicates a bright portion of the point image. The number N of rays is typically 30 to a few hundreds.

The relationship between lateral aberrations ξ, η and the derivatives $\frac{\partial W}{\partial x}$ and $\frac{\partial W}{\partial y}$ of the wave aberrations can be obtained also by a wave-optical computation. One sets $e^{ikW(x,y)}$ on

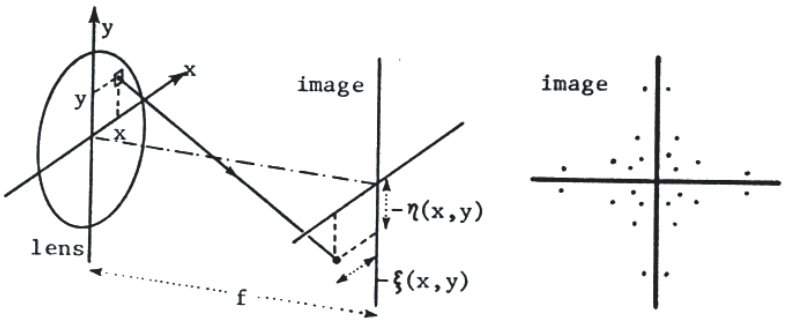

Figure 26.10: The spot diagram for description of the lens quality.

the reference sphere and computes $u(\xi, \eta)$ in the rear focal plane by means of a somewhat modified HFK approach.

26.8 The OTF of a perfect lens

The filter function of a perfect lens is:

$$\tilde{F}(x,y) = \begin{cases} +1 & \text{if } x^2 + y^2 \leq \frac{B}{2} \\ 0 & \text{otherwise;} \end{cases} \tag{26.43}$$

In other words the lens has no aberrations W. The amplitude transmittance is 1 within a circle of diameter B (Fig. 26.11).

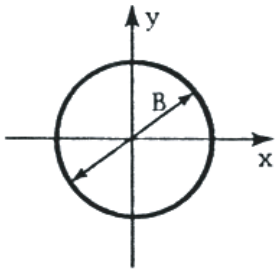

Figure 26.11: The filter function of a perfect lens.

Duffieux:

$$\tilde{D}(\nu,\mu) = \frac{\iint \tilde{F}\left(x+\frac{\lambda f\nu}{2}, y+\frac{\lambda f\mu}{2}\right)\tilde{F}^*\left(x-\frac{\lambda f\nu}{2}, y-\frac{\lambda f\mu}{2}\right)\mathrm{d}\nu'\mathrm{d}\mu'}{\iint |\tilde{F}(x,y)|^2 \mathrm{d}x\mathrm{d}y} \tag{26.44}$$

The denominator yields simply $\pi\left(\frac{B}{2}\right)^2$. The numerator is given by the overlap area of two shifted circles with diameters B and center positions $\left(\frac{\lambda f\nu}{2}, \frac{\lambda f\mu}{2}\right)$ and $\left(-\frac{\lambda f\nu}{2}, -\frac{\lambda f\mu}{2}\right)$. The resulting OTF is a conical pyramid, which is slightly sagging (Fig. 26.12).

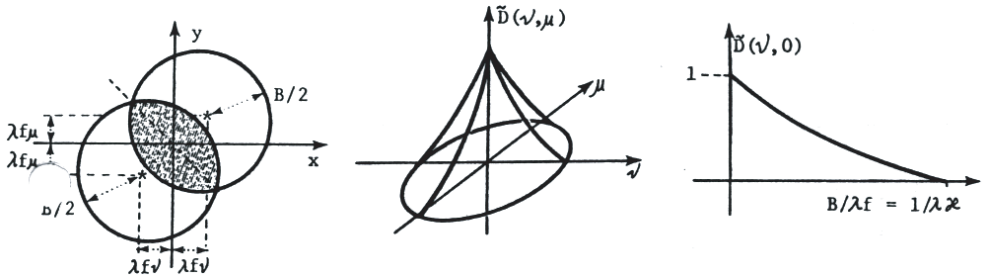

Figure 26.12: Derivation of the OTF of the ideal lens.

$\chi = \frac{f}{B}$ is the stop number or F-number.

The computation of $\tilde{D}(\nu,\mu)$ of the perfect lens is an exercise in trigonometry, not very interesting. More interesting is the following intuitive derivation. We assume an object with amplitude transmittance $u_0(x,y) = \cos(\pi\nu x)$; $I_0(x,y) = |u_0(x,y)|^2 = \frac{1}{2} + \frac{1}{2}\cos(2\pi\nu x)$. At first we consider only a single source point on axis. The spatial frequency of $\cos(\pi\nu x)$ is $\frac{\nu}{2}$ or the grating constant $d_0 = \frac{2}{\nu}$. Hence the first diffraction orders are deviated by angles $\sin\alpha = \pm\frac{\lambda}{d_0}$. Two bright points will appear in the aperture plane at $x_F = \pm\frac{f\lambda\nu}{2}$, separated by $\lambda f\nu$. If the aperture diameter B is wider than B the object will be resolved. But if $\lambda f\nu$, all the light is stopped in the aperture plane.

Now let us consider a source point off-axis. The cosine grating object will cause two bright spots in the aperture plane. Three cases might occur:

1. both outside the aperture: $\left||x_S| - \lambda f\frac{|\nu|}{2}\right| > \frac{B}{2}$
2. both inside the aperture: $|x_S| + \lambda f\frac{|\nu|}{2} < \frac{B}{2}$
3. one inside one outside of aperture: $\left||x_S| - \lambda f\frac{|\nu|}{2}\right| < \frac{B}{2}$ and $|x_S| + \lambda f\frac{|\nu|}{2} > \frac{B}{2}$

(1) means darkness in the image plane; (2) the cosine fringes are produced; but in the case of (3) a constant "d.c." illumination appears in the image plane, since the single plane wave

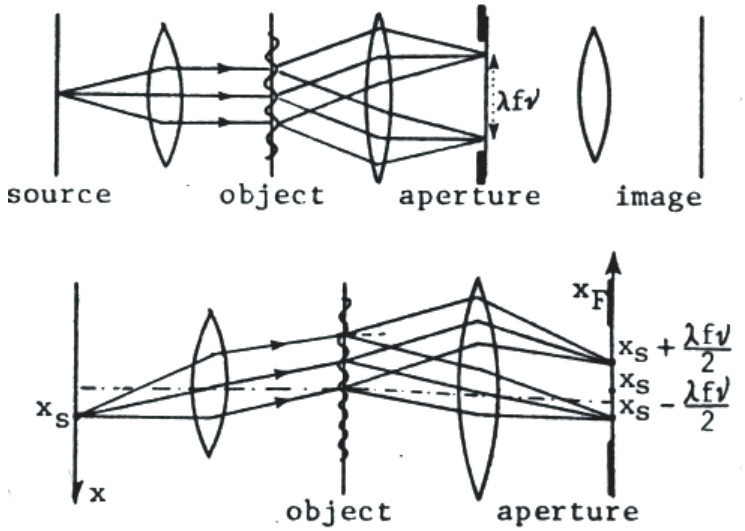

Figure 26.13: Incoherent image formation.

has nothing to interfere with. At least two plane waves are needed for producing interference fringes. The total intensity distribution in the image plane consists of intensity contributions of types (2) and (3). The contrast is high if there are many type (2) contributions, but only few type (3) contributions.

Now let us be somewhat more quantitative (Fig. 26.14):
region 2:

$$\begin{aligned} |x_S| + \frac{\lambda f}{2}|\nu| &\leq \frac{B}{2} \\ |y_S| &\leq \frac{1}{2}\sqrt{B^2 - (\lambda f \nu)^2} \end{aligned} \tag{26.45}$$

region (3) plus region (2) consists of two circles, $\left(x_S \pm \frac{\lambda f \nu}{2}\right)^2 + y_S^2 \leq \left(\frac{B}{2}\right)$

A point (x_S, y_S) in the source plane produces two point sources $(x_S + \frac{\lambda f \nu}{2}, y_S)$ and $(x_S - \frac{\lambda f \nu}{2}, y_S)$ within the aperture plane *if* (x_S, y_S) was in region (2):

$$\delta\left(x_F - x_S - \frac{\lambda f \nu}{2}, y_F - y_S\right) + \delta\left(x_F - x_S + \frac{\lambda f \nu}{2}, y_F - y_S\right) \tag{26.46}$$

As a result two plane waves will appear in the image plane:

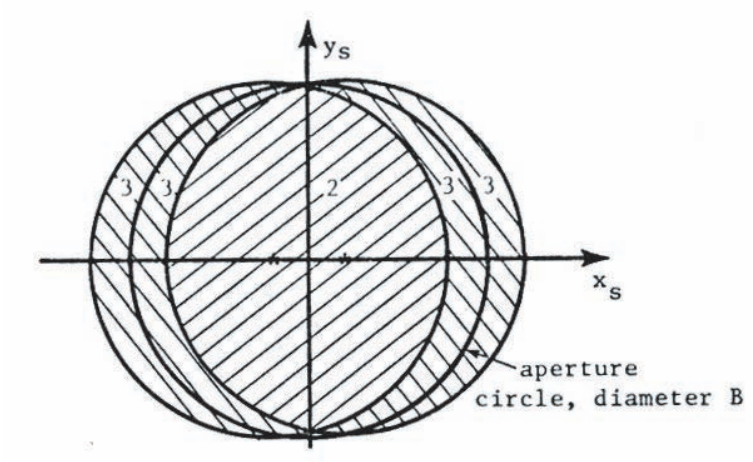

Figure 26.14: Illustrating the incoherent OTF of a perfect lens.

$$e^{2\pi i \frac{x\left(x_S+\frac{\lambda f\nu}{2}\right)+yy_S}{\lambda f}} + e^{2\pi i \frac{x\left(x_S-\frac{\lambda f\nu}{2}\right)+yy_S}{\lambda f}} \tag{26.47}$$

which result in an intensity distribution:

$$\left| e^{2\pi i \frac{x\left(x_S+\frac{\lambda f\nu}{2}\right)+yy_S}{\lambda f}} + e^{2\pi i \frac{x\left(x_S-\frac{\lambda f\nu}{2}\right)+yy_S}{\lambda f}} \right|^2 = (2\cos\pi\nu x)^2 = 2+2\cos(2\pi\nu x) \tag{26.48}$$

All intensity contributions from area S_2 of the source added together yield $S_2[2+2\cos(2\pi\nu x)]$. We have assumed uniform brightness of the source. If (x_S, y_S) belongs to (3), then we get:

$$\delta\left(x_F - x_S \mp \frac{\lambda f\nu}{2}, y_F - y_S\right) \quad \text{in the aperture} \tag{26.49}$$

$$e^{2\pi i \frac{x\left(x_S\pm\frac{\lambda f\nu}{2}\right)+yy_S}{\lambda f}} \longrightarrow \left| e^{2\pi i \frac{x\left(x_S\pm\frac{\lambda f\nu}{2}\right)+yy_S}{\lambda f}} \right|^2 = 1 \quad \text{in the image plane} \tag{26.50}$$

The (3) region (see Fig. 26.14) consists of a right-hand and a left-hand part, each of them being $A - S_2$ large, where $A = \pi\frac{B}{2}$ is the area of the circular pupil. Hence $S_3 = 2(A - S_2)$. The total image intensity is:

$$\begin{aligned} I_B(x) \propto 1S_3 + [2 + 2\cos(2\pi\nu x)]S_2 &= 2A - 2S_2 + 2S_2 + 2S_2\cos(2\pi\nu x) = \\ &= 2[A + S_2\cos 2\pi\nu x] \end{aligned} \tag{26.51}$$

or

$$I_B(x) = 2A[1 + \frac{S_2}{A}\cos(2\pi\nu x)] \tag{26.52}$$

Hence $\frac{S_2}{A}$ is the image contrast, while the object contrast was 1. Therefore $\frac{S_2}{A}$ is the OTF, just as we had derived a few pages earlier in a more formal way.

26.9 Some specific OTF's

26.9.1 Defocussing

Defocussing can be described as a particular wave aberration:

$$W(x,y) = \frac{\Delta z}{2}\frac{(x^2+y^2)}{f^2} \tag{26.53}$$

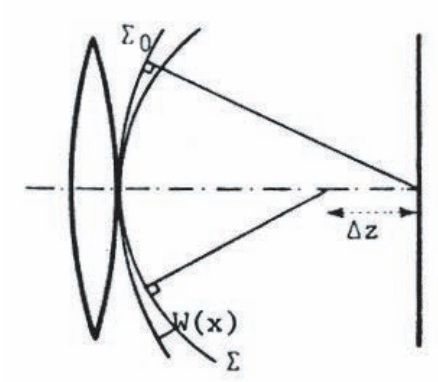

Figure 26.15: Defocussing as a wavefront aberration.

Here the wave aberration is the distance between the two spheres Σ and Σ_0. A useful approximation for the derivation of W is:

$$R - r = \frac{R^2 - r^2}{r + R} \approx \frac{R^2 - r^2}{2R} \tag{26.54}$$

If

$$\tilde{F}(x,y) = e^{ikW(x,y)} \cdot \begin{cases} +1 & \text{if } (x,y) \text{ in } x^2+y^2 \le \left(\frac{B}{2}\right)^2 \\ 0 & \text{if } (x,y) \text{ not in } x^2+y^2 \le \left(\frac{B}{2}\right)^2 \end{cases} \tag{26.55}$$

then the Duffieux formula reduces to:

$$\boxed{\tilde{D}(\nu,\mu)=\left(\frac{1}{A}\right)\iint\limits_{S_2} e^{ik\left[W\left(x+\lambda f\frac{\nu}{2},y+\lambda f\frac{\mu}{2}\right)-W\left(x-\lambda f\frac{\nu}{2},y-\lambda f\frac{\mu}{2}\right)\right]}\mathrm{d}x\mathrm{d}y} \tag{26.56}$$

With the specific aberration for defocussing the exponent is $ik2\lambda f\left(\frac{\Delta z}{2f^2}\right)(x\nu+y\mu)=2\pi i\left(\frac{\Delta z}{f}(x\nu+y\mu)\right)$. Notice that the λ dropped out; however, the wavelength influences the region S_2 of integration. This suggest as an approximate formula:

$$\tilde{D}\approx\frac{S_2}{A}\iint\limits_{(A)} e^{2\pi i\frac{\Delta z(x\nu+y\mu)}{f}}\mathrm{d}x\mathrm{d}y \tag{26.57}$$

The exact integral looks simpler than it really is, because the integration limits (region S_2) depend on the spatial frequency too. But it is possible to solve this integral analytically with the help of Bessel functions (Hopkins 1955). Today one would probably use a digital computer.

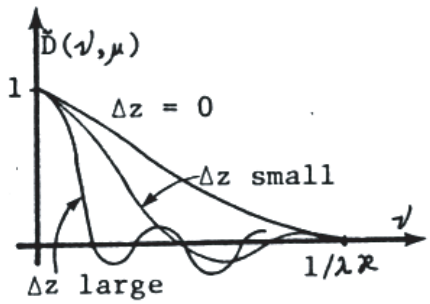

Figure 26.16: The effect of defocussing on the OTF.

Actually, when computing digitally the OTF $\tilde{D}$ from given aberrations W one does not use the Duffieux formula anymore because the Fast-Fourier-Transform algorithm (Cooley-Tukey) is so very efficient. One computes in these steps:

$$W(x)\longrightarrow\tilde{F}(x)=e^{ikW(x)}\mathrm{rect}\left(\frac{x}{\Delta x_F}\right)\overset{\mathrm{FOU}}{\longrightarrow}F(x)\longrightarrow|F(x)|^2=D(x)\overset{\mathrm{FOU}}{\longrightarrow}\tilde{D}(\nu) \tag{26.58}$$

26.9.2 Other lens aberrations

Spherical aberration:

$$W_S = W_{40}(x^2+y^2)^2 + W_{60}(x^2+y^2)^3 \tag{26.59}$$

Astigmatism:

$$W_A = \frac{1}{2}(W_{20}-W_{02})(x^2-y^2) + \frac{1}{2}(W_{40}-W_{04})(x^2-y^2)(x^2+y^2) \tag{26.60}$$

Coma:

$$W_C = W_{30}x(x^2+y^2) + W_{50}x(x^2+y^2)^2 \tag{26.61}$$

In the case of coma the $D(x,y)$ is not centersymmetric anymore, and hence $\tilde{D}$ will be complex. Astigmatism and coma vary slowly as a function of the lateral coordinate in the image plane. On-axis W_A and W_C are zero for axial-symmetric lenses.

26.9.3 Rough lens surface

$$W = W_{\text{aberr}} + W_{\text{rough}} \tag{26.62}$$

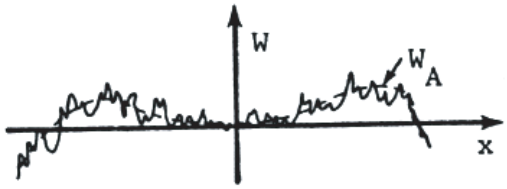

Figure 26.17: The effect of a rough lens surface.

We call the exponent of the Duffieux formula briefly:

$$k[W(+) - W(-)] = \Phi = \Phi_{\text{ab}} + \Phi_{\text{ro}} \tag{26.63}$$

We assume $\overline{W_{\text{ro}}} = 0$, but $\overline{W_{\text{ro}}^2} = \sigma^2$. The bars indicate a spatial average. For the following derivation it is important that $W_{\text{ro}}(x)$ varies much faster than $W_{\text{ab}}(x)$. We assume $|W_{\text{ro}}(x)| < \frac{\lambda}{4}$. Otherwise the lens grinder forgot to polish the lens.

$$e^{i\Phi_{\text{ro}}} \approx 1 + i\Phi_{\text{ro}} - \frac{\Phi_{\text{ro}}^2}{2}, \qquad \overline{e^{i\Phi_{\text{ro}}}} \approx 1 - \frac{1}{2}\overline{\Phi_{\text{ro}}^2} \tag{26.64}$$

$$\Phi_{\rm ro} = k[W_R(+) - W_R(-)]; \Phi_{\rm ro}^2 = k^2[W_R^2(+) + W_R^2(-) - 2W_R(+)W_R(-)] \quad (26.65)$$

$$\overline{W_R\left(x+\frac{f}{2}\right)W_R\left(x-\frac{f}{2}\right)} = \begin{cases} 1 & \text{if } \nu \text{ very small} \\ 0 & \text{if } |\lambda f \nu| \text{ is bigger than grain size.} \end{cases} \quad (26.66)$$

In the latter case:

$$\overline{\Phi_{\rm ro}^2} = 2k^2\overline{W_R^2} = 2k^2\sigma^2; \qquad \overline{e^{i\Phi_{\rm ro}}} = \begin{cases} +1 & \text{if } \nu \text{ very small} \\ 1-k^2\sigma^2 & \text{if } \lambda f|\nu| > \text{grain size} \end{cases} \quad (26.67)$$

we call: $\overline{e^{i\Phi_{\rm ro}}} = \tilde{D}_R(\nu)$.

Now we claim:

$$\tilde{D}(\nu) \approx \tilde{D}_A(\nu)\tilde{D}_R(\nu) \quad (26.68)$$

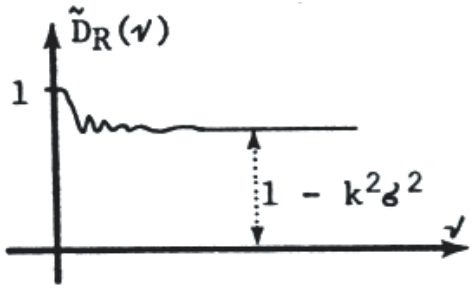

Figure 26.18: The effect of surface roughness on the OTF.

A loss $k^2\sigma^2$ of about 0.05 occurs even for good lenses. For the derivation we assume that $W_{\rm ro}$ is stationary. We subdivide S into areas, in which $W_A \approx$ const., but these areas are large enough so that the part-area integrals are proportional to $e^{iW_A}e^{iW_R}$. Then we sum up the small-area-integrals. Essentially the same approach can be used when computing the OTF of a dusty lens. The assumed value of $k^2\sigma^2 = 0.05$ corresponds to a roughness of $\sigma = 0.03\lambda$.

26.9.4 Double-slit aperture

$$\tilde{F}(x,y) = \text{rect}\left(\frac{y}{A}\right)\left\{\text{rect}\left[\frac{x-\frac{B}{2}+\frac{C}{2}}{C}\right] + \text{rect}\left[\frac{x+\frac{B}{2}-\frac{C}{2}}{C}\right]\right\} \quad (26.69)$$

This case occurs in the Michelson Star-Diameter Interferometer. A ring aperture is common in reflecting astronomical telescopes. The computation of the associated OTF is an exercise in the manipulation of Bessel functions.

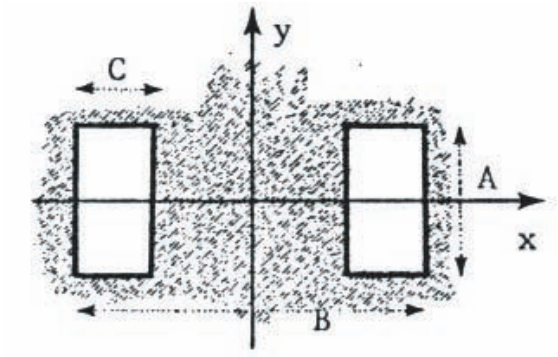

Figure 26.19: The shape of a double slit aperture.

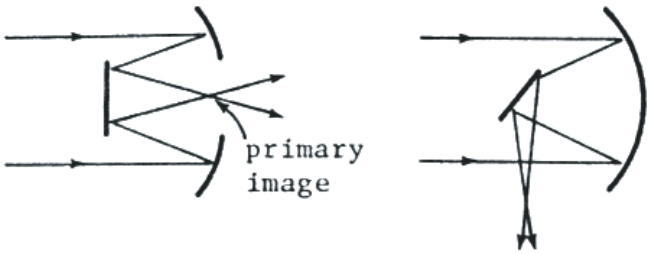

Figure 26.20: The Michelson Star-Diameter Interferometer.

26.9.5 Object Motion

First we consider the fate of a single object point at x'.

Instantaneous: $\delta(x - x') \longrightarrow D_L(x - x' - \xi(t))$.

The function $\xi(t)$ describes the time dependent shift. $D_L(x)$ is the p.s.f. of the *static* process of image formation.

$$I_0(x) \longrightarrow \int I_0(x')D_L(x - x' - \xi(t))\mathrm{d}x' = I_B(x,t) \tag{26.70}$$

The photographic plate will record during the exposure time T:

$$I_B(x) = \int_{-\frac{T}{2}}^{+\frac{T}{2}} I_B(x,t)\mathrm{d}t = \int_{(x')} I_0(x') \left[\int_{(t)} D_L(x - x' - \xi(t))\mathrm{d}t \right] \mathrm{d}x' \tag{26.71}$$

The square bracket describes the overall p.s.f. $D_{\mathrm{total}}(x - x') = D_{\mathrm{T}}(x - x')$.

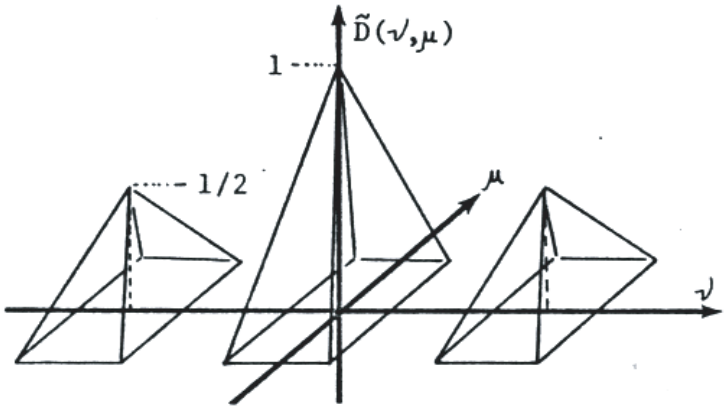

Figure 26.21: The OTF of a double slit aperture.

$$\begin{aligned}\tilde{D}_{\mathrm{T}}(\nu) &= \int D_{\mathrm{T}}(x)e^{-2\pi i\nu x}\mathrm{d}x = \iint D_L(x-\xi(t))e^{-2\pi i\nu x}\mathrm{d}t\,\mathrm{d}x \\ &= \iiint D_{\mathrm{L}}(\nu')e^{2\pi i[-\nu x+\nu'\{x-\xi(t)\}]}\mathrm{d}(x,\nu',t)\end{aligned} \tag{26.72}$$

$$\boxed{\tilde{D}_{\mathrm{T}} = \tilde{D}_{\mathrm{L}}(\nu)\tilde{D}_{\mathrm{motion}}(\nu)} \qquad \boxed{\tilde{D}_{\mathrm{M}}(\nu) = \frac{1}{T}\int_{-\frac{T}{2}}^{\frac{T}{2}} e^{-2\pi i\nu\xi(t)}\mathrm{d}t} \tag{26.73}$$

Here we encounter again the nice feature that OTF's tend to combine as products. In other words we can understand the impact of motion blur without having to specify any particular lens system with its OTF $\tilde{D}_{\mathrm{L}}$. Obvious special cases to be considered are linear motion $\xi(t) = vt$ and oscillations $\xi(t) = a\sin(\omega t)$. A fairly obvious generalization takes into account a time-varying illumination $L(t)$ of the object.

$$\tilde{D}_{\mathrm{LM}}(\nu) = \frac{\int L(t)e^{-2\pi i\nu\xi(t)}\mathrm{d}t}{\int L(t)\mathrm{d}t} \tag{26.74}$$

The special case $L(t) = \frac{1}{T}\mathrm{rect}\left(\frac{t}{T}\right)$ leads back to $\tilde{D}_{\mathrm{M}}$.

26.9.6 Photography

Let us assume that the lens converts the object intensity $I_0(x)$ into the "aerial image" $I_A(x) = \int I_0(x')D_{\mathrm{L}}(x-x')\mathrm{d}x'$. This energy distribution then strikes the photographic plate where

it will be somewhat blurred by scattering on the grains of the emulsion. After scattering the light settles down and activates silver halide grains according to the distribution $I_E = \int I_{\mathrm{A}}(x')D_{\mathrm{P}}(x-x')\mathrm{d}x'$. We call I_{E} the "effective intensity". The process of imaging and scattering is described by:

$$\tilde{D}(\nu) = D_{\mathrm{L}}(\nu)\tilde{D}_{\mathrm{P}}(\nu) \tag{26.75}$$

More details about the photographic process will follow in Chapter 34. Usually the photographic OTF can be described by $\tilde{D}(\nu,\mu) = \left[1+\frac{\nu^2+\mu^2}{\nu_P^2}\right]^{-1}$ with $\tilde{D}(\nu_{\mathrm{P}},0) = \frac{1}{2}$. The characteristic frequency ν_{P} is anywhere between 50 mm^{-1} and 2000 mm^{-1} depending on the resolution of the film or plate.

26.9.7 The OTF-chain of TV

Fig. 26.22 illustrates the long OTF chain of a total TV system. If 500 lines per format are on a cathode of 20 mm diameter the TV cutoff frequency is 25 lines per millimeter, which is certainly small compared to the cutoff frequency of any decent lens.

$$\tilde{D}_{\mathrm{TV}} = \tilde{D}_{\mathrm{L}}\tilde{D}_{\mathrm{scan}}\tilde{D}_{\mathrm{tape}}\tilde{D}_{\mathrm{transm.}}\tilde{D}_{\mathrm{display}}\tilde{D}_{\mathrm{eye}} \tag{26.76}$$

Figure 26.22: The OTF-chain of TV.

26.10 Quality criteria based on the OTF

Aberrations are always bad, as can be seen from $|\tilde{D}(\nu)| \leq \tilde{D}_0(\nu)$. We call the OTF of an aberration-free lens $\tilde{D}_0(\nu)$.

$$|\tilde{D}(\nu)| = \frac{1}{A}\int\limits_{(\mathrm{S})} e^{ik[W(+)-W(-)]}\mathrm{d}x \leq \frac{1}{A}\int\limits_{(\mathrm{S})} |e^{ik[\ldots]}|\,\mathrm{d}x = \frac{S}{A} = \tilde{D}_0(\nu) \tag{26.77}$$

Hence aberration-free lenses are desirable, but they are not obtainable in most cases. In case of photographic lenses one can say as a rule of thumb that the aberrations are negligible, if the aperture is closed by two or three stops. For example an $F/2$ lens is pretty good at $F/4$

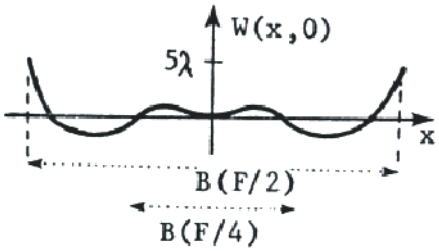

Figure 26.23: Typical aberrations $W(x)$ of a lens or lens system.

or $F/5.6$. (Each stop reduces the diameter by $\frac{1}{\sqrt{2}}$ and hence the area by $\frac{1}{2}$.) The reason is that the aberrations are worst close to the outer margin of the lens (Fig. 26.23). When reducing the aperture from $F/2$ to $F/4$ one pays two prices: the light thru-put is reduced by $\frac{1}{4}$; the cutoff frequency only by $\frac{1}{2}$. The cutoff frequency $\nu_{\rm A} = \frac{1}{\lambda\mathcal{X}}$ is for green light ($\lambda = 0.5 \cdot 10^{-3}$) and $F/2$: $\nu_{\rm A}$ =1000 mm^{-1}.

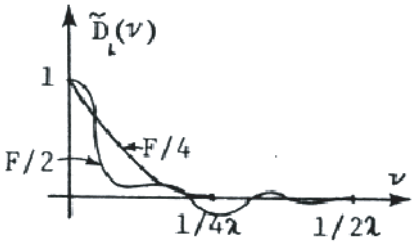

Figure 26.24: The shape of the OTF for aberrations shown in Fig. 26.23 and different aperture stops.

There exist quite a few different quality criteria for $\tilde{D}_{\rm lens}$ (Fig. 26.24). This is not only due to the tastes of the inventors of those criteria, but largely due to the different receivers (photographic emulsion, eye, TV, etc.) which follow after the lens. $\tilde{D}_{\rm total}(\nu) = \tilde{D}_{\rm lens}(\nu)\tilde{D}_{\rm rcv}(\nu)$. If the bandwidth of the receiver is only 25 mm^{-1} (typical for TV system) only the first twenty five spatial frequencies of $\tilde{D}_{\rm lens}(\nu)$ matter. Obviously the OTF (1) is better for this purpose than OTF (2) (Fig. 26.25). But for a 35 mm camera with medium-fast black-and-white film, the OTF (2) is better matched to the capabilities of the receiver.

If only the low frequencies are important one may use the following criterion, based on the Taylor expansion of the OTF:

$$\tilde{D}(\nu) \approx \tilde{D}(0) + \tilde{D}'(0)|\nu| + \tilde{D}''(0)\frac{\nu^2}{2} \tag{26.78}$$

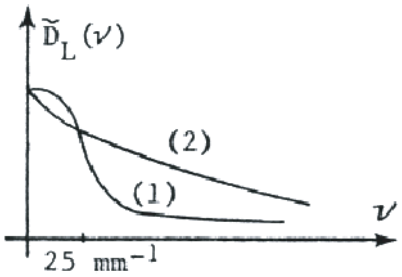

Figure 26.25: Detail of the shapes of the OTF for the cases shown in Fig. 26.24.

The absolute-bars around the $|\nu|$ in the linear term are necessary in order to satisfy the reality symmetry $\tilde{D}(\nu) = \tilde{D}^*(-\nu)$. Or in other words, $\tilde{D}(\nu)$ is not continuous at $\nu = 0$. But:

$$\lim_{\epsilon \to 0} \left\{ \frac{\tilde{D}(+\epsilon) - \tilde{D}(0)}{\epsilon} \right\} = - \lim_{\epsilon \to 0} \left\{ \frac{\tilde{D}(0) - \tilde{D}(-\epsilon)}{|\epsilon|} \right\} \tag{26.79}$$

For the circular pupil with aberrations we have:

$$\begin{aligned} \tilde{D}(0) &= 1; \qquad \tilde{D}'(0) = -\frac{4\lambda\mathcal{X}}{\pi} \\ \tilde{D}''(0) &= -8\pi^2\mathcal{X}^2 \overline{\left[\frac{\partial W}{\partial x} - \overline{\frac{\partial W}{\partial x}} \right]^2} = -8 \left(\frac{\pi}{B} \right)^2 \overline{(\xi - \overline{\xi})^2} \end{aligned} \tag{26.80}$$

Here B = pupil diameter; $\mathcal{X} = \frac{f}{B}$; ξ =lateral aberration. The top-bar means averaging over the aperture. The linear term is due to diffraction on the aperture, since it contains the wavelength and the aperture diameter. The quadratic term considers ray deviations as the Gaussian mean square. That term is of purely geometrical nature since it does not contain the wavelength. Only the second derivative is under the control of the lens designer. Nowadays they let vary all relevant parameters like lens curvatures, lens element distances, refractive indices and perhaps pupil diameter till a minimum of the gaussian spread of the spot diagram is found.

Some lens designer utilize another criterion based on the following approximation:

$$\begin{aligned}
\tilde{D}(\nu,0) &= \frac{1}{A}\iint\limits_{(\mathrm{S})} e^{ik\left[W\left(x+\frac{\lambda f\nu}{2},y\right)-W\left(x-\frac{\lambda f\nu}{2},y\right)\right]}\mathrm{d}x\,\mathrm{d}y \qquad (26.81)\\
&\approx \frac{1}{A}\iint\limits_{(\mathrm{A})} e^{ik[W(+)-W(-)]}\mathrm{d}x\,\mathrm{d}y\\
&\approx \frac{1}{A}\iint\limits_{(\mathrm{A})} \left\{1+ik[\ldots]-\frac{k^2}{2}[\ldots]\right\}\mathrm{d}x\,\mathrm{d}y\\
\tilde{D}(\nu,0) &\approx 1-\frac{k^2}{2A}\iint\limits_{(\mathrm{A})}[\ldots]^2\mathrm{d}x\,\mathrm{d}y
\end{aligned}$$

The linear term often drops out due to symmetry, or is very small anyway. Hence the goal is to minimize $\overline{[\ldots]^2}$. If

$$W\left(x+\frac{\lambda f\nu}{2},y\right)\approx W(x,y)+\frac{\lambda f\nu}{2}\frac{\partial W(x,y)}{\partial x}+\frac{(\lambda f\nu)^2}{8}\frac{\partial^2 W}{\partial x^2} \qquad (26.82)$$

is justified this criterion is identical to the previous one. This criterion is good only for lenses to be used only at low frequencies $|\nu|\ll\nu_{\mathrm{A}}=\frac{1}{\lambda\mathcal{X}}$.

If the small-frequency assumption is not justified one may consider the correlation of object and image, of course normalized.

$$\frac{\int I_0(x)I_{\mathrm{B}}(x)\mathrm{d}x}{\int I_0^2(x)\mathrm{d}x}=\frac{\int|\tilde{I}_0(\nu)|^2\tilde{D}(\nu)\mathrm{d}\nu}{\int|\tilde{I}_0(\nu)|^2\mathrm{d}\nu} \qquad (26.83)$$

A high degree of correlation means the image is very similar to the object. For an object with a "white" spatial power spectrum (which rarely exists, except for the snow on the TV-screen; but it yields a nice criterion) we get $\int\tilde{D}(\nu)\mathrm{d}\nu$ as a measure of quality.

This quality $\int\tilde{D}(\nu)\mathrm{d}\nu=D(0)$ is also the peak intensity of the point spread function. Case (1) is considered to be better then case (2). $\frac{D(0)}{\int D(x)\mathrm{d}x}$ is called the "Strehl definition" or "Strehl intensity". But if the gaussian mean square measure:

$$\overline{(\xi-\overline{\xi})^2}=\frac{\int x^2D(x)\mathrm{d}x}{\int D(x)\mathrm{d}x} \qquad (26.84)$$

were relevant case (2) would be preferable.

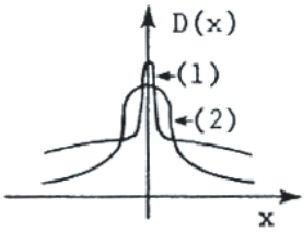

Figure 26.26: The point spread functions for two different OTFs.

I purposely stressed that "lens quality" is a somewhat ambiguous matter. However the ambiguity is removed in most situations if it is specified which receiver will be used in connection with the lens. Sometimes also a specification of the class of relevant or interesting objects influences the selection of a suitable quality criterion. For example the esthetic features of a portrait are usually confined to rather low frequencies. Therefore some professional photographers put a nylon stocking over the lens since their aging customers will never return if too many high frequency details are reproduced. The nylon stocking is not used while taking picture. That would be too obvious. Instead it is done in secrecy of the darkroom when the prints are copied.

Another criterion considers the mean square deviation of object and image.

$$\begin{aligned} \int (I_0 - I_B)^2 \mathrm{d}x &= \int I_0^2 \mathrm{d}x + \int I_\mathrm{B}^2 \mathrm{d}x - 2\int I_0 I_\mathrm{B} \mathrm{d}x \\ &= \int |\tilde{I}_0(\nu)|^2 [1 + |\tilde{D}(\nu)|^2 - 2\tilde{D}(\nu)] \mathrm{d}\nu \end{aligned} \tag{26.85}$$

This criterion is popular in electrical engineering (EE) circles, where mean squares have almost a religious status. However I doubt that the eye makes judgment based on mean square deviations. Instead it picks out details of subjective significance when saying a picture is good or bad.

The term $\frac{\int I_\mathrm{B}^2 \mathrm{d}x}{\int I_0^2 \mathrm{d}x} = \frac{|\int \tilde{I}_0 \tilde{D}|^2 \mathrm{d}\nu}{\int |\tilde{I}_0|^2 \mathrm{d}\nu}$ is called the "structure content". It reduces to $|\tilde{D}|^2$ for objects with "white" spatial power spectrum. I am skeptical about this term too since it ignores the phase of the OTF. Such phase defects don't diminish the information in the Shannon sense, but they encode the information. In principle this coding process is reversible. But this statement is useless for the eye, which does not know how to decode.

26.11 OTF synthesis

What we have done so far with the OTF can be called "*analysis*". Now we want to *synthesize* OTF's. In other words so far the situation was like this: given the aberrations, aperture size,

image motion, etc. what is the OTF like under these circumstances? Now we assume the opposite attitude: we want an OTF with a specific shape in order to do a certain job. How must the lens be made such that its OTF is as wanted? We talk about "analysis" and "synthesis" in the same sense as in circuit theory. There "analysis" means: given a network with known RCL-components, wanted the resulting transfer function for temporal frequencies. The more challenging problem is the "synthesis" of circuits. The customer prescribes a filter function and leaves it to the designer to find a circuit with that filter function. As you may know there exist elegant methods for solving the synthesis problem of circuit theory.

The synthesis problem for *coherent* spatial filtering is very simple, at least for the theoretician. The spatial frequencies are nicely displayed in the Fourier domain. If you want to block out certain frequency bands you simply insert a piece of cardboard. The transmittance distribution of that piece of cardboard represents *directly* the coherent filter function. For the experimentalist the problem becomes somewhat more complicated if phase shifting is required in order to get a complex filter function.

The synthesis problem of *incoherent* spatial filtering is more involved even for the theoretician, because there is no nice display of spatial frequencies, where the incoherent filter function or OTF could be implemented directly. Therefore you will find statements in some books saying that OTF synthesis is *impossible*. Such a statement provokes inventors, of course; usually "impossible" stands for "not always possible under the most general conditions". The obvious but rare reaction should be to look for those special conditions under which things are possible indeed. Sometimes the special conditions are incompatible with practical applications, but often they are not. We will present now three special cases where it is possible indeed to synthesize a useful OTF.

26.11.1 Apodisation

The word "apodisation" is an artifical Greek word which means literally "cutting off the feet". Not so literally it means a point-spread function (or line spread function) without secondary diffraction maxima as shown in Fig. 26.27 on the left. Apodisation is useful for grating or prism spectrographs where every sharp spectral line appears as a line spread function on the photographic plate. Sometimes a weak isotope line is to be detected very close to a strong isotope line. Without apodisation it would be difficult to distinguish between the weak isotope line and the secondary diffraction maximum of the strong isotope line. A line spread function $L(x)$ without secondary maxima (Fig. 26.27 a)) is obtained if the pupil function has soft transmittance edges (Fig. 26.27 b)). This is plausible since the diameter of the usual pupil function $\tilde{F}(x) = \mathrm{rect}\left(\frac{x}{\Delta x}\right)$ determines the location $\frac{\lambda f}{\Delta x}$ of the diffraction minima. A soft edge is not well defined. Hence no well-defined diffraction maxima will arise. One pays two prices for the advantages of apodisation: less light efficiency $\int |\tilde{F}(x)|^2 \mathrm{d}x$ and somewhat less resolution as indicated by the increased width of the central maximum of $L(x)$ and by the decreased OTF at high frequencies (Fig. 26.27c)). What has been said so far for the line images holds as well for point images. A situation where diffraction rings around point images are undesirable arises in astronomy, where objects are points. The detection of a weak satellite

close to a bright star is facilitated by introducing an apodisation mask with circular symmetry into the pupil plane of the telescope.

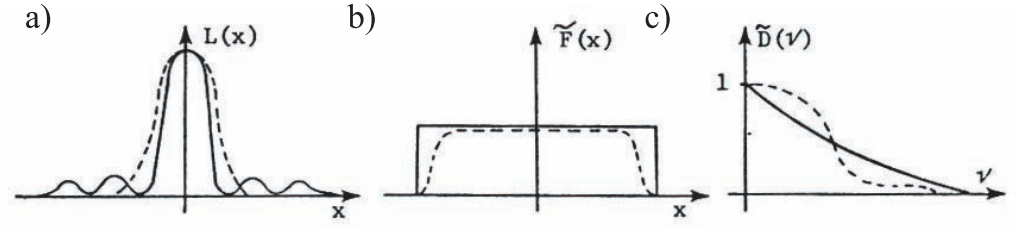

Figure 26.27: Apodisierung: a) point-spread-function; b) filter function; c) OTF.

26.11.2 Pseude-coherent image formation

As you know in *coherent* image formation the pupil transmittance function $\tilde{F}(\nu)$ acts directly as the filter function. But in *incoherent* image formation it is the autocorrelation function of the pupil function which is the filter function or OTF. Nevertheless we can "linearize" the autocorrelation integral in a way which is formally similar to holography. We modify the original pupil function $\tilde{F}_0(x)$ by superposing a mask with an amplitude transmittance which is almost everywhere $A(A^2 \ll 1)$, but unity within a pinhole at the center or at the edge (Fig. 26.28b). In abbreviated mathematics we use a delta function for describing the pinhole.

$$\begin{aligned} \tilde{F}(x) &= A\tilde{F}_0(x)\mathrm{rect}\left(\frac{x}{\Delta x}\right) + \delta\left(x - \frac{\Delta x}{2}\right) \\ \tilde{D}(\nu) &\propto \int \tilde{F}\left(x + \frac{\lambda f \nu}{2}\right)\tilde{F}\left(x - \frac{\lambda f \nu}{2}\right)\mathrm{d}x \\ &\propto \delta(\nu) + A\tilde{F}_0\left(\lambda f \nu + \frac{\Delta x}{2}\right) + A\tilde{F}_0^*\left(-\lambda f \nu + \frac{\Delta x}{2}\right) \end{aligned} \tag{26.86}$$

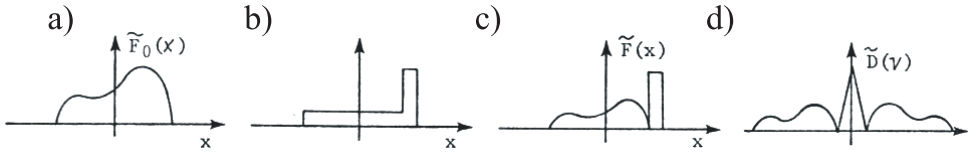

Figure 26.28: OTF synthesis for pseudo-coherent imaging.

Now the OTF is essentially proportional to the original pupil function $\tilde{F}_0$ (Fig. 26.28d). However one pays two prices for this achievement. The light transmittance of the pupil has been reduced by the factor A, and the delta term of the OTF results in a constant background term of the point spread function and also of the image intensity. This background light can be suppressed photographically by using a film with a high threshold or with TV technology.

26.11.3 Synthesis of incoherent matched filters

In the coherent case the filter function which helps us to detect an object $u(x-x_0)$ by producing an intensity peak at x_0 in the image plane is $\tilde{F}(\nu) = \tilde{u}^*(\nu)$. The theoretical background and the experimental verification of coherent matched filtering has been presented by A. Vander Lugt. That method is one of the most brilliant achievements in coherent optics. However that method has two drawbacks: the object must exist as a transparency in order to make it possible to create a coherent input signal by means of coherent illumination of that transparency. This requirement excludes texts printed on paper, signals on a CRT and natural scenes from coherent matched filtering. Furthermore the positioning of the matched filter is quite critical. We will now explain why the positioning is so critical. Thereafter we will show how an incoherent matched filter can be synthesized. It does not suffer from the two disadvantages. More details are presented in Appl. Opt. 10, 670 (1971).

Suppose the coherent object is $u(x-x_0)$. From it a complex amplitude $\tilde{u}(\nu)e^{-2\pi i\nu x_0}$ results in the Fourier plane. Multiplication with the filter function $\tilde{F}$ which might be somewhat shifted accidentally yields $\tilde{u}(\nu)e^{-2\pi i\nu x_0}\tilde{F}(\nu-\nu_0) = \tilde{u}(\nu)\tilde{u}^*(\nu-\nu_0)e^{-2\pi i\nu x_0}$. The final lens of the telecentric image forming system produces another Fourier transform and hence the image amplitude $v(x)$.

$$\begin{aligned} v(x) &= \int \tilde{u}(\nu)\tilde{u}^*(\nu-\nu_0)e^{2\pi i\nu(x-x_0)}\mathrm{d}\nu \\ &= \int u(x')u^*(x'+x_0-x)e^{-2\pi i\nu(x'-x_0-x)}\mathrm{d}x' \end{aligned} \tag{26.87}$$

The detection peak is expected at $x = x_0$. Hence we compute the image amplitude for that point:

$$v(x_0) = \int \tilde{u}(\nu)\tilde{u}^*(\nu-\nu_0)\mathrm{d}\nu = \int |u(x')|^2 e^{-2\pi i\nu_0 x'}\mathrm{d}x' \tag{26.88}$$

The second integrand consists of a real-nonnegative and of a phase factor. The integral will be biggest if the phase factor is always $+1$ due to $\nu_0 = 0$ (perfect adjustment of the spatial filter). But with $\nu_0 \neq 0$ the phase factor might be negative for some x'-values. Hence the peak $v(x_0)$ will diminish. How much maladjustment can we tolerate? If the phase $2\pi\nu_0 x'$ never exceeds $\pm\frac{\pi}{4}$ the damage will be tolerable. Assuming that the object $u(x')$ has a finite width Δx it follows $|x'| \leq \frac{\Delta x}{2}$ and $|2\pi\nu_0 x'| \leq \pi\nu_0\Delta x$. The $\frac{\pi}{4}$ tolerance is satisfied if the shift ν_0 and the object size Δx are related like $\nu_0 \leq \frac{1}{4\Delta x}$. A shift ν_0 in frequency coordinates

is equivalent to a shift $\lambda f \nu_0 = \delta x_F$ in spatial coordinates. Hence we obtain $\delta x_F \leq \frac{\lambda f}{4\Delta x}$. With $\lambda \frac{1}{2000}$ mm^{-1}, $f = 80$ mm, $\Delta x = 10$ mm we get $\delta x_F = \frac{1}{1000}$ mm $= 1\mu$m, which is indeed a difficult tolerance.

Now we are sufficiently motivated to develop or synthesize an incoherent matched filter system. We want this system to respond to the target or object intensity $I_0(x - x_0)$ with an intensity peak at x_0 in the output or image plane. Since the mathematical formalism of incoherent image formation is the same as for coherent image formation we can immediately specify which incoherent filter function or OTF is needed for the job.

Coherent:

$$u(x - x_0) \longrightarrow v(x) = \int u(x' - x_0) F(x - x') \mathrm{d}x' \tag{26.89}$$

$$= \int \tilde{u}(\nu) \tilde{F}(\nu) e^{2\pi i \nu (x - x_0)} \mathrm{d}\nu \tag{26.90}$$

$$\boxed{\tilde{F}(\nu) = \tilde{u}^*(\nu)} \tag{26.91}$$

Incoherent:

$$I_0(x - x_0) \longrightarrow I_\mathrm{B}(x) = \int I_0(x' - x_0) D(x - x') \mathrm{d}x' \tag{26.92}$$

$$= \int \tilde{I}_0(\nu) \tilde{D}(\nu) e^{2\pi i \nu (x - x_0)} \mathrm{d}\nu$$

$$\boxed{\tilde{D}(\nu) = \tilde{I}_0^*(\nu)} \tag{26.93}$$

So far the theory of incoherent matched filtering was simple. But now comes the problem, that is, how to implement the wanted OTF $\tilde{D}$? What we physically implement is the pupil function $\tilde{F}$ which is related to the OTF by Duffieux' autocorrelation formula.

$$\begin{array}{ccc} \tilde{D}(\nu) = \displaystyle\int \tilde{F}\left(\nu' + \frac{\nu}{2}\right) \tilde{F}^*\left(\nu' - \frac{\nu}{2}\right) \mathrm{d}\nu' & \overset{\text{synthesis}}{\underset{\text{analysis}}{\longrightarrow\!\!\!\!\!\!\longleftarrow}} & \tilde{F}(\nu) \\ \Big\downarrow \text{Fourier} & & \Big\uparrow \text{Fourier} \\ D(x) \qquad \longrightarrow \qquad \sqrt{D(x)} e^{i\varphi(x)} = & & F(x) \end{array} \tag{26.94}$$

The path from $\tilde{F}$ to $\tilde{D}$ (called OTF analysis) is unique and straightforward. But the path from $\tilde{D}$ to $\tilde{F}$ is ambiguous. More than one pupil function $\tilde{F}$ leads to the same OTF $\tilde{D}$. Some

people are shocked when the advice from the theoreticians becomes ambiguous. Actually they should be happy, since ambiguity means a certain amount of freedom for the experimentalist, who now is free to look for the most convenient form of $\tilde{F}$ which leads to the specified $\tilde{D}$. But this still leaves the question open as to how to find $\tilde{F}$. Since $\tilde{D} \rightarrow \tilde{F}$ in the frequency domain is ambiguous we translate the problem into the other Fourier domain, the space domain. There it becomes evident where the ambiguity enters into the problem, namely when going from $D(x)$ to $F(x) = \sqrt{D((x)}e^{i\varphi(x)}$. We are free to choose any phase we like because it is always $|\sqrt{D}e^{i\varphi}|^2 = |F|^2 = D$. We soon will explore the options.

When going from D to F we pulled a root $\sqrt{D}$ which could be imaginary in principle. This would not prevent us from constructing F and $\tilde{F}$. However $D(x)$ is the incoherent point spread function, which is inherently nonnegative because intensity is an energy quantity. Hence we conclude that only those OTF's, $\tilde{D}$, can by synthesized which correspond to a real-nonnegative point spread function D.

Now let us discuss the implications of choosing various phases $\varphi(x)$. We may of course simply set $\varphi = 0$. The next most imaginative thing to do is to take a linear phase $\varphi(x) = 2\pi\nu_0 x$. When changing $F(x)$ to $F(x)e^{2\pi i\nu_0 x}$ the corresponding pupil function changes from $\tilde{F}(\nu)$ into $\tilde{F}(\nu - \nu_0)$, which is nothing but a lateral shift. Since no phase $\varphi(x)$ can deteriorate the incoherent filter operation, and since this is true for the particular phase $\varphi(x) = 2\pi\nu_0 x$ we may conclude that the corresponding shift $\tilde{F}(\nu) \rightarrow \tilde{F}(\nu - \nu_0)$ of the pupil function is completely harmless too. In other words the lateral position of the pupil function is completely uncritical now, while the lateral adjustment of the pupil was extremely delicate in the case of coherent spatial filtering.

Next we consider a quadratic phase $\varphi(x) = \pi z_0 \frac{x^2}{\lambda f^2}$. As we know from the considerations of wave aberrations a quadratic phase in one domain corresponds to a longitudinal shift ("defocussing") in the other Fourier domain. This implies that the longitudinal position of the pupil function is uncritical, which makes life easier for the experimentalist. When looking somewhat closer into the theory of a longitudinal shift of a pupil function we find that the statement just made is strictly true only in a telecentric image forming system. In other systems such as one with a single lens between object and image a longitudinal shift of the pupil function creates a magnification or reduction of the point spread function. This is sometimes a desirable feature in matched filtering if the magnification of the target is unknown. Longitudinal shifting of the pupil function then provides the opportunity to perform "scale searching". Finally we should mention briefly that $\varphi(x)$ might also be a random phase as it occurs experimentally behind a ground glass. This is important if $\tilde{F}(\nu)$ is produced as a Fourier hologram from the object $F(x)$. The advantages and disadvantages of a ground glass in holography will be explained in Chapter 32.

27 Theory of Image Formation in Partially-Coherent Light

The motivation for studying this subject is mainly due to the microscope, where partial coherence occurs rather frequently. In other situations like photography, spectroscopy, and spatial filtering in laser light, we usually approach one of the two extreme cases, complete incoherence or complete coherence. One would like to do that in microscopy too, since image evaluation in the case or partially-coherent illumination is messy, as we will see shortly. However the case of complete incoherence is not easy to implement if lenses with very large numerical apertures (NA>0.8) are used, as is common in microscopy. Complete coherence was not easy to implement before the laser was available. But even now many experimentalists shy away from completely coherent illumination, since the image suffers from speckling or from so-called out-of-focus noise. The latter means that object details somewhat above and below the focused object plane show up in a fuzzy form, thereby making the observation of the in-focus object details difficult. This out-of-focus noise disappears gradually as the spatial coherence decreases. But spatial coherence is necessary if phase contrast, or knife edge- or darkfield- or any other spatial filtering method is necessary for detecting certain object details such as phase structures.

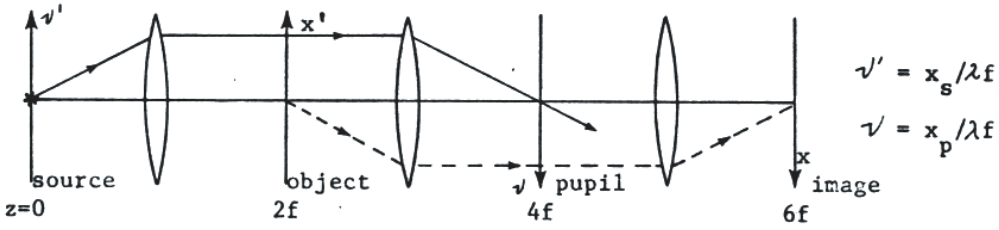

Figure 27.1: Schematic setup for analysis of partially coherent image formation.

We will develop the theory around Fig. 27.1, although a more realistic setup is as shown in Fig. 27.2. The differences are mainly of a practical nature, like the minification of the original source into the effective source. But both setups (Figs 27.1 and 27.2) have in common that the source is imaged into the pupil plane (solid rays in Fig. 27.1) and the object into the image plane (dotted rays). In Fig. 27.2 both steps occur twice in a row. If we would actually compute the process of image formation for the realistic setup (Fig. 27.2), we would encounter the magnification explicitly and also some quadratic phase factors (which however drop out

anyway when the modulus square step is applied in the final image plane, the retina).

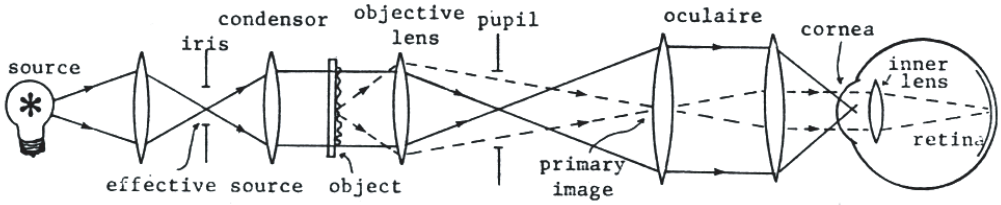

Figure 27.2: The realistic setup for partial coherent image formation.

The principle of our theory is as follows. We start with a source point and compute the resulting image amplitude.

$$\delta(\nu - \nu') \quad \text{in source converted into} \quad u_B(x, \nu') \quad \text{in image} \tag{27.1}$$

This is done in the standard fashion of coherent optics where the light propagation from source to object (see Fig. 27.1), from object to pupil, and from pupil to image is mathematically described by a Fourier transform. The impact of the object is described by a multiplication.

$$\begin{aligned} u(x', 2f - 0) \quad & \text{before object converted into} \\ u(x', 2f + 0) = u(x', 2f - 0)u_0(x') \quad & \text{behind object} \end{aligned} \tag{27.2}$$

The pupil function or filter function $\tilde{p}(\nu)$ also is taken into account as a multiplication.

$$\begin{aligned} u(\nu, 4f - 0) \quad & \text{before pupil converted into} \\ u(\nu, 4f + 0) = u(\nu, 4f - 0)\tilde{p}(\nu) \quad & \text{behind pupil} \end{aligned} \tag{27.3}$$

Knowing the image amplitude $u_B(x, \nu)$ as produced by the source point ν' we get the corresponding image intensity by a modulus square operation.

$$\begin{aligned} u_B(x, \nu) \quad & \text{complex amplitude converted into} \\ |u_B(x, \nu)|^2 \quad & \text{elementary intensity in image} \end{aligned} \tag{27.4}$$

Next we add (or integrate) all the intensity contributions from different source points ν' with the source intensity $S(\nu')$ as weighting factor.

$$\begin{aligned} |u_B(x', \nu')|^2 \quad & \text{elementary intensity in image summed up to} \\ \int S(\nu')|u_B(x, \nu')|^2 \mathrm{d}\nu' = I_B(x) \quad & \text{total intensity in image} \end{aligned} \tag{27.5}$$

To add the contributions from various points as intensities is justified since there is no mutual coherence between different source points, which get their light from different atoms that oscillate independently from each other.

So far we have assumed that the source is monochromatic. This is not realistic unless a laser is employed. Hence we must integrate once more over all wavelengths, again adding up intensities, since light of different wavelengths does not interfere.

$$\begin{array}{rcll} |u_B(x,\nu',\lambda)|^2 & & \text{monochromatic elementary intensity in image,} & \\ \text{summed up to} & & & (27.6) \\ \iint S(\nu',\lambda)|u_B(x,\nu',\lambda)|^2 \mathrm{d}\nu'\mathrm{d}\lambda & = & I_B(x) \quad \text{polychromatic total intensity in image} & \end{array}$$

This last step is rarely performed in the literature, not because it would not correspond to reality but because it would not change the result very much in most cases because $|u_B(x,\nu',\lambda)|^2$ tends to be almost independent of the wavelength. However there are exceptions. For example G. Hansen observed that black-and-white objects when illuminated in white light appear sometimes in colour in the image plane. What happens is that the object spectrum $u_0\left(\frac{x}{\lambda f}\right)$ in the pupil plane is larger for the long wavelengths. Hence a certain high frequency details of the object might be resolved in blue (short λ) but not in red (long λ).

Before actually starting we will introduce a somewhat modified terminology which is commonly used in the theory of partial coherence.

- Normalized monochromatic source intensity $\gamma(\nu')$; $(\int \gamma(\nu')\mathrm{d}\nu' = 1)$
- Degree of coherence $\Gamma_{12} = \Gamma(x_1' - x_2') = \int \gamma(\nu') e^{2\pi i \nu'(x_1' - x_2')} \mathrm{d}\nu'$.
- Complex amplitude transmittance of object: $u_0(x')$
- Complex amplitude transmittance of pupil: $\tilde{p}(\nu)$
- Coherent point spread function (psf) $p(x) = \int \tilde{p}(\nu) e^{2\pi i \nu x} \mathrm{d}\nu$.
- Incoherent point spread function $F(x) = |p(x)|^2$.
- Wave from source point ν', in $z = 2f - 0$, illuminating the object is $u(x', \nu') = e^{2\pi i x' \nu'}$.

The normalized cross-illumination in the object plan $z = 2f - 0$ is:

$$\frac{\int u(x_1', \nu')u^*(x_2', \nu')\gamma(\nu')\mathrm{d}\nu'}{\left[\int \underbrace{|u(x_1', \nu')|^2}_{=1}\gamma(\nu')\mathrm{d}\nu'\right]^{\frac{1}{2}}\left[\underbrace{\int |u(x_2', \nu')|^2\gamma(\nu')\mathrm{d}\nu'}_{=1}\right]^{\frac{1}{2}}}$$
$$= \int \gamma(\nu')e^{2\pi i\nu'(x_1'-x_2')}\mathrm{d}\nu' = \Gamma(x_1' - x_2') \tag{27.7}$$

Now we compute the process of image formation. A point ν' in the source plane produces a titled plane wave $u(x', \nu') = e^{2\pi i x'\nu'}$ in $z = 2f - 0$. Behind the object in $z = 2f + 0$ the field is $u_0(x')u(x', \nu')$. The propagation from there to the image plane is expressed by means of a convolution:

$$\int u_0(x')u(x', \nu')p(x - x')\mathrm{d}x' \tag{27.8}$$

the corresponding elementary intensity, $I(x; \nu')$, is:

$$I(x, \nu') = |\int \ldots \mathrm{d}x'|^2 = \iint u_0(x')u^*(x'')u(x', \nu')u^*(x'', \nu')p(x-x')p^*(x-x'')\mathrm{d}x'\mathrm{d}x'' \tag{27.9}$$

Finally the total intensity with contributions from all source points is $I(x) = \int \gamma(\nu')$ $I(x, \nu')\mathrm{d}\nu'$. Inserting $u(x', \nu') = e^{2\pi i\nu'(x'-x'')}$ for the illuminating plane waves enables us to perform the $\nu-$ integration $\int \gamma(\nu')e^{2\pi i\nu'(x'-x'')}\mathrm{d}\nu' = \Gamma(x' - x'')$. This leads to a simple formula for the total image intensity, expressed in quantities from the object and image planes. This is the fundamental formula for the theory of image formation in partially coherent light.

$$\boxed{I(x) = \iint \Gamma(x' - x'')u_0(x')u_0^*(x'')p(x - x')p^*(x - x'')\mathrm{d}x'\mathrm{d}x''} \tag{27.10}$$

Two important extreme cases are:

1. $\gamma(\nu') = \delta(\nu') \longrightarrow \Gamma(x' - x'') = 1$ (point source; the coherent case)

$$I_{\mathrm{coherent}}(x) = |\int u_0(x')p(x - x')\mathrm{d}x'|^2 \tag{27.11}$$

note we first integrate, then apply the modulus square!

2. $\gamma(\nu') = 1 \longrightarrow \Gamma(x' - x'') = \delta(x' - x'')$; large source; the incoherent case.

$$I_{\text{incoherent}}(x) = \int |u_0(x')|^2 |p(x - x')|^2 \mathrm{d}x' = \int I_0(x') F(x - x') \mathrm{d}x' \quad (27.12)$$

Now we consider some specific objects, at first a double slit:

$$\begin{aligned} u_0(x') &= e^{i\varphi}\delta(x' - x_0) + e^{-i\varphi}\delta(x' + x_0) \quad (27.13)\\ u_0(x')u_0^*(x'') &= \delta(x' - x_0)\delta(x'' - x_0) + \delta(x' + x_0)\delta(x'' + x_0) + \\ &+ e^{2i\varphi}\delta(x' - x_0)\delta(x'' + x_0) + e^{-2i\varphi}\delta(x' + x_0)\delta(x'' - x_0) \end{aligned}$$

We insert into the general formula for the image intensity related to a partially coherent-illuminated object.

$$\begin{aligned} I(x) &= |p(x - x_0)|^2 + |p(x + x_0)|^2 + e^{2i\varphi}\Gamma(2x_0)p(x - x_0)p^*(x + x_0) + \\ &+ e^{-2i\varphi}\Gamma(-2x_0)p(x + x_0)p^*(x - x_0) \quad (27.14) \end{aligned}$$

We remember that the source intensity $\gamma(\nu') = \gamma^*(\nu')$ is real; hence the degree of coherence obeys reality symmetry $\Gamma(-2x_0) = \Gamma^*(+2x_0) = |\Gamma|e^{-i\sigma}$. This property allows us to simplify the expression for the image intensity.

$$\begin{aligned} I(x) &= F(x - x_0) + F(x + x_0) + 2|\Gamma(2x_0)| \left[F(x - x_0)F(x + x_0)\right]^{\frac{1}{2}} \cdot \quad (27.15)\\ &\cdot \cos(2\varphi + \sigma(2x_0) + \varrho(x - x_0) - \varrho(x + x_0)) \end{aligned}$$

where:

$$p(x - x_0) = |p(x - x_0)|e^{i\varrho(x - x_0)} = \sqrt{F(x - x_0)}e^{i\varrho(x - x_0)} \quad (27.16)$$

Assume now that the point spread function is symmetrical, $F(x) = F(-x)$, then we get at the center of the image plane:

$$I(0) = 2F(x_0) + 2|\Gamma(2x_0)|F(x_0)\cos(2\varphi + \sigma + \varrho(-x_0) - \varrho(x_0)) = 2F(x_0)[1 + |\Gamma|\cos(\ldots)] \quad (27.17)$$

Assuming $F(x_0) \neq 0$, then $I(0)$ can be zero only if $|\Gamma| = 1$ (perfect coherence) and if $\{\ldots\} = \pm\pi$ (commonly but not necessarily $\sigma = 0$ and $\varrho(x_0) = \varrho(-x_0)$). In that case complete darkness midway between the two image points occurs if the phase difference 2φ between the two object points is 180°.

Now we consider a periodic object with amplitude $u_0(x') = \cos(2\pi\nu_0 x')$ and with object intensity

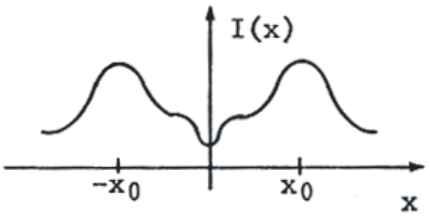

Figure 27.3: Intensity distribution behind a double slit.

$$I_0(x') = |u_0(x')|^2 = \cos^2(\pi\nu_0 x') = \frac{1}{2}[1 + \cos(2\pi\nu_0 x')] \tag{27.18}$$

Basically we insert this $u_0(x')$ value into the fundamental $I(x)$ equation. But that does not seem to be very sensible after thinking a moment about the situation. The object is a "spatial monofrequency object". Hence the result will probably look simpler in the frequency domain, where we may expect delta functions. Hence let us compute first $\tilde{I}(\mu) = \int I(x)e^{-2\pi i\mu x}\mathrm{d}x$, and $I(x)$ maybe later. Basically we now could insert the $I(x) = \iint \Gamma(x' - x'')\ldots \mathrm{d}x'\mathrm{d}x''$ into the $\tilde{I}(\mu) = \int I(x)e^{-2\pi i\mu x}\mathrm{d}x$ integral. But this would not be quite consistent with our intention to compute something which relates in the most sensible way to our experiment. For every source point ν', only two spots will appear in the pupil plane, at $\nu = \nu' + \frac{\nu_0}{2}$ and at $\nu = \nu' - \frac{\nu_0}{2}$. Hence let us try to formulate $\tilde{I}(\mu) = \mathrm{functional}[\gamma(\nu'), \tilde{u}_0(\nu), p(\nu)]$. In other words we now want to express $\tilde{I}$ in terms of the properties in the Fourier domain, which physically appears in the source plane and in the pupil plane. We could do this by replacing Γ, u_0 and p in the fundamental formula by their Fourier integrals and then trying to find hidden delta functions in:

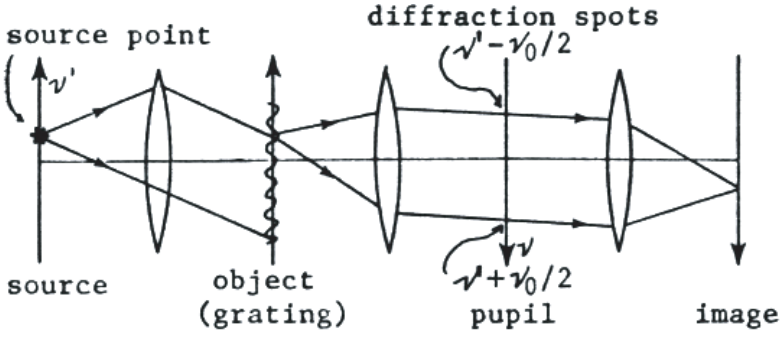

Figure 27.4: Imaging of a periodic object under partially coherent illumination.

$$I(\tilde{\mu}) = \iiiiiiii \gamma\ \tilde{u}_0\ \tilde{u}_0^*\ \tilde{p}\ \tilde{p}^* e^{2\pi i[\ldots]} \mathrm{d}(x'\ x''\ x\ \nu'\ \overline{\nu}\ \overline{\nu}'\ \overline{\overline{\nu}}\ \overline{\overline{\nu}}') \tag{27.19}$$

But instead we will start from the beginning and get the result more directly, because that approach provides more physical insights. The fields are, in $z = 0$: $\delta(\nu - \nu')$ and in $z = 2f - 0 : e^{2\pi i x'\nu}$.

In $z = 2f + 0$:

$$\begin{aligned} u_0(x')e^{2\pi i x'\nu'} &= \int \tilde{u}_0(\overline{\nu})e^{2\pi i x'(\overline{\nu}+\nu')}\mathrm{d}\overline{\nu} \\ &= \int \tilde{u}_0(\nu - \nu')e^{2\pi i x'\nu}\mathrm{d}\nu \end{aligned} \tag{27.20}$$

In $z = 4f - 0$: $\tilde{u}_0(\nu - \nu')$,
in $z = 4f + 0 : \tilde{u}_0(\nu - \nu')p(\nu)$;
in $z = 6f : \int \tilde{u}(\nu - \nu')\tilde{p}(\nu)e^{2\pi i\nu x}\mathrm{d}\nu$.

The corresponding elementary intensity distribution in the image plane is:

$$I(x, \nu') = |\int \ldots \mathrm{d}\nu|^2 = \iint \tilde{u}_0(\overline{\nu} - \nu')\tilde{u}_0^*(\overline{\overline{\nu}} - \nu')\tilde{p}(\overline{\nu})\tilde{p}^*(\overline{\overline{\nu}})e^{2\pi i x(\overline{\nu}-\overline{\overline{\nu'}})}\mathrm{d}\overline{\nu}\ \mathrm{d}\overline{\overline{\nu}} \tag{27.21}$$

Total intensity:

$$I(x) = \int \gamma(\nu')I(x, \nu')\mathrm{d}\nu' \tag{27.22}$$

We get the spatial spectrum of $I(x)$ by means of a Fourier transform:

$$\begin{aligned} \tilde{I}(\nu) &= \int e^{-2\pi i x\mu} \int \varrho(\nu')I(x, \nu')\mathrm{d}\nu'\mathrm{d}x = \\ &= \iiii \gamma(\nu')\tilde{u}_0(\overline{\nu} - \nu')\tilde{u}_0^*(\overline{\overline{\nu}} - \nu')\tilde{p}(\overline{\nu})\tilde{p}^*(\overline{\overline{\nu}})e^{2\pi i x(\overline{\nu}-\overline{\overline{\nu}}-\mu)}\mathrm{d}(\overline{\nu}\ \overline{\overline{\nu}}\ \nu'\ x) \end{aligned} \tag{27.23}$$

We recognize a hidden delta function and its impact.

$$\begin{aligned} \int \ldots \mathrm{d}x &= \delta(\overline{\nu} - \overline{\overline{\nu}} - \nu'); \qquad \int \ldots \mathrm{d}\overline{\overline{\nu}} \sim \overline{\overline{\nu}} \longrightarrow \overline{\nu} - \mu \\ \tilde{I}(\mu) &= \iint \gamma(\nu')\tilde{u}_0(\overline{\nu} - \nu')\tilde{u}_0^*(\overline{\nu} - \mu - \nu')\tilde{p}(\overline{\nu})\tilde{p}^*(\overline{\nu} - \mu)\mathrm{d}\nu'\mathrm{d}\overline{\nu} \end{aligned} \tag{27.24}$$

It is common and convenient to shift the integration variable $\overline{\nu} = \nu + \frac{\mu}{2}$.

$$\boxed{\begin{array}{c}\tilde{I}(\mu)=\iint\gamma(\nu')\tilde{u}_0\left(\nu+\frac{\mu}{2}-\nu'\right)\tilde{u}_0^*\left(\nu-\frac{\mu}{2}-\nu'\right)\\ \tilde{p}\left(\nu+\frac{\mu}{2}\right)\tilde{p}^*\left(\nu-\frac{\mu}{2}\right)\mathrm{d}\nu'\mathrm{d}\nu\end{array}} \tag{27.25}$$

This formula describes the spatial frequency spectrum of the image intensity in case of partial coherence. So far the object was general. Now insert the special object $u_0(x')=\cos(\pi\nu_0 x')$, which is a grating with only plus-first and minus-first diffraction orders.

$$\begin{aligned}
&\tilde{u}_0(\nu)=\frac{1}{2}\delta\left(\nu+\frac{\nu_0}{2}\right)+\frac{1}{2}\delta\left(\nu-\frac{\nu_0}{2}\right); \qquad (27.26)\\
&\tilde{u}_0\left(\nu+\frac{1}{2}\mu-\nu'\right)\tilde{u}_0^*\left(\nu-\frac{1}{2}\mu-\nu'\right)=\\
=\;&\frac{1}{4}\,\delta\left(\nu+\frac{1}{2}\mu-\nu'+\frac{1}{2}\nu_0\right)\delta\left(\nu-\frac{1}{2}\mu-\nu'+\frac{1}{2}\nu_0\right)+\\
+\;&\frac{1}{4}\,\delta\left(\nu+\frac{1}{2}\mu-\nu'+\frac{1}{2}\nu_0\right)\delta\left(\nu-\frac{1}{2}\mu-\nu'-\frac{1}{2}\nu_0\right)+\\
+\;&\frac{1}{4}\,\delta\left(\nu+\frac{1}{2}\mu-\nu'-\frac{1}{2}\nu_0\right)\delta\left(\nu-\frac{1}{2}\mu-\nu'-\frac{1}{2}\nu_0\right)+\\
+\;&\frac{1}{4}\,\delta\left(\nu+\frac{1}{2}\mu-\nu'-\frac{1}{2}\nu_0\right)\delta\left(\nu-\frac{1}{2}\mu-\nu'+\frac{1}{2}\nu_0\right)
\end{aligned}$$

Before continuing we remember what happens if two delta functions occur in an integral, $\iint f(\alpha,\beta)\delta(\alpha-\beta)\delta(\alpha+\beta)\mathrm{d}\alpha\mathrm{d}\beta=\frac{f(0,0)}{2}$. This result can be obtained simply by considering at first $f(\alpha,\beta)\delta(\alpha+\beta)$ as a function $g(\alpha,\beta)$ while executing the inner integral $\int g(\alpha,\beta)\delta(\alpha-\beta)\mathrm{d}\alpha=g(\beta,\beta)=f(\beta,\beta)\delta(2\beta)=f(\beta,\beta)\frac{\delta(\beta)}{2}$. After integrating also over β we conclude that we might have gotten the same result more simply by setting $\delta(\alpha-\beta)\delta(\alpha+\beta)=\delta(\alpha)\frac{\delta(\beta)}{2}$. Using this rule we may reformulate the square bracket as:

$$2[\ldots]\delta\left(\nu-\nu'+\frac{1}{2}\nu_0\right)\delta(\mu)+\delta(\nu-\nu')\delta(\mu-\nu_0)+\delta\left(\nu-\nu'-\frac{1}{2}\nu_0\right)\delta(\mu)+\delta(\nu-\nu')\delta(\mu-\nu_0) \tag{27.27}$$

Now we can compute the image spectrum.

$$\begin{aligned}
8\tilde{I}(\mu)\;&=\;\delta(\mu)\int\gamma(\nu')\left[\left|\tilde{p}\left(\nu'-\frac{1}{2}\nu_0\right)\right|^2+\left|\tilde{p}\left(\nu'+\frac{1}{2}\nu_0\right)\right|^2\right]\mathrm{d}\nu'+ \qquad (27.28)\\
&+\;\delta(\mu+\nu_0)\int\gamma(\nu')\tilde{p}\left(\nu'-\frac{1}{2}\nu_0\right)\tilde{p}^*\left(\nu'+\frac{1}{2}\nu_0\right)d\nu'\\
&+\;\delta(\mu-\nu_0)\int\gamma(\nu')\tilde{p}\left(\nu'+\frac{1}{2}\nu_0\right)\tilde{p}\left(\nu'-\frac{1}{2}\nu_0\right)d\nu'\\
&=\;\delta(\mu)A_0+\delta(\mu-\nu_0)A_1+\delta(\mu-\nu_0)A_1^*
\end{aligned}$$

$$
\begin{aligned}
I(x) &= \int \tilde{I}(\mu) e^{2\pi i \mu x} \mathrm{d}\mu = \qquad (27.29)\\
&= \frac{1}{8} \int \left[A_0 \delta(\mu) + A_1 \delta(\mu - \nu_0) + A_1^* \delta(\mu - \nu_0) \right] e^{2\pi i \mu x} \mathrm{d}\mu \\
&= \frac{A_0}{8} \left[1 + \frac{2|A_1|}{A_0} \cos(2\pi \nu_0 x - \alpha_1) \right]; \qquad A_1 = |A_1| e^{i\alpha_1}
\end{aligned}
$$

The coefficients A_0 and A_1 have a simple interpretation. For example the integral $\int \gamma(\nu') \left| \tilde{p}\left(\nu' + \frac{1}{2}\nu_0\right) \right|^2 \mathrm{d}\nu'$ counts how much of the source light fits as plus-first diffraction order through the pupil. Hence the meaning of A_0 is that either the plus-first order $\left(\nu' + \frac{1}{2}\nu_0\right)$ or the minus-first order $\left(\nu' - \frac{1}{2}\nu_0\right)$ or both fit through the pupil function $\tilde{p}(\nu)$, which is usually $\tilde{p}(\nu) = \mathrm{rect}\left(\frac{\nu}{\Delta\nu}\right)$. On the other hand A_1 counts how often *both* $\left(\nu' + \frac{1}{2}\nu_0\right)$ and $\left(\nu' - \frac{1}{2}\nu_0\right)$ fit through $\tilde{p}(\nu)$. If both diffraction spots fit through the pupil then these two mutually coherent light sources at $\nu = \nu' + \frac{1}{2}\nu_0$ and at $\nu = \nu' - \frac{1}{2}\nu_0$ will produce two titled plane waves in the image plane $e^{2\pi i x(\nu' + \frac{1}{2}\nu_0)} + e^{2\pi i x(\nu' - \frac{1}{2}\nu_0)} = e^{2\pi i x \nu''} 2\cos(\pi x \nu_0)$ with the corresponding intensity $\cos^2(\pi \nu_0 x) = \frac{1}{2}[1 + \cos(2\pi \nu_0 x)]$. The A_0 cases which do not also belong to the A_1-cases mean that only one diffraction spot fits through the pupil. In that case only a uniform brightness is contributed to the total image intensity. If those latter contributions dominate, the contrast of the image deteriorates. The geometric meanings of A_0 and A_1 can be inferred by comparing the $\int \ldots \mathrm{d}\nu'$ with Fig. 27.5. These shifted circles (= pupils) and the centered square (= source) indicate where the various factors in the A_0 and A_1 integrals are non-zero. This result can be compared with another treatment on p. 298

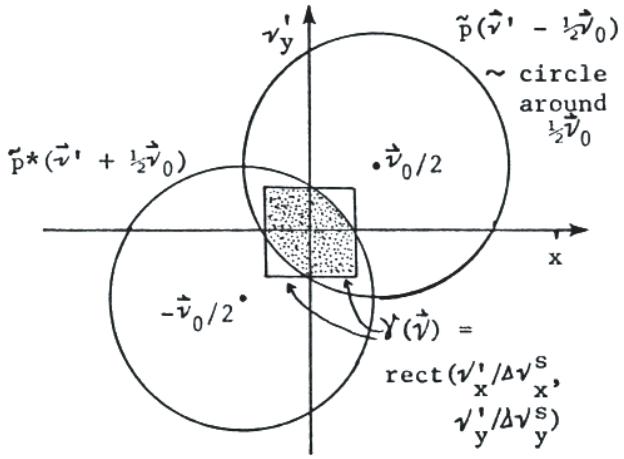

Figure 27.5: Geometrical interpretation of the various parts of the intensity distribution of the partially coherent image.

Preface to volume 2

Theses course notes are the continuation of Volume I of “Optical Information Processing”. The main goal is to provide a good basis in physical optics, which then can be used for holography. To achieve this goal it is not necessary to present the fundamentals of physical optics in its entirety. But it is advisable for students to have a more complete survey of physical optics handy.

Holography is not treated completely either, since that is well done for example by Collier, Burckhardt and Lin in “Optical Holography”. Furthermore, a third volume of these notes will follow which will cover those parts of holography which are particularly relevant to “optical information processing”. Other non-holographic contributions to the main theme of these lecture notes will be discussed also.

I have to thank Mrs. Linda Gail Chen and Curtis Shuman for their friendly cooperation.

OPTICS II: IMAGE INFORMATION

These course notes for 205B are the continuation of the 205A notes on “Optical Information Processing”, Volume I. The majority of 205B will be devoted to Holography, but first we have to add a few more fundamentals of wave optics. We will go quickly through these fundamentals, since they are well covered in standard books such as Born & Wolf or Klein.

28 Boundary Conditions

28.1 Discontinuities of the Medium

So far we have considered solutions of the wave equation in a medium in which $\epsilon = \text{const.}$, $\mu = \text{const.}$, $\sigma = 0$ (no conductivity) and $\varrho = 0$ (no charges). Now we assume still $\sigma = 0 = \varrho$, but ϵ and μ are different in $z > 0$ and $z < 0$. Then we only know how to find two solutions, one for $z > 0$, another one for $z < 0$. At the boundary ($z = 0$) will be some interaction between the two solutions. In other words, the field from $z > 0$ will partially penetrate into $z < 0$ and vice versa. To my taste it would be most desirable if one could derive the well-established boundary conditions based on conservation of energy, momentum and angular momentum. In other words, all the energy leaving the upper half space ($z > 0$) has to show up in the lower half space ($z < 0$) and so on. To my knowledge no one has derived the boundary conditions in this way. Occasionally someone has done, at least partially, the opposite, namely: suppose the boundary conditions are true, does energy conservation follow from it? That is much simpler, because the boundary conditions are *linear* in E and H, whereas energy, momentum, and angular momentum consist of second order terms like $E_x E_x, E_y H_z, \ldots$. Naturally it is more difficult to extract *linear* conditions out of some quadratic laws. If one would attempt to do it, one probably should use the so-called four-dimensional formulation of Maxwell's equations, built around the vector potential A and the scalar potential Φ. The four-dimensional formulation is mathematically simpler, although perhaps not so easy to visualize.

The more traditional way for deriving the boundary conditions is based on the postulate that the field remains finite in the boundary plane. This postulate is verified indirectly, since all the consequences of this postulate agree with experimental experience.

Assume ϵ, μ to be ϵ_1, μ_1 in $z > 0$, and ϵ_2, μ_2 in $z < 0$. Now some more assumptions, which are typical for many theoretical "proofs". I don't like it this way, but I can't present it any better. Fortunately the consequences support this shaky approach. Although ϵ, μ are supposed to be discontinuous, they should not be completely discontinuous, otherwise Maxwell's equations, which are *differential* equations, could not hold at the places of the discontinuities.

Consider a closed path of height h and length L. h should be small enough so that within h the normal field components don't change very much; so h probably should be less than λ. The length L might be thought of as being a few λ long, yet short enough that the field $E(x, y, z)$ does not change very much in $|x| \leq \frac{L}{2}$. According to Maxwell:

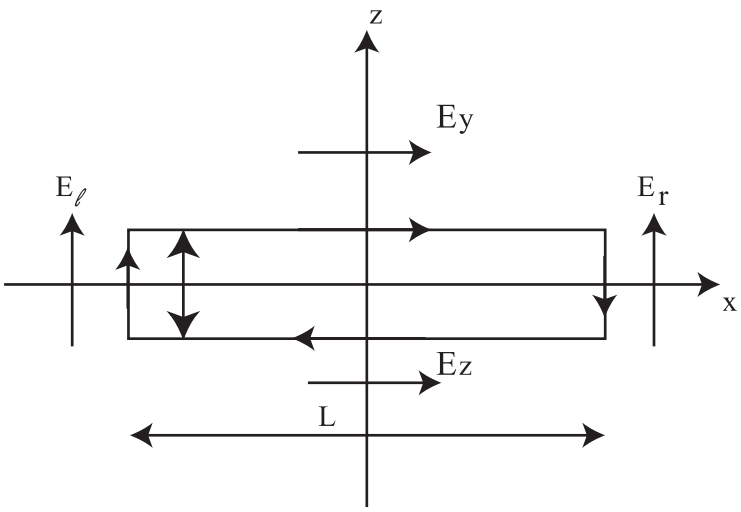

Figure 28.1: Orientations of the electrical field vectors relative to the boundary.

$$\mathrm{curl}\vec{E} = -\dot{\vec{B}} \tag{28.1}$$

This can be changed into an integral law by using the (mathematical) formula of Stokes:

$$\underbrace{\oint \vec{V} \cdot d\vec{s}}_{\text{along a closed path around an area}} = \underbrace{\iint \mathrm{curl}\vec{V} \cdot \mathrm{d}\vec{a}}_{\text{over the same area; d}\vec{a}\text{ perpendicular to surface}} \tag{28.2}$$

For the electric field vector $\vec{E}$ this gives:

$$\oint \vec{E} \cdot \mathrm{d}\vec{s} \underbrace{=}_{\text{Stokes}} \iint \mathrm{curl}\vec{E} \cdot \mathrm{d}\vec{s} \underbrace{=}_{\text{Maxwell}} -\iint \dot{\vec{B}} \cdot \mathrm{d}\vec{s} \tag{28.3}$$

Now we perform the integrations for the specific case sketched in Fig. 28.1, going clockwise.

$$\begin{aligned} &\oint \vec{E} \cdot \mathrm{d}\vec{s} \approx E_1 L - E_r h - E_2 L + E_\ell h; \\ &-\iint \dot{\vec{B}} \cdot \mathrm{d}\vec{a} \approx -\dot{B}_y \iint \mathrm{d}\vec{a} = -B_y h L \end{aligned} \tag{28.4}$$

y is the normal direction of the closed path area.

Now the integral form $\oint \vec{E} \cdot \mathrm{d}\vec{s} = -\int \dot{\vec{B}} \cdot \mathrm{d}\vec{a}$ of Maxwell's equation leads to

$$E_1 - E_2 \approx h \left\{ \frac{E_r - E_\ell}{L} - \dot{B}_y \right\} \tag{28.5}$$

$E_r - E_1$ can be replaced by $E_r - E_\ell \approx \frac{\partial E_z}{\partial x} \cdot L$. Hence we get

$$E_r - E_\ell \approx h \left\{ \frac{\partial E_z}{\partial x} - \frac{\partial B_y}{\partial t} \right\} \tag{28.6}$$

Now we assume $\frac{\partial E_z}{\partial x}$ and $\frac{\partial B_y}{\partial t}$ to be finite; next we let h go to zero, so that $E_1 = E_2$ remains. This means continuity of the tangential component of E.

$$\boxed{E_{\mathrm{tang}} : \text{ continuous}} \tag{28.7}$$

If there are no currents ($\vec{I} = 0$) in the plane of discontinuity, then Maxwell's second equation has the same form $\mathrm{curl}\vec{H} = \dot{\vec{D}}$ as the first equation $\mathrm{curl}\vec{E} = -\dot{\vec{B}}$. We can go through the same motions and get:

$$\boxed{B_{\mathrm{tang}} : \text{ continuous}} \tag{28.8}$$

Another boundary condition can be found on the basis of the 3rd Maxwell equation, $\mathrm{div}\vec{B} = 0$ which can be written also in integral form, and then modified on the basis of the Gauss formula:

$$0 = \underbrace{\iiint}_{(\mathrm{volume})} \mathrm{div}\vec{B}\mathrm{d}v = \underbrace{\oiint \vec{B} \cdot \mathrm{d}\vec{a}}_{\substack{\text{surface of volume} \\ \mathrm{d}\vec{a} \text{ in normal direction}}} \tag{28.9}$$

Now let us take a very specific volume which encloses a small portion L^2 of the boundary plane $z = 0$. The height of the volume h, is *very* small, the length and width L is fairly small, in the same sense as in the previous consideration.

$$\begin{aligned} \oiint \vec{B} \cdot \mathrm{d}\vec{a} &\approx B_{1z}L^2 - B_{2z}L^2 + hL\{\underbrace{B_x - B_{-x}}_{\approx \frac{\partial B_x}{\partial x} L} \underbrace{B_y - B_{-y}}_{\approx \frac{\partial B_y}{\partial y} L}\} \approx \\ &\approx L^2 \left[B_{1z} - B_{2z} + h \left\{ \frac{\partial B_x}{\partial x} + \frac{\partial B_y}{\partial y} \right\} \right] \end{aligned} \tag{28.10}$$

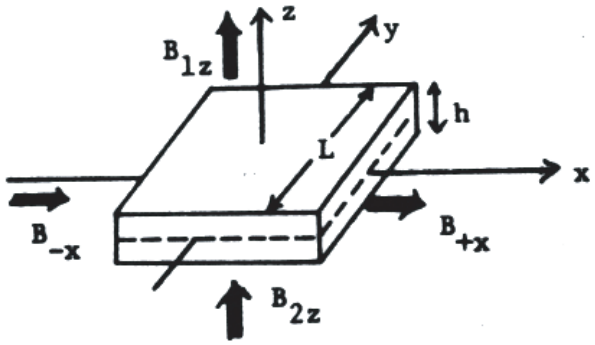

Figure 28.2: Definition of the geometrical parameters for the volume and path integrals in Eqs. 28.9 and 28.10.

From Maxwell's 3rd equation div$\vec{B} = 0$ follows $\oiint \vec{B} \cdot \mathrm{d}\vec{a} = 0$, hence $[\ldots] = 0$. Now we assume $\frac{\partial B_x}{\partial x}$ and $\frac{\partial B_y}{\partial y}$ to be finite, and then we let h go to zero. What remains is $B_{1z} - B_{2z} = 0$, which means

$$\boxed{B_{\mathrm{normal}}:\ \text{continuous}} \tag{28.11}$$

If there are no charges at the surface, Maxwell states div$\vec{D} = 0$, from which follows similarly

$$\boxed{D_{\mathrm{normal}}:\ \text{continuous}} \tag{28.12}$$

(Born and Wolf treat also the more general case, where there is some charge at the surface.)

28.2 Consequences of the boundary conditions

Now we want to list some consequences of the boundary conditions, but without proof, since this topic is presented fairly well almost everywhere, and, furthermore, it is not of central importance for our purpose.

A plane wave, falling onto a plane boundary is partially reflected, and partially refracted. The laws of reflection and refraction (Snellius) say that $\vec{K_T}$ and $\vec{K_R}$ are in the same plane as $\vec{K_1}$ and $\vec{S}$, which is the surface normal. Furthermore, $K_{1\,\tan} = K_{R\,\tan} = K_{T\,\tan}$.

$$\vec{K_1}\cdot\vec{K_1}=\vec{K_R}\cdot\vec{K_R};\quad \frac{K_1}{n_1}=\frac{K_T}{n_T}=\frac{2\pi}{\lambda_{\text{vacuum}}} \tag{28.13}$$
$$K_{1\,\tan}=K_{R\,\tan}\longrightarrow \alpha_1=-\alpha_R;$$
$$K_{1\,\tan}=K_{T\,\tan}\longrightarrow n_1\sin\alpha_1=n_T\sin\alpha_T$$

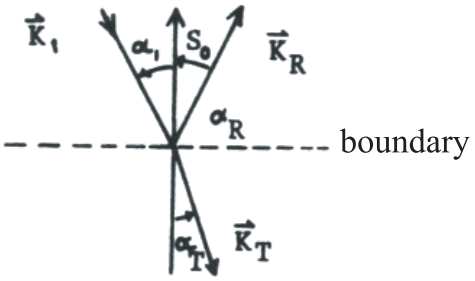

Figure 28.3: The k-vectors at a boundary between two media.

These laws are several centuries old*. Snell's law and the reflection law are supplemented by Fresnel's formulas (1823), which state how much light is directed into the reflected and into the transmitted beam.

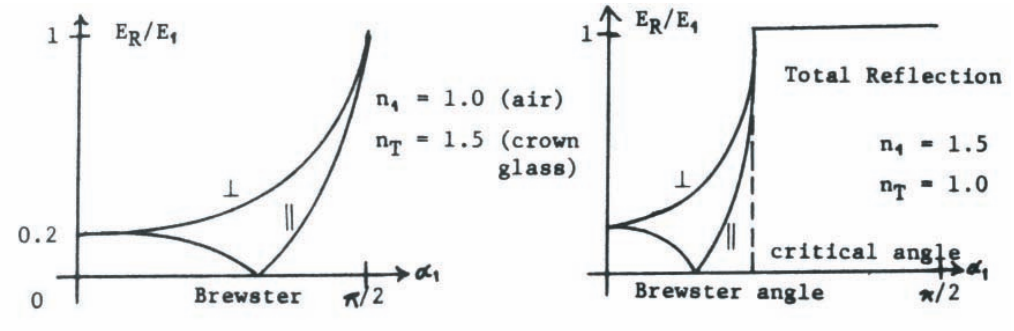

Figure 28.4: Reflection coefficient at the boundary between two media; ∥ means $\vec{E}$ is in the plane of $\vec{K_1}$ and $\vec{S_0}$. ⊥ means $\vec{E}$ is perpendicular to the plane of $\vec{K_1}$ and $\vec{S_0}$.

* A modern derivation is contained in H. G. Zimmer's Geometrical Optics (published by Springer, N. Y. 1969). Snell's law follows from energy conservation.

Another application of the Fresnel formulas occurs in connection with *thin films*.

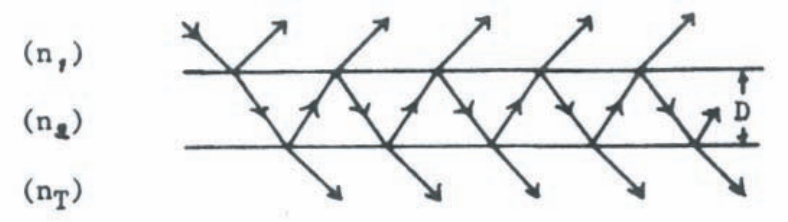

Figure 28.5: Multiple beam interference in a thin film.

In this approach (Airy, about 100 years ago) one computes first the split at the (1, 2) surface into reflected and transmitted light. Next the transmitted light travels to the (2, T) boundary, while its phase advances according to the path. Then again the light is split up, and so on. Finally one sums up all the reflected portions, with proper phase factors, and also all the transmitted portions. This turns out to be fairly simple. Mathematically speaking it is a "geometric series".

A more modern approach, which leads to the same result, consists of a simultaneous satisfaction of the boundary conditions on both surfaces (1, 2) and (2, T). One makes the "ANSATZ"** $\vec{E_1}$ (known), $\vec{E_{1R}}$ (yet unknown in amplitude and phase, but with a $\vec{K_{1R}}$ vector according to the law of reflection).
(** "Ansatz" (German) means an intelligent guess of the solution, usually with a few open parameters. For example $u = A\cos(\omega t + \varphi)$ is a good "Ansatz" for $u + B\ddot{u} = 0$).

$$\vec{K_{1R}} = \vec{K_1} - 2\vec{S_0} \cdot (\vec{S} \cdot \vec{K_1}) \tag{28.14}$$

Furthermore, one assumes a forward wave within the film, and another forward wave beyond the film, both forward waves having $\vec{K}$ vectors in accordance with the refraction law. Finally there has to be a backward wave with $\vec{K}_{2R} = \vec{K}_2 - 2\vec{S_0}(\vec{S_0} \cdot \vec{K}_2)$ within the film. The waves with $\vec{K_{1R}}$ and $\vec{K}$, $\vec{K_{2R}}$ and $\vec{K_T}$ respectively consist of many waves sketched in Fig. 28.5 on the zig-zag approach. Anyway, it turns out that one has just enough equations from the boundary conditions to find all components of the vector fields $\vec{E_{1R}}$, $\vec{E}_2$, $\vec{E_{2R}}$ and $\vec{E_T}$, when $\vec{E_1}$, D, n_1, n_2, n_T are known*. (* Sommerfeld comments extensively on this equivalence of the zig-zag and boundary condition approaches)

H. Wolter (in Progress in Optics, Volume 1, E. Wolf editor, North Holland Publishing Co., 1966) has developed a network theory for treating a stack of multilayers. Experimentally more than 120 layers can be put on top of each other. This is done for creating well defined reflection or transmittance curves over wide ranges of λ. Wolter developed a matrix treatment just as in the electrical 4-pole network theory. As you know, a 2 x 2 matrix connects the two output functions (voltage and current) with the two input functions. In the case of thin films one needs two independent matrices, one for the so-called TE case (E-vector perpendicular to the plane of incidence), and another matrix for the TH case (H-vector perpendicular to

the plane of incidence). The voltage corresponds formally to a magnetic field component, and the current is replaced in this analogy by an electric field component. All the techniques for getting broadband, or narrow band filters can be translated into optics immediately.

A particularly interesting case of a thin film arises if the angle of incidence is beyond the "critical angle", that is, in the angular region of total reflection (Fig. 28.6). Moving the upper prism piece electrically, in proportion to an audio signal picked up by a microphone, this device served 25 years ago as the emitter of a "light telephone". A similar scheme is used also as a variable "output coupler" of laser resonators. By the way, this effect is for electromagnetic waves, what for Ψ waves (Schrödinger) is generally called the "tunnel effect".

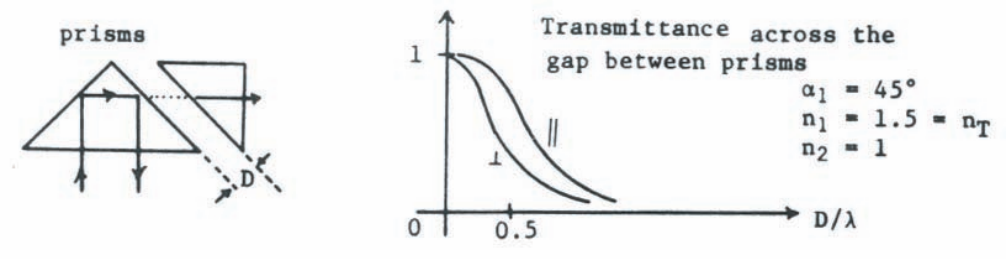

Figure 28.6: Optical tunneling.

Most recently Tien (Bell Telephone Laboratories) and others have used a similar effect for mode launching in thin films. This is used for "planar optics", a very new field, which might possibly lead to a technology which would replace electronic integrated circuits by optical integrated circuits. For getting an idea about "planar optics" read the Bell Telephone ads in Applied Optics, Physics Today, etc. These ads are usually quite clear and informative.

29 Interference

29.1 Division of Wavefront and Division of Amplitude

In optics the word "interference" means that the joint intensity I of two complex amplitudes u_1 and u_2 is in general different from the sum of the two single intensities:

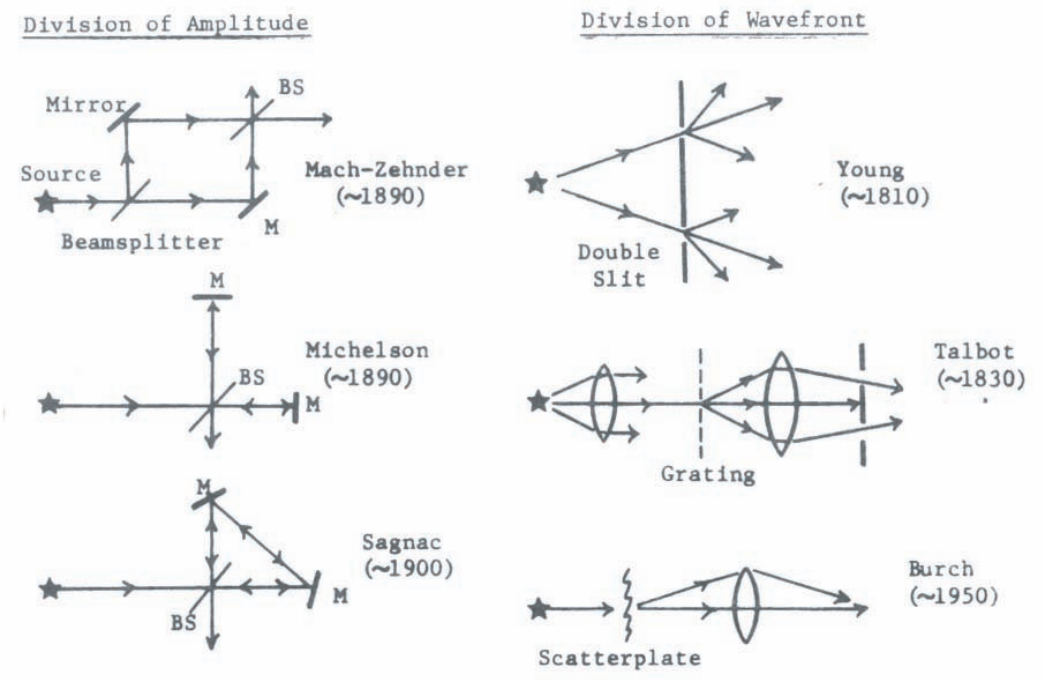

Figure 29.1: Various setups for interferometers based on amplitude division (left) or wavefront division (right).

$$I_1 = |u_1|^2 \quad \text{and} \quad I_2 = |u_2|^2 \tag{29.1}$$

$$I = |u_1 + u_2|^2 = |u_1|^2 + |u_2|^2 + \underbrace{u_1 u_2^* + u_1^* u_2}_{\text{interference term}}$$

In most textbooks the different interference effects are classified into these two groups: “division of amplitude” and “division of wavefront”.

In the Fig. 29.1 lenses are omitted (except for one example), which is very unrealistic. We will come back to this point later.

Another classification takes into account the relative position of the “object” (under investigation) and the plane of observation. This relationship might be (1) imaging, (2) Fraunhofer diffraction, or (3) Fresnel diffraction. From now on (as before, too) I will give only some representative examples. Details can be found for example in M. Francon’s Optical Interferometry.

1. Imaging interferometer, say for the study of phase objects $u(x,y) = e^{i\varphi(x,y)}$.

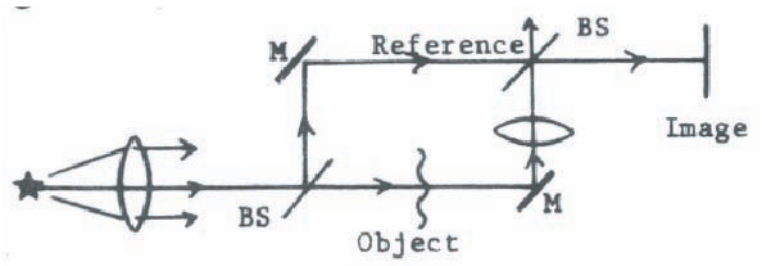

Figure 29.2: Imaging interferometer based on the Mach-Zehnder configuration.

In the image plane the object amplitude $u(x,y)$ is reproduced due to the action of the lens. Furthermore a plane wave arrives via the other arm of the interferometer.

Special cases:

(a)

$$I(x,y) = \underbrace{|1+u|^2}_{\substack{\text{plane wave} \\ in \text{ phase, not} \\ \text{tilted}}} = 1 + u + u^* + |u|^2 = 1 + 2\mathrm{Re}\{u\} + |u|^2 \tag{29.2}$$

if $u = e^{i\varphi(x,y)}$ (phase object):

$$I = 2[1 + \cos\varphi] \tag{29.3}$$

(b)

$$I(x,y) = |i+u|^2 = 1 + |u|^2 - iu + iu^* = 1 + |u|^2 + 2\mathrm{Im}\{u\} \tag{29.4}$$
$$\Longrightarrow 2[1 + \sin\varphi]$$

(c)

$$I(x,y) = |e^{2\pi i\nu_0 x} + u(x,y)|^2 = 1 + |u|^2 + ue^{-2\pi i\nu_0 x} + u^* e^{2\pi i\nu_0 x} \qquad (29.5)$$
$$\Longrightarrow 2[1 + \cos[2\pi\nu_0 x - \varphi(x,y)]]$$

For a piece of glass with a triangular groove of depth $L_{\max}(x,y) = \frac{3}{2}\frac{\lambda}{n-1}$ (Fig. 29.3) the resulting phase profile would be (n: index of refraction):

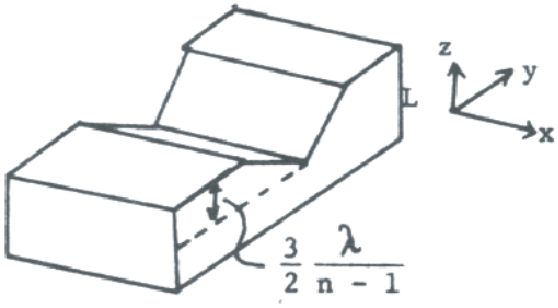

Figure 29.3: The shape of a glass substrate with triangular grooves.

$$\varphi(x,y) = \frac{2\pi}{\lambda}(n-1)L(x,y) \qquad (29.6)$$

Thus the maximum phase variation spans over 3π.

The corresponding interference pattern would look like shown in Fig. 29.4.

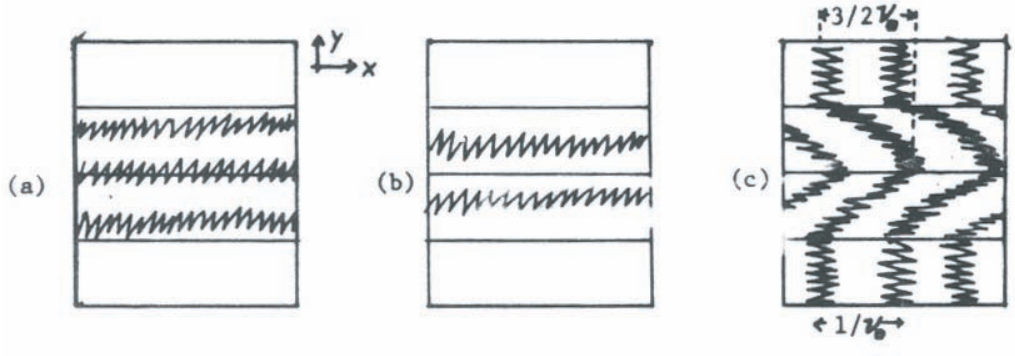

Figure 29.4: Interference fringes of the structured glass substrate.

The interference fringes indicate height profiles, untilted or tilted.

So far in the image plane, the object wave has been superposed by a plane wave, tilted or not. A slight modification would be to take as the so-called "reference wave" now a spherical wave instead of a plane wave. This makes sense if one wants to test how much the object deviates from a perfect sphere.

A more drastic departure from classical interferometry is the so-called "shearing" interferometry, whereby the object wave interferes with a duplicate of the object wave, which however is somehow displaced:

(a) Lateral shearing:

$$I = |u(x, y) + u(x \pm \Delta x, y)|^2 \tag{29.7}$$

(b) Radial shearing with differential magnification:

$$I = \left| u(r, \varphi) \pm u\left(\frac{r}{M}, \varphi\right) \right|^2 \tag{29.8}$$

(c) Radial shearing with constant shift:

$$I = |u(r + \Delta r, \varphi) \pm u(r, \varphi)|^2 \tag{29.9}$$

(d) Radial-inverted shearing:

$$I = |u(r, \varphi) \pm u(r - r_0, \varphi)|^2 \tag{29.10}$$

(e) Longitudinal shearing:

$$I = |u(x, y, z) \pm u(x, y, z + \Delta z)|^2 \tag{29.11}$$

(f) Lateral inversion shearing

$$I = |u(x, y) + u(-x, +y)|^2 \tag{29.12}$$

(g) Angular shearing

$$I = |u(r, \varphi) + u(r, \varphi + \Delta\varphi)|^2 \tag{29.13}$$

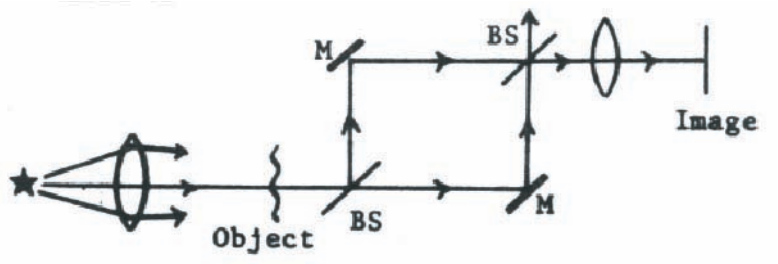

Figure 29.5: Lateral shearing interferometer based on the Mach-Zehnder configuration.

The most developed type is "lateral shearing", which can be achieved for example by putting the object not *into* but *in front of* the interferometer (for example Mach-Zehnder) (Fig. 29.5).

The two mirrors and the two beam-splitters provide more than enough degrees of freedom to shift and tilt the two images. Two special cases are of particular importance, because they lead to easy-to-interpret results.

Total shear

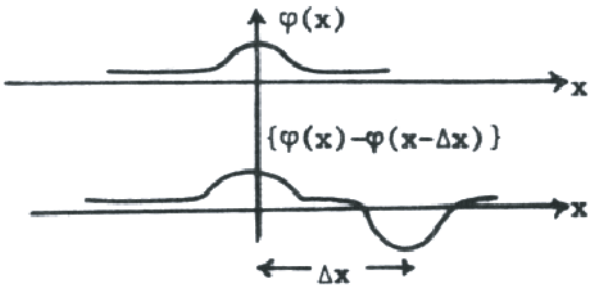

Figure 29.6: The result of a total shearing interferometer.

$$\begin{aligned} \text{object}: \ & u(x) = e^{i\varphi(x)} \\ \text{image intensity}: \ & I(x) = |u(x) - u(x-\Delta x)|^2 = 2[1-\cos(\varphi(x)-\varphi(x-\Delta x))] \end{aligned} \tag{29.14}$$

Δx is so large that the essential part of the object, which has only a moderate extension,

will fall upon another part of the "object" (Fig. 29.6), which is constant, hence acts like a simple plane reference wave as in classical interferometry. In other words the supporting glass plate is only half covered by the object.

Differential shear

Now the shift Δx is small compared with the typical object dimensions. Furthermore it is assumed now that the two images have a "total phase shift", which introduces a minus-sign.

$$I = |u(x,y) - u(x-\Delta x, y)|^2 \approx \left|\frac{\partial u(x,y)}{\partial x}\Delta x\right|^2 = \tag{29.15}$$

$$= \left|\frac{\partial u}{\partial x}\right|^2 (\delta x)^2; \qquad \text{with}: \quad u(x,y) = e^{i\varphi(x,y)}$$

$$I(x,y) = \left(\frac{\partial \varphi}{\partial x}\right)^2 (\Delta x)^2 \qquad \frac{\partial u}{\partial x} = ie^{i\varphi}\frac{\partial \varphi}{\partial x}$$

Later, in connection with polarization, we will describe other ways for producing differential shear.

2. Fraunhofer diffraction interferometer

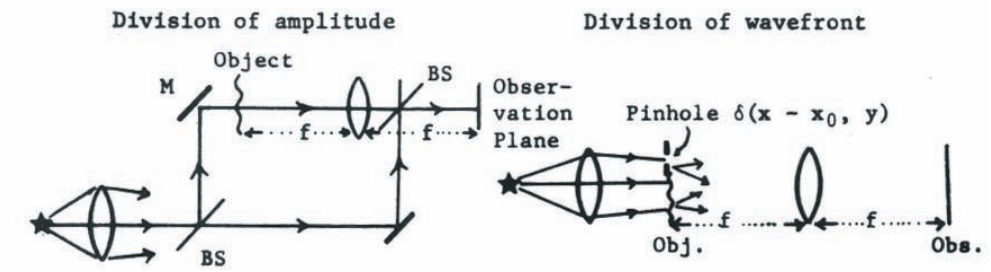

Figure 29.7: Two examples for configurations for Fraunhofer diffraction interferometers.

As almost always in interferometry the goal is to record the phase of a wave front in the form of more or less deformed interference fringes. Zernike and his co-workers did this first in 1948 in connection with Fraunhofer diffraction (Fig. 29.7).

In both cases one observes:

$$I = \left| \underbrace{\tilde{u}\left(\frac{x}{\lambda f}, \frac{y}{\lambda f}\right)}_{\text{Fourier spectrum of object}} + \underbrace{e^{-2\pi m i \nu_0 x}}_{\text{plane waves}} \right|^2 \tag{29.16}$$

Some of you might have seen for example in Goodman's book similar setups for recording holograms. This is no accidental coincidence since holograms are interferograms. They are called differently because they are used differently. An interferogram is the end product of an experiment, while a hologram is used for the reconstruction of a wavefront as we will see later in detail.

3. Fresnel diffraction interferometer

   Let us take the lens between OBJ and OBS out of the "division of amplitude" setup (Fig. 29.7); then the complex amplitude in the observation plane is the Fresnel transform u of the object u, hence $I = |\hat{u} + e^{-2\pi i \nu_0 x}|^2$.

   If we take a lens between OBJ and OBS out of the "division of wavefront" scheme, then the lens-action is removed both for the wave coming from the object, and for the reference wave. Hence this time the lens removal means something different.

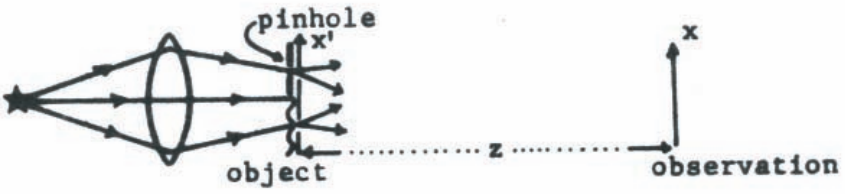

Figure 29.8: Fresnel diffraction interferometry.

We call the object $u(x, y)$; each object point (x', y') produces a spherical wave, which can be described far away, and at not too large an angle as:

$$\approx e^{i\pi \frac{[(x-x')^2+(y-y')^2]}{\lambda z}} \tag{29.17}$$

All the spherical waves together, plus the spherical wave from the pinhole, produce in the plane of observation:

$$\iint u(x', y') e^{i\frac{\pi}{\lambda z}[(x-x')^2+(y-y')^2]} \mathrm{d}x' \mathrm{d}y' + e^{i\frac{\pi}{\lambda z}[(x-x_0)^2+(y-y_0)^2]} \tag{29.18}$$

The corresponding intensity is:

$$I = 1 \quad + \quad \left| \iint \dots \right|^2 + \iint u(x',y') e^{i\frac{\pi}{\lambda z}[-2x(x'-x_0)-2y(y'-y_0)+x'^2-x_0^2+y'^2-y_0^2]} \mathrm{d}x'\mathrm{d}y' + \\ + \quad \text{c. c.} \tag{29.19}$$

Let us now assume $|\iint \dots|^2 \ll 1$ to be small. Another specification, which leads to an important special case is:

$$u(x',y') \neq 0 \qquad \text{only in} \qquad |x'| \leq \frac{\Delta x}{2}, \quad |y'| \leq \frac{\Delta y}{2} \tag{29.20}$$

and the distance z may be fairly large:$\lambda z > (\Delta x)^2 + (\Delta y)^2$. Then the part of the phase term $e^{i\frac{\pi}{\lambda z}(x'^2+y'^2)}$ is not too much different from 1 for all:

$$x'^2 + y'^2 \leq \frac{(\Delta x)^2 + (\Delta y)^2}{4} \tag{29.21}$$

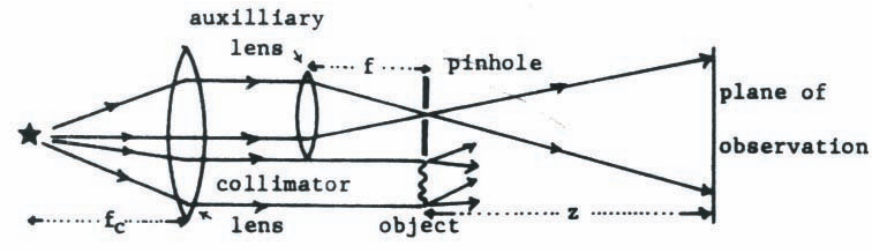

Figure 29.9: Setup for Fourier holography, i.e. modified setup for Fresnel interferometry.

Hence we drop this term, and also the $x_0^2 + y_0^2$ term for similar reasons. Now the intensity is:

$$\begin{aligned} I(x,y) &\approx 1 + \iint u(x',y') e^{2\pi i \frac{x(x'-x_0)+y(y'-y_0)}{\lambda z}} \mathrm{d}x'\mathrm{d}y' + \text{c. c.} \\ &= 1 + e^{2\pi i \frac{xx_0+yy_0}{\lambda z}} \tilde{u}\left(\frac{x}{\lambda z}, \frac{y}{\lambda z}\right) + \text{c. c.} \\ &= 1 + 2\left|\tilde{u}\left(\frac{u}{\lambda z}, \frac{y}{\lambda z}\right)\right| \cos\left[2\pi\left(\frac{x_0}{\lambda z}x + \frac{y_0}{\lambda z}y\right)\right] + \varphi\left(\frac{x}{\lambda z}, \frac{y}{\lambda z}\right) \end{aligned} \tag{29.22}$$

where $\varphi(\nu, \mu) = \arg(\tilde{u}(\nu, \mu))$.

This is a fringe system with a carrier frequency $\nu_c = \frac{x_0}{\lambda z}, \mu_c = \frac{y_0}{\lambda z}$ which is amplitude modulated by the modulus of the spatial frequency spectrum, and phase modulated by the phase of $\tilde{u}(\nu, \mu)$. In other words, the *intensity* distribution $I(x, y)$ displays essentially the Fourier transform $\tilde{u}(\nu, \mu)$ of the *complex amplitude* $u(x', y')$ of our "object". This experiment is also called "lens-less Fourier holography".

You might wonder why it was justified to neglect the quadratic term $|\iint \ldots|^2$, which implies that more light comes out of the pinhole than altogether from the object. This is quite reasonable when the setup in Fig. 29.8 is modified as shown in Fig. 29.9. Now a very large portion of the collimated beam is forced to go through the pinhole.

30 Coherence

30.1 Fundamentals of coherence theory

When talking about interference we assumed tacitly that the two light waves, which overlapped in the plane of observation, were mutually *coherent*. Not always are two light waves coherent; sometimes they are incoherent, which means no interference fringes occur. Sometimes the interference fringes might be barely visible, having only low contrast. This situation is called "partial coherence". The subject of coherence theory is considered by most students the most difficult subject in optics. I think this is partially due to the fact that many textbooks try to present the topics in an elegant and abstract manner, rather than intuitively, as I will attempt to do now. First we have to talk about atomic emission processes, later about macroscopic effects as the result of the orderliness of many emission acts. Let us start with a very simple case, and then gradually increase the complexity, such making it more and more realistic.

A single atom, which might have been excited (that means brought into a state of elevated energy) may start to irradiate at any moment. The starting moment, which determines the phase of the emitted wave, is unpredictable in the case of the so-called "spontaneous" emission, which is typical for *thermal* light sources, where the excitation is provided by collision, by photon absorption, or by a chemical process like ionization.

Besides *spontaneous* emission there is so-called *stimulated* emission, an effect which had been predicted 50 years ago by Einstein. It means that an atom, which is ready to emit any moment, is exposed to a by-passing wave of the proper frequency. This by-passing wave, if it is strong enough, has a fair chance of initiating the emission of the waiting atom in such a way that both waves will be *in-phase*. It is the essence of a laser that almost all atoms will be *stimulated in* phase. Hence the name "Light Amplification by Stimulated Emission of Radiation". But presently we are not so much interested in a laser, which is easier to understand in connection with coherence than an ordinary thermal light source.

The wave train leaving a radiating atom might last for 10^{-8} seconds, which corresponds to a train length of 300 cm. If many atomic collisions occur the interval of undisturbed emission might be only 10^{-11} seconds (~ 0.3 cm) or even shorter. Such intervals are typical for a gas discharge lamp, filled for example with mercury. The longest wave trains occur only in very low pressure lamps, which contain only relatively few atoms. Hence the process of emission is not so likely to be interrupted by a collision process as in high pressure lamps, which there-

fore emit (on the average) much shorter wave trains, but also many more of them.

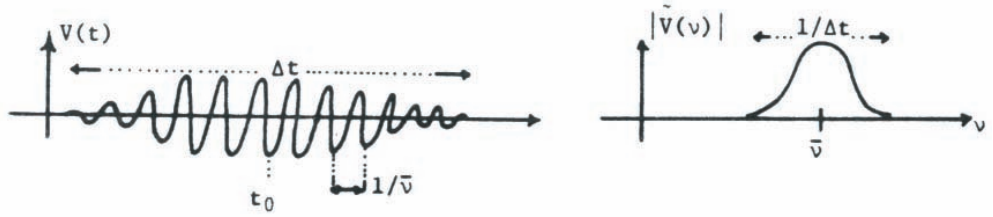

Figure 30.1: A wave train emitted by a thermal light source and the corresponding spectral distribution.

$$\tilde{V}(\nu) = e^{2\pi i \nu t_0} \tilde{V}(\nu - \overline{\nu}) \qquad \tilde{V}(\nu) = \int V(t) e^{-2\pi i \nu t} \mathrm{d}t \tag{30.1}$$

Now let us set up an interference experiment.

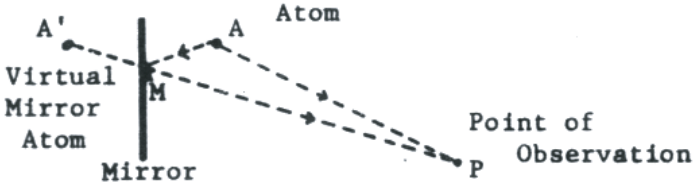

Figure 30.2: A basic interference experiment.

$$\overline{\mathrm{A'M}} = \overline{\mathrm{AM}} \text{ (equal length)} \qquad \overline{\mathrm{AP}} = \mathrm{R}; \qquad \overline{\mathrm{A'P}} = \mathrm{R'} \tag{30.2}$$

At point P the total field V_T will be $V_T = V(t) + V\left[t - \frac{R'-R}{c}\right]$; where $\frac{R'-R}{c}$ is the time delay between the direct wave and the reflected wave. The "instantaneous intensity" is $B = |V_T|^2$ and the resulting intensity is:

$$I(t_0) = \frac{1}{T} \int_{t_0 - \frac{T}{2}}^{t_0 + \frac{T}{2}} B(t) \mathrm{d}t \tag{30.3}$$

Herein T has to be large enough to enclose the whole wave train $V(t)$ and $V\left[t - \frac{R'-R}{c}\right]$. Call $\frac{R'-R}{c}$ from now on the "delay" time τ, and omit the factor $\frac{1}{T}$.

$$I(t) = \int |V(t)|^2 \mathrm{d}t = \int |V(t-\tau)|^2 \mathrm{d}t + 2\mathrm{Re}\left\{ \int V(t) V^*(t-\tau) \mathrm{d}t \right\} \tag{30.4}$$

With $\tilde{V}(\nu) = \int V(t) e^{-2\pi i \nu t} \mathrm{d}t = e^{2\pi i \nu t_0} \tilde{V}_0(\nu - \overline{\nu})$ this will be, setting $\nu - \overline{\nu} \longrightarrow \nu' \longrightarrow \nu$,

$$I(t) = 2 \int |\tilde{V}_0(\nu)|^2 \mathrm{d}\nu + 2\mathrm{Re}\left\{ e^{2\pi i \overline{\nu} \tau} \int |\tilde{V}_0(\nu)|^2 e^{2\pi i \nu \tau} \mathrm{d}\tau \right\} \tag{30.5}$$

Herein $\overline{\nu}$ is the mean-frequency. Looking at the sketch of $V(t)$ in Fig. 30.1, it is clear that the interference term $\int |\tilde{V}_0(\nu)|^2 e^{2\pi i \nu \tau} \mathrm{d}\nu$ will be essentially $\neq 0$ only in $|\tau| \leq \Delta t$.

What does that mean? Only for time delays $\tau = \frac{R' - R}{c}$, which do not exceed the time duration Δt of the wave train, one might expect to have a non-vanishing interference term $\int V(t) V^*(t-\tau) \mathrm{d}t$.

So we get as an *necessary* (not sufficient!) condition for the interference interaction between two wave trains, which stem from the same atom, and not only that, but also from the same emission act, that these two wave trains *overlap in time* (which is another way of stating the condition $|\tau| \leq \Delta t$).

What we have said so far is not really wrong but highly unrealistic. What could we expect to see, if only one atom emits only once a wave train? The probability that a photon is observed at the point P is very, very low. So let the atom emit some more wave trains. Even the most diligent atoms will emit during less than a millionth of the time. Hence it might happen only once in a year or so that two wave trains, coming from the same atom but from different emission acts, will meet somewhere, say at point P. It is not impossible, though, that this occurs, assuming that the late wavetrain from an earlier emission (going A - M - P) meets the early wave train (going directly A - P) from the next emission process. Even so, we can forget about these events for yet another reason. Since we assumed that the emission processes are all spontaneous, the time difference between starting moments of subsequent emission acts varies at random. Hence the type of interaction between parts from different emission acts will ultimately cancel out if it happens often enough, because the time difference might sometimes produce a *constructive* interaction, but equally likely a *destructive* interaction. You might imagine as time-integration interval a fraction of a second (say 1/10), which might be needed for the exposure of a photographic plate, or for the perception of an image by the eye. All this means is that the *repetition* of the emission act does not change our coherence considerations.

But to be more correct, we should modify the condition τ (delay) $< \Delta t$ (wave train duration). What is observable is not $V(t)$ but only $I(t_0)$; in other words, $\tilde{V}(\nu)$ is not really important here, only $|\tilde{V}_0(\nu)|^2$.

For $\int |\tilde{V}_0(\nu)|^2 e^{2\pi i \nu \tau} \mathrm{d}\nu$ to be $\neq 0$ (which means interference will be observed) it is sufficient that the spectral width $\Delta\nu$ of the temporal power spectrum $|\tilde{V}_0(\nu)|^2$ is small enough

$\Delta\nu < \frac{1}{\tau}$. This can certainly be satisfied by a wave train of duration $\Delta\tau \approx \frac{1}{\Delta\nu}$, as pointed out, but completely different waves $V(t)$, which are $\neq 0$ over much longer intervals, can have the same power spectrum $|\tilde{V}(\nu)|^2$. Of course, these other wave trains would have a different $\arg\{\tilde{V}(\nu)\}$, but that is of no consequence for our experiment. Hence we had better generalize the older condition $\tau < \Delta t$ into $\Delta\nu < \frac{1}{\tau}$.

It is more traditional to formulate this condition slightly differently. For one thing we replace the delay time τ by the path difference $R' - R = c\tau$, and call $R' - R = \Delta L$. Also it is more common to use the wavelength λ rather than the temporal frequency ν for the specification of the "spectrum" $|\tilde{V}(\nu)|^2$. Because of $\lambda\nu = c$ it is $|\Delta\nu| = |\frac{\Delta\lambda}{\lambda^2}|$, where λ stands briefly for $\overline{\lambda} = \frac{c}{\overline{\nu}}$. Then $\Delta\nu < \frac{1}{\tau}$ goes over into $\frac{\Delta L}{\lambda} < \frac{\lambda}{\Delta\lambda}$.

In other words, it is necessary for the observation of interference that the path difference ΔL, measured in mean-wavelengths $\overline{\lambda}$, is less than the "spectral purity" $\frac{\lambda}{\Delta\lambda}$ of the source.

Now let us state three more conditions, which are essential for interference to occur. Then we have learned enough for our purpose about the physics underlying the coherence theory.

Two waves which are polarized perpendicularly cannot interfere:

$$\begin{aligned} &\vec{V} = \vec{x}\overline{V_x} + \vec{y}\overline{V_y}; \qquad I = \vec{V}\cdot\vec{V}^* \\ &I = |V_x|^2 + |V_y|^2 \qquad (\text{no } V_xV_y) \end{aligned} \tag{30.6}$$

The reason is that it is the electric field, which exerts a force upon electrons in the receiver, which creates an observable effect. Destructive interference occurs if at a certain point two fields are oriented just in opposite directions. However, if the fields are perpendicular, as assumed above, nothing like that could occur.

Two waves coming from different atoms which emit spontaneously cannot interfere (time-integrated over many emission processes) because the phase differences are uncorrelated, and furthermore, the chance for overlapping in time is not very high. (Note: such a rule does not apply for stimulated emission from a laser.)

Two waves, emitted from the same atom, but with different temporal frequencies $\nu,\ \nu+\delta\nu$, cannot interfere, if the duration of observation (time integral) T is $T \gg \frac{1}{\delta\nu}$. The reason? These two waves produce a beat frequency $\cos(2\pi t\delta\nu)$, which however is too fast to be observed with an integrating time $T \gg \frac{1}{\delta\nu}$. Notice: it is quite simple (but of no interest in this context) to create conditions $T < \frac{1}{\delta\nu}$ such that the beat frequency is observable (see T. Suzuki et al. JOSA **51**, 253, 1961).

In order to get a feel for the macroscopic consequences of our so far microscopic considerations we will now discuss some simple but representative interference experiments.

30.2 Coherence and interference by division of amplitude

The simplest setup is a source in front of a mirror (Fig. 30.3). The source may be extended in space (x', y', z') as well as in temporal frequencies ν_t.

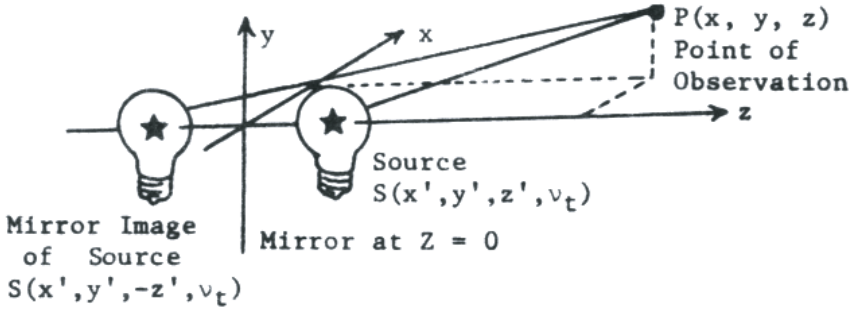

Figure 30.3: Interference by division of amplitude.

The functions S represents the energy emission at point (x', y', z') and at frequency ν_t. Let us assume that the spectral sensitivity of the receiver is $R(\nu_t)$. Then the intensity at P is:

$$I(x,y,z) = \iiint\!\!\!\!\iint S(x',y',z',\nu_t)R(\nu_t)\left|\frac{e^{ikr_+}}{r_+} + \frac{e^{ikr_-}}{r_-}\right|^2 \mathrm{d}(x'\ y'\ z'\ \nu_t) \tag{30.7}$$

This means that always a pair of spherical waves, coming from the point pair $(x', y', +z')$ and $(x', y', -z')$ will interact, of course assuming the same frequency ν_t, which is contained in:

$$K = \frac{2\pi}{\lambda} = \frac{2\pi\nu_t}{c}; \qquad r_\pm = \sqrt{(x-x')^2 + (y-y')^2 + (z \pm z')^2} \tag{30.8}$$

$$\left|\frac{e^{ikr_+}}{r_+} + \frac{e^{ikr_-}}{r_-}\right|^2 = \frac{1}{r_+^2} + \frac{1}{r_-^2} + \frac{\cos\{k(r_+ - r_-)\}}{r_+ r_-}$$

This general formula is not easy to grasp, so let us study some instructive special cases.

30.2.1 Monochromatic point source

$$\begin{aligned} S(x',y',z',\nu_t)R(\nu_t) &= \delta(x',y',z'-z,\nu_t-\nu_0) \qquad (30.9)\\ I &= \frac{1}{r_+^2} + \frac{1}{r_-^2} + \frac{\cos\{k(r_+ - r_-)\}}{r_+ r_-} \\ k_0 &= 2\pi\frac{\nu_0}{c} \qquad r_\pm = \sqrt{x^2 + y^2 + (z \pm z_0)^2} \end{aligned}$$

The maxima of the interference fringes occur where the cosine is $+1$. That is at $k_0|r_+ - r_-| = 0, 2\pi, 4\pi \ldots$ or $|r_+ - r_-| = 0, \lambda_0, 2\lambda_0, 3\lambda_0, \ldots$.

These are rotational hyperboloids around the z-axis (Fig. 30.4).

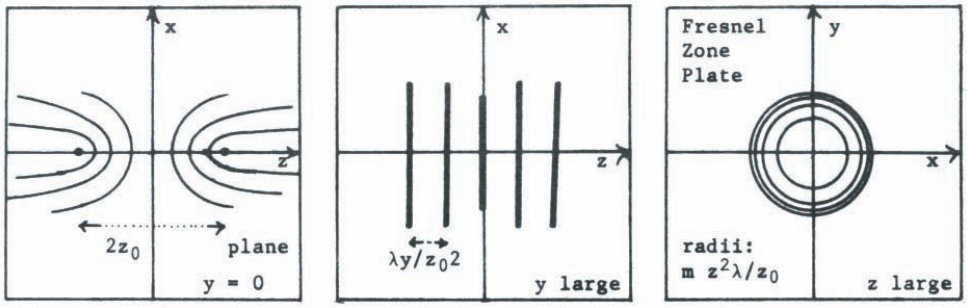

Figure 30.4: Interference finges according to Eq. 30.9 in different approximations.

If y is very large, then $I \approx \frac{2}{r^2}\left[1 + \cos\left(\frac{4\pi z z_0}{\lambda y}\right)\right]$, $(r \approx y)$

If z is very large, then $I \approx \frac{2}{z^2}\left[1 + \cos\left(2\pi \frac{z_0(x^2+y^2)}{\lambda z^2}\right)\right]$.

30.2.2 Polychromatic point source

$$S(x', y', z', \nu_t)R(\nu_t) = \delta(x', y', z' - z_0)S_2(\nu_t) \tag{30.10}$$

remember: $\nu_t = \frac{c}{\lambda}$; Compare Eq. 30.10 with the main formula Eq. 30.7 for the intensity at P.

If y is very large then :

$$\begin{aligned} I &\approx \frac{2}{r^2}\int S_2(\nu_t)\left[1 + \cos\left(2\pi\frac{2zz_0}{cy}\right)\right]\mathrm{d}\nu_t \\ &= \frac{2}{r^2}\left[\tilde{S}_2(0) + |\tilde{S}_2\left(\frac{2zz_0}{cy}\right)|\cos\left[\sigma_2\left(\frac{2zz_0}{cy}\right)\right]\right] \end{aligned} \tag{30.11}$$

whereby $\tilde{S}_2(\varrho) = |\tilde{S}_2(\varrho)|e^{i\sigma_2(\varrho)} = \int S_2(\nu_t)e^{-2\pi i\varrho\nu_t}\mathrm{d}\nu_t$

Herein we made use of the reality of $S_2 = S_2^*$. Furthermore we might assume that $S_2(\nu_t)$ has a mean frequency $\overline{\nu}_t$.

Call $S_2(\nu_t) = S_{20}(\nu - \overline{\nu}_t) \Rightarrow |\tilde{S}_{20}(\varrho)| = |\tilde{S}_2(\varrho)|$:

$$\sigma_{20}(\varrho) = \sigma_2(\varrho) + 2\pi\overline{\nu_t}\varrho \tag{30.12}$$

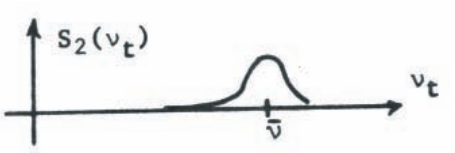

Figure 30.5: The source spectrum.

$$I(z) = \frac{2}{r^2}\tilde{S}_2(0)\left[1 + \frac{|\tilde{S}_2\left(\frac{2zz_0}{cy}\right)|}{\tilde{S}_2(0)}\cos\left\{2\pi\overline{\nu_t}\frac{2zz_0}{cy} - \sigma_{20}\left(\frac{2zz_0}{cy}\right)\right\}\right] \tag{30.13}$$

The contrast goes down with z; there might be a fringe shift $\frac{\sigma_{20}}{2\pi\overline{\nu_t}}$.

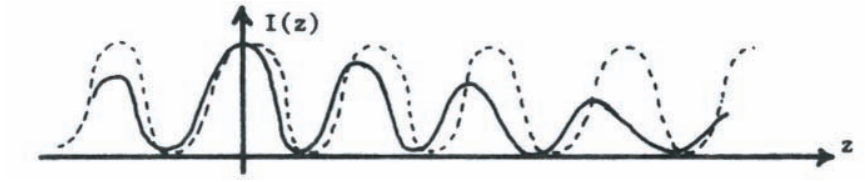

Figure 30.6: The interference pattern for the case of a polychromatic source.

Similarly at a plane $z =$ constant (very large):

$$I(x,y) \approx \frac{2\tilde{S}_2(0)}{z^2}\left[1 + \underbrace{\frac{|\tilde{S}_{20}\left(\frac{z_0(x^2+y^2)}{cz^2}\right)|}{\tilde{S}_2(0)}}_{\text{contrast}}\cos\left\{2\pi\frac{\overline{\nu_t}z_0(x^2+y^2)}{cz^2} + \sigma_{20}(\ldots)\right\}\right] \tag{30.14}$$

($\sigma_{20} \sim$ shift of fringes.)

$\frac{\tilde{S}(\tau)}{\tilde{S}(0)}$ is what is called the "temporal degree of partial coherence". A fringe shift due to σ_{20} will occur if $S_{20}(\nu_t)$ is not symmetrical, i.e. $S_{20}(\nu_t) \neq S_{20}(-\nu_t)$. Basically this whole treatment (2) of interference from a polychromatic source consists of two parts: microscopic assumptions, as in the first part of this chapter on coherence; and macroscopic overlapping. The microscopic rules say that there are coherent point pairs $(x', y', +z')$ and $(x', y', -z')$ due to the mirror at $z' = 0$. No other point pairs can produce waves which mutually interfere. Now comes the macroscopic part of the coherence problem. The interference fringes from theses various point pairs are very similar, except that different frequencies ν_t cause a mismatch in scale, and (as we will elaborate next), different point pairs produce fringe systems

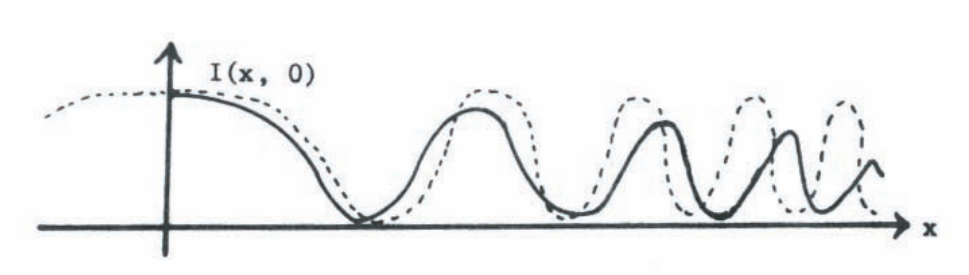

Figure 30.7: The interference pattern for the case of a polychromatic point source at $z = \text{const}$.

which coincide only imperfectly, such reducing the contrast of the total fringe system.

30.2.3 Monochromatic extended source extended perpendicular to the mirror

$$S(x', y', z', \nu_t) = \delta(x', y', \nu_t - \nu_0)\text{rect}\left(\frac{z' - z_0}{\Delta z}\right) \tag{30.15}$$

or somewhat more general: $S_3(z' - z_0)$

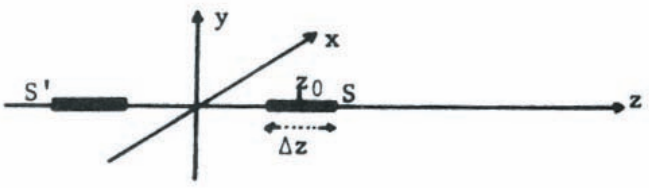

Figure 30.8: Source distribution of a monochromatic extended source including the mirror image of the source.

$$I(x, y, z) = \int S_3(z' - z_0)\left|\frac{e^{ik_0 r_+}}{r_+} + \frac{e^{ik_0 r_-}}{r_-}\right|^2 \mathrm{d}z' \tag{30.16}$$

$$k_0 = 2\pi\frac{\nu_0}{c} \qquad r_\pm\sqrt{x^2 + y^2 + (z \pm z')^2}$$

If y is very large, then:

$$I(x,y,z) \approx \frac{2}{y}\int S_3(z'-z_0)\left[1+\cos\left(2\pi z'\frac{z\nu_0}{cy}\right)\right]\mathrm{d}z' \tag{30.17}$$
$$= \frac{2\tilde{S}_3(0)}{y}\left[1+\frac{\left|\tilde{S}_3\left(\frac{z\nu_0}{cy}\right)\right|}{\tilde{S}_3(0)}\cos\left\{2\pi z\frac{z_0\nu_0}{cy}-\sigma_3\left(\frac{z\nu_0}{cy}\right)\right\}\right]$$

30.2.4 Monochromatic extended source extended parallel to mirror, observed at large z

$$S(x',y',z',\nu_t) = \delta(\nu_t-\nu_0, z'-z_0)S_4(x',y') \tag{30.18}$$

(Do it yourself as a homework problem)

30.3 Tolerances

We found that all the various deviations from the ideal case, where the light comes from a monochromatic point source, manifest themselves in a reduced contrast of the fringes, as well as in a fringe shift:

Ideal: $I = I_0\,[1+\cos(2\pi\nu_c x)]$

Imperfect: $I = I\,[1+V_{21}\cos(2\pi\nu_c x+\sigma_{21})]$

$0 \le V_{12} \le 1$; V_{12} and σ_{12} may be functions of x. V_{21} is sometimes called "contrast"$=\frac{I_{\max}-I_{\min}}{I_{\max}+I_{\min}}$; $I_{\max}\sim\cos=+1$, $I_{\min}\sim\cos=-1$.

It is standard practice to say that $V_{21}\ge 0.8$ is a tolerance, which assures pretty well fringe visibility. Actually, one can see fringes at much lower contrast (or modulation) quite well, and one can pick them up by photoelectric detection too. But 0.8 tolerance criteria are in fashion, I guess, because they lead to simple formulas.

For example consider the case of the polychromatic point source (example # 2 on page 332). Let us specialize:

$$S_{20}(\nu_t) = \mathrm{rect}\left(\frac{\nu_t}{\Delta\nu}\right) \tag{30.19}$$
$$\tilde{S}_{20}(\varrho) = \Delta\nu\,\mathrm{sinc}\,(\varrho\Delta\nu)\,; \qquad |\tilde{S}_2(\varrho)| = |\tilde{S}_{20}(\varrho)|$$
$$\text{contrast} = \frac{|\tilde{S}_2(\varrho)|}{|\tilde{S}_2(0)|} = \mathrm{sinc}(\varrho\Delta\nu) \approx 1-\frac{\pi\varrho\Delta\nu}{3}!$$

It will be >0.8, if $\pi\varrho\Delta\nu<1$. Here we have to insert $\varrho\longrightarrow 2\frac{zz_0}{cy}$. Let us replace $\Delta\nu$ by a corresponding measure expressed in wavelengths. Due to $\nu_t\lambda = c$ it is $\Delta\nu = c\frac{\Delta\lambda}{\lambda}$; hence:

$$\pi\left|\frac{2zz_0}{cy}\right|\cdot c\frac{\Delta\lambda}{\lambda}\le 1; \qquad \text{or} \quad \frac{\Delta\lambda}{\lambda}\ge\left|\frac{2\pi zz_0}{\lambda y}\right| \tag{30.20}$$

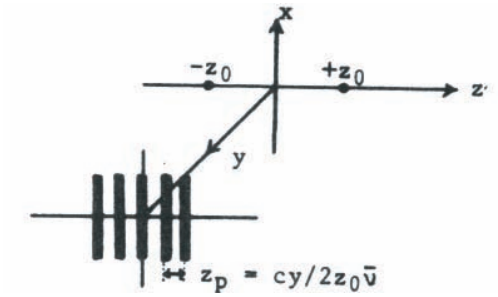

Figure 30.9: Geometry of the fringes formed by a polychromatic point source and its mirror image.

This is a tolerance for the "spectral purity $\frac{\Delta\lambda}{\lambda}$", which is needed for having a fringe contrast ≥ 0.8 at a distance y away from a polychromatic point source, which is doubled into two sources at $z = +z_0$ and $z = -z_0$, both at $x = 0$, $y = 0$. A somewhat different form of the same tolerance can be obtained from observing that the fringe period is $z_P = \frac{cy}{2} z_0 \overline{\nu_t} = \frac{\lambda y}{2 z_0}$. Hence we get:

$$\frac{\lambda}{\Delta\lambda} \geq \pi \left| \frac{z}{z_p} \right| \tag{30.21}$$

That means that within $-z_{\max}$ and $+z_{\max}$ there will be fringes with contrast better than 0.8. $z_{\max}$ is given by $\frac{\lambda}{\Delta\lambda} = \pi \frac{z_{\max}}{z_P}$; $2\frac{z_{\max}}{z_P}$ is the number of high contrast fringes. This number will be $2\frac{z_{\max}}{z_P} = \frac{2}{\pi}\frac{\lambda}{\Delta\lambda}$. Hence you may remember as a rule of thumb that the number of high-contrast fringes equals about the spectral purity of the source.

30.4 Solution of the example # 4, suggested for self-study:

Remember some facts about the Fresnel transform:

$$\breve{u}(x,y,\eta) = \frac{1}{\lambda\eta} \iint u(x',y') e^{-\frac{i\pi}{\lambda\eta}\{(x-x')^2+(y-y')^2\}} \mathrm{d}x'\mathrm{d}y' \tag{30.22}$$

$$\hat{u}(x,y,\eta) = \frac{1}{\lambda\eta} \iint \ldots e^{+\cdots} \ldots \mathrm{d}x'\mathrm{d}y'$$

$$\{\breve{u}^*\} = \{\hat{u}\}^* \qquad \text{and} \qquad \hat{\{u^*\}} = \{\breve{u}\}^*$$

If $u = u^*$ (real), then $\breve{u} = \hat{u}^*$ and $\hat{u} = \breve{u}^*$.

In the problem the source was described as:

$$S(x',y',z',\nu_t) = \delta(\nu_t - \nu_0, z' - z_0) S_4(x',y') \tag{30.23}$$

z very large:

$$\frac{1}{r_\pm} \approx \frac{1}{z}; \qquad r_\pm = \sqrt{(z \pm z_0)^2 + (x-x')^2 + (y-y')^2} \tag{30.24}$$

$$r_\pm \approx z \pm z_0 + \frac{(x-x')^2 + (y-y')^2}{2(z \pm z_0)}$$

$$r_+ - r_- \approx 2z_0 - \frac{(x-x')^2 + (y-y')^2}{\frac{z^2}{z_0}}$$

abbreviate: $\frac{z^2}{z_0} = \eta$.

$$\begin{aligned} I(x,y) &\approx \frac{2}{z^2} \iint S_4(x',y') \left[1 + \cos\left\{\frac{2\pi\nu_0}{c}\left(2z_0 - \frac{(x-x')^2 + (y-y')^2}{\frac{z^2}{z_0}}\right)\right\}\right] \mathrm{d}x'\mathrm{d}y' \\ &= 2\frac{\tilde{S}_4(0,0)}{z^2} + \frac{1}{z^2}\iint S_4(x',y') e^{+i\{\ldots\}} \mathrm{d}x'\mathrm{d}y' + \qquad (30.25) \\ &+ \frac{1}{z^2}\iint S_4 e^{-i\{\ldots\}} \mathrm{d}x'\mathrm{d}y' = \\ &= \frac{2\tilde{S}_4(0,0)}{z^2} + \frac{e^{2\pi i\nu_0 2\frac{z_0}{c}}}{z^2}\lambda\eta\check{S}_4(x,y) + \frac{e^{-2\pi i\nu_0 2\frac{z_0}{c}}}{z^2}\lambda\eta\hat{S}(x,y) \end{aligned}$$

$\check{S}_4 = |\check{S}_4| e^{i\sigma_4}$; due to $S_4 = S_4^*$ it is $\hat{S}_4 = \check{S}_4^* = |\check{S}_4| e^{-i\sigma_4}$, hence:

$$I(x,y) = \frac{2\tilde{S}_4(0,0)}{z^2} + \frac{2\lambda}{z_0}\left|\check{S}_4(x,y;\frac{z^2}{z_0})\right| \cos\left\{2\pi\nu_0\frac{2z_0}{c} + \sigma_4(\ldots)\right\} \tag{30.26}$$

(herein we replace $\eta = \frac{z^2}{z_0}$, hence $\frac{\lambda\eta}{z^2} = \frac{\lambda}{z_0}$).

In this problem the method of stationary phase yields a very poor result, since with $z \gg z_0$ (observation far away) the exponential function does not oscillate wildly, only mildly. The method of stationary phase requires that the exponent varies over many 2πs within the region of integration.

30.5 Coherence — Division of the Wavefront

For example, double-slit diffraction.

Coordinate system:

Start with a monochromatic component $\overline{\nu_t}$ of a single source point $(\overline{x}, \overline{y})$.

$$\iiint S(\overline{x},\overline{y},\overline{\nu_t})\delta(x-\overline{x}, y-\overline{y}, \nu_t - \overline{\nu_t})\, \mathrm{d}\overline{x}\, \mathrm{d}\overline{y}\, \mathrm{d}\overline{\nu_t} \tag{30.27}$$

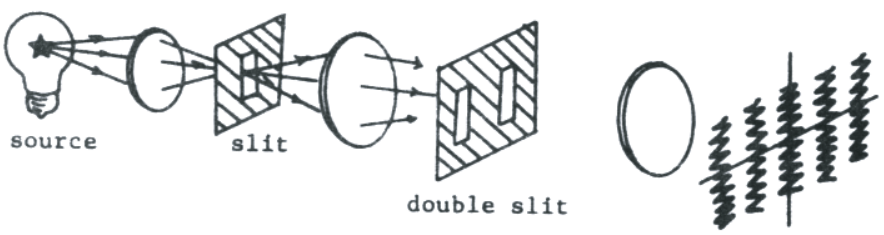

Figure 30.10: The optical setup of the double slit experiment.

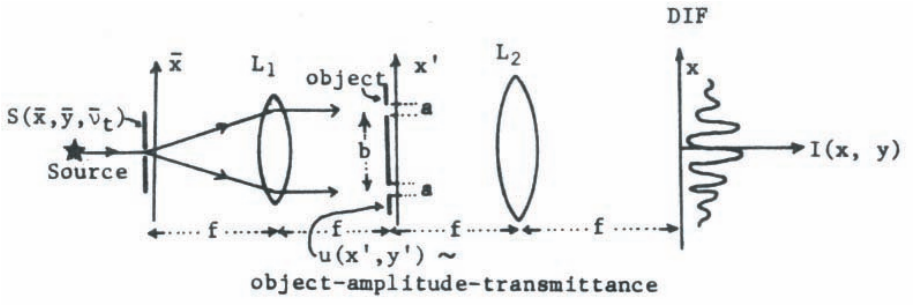

Figure 30.11: The parameters in the double slit experiment.

Monochromatic tilted plane wave falling onto the object:

$$\delta \text{ (in source)} \longrightarrow e^{-2\pi i\left(\frac{\overline{\nu_t}}{c\overline{t}}\right)(\overline{x}x'+\overline{y}y')} \text{ (before object)} \tag{30.28}$$

Let us assume an object which has the same amplitude transmittance $u(x', y')$ for every ν_t. Behind the object we have:

$$u(x', y')e^{-2\pi i\left(\frac{\overline{\nu_t}}{c\overline{f}}(\overline{x}x'+\overline{y}y')\right)} \tag{30.29}$$

The lens L_2 performs another Fourier transformation:

$$\begin{aligned} &\iint u(x', y')e^{-2\pi i\left(\frac{\overline{\nu_t}}{c\overline{f}}(\overline{x}x'+\overline{y}y'+x'x+y'y)\right)}\,\mathrm{d}x'\,\mathrm{d}y' = \\ = \quad &\iiiint \tilde{u}(\nu,\mu)e^{-2\pi i\left(\frac{\overline{\nu_t}}{c\overline{f}}(\ldots)\right)}e^{+2\pi i(\nu x'+\mu y')}\mathrm{d}(x'\ y'\ \nu\ \mu); \end{aligned} \tag{30.30}$$

Herein: $\int \ldots \mathrm{d}x' = \delta\left(\nu - \left(\frac{\overline{\nu_t}}{c\overline{f}}\right)(\overline{x}+x)\right)$; $\int \ldots \mathrm{d}\nu \sim \nu \rightarrow \frac{\overline{\nu_t}}{c\overline{f}}(\overline{x}+x)$.

Similarly, $\iint \ldots \mathrm{d}y'\mathrm{d}\mu \sim \mu \to \frac{\overline{\nu_t}}{cf}(y+\overline{y})$; hence as complex amplitude in plane DIF,

$$\tilde{u}\left(\frac{\nu_t}{cf}(x+\overline{x}, \frac{\nu_t}{cf}(y-\overline{y}))\right) \tag{30.31}$$

This is the Fourier transform of u as expected but with theses two features:

1. shifted sidewise according to the source point position $\overline{x}, \overline{y}$;
2. a wavelength-proportional magnification. ($\frac{\overline{\nu_t}}{c} = \frac{1}{\lambda}$; magnification appears as a denominator of the coordinate.)

Now let us take into account not only the one source point $\overline{x}, \overline{y}$ and not only one spectral component $\overline{\nu_t}$, but all radiation emitted by the source. As we have discussed before, different frequencies $\overline{\nu_t}$ do not interfere. Also light from different atoms does not interfere. Since the source-slit (or any other shape of source mask) is illuminated by an image of the original source (see Fig. 30.10), different points $(\overline{x}, \overline{y})$ correspond to different atoms of the original source. Hence we must add up intensities (rather than complex amplitudes) from different sources:

$$I(x,y) = \iiint \left|\tilde{u}\left(\frac{\overline{\nu_t}}{cf}(x+\overline{x}), \frac{\overline{\nu_t}}{cf}(y+\overline{y})\right)\right|^2 S(\overline{x}, \overline{y}, \overline{\nu_t})\, \mathrm{d}\overline{x}\, \mathrm{d}\overline{y}\, \mathrm{d}\overline{\nu_t} \tag{30.32}$$

In this context the following nomenclature is commonly used:

coherent integration: $\left|\int u \mathrm{d}x\right|^2$; incoherent integration: $\int |u|^2 \mathrm{d}x$,
whereby $u = u(x)$ is a complex amplitude. The difference is in the *sequence* of addition (= integration) and modulus-squaring.

To appreciate this general formula better, we will discuss some special cases.

30.5.1 Polychromatic point source

$$S(\overline{x}, \overline{y}, \overline{\nu_t}) = \delta(\overline{x}, \overline{y}) S_2(\overline{\nu_t}) \tag{30.33}$$
$$\longrightarrow I(x,y) = \int \left|\tilde{u}\left(\frac{\overline{\nu_t x}}{cf}, \frac{\overline{\nu_t y}}{cf}\right)\right| S_2(\overline{\nu_t})\, \mathrm{d}\overline{\nu_t}$$

In general this will not be a clean picture $I(x,y)$ of the spatial power spectrum $|\tilde{u}(\nu,\mu)|$ because during the integration several such spatial power spectra will overlap, with magnification mismatch, which will cause a blur. The magnification is $M = \frac{cf}{\overline{\nu_t}}$. The damage caused by this magnification mismatch will become clearer, if we specialize even further by assuming as object a double slit (Fig. 30.12).

$$u(x',y') = \left[\mathrm{rect}\left(\frac{x-b/2}{a}\right) + \mathrm{rect}\left(\frac{x+b/2}{a}\right)\right] \mathrm{rect}\left(\frac{y}{h}\right) \tag{30.34}$$
$$\tilde{u}(\nu,\mu) = 2a\, h\, \mathrm{sinc}(\nu a)\, \mathrm{sinc}(\mu h)\, \cos(\pi \nu b)$$
$$|\tilde{u}(\nu,\mu)|^2 = 2(a\, h)^2\, \mathrm{sinc}^2(\nu\, a)\, \mathrm{sinc}^2(\mu h)[1+\cos(2\pi\nu b)]$$

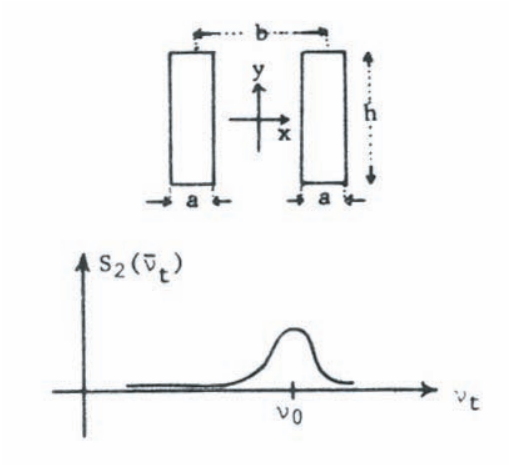

Figure 30.12: The parameters for the doubleslit experiment with a polychromatic point source.

Now set $\mathrm{sinc}^2\left(\frac{\overline{\nu_t}x}{cf}a\right) \approx \mathrm{sinc}^2\left(\frac{\nu_0 x}{cf}a\right)$ and $\mathrm{sinc}^2\left(\frac{\overline{\nu_t}y}{cf}h\right) \approx \mathrm{sinc}^2\left(\frac{\nu_0 y}{cf}h\right)$. Then we can pull these factors in front of the integral, to make it more tractable. This is justified since sinc is a smooth function, almost constant, if ν_t does not vary much in the region of interest.

$$I(x,y) \approx \mathrm{sinc}^2 \ldots \mathrm{sinc}^2 \ldots 2(ah)^2 \int \left[1 + \cos\left(2\pi \frac{\overline{\nu_t}x}{cf} b\right)\right] S_2(\overline{\nu_t}) \mathrm{d}\overline{\nu_t} \tag{30.35}$$

$$I(x,y) = \underbrace{I_0(x,y)}_{\substack{\text{smooth enve-}\\ \text{lope}}} \left[1 + \underbrace{V_2\left(\frac{x}{x_p \nu_o}\right)}_{\text{contrast}} \cos\left\{2\pi \frac{x}{x_P} - \underbrace{\sigma_2\left(\frac{x}{x_P \nu_0}\right)}_{\substack{\text{causes fringe}\\ \text{shift}}}\right\}\right]$$

Herein we assumed again $S_2(\overline{\nu_t}) = S_{20}(\overline{\nu_t - \nu_0}) \longrightarrow \tilde{S}_2(\varrho) = \tilde{S}_2(\varrho) = \tilde{S}_{20}(\varrho) e^{-2\pi i \nu_0 \varrho}$; $\overline{\nu_0} = \frac{\int \overline{\nu_t} S_2(\overline{\nu_t}) \mathrm{d}\overline{\nu_t}}{\int S_2(\overline{\nu_t}) \mathrm{d}\overline{\nu_t}}$; $\tilde{S}_{20} = |\tilde{S}_{20}| e^{i\sigma_2}$.

We used the following abbreviations:

$$\begin{aligned} &2(ah)^2 \mathrm{sinc}^2 \ldots \mathrm{sinc}^2 \ldots \tilde{S}_2(0) = I_0(x,y) \\ &\frac{cf}{\nu_0 b} = x_p \text{ (period)}; \quad \frac{|\tilde{S}_{20}(\varrho)|}{\tilde{S}_{20}(0)} = V_2(\varrho) \end{aligned} \tag{30.36}$$

In other words, the "contrast" of these fringes yields the modulus $|S_2(\varrho)|$ of the Fourier transform of the source spectrum $S_2(\overline{\nu_t})$ and the fringe shifts $\frac{\sigma_2}{2\pi x_P}$ indicate the argument of

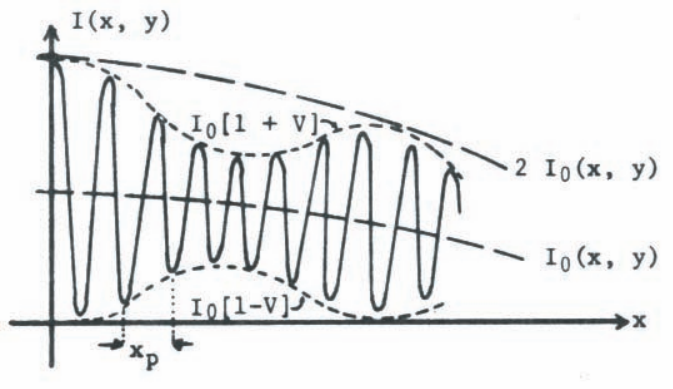

Figure 30.13: Interference pattern generated by a double slit illuminated by a polychromatic point source.

that Fourier transform. From measuring both quantities one can deduce $\tilde{S}_2$, and the source spectrum $S(\overline{\nu_t})$ itself by means of a Fourier transformation. This is another example of Fourier spectrometry.

30.5.2 Extended monochromatic source

$$S(\overline{x},\overline{y},\overline{\nu_t}) = S(\overline{x},\overline{y})\delta(\overline{\nu_t}-\nu_0) \tag{30.37}$$

We insert this into the general formula on Eq. 30.32, which becomes now

$$I(x,y) = \iint \left|\tilde{u}\left(\frac{\nu_0}{cf}(x+\overline{x}),\frac{\nu_0}{cf}(y+\overline{y})\right)\right|^2 S_3(\overline{x},\overline{y})\mathrm{d}\overline{x}\mathrm{d}\overline{y} \tag{30.38}$$

let us take again the double slit as object and set $\frac{\nu_0}{cf} = \frac{1}{\lambda f}$.

$$I_0(x,y) = I_0(x,y)\iint\left[1+\cos\left\{2\pi\frac{b(x+\overline{x})}{\lambda f}\right\}S_3(\overline{x},\overline{y})\right]\mathrm{d}\overline{x}\mathrm{d}\overline{y} \tag{30.39}$$

within the small region where $S_3(\overline{x},\overline{y})$ may be $\neq 0$. The smooth function $I_0(x,y)$ was obtained again by pulling two sinc-functions in front of the integral, which is justified. Now we define:

$$\tilde{S}_3(\nu,\mu) = \iint S_3(\overline{x},\overline{y})e^{-2\pi i(\overline{x}\nu+\overline{y}\mu)}\,\mathrm{d}\overline{x}\,\mathrm{d}\overline{y} = |\tilde{S}_3|e^{i\sigma_3} \tag{30.40}$$

$$\text{(and)}\qquad I_0(x,y) = \tilde{S}_3(0,0)\,\mathrm{sinc}^2(\frac{ax}{\lambda f})\,\mathrm{sinc}^2(\frac{hy}{\lambda f})2(ah)^2$$

Then we obtain after using the ordinary Fourier-δ tricks:

$$I(x,y) \approx I_0(x,y)\left[1 + \frac{|\tilde{S}_3\left(\frac{b}{\lambda},0\right)|}{\tilde{S}_3(0,0)}\cos\left\{2\pi\frac{bx}{\lambda f} - \sigma_3\left(\frac{b}{\lambda f},0\right)\right\}\right] \tag{30.41}$$

By measuring the contrast and fringe shift of $I(x,y)$ one can determine the spatial spectrum $\tilde{S}_3$ of the source. Michelson did this in his famous Stellar Interferometer experiments ($\sim$ 1900 in Cleveland, $\sim$ 1920 in Pasadena). His source was a star whose diameter was too small to be measured in an ordinary telescope. He started from the assumption that his source is rotationally symmetric:

$$S(x,y) = \begin{cases} +1, & \text{if } \overline{x}^2 + \overline{y}^2 \le r_0^2 \\ 0, & \text{otherwise;} \end{cases} \tag{30.42}$$

Hence it is enough to know $S_3(\nu,0)$ only along the ν-axis since $\tilde{S}_3$ also is rotationally symmetric. For objects without rotational symmetry one has to perform a whole series of experiments with different orientations of the double slit (Fig. 30.14).

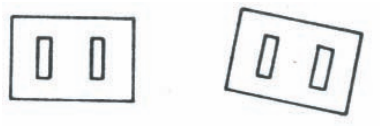

Figure 30.14: Double slit at different angular orientations.

A simple Fourier calculation of a type we have done before shows that a disk object $S_3(\overline{x},\overline{y})$ has as its transform $\nu^2 + \mu^2 = \varrho^2$; $\frac{\mu}{\nu} = \tan(\theta)$.

$$\begin{aligned} \tilde{S}_3(\nu,0) &= \tilde{S}_3(\varrho,\theta) = \tilde{S}_3(\varrho,0) \\ \tilde{S}_3(\varrho) &= \tilde{S}_3(0)\frac{J_1(2\pi r_0\varrho)}{\pi r_1\varrho}; \end{aligned} \tag{30.43}$$

in our case: $\varrho \to \frac{b}{\lambda f}$.

Michelson varied the distance b of the two slits and looked for the contrast to go down to the first zero of the $2\frac{J_1(z)}{z}$ function. He also had to use spectral filters to monochromatize the light. The observations required quite a bit of diligence, because the fringes were dancing due to turbulence. Only a few people dared to take up Michelson's difficult technique. A modern continuation, which uses rooms full of electrics, is the Hanbury Brown-Twiss stellar diameter method, where intensity fluctuations as measured at two points (maybe 100 m apart) are correlated. HB still believes it is a good method since he works on it in the middle of the lonely bush country in Australia. T thinks it is hopeless, as he expressed in Optica Acta, 1968. T lives in London.

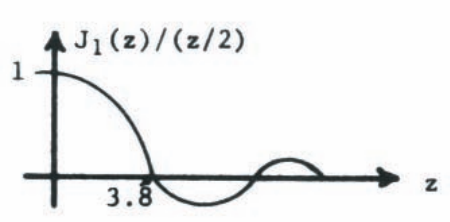

Figure 30.15: The shape of the first order Bessel function J_1.

30.6 Coherence — division by grating diffraction

This type of beam-splitting is omitted in most treatments of interference, but as Leith & Upatnieks have shown in JOSA 57, 975 (1967) it is in a way the best way for holography with thermal light sources. We will come back to this subject. At the present time let us discuss the coherence properties of this type of interference setup, which are responsible for its usefulness (Optica Acta 9, 1, 1962).

30.7 Coherence—Division by a scatter plate (Jim Burch ∼1950)

The scatter plate interferometer is nice and cheep but rarely used or mentioned in the literature. My guess is that most scientists mistrust instruments with statistical components, and dislike statistics even in those rare occasions where it is constructively useful, not merely stating how bad things are in average.

30.8 Partial Coherence in Case of Wavefront Division

This is a repetition, but in a slightly different form, more similar to the Born & Wolf style. The (normalized) complex degree of coherence is defined as the "complex contrast" of a fringe system in the observation plane, produced by the source S, which illuminates two pinholes at (x_1, y_1) and (x_2, y_2) in the object plane. "Complex contrast" means contrast in the ordinary sense, multiplied by a phase factor, which accounts for a fringe shift.

$$\begin{aligned} \text{ideal}: 1+\cos(2\pi\nu_x x) \qquad & \text{actual}: 1+\mathrm{Re}\left\{\gamma e^{2\pi i\nu_x x}\right\} = \\ = 1+\mathrm{Re}\left\{V_{12}e^{i\beta_{21}}e^{2\pi i\nu_x x}\right\} \quad &= \quad 1+V_{21}\cos(2\pi\nu_x+\beta_{21}) \\ \gamma_{21}=V_{21}e^{i\beta_{21}} \qquad & \text{is a "complex contrast"} \end{aligned} \tag{30.44}$$

For determining γ we compute the output intensity $I(x, y)$ for a *particular* "object" out of two pinholes.

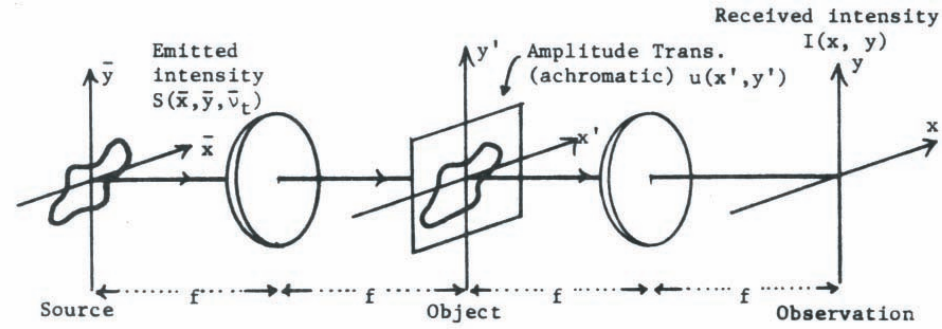

Figure 30.16: Schematic of the experimental setup for analyzing partial coherence.

$$\begin{aligned} u(x',y') &= \delta(x'-x_1,y'-y_1)+\delta(x'-x_2,y'-y_2) \\ &\Longrightarrow \tilde{u}(\nu,\mu) = e^{-2\pi i(\nu x+\mu y)}+e^{2\pi i(\nu x+\mu y)} \\ &\Longrightarrow |\tilde{u}(\nu,\mu)|^2 = 2\left[1+\cos\left\{2\pi[\nu(x_1-x_2)+\mu(y_1-y_2)]\right\}\right] \end{aligned} \tag{30.45}$$

The spatial frequency ν is displayed at $x = \lambda f\nu$. For λ we write now better $\lambda = \frac{c}{\nu_t}$, because λ would occur in the denominator of the exponent. When inserting this specific $|\tilde{u}|^2$ into the main formula Eq. 30.32, we have to replace ν and μ according to $\nu \to \overline{\nu_t}\frac{x+\overline{x}}{cf}$; $\mu \to \overline{\nu_t}\frac{y+\overline{y}}{cf}$.

$$\begin{aligned} I(x,y) &= 2\iiint \left[1+\cos\{\ldots\}\right] S(\overline{x},\overline{y},\overline{\nu_t})\,\mathrm{d}\overline{x}\,\mathrm{d}\overline{y}\,\mathrm{d}\overline{\nu_t} \\ &= 2\iiint S(\overline{x},\overline{y},\overline{\nu_t})\,\mathrm{d}\overline{x}\,\mathrm{d}\overline{y}\,\mathrm{d}\overline{\nu_t}\left[1+\mathrm{Re}\left\{\gamma_{12}e^{2\pi i\frac{\nu_0}{cf}[x(x_1-x_2)+y(y_1-y_2)]}\right\}\right] \end{aligned} \tag{30.46}$$

with $\nu_0 = \frac{\iiint \overline{\nu_t}\,S\,\mathrm{d}\overline{x}\,\mathrm{d}\overline{y}\,\mathrm{d}\overline{\nu_t}}{\iiint S\,\mathrm{d}\overline{x}\,\mathrm{d}\overline{y}\,\mathrm{d}\overline{\nu_t}}$.

In the two special cases:

$$\begin{aligned} S &= \delta(\overline{x},\overline{y})S_2(\overline{\nu_t}) && \text{polychromatic point source} \\ S &= S_3(\overline{x},\overline{y})\delta(\overline{\nu_t}-\nu_0) && (\text{extended monochromatic source}) \end{aligned} \tag{30.47}$$

one gets a Fourier relationship between γ_{21} and S, which is in the case of the extended monochromatic source referred to as Zernike-Van Cittert theorem. Actually both Fourier relationships were known already to Michelson, who made practical use of them in his stellar diameter interferometer and in his experiments on Fourier spectrometry.

γ and Γ are (in most books) connected like $\gamma(x_1-x_2) = \frac{\Gamma(x_1-x_2)}{\Gamma(0)}$. Yet another way to arrive at the same goal is by replacing in the main formula (Eq. 30.32):

$$|u(\nu,\mu)|^2 \quad = \quad \iiiint u(x',y')\; u^*(x'',y'')e^{-2\pi i[\nu(x'-x'')+\mu(y'-y'')]}\;\mathrm{d}(x'\;y'\;x''\;y'')$$

$$\text{with}: \gamma \quad \longrightarrow \quad \frac{\overline{\nu_t}}{cf}(x+\overline{x}) \quad \text{and}\; \mu \longrightarrow \frac{\overline{\nu_t}}{cf}(y+\overline{y}) \tag{30.48}$$

$$I(x,y) \quad = \quad \iiiint u(x',y')\; u^*(x'',y'')\Gamma(x'-x'',y'-y'')\cdot \tag{30.49}$$

$$\cdot \quad e^{2\pi i\frac{\nu_0}{cf}[x(x'-x'')+y(y'-y'')]}\;\mathrm{d}(x'\;y'\;x''\;y'')$$

$$\Gamma = \iint S(\overline{x},\overline{y},\overline{\nu_t})e^{\frac{2\pi i}{cf}[\ldots]}\;\mathrm{d}(\overline{x}\;\overline{y}\;\overline{\nu_t}) \tag{30.50}$$

$$[\ldots] = (x'-x'')(\overline{x\nu_t}+x\overline{\nu_t}-x\nu_0)+(y'-y'')(\overline{y\nu_t}+y\overline{\nu_t}+y\nu_0)$$

Notice: sometimes the "carrier frequency factor" $e^{2\pi i\frac{\nu_0}{cf}[x(x'-x''\ldots)]}$ is also included into the definition of Γ, which is then called "mutual intensity".

30.9 A Final Look at Coherence Theory

Before closing the chapter on coherence theory let us once more treat the general case of two-beam interferences as produced by an extended polychromatic source. At proper points of this theory we will utilize the atomistic properties of thermal light. The setup consists of a source, an interferometer, and a plane of observation (Fig. 30.17). Due to the two-beam interferometer light from the source point x' can reach the observation point x along two different paths. The two optical path lengths are called $L_1(x,x')$ and $L_2(x,x')$. "Optical path" means "geometrical path" times "index of refraction". This definition of optical path length is meaningful since it is proportional to the travel time of a wave crest.

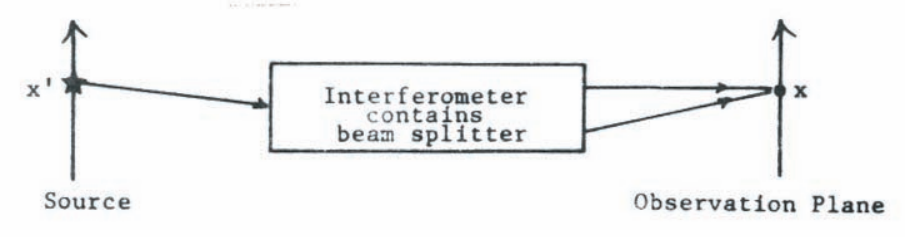

Figure 30.17: Schematic of a two beam interferometer.

$$\mathrm{d}L = n\mathrm{d}s; \qquad \frac{\mathrm{d}L}{c} = \frac{\mathrm{d}s}{\frac{c}{n}} = \frac{\mathrm{d}s}{v} = \mathrm{d}t \tag{30.51}$$

The amplitude may be attenuated by factors $A_1(x,x'')$ and $A_2(x,x')$ in these two paths. If the complex amplitude of the source is $V_S(x',t)$, then the complex amplitude at the observation point x is:

$$V(x,t) = V_1(x,t) + V_2(x,t); \tag{30.52}$$
$$V_1(x,t) = \int A_1(x,x')V_S(x',t-\frac{L_1(x,x')}{x})\mathrm{d}x'$$

V_2 correspondingly; $\frac{L}{c}$ = travel time from x' to x.
The recorded intensity (for example on a photograph) is:

$$\begin{aligned} I(x) &= \int_0^T |V(x,t)|^2\mathrm{d}t = \int |V_1|^2\mathrm{d}t + \int |V_2|^2\mathrm{d}t + \int V_1V_2^*\mathrm{d}t + \int V_1^*V_2\mathrm{d}t \\ &= I_1(x)I_2(x) + 2I_{12}(x) \end{aligned} \tag{30.53}$$

Actually $|V|^2$ should be called "intensity" and $\int |V|^2\mathrm{d}t$ the "exposure". But it is quite common to call almost every modulus-square term an "intensity". The interference term I_{12} is called "mutual intensity". Its normalized version is the "degree of partial coherence" $\frac{I_{12}}{\sqrt{I_1I_2}}$, which is usually indicated as "gamma" (upper case or lower case).

Now let us discuss $I(x)$ in more detail. We will compute $\int V_1V_2^*\mathrm{d}t$. This is enough calculation labor since the other three terms of $I(x)$ can be deduced formally by changing the indices "1" and "2" accordingly. As a first step we represent the source amplitude by its temporal frequency composition:

$$V_S(x',t) = \int \tilde{V}_S(x',\nu')e^{2\pi i\nu' t}\mathrm{d}\nu' \tag{30.54}$$

Inserting now V_S into $\int V_1V_2^*\mathrm{d}t$ we get:

$$\int V_1V_2^*\mathrm{d}t = \tag{30.55}$$
$$= \iint A_1(x,x')A_2(x,x')V_S\left(x',t-\frac{L_1(x,x')}{c}\right)V_S^*(x'',t-\frac{L_2(x,x'')}{c})\ \mathrm{d}(x'\ x''\ t)$$
$$= \iiiint A_1A_2\tilde{V}_S(x',\nu')\tilde{V}_S(x'',\nu'')e^{2\pi i[\ldots]}\ \mathrm{d}(x'\ x''\ \nu'\ \nu''\ t) \tag{30.56}$$

where: $[\ldots] = \nu'\left\{t-\frac{L_1(x,x')}{c}\right\} - \nu''\left\{t-\frac{L_1(x,x'')}{c}\right\}$

The exposure time T must always be *very* large compared to the light period $\frac{1}{\nu'}$. Otherwise we would not collect enough photons for the plate. Hence the t-integral is essentially a δ-function.

$$\int e^{2\pi i t(\nu'-\nu'')}\mathrm{d}t = \delta(\nu'-\nu''); \qquad \int \ldots \mathrm{d}\nu'' \sim \nu'' \longrightarrow \nu' \tag{30.57}$$

Now we get:

$$\int V_1 V_2^* \mathrm{d}t = \iiint A_1 A_2 \tilde{V}_S(x',\nu)\tilde{V}_S^*(x'',\nu) e^{-2\pi i \nu \frac{L_1-L_2}{c}} \,\mathrm{d}(x'\; x''\; \nu) \tag{30.58}$$

To get ahead we must now make some specific assumptions about the source. The following model is general enough but still manageable. Two types of wave trains $V_A(t)$ and $V_B(t)$ can be produced at any point x' of the source. But the beginnings of the spontaneous emission acts are assumed to be at random. Hence we write:

$$V_S(x',t) = \sum_{n=0}^{N(x')} V_A(t-\tau_n(x')) + \sum_{m=0}^{M(x')} V_B(t-\tau_m(x')) \tag{30.59}$$

In other words at point x' there will be $N(x')$ emissions of wave train type A during the exposure time and $M(x')$ wave trains of type B. The starting times are indicated by $\tau_n(x')$ and $\tau_m(x')$. (Actually τ_n should have an index A, and τ_m an index B. That would look clumsy in writing, but it should be understood.) For $\int V_1 V_2^*$ we need the temporal spectrum $\tilde{V}_S(x',\nu)$.

$$\begin{aligned}
\tilde{V}_S(x',\nu) &= \tilde{V}_A(\nu)\sum_{(m)} e^{-2\pi i\nu\tau_n(x')} + \tilde{V}_B(\nu)\sum_{(m)} e^{-2\pi i\nu\tau_m(x')}; \qquad (30.60)\\
\tilde{V}_S(x',\nu)\tilde{V}_S^*(x'',\nu) &= |\tilde{V}_A(\nu)|^2 \sum_{(n)}\sum_{(\overline{n})} e^{-2\pi i\nu[\tau_n(x')-\tau_{\overline{n}}(x'')]} + \\
&+ |\tilde{V}_B(\nu)|^2 \sum_{(m)}\sum_{(\overline{m})} e^{-2\pi i\nu[\tau_m(x')-\tau_{\overline{m}}(x'')]} + \\
&+ \tilde{V}_A(\nu)\tilde{V}_B^*(\nu)\sum_{(n)}\sum_{(m)} e^{-2\pi i\nu[\tau_n(x')-\tau_m(x'')]} + \text{c. c.}
\end{aligned}$$

This expression will now be inserted into:

$$\int V_1 V_2^* \mathrm{d}t = \iiint A_1 A_2 \tilde{V}_S(x',\nu)\tilde{V}_S^*(x'',\nu) e^{-2\pi i \nu \frac{L_1-L_2}{c}} \mathrm{d}(x'\; x''\; \nu) \tag{30.61}$$

Now we utilize the random properties of τ_n and τ_m. The exponent of the first term contains $\tau_n(x') - \tau_{\overline{n}}(x'')$ which is a random variable if $x' \neq x''$ because atoms at x' are unrelated to atoms at x''. Hence that double sum must be proportional to $\delta(x'-x'')$. Now the exponent

contains $\tau_n(x') - \tau_{\overline{n}}(x')$, which is the time delay between the n-th and the $\overline{n}$-th emission (type A) from the atom at x'. Since the emissions occur spontaneously in a thermal source this time delay is a random quantity except for the $n = \overline{n}$ cases of the $\sum_{(n)} \sum_{(\overline{n})}$. The $(n = \overline{n})$ case occurs $N(x')$ times. Hence:

$$\sum_{n=1}^{N(x')} \sum_{\overline{n}}^{N(x'')} e^{-2\pi i \nu [\tau_n(x') - \tau_n(x'')]} = N(x') \delta(x' - x'') \tag{30.62}$$

In general the case $(\nu = 0)$ would deserve a special treatment. But for optical wave trains it is $\tilde{V}(x, 0) = 0$ for $\nu = 0$ (zero time frequency). This number $N(x')$ indicates how many wave trains type A leave point x' during T. The second term of $\tilde{V}_S \tilde{V}_S^*$ yields in the same manner

$$\sum_{(m)} \sum_{(\overline{m})} = M(x') \delta(x' - x'') \tag{30.63}$$

Next we discuss the interaction of the two types (A and B) of wave trains. In the double sum we consider the time difference between the n-th A-emission at x' and the m-th B-emission at x''. Since these two emissions are completely unrelated we get

$$\sum_{(n)} \sum_{(m)} e^{-2\pi i \nu [\tau_n(x') - \tau_m(x'')]} = 0 \tag{30.64}$$

What remains is:

$$\tilde{V}_S(x', \nu) \tilde{V}_S^*(x'', \nu) = [|\tilde{V}_A(\nu)|^2 N(x') + |\tilde{V}_B(\nu)|^2 M(x')] \delta(x' - x'') \tag{30.65}$$

Inserting this into $\int V_1 V_2^* \mathrm{d}t$ we get:

$$\iint A_1(x, x') A_2(x, x') [|\tilde{V}_A(\nu)|^2 N(x') + |\tilde{V}_B(\nu)|^2 M(x')] e^{-2\pi i [\ldots]} \, \mathrm{d}x' \, \mathrm{d}y' \tag{30.66}$$

$[\ldots] = \nu \frac{L_1(x,x') - L_2(x,x')}{c} = \nu \Delta t(x, x')$

Δt is the difference of travel times from source point x' to observation point x along the two paths. Now let us discuss $[|\tilde{V}_A|^2 N + |\tilde{V}_B|^2 M]$ with the goal in mind to generalize our result beyond the specific source model which we have used so far.

$$V_S(x', t) = \sum_{(n)} V_A(t - \tau_n(x')) + \sum_{(m)} V_B(t - \tau_m(x')) \tag{30.67}$$

The term $|\tilde{V}_A(\nu)|^2$ describes the energy between ν and $\nu + d\nu$ from a single emission act of type A. This becomes plausible when the total energy within one wave train type A is computed:

$$\int |V_A(t)|^2 \mathrm{d}t = \int |\tilde{V}_A(\nu)|^2 \, \mathrm{d}\nu \tag{30.68}$$

The term $|\tilde{V}_A(\nu)|^2 N(x')$ describes all the energy in the frequency band $(\nu, \nu + d\nu)$ which comes from type A emissions at the source region $(x', x' + \mathrm{d}x')$ during the whole integration time T. Remember that $N(x')$ was the number of emission acts type A in $(x', x' + \mathrm{d}x')$ during T. Combining $|\tilde{V}_A(\nu)|^2 N(x')$ with $|\tilde{V}_B(\nu)|^2 M(x')$ we get all the source energy in $(x', x' + \mathrm{d}x')$ and in $(\nu, \nu + \mathrm{d}\nu)$ during T, no matter what type of emission generated that energy. In earlier sections we called this quantity $S(x', \nu)$. Hence we write now for the general source which emits $S(x', \nu)$ from $(x', x' + \mathrm{d}x')$ into the temporal frequency band $(\nu, \nu + \mathrm{d}\nu)$ during the total exposure time T:

$$\begin{aligned} \int_0^T V_1(x, x', t) V_2^*(x, x', t) \mathrm{d}t &= \iint A_1(x, x') A_2(x, x') S(x', \nu) e^{-2\pi i \nu \Delta t(x, x')} \, \mathrm{d}x' \, \mathrm{d}\nu \\ \Delta t &= \frac{L_1(x, x') - L_2(x, x')}{c} \end{aligned} \tag{30.69}$$

When adding the conjugate complex $\int V_1^* V_2 \mathrm{d}t$ we get the mutual intensity $I_{12}(x)$, while $I_1(x)$ is simply:

$$\begin{aligned} I_1(x) &= \iint A_1^2(x, x') S(x', \nu) \, \mathrm{d}x' \, \mathrm{d}\nu; \qquad I_2(x) = \iint A_2^2 \, S \, \mathrm{d}x' \, \mathrm{d}\nu \\ I(x) &= I_1(x) + I_2(x) + I_{12}(x) \end{aligned} \tag{30.70}$$

Our result justifies the following general approach to any image formation or diffraction problem where the source is not a point-source and is not monochromatic. First we consider only a single point x' of the source and assume that the light emitted from there is purely monochromatic $e^{2\pi i \nu t}$. This emerging monochromatic spherical wave propagates through lenses, mirrors, prisms, gratings, diffusers, etc. to the observation point x. In case of two-beam interferences there are two distinct paths from x' to x, which is accomplished by some kind of beam-splitter. The amplitude attenuations along those paths are called $A_1(x, x')$ and $A_2(x, x')$, and the optical path lengths $L_1(x, x')$. The arriving complex amplitude is therefore

$$A_1(x, x') e^{2\pi i \nu \left(t - \frac{L_1}{c}\right)} + A_2 e^{2\pi i \nu \left(t - \frac{L_2}{c}\right)} = u(x, x', \nu) \tag{30.71}$$

The path length L introduces a time delay $\frac{L}{c}$ between source and observation point. In the most general case A and L will depend also on the time frequency ν. For example colored glass requires $A = A(x, x', \nu)$, and a dispersive material with refractive index $n = n(\nu)$ will

result in $L = L(x, x', \nu)$. The case we have treated was not so general. It can be called a system with "non-dispersive and achromatic transmission properties".

Now comes the important step. We conclude that different frequencies ν, ν' are unrelated, and also different source points are unrelated. Hence we add intensities $|u(x, x', \nu)|^2$ which arrive from various source points x' with monochromatic oscillators. The weighting function $S(x', \nu)$ describes how much intensity the source at x' emits at frequency ν. The total observed intensity is now

$$I(x) = \iint S(x', \nu)|u(x, x', \nu)|^2 \, \mathrm{d}x' \, \mathrm{d}\nu \tag{30.72}$$

This formula is the same as the previous one, only

$$I(x) = I_1(x) + I_2(x) + 2I_{12}(x) \tag{30.73}$$

is arranged somewhat differently in order to show how the source intensity S and the "impulse response" $|u(x, x', \nu)|^2$ of the propagation system between source and observation point contribute together to the observed intensity. Two more generalizations are conceivable. The sensitivity of the receiver might vary for different frequencies ν and as a function of the observation point. This can be described by a function $R(x, \nu)$:

$$I(x) = \iint S(x', \nu)|u(x, x', \nu)|^2 R(x, \nu) \, \mathrm{d}x' \, \mathrm{d}\nu \tag{30.74}$$

Finally S, u, and/or R may vary as a function of time, and hence also $I(x, t)$. This time-variation generalization is straight forward if all time constants are large to the period of the light frequency. The very last generalization would consider also polarization, which requires a vectorial treatment. One chapter of O'Neill's book is devoted to this subject.

30.10 Group velocity

In a non-dispersive medium (defined as $n(\nu_t) =$ constant) a wave train maintains its shape while propagating. Assume for simplicity only z-dependence, so that the wave equation is simply

$$\frac{\partial^2 V(z,t)}{\partial z^2} - \left(\frac{n}{c}\right)^2 \frac{\partial^2 V}{\partial t^2} \tag{30.75}$$

Any $V(z,t) = V\left(z \pm \frac{ct}{n}\right)$ solves this equation. This means that a given wave train (at $t = 0$) is shifted without losing shape while time progresses (Fig. 30.18).

But if there is dispersion, $n(\nu_t) \neq$ constant, then the wave train changes its shape. To show this we insert $V(z,t) = \int \tilde{V}(z, \nu_t) e^{-2\pi i \nu_t t} \mathrm{d}\nu_t$ into the wave equation:

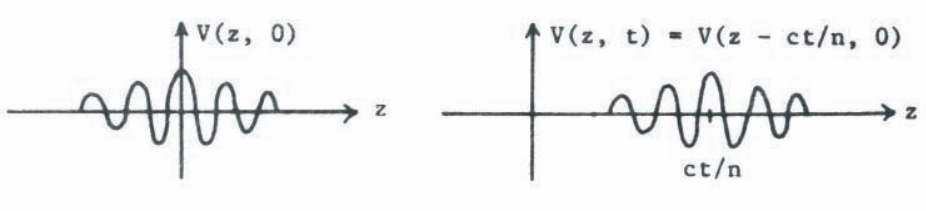

Figure 30.18: A light pulse travelling through a non-dispersive medium.

$$\frac{\partial^2 \tilde{V}}{\partial z^2} + \left(2\pi n \frac{\nu_t}{c}\right)^2 \tilde{V} = 0 \longrightarrow \tilde{V}(z,\nu_t) = \tilde{V}(0,\nu_t) e^{\pm 2\pi i n(\nu_t)\nu_t \frac{z}{c}}$$
$$\Longrightarrow |\tilde{V}(z,\nu_t)|^2 = |\tilde{V}(0,\nu_t)|^2 \tag{30.76}$$

but:

$$V(z,t) = \int \tilde{V}(0,\nu_t) e^{2\pi i \left\{ \left[\nu_t \frac{n(\nu_t)}{c}\right]\left(z - \frac{ct}{n(\nu_t)}\right)\right\}} \mathrm{d}\nu_t. \tag{30.77}$$

The phase velocity $\frac{c}{n(\nu_t)}$ differs for different Fourier components. If for example many Fourier components were *in phase* at $t = 0$, they would build up a strong pulse at $z = 0$, where the maxima of all cosine components coincide. But this coincidence of maxima falls apart as t increases. Hence the pulse will "disperse". What happens in detail to the pulse cannot be said without knowing more about the specific dispersion $n(\nu_t)$. But two things of some generality can be said anyway. The one thing is that the *signal velocity* cannot exceed c in any case. This means that no portion of the light energy can travel faster than c. So, Maxwell's equations are compatible with Einstein's first postulate of his special relativity theory. The proof, which is presented nicely in Sommerfeld's Optics (Theor. Physics, Vol. IV), is based on integration along a path in the complex ν_t domain. Those familiar with Laplace transforms will appreciate the proof easily. The other comment is related to the *group velocity* G. Again look at

$$V(z,t) = \int \tilde{V}(0,\nu_t) e^{2\pi i \left(\nu_t n(\nu_t)\frac{z}{c} - \nu_t t\right)} \mathrm{d}\nu_t \tag{30.78}$$

Assume $\tilde{V}(0,\nu_t)$ broad enough so that this integrand has enough oscillations to justify the method of stationary phase.

$$\frac{\mathrm{d}\left\{\nu_t n(\nu_t)\frac{z}{c} - \nu_t t\right\}}{\mathrm{d}\nu_t} = 0 \longrightarrow \frac{z}{t} = \frac{c}{\frac{\mathrm{d}\{\nu_t n(\nu_t)\}}{\mathrm{d}\nu_t}} = G = \text{group velocity} \tag{30.79}$$

More often it is derived in the form:

$$V = \int \tilde{V} e^{i\{K(\omega)z - \omega t\}} \frac{\mathrm{d}\omega}{2\pi}; \quad G = \frac{\mathrm{d}\omega}{\mathrm{d}K}; \quad \omega = 2\pi\nu_t \tag{30.80}$$

For better visualization assume a fairly sharp pulse shape while $V(z,t)$ is at $z = 0$:

$$V(0,t) = \int \tilde{V}(\omega) e^{-i\omega t} \frac{\mathrm{d}\omega}{2\pi} \tag{30.81}$$

For a pulse, $\tilde{V}(\omega) \approx$ constant, at least around a fairly wide region around the mean frequency ω_0. Now we observe $V(z,t)$ at $z > 0$. We approximate $K(\omega) \approx K(\omega_0) + K'(\omega_0)(\omega - \omega_0)$. The exponent now becomes $K_0 z - K'\omega_0 z + \omega(K'z - t)$. In so far as the linear $K(\omega)$ approximation is good $V(z,t)$ will be the same except for an unimportant factor in all space-time points with the same value of $K'z - t$. These space-time points evolve sequentially at different places according to $\mathrm{d}(K'z - t) = 0 = K'\mathrm{d}z - \mathrm{d}t$, or $\frac{\mathrm{d}z}{\mathrm{d}t} = K'$. An observer moving with velocity K' would see only a static EM field.

31 Polarization

31.1 Polarization and Crystal Optics

You certainly know about the *vectorial* character of electromagnetic waves and you also have heard about "polarization", for example when the Brewster effect was mentioned in connection with the reflection on a boundary between two dielectric media. From the information point of view polarization means that there can be carried twice as many parameters on a vectorial wavefield with two components as compared to a scalar field. In other words a radio wave can carry two messages on its two polarization components. But more important is that some polarization tricks are very useful means for manipulation of a light wave.

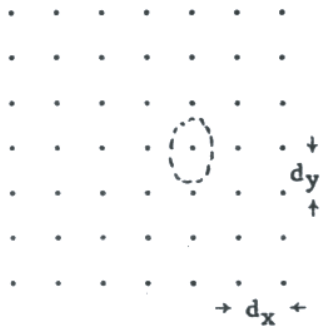

Figure 31.1: Schematic of a crystal lattice.

First let me try to explain qualitatively how double-refraction, the main effect of crystal optics, occurs. Before that we must understand how it comes about that in an isotropic material the phase velocity is reduced from c to $\frac{c}{n}$. The dielectric medium contains many electrons, which are tied to the atoms. These electrons can oscillate if pushed. Their resonance frequency is usually higher than the frequency of visible light. When light passes through such a dielectric material the electrons are forced to join the oscillations of the travelling electric wavefield. Since the forcing frequency does not match the resonance frequency, the electron oscillations will be somewhat out of step. You might have learned this already in connection with forced oscillations in mechanics. Anyway, the forced oscillator will radiate like a dipole, such getting rid again of the energy, which it temporarily extracted from the travelling electric

wave. The remainder of the travelling wave plus the re-radiated wave make up a joint wave, which contains again all the energy, but which is a little bit delayed each time that interaction with so-called "dispersion-electrons" takes place. That is why the phase velocity is reduced from c to $\frac{c}{n}$. A travel time is proportional to the inverse velocity. Hence the time delay due to the dielectric medium is proportional to $n-1$. The more atoms there are the greater the delay. Hence it is plausible that $n-1$ is proportional to the number of electrons per unit volume.

Now imagine a crystal lattice, seen in the direction of light propagation in Fig. 31.1. A typical electron, or maybe a Ψ-wave cloud, around a certain nucleus of the lattice, might have an *elliptical* area to swing in if $d_y > d_x$ (non-cubic crystal). Since the x-neighbours are closer, the Coulomb repulsion in the x-direction will be stronger than in the y-direction. Since the "elastic constant" influences the resonance frequency, and since the difference between resonance frequency and forcing frequency determines the phase delay of the forced oscillation, it should be plausible that the propagation for light with an E-vector in the x-direction will be different from a light-wave with y-polarization. This can be expressed as $n_x \neq n_y$; $\frac{c}{n_x} \neq \frac{c}{n_y}$, which is called "double refraction" or "birefringence". The geometrical dominant directions of the lattice are called "crystal-axis".

31.2 Some crystal-optical elements

31.2.1 Quater-wave plate

Assume $\Delta n \cdot D = \frac{\lambda}{4}$, where $\Delta n = n_x - n_y$. $\Delta\varphi = \frac{2\pi}{\lambda}\Delta n \cdot D = \frac{\pi}{2}$:

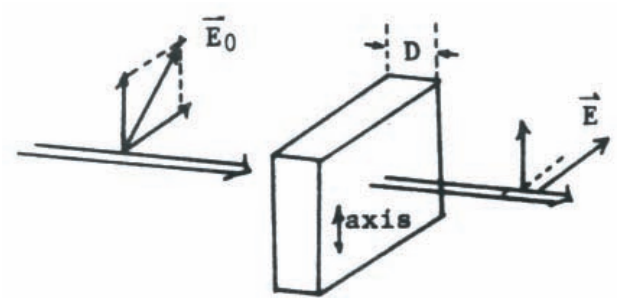

Figure 31.2: The effect of a quater- wave plate.

Before the quater-wave plate assume a *linear* polarization, $45°$ azimuth.

$$\vec{E_0} = \vec{x}_0 \cos(\omega t) + \vec{y} \cos(\omega t) \tag{31.1}$$

After propagation through the quater-wave plate (Fig. 31.2):

$$\begin{aligned} \vec{E} &= \vec{x}_0 \cos(\omega t) + \vec{y}_0 \cos\left(\omega t - \frac{\pi}{2}\right) \\ &= \vec{x}_0 \cos(\omega t) + \vec{y}_0 \sin(\omega t) \end{aligned} \tag{31.2}$$

This corresponds to a *circular* polarization.
A quarter-wave plate can also convert circular-polarized light into linear-polarized light.

31.2.2 Half-wave plate

$\delta n \cdot D = \frac{\lambda}{2}$; $\Delta\varphi = \pi$

$$\begin{aligned} \text{Before}: \quad \vec{E_0} &= \{\vec{x}_0 \cos\theta + \vec{y}_0 \sin\theta\} \cos(\omega t) \\ \text{After}: \quad \vec{E} &= \vec{x}_0 \cos\theta \cos(\omega t) + \vec{y}_0 \sin\theta \cos(\omega t - \pi) = \\ &= \{\vec{x}_0 \cos\theta - \vec{y}_0 \sin\theta\} \cos(\omega t) \end{aligned} \tag{31.3}$$

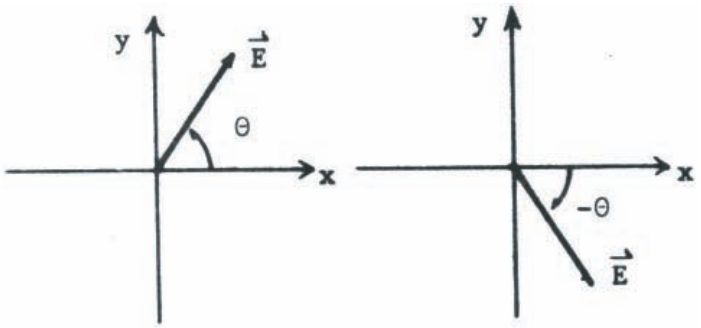

Figure 31.3: Pointer diagram of the polarization directions in front of and behind the half-wave plate.

In other words a half-wave plate performs a flip of the polarization direction.

Δn can be controlled by static electric or magnetic fields. "Static" means that it changes slowly compared to the period of the light itself. Polarization flipping in microseconds and even faster is quite feasible. It is used in "digital light deflectors" which consist of an alternating sequence of pol-flippers and Wollaston prisms. The deflection angle of the n-th Wollaston prism is $\alpha_n = \alpha_1 2^n$. Hence N sequential Wollaston prism with N pol-flippers can "address" 2^N different angles.

The index "n" does not influence only the phase velocity, but it can also cause a deviation of a light beam, called refraction. Already Huygens knew how refraction can be explained in terms of the phase velocity $\frac{c}{n}$. Refraction is pretty much the same as what you experience

when your left car wheel gets onto ice. In generalization of isotropic refraction, the two polarization components of a light wave might experience different amounts of refraction and hence go off into different directions.

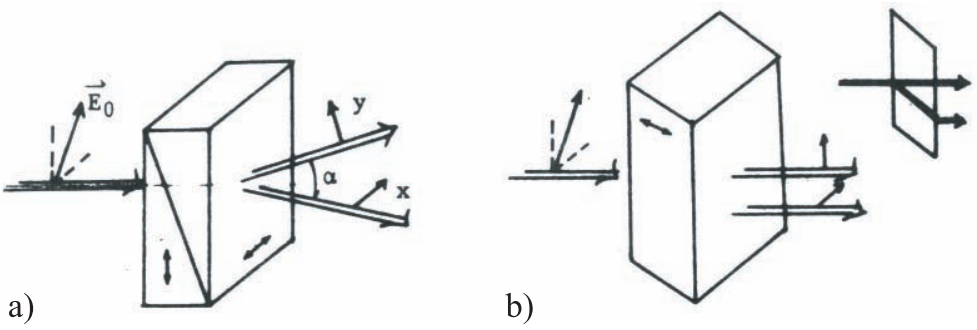

Figure 31.4: Two important polarization optical elements: a) Wollaston prism consisting of two prisms with orthogonal oriented axis; b) Savart plate consisting of a single quartz plate. The entrance and exit surfaces are parallel but the crystal axis is off-orthogonal.

The split angle α of the Wollaston prism (Fig. 31.4 a) is $\alpha \approx 2\beta\Delta n$ where β is the wedge angle. The highest Δn ($CaCO_3$: Calcite) is about $\Delta n = \frac{1}{7}$. More typical is quartz, $\Delta n \approx 0.04$.

31.2.3 Refraction in the Wollaston prism

For the x-component the first wedge may have the refractive index $n_0 + \frac{\Delta n}{2}$, and the second wedge $n_0 - \frac{\Delta n}{2}$, while the y-component of the E-field encounters first $n_0 - \frac{\Delta n}{2}$, and later $n_0 + \frac{\Delta n}{2}$. The first surface may be in normal incidence, hence both "rays" continue straight. The next surface is approached then under an angle β (Fig. 31.5 b):

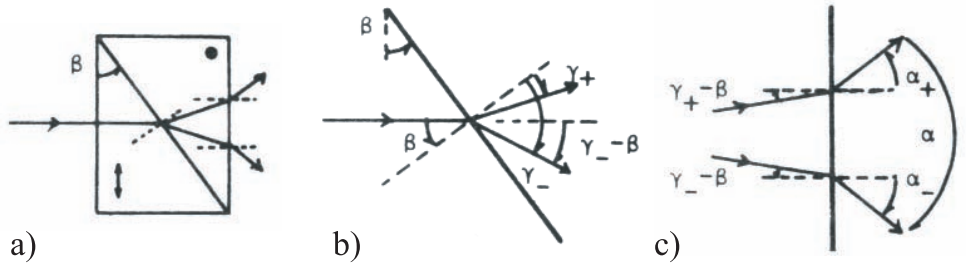

Figure 31.5: Refraction at the Wollaston prism: a) total view; b) refraction at the prism boundary; c) refraction at the exit surface.

x-polarization:

$$\begin{aligned}\left(n_0+\frac{\Delta n}{2}\right)\sin\beta &= \left(n_0-\frac{\Delta n}{2}\right)\sin\gamma_- \\ \left(n_0+\frac{\Delta n}{2}\right)\beta &\approx \left(n_0-\frac{\Delta n}{2}\right)\gamma_- \\ \gamma_- &\approx \beta\frac{n_0+\frac{\Delta n}{2}}{n_0-\frac{\Delta n}{2}}; \\ \gamma_--\beta &\approx \beta\left(\frac{n_0+\frac{\Delta n}{2}}{n_0-\frac{\Delta n}{2}}-1\right)=\frac{\beta\Delta n}{n_0-\frac{\Delta n}{2}}\end{aligned} \tag{31.4}$$

Similarly the y-polarization:

$$\begin{aligned}\left(n_0-\frac{\Delta n}{2}\right)\sin\beta &= \left(n_0-\frac{\Delta n}{2}\right)\sin\gamma_+ \\ \gamma_+-\beta &\approx \frac{-\beta\Delta n}{n_0+\frac{\Delta n}{2}}\end{aligned} \tag{31.5}$$

Next comes the surface towards the air (Fig. 31.5 c):
x-polarization:

$$\left(n_0-\frac{\Delta n}{2}\right)\sin(\gamma_--\beta)=\sin\alpha_-\left(n_0-\frac{\Delta n}{2}\right)(\gamma_--\beta)\approx\alpha_-\approx\beta\Delta n \tag{31.6}$$

y-polarization:

$$\left(n_0+\frac{\Delta n}{2}\right)\sin(\gamma_+-\beta)=\sin\alpha_+\left(n_0+\frac{\Delta n}{2}\right)(\gamma_+-\beta)\approx\alpha_+\approx-\beta\Delta n \tag{31.7}$$

Total angle:

$$\boxed{\alpha=\alpha_--\alpha_+\approx 2\beta\Delta n} \tag{31.8}$$

31.2.4 Circular birefringence

It is most common to decompose the polarization vector or electrical field vector into orthogonal *linear* components.

$$\vec{E}(t)=\vec{x}E_x\cos(\omega t-\varphi_x)+\vec{y}_0E_y\cos(\omega t-\varphi_y) \tag{31.9}$$

Instead of using linear unit polarization vectors one may equally well use *circular* unit polarization vectors.

$$\begin{aligned}\vec{C}_R(t) &= \vec{x}_0\cos(\omega t)+\vec{y}_0\sin(\omega t)\\ \vec{C}_L(t) &= \vec{x}_0\cos(\omega t)-\vec{y}_0\sin(\omega t)\\ \vec{E}(t) &= E_R\vec{C}_R(t-t_R)+E_L\vec{C}_L(t-t_L)\end{aligned} \tag{31.10}$$

These circular unit polarization vectors spin around the z-axis in opposite directions. Orthogonality and normality are defined in the time-average sense.

$$\begin{aligned}\frac{1}{\tau}\int_0^\tau \vec{C}_R\cdot\vec{C}_L\mathrm{d}t &= \frac{1}{\tau}\int\cos(2\omega t)\mathrm{d}t=0; \qquad \tau=\frac{2\pi}{\omega}\\ \frac{1}{\tau}\int_0^\tau \vec{C}_R\cdot\vec{C}_R\mathrm{d}t &= 1=\frac{1}{\tau}\int_0^\tau \vec{C}_L\cdot\vec{C}_L\mathrm{d}t\end{aligned} \tag{31.11}$$

The linear unit polarization vectors can be composed out of the circular unit polarization vectors and vice versa.

$$\begin{aligned}&\frac{\vec{C}_R(t)+\vec{C}_L(t)}{\sqrt{2}}=\sqrt{2}\vec{x}_0\cos(\omega t); \qquad \frac{\vec{C}_R(t)-\vec{C}_L(t)}{\sqrt{2}}=\sqrt{2}\vec{y}_0\sin(\omega t)\\ &\vec{x}_0\cos(\omega t)+\vec{y}_0\sin(\omega t)=\vec{C}_R(t); \qquad \vec{x}_0\cos(\omega t)-\vec{y}_0\sin\omega t=\vec{C}_L(t)\end{aligned} \tag{31.12}$$

Sometimes an abbreviated complex notation is used, where the complex unit "i" means a time lag of a quarter period. The $\sqrt{2}$-factors are now somewhat different due to a different rule of multiplication.

$$\begin{aligned}\vec{C}_R=\frac{\vec{x}_0+i\vec{y}_0}{\sqrt{2}}; \qquad &\vec{C}_L=\frac{\vec{x}_0-i\vec{y}_0}{\sqrt{2}}\\ \vec{C}_R\cdot\vec{C}_R^*=1=\vec{C}_L\cdot\vec{C}_L^*; \qquad &\vec{C}_R\cdot\vec{C}_L^*=\vec{C}_R^*\cdot\vec{C}_L=0\end{aligned} \tag{31.13}$$

One can go one step further and chose a pair of elliptical unit polarization vectors as basis for composing the electrical field vector.

$$\begin{aligned}\sqrt{2}\vec{\epsilon}_1(t) &= \cos\alpha\vec{x}_0\cos(\omega t)+\sin\alpha\vec{y}_0\sin(\omega t);\\ \sqrt{2}\vec{\epsilon}_2(t) &= \sin\alpha\vec{x}_0\cos(\omega t)-\cos\alpha\vec{y}_0\sin(\omega t)\end{aligned} \tag{31.14}$$

Again these unit vectors are orthonormal in the time-average sense. The vector $\vec{\epsilon}_1(t)$ represents an elliptical path in the (x,y) domain. The $\vec{\epsilon}_2(t)$ vector represents another ellipse with the same shape but rotated by 90° and with the opposite sense of rotation.

These unusual ways of representing the electrical field $\vec{E}(t)$ are justified whenever a certain physical effect can be described most easily with their help. A case in point is the *circular birefringence*, which means that the index of refraction differs for the two polarization components. Hence the right-hand circular light will travel more slowly than the left-hand circular component or vice versa.

$$\Delta n_C = n_R - n_L \qquad \Delta\varphi_C = \frac{2\pi}{\lambda} D \Delta n_C \tag{31.15}$$
$$\vec{E}_0 = \vec{C}_R E_{0R} + \vec{C}_L E_{0L} \qquad \vec{E} = \vec{C}_R E_{0R} e^{i\Delta\varphi_C} + \vec{C}_L E_{0L}$$

Circular birefringence occurs in sugar-water solutions. Dextrose-sugar has $\Delta n_C > 0$. For some reason $\Delta n_C < 0$-sugar is unhealthy. Fortunately, sugarcane plants and bees specialize in $\Delta n_C > 0$.

31.3 Compensators

In polarization optics one calls a method for varying the phase difference between the two polarization components a ‘compensator”.

$$\vec{E}_{\text{in}} = \vec{x}_0 A + \vec{y}_0 B; \qquad \vec{E}_{\text{out}} = e^{i\varphi_{\text{abs}}} \left[\vec{x}_0 A + \vec{y}_0 B e^{i\varphi_{\text{rel}}}\right] \tag{31.16}$$

The “absolute phase” is seldom of interest, only the so-called “relative phase”, which is variable in a compensator. The two most common compensators are due to Babinet and due to Babinet & Soleil (Fig. 31.6 a). The latter consists of two crystal plates with orthogonal crystal axis (indicated by a double arrow). The one plate consists of two wedges in order to vary the plate thickness by lateral shifts of the two wedges. Simpler is the Berek compensator which consists of a crystal plate with variable tilt (Fig. 31.6 b). The effective thickness of this plate varies like cosφ for the y-component of the polarization vector.

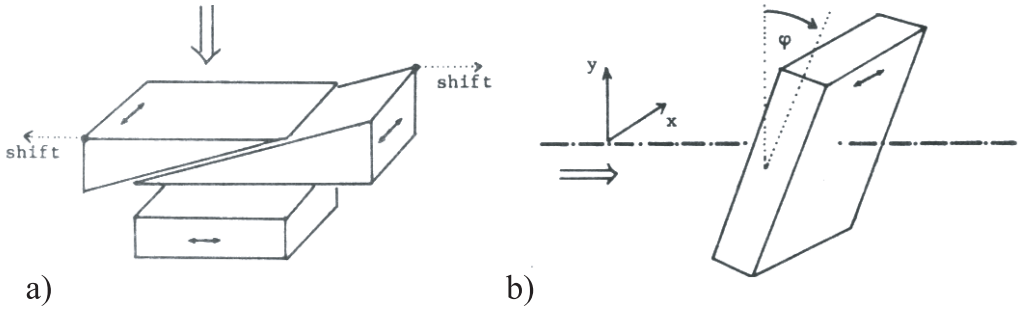

Figure 31.6: The most common compensator principles: a) Babinet-Solei compesator; b) Berek compensator.

We want to study now a particular compensator for two reasons: it is a useful component of a device to be described later; it gives us an opportunity to get familiar with calculations in polarization optics.

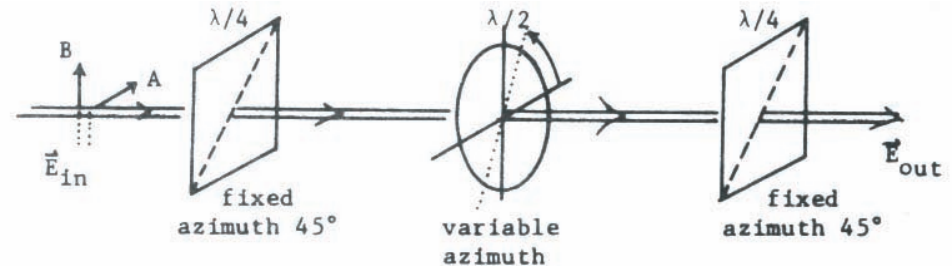

Figure 31.7: The geometry of a particular compensator.

$$\vec{E}_{\text{in}} = A\vec{x}_0 + B\vec{y}_0 \tag{31.17}$$

where A, B might be complex values.

For calculating the influence of the fixed $\frac{\lambda}{4}$ with $45°$ azimuth, we rewrite $\vec{E}_{\text{in}}$ such that the basic vector components are now parallel or perpendicular to the crystal axis of the $\frac{\lambda}{4}$ plate.

Figure 31.8: Vector decomposition of the incident polarization directions.

$$\vec{x}_0 = \frac{\vec{x}_0 + \vec{y}_0}{2} + \frac{\vec{x}_0 - \vec{y}_0}{2}; \qquad \vec{y}_0 = \frac{\vec{x}_0 + \vec{y}_0}{2} - \frac{\vec{x}_0 - \vec{y}_0}{2} \tag{31.18}$$

$$\vec{E}_{\text{in}} = \frac{\vec{x}_0 + \vec{y}_0}{2}(A + B) \quad + \quad \frac{\vec{x}_0 - \vec{y}_0}{2}(A - B)$$

The quarter-wave plate shifts the phase of the component along its axis (45°) by 90°, which can be described by a multiplication of that component by $e^{\frac{i\pi}{2}} = i$

$$\vec{E}_1 = i\frac{\vec{x}_0 + \vec{y}_0}{2}(A + B) + \frac{\vec{x}_0 - \vec{y}_0}{2}(A - B) \tag{31.19}$$

Next we reconvert this expression for $\vec{E}_1$ into a form with $\vec{x}_0$ and $\vec{y}_0$ as unit vector components:

$$\vec{E}_1 = \frac{\vec{x}_0}{2}\{A(i+1)+B(i-1)\} + \frac{\vec{y}_0}{2}\{A(i-1)+B(i+1)\} \tag{31.20}$$

It simplifies things to draw $(i+1)$ out of the whole expression:

$$\vec{E}_1 = \frac{i+1}{2}\left[\vec{x}_0(A+iB)+\vec{y}(iA+B)\right]; \qquad \frac{i-1}{i+1} = i \tag{31.21}$$

Now we have to transform $\vec{E}_1$ into a form which is adapted to the crystal-axis of the rotatable $\frac{\lambda}{2}$-plate.

$$\begin{aligned} \vec{x}_0 &= \vec{a}_0\cos\vartheta - \vec{b}_0\sin\vartheta \\ \vec{y}_0 &= \vec{a}_0\cos\vartheta + \vec{b}_0\sin\vartheta \end{aligned} \tag{31.22}$$

$$\begin{aligned} E &= \frac{i+1}{2}\left[\vec{a}_0\{(A+iB)\cos\vartheta + (iA+B)\sin\vartheta\} + \right. \\ &+ \left. \vec{b}_0\{-(A+iB)\sin\vartheta + (iA+B)\cos\vartheta\}\right] = \\ &= \frac{i+1}{2}\left[\vec{a}_0\left\{Ae^{i\vartheta}+iBe^{-i\vartheta}\right\} + \vec{b}_0\left\{iAe^{i\vartheta}+Be^{-i\vartheta}\right\}\right] \end{aligned} \tag{31.23}$$

(By the way, here is again an example where complex notation pays off. Imagine the mess in real trigonometry). Now we can consider the influence of the $\frac{\lambda}{2}$-plate which shifts the phase of the $\vec{a}_0$-component by π. Since $e^{i\pi} = -1$, all we have to do is $\vec{a}_0 \longrightarrow -\vec{a}_0$.

$$\vec{E}_2 = \frac{i+1}{2}\left[-\vec{a}_0\left\{Ae^{i\vartheta}+iBe^{-i\vartheta}\right\} + \vec{b}_0\left\{iAe^{i\vartheta}+Be^{-i\vartheta}\right\}\right] \tag{31.24}$$

Now the $\vec{a}_0, \vec{b}_0$ coordinate system is not useful anymore, so we go back to $\vec{x}_0$, $\vec{y}_0$:

$$\begin{aligned} \vec{a}_0 &= \vec{x}_0\cos\vartheta + \vec{y}_0\sin\vartheta; \qquad \vec{b}_0 = -\vec{x}_0\sin\vartheta + \vec{y}_0\cos\vartheta \\ \vec{E}_2 &= \frac{1+i}{2}\left[\vec{x}_0\left(-\cos\vartheta Ae^{+i\vartheta} - i\cos\vartheta Be^{-i\vartheta} - i\sin\vartheta Ae^{+i\vartheta} - \sin\vartheta\, Be^{-i\vartheta}\right) + \right. \\ &\left. +\vec{y}_0\left(-\sin\vartheta\, Ae^{+i\vartheta} - i\sin\vartheta\, Be^{-i\vartheta} + i\cos\vartheta Ae^{+i\vartheta} + \cos\vartheta\, Be^{-i\vartheta}\right)\right] = \\ &= \frac{1+i}{2}\left[-\vec{x}_0\left(Ae^{2i\vartheta}+iBe^{-2i\vartheta}\right) + \vec{y}_0\left(iAe^{2i\vartheta}+Be^{-2i\vartheta}\right)\right] \end{aligned} \tag{31.25}$$

Next we transform into the $(\vec{x}_0+\vec{y}_0, \vec{x}_0-\vec{y}_0)$ system, which fits the orientation of the final $\frac{\lambda}{4}$-plate

$$\begin{aligned}
\vec{x}_0 &= \frac{\vec{x}_0+\vec{y}_0}{2}+\frac{\vec{x}_0-\vec{y}_0}{2}; \qquad \vec{y}_0=\frac{\vec{x}_0+\vec{y}_0}{2}-\frac{\vec{x}_0-\vec{y}_0}{2} \qquad (31.26)\\
\vec{E}_2 &= \frac{1+i}{2}\left[\frac{\vec{x}_0+\vec{y}_0}{2}(-Ae^{i\vartheta}-iBe^{-i\vartheta}+iAe^{i\vartheta}+Be^{-i\vartheta})\right.\\
&\quad \left.+\frac{\vec{x}_0-\vec{y}_0}{2}(-Ae^{i\vartheta}-iBe^{-i\vartheta}-iAe^{i\vartheta}+Be^{-i\vartheta})\right]\\
&= \frac{1+i}{4}\left[(\vec{x}_0+\vec{y}_0)\left\{Ae^{i\vartheta}(-1+i)+Be^{-i\vartheta}(1-i)\right\}+\right.\\
&+ \left.\left[(\vec{x}_0-\vec{y}_0)\left\{Ae^{i\vartheta}(-1-i)+Be^{-i\vartheta}(-1-i)\right\}\right]\right.
\end{aligned}$$

Now we consider the final $\frac{\lambda}{4}$-plate by changing $(\vec{x}_0+\vec{y}_0) \longrightarrow i(\vec{x}_0-\vec{y}_0)$ [$i(-1+i)=-1-i;\ i(1-i)=i+1=-(-1-i)$].

$$\begin{aligned}
\vec{E}_{\rm out} &= \frac{1+i}{4}(-1-i)\left[(\vec{x}_0+\vec{y}_0)\left(Ae^{2i\vartheta}-Be^{-2i\vartheta}\right)+\right. \qquad (31.27)\\
&\quad \left.+(\vec{x}_0-\vec{y}_0)\left(Ae^{2i\vartheta}+Be^{-2i\vartheta}\right)\right]\\
&= -i\left[\vec{x}_0Ae^{2i\vartheta}-\vec{y}_0Be^{-2i\vartheta}\right]
\end{aligned}$$

$$\vec{E}_{\rm out}=-ie^{2i\vartheta}\left[\vec{x}_0A-\vec{y}_0Be^{-4i\vartheta}\right]=e^{i\left(2\vartheta-\frac{\pi}{2}\right)}\left[\vec{x}_0A+\vec{y}_0Be^{-i(4\vartheta+\pi)}\right] \qquad (31.28)$$

Comparing $\vec{E}_{\rm out}$ with $\vec{E}_{\rm in}$ we get as "absolute phase" $2\vartheta-\frac{\pi}{2}$, and as a *relative phase* $-4\vartheta-\pi$.

32 Holography

Other names for this illustratious field are “two-step imaging”, “lens-less photography”, and “wavefront reconstruction”. It started in 1948 when D. Gabor wanted to improve the electron microscope. While in light microscopy the resolution is about one light wavelength, with electron lenses one achieves only resolutions of hundreds to thousands of electron wavelengths. Both electrical and magnetic lenses are very poor comparatively, about as good as a milk bottle filled with water. You should not blame the designers of lenses or electron microscopes for this relatively poor state of the art, because Maxwell does not allow them to do it better. Due to div$\vec{E} = 0$ and $\vec{E} = -\mathrm{grad}\Phi$, is div grad $\Phi = 0$. An electrostatic lens has a potential Φ which is symmetrical around the optical axis $\Phi = \Phi(r, z)$. Hence, if $\Phi(r, z)$ is given along the axis, then $\Phi(r, z)$ is determined everywhere. To comprehend how little freedom that means imagine that in analogy a whole lens system would be completely specified in any point (r, z) by fixing it only on axis $(r = 0)$. Gabor knew that electron lenses are poor for fundamental reasons, but optical lenses are fairly good. Furthermore optical lenses can be made with any amount and shape of aberrations. Hence he decided to use somehow optical lenses for the process of image formation in the electron microscope. An encouraging fact is that in the time-stationary case the differential equation for electrons (Schrödinger) is the same as for electromagnetic waves: $\nabla^2 u + k^2 u = 0$. Hence, if one could somehow intercept u_{electron}, store it, and then reproduce an optical wave u_{opt} just like u_{el}, maybe different only by a scale-factor, one could then introduce an optical lens, which has aberrations just compensating the electron aberrations.

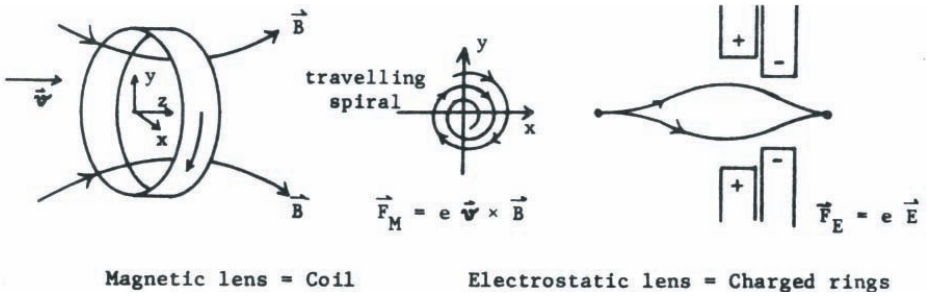

Figure 32.1: Typical realizations for lenses in electron microscopy: a) magnetic lens = Coil; b) Electrostatic lens = charged rings.

Or perhaps there would be no electron lens L_{E} at all. Then the optical lens alone carries the burden of producing an image. In 1920 the Polish physicist M. Wolfke was already thinking of doing something very similar, namely with X-rays as primary radiation, and light as secondary radiation. He already realized then that such a two-step imaging system would have an inbuilt magnification equation to the ratio of the wavelength: $M = \frac{\lambda_{\mathrm{light}}}{\lambda_{x-ray}}$ (typically 10^4). But Wolfke also realized why it would not work. The trouble is that all our receivers, be they for X-rays, visible light, or for electron waves, do not record the phase $\arg\{u\}$, but only the amplitude square $|u|^2$ of the wavefield. Without knowing the phase one is lost, at least in general. Gabor, however, found a trick to avoid the loss of the phase. For understanding this trick we will simplify the situation and assume that both the primary and the secondary waves consist of visible light, which furthermore is supposed to be perfectly coherent, both spatially and temporally. We will explain Gabor's trick more than once, in that way bringing out several facets of this idea, which is really brilliant, because the idea was possible already at the beginning of the century if not earlier. Although Wolfke (1920) and since then several others had clearly said how desirable it would be if anybody would have an idea with those features of Gabor's trick, no one before Gabor knew how to save the phase through the temporary recording step.

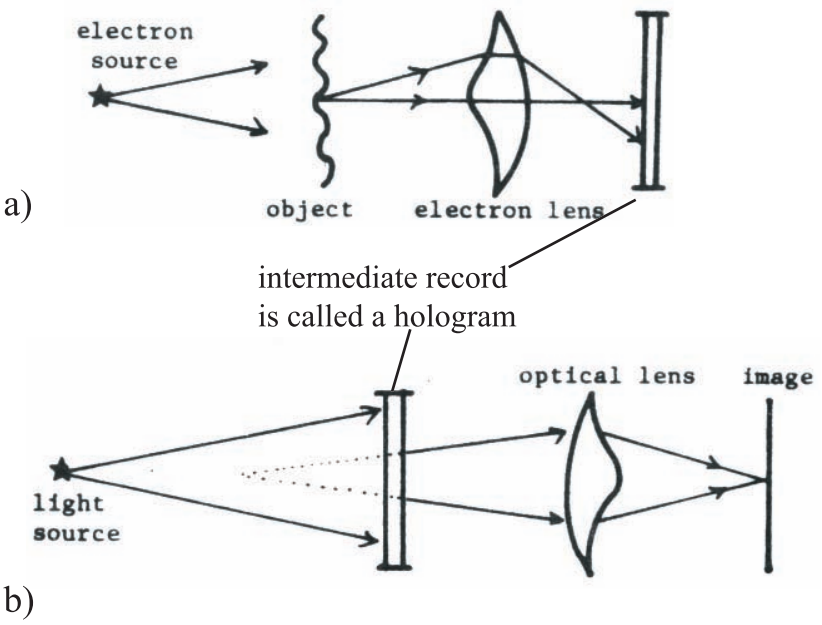

Figure 32.2: Holography for enhancement of electron microscopic images: a) recording step; b) reconstruction.

Before explaining the idea, let us shortly mention that "hologram" means "total recording" (replacing an artificial Latin word with an artificial Greek word). Implicitly a photograph is a

non-total recording, becauses it catches the amplitude only, not the phase, as a hologram does.

32.1 Rogers' Explanation

Suppose the object consists of a glass plate, which is perfectly flat and clean, except for one little dot, where the transmittance for the complex light amplitude is $Ae^{i\alpha}$ (maybe zero or not).

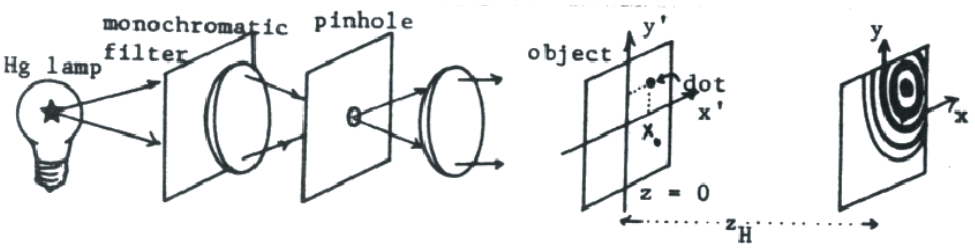

Figure 32.3: Rogers' explanation of holography.

The illumination in $z = -0$ is $u_L = 1$; hence immediately behind the object we have

$$\begin{aligned} u(x', y', +0) &= u_0(x', y') = \begin{cases} Ae^{i\alpha} & (\text{at the dot}) \text{ at } (x_0, y_0) \\ 1 & (\text{beside the dot}); \end{cases} \\ u_0(x', y') &= 1 + \begin{cases} Ae^{i\alpha} - 1 & \text{dot} \\ 0 & \text{not dot}; \end{cases} \end{aligned} \tag{32.1}$$

The "1" is called the "background wave" or coherent background, the rest is called the "diffracted or scattered light". Since the wave equation is linear, we may for a moment consider both parts of $u(x', y', +0)$ independently. The background term "1" will cause simply a plane wave which will be $e^{2\pi i \frac{z_H}{\lambda}}$ when reaching the hologram. If we consider the dot to be a point, then a spherical wave will emerge from it, which will be

$$u_S(x, z_H) \approx \frac{Ae^{i\alpha} - 1}{z_H} e^{2\pi i \frac{r}{\lambda}}; \qquad r^2 = z_H^2 + (x - x_0)^2 + (y - y_0)^2 \tag{32.2}$$

The total amplitude falling onto the hologram is:

$$u(x, y, z_H) = e^{ikz_H} + ae^{ikr}; \quad a = \frac{Ae^{i\alpha} - 1}{z_H}; \qquad k\frac{2\pi}{\lambda} \tag{32.3}$$

As always, it is the intensity $I_H = |u_H|^2$ which triggers the receiver:

$$I_H = |u(x, y, z_H)|^2 = 1 + ae^{ik(r - z_H)} + a^* e^{-ik(r - z_H)} + |a|^2 \tag{32.4}$$

For Gabor's version of holography (not so for newer versions) it is essential that we may drop $|a|^2 \ll 1$:

$$I_H \approx 1 + 2|a| \cos\{k(r - z_H) + \beta\}; \qquad \beta = \arg(a) \tag{32.5}$$

Herein we may approximate:

$$r - z_H = \sqrt{z_H^2 + (x - x_0)^2 + (y - y_0)^2} - z_H \approx \frac{(x - x_0)^2 + (y - y_0)^2}{2z_H} \tag{32.6}$$

if:

$$\frac{k(x - x_0)^2 + (y - y_0)^2}{8z_H^3} \ll 2\pi \tag{32.7}$$

$$I_H(x, y) \approx 1 + 2|a| \cos\left\{\frac{\pi}{\lambda z_H}[(x - x_0)^2 + (y - y_0)^2 + \beta]\right\} \tag{32.8}$$

This is what we called earlier a "Fresnel zone pattern", which is not surprising at all, since what we considered, so far was nothing but Fresnel diffraction. So we conclude that in Gabor's recording process the object dot gives rise to a zone plate pattern with a focal length $f = z_H$, and centered around x_0, y_0, which is the forward-projected place of the dot.

The phase information of the scattered wave ae^{ikr} has been preserved indirectly, since the phase *difference* between the scattered wave and the background wave $k(r - z_H)$ is responsible for the position of the interference fringes. Since the phase kz_H of the background wave is known due to the geometry, and since we can measure that phase difference $k(r - z_H) + \beta$ from the position of the maxima of the interference fringes, we obviously can deduce the phase $kr + \beta$ itself.

This leaves at the moment two questions unanswered: Could we deduce similarly also the phase from a more complicated diffracted wave, coming from an object which consists of more than a single dot? And even if we know the phase of the wave while it hits the hologram during the recording process, are we able to recreate the same phase in the reconstruction process? Furthermore, since the intensity contains the *cosine* of the phase $k(r - z_H)$ we are left with a $(\pm)$-ambiguity. As we will see shortly we will suffer somewhat from this $\pm$-ambiguity.

Let us answer the second question first, but for the time being only for our very simply object with a single dot. The setup used for reconstruction is very practically the same as the one used for recording. We show it in two views.

The photographic plate, which we called a hologram, has been developed, and we assume it has an amplitude transmittance which is proportional to the intensity which has been recorded on it. (Later on we will discuss how true this assumption is, and what happens if this

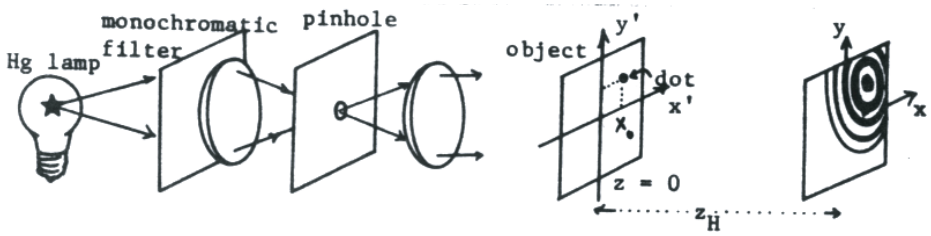

Figure 32.4: Hologram reconstruction setup according to Rogers.

assumption is fulfilled only crudely).

$$u_H(x,y) = I_H(x,y) \qquad \text{(proportionality factor omitted)} \tag{32.9}$$

The hologram is illuminated by a plane wave, which is at $z = z_H - 0 :\ u_L = e^{ikz_H}$. Right behind the hologram we have:

$$\begin{aligned} u(x,y,z_H+0) &= u_H(x,y)u_L(x,y,z_H-0) \approx [1 + a^{ik(r-z_H)} + a^* e^{-ik(r-z_H)}]e^{ikz_H} \\ &= e^{ikz_H} + ae^{ikr} + a^* e^{ik(2(z_H-r))} \end{aligned} \tag{32.10}$$

Without making explicit use of the last formula we can predict what will happen already based on our knowledge of the Fresnel zone plate (Chapter 19). We remember that a FZP acts simultaneously as a plane glass plate, as a positive lens with $f = +2\frac{r_1^2}{\lambda}$, and as a negative lens with $f = -2\frac{r_1^2}{\lambda}$. Herein r_1^2 was the pseudo-period of the FZP, expressed as a function of $(x^2 + y^2)$. These three contributions can be understood also in terms of grating diffraction, when considering the FZP as a grating with slowly varying magnitude and orientation of the grating period. The "plane glass plate" contribution corresponds to the zeroth grating diffraction order, while the two other terms can be interpreted as "inward" and "outward" diffraction, as indicated in the figure of the reconstruction process. The inward diffraction creates a focal point at $z = +2z_H$, which is called the "conjugate image" or the "real image" of the original dot, while the outward diffraction seems (for anyone at $z > z_H$) to stem from a point at $z = 0$, $x = x_0$, $y = y_0$, which is the place of the original dot. In fact the first two terms $e^{ikz_H} + ae^{ikr}$ are a true replica of the original wavefield. We can do with it whatever we might have intended to do with the original wavefield. For example we might insert a lens anywhere at $z > z_H$ with proper focal length and observe what is called the "true image" or the "virtual image", located at $z = 0$.

The fact that we got two images (also called "twin images") is a direct consequence of the $\pm$-ambiguity of the cosine. The cosine contains:

$$2\cos\{k(r - z_H)\} = e^{ik(r-z_H)} + e^{-ik(r-z_H)} \tag{32.11}$$

both unambiguous functions in linear superposition. Consequently a hologram with cosine-transmittance produces the linear superposition of a *divergent* and a *convergent* spherical wave.

32.2 Discussion of the phase loss

Let us consider once more why the loss of the phase during photographic recording did not prevent the formation of an image in the reconstruction process. The complex amplitude $u(x, y, z_H)$ falls onto the photographic plate, which later serves as the hologram in the reconstruction process. The photographic plate is "phase-blind"; it can record only $I_H(x, y) = |u(x, y, z_H)|^2$. After development (say on positive film, ideally linear) the amplitude transmittance is $u_H(x, y) = I_H(x, y) = |u(x, y, z_H)|^2$. However in the ideal (and impossible) case of a phase-sensitive recording medium the amplitude transmittance would have to be:

$$\begin{aligned} u_H(x,y) &= u(x,y,z_H) \qquad (\text{ideal, impossible}) \\ u_H(x,y) &= |u(x,y,z_H)|^2 \qquad (\text{reality, somewhat simplified}) \end{aligned} \tag{32.12}$$

It is always allowed to split up "reality" into the "ideal world" and "the rest". (Idealism means ignoring "the rest".) In our case,

$$\underbrace{u_H(x,y)}_{\substack{\text{real, since it is a photographic film transmittance; also non-negative}}} = |u(x,y,z_H)|^2 = \underbrace{u(x,y,z_H)}_{\substack{\text{ideal; in general complex}}} + \underbrace{\text{“the rest”}}_{\substack{\text{must be the complex conjugate of } u(x,y,z_H) \text{ to make sum real; in addition to a real-positive part might be needed to make the sum non-negative}}} \tag{32.13}$$

The term u_H is "real" both in the mathematical as well as in the philosophical sense. It is always allowed to split the real world into an ideal world and "the rest", but this conceptual split is of practical use only *if "the rest" can be neglected somehow*. This is indeed the case in the example we have studied (see figure 32.4) and it is Gabor's achievement to have recognized it. Ideally the reconstructed wavefield should be $u_{\mathrm{id}}(x, y, z_H) = e^{ikz_H} + ae^{ikr}$ (see Eq. 32.3 and Fig. 32.4), but in actuality the wavefield behind the hologram is:

$$u_{\mathrm{reconstr}}(x,y,z_H+0) = \underbrace{e^{ikz_H} + ae^{ikr}}_{\substack{\text{“ideal” plane wave + spherical wave, seemingly coming from the object (which actually is not there anymore during the reconstruction)}}} + \underbrace{a^* e^{ik(2z_H - r)}}_{\substack{\text{“the rest” another spherical wave converging at } z = 2z_H}} \tag{32.14}$$

Let us repeat the drawing in Fig. 32.4, but now supplement it with a "telecentric lens system" for imaging purposes. (A telecentric system keeps plane waves as plane waves.) The drawing tells us that the diverging spherical wave, after leaving the hologram and passing through the telecentric system, will converge in the image plane ($z = 4f$) at x_0 exactly as if

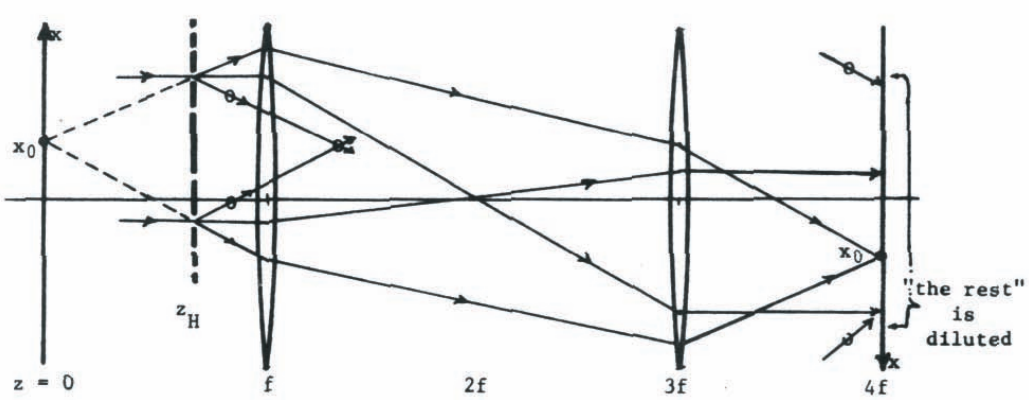

Figure 32.5: Reconstruction of object and twin image.

the hologram were not there, but the object still in place, with its dot at x_0 in $z = 0$. Also the plane wave which emerged from the original object is "reconstructed" in the image. "The rest" is another spherical wave, which however is hardly noticable in the image plane $z = 4f$, because it is spread out and hence diluted. However in another plane behind, at $z = 4f + 2z_H$, "the rest" will converge, also at x_0. The plane wave will arrive in that plane too, assuming that we did not intercept anything. On the other hand the original spherical wave, which formed an image of the dot at x_0 in $z = 4f$, will be widely spread out and diluted. Hence we see in $z = 4f + 2z_H$ another "image". In other words, "the rest" is not complete nonsense in terms of image formation. This is not surprising, since "the rest" was something which had supplemented the "ideal part" $e^{ikz_H} + ae^{ikr}$ of the wavefront such that it was *real* directly behind the hologram: "the rest" $= a^* e^{ik(2z_H - r)}$. In other words "the rest" is the complex conjugate; after all, two functions which are a pair of complex conjugate functions are very, very similar. Hence the two physical effects described by two complex conjugate functions can be expected to be similar also. Only one thing was omitted so far, the quadratic term $|a|^2$; the justification for this omission is plausible, if $|a|^2$ comes from a little dot in a wide bright object field. We will discuss this omission again later on a more general level.

32.3 Generalized Rogers' Explanation

see: Proc. Roy. Soc. Edinburgh, A63, 193, 1952.

So far we have assumed a very special object: a small dot, surrounded by a clear background. Now let us take a more general object, one with a strong background, but otherwise arbitrary. "Background" means average, which we set $= 1$, for the sake of simplicity: $u_0(x, y) = 1 + \Delta u_0(x, y)$; $\iint u_0(x, y)\, \mathrm{d}x\, \mathrm{d}y = \iint\limits_{\text{obj.}} \mathrm{d}x\, \mathrm{d}y$ (the $\iint$ over the object area). "Strong" background means $|\Delta u_0|^2 \ll 1$, at least at most position (x, y). Actually $\iint\limits_{\text{obj.}} |\Delta u_0|^2\, \mathrm{d}x\, \mathrm{d}y \ll \iint\limits_{\text{obj.}} \mathrm{d}x\, \mathrm{d}y$ is a more suitable condition.

What result can we expect? In a linear and space-invariant system (whatever it may be) we know everything about the system already, if we know only what the system does to a single point input:

input	output	condition used
single point at x' : $\delta(x-x')$	$A(x-x')$	space invariance
stronger single point: $u(x')\delta(x-x')$	u(x')A(x-x')	homogeneity
many single points building up the general object: $u(x)=\iint u(x')\delta(x-x')\,\mathrm{d}x'$	many point responses building up the image $u_B=\int u(x')\,A(x-x')\,\mathrm{d}x'$	additivity

Table 32.1: Generalizing the Rogers explanation of holography.

Additivity + Homogeneity = Linearity

So far we studied only the formation of a holographic image for a single point object. We would like to generalize this result in the spirit of linear filter theory. However the total holographic system is not linear. (Total system: from object, via hologram, to reconstructed image.) The reason is the non-linear recording process of the photographic emulsion, whereby the phase is lost, as part of the modulus-square operation.

But a system which is not linear for the most general set of inputs might neverless be linear for a restricted set of objects. This is in fact the case in holography, at least in approximation.

If this is true, then we can understand holography in this way: each object point emits a spherical wave. When this spherical wave arrives at the hologram plate it interferes with a plane wave which comes from the strong background of the object. (Remember, the set of permissible objects has a strong background.) Interferences between a spherical wave and a plane wave gives a Fresnel zone pattern. In reconstruction each Fresnel zone patterns acts like a lens (deflection of light by diffraction instead of refraction), focussing a portion of the incoming light into a point, which then is the image point of that object point which was responsible for that particular Fresnel zone pattern.

Another way to say all this is that the recording process is a particular encoding process, whereby each object point is converted into a FZ pattern, which can be described (as we will see shortly) as a convolution of object and FZP. Reconstruction then is a decoding process, whereby each FZP is reconverted into a point. These convolution operations are performed physically by propagation of light from one plane to another plane, called Fresnel diffraction.

Now we will treat all this quantitatively, mentioning the instance where we approximate. But before that a quick reminder about Fresnel transformation and Fresnel diffraction. The two transformations are defined as:

$$\begin{aligned}
\hat{u}(x,y,z+\eta) &= \frac{1}{|\lambda\eta|}\iint u(x',y',z)e^{i\frac{\pi}{\lambda\eta}\{(x'-x)^2+(y-y')^2\}}\,\mathrm{d}x'\,\mathrm{d}y' \\
\check{u}(x,y,z+\eta) &= \frac{1}{|\lambda\eta|}\iint u(x',y',z)e^{-i\frac{\pi}{\lambda\eta}\{(x'-x)^2+(y-y')^2\}}\,\mathrm{d}x'\,\mathrm{d}y' \\
\{\check{u^*}\} &= \{\hat{u}\}^*; \qquad \{\hat{u^*}\} = \{\check{u}\}^*; \\
\hat{u}(x,y,z-\eta) &= \check{u}(x,y,z+\eta); \qquad \hat{u}(x,y,z+\eta) = \check{u}(x,y,z-\eta)
\end{aligned} \tag{32.15}$$

The wave propagation *FORWARD* from plane z to $z+\eta$ can be described by:

$$u(x,y,z) \longrightarrow u(x,y,z+\eta) = e^{ik\eta}\hat{u}(x,y,z+\eta) \tag{32.16}$$

Similarly we can describe the *BACKWARD* propagation ("virtual") from z to $z-\eta$ as:

$$\begin{aligned}
u(x,y,z) \longrightarrow u(x,y,z-\eta) &= e^{-ik\eta}\check{u}(x,y,z+\eta) = e^{-ik\eta}\hat{u}(x,y,z-\eta) \\
\left\{e^{ik\eta}\hat{u}(x,y,z+\eta)\right\}^* &= e^{-ik\eta}\left\{u^*(x,y,z+\eta)\right\}^{\check{}}
\end{aligned} \tag{32.17}$$

Now we are well prepared for the theory of Fresnel-Holography.

Illumination of the object by a plane wave:

$$\begin{aligned}
u_L(x,y,z) &= e^{ikz} \quad \text{in } z<0; \qquad u_L(x,y,-0)=1 \quad \text{directly before object} \\
u(x,y,+0) &= u_L(x,y,-0) \qquad \underbrace{u_0(x,y)}_{\text{obj.-ampl.-transm.}} \qquad = u_0(x,y)
\end{aligned} \tag{32.18}$$

The object is supposed to have a strong background:

$$u_0(x,y) = 1 + \Delta u_0(x,y) \tag{32.19}$$

Propagation from $z=+0$ to $z=z_H$:

$$u_0(x,y) \longrightarrow u(x,y,z_H) = e^{ikz_H} + e^{ikz_H}\Delta\hat{u}(x,y,z_H) = e^{ikz_H}[1+\Delta\hat{u}_0] \tag{32.20}$$

The intensity which triggers the photographic plate is:

$$I_H(x,y) = |u(x,y,z_H)|^2 = |1+\Delta\hat{u}_0|^2 = 1 + \Delta\hat{u}_0 + \Delta\hat{u}_0^* + |\Delta\hat{u}_0|^2 \tag{32.21}$$

Now we assume that the background is so strong that $|\Delta\hat{u}_0|^2$ can be neglected. This avoids any nonlinearity. Next we have to consider the conversion of the incident recorded intensity into the resulting amplitude transmission of the hologram. From now on we will indicate the complex amplitudes occurring in the reconstruction process by $\mathcal{V}$ (with index if

applicable); in particular the amplitude transmittance of the hologram is called $\mathcal{V}_H(x,y)$. We assume a linear relationship between received intensity and resulting amplitude transmittance: $\mathcal{V}_H(x,y) = I_H(x,y)$. (A more accurate formula, $\mathcal{V}_H = \sum_{m=1}^{3} c_n I_H^n$, will be discussed later.)

Now we put the hologram in its old place $z = z_H$ and illuminate it with the same illumination wave as in the recording step. But the object is removed.

$$\mathcal{V}_H(x,y,z) = u_L(x,y,z) = e^{ikz} \quad \text{in} \quad z \le z_H \tag{32.22}$$

(In $z \le z_H$ there is no obstruction which could do something to this plane wave.) Immediately before the hologram in $z = z_H - 0$ it is $\mathcal{V}_L(x,y,z_H-0) = e^{ikz_H}$ and immediately after:

$$\begin{aligned}
\mathcal{V}(x,y,z_H+0) &= \mathcal{V}(x,y,z_H-0)\mathcal{V}_H(x,y) = \\
&= e^{ikz_H}\mathcal{V}_H(x,y) = e^{ikz_H} I_H(x,y) = \\
&= e^{ikz_H}[1 + \Delta\hat{u}_0 + \{\Delta\hat{u}_0\}^*] = e^{ikz_H} + e^{ikz_H}\Delta\hat{u}_0 + e^{ikz_H}\{\Delta\hat{u}_0\}^* \\
&= u(x,y,z_H) + \text{“the rest”}; \quad \text{“the rest”} = e^{ikz_H}\Delta\hat{u}_0^*
\end{aligned} \tag{32.23}$$

Neglecting for a moment “the rest”, this equation says that behind the hologram we have the same wave as there was originally, while the object was still in place. Having the same wave again allows us to do everything with it which we might have wanted to do with the original wave u. The most obvious thing one might want to do is to form an image. This can be done (for example) by a telecentric system of 1:1 magnification, the two lenses being positioned at $z = f$ and $z = 3f$. This system would have formed from the object $u(x,y)$ in $z = 0$ an image in $z = 4f$. Since the telecentric system cannot perceive any difference (neglecting “the rest”) between the original wave and the reconstructed wave, it will do to the reconstructed wave exactly what it would have done to the original wave, that is to form an image at $z = 4f$. This image will be called “the image of the virtual image”, the “virtual image” being exactly where the object had been originally.

The use of the telecentric system makes all the image formation equations simpler (we did not even write down in detail what happens to $\mathcal{V}$ at $z = z_H$, since we did this type of calculation in connection with the theory of coherent image formation in Chapter 24). Any other lens system would have been useful as well, for example the eye. Also the eye lens (at $z > z_H$) could not decide if it looks at the original object (without hologram) or at the hologram (without the object actually there).

The last statement is true, if the previous assumptions are valid, and if “the rest” does not cause any confusion. What is this “the rest”?

$$\begin{aligned}
\text{the rest} &= \{\Delta\hat{u}_0(x,y,z_H)\}^* e^{ikz_H} \overset{\text{make use of Eq. 32.16}}{=} \\
&= e^{ikz_H}\{\Delta u_0^*(x,y,-z_H)\}\hat{} = e^{2ikz_H}[e^{-ikz_H}\{\Delta u_0^*(x,y,-z_H)\}\check{}]
\end{aligned} \tag{32.24}$$

This is what one would see "virtually", or as backward-propagation at a plane which is at a distance z_H *in front of* the plane, from where the complex amplitude $\Delta u_0^*(x,y)$ would start its backward propagation. In other words, the "the rest" term behaves in reconstruction *as if* in recording there would have been a "rest" object $\Delta u^*(x,y)$ in plane $z = 2z_H$ *behind* the hologram at z_H. This "rest" object seemingly had been illuminated by what u_L would have been in that plane $2z_H$ that is, $u_L(x,y,2z_H) = e^{2ikz_H}$.

The e^{ikz_H}-term or background term in $\mathcal{V}(x,y,z_H+0)$ (see Eq. 32.24), which so far had been as part of the "reconstructed wave" $u(x,y,z_H)$, can also, if we wish to consider it this way, be counted together with "the rest".

$$\mathcal{V}(x,y,z_H+0) = e^{ikz_H}\Delta\hat{u}_0 + \underbrace{e^{ikz_H} + \overbrace{e^{ikz_H}\{\Delta\hat{u}_0\}^*}^{\text{"the rest}''}}_{\text{"the rest}'' \text{ with background}} \tag{32.25}$$

The combination of "the rest" and background wave behaves as if $1+\Delta u_0^*(x,y)$ had been put as "object" into plane $z = +2z_H$ during recording. This $1 + \Delta u_0^*(x,y)$ is the complex conjugate of the actual original object. Again, we can do anything we want to do with "the rest" with background, for example use the telecentric lens system and form an "image" of $u_0^*(x,y)$ at $2z_H + 4f$. Without the telecentric system it is even easier to get $u_0^*(x,y)$, simply by holding some cardboard at $z = +2z_H$, where $|u_0^*(x,y)|^2$ will be the visible intensity. Of course now the other term $e^{ikz_H}\Delta\hat{u}_0$ might be bothersome, when observing this so-called "real image". This is "real" in the sense of ray-optics, not as a complex classification.

In the older literature the u_0^*-term is called the "real-image wave" and the u_0-term the "virtual-image wave". Now many authors call u_0^* the *"conjugate wave"* and u_0 the *"true wave"*. Similarly one refers to the true and conjugate images. This pair of images is also called the "twin images". Coming back now to the observation of the "conjugate image" at $z = z_H$, the contribution from $e^{ikz_H}\hat{u}_0$ will be out of focus by a distance of $2z_H$. Hence one hopes that the unsharp "twin image" is so much blurred that it does not bother too much. Actually it does bother in most cases, enough that this twin image problem was the second most important hindrance of progress. The most severe handicap for Gabor and his early successors was the lack of a good coherent light source such as the laser.

One additional comment on the theory of Fresnel-Holography: On page 372 it was said, based on qualitative arguments, that the recording process can be considered as an *encoding* process, more specifically as a conversion of each object point into its own FZP of appropriate "strength" and position. Mathematically this is meant to be a convolution, which we now want to write down explicitly.

On page 372 we had found that the complex object amplitude $u_0(x,y) = 1 + \Delta u_0(x,y)$ causes the intensity falling onto the photographic plate (which later is the hologram) to be:

$$
\begin{aligned}
I_H(x,y) &= 1 + \Delta\hat{u}_0 + \{\Delta\hat{u}_0\}^* + \overbrace{|\Delta\hat{u}_0|^2}^{\text{negligible}} \\
&\approx 1 + \frac{1}{\lambda z_H} \iint \Delta u_0(x',y') e^{\frac{i\pi}{\lambda z_H}\{(x-x')^2+(y-y')^2\}}\, \mathrm{d}x'\, \mathrm{d}y' + \text{c. c.}
\end{aligned}
\tag{32.26}
$$

No we rewrite $\Delta u_0 = |\Delta u_0| e^{i\varphi}$, and then combine the $\iint \ldots$ term and its complex conjugate:

$$
\begin{aligned}
I_H(x,y) &\approx 1 + \frac{2}{\lambda z_H} \iint |\Delta u_0(x',y')| \\
&\qquad \cos\left[\frac{\pi}{\lambda z_H}\left\{(x-x')^2 + (y-y')^2\right\} + \varphi(x',y')\right] \mathrm{d}x'\, \mathrm{d}y'
\end{aligned}
\tag{32.27}
$$

We recognize that each "object dot" at (x', y') with its complex amplitude $|\Delta u_0| e^{i\varphi}$ forms its own FZP in the hologram plane centered appropriatly at (x', y').

32.4 Some attempts to remove the twin-image

It is a very interesting question, at least for me, why Gabor's original papers on holography (1948 - 51) had so relatively little impact. Before 1962 only three other groups (Edinburgh, Stanford, Braunschweig) published anything about holography. Of course, the availability of the laser helped later a great deal in promoting holography. But one can make excellent holograms without a laser. I consider two other points to be equally important for the long delay of holography's popularity: the trouble with the twin-image, and Gabor's superiority above the average optical scientist's level of competence. Gabor had so many little additional ideas, which he also wanted to put into his papers, that he had to condense quite a bit. Hence his papers are not easy to read. Many of his little side remarks have been re-discovered and published as elaborate papers by others, who then cited Gabor as the inventor-at-large, but did not mention that Gabor had also invented that particular bit of progress. These people were sincere, they just could not appreciate all the little facets. It did happen to me, and also to Leith & Upatnieks in their paper on *off-axis holography*, which is the most important innovation since Gabor's original paper. Actually, Gabor was fully aware of it, which one finds out whenreading his papers carefully. He did not pursue off-axis holography, because at that time there were no beam-splitters for electron-waves available. On the other hand E. Leith (U. of Michigan, Ann Arbor) showed to me recently a report he wrote in 1952, which had been de-classified only recently, in which he described clearly off-axis holography, but in completely non-optical terms, as a method for data processing in connection with side-looking radar. Only much later did he become aware of Gabor's paper, when he realized that side-looking radar with optical data processing can be considered as holography, whereby the hologram is recorded with radar waves, and reconstructed with light waves.

The first three out of four attempts to remove the twin image have basically only historical significance, but they help to provide more insight, and they demonstrate experimental trickology and valuable theoretical tools. The first attempt to be explained is mentioned by Gabor in a footnote of 1 1/2 lines!

(Note added in 1986): Recently I re-read the earliest papers of Gabor and of Leith and Upatnieks. In order to clarify for myself the matter of priorities, I also looked at the early patents. It is my conviction now, that Gabor is the prime inventor, of course. Leith and Upatnieks contributed off-axis holography and diffuse illumination, Denisyuk invented the BRAGG-holograms.

Gabor's first attempt to remove the twin-images (published in Proc. NBS Symp. Electron Microscopy, Washington, D.C., Nov. 1951) can be called "optical interpolation". It is more involved than his second attempt, which I will present first. The second attempt was published in the same place, and again a few year ago in JOSA 56, 849 (1966). Basically the idea is to record *two* holograms from one object, one hologram for the real part, and another one for the imaginary part of the wavefront. This pair of holograms contains everything about the wavefield, without ambiguity. Hence it must be possible to reconstruct the original wavefield perfectly. At this moment we do not have to assume that the object has a strong background of its own, because a background wave is provided externally.

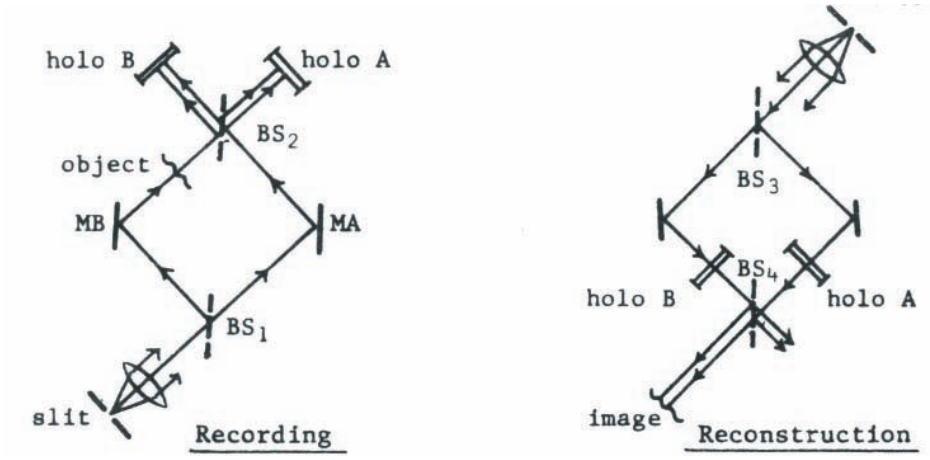

Figure 32.6: Recording and reconstruction schemes of two holograms of the same object in order to avoid the twin image.

For the sake of simplicity let us assume (which is not essential) that the optical path length from the object to hologram A is the same as from the object to hologram B. Hence in both hologram planes the same complex amplitude u_H arrives from the object. But the plane reference waves, coming along mirror MA and beamsplitter BS, may arrive at holo A and

holo B at different times, delayed by a quarter-wavelength, which corresponds to a phase factor $e^{i\frac{\pi}{2}} = i$. At holo A the intensity I_A will be.

$$I_A = |1 + u_H|^2 \approx 1 + 2\mathrm{Re}\{u_H\} \tag{32.28}$$

and at holo B:

$$I_B = |i + u_H|^2 \approx 1 + 2\mathrm{Im}\{u_H\}; \quad \text{where :} u_H = \mathrm{Re}\{u_H\} + i\mathrm{Im}\{u_H\} \tag{32.29}$$

Next the two holograms are developed, again *linear* in terms of amplitude transmittance versus exposure. Now both holograms with their amplitude transmittances $\mathcal{V}_A \approx I_A$ and $\mathcal{V}_B = I_B$ are illuminated by plane waves, which however are again 90° out of phase. After combining both waves in BS4 the joint wave is $\mathcal{V}_A + i\mathcal{V}_B$.

$$\mathcal{V}_A + i\mathcal{V}_B = I_A + iI_B \approx 1 + \mathrm{Re}\{u_H\} + i[1 + 2\mathrm{Im}\{u_H\}] = \underbrace{1+i}_{\substack{\text{surplus plane}\\ \text{wave}}} + \underbrace{2u_H}_{\substack{\text{reconstructed}\\ \text{image}}} \tag{32.30}$$

This experiment is very delicate, since it is difficult to produce the two wavefronts $\mathcal{V}_A$ and $\mathcal{V}_B$ without any relative tilt, and with exactly the same scale.

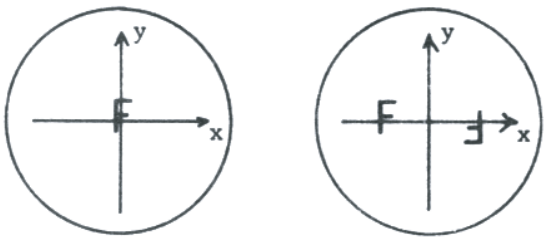

Figure 32.7: Specific objects for holographic recording.

It is not clear to me whether Gabor's first attempt will work the way it has been published. But I can show that it will work if the class of admissable objects is further restricted. Gabor assumed only a strong background-type object $u_0(x, y) = 1 + \Delta u_0(x, y)$; now we assume in addition the following symmetry property: $\Delta u_0(x, y) = \Delta u_0^*(-x, -y)$. This can be achieved very simply, if Δu_0 happens to be real. Assume as object (originally) for example the letter 'F', opaque on a transparent background. Now we shift the 'F' and add an additional 'F', but 180 inverted (Fig. 32.7). The new Δu_0, which describes the 'double-F', is actually symmetrical $\Delta u_0(x, y) = \Delta u_0(-x, -y)$. If in addition $\Delta u_0 = \Delta u_0^*$ we get

$\Delta u_0(x,y) = \Delta u_0^*(-x,-y)$ which is equivalent to $\Delta\tilde{u}_0(\nu,\mu) = \Delta\tilde{u}_0^*(\nu,\mu)$.

The combined assumptions: strong background, real, center-symmetrical, might reduce the set of admissable objects so severely that the method is of little practical value, but it is nevertheless instructive for the following reason. Many inventions (like this one) were made when everybody knew that some desirable effect is impossible *in general*. The inventor then realized that this effect is not impossible *in special circumstances*. The inventor's problem is to find such special circumstances and then check if the invention is still useful under these special circumstances.

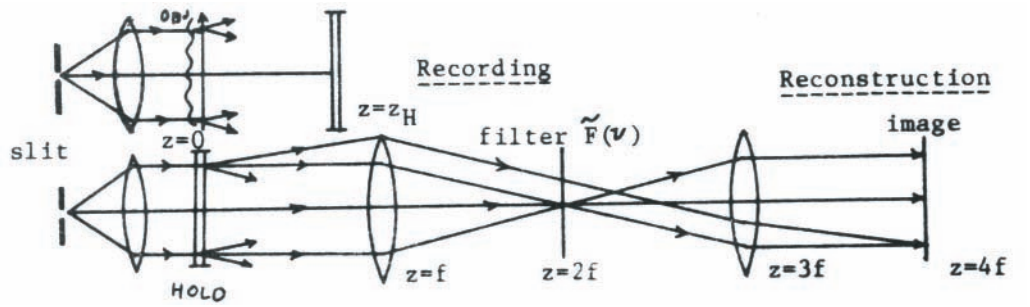

Figure 32.8: Illustration of the hologram recording and reconstruction.

We will use the Rayleigh-Sommerfeld-Debye approach to diffraction theory (Chapter 18.2), which means superposition of *plane waves* (Fig. 32.8).

Illumination in recording: $u_L(x,y,z) = e^{ikz}$ in $z < 0$;

Immediately before the object: $u_L(x,y,-0) = 1$;

Behind the object: $u(x,y,+0) = u_L(x,y,-0)u_O(x,y) = u_O(x,y)$;

Assumption (strong background):

$$u_O(x,y) = 1 + \Delta u_O(x,y) = \iint \underbrace{[\delta(\nu,\mu) + \Delta\tilde{u}(\nu,\mu)]}_{\tilde{u}_O(\nu,\mu)} e^{2\pi i(\nu x,\mu y)}\,\mathrm{d}\nu\,\mathrm{d}\mu \qquad (32.31)$$

Propagation from $z = 0$ to $z = z_H$:

$$u(x,y,+0) = u_O(x,y) \longrightarrow u(x,y,z_H) \qquad (32.32)$$

This is equivalent to:

$$\tilde{u}(\nu,\mu) \longrightarrow \tilde{u}(\nu,\mu)e^{ik\sqrt{1-\lambda^2(\nu^2+\mu^2)}z_H} \tag{32.33}$$

A simplifying assumption: Fresnel diffraction in the nearfield, which means that z_H is small enough to justify:

$$e^{ik\sqrt{1-\lambda^2(\nu^2+\mu^2)}z_H} \approx e^{ikz_H}e^{-i\pi\lambda z_H(\nu^2+\mu^2)} \tag{32.34}$$

Hence propagation is described by:

$$\begin{aligned}\tilde{u}(\nu,\mu) &\longrightarrow \tilde{u}_0(\nu,\mu)e^{ikz_H}e^{i\pi\lambda z_H}(\nu^2+\mu^2) = \\ &= e^{ikz_H}\left[\delta(\nu,\mu)+\Delta\tilde{u}_O(\nu,\mu)e^{-i\pi\lambda z_H(\nu^2+\mu^2)}\right]\end{aligned} \tag{32.35}$$

Inserting this we get:

$$u(x,y,z_H) = e^{ikz_H}\left[1+\iint \Delta\tilde{u}_O e^{-i\pi\lambda z_H(\nu^2+\mu^2)}e^{2\pi i(x\nu+y\mu)}\,\mathrm{d}\nu\,\mathrm{d}\mu\right] \tag{32.36}$$

and:

$$I_H(x,y) = |u(x,y,z_H)|^2 \approx 1+\ldots\iint\ldots+\left\{\iint\ldots\right\}^* + \text{negligible} \tag{32.37}$$

Herein one can reformulate:

$$\left\{\iint\ldots\right\}^* = \iint \Delta\tilde{u}_O(\nu,\mu)e^{+i\cdots}e^{-i\cdots}\,\mathrm{d}\nu\,\mathrm{d}\mu \tag{32.38}$$

Now with the coordinate transforms: $\nu \longrightarrow -\nu' \longrightarrow -\nu$ and $\mu \longrightarrow -\mu' \longrightarrow -\mu$

$$\left\{\iint\ldots\right\}^* = \iint \Delta u_O^*(-\nu,-\mu)e^{+i\pi\cdots}e^{+2\pi i(\ldots)}\,\mathrm{d}\nu\,\mathrm{d}\mu \tag{32.39}$$

and: $\Delta\tilde{u}_O^*(-\nu,-\mu) = \Delta\tilde{u}_0(+\nu,+\mu)$ due to the assumption $u_0 = u_0^*$.
Hence one can combine the two $\iint$ and $\iint^*$ with $e^{+i\pi\cdots}+e^{-i\pi\cdots} = 2\cos(\pi\ldots)$:

$$I_H(x,y) \approx 1+2\iint \Delta\tilde{u}_O(\nu,\mu)\cos\left[\pi\lambda z_H(\nu^2+\mu^2)\right]e^{2\pi i(x\nu+y\mu)}\,\mathrm{d}\nu\,\mathrm{d}\mu \tag{32.40}$$

After the photographic development process the recorded hologram intensity $I_H(x,y)$ appears as the hologram-amplitude transmittance, if the photographic process was linear, $\mathcal{V} = I_H(x,y)$. We insert the hologram at $z = 0$ in the reconstruction setup (Fig. 32.8).

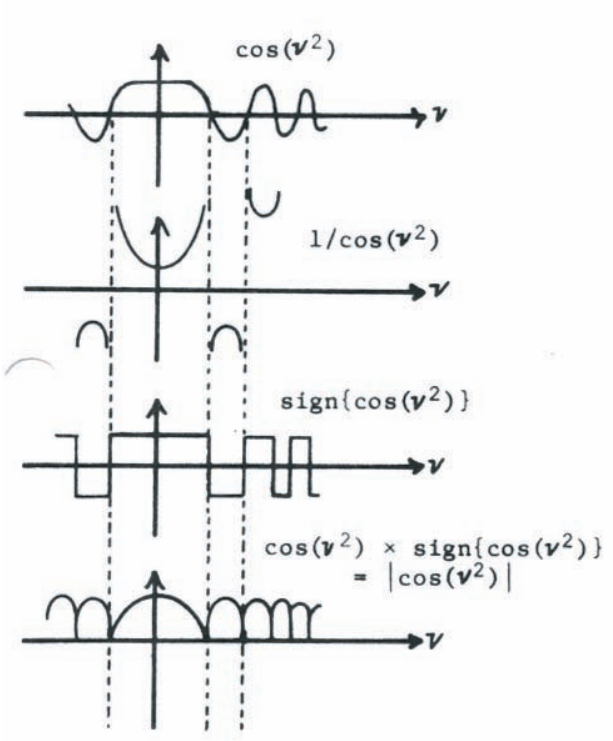

Figure 32.9: Filtering in order to remove the twin image.

$\mathcal{V}(x,y)$ is different from the wanted $u_o(x,y)$ because the frequency spectrum $\Delta\tilde{u}(\nu,\mu)$ has been multiplied by $2\cos[\pi\lambda z_H(\nu^2+\mu^2)]$. We will repair this by means of a compensating filter $\tilde{F}(\nu,\mu)$, inserted into the Fourier plane of the reconstruction setup.

The ideal compensation filter would be $\tilde{F} = \frac{1}{2\cos[\pi\lambda z_H(\nu^2+\mu^2)]}$. But that is not realizable because $\tilde{F}$ is infinite where the $\cos[\ldots]$ goes to zero. To avoid this problem Gabor suggested (in the previously mentioned $1\frac{1}{2}$ lines of footnote) to take instead a filter $\tilde{F}_G = \mathrm{sign}(\cos)$, which could be made by rings of thin transparent film (Fig. 32.9). At least that is the way I interpret Gabor's footnote which reads, "Note added in proof (Feb. 2, 1952). In the meantime I have found it is, in fact, possible to construct zone filters that reduce the disturbing effect of the conjugate image to a small fraction." The sign-function can be realized as a filter consisting of rings of transparent film of a thickness $D = \frac{\lambda}{2(n-1)}$ leading to a $180°$ phase shift. The mathematics now to be used is the same as needed for the process of rectification:

$$\begin{aligned} \cos x &= \frac{1}{2}e^{ix} + \frac{1}{2}e^{-ix} \\ |\cos x| &= \frac{2}{\pi} + \frac{2}{3\pi}e^{2ix} + \frac{2}{3\pi}e^{-2ix} - \frac{2}{15\pi}e^{4ix} - \frac{2}{15\pi}e^{-4ix}\text{etc.} \end{aligned} \tag{32.41}$$

We get the same type of Fourier series if x is replaced by $\pi\lambda(\nu^2+\mu^2)$. (Remember, this treatment is like the pseudo-periodic functions which we represented in Chap. 2 as Fourier series).

Hence the action of the filter $\tilde{F}_G(\nu,\mu) = \text{sign}\{\cos[\pi\lambda z_H(\nu^2+\mu^2)]\}$ changes the factor $\cos[\ldots]$ of the I_H spectrum into:

$$\begin{aligned} &\cos[\ldots]\tilde{F}_G = |\cos[\ldots]| = \\ = \quad &\frac{2}{\pi}\left[1 + \frac{1}{3}e^{i\pi\lambda 2 z_H(\nu^2+\mu^2)} + \frac{1}{3}e^{-i\pi\lambda 2 z_H(\nu^2+\mu^2)} + \ldots\right] = \frac{2}{\pi}[\ldots] \end{aligned} \tag{32.42}$$

$$\mathcal{V}(x,y) = I_H(x,y) = 1 + \frac{4}{\pi}\iint \Delta\tilde{u}(\nu,\mu)[\ldots]e^{2\pi m i(x\nu+y\mu)}\,\mathrm{d}\nu\,\mathrm{d}\mu \tag{32.43}$$

The strongest term in $[\ldots]$ (Eq. 32.43) is the "1", which yields a regular image of the original object $1 + \iint \Delta\tilde{u}_o e^{2\pi i(x\nu+y\mu)}\,\mathrm{d}\nu\,\mathrm{d}\mu$, except for the contrast-enhancing factor $\frac{4}{\pi}$. The other terms will produce defocused spurious images, for example $\frac{1}{3}e^{i\pi\lambda 2 z_H(\nu^2+\mu^2)}$ at a plane $4f - 2z_H$, but with a three-times weaker amplitude, and nine-times weaker intensity. Other spurious images will be at $4f + 2z_H$, $4f \pm 4z_H$, $4f \pm 6z_H$, etc., but these higher spurious images will be very soft. The intensity fraction of the main image is $\frac{8}{\pi^2} = 0.81$.

The third attempt to remove the twin image was conceived in 1955. It is called "Single-Sideband-Holography". Originally it was restricted to real (= phase-free) objects with a strong background. Recently Olof Bryngdahl and I found extensions which can handle any object, but not as well as Leith's & Upatniek's off-line approach, which will be discussed soon as the fourth and best attempt to remove the twin image. (Recommended reading: "Single-Sideband Holography", J. Opt. Soc. Am. 58, 620 (1968).)

32.5 Wave Propagation and Fresnel Transformation

This subject is important for several topics to be considered soon, among others for Leith & Upatnieks' off-axis holography. Although treated before I will present it again, but somewhat differently, in two ways: firstly I will give a somewhat cleaner definition of the Fresnel transformation; secondly, the method of stationary phase is not really needed, at least not explicitly.

Definition: when the complex amplitude $u(x,y,z)$ in plane z propagates into the plane $z+\eta$, where it will be $u(x,y,z+\eta)$, then the Fresnel-transform is defined as $u(x,y,z+\eta) =$

$e^{ik\eta}\underline{P}[u(x,y,z);\eta]$. $\underline{P}$ is meant to be an operator. From the Rayleigh-Sommerfield-Debye diffraction theory (Chapter 18.2) we know:

$$u(x,y,z+\eta) = \iiiint u(x',y',z)e^{2\pi i[\nu(x-x')+\mu(y-y')+\sqrt{1-\lambda^2(\nu^2+\mu^2)}\frac{\eta}{\lambda}]}\mathrm{d}(x'\ y'\nu\mu) \tag{32.44}$$

Proof : since the exponential function by itself satisfies the wave equation, and since the wave equation $\Delta u + k^2 u = 0$ is linear, also the superposition of all exponential functions in the fourfold integral satisfies the wave equation. It is not just any old solution, but the one we are interested in, namely the one which is launched by the boundary value $u(x',y',z')$ in plane z. This can be verified by letting $\eta \longrightarrow 0$, whereby the fourfold integral collapses into a trivial identity. Having now proven the fourfold integral formula, we find by comparision that the $\underline{P}$ operator performs a convolution.

$$\underline{P}(u(x,y,z),\eta) = \iint u(x',y',z')\cdot \tag{32.45}$$
$$\cdot \quad \left\{\iint e^{2\pi i[\nu(x-x')+\mu(y-y')+\frac{\eta}{\lambda}(\sqrt{1-\lambda^2(\nu^2+\mu^2)}-1)]}\mathrm{d}\nu\ \mathrm{d}\mu\right\}\ \mathrm{d}x\ \mathrm{d}y$$

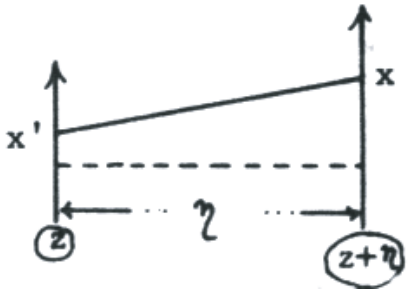

Figure 32.10: Geometrie for the Fresnel propagation.

The "-1" in the exponent is due to the fact that we pulled $e^{ik\eta}$ out of the integral when defining $\underline{P}$. So far this is still rigorous, but now let us approximate, whereby we will come back to our more familiar formulation of the Fresnel transformation. In $\{\iint \ldots \mathrm{d}\nu\ \mathrm{d}\mu\}$ we set $\sqrt{1-\lambda^2(\nu^2+\mu^2)}-1 \approx \frac{\lambda^2}{2}(\nu^2+\mu^2)$. This can be justified in the spirit of the method of the stationary phase, which said that an integral of the type $\int e^{ikf(\nu)}\mathrm{d}\nu$ will be $\approx e^{ikf(\nu_0)}\cdot$ const., where ν_0 follows from $\frac{df}{d\nu}=0$, and $f(\nu)$ has been replaced by $f(\nu_0)+\frac{f''(\nu_0)}{2}(\nu-\nu_0)^2$. This means that the integrand $e^{ikf(\nu)}$ oscillates rapidly, except around ν_0, where $f(\nu)$ changes only slowly. Looking at the specific exponent above, it is seen that

$$\frac{\partial f(\nu,\mu)}{\partial \nu} = \lambda(x-x') - \frac{\lambda^2 \eta \nu}{\sqrt{1-\lambda^2(\nu^2+\mu^2)}}; \qquad \text{or} \qquad \frac{\lambda\nu_0}{\sqrt{1-\lambda^2(\nu^2+\mu^2)}} = \frac{x-x'}{\eta} \tag{32.46}$$

(similar $\frac{\partial f}{\partial \mu}$)

Remembering the significance of x, x', η: $\frac{(x-x')}{\eta}$ can be identified as a tangent. If now the lateral extension $\Delta x'$ of the input and the lateral extension Δx of the output are both smaller than η (and only then should we use the approximation now under consideration), it is clear that $|\lambda\nu_0|$ and $|\lambda\mu_0|$ will be smaller than unity, hopefully small enough so that $\sqrt{1-\lambda^2(\nu^2+\mu^2)} \approx 1 - \frac{\lambda^2}{2}(\nu^2+\mu^2)$ is justified. For this to be true the next term of the Taylor expansion has to be small compared to π, that is $k\eta\frac{\lambda^4}{8}(\nu^2+\mu^2) \ll \pi$. Now the convolution kernel assumes the form

$$\begin{aligned} \{\} &\approx e^{2\pi i[\nu(x-x')+\mu(y-y'-\frac{\lambda\eta}{2}(\nu^2+\mu^2))]}\mathrm{d}\nu\,\mathrm{d}\mu = \\ &= \int e^{2\pi i[\nu(x-x')-\lambda\eta\frac{\nu^2}{2}]}\mathrm{d}\nu \int e^{2\pi i[\mu(y-y')-\lambda\eta\frac{\eta^2}{2}]}\mathrm{d}\mu \end{aligned} \tag{32.47}$$

So far we did not really say anything about the limits of integration, which actually should be given by $\nu_L^2+\mu_L^2=1$, such *in*cluding all plane waves, but *ex*cluding all evanescent waves, which stick closely to $u(x,y,z)$, and hence cannot contribute to $u(x,y,z+\eta)$ at distances $\eta \gg \lambda$. However, now we let the integrals go from $-\infty$ to $+\infty$, which will not change the result because the integrand oscillates heavily outside of $\nu^2+\mu^2=1$. This may seem fishy. As long as the root in the exponent $\sqrt{1-\lambda^2(\nu^2+\mu^2)}$ was still intact we did stick to the $\nu^2+\mu^2 \le 1$ region of integration, but now with $\sqrt{\dots} = 1-\frac{\lambda^2}{2}(\nu^2-\mu^2)$ we just ignore the plane wave limitation $\nu^2+\mu^2 \le 1$ by integrating over the whole (ν,μ) domain. If the integrand oscillates, except around the saddlepoint (ν_0,μ_0), then a change of the region of integration does not matter, as long as the saddle point stays inside of the legitimate bounds $\nu^2+\mu^2 \le 1$.

$$\iint\limits_{\mathrm{A}_1} e^{ikf(\nu)}\mathrm{d}\nu\,\mathrm{d}\mu \approx \int\limits_{\mathrm{A}_1+\mathrm{A}_2}\int e^{ikf(\nu,\mu)}\mathrm{d}\nu\,\mathrm{d}\mu \tag{32.48}$$

if $e^{ikf(\nu)}$ oscillates except at (ν_0,μ_0) which is within region A_1.

We did all this in order to get our unknown integrals into the shape of the Fresnel integral:

$$\int\limits_{-\infty}^{+\infty} e^{i\alpha x^2} = \sqrt{\frac{i\pi}{\alpha}} \tag{32.49}$$

We do this by filling up the exponent into a quadratic expression:

$$2\pi\left[\nu(x-x')-\lambda\eta\frac{\nu^2}{2}\right] = -[\nu^2\pi\lambda\eta-2\nu\pi(x-x')] = \tag{32.50}$$

$$= -\pi\lambda\eta\left[\nu^2+2\nu\frac{x-x'}{\lambda\eta}\right] = -\pi\lambda\eta\left[\nu-\frac{x-x'}{\lambda\eta}\right]^2+\pi\lambda\eta\left[\frac{x-x'}{\lambda\eta}\right]^2$$

$$\int_{-\infty}^{\infty} e^{2\pi i[\nu(x-x')-\lambda\eta\frac{\nu^2}{2}]}\mathrm{d}\nu = e^{i\pi\frac{(x-x')^2}{\lambda\eta}}\int_{-\infty}^{\infty} e^{-i\pi\lambda\eta[\nu-\frac{(x-x')}{\lambda\eta}]^2}\mathrm{d}\nu = \tag{32.51}$$

$$= e^{i\pi\frac{(x-x')^2}{\lambda\eta}}\int_{-\infty}^{\infty} e^{-i\pi\lambda\eta\nu'^2}\mathrm{d}\nu' = e^{i\pi\frac{(x-x')^2}{\lambda\eta}}\sqrt{\frac{i\pi}{-\pi\lambda|\eta|}} = e^{+\dots}\sqrt{\frac{-i}{\lambda|\eta|}}$$

where $\nu' = \nu - \frac{x-x'}{\lambda\eta}$.

In the same way one gets for the second integral:

$$\int e^{2\pi i\left[\mu(y-y')-\frac{\lambda\eta\mu^2}{2}\right]}\mathrm{d}\mu \approx e^{i\pi\frac{(y-y')^2}{\lambda\eta}}\sqrt{\frac{-i}{\lambda|\eta|}} \tag{32.52}$$

and as their product:

$$\approx \frac{-i}{\lambda|\eta|}e^{i\pi\frac{(x-x')^2+(y-y')^2}{\lambda\eta}} \tag{32.53}$$

Inserting this result into the original formula 32.46 of the Fresnel- or propagation operator $\underline{P}$, we get:

$$\underline{P}[u(x,y,z),\eta] \approx \frac{-i}{\lambda|\eta|}\iint u(x',y',z)e^{i\pi\frac{(x-x')^2+(y-y')^2}{\lambda\eta}}\,\mathrm{d}x'\,\mathrm{d}y' \tag{32.54}$$

$$u(x,y,z+\eta) = e^{ik\eta}\underline{P}[u(x,y,z),\eta]$$

Connecting this with our earlier notation it is
$\underline{P}[\dots,+\eta] \sim .\hat{.}.$ (forward propagation), $\underline{P}[\dots,-\eta] \sim .\check{.}.$ (backward propagation).

32.6 Off-Line Fresnel Holography

Leith & Upatnieks, JOSA 52, 1123 (1962)

This is the fourth and by far the most important attempt to overcome the twin-image problem. It is probably the most important achievement in holography since Gabor's original invention. First I will explain it qualitatively in terms of Fresnel zone plates, later in a more quantitative way.

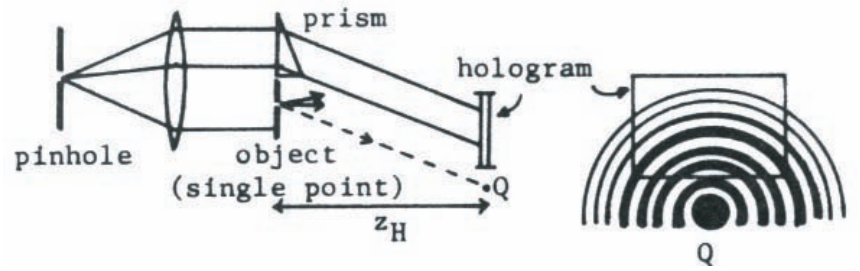

Figure 32.11: The interference formed during hologram recording (Notice: the FZP center Q is not on the hologram).

32.6.1 Recording Step

An off-center portion of a FZP interference fringe system is recorded on the hologram (Fig. 32.11). The FZP-center would appear where the plane reference wave, coming from the prism, is parallel to the spherical wave, coming from the object point. Important: the hologram is as wide as the reference beam. (Making the hologram smaller would waste some light from the reference beam; making it wider is not meaningful, because we get the phase information from the object wave only by way of interference with the reference wave.) Under these circumstances the FZP-center Q for any object point besides the prism will be outside of the hologram.

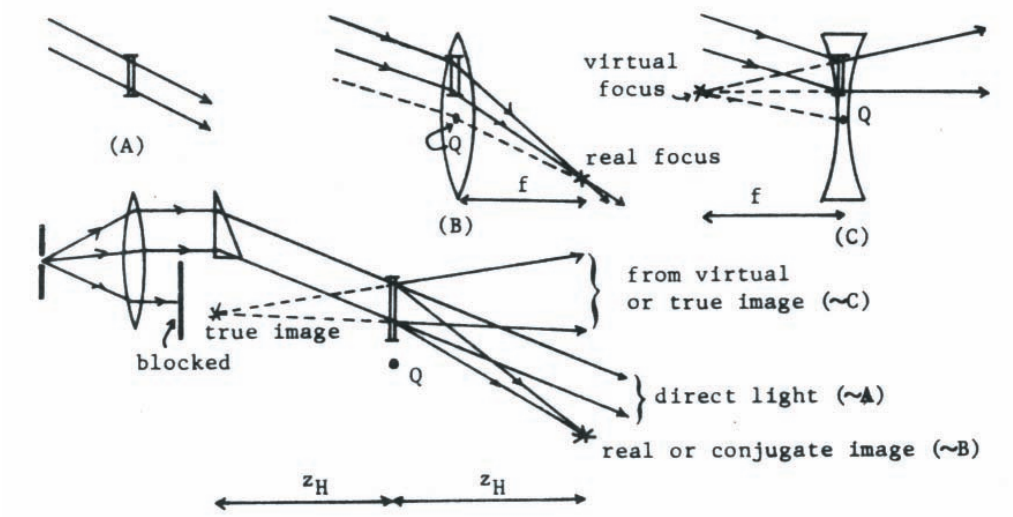

Figure 32.12: Reconstruction of the off-axis hologram.

32.6.2 Reconstruction

For understanding the reconstruction process remember that FZP acted simultaneously like a plane plate (a), like a positive lens (B), and like a negative lens (C) (Fig. 32.12). The lens center is at the FZP center.

The virtual image point, the FZP center point Q, and the real image point are on a joint straight line. This follows from considering the FZP (same as the hologram) as a pair of positive and negative lenses. (Rays going through a lens center are not deviated by refraction.) Looking at the reconstruction figure (Fig. 32.12) tells us that the three beams (*true* or *virtual*, *conjugate* or *real*, *direct*) can be separated at a suitable z-plane, if and only if Q is off the hologram. But this is assured if the (plane) reference wave in the recording process comes from *beside* the object. As we will see later, it is not necessary in general that the plane wave used for reconstruction duplicates the plane reference reference wave of the recording process.

32.6.3 Theory of Off-Line-Fresnel Holography

The object in $z = 0$ is illuminated by means of $u_L(x, y, z) = e^{ikz}$;
immediately before the object: $u_L(x, y, z) = 1$;
immediately behind the object with
complex amplitude transmission u_0: $u(x, y, +0) = u_L(x, y, -0)u_0(x, y) = u_0(x, y)$;
$u_0(x, y) = \iint \tilde{u}_0(\nu, \mu)e^{2\pi i(x\nu+y\mu)}\mathrm{d}\nu\ \mathrm{d}\mu$;

Propagation to the hologram plane $z = z_H$;

$$u(x, y, z_H) = \iint \tilde{u}_0(\nu, \mu)e^{2\pi i\left[x\nu+y\mu+\sqrt{1-\lambda^2(\nu^2+\mu^2)}\frac{z_H}{\lambda}\right]}\mathrm{d}\nu\ \mathrm{d}\mu \tag{32.55}$$

There also a tilted plane wave arrives from the prism.
Both waves together (object wave + reference wave) are: $u_H(x, y) = u(x, y, z_H) + e^{-2\pi ix\nu_R}$.

Recorded will be the intensity:

$$I_H(x, y) = |u_H(x, y)|^2 = 1+u(x, y, z_H)e^{2\pi ix\nu_R}+u^*(x, y, z_H)e^{-2\pi ix\nu_R}+|u(x, y, z_H)|^2 \tag{32.56}$$

Next we develop the hologram photographically, again *linearly*; that means the (complex) amplitude transmittance after developing is equal to the recorded intensity, $\mathcal{V}_H(x, y) = I_H(x, y)$.

Will it be possible to separate the various terms of V_H?

$$\mathcal{V}_H = \underbrace{1}_{\text{direct}} + \underbrace{u e^{2\pi i x \nu_R}}_{\substack{\text{true or} \\ \text{virtual}}} + \underbrace{u^* e^{-2\pi i x \nu_R}}_{\substack{\text{conjugate or} \\ \text{real}}} + \underbrace{|u|^2}_{\text{intramodulation}} \tag{32.57}$$

The intramodulation term is often but not always negligible! (From now on we will use only the newer names *true* and *conjugate* instead of the old ones *virtual* and *real*).

Looking at the reconstruction figure (Fig. 32.12) tells us that the chances for cutting out all but one term, say *true*, are the better the farther we are away from the hologram. Hence it might be best at infinity, which can be realized in the rear focal plane of a lens. But there one would observe the Fourier transform (due to Fraunhofer diffraction) of the hologram transmittance $\mathcal{V}_H$. Let's compute $\tilde{\mathcal{V}}_H$.

$$\tilde{\mathcal{V}}(\nu,\mu) = \iint I_H(x,y) e^{-2\pi i(x\nu+y\mu)} \mathrm{d}x\, \mathrm{d}y = \tag{32.58}$$

$$= \delta(\nu,\mu) +$$

$$+ \iiiint \tilde{u}_0(\nu',\mu') e^{2\pi i\left[\nu' x+\mu' y+\sqrt{1-\lambda^2(\nu'^2+\mu'^2)}\frac{z_H}{\lambda}+\nu_R x-\nu x-\mu y\right]} \mathrm{d}(\nu'\ \mu'\ x\ y)$$

$$+ \iiiint \tilde{u}_0^*(\nu',\mu') e^{2\pi i\left[-\nu' x-\mu' y-\sqrt{1-\lambda^2(\nu'^2+\mu'^2)}\frac{z_H}{\lambda}-\nu_R x-\nu x-\mu y\right]} \mathrm{d}(\nu'\ \mu'\ x\ y)$$

$$+ \iiiiii \tilde{u}_0(\nu',\mu')\tilde{u}_0^*(\nu'',\mu'') \cdot$$

$$\cdot\ e^{2\pi i\left[\nu' x+\mu' y+\sqrt{1-\lambda^2(\nu'^2+\mu'^2)}\frac{z_H}{\lambda}-\{\nu'' x+\mu'' y+\sqrt{1-\lambda^2(\nu''^2+\mu''^2)}\frac{z_H}{\lambda}\}-\nu x-\mu y\right]} \mathrm{d}(\nu'\mu'\nu''\mu'' xy)$$

$$= \overbrace{\delta(\nu,\mu)}^{\text{direct}} + \overbrace{\tilde{u}_0(\nu-\nu_R,\mu)}^{\text{true}} e^{\pi i\sqrt{1-\lambda^2\{(\nu-\nu_R)^2+\mu^2\}}\frac{z_H}{\lambda}} +$$

$$+ \overbrace{\tilde{u}_0^*(-\nu-\nu_R,-\mu_R)}^{\text{conjugate}} e^{-2\pi i\sqrt{1-\lambda^2\{(\nu+\nu_R)^2+\mu^2\}}\frac{z_H}{\lambda}} +$$

$$+ \overbrace{\iint \tilde{u}_0(\nu',\mu')\tilde{u}_0^*(\nu'-\nu,\mu'-\mu)}^{\text{intramodulation}} e^{2\pi i\frac{z_H}{\lambda}\left[\sqrt{1-\lambda^2(\nu'^2+\mu'^2)}-\sqrt{1-\lambda^2\{(\nu'-\nu)^2+(\mu'-\mu)^2\}}\right]} \mathrm{d}\nu'\, \mathrm{d}\mu'$$

Consequences: *true* and *conjugate* are separable from *direct* if $|\nu_R| \geq \frac{\Delta\nu}{2}$, where $\Delta\nu$ is the spectral width of the object (Fig. 32.13). If the *intramodulation* term is not negligible, one has to require even more for *true-intramodulation* separation, $|\nu_R| \geq \frac{3\Delta\nu}{2}$. If the object spectrum $\tilde{u}_0(\nu,\mu)$ does not simply cover a square or a circular region of the frequency domain (ν,μ), it might pay off to rotate the object $u_0(x,y)$ around the z-axis. This becomes clear in the following case, where (at left) the (ν,μ) - domain is better utilized. This will become even clearer when we discuss later the influence of the photographic material.

Here, as well as in connection with the previous figure, it was tacitly assumed to be know that the intramodulation integral can cover a (ν,μ) area of twice the diameter of the (ν,μ)

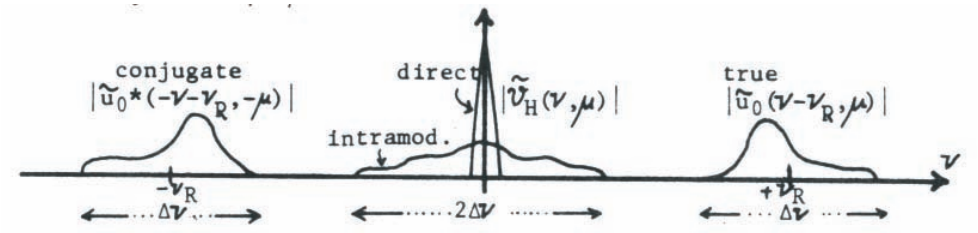

Figure 32.13: The diffraction pattern (1D) of an off-line hologramm — location of the various distributions (terms in Eqs 32.58).

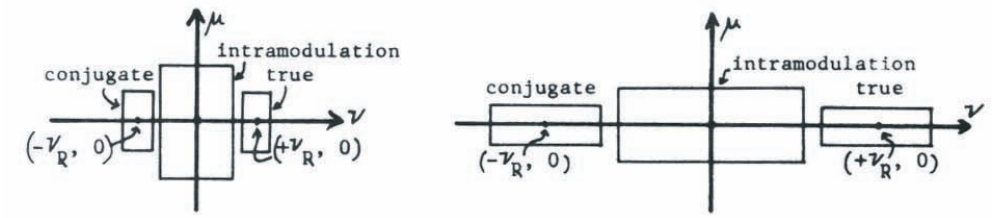

Figure 32.14: The diffraction pattern (2D) of an off-line hologramm — location of the various distributions (terms in Eqs 32.58).

area from $|\tilde{u}_0(\nu,\mu)|$. This is quite plausible, if the intramodulation integral is visualized in the following steps: take $\tilde{u}_0(\nu',\mu')$, then take $\tilde{u}_0^*$, but shift it by a vector (ν,μ), overlap (= multiply) $\tilde{u}_0(\nu',\mu')$ and $\tilde{u}_0^*(\nu'-\nu,\mu'-\mu)$. This product can be non-zero only if $\tilde{u}_0(\nu',\mu')$ and $\tilde{u}_0^*(\nu'-\nu,\mu'-\mu)$ overlap in the (ν',μ') domain. For this to be true the shift of $\tilde{u}_0$ and $\tilde{u}_0^*$ should not exceed the diameter of $\tilde{u}_0$ itself. But the shift might go into positive and into negative direction, hence the autocorrelation integral of u_0 might extend from $-\Delta\nu$ to $\Delta\nu$.

32.6.4 Theory of the reconstruction process

Illuminate the hologram (in $z = z_H - 0$) with: $e^{-2\pi i x \nu_R}$;
immediately behind the hologram: $\mathcal{V}(x,y,z_H+0) = \mathcal{V}(x,y)e^{-2\pi i x\nu_R}$;

$$\mathcal{V}(x,y,z_H{+}0) = e^{-2\pi i x\nu_R} + u(x,y,z_H) + u^*(x,y,z_H)e^{-4\pi i x\nu_R} + |u(x,y,z_H)|^2 e^{-2\pi i x\nu_R} \tag{32.59}$$

The second term is a perfect replica of the original object wavefront. As long as we observe only in $z > z_H$ it is impossible to say if this wavefront comes directly from the original object (without the hologram), or if this wavefront is formed by the hologram (and no

object is around). $u(x, y, z_H)$ is now called the true or virtual wavefield. "Virtual" refers to the fact that we cannot catch an image on a screen from this wavefront. A lens is needed, for example the eye's lens, to produce an image, which is called "the image of the virtual or true image". In the reconstruction setup shown in Fig. 32.15 it is possible to block the direct light in the rear focal plane of the lens where the direct light is focussed. And the conjugate image can be rejected in $z = \frac{2f}{3}$.

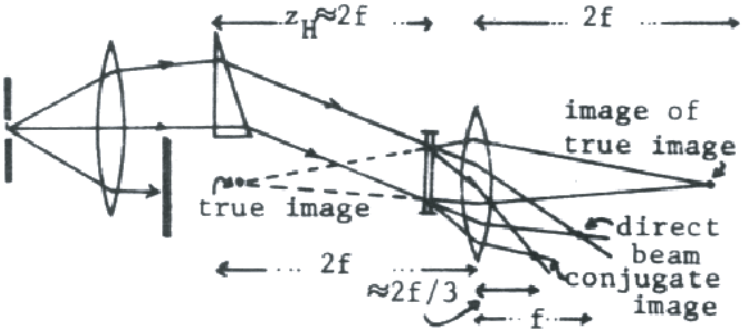

Figure 32.15: Reconstruction of an off-line hologramm.

Now let us discuss the wavefront, which would create the conjugate image, in some detail.

$$u_0^*(x, y, z_H)e^{-4\pi i x\nu_R} = \iint \tilde{u}_0^*(\nu, \mu)e^{2\pi i\left[-x\nu - y\mu - \sqrt{1-\lambda^2(\nu^2+\mu^2)}\frac{z_H}{\lambda} - 2x\nu_R\right]}\mathrm{d}\nu\ \mathrm{d}\mu \tag{32.60}$$

Let us assume the reconstruction setup of Fig. 32.15, but *without* the lens behind the hologram. We know from our qualitative FZP discussion, that the real image will appear in $z = 2z_H$. This time I will do it in a somewhat different style, a style which sometimes is more practical, but nevertheless the same as Rayleigh-Sommerfeld-Debye, fundamentally. Instead of computing the propagation process for the *whole* complex amplitude, we compute it first for convenient parts, and then add up the result. This is allowed because the propagation operator is a *linear* operator, more specifically a convolution. For a *linear* operator $\underline{P}$: $\underline{P}[u_1(x) + u_2(x); \eta] = \underline{P}[u_1(x); \eta] + \underline{P}[u_2(x); \eta]$. This can be generalized to include also integration, which is a summation of infinitely many terms:

$$\text{if} \qquad u(x) = \int u(\sigma)\Psi(\sigma, x)\mathrm{d}\sigma; \quad \text{then} \tag{32.61}$$
$$\underline{P}\left[\int u(\sigma)\Psi(\sigma, x)\mathrm{d}\sigma; \eta\right] = \int u(\sigma)\left\{\underline{P}[\Psi(\sigma, x); \eta]\right\}\mathrm{d}\sigma$$

This might simplify things if $\underline{P}[\Psi(\sigma, x); \eta]$ is easy to get. In our case, where we want to compute the propagation from z_H to $2z_H$ we have to apply $e^{ikz_H}\underline{P}[\ldots; \eta]$ upon

$$\iint \tilde{u}_0^*(\nu,\mu) e^{2\pi i\left[-x\nu-y\mu-\sqrt{1-\lambda^2(\nu^2+\mu^2)}\frac{z_H}{\lambda}-2x\nu_R\right]} \mathrm{d}\nu\ \mathrm{d}\mu.$$

As justified on the previous page, we may go with the operator into the integral, where we have to evaluate:

$e^{ikz_H}\underline{P}[e^{-2\pi i[x(\nu+2\nu_R)+y\mu]}; z_H] = e^{2\pi i\left[-x(\nu+2\nu_R)-y\mu+\sqrt{1-\lambda^2\{(\nu+2\nu_R)^2+\mu^2\}}\frac{z_H}{\lambda}\right]}$
which is multiplied by the not-(x,y) dependent factor
$\tilde{u}_0^*(\nu,\mu)e^{-2\pi i\sqrt{1-\lambda^2(\nu^2+\mu^2)}\frac{z_H}{\lambda}}$, and integrated $\iint \ldots \mathrm{d}\nu\ \mathrm{d}\mu$:

$$\iint u_0^*(\nu,\mu) e^{2\pi i\left[-x(\nu+2\nu_R)-y\mu+\frac{z_H}{\lambda}\left(\sqrt{1-\lambda^2\{(\nu+2\nu_R)^2+\mu^2\}}-\sqrt{1-\lambda^2(\nu^2+\mu^2)}\right)\right]} \mathrm{d}\nu\ \mathrm{d}\mu \tag{32.62}$$

$$\left(\sqrt{1-\lambda^2\{(\nu+2\nu_R)^2+\mu^2\}}-\sqrt{1-\lambda^2(\nu^2+\mu^2)}\right) \approx \tag{32.63}$$
$$\approx 1-\frac{\lambda^2}{2}\left\{(\nu+2\nu_R)^2+\mu^2\right\}+\frac{\lambda^4}{8}\{\ldots\}^2-1+\frac{\lambda^2}{2}(\nu^2+\mu^2)-\frac{\lambda^4}{8}(\nu^2+\mu^2)=$$
$$-2\lambda^2(\nu_R\nu+\nu_R)+\lambda^4\epsilon(\nu,\mu)$$

The term ϵ which contains the higher orders is sometimes called "holographic wave aberrations" (R. W. Meier, 1965). Now let us pull in front of the integral in Eq. 32.65 whatever possible.

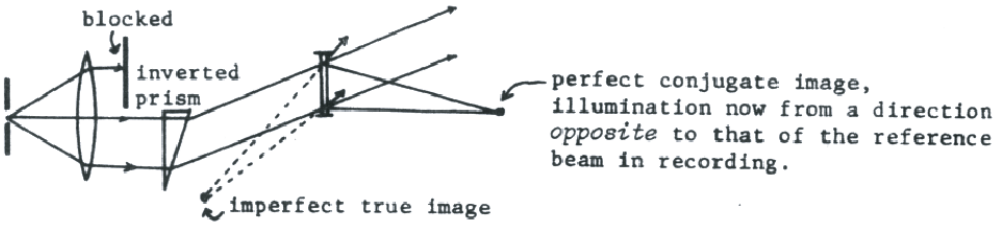

Figure 32.16: Modified reconstruction setup in order to avoid the phase error on the *conjugate* image.

$$e^{-2\pi i(2\nu_R x-2z_H\lambda\nu_R^2)}\iint \tilde{u}_0^*(\nu,\mu)\overbrace{e^{-2\pi i[\nu(x+2\lambda z_H\nu_R)+y]}}^{\text{lateral shift}}\overbrace{e^{2\pi i\lambda^3 z_H\epsilon(\nu,\mu)}}^{\text{phase error}}\mathrm{d}\nu\ \mathrm{d}\mu \approx$$
$$\approx u_0^*(x+2\lambda z_H\nu_R, y) \quad [\epsilon \text{ neglected}] \tag{32.64}$$

We see that the conjugate image is not perfect due to the phase factor with ϵ. The phase factor in front of the integral is harmless, because it drops out when we compute the intensity of the conjugate image by forming the modulus square. However, it is quite easy to

get a perfect conjugate image by illuminating the hologram transmittance $\mathcal{V}_H(x,y)$ not with $e^{-2\pi i x \nu_R}$ but with $e^{+2\pi i x \nu_R}$:

$$\mathcal{V}_H(x,y,z_H+0) = \mathcal{V}_H(x,y)e^{2\pi i x\nu_R} + u(x,y,z_H)e^{4\pi i x\nu_R} + \\ +u^*(x,y,z_H) + |u(x,y,z_H)|^2 e^{2\pi i x\nu_R} \tag{32.65}$$

The third term is perfect for getting a conjugate image at $2z_H$. But now the true image will suffer from an ϵ-phase factor, and it will be laterally shifted $x \longrightarrow x + 2\lambda\nu_R z_H$. What really changed was only the angle of incidence.

32.6.5 About the Pseudoscopic Structure of the Conjugate Image

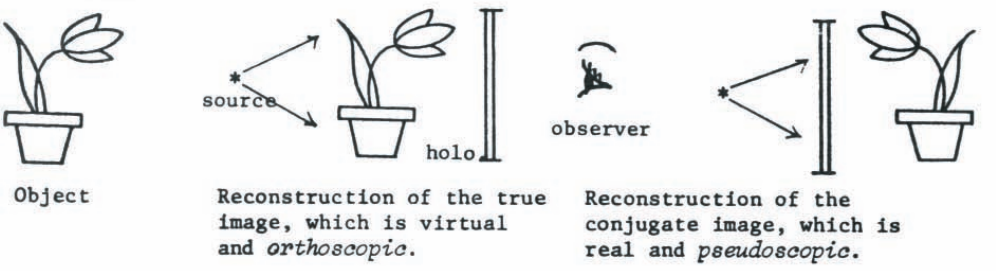

Figure 32.17: Virtual and real images during hologram reconstruction.

To avoid confusion it is desirable to again make some remarks about the nomenclature. If the illumination wave used in reconstruction is a replica of the reference wave of the recording process, then the complex conjugate in $I_H \approx 1 + ue^{+\cdots} + u^*e^{-\cdots}$ will create a *real* image, while the term without the star will be responsible for the *virtual* image. *"Real"* in the sense of geometrical optics means that this image is located *outside* of the area between source and hologram, so that it is accessible for an observer. For example this image can be captured on a screen. But the *virtual* image will be created somewhere between source and hologram, where it is not accessible. If you would put there a white screen, you would not see the virtual image because at that place the light did not yet have the opportunity to get any information about the original object out of the hologram. However, behind the hologram, the wave behaves as if there had been an object (= virtual image) in front of the hologram. The "as if" is a *complete* simulation, since one can do everything with the virtual wavefield one could have done with the original wavefield which came directly from an actual object. If you reach around the hologram, as most first-time viewers do, you will find that the "as if" simulation is complete only in $z \geq z_H$.

"Pseudoscopic" means a depth inversion. For example, when looking at the pseudoscopic image of a face the nose does not appear as the usual prominence but as a dent.

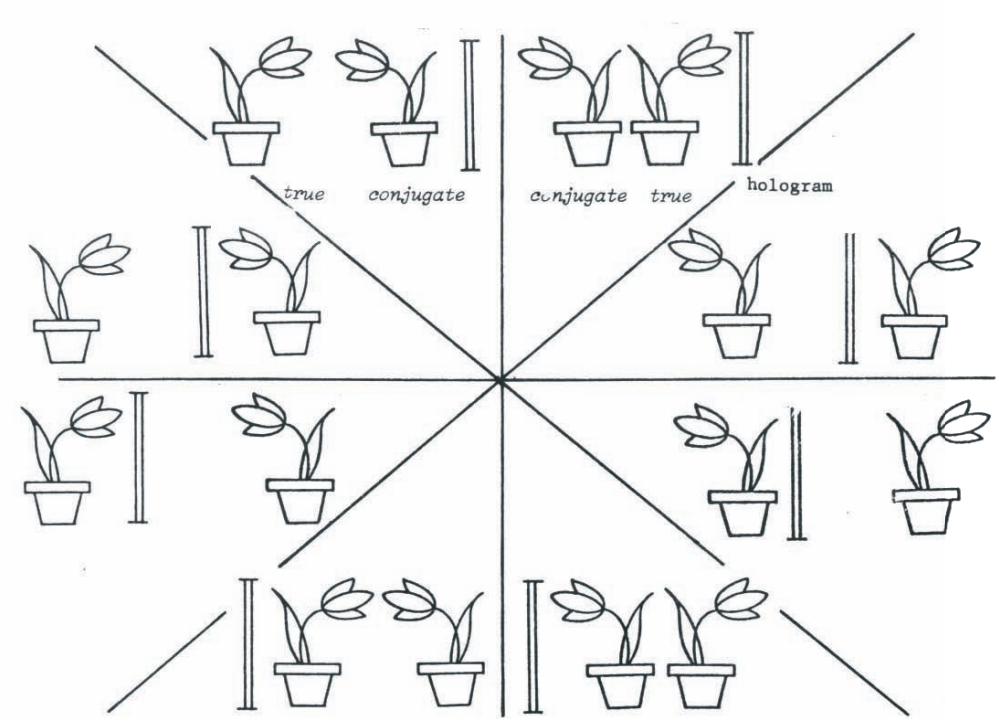

Figure 32.18: Variety of possible reconstruction situations of an object from the recorded hologram.

One reason why the u^*-term should not be called the *real* wavefield and the u-term called the *virtual* wavefront anymore is that these terms are ambiguous as R. W. Meier (JOSA, 55, 987, 1965) has shown. This ambiguity may occur if the curvature of the reference wave is different from the curvature of the re-illuminating wave. In this more general case it is possible to have the conjugate image (from $u*$) appear *in front of* the hologram, such that it is actually *virtual* in the sense of geometrical optics. But it will always be pseudoscopic, while the "true image" (from u) will create always an orthoscopic image, which may be located in front of the hologram (=virtual) or behind the hologram (= real). This depends on the curvatures of the reference and re-illumination waves as we will see soon. All conceivable situations might actually occur as shown in the Fig. 32.18. The object is a flower pot with the blossom bent to the right. Both the object and later the hologram are illuminated from the left.

For the proof it is important to recognize the difference between a *divergent* and a *convergent* spherical wave (Fig. 32.19).

divergent: $e^{+ikr} = e^{ik\sqrt{x^2+y^2+z^2}} \approx e^{ikz} e^{\frac{i\pi}{\lambda z}(x^2+y^2)}$

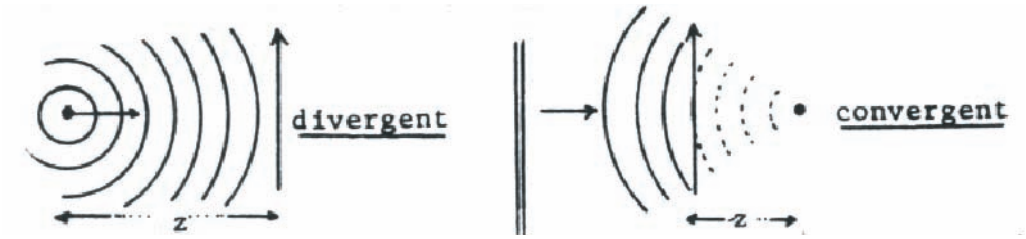

Figure 32.19: Convergent and divergent spherical waves.

convergent: $e^{-ikr} = e^{-ik\sqrt{x^2+y^2+z^2}} \approx e^{-ikz} e^{-\frac{i\pi}{\lambda z}(x^2+y^2)}$

It is the $\pm$-sign of the quadratic portion of the exponent which indicates the property: divergent $(+)$, or convergent $(-)$. The $e^{\pm ikz}$ is merely an uninteresting constant in this context. Now let us assume the recording setup illustrated in Fig. 32.20:

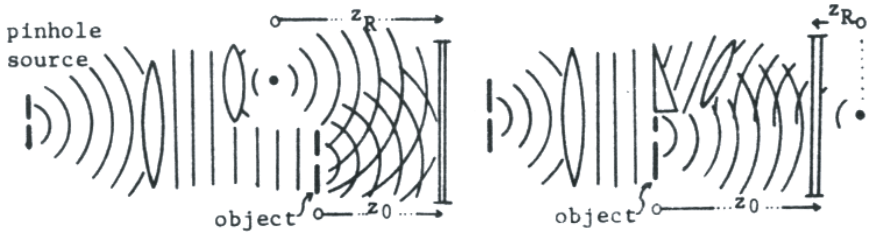

Figure 32.20: Setups for recording with divergent and convergent illumination.

The object may consist of a single point, which creates a spherical wave (divergent) in the hologram plane. The reference wave is also a divergent spherical wave, but with a different curvature. But the reference wave could be also convergent, as in the right-hand section of Fig. 32.20. (Notice: a length is counted positive if indicated as $\longrightarrow$, and negative if $\longleftarrow$).

$$u(x,y,z_H) = \overbrace{e^{i\pi\frac{(x-x_R)^2+y^2}{\lambda z_R}}}^{\text{reference wave}} + \overbrace{a e^{\frac{i\pi}{\lambda z_0}}}^{\text{object wave}} \tag{32.66}$$

$$\begin{aligned} I_H(x,y) &= |u(x,y,z_H)|^2 \qquad (32.67)\\ &\approx 1 + a e^{i\frac{\pi}{\lambda}\left[\frac{x^2+y^2}{z_0} - \frac{(x-x_R)^2+y^2}{z_R}\right]} + a^* e^{-i\frac{\pi}{\lambda}\left[\frac{x^2+y^2}{z_0} - \frac{(x-x_R)^2+y^2}{z_R}\right]} \\ &= 1 + a e^{i\frac{\pi}{\lambda}\left[(x^2+y^2)\left(\frac{1}{z_0}-\frac{1}{z_R}\right)+\text{something}\right]} + a^* e^{-i\frac{\pi}{\lambda}\left[(x^2+y^2)\left(\frac{1}{z_0}-\frac{1}{z_R}\right)+\text{something}\right]} \end{aligned}$$

"Something" stands for everything which is not quadratic in (x, y), and which has therefore no influence on the *curvature* of the wave. After linear photographic development we get $I_H(x, y) = \mathcal{V}_H(x, y)$. Next we illuminate the hologram with a spherical wave:

$$\mathcal{V}_L(x, y, z_H - 0) = e^{i\frac{\pi(x+y)}{\lambda z_L}} = \begin{cases} z_L > 0 & \sim \text{ divergent} \\ z_L < 0 & \sim \text{ convergent} \\ z_L = \infty & \sim \text{ plane wave} \end{cases} \tag{32.68}$$

This spherical illumination wave has its convergent point on the z-axis somewhere. This specialization is unimportant in this context since only the *quadratic* phase terms determine the z-locations of the images. Behind the hologram the complex amplitude is:

$$\begin{aligned} \mathcal{V}_H(x, y, z_H + 0) &= \mathcal{V}(x, y, z_H - 0)\mathcal{V}_H(x, y) = e^{i\pi\frac{x^2+y^2}{\lambda z_L}} + \\ &+ \underbrace{a e^{i\frac{\pi}{\lambda}\left[\left(x^2+y^2\right)\left(\frac{1}{z_0}-\frac{1}{z_R}+\frac{1}{z_L}\right)+\text{something}\right]}}_{\text{I}} \\ &+ \underbrace{a^* e^{i\frac{\pi}{\lambda}\left[\left(x^2+y^2\right)\left(-\frac{1}{z_0}+\frac{1}{z_R}+\frac{1}{z_L}\right)+\text{something}\right]}}_{\text{II}} \end{aligned} \tag{32.69}$$

The term I is called the *true* wavefront; it is convergent if $\frac{1}{z_0} - \frac{1}{z_R} + \frac{1}{z_L} < 0$ and divergent if $\frac{1}{z_0} - \frac{1}{z_R} + \frac{1}{z_L} > 0$.

The term II is called the *conjugate* wavefront; it is convergent if $-\frac{1}{z_0} + \frac{1}{z_R} + \frac{1}{z_L} < 0$ and divergent if $-\frac{1}{z_0} + \frac{1}{z_R} + \frac{1}{z_L} > 0$.

A *convergent* wave will come to a focus to the right of the hologram, while a *divergent* wave has a virtual focus to the left of the hologram (focus "as if"). The "something" term might be linear in x and y, and also contain constants. The linear x, y terms describe merely a lateral (x, y) shift of the focal points. It is now convenient to describe the spherical wavefronts in curvatures $c = \frac{1}{z}$ instead of the distance z from the spherical wave center to the plane of observation.

$$c_0 = \frac{1}{z_{\text{obj}}}; \quad c_R = \frac{1}{z_{\text{ref}}}; \quad c_L = \frac{1}{z_{\text{illum.}}}; \quad c_1 = \frac{1}{z_{\text{conj.}}}; \quad c_2 = \frac{1}{z_{\text{true}}}; \tag{32.70}$$

Two more abbreviations: $x^2 + y^2 = \varrho^2$; "something not quadratic in (x, y)" $= s$. In this notation the wavefield behind the hologram during reconstruction is:

$$\mathcal{V}_H(x, y, z_H + 0) = \underbrace{e^{i\frac{\pi c_L \varrho^2}{\lambda}}}_{\text{direct}} + a\underbrace{e^{i\frac{\pi}{\lambda}\left[(+c_0-c_R+c_L)\varrho^2+s\right]}}_{\text{true}} + a^*\underbrace{e^{i\frac{\pi}{\lambda}\left[(-c_0+c_R+c_L)\varrho^2+s\right]}}_{\text{conjugate}} \tag{32.71}$$

The term "true" with $+c_0$ must be *orthoscopic* (= no depth inversion), because c_0 appeared with + in front of it in the original wavefield.

Let me explain this in some more detail. Suppose the object consisted of two points at different depth positions z_{01}, z_{02} (Fig. 32.21), where $z_{02} > z_{01} \Longrightarrow c_{02} < c_{01}$:

$$\begin{aligned} u(x,y,z_H) &= u_{\rm ref} + a_1 e^{i\frac{\pi}{\lambda}(c_{01}\varrho^2+s)} + a_2 e^{i\frac{\pi}{\lambda}(c_{02}\varrho^2+s)} \\ \mathcal{V}_H(x,y) &= |u(x,y,z_H)|^2 \approx |u_{\rm ref}|^2 + u^*_{\rm ref}(a_1 e^+ + a_2 e^+) + u_{\rm ref}(a_1^* e^- + a_2^* e^-); \\ \mathcal{V}(x,y,z_H+0) &= \mathcal{V}(x,y,z_H-0)\mathcal{V}_H(x,y) \\ u_{\rm ref} &= e^{i\frac{\pi}{\lambda}(c_R\varrho^2+s)}; \mathcal{V}_L = e^{i\frac{\pi}{\lambda}(c_L\varrho^2+s)} \end{aligned} \tag{32.72}$$

Figure 32.21: Object with two points at different depth positions.

$$\begin{aligned} \mathcal{V}(x,y,z_H+0) &= e^{i\frac{\pi}{\lambda}(c_L\varrho^2+s)} + \\ &+ \underbrace{e^{i\frac{\pi}{\lambda}[(c_L-c_R)\varrho^2+s]}\left[a_1 e^{i\frac{\pi}{\lambda}(c_{01}\varrho^2+s)} + a_2 e^{i\frac{\pi}{\lambda}(c_{02}\varrho^2+s)}\right]}_{\text{true}} + \\ &+ \underbrace{e^{i\frac{\pi}{\lambda}[(c_L+c_R)\varrho^2+s]}\left[a_1^* e^{i\frac{\pi}{\lambda}(-c_{01}\varrho^2+s)} + a_2^* e^{i\frac{\pi}{\lambda}(-c_{02}\varrho^2+s)}\right]}_{\text{conjugate}} = \\ &= e^{i\frac{\pi}{\lambda}(c_L\varrho^2+s)} + \\ &+ \underbrace{a_1 e^{i\frac{\pi}{\lambda}[(c_{01}+c_L-c_R)\varrho^2+s]} + a_2 e^{i\frac{\pi}{\lambda}\left[(c_{02}+c_L-c_R)\varrho^2+s\right]}}_{\text{true}} + \\ &+ \underbrace{a_1^* e^{i\frac{\pi}{\lambda}[(-c_{01}+c_L+c_R)\varrho^2+s]} + a_2^* e^{i\frac{\pi}{\lambda}\left[(-c_{02}+c_L+c_R)\varrho^2+s\right]}}_{\text{conjugate}} \end{aligned} \tag{32.73}$$

The true term with a_1 and a_2 *without* $*$ must be *orthoscoic* for the following reason. Since by assumption $c_{01} > c_{02}$, it is also true that $(c_{01} + c_L - c_R) > (c_{02} + c_L - c_R)$. Hence it follows $z_{11} < z_{12}$ and $z_{01} < z_{02}$, which means that the depth-order in the true image is the

same as in the object. Similarly we find for the conjugate terms with a_1^* and a_2^*: $z_{01} < z_{02}$ and $z_{21} < z_{22}$. This means that the depth-order in the conjugate image is opposite from the depth order in the object.

One can show the same thing much more briefly: the object wave $ae^{i\frac{\pi}{\lambda}(c_O\varrho^2+s)}$ is reconstructed as:

$$\underbrace{ae^{i\frac{\pi}{\lambda}(c_1\varrho^2+s)}}_{\text{true}} + \underbrace{a^*e^{i\frac{\pi}{\lambda}(c_1\varrho^2+s)}}_{\text{conjugate}} \tag{32.74}$$

Herein the curvatures c_1 and c_2 are:

$$c_1 = c_0 - c_R + c_L; \qquad c_2 = -c_0 + c_R + c_L \tag{32.75}$$

We compare these two image wave curvatures with the object wave curvature by computing the derivatives $\frac{\mathrm{d}c_1}{\mathrm{d}c_0} = +1$ and $\frac{\mathrm{d}c_2}{\mathrm{d}c_0} = -1$. Translating these curvature statements we get on the basis of the definition $c = \frac{1}{z}$:

$$\begin{aligned}
\frac{\mathrm{d}z_1}{\mathrm{d}z_0} &= \left(\frac{\mathrm{d}z_1}{\mathrm{d}z_0}\right)^2 \frac{\mathrm{d}c_1}{\mathrm{d}c_0}; \quad \frac{\mathrm{d}c_1}{\mathrm{d}c_0} = +1 \implies \frac{\mathrm{d}z_1}{\mathrm{d}z_0} > 0 \quad \text{true is orthoscopic} \\
\frac{\mathrm{d}z_2}{\mathrm{d}z_0} &= \left(\frac{\mathrm{d}z_2}{\mathrm{d}z_0}\right)^2 \frac{\mathrm{d}c_2}{\mathrm{d}c_0}; \quad \frac{\mathrm{d}c_2}{\mathrm{d}c_0} = -1 \implies \frac{\mathrm{d}z_2}{\mathrm{d}z_0} < 0 \quad \text{conjugate is pseudoscopic}
\end{aligned} \tag{32.76}$$

Now let us return to the question of whether the true and conjugate images will appear in front of or behind the hologram.

true	left from hologram	if	$c_1 > 0 \longrightarrow +c_0 - c_R + c_L > 0;$
true	right from hologram	if	$c_1 < 0 \longrightarrow +c_0 - c_R + c_L < 0;$
conjugate	left from hologram	if	$c_2 > 0 \longrightarrow -c_0 + c_R + c_L > 0;$
conjugate	right from hologram	if	$c_2 < 0 \longrightarrow -c_0 + c_R + c_L < 0;$
center gravity	left from hologram	if	$c_1 + c_2 > 0 \longrightarrow c_L > 0;$

These results are summarized in Fig. 32.22. The (c_R, c_L) domain is divided into eight equal octants around $(c_L = 0)$, $c_R = c_0$. The eight corresponding configurations of true image, conjugate image and hologram had been shown before in a corresponding arrangement in Fig. 32.18. Although this classification in terms of curvatures c gives a neater result, the corresponding classification in depth coordinates $z = \frac{1}{c}$ is easier to relate to a given experimental situation.

Two more topics in connection with the pseudoscopic property of the conjugate image should be discussed, firstly a more general and elegant proof of the pseudoscopic feature, and secondly an attempt to explain why it is so hard to observe visually the pseudoscopic image.

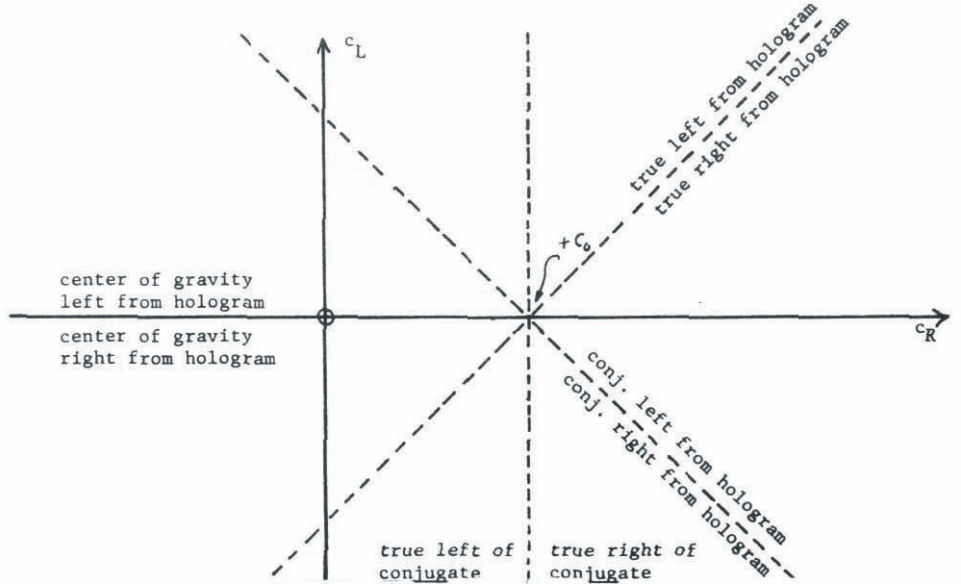

Figure 32.22: Hologram reconstruction in the (c_R, c_L) domain.

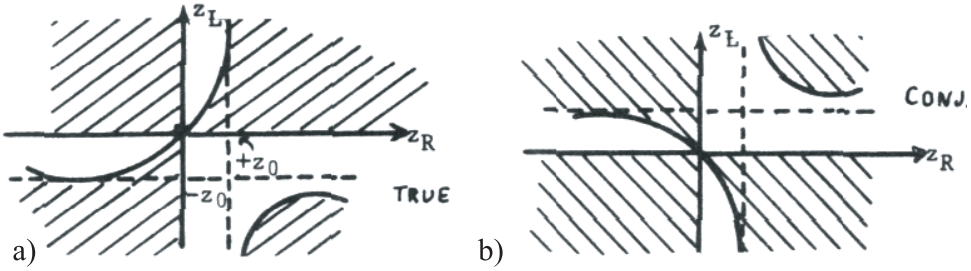

Figure 32.23: Hologram reconstruction in the (z_L, z_R)-domain: a) shaded area: $\frac{1}{z_0} - \frac{1}{z_R} + \frac{1}{z_L} > 0$ means true image *left* of hologram. The conjugate image is right of the image if $z_R > z_0$; b) Shaded area: $-\frac{1}{z_0} + \frac{1}{z_R} + \frac{1}{z_L} < 0$ means conjugate image *right* of hologram. Center of gravity left of the hologram in $z_L < 0$. (Sign convention: the hologram is at $z = 0$. Positive z-values are left of the hologram, negative z-values to the right of it)

As we will see, the occurrence of the pseudoscopic by-product is due to the fact that a hologram transmittance is real. (Complex holograms are exceptions to be treated later.) A wave amplitude $v(x, y)$ in plane z is assumed to be real: $v(x, y) = v^*(x, y)$. Another way to state the reality of $v(x, y)$ is to split it up into two conjugate portions: $v(x, y) = u(x, y) + u^*(x, y)$. This can be done of course in many different ways, but you might think of $u(x, y)$ as

coming from the "true" portion of $I_H(x,y)$ and u^* from the "conjugate" portion. The direct term of I_H is of no interest in this context. Let us call temporarily $u(x,y) = u_1(x,y)$ and $u^*(x,y) = u_2(x,y)$. From these definitions it follows immediately that it is $u_1^* = u_2$. Now we compute two propagations; one forward, and another backwards:

$$\begin{aligned} &u_1(x,y) \text{ from } z \text{ to } z-\eta: \quad u_1(x,y,z-\eta) \\ &u_2(x,y) \text{ from } z \text{ to } z+\eta: \quad u_1(x,y,z+\eta) \end{aligned} \tag{32.77}$$

According to Eq. 32.42:

$$\begin{aligned} u_1(x,y,z-\eta) &= e^{-ik\eta}\underline{P}\left[u_1(x,y);-\eta\right] \\ u_2(x,y,\eta) &= e^{+ik\eta}\underline{P}\left[u_1(x,y);+\eta\right] \end{aligned} \tag{32.78}$$

Now we want to make use of a symmetry property of $\underline{P}$, which holds for any function inside of []. Using this for $u_1(x,y,z-\eta)$ we get:

$$\begin{aligned} u_1(x,y,z-\eta) = e^{-k\eta}\underline{P}[u_1(x,y);-\eta] = e^{-ik\eta}\left\{\underline{P}[u_1^*(x,y);+\eta]\right\}^* = \\ = \left\{e^{+ik\eta}\underline{P}[u_1^*(x,y);+\eta]\right\}^* \end{aligned} \tag{32.79}$$

Insert now the assumption $u_1^* = u_2$, which yields $= \{u_2(x,y,z+\eta)\}^* = u_1(x,y,z-\eta)$. This says what is forward propagated $(z \longrightarrow -\eta)$ from $u^*(x,y)$ is the same (except for a^*) as what is backward propagated $(z \longrightarrow +\eta)$ from $u(x,y)$. Hence u and u^* create wavefields which are symmetrical to each other, folded around plane z. This z-folding means depth inversion. In other words, while an object $u_O(x)$ in $z=0$ might create $u(x,z)$ in $z \neq 0$, the associated complex conjugate object $u^*(x)$ will create a wavefield $u^*(x,-z)$.

Methods of *linear* optics (lenses, transparencies, polarizers, waveplates, phase-shifters, etc.) cannot produce a $(^*)$-operation. Hence no depth-inversion can be produced with those components. For a depth inversion it takes something *non-linear* like the modulus-square process to create a $(*)$. A mirror is an interesting case to study. After reflection the z-coordinate of the object is inverted, if $\vec{z}_0$ is the surface normal vector. But also the z-component of all the k-vectors have been inverted. Hence $zk_z = z'k'_z$. In that case no pseudoscopic effect occurs. The ortho-pseudo transformation $z''k'_z = -zk_z$.

32.6.6 Why is it so tricky to see the pseudoscopic image?

There are two reasons for the difficulty of seeing the pseudoscopic image, in my opinion (which differs from what you might find in the literature), firstly a simple geometrical reason, and then, our brain computer is confused when presented with pseudoscopic information. To understand the geometrical reason let us assume that the pseudoscopic or conjugate image is between hologram and eye, as is common in practice since mostly $c_R \approx c_L$ applies. To emphasize this geometrical reason let the object be much wider than the hologram. The distance eye-image z_E (conjugate or true) may be the same for both cases (see Figs 32.24).

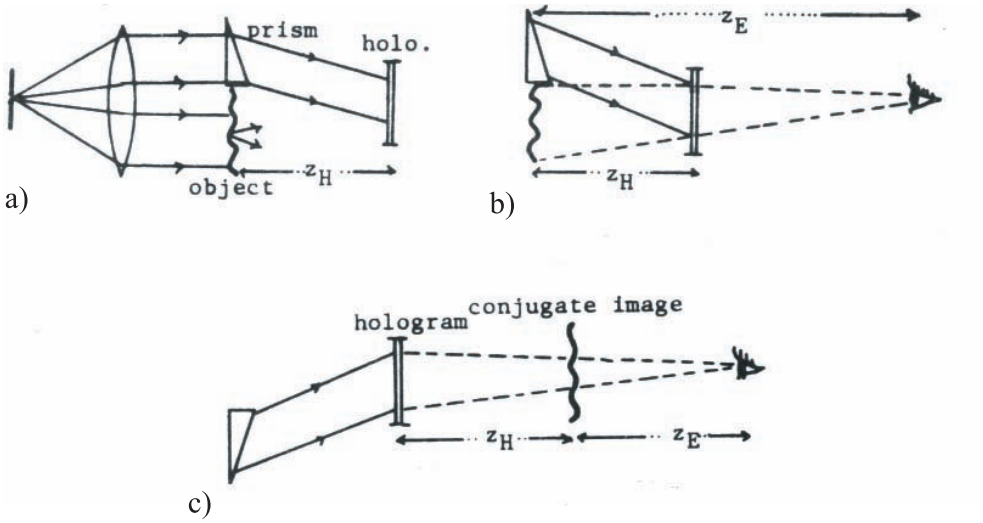

Figure 32.24: Observation of pseudoscopic images: a) recording process; b) observation of the true image: *all* of the object is visible from one eye position; c) observation of the conjugate image: observation from the same distance image-to-eye. Now only a small portion of the image is back illuminated for any particular eye position. One cannot see the whole image simultaneously.

These figures show that one cannot see all parts of the *conjugate* image at the same time, only sequentially by moving the head sidewise. This is a handicap for comprehending the image, even if the object is flat. Even for the comprehension of a local detail (say a single letter in a written word) it is very desirable, and often necessary to see simultaneously the environment, the "context". The "geometrical reason" we have just considered occurs whenever an image is located *in front of* the hologram as seen from the eye. This situation can happen both for the true and for the conjugate image. Hence this reason is not necessarily connected with the *pseudoscopic* (= conjugate) image. However, in practice the conjugate image is usually *in front of* the hologram and the true image behind it. One reason for doing it this way is that the "holographic aberrations" (see page 389) will be small in that configuration.

To explain the second reason it is necessary to comment first on how we perceive depth visually. To a certain degree we can vary the focal power of our eye lens, till we find a sharp position. But as depth-locating method this approach is probably useless beyond arm's length. More far-reaching is binocular triangulation, but not beyond a few meters. Thereafter we rely on dynamic experiences.

Apparent angular velocity	Obscuration
object is still eye moves (Fig. 32.25)	
Observation: $\left\|\frac{\mathrm{d}\alpha}{\mathrm{d}x}\right\| < \left\|\frac{\mathrm{d}\beta}{\mathrm{d}x}\right\|$	Observation: B-object obscures A
Conclusion: $z_A > z_B$	Conclusion: $z_A < z_B$

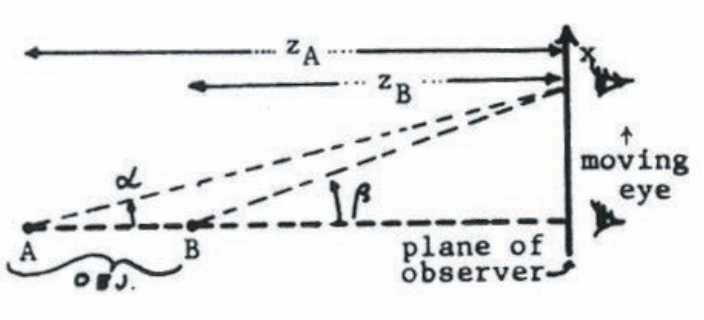

Figure 32.25: Perception of depth through trinagulation.

32.6.7 Dynamic angular velocity

Also longitudinal movements of the eye provide a depth clue. If the angular extent of object A at distance z_A, is α and for B at z_B it is β, then $\left|\frac{\mathrm{d}\alpha}{\mathrm{d}x}\right| < \left|\frac{\mathrm{d}\beta}{\mathrm{d}x}\right| \longrightarrow z_A > z_B$.

Whenever we can apply these two dynamic schemes and draw conclusions from obscuration observations, even at short distances we probably do better than with focusing and triangulation.

Observation of the true image (Fig. 32.26 a)):

1. relative angular velocity $\left|\frac{\mathrm{d}\alpha}{\mathrm{d}x}\right| < \left|\frac{\mathrm{d}\beta}{\mathrm{d}x}\right| \longrightarrow z_A > z_B$.
2. B can obscure A $\longrightarrow z_A > z_B$.

Observation of the conjugate image (Fig. 32.26 b)):

3. $\left|\frac{\mathrm{d}\alpha'}{\mathrm{d}x}\right| > \left|\frac{\mathrm{d}\beta'}{\mathrm{d}x}\right| \longrightarrow z'_A < z'_B$
4. B' (which is wider than A') can obscure A' $\longrightarrow z'_B < z'_A$

(3) and (4) are contradictory!

The longitudinal movement yields the same conclusion as the lateral movement of the eye. When two indirect means of assessing depth give contradicting results, the brain-computer's diagnostic message is "execution inhibited". The final, mental act of synthesizing a hypothesis of the 3D structure of the outer world is not possible, because the input data are logically inconsistent. This experience is as confusing as if you were to look at a candle, and whenever you held your hand *behind* the candle, the candle was obscured (Fig. 32.27).

Maybe someone could make a hologram with c_O, c_R, c_L parameters such that the "geometrical trouble" is not severe. Take a cardboard model of the hand and of the candle.

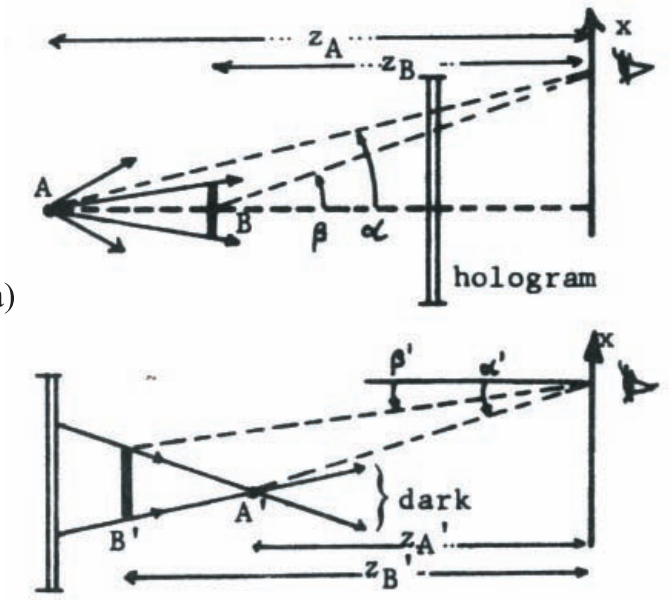

Figure 32.26: Observation of the a) real and b) pseudoscopic image reconstructed by a hologram.

Figure 32.27: Watching a candle in front of the hand.

Finally a remark on how to get the most striking 3D effects: take in two steps the conjugate image of the conjugate image, which will be *orthoscopic* again. Set it up so that it appears a short distance before the second-generation hologram as seen from the eye.

32.7 Classification of holographic setups

As we have said many times before the basic trick to holography, which enables us to preserve phase information despite a photographic recording process (modulus square sensitive), is to

superpose upon the unknown object wave a known reference wave, which in the recording process acts like the local oscillator of a heterodyne receiver. Re-illuminating the hologram with a wave which is a replica of the former reference wave is all we have to do to recreate the former object wave. In this recipe it is never said where in the optical setup we should place the hologram. We can do it everywhere in principle, although from a practical point of view the four setups shown in Fig. 32.28 each have their own merits. In Fig. 32.28 we only sketch the off-line setups.

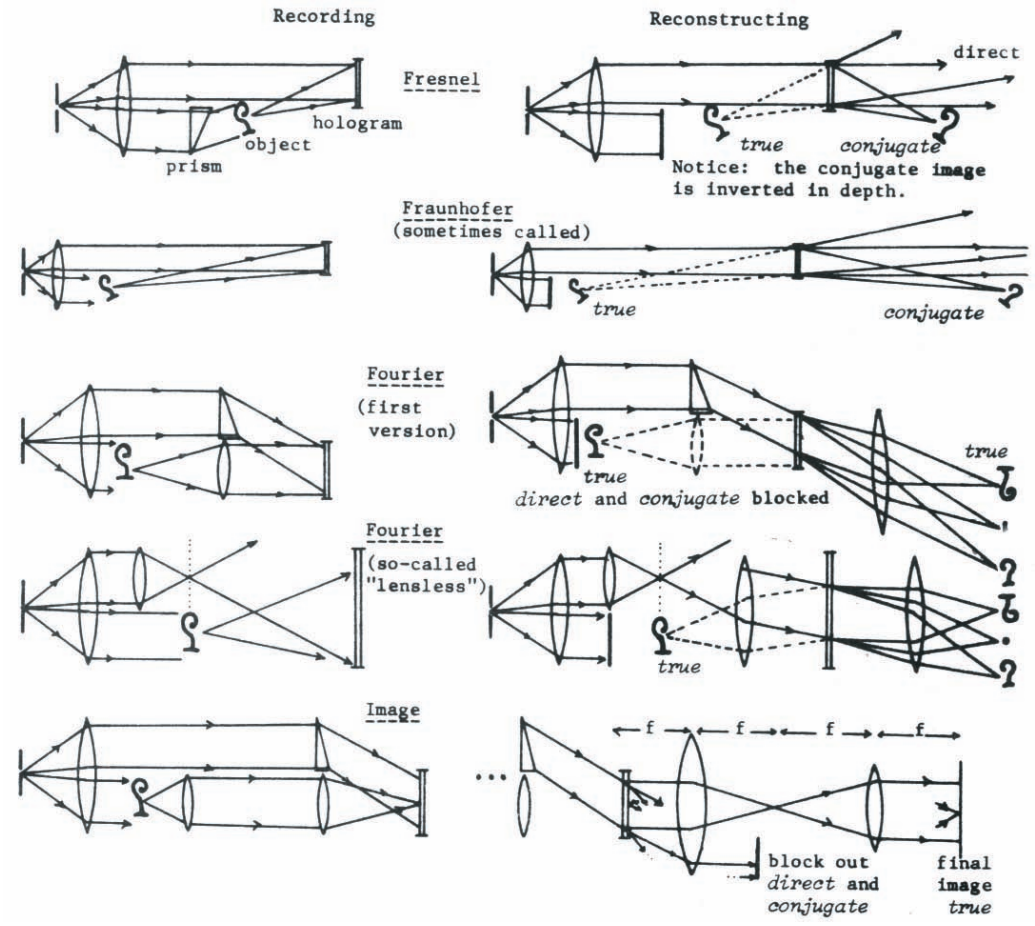

Figure 32.28: Various configurations for off-line holography.

32.7.1 Fraunhofer off-line holography

You might find the nomenclature confusing. It really is, mainly due to lack of coordination, but perhaps also due to personal vanity, or for making patent claims seem novel. Anyway, Fraun-

hofer diffraction is the *very-far* version of Fresnel diffraction. "Very far" means that if the object $u_O(x,y) \neq 0$ only in $|x| \leq \frac{\Delta x_0}{2}, |y| \leq \frac{\Delta y_0}{2}$, then the distance from object to hologram (where the Fraunhofer diffraction pattern is recorded) shall be large: $2z_H \geq \frac{(\Delta x_0)^2+(\Delta y_0)^2}{\lambda}$. This is the condition under which the Fresnel transformation can be approximated by a Fourier transformation.

Illumination:	$u_L(x,y,z) = e^{ikz} \quad \text{in} \quad z \leq 0$
in $z=-0$, in front of the object:	$u_L(x,y,-0) = 1$
behind the object:	$u(x,y,0) = u_L(x,y,-0)u_0(x,y) = u_0(x,y)$

After propagation from $z=0$ to $z=z_H$ (see Eq. 32.63):

$$\begin{aligned} u(x,y,z_H) &= e^{ikz_H}\underline{P}[u(x,y,+0),z_H] = \\ &\approx \frac{-ie^{ikz_H}}{\lambda|z_H|}\iint u_0(x',y')e^{i\frac{\pi}{\lambda z_H}\left\{(x-x')^2+(y-y')^2\right\}}\mathrm{d}x'\mathrm{d}y' \end{aligned} \tag{32.80}$$

where $\left\{(x-x')^2+(y-y')^2\right\} = x^2+y^2-2(xx'+yy')+x'^2+y'^2$

The (x^2+y^2) term can be pulled out of the integral. The $(x'^2+y'^2)$ term can be neglected if the object size is limited by $(\Delta x_0)^2+(\Delta y_0)^2 \leq 2\lambda z_H$.

$$\begin{aligned} u(x,y,z_H) &\approx \frac{-i}{\lambda|z_H|}e^{ik\left(z_H+\frac{x^2+y^2}{2z_H}\right)}\iint u_0(x',y')e^{-2\pi i\frac{xx'+yy'}{\lambda z_H}}\mathrm{d}x'\mathrm{d}y' \\ &= \frac{-i}{\lambda|z_H|}e^{ik\left(z_H+\frac{x^2+y^2}{2z_H}\right)}\tilde{u}_0\left(\frac{x}{\lambda z_H},\frac{y}{\lambda z_H}\right) \end{aligned} \tag{32.81}$$

This wave arrives from the object at the hologram. In addition a plane reference wave will be there: e^{ikz_H}. Both together form the exposing intensity $I_H = |e^{ikz_H} - \frac{i}{\lambda z_H}\ldots|^2$.

$$I_H(x,y) \approx \underbrace{1}_{direct} - \underbrace{\frac{i}{\lambda|z_H|}e^{ik\frac{(x^2+y^2)}{2z_H}}\tilde{u}_0\left(\frac{x}{\lambda z_H},\frac{y}{\lambda z_H}\right)}_{true} + \underbrace{\frac{i}{\lambda|z_H|}e^{-\cdots}\tilde{u}_0^*}_{conjugate} + \underbrace{\frac{|\tilde{u}_0|^2}{(\lambda z_H)^2}}_{intramodulation} \tag{32.82}$$

In reconstruction the true and the conjugate images are at distances z_H in front of and behind the hologram as shown in Fig. 32.28. If the two twin images are so very far ($2z_H$) apart one can afford not to bother about any mutual disturbance even for in-line Fraunhofer holography. This case has been studied in particular by B. J. Thompson et al. The Reynolds & DeVelis book contains a detailed discussion.

32.7.2 Fourier holography (off-line)

Both in Fourier holography and in Fraunhofer holography the Fourier transform $\tilde{u}_0$ of the object u_0 falls onto the hologram. That is why many people feel there should only be one name

for both. But there are two differences, although minor ones: the production of the reference wave happens in a different way (see Fig. 32.28); furthermore in Fraunhofer holography it is not $\tilde{u}_0$ itself, but $\tilde{u}_0\left(\frac{x}{\lambda z_H}, \frac{y}{\lambda z_H}\right) e^{i\left(\frac{\pi}{\lambda z_H}\right)(x^2+y^2)}$ which arrives from the object at the hologram plane. It is a matter of taste whether this quadratic phase factor should justify a whole new category in holography. Such a phase factor can occur also if any one of the lenses in the Fourier-recording setup is shifted longitudinally.

The theory of Fourier holography is very simple, and similar to previous Fourier manipulations:

Recording:

$$u(x,y) \longrightarrow \tilde{u}\left(\frac{x}{\lambda f}, \frac{y}{\lambda f}\right) \longrightarrow \left|\tilde{u}\left(\frac{x}{\lambda f}, \frac{y}{\lambda f}\right) + e^{2\pi i \frac{xx_0+yy_0)}{\lambda f}}\right|^2 = \tag{32.83}$$

$$= \quad I_H(x,y) = \tilde{u}_0 e^- + \tilde{u}_0 e^+ + 1 + |\tilde{u}_0|^2; \qquad I_H \longrightarrow \mathcal{V}_H = I_H$$

Reconstruction:

Another Fourier transform for $\mathcal{V}_H$, which might be illuminated under normal incidence (but not necessarily).

$$\frac{1}{(\lambda f)^2} \iint \mathcal{V}_{\mathcal{H}}(x',y') e^{-2\pi i \frac{xx'+yy'}{\lambda f}} \mathrm{d}x' \, \mathrm{d}y' = \tag{32.84}$$

$$= \underbrace{\delta(x,y)}_{direct} + \underbrace{u_0(-x-x_0,-y-y_0)}_{true} + \underbrace{u_0^*(x-x_0,y-y_0)}_{conjugate} +$$

$$+ \underbrace{\iint u_0(\overline{x},\overline{y}) u_0^*(\overline{x}+x,\overline{y}+y) \mathrm{d}\overline{x}\mathrm{d}\overline{y}}_{intramodulation}$$

32.7.3 Lensless Fourier holography

The setups shown for lensless Fourier holography in Fig. 32.28 were incomplete. Reconstruction can be achieved in different ways (Fig. 32.29).

Recording theory: in $z = 0$ the object $u_0(x,y)$ and a point source beside it are $u(x,y,+0) = u_0(x,y) + \delta(x-x_0, y-y_0)$. Propagation to the plane of the hologram:

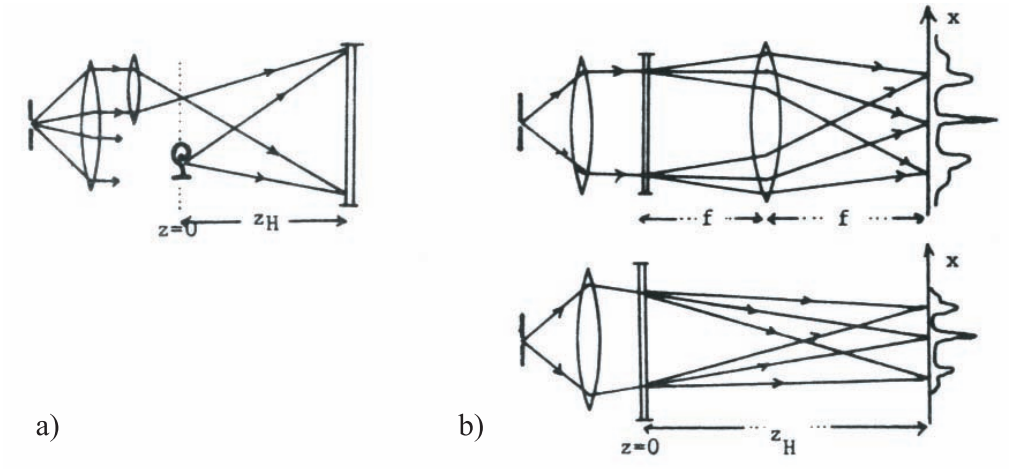

Figure 32.29: Setups for recording (a) and reconstruction (b) of lensless Fourier holograms.

$$
\begin{aligned}
u(x,y,z_H) &= e^{ikz_H}\underline{P}\,[u(x,y,+0);z_H] = \qquad (32.85)\\
&= \frac{-ie^{ikz_H}}{\lambda|z_H|}\iint u(x',y',+0)e^{i\frac{\pi}{\lambda z_H}[(x-x')^2+(y-y')^2]}\mathrm{d}x'\,\mathrm{d}y' =\\
&= \frac{-ie^{ik\left(z_H\frac{x'+y'}{z_H}\right)}}{\lambda|z_H|}\iint u(x',y',+0)e^{i\frac{\pi}{\lambda z_H}(-2xx'-2yy'+x'^2+y'^2)}\mathrm{d}x'\,\mathrm{d}y' =\\
&= \frac{-ie^{ik\left(z_H\frac{x'+y'}{z_H}\right)}}{\lambda|z_H|}\left\{\iint u(x',y')e^{i\frac{\pi}{\lambda z_H}(-2xx'-2yy'+x'^2+y'^2)}\mathrm{d}x'\,\mathrm{d}y' +\right.\\
&+ \left. e^{i\frac{\pi}{\lambda z_H}(-2xx'-2yy'+x'^2+y'^2)}\right\}
\end{aligned}
$$

Now we assume that the object u_0 is small compared to the distance z_H from object to hologram. More precisely, $u_0(x',y') \neq 0$ only in $|x'| \leq \frac{\Delta x_0}{2}; |y'| \leq \frac{\Delta y_0}{2}$;

$$\frac{\pi(x'^2+y'^2)}{\lambda|z_H|} \leq \frac{\pi\{(\Delta x_0)^2+(\Delta y_0)^2\}}{4\lambda|z_H|} \leq \frac{\pi}{4} \qquad (32.86)$$

This assumption (made before on other occasions of diffraction at "very far distances") is

$$(\Delta x_0)^2+(\Delta y_0)^2 \leq \lambda|z_H| \qquad (32.87)$$

If this assumption is justified we can neglect $(x'^2+y'^2)$-term in the exponent of the $\int\int u_0 \ldots \mathrm{d}x'\,\mathrm{d}y'$, which now becomes:

$$\iint u_0(x',y')e^{-2\pi i\frac{(xx'+yy')}{\lambda z_H}}\,\mathrm{d}x'\,\mathrm{d}y' = \tilde{u}_0\left(\frac{x}{\lambda z_H},\frac{y}{\lambda z_H}\right) \tag{32.88}$$

The intensity falling onto the hologram is

$$\begin{aligned} I_H(x,y) &= |u(x,y,z_H)|^2 = \frac{1}{(\lambda z_H)^2}|\{\ldots\}|^2 = \\ &= \frac{1}{(\lambda z_H)^2}\left[1+\tilde{u}_0\left(\frac{x}{\lambda z_H},\frac{y}{\lambda z_H}\right)e^{-i\frac{\pi}{\lambda z_H}(x_0^2+y_0^2-2xx_0-2yy_0)}+\text{c.c.}+|\tilde{u}_0|^2\right] \end{aligned} \tag{32.89}$$

The "1" corresponds to the "direct light", the $\tilde{u}_0$ to the "true" image, the $\tilde{u}_0^*$ to the "conjugate" image, and $|\tilde{u}_0|^2$ is the "intramodulation term".

Now comes the photographic development process, which we assume to be *linear*, that is the amplitude transmittance $V_H(x,y)$ after development is assumed to be proportional to the intensity $I_H(x,y)$ before exposure:

$$V_H(x,y) = I_H(x,y) \tag{32.90}$$

In reconstruction let us this time compute the simpler setup (Fig. 32.29), which contains only one lens. By the way, the term "lensless" refers to the fact that no lens is between object and hologram in the recording process. The nomenclature "lensless" is misleading. When reading some of the literature one might make the following invalid conclusion. For X-rays we do not have lenses, at least not good lenses. Hence a lensless recording setup is highly desirable for X-ray holography. However the fact that in the so-called "lensless" scheme no lens is needed between object and hologram does not make this scheme suitable for X-ray holography because a lens is needed *in front of* the object.

The hologram in $z=0$ is illuminated by a convergent spherical wave: $\mathcal{V}_H(x,y,-0) = e^{-i\pi\frac{x'^2+y'^2}{\lambda z_H}}$. This wave would come to a focus at a distance which is assumed to be equal to z_H, the distance between object and hologram during recording. Behind the hologram the complex amplitude is $\mathcal{V}(x,y,+0) = \mathcal{V}_L(x,y,-0)\mathcal{V}_H(x,y)$. We will find the two images at $z=z_H$, which can be computed by applying the propagation operator:

$$\begin{aligned} \mathcal{V}_H(x,y,z_H) &= e^{ikz_H}\underline{P}[\mathcal{V}(x,y,+0);z_H] \approx \\ &\approx \frac{-ie^{ikz_H}}{\lambda|z_H|}\iint \mathcal{V}(x',y',+0)e^{i\pi\frac{(x-x')^2+(y-y')^2}{\lambda z_H}}\,\mathrm{d}x'\,\mathrm{d}y' = \\ &= \frac{-ie^{ik\left(z_H+\frac{x'+y'}{\lambda z_H}\right)}}{\lambda|z_H|}\iint \mathcal{V}(x',y',+0)e^{i\frac{\pi}{\lambda z_H}(-2xx'-2yy'+x'^2+y'^2)}\mathrm{d}x'\,\mathrm{d}y' \end{aligned} \tag{32.91}$$

At this point we do not make any assumption about the width of $\mathcal{V}(x',y',+0)$ which would allow us to drop the $x'^2+y'^2$ term in the exponent. This means, although our object u_0 had to

be limited in lateral size, our hologram $\mathcal{V}_H$ can be as wide as we want it to be. In actuality the hologram is mostly wider than the object, so that the viewing angle is large, which allows us to enjoy parallax observation. Now let us insert $\mathcal{V}(x', y', +0)$ from Eq. 32.89. It is convenient to change the integration variables: $x' \longrightarrow \lambda\nu z_H$; $y' \longrightarrow \lambda\nu z_H$; $\mathrm{d}x'\mathrm{d}y' \Longrightarrow (\lambda z_H)^2 \mathrm{d}\nu\mathrm{d}\mu$.

$$\begin{aligned}\mathcal{V}_H(x,y,z_H) \quad = \quad & \frac{-ie^{ik\left(z_H+\frac{x'^2+y'^2}{z_H}\right)}}{\lambda|z_H|} \iint \underbrace{e^{-i\pi\lambda z_H(\nu^2+\mu^2)}}_{\mathcal{V}_L} \ldots \\ & \ldots \underbrace{\left[1+\tilde{u}_0(\nu,\mu)e^{2\pi i(x_0\nu+y_0\mu)}e^{-i\pi\frac{(x_0^2+y_0^2)}{\lambda z_H}} + \text{c.c.} + |\tilde{u}_0|^2\right]}_{\mathcal{V}_H} \ldots \\ & \ldots \underbrace{e^{-2\pi i(x\nu+y\mu)}e^{i\pi\lambda z_H(\nu^2+\mu^2)}}_{\text{from propagation operator}} \mathrm{d}\nu\mathrm{d}\mu \end{aligned} \tag{32.92}$$

The $e^{\pm i\pi\lambda z_H(\nu^2+\mu^2)}$ terms cancel each other. Hence we get

$$\begin{aligned} & \frac{-ie^{ik\left(z_H+\frac{x^2+y^2}{z_H}\right)}}{\lambda|z_H|} \left[\iint e^{-2\pi i(x\nu+y\mu)}\mathrm{d}\nu\mathrm{d}\mu + \right. \\ + \quad & e^{-i\pi\frac{(x_0^2+y_0^2)}{\lambda z_H}} \iint \tilde{u}_0(\nu,\mu)e^{2\pi i\{\nu(x_0-x)+\mu(y_0-y)\}}\mathrm{d}\nu\mathrm{d}\mu + \\ + \quad & e^{i\pi\frac{(x_0^2+y_0^2)}{\lambda z_H}} \iint \tilde{u}_0^*(\nu,\mu)e^{-2\pi i\{\nu(x_0+x)+\mu(y-y_0)\}}\mathrm{d}\nu\mathrm{d}\mu + \\ + \quad & \left.\iint |\tilde{u}_0(\nu,\mu)|^2 e^{-2\pi i(x\nu+y\mu)}\mathrm{d}\nu\,\mathrm{d}\mu\right] = \\ = \quad & \frac{-ie^{ik\left(z_H+\frac{x^2+y^2}{z_H}\right)}}{\lambda|z_H|} \left[\delta(x,y) + e^{-i\frac{\pi}{\lambda z_H}(x_0^2+y_0^2)}u_0(-x+x_0,-y+y_0) + \right. \\ + \quad & \left. e^{i\frac{\pi}{\lambda z_H}(x_0^2+y_0^2)}u_0^*(+x+x_0,+y+y_0) + \iint u_0(x',y')u_0^*(x'+x,y'+y)\mathrm{d}x'\,\mathrm{d}y'\right] \end{aligned} \tag{32.93}$$

We have again the same rules for avoiding overlap between the "true" and the "conjugate" images. In the case of Fourier holography these two images appear in the same place. This might seem somewhat inconsistent since (with plane reference and illumination wave) the two images occurred in front of and behind the hologram at equal distance. This is true too. The "true" image is at $-\infty$ and the "conjugate" image at $+\infty$ from the hologram. The location $-\infty$ is in the front focal plane of the lens in front of the hologram, in other words in the object plane. From there it is imaged into the plane where the conjugate image occurs, which is the back focal plane of the lens behind the hologram.

The rule for avoiding overlapping is now $x_0 \geq \frac{\Delta x_0}{2}$, which means the reference point $\delta(x-x_0)$ has to be outside of the object $u_0(x)$ ($\neq 0$ in $|x| \leq \frac{\Delta x_0}{2}$). If furthermore separation from the intramodulation terms is wanted, one has to shift the reference point even farther out:

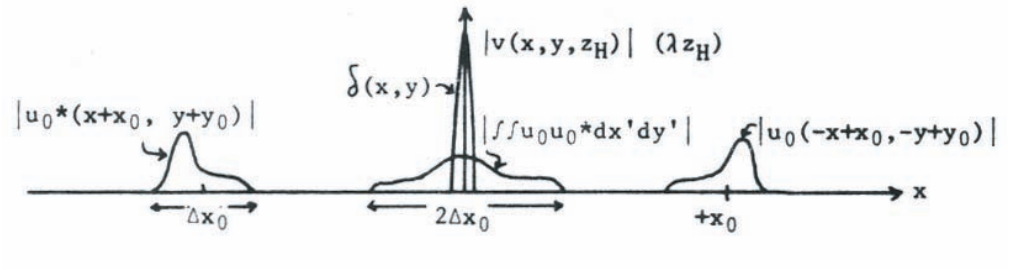

Figure 32.30: The reconstruction plane of a lensless Fourier hologram.

$x_0 \geq 3\frac{\Delta x_0}{2}$

There were several phase factors in Eq. 32.92 for $\mathcal{V}(x,y,z_H)$, all of which are unimportant, although for different reasons. What we observe is the intensity $|\mathcal{V}(x,y,z_H)|^2$.

$$|\mathcal{V}(x,y,z_H)|^2 = \left|\frac{-ie^{ik\left(z_H+\frac{x^2+y^2}{z_H}\right)}}{\lambda|z_H|}[\ldots]\right|^2 = |[\ldots]|^2\frac{1}{(\lambda z_H)^2} \tag{32.94}$$

Hence the phase factor $\frac{-ie^{ik\left(z_H+\frac{x^2+y^2}{z_H}\right)}}{\lambda|z_H|}$ is not observable. Inside of $[\ldots]$ we have phase factors

$$e^{\mp i\pi\frac{(x_0^2+y_0^2)}{\lambda z_H}} = e^{\mp i\varphi}; \tag{32.95}$$
$$|[\ldots]|^2 = \delta^2 + |u_0|^2 + |u_0^*|^2 + |u_0 \otimes u_0^*|^2 +$$
$$2\mathrm{Re}\left\{u_0e^{-i\varphi}\delta + u_0^*e^{i\varphi}\delta + u_0e^{-i\varphi}(u_0^*e^{i\varphi})^* + \iint \ldots \mathrm{d}x'\mathrm{d}y'(\delta + u_0e^{-i\varphi} + u_0^*e^{i\varphi})^*\right\}$$

The φ appears only in the *mixed* terms of $2\mathrm{Re}\{\ldots\}$, which however are all zero, because each term in $2\mathrm{Re}\{\ldots\}$ consists of a product of two factors which are shifted and do not overlap in (x,y). Hence φ is of no consequence for $|\mathcal{V}(x,y,z_H)|^2$. The square of the δ-function is mathematically nonsense. But the physicists' δ-function is a narrow and rectangular function or a skinny sinc-function may very well be squared. Since only the physical δ-function exists in reality, a δ^2 is nonsense only in the unreal world of a pure mathematician.

32.7.4 Image holography

The main point of that paper was: an interferogram is a special type of a hologram, an image-hologram, recorded in the image plane of the object. Historically this means that "holograms" have been made long before Gabor realized that one can reconstruct a wavefront which has

been recorded as a hologram. However non of the interferogram-makers realized that he could reconstruct the wave if he wanted to. Practically this means that we can *now* apply modern methods for the investigation of a wavefront, which did exist long before these methods, like phase contrast, had been invented. The same thing in more general terms: holography offers the opportunity for a posteriori processing. For example a transient windtunnel event, recorded on a hologram, can later be processed in leisure by all kinds of Schlieren methods, etc. We do not have to select the processing method before the unknown event takes place. Also we do not have to know the depth position of the event to be recorded on a hologram. Fig. 32.31 shows a typical setup for image holography. (recommended reading: "Interferograms are Image Holograms", JOSA 58 (1968), 141, see Appendix page 486)

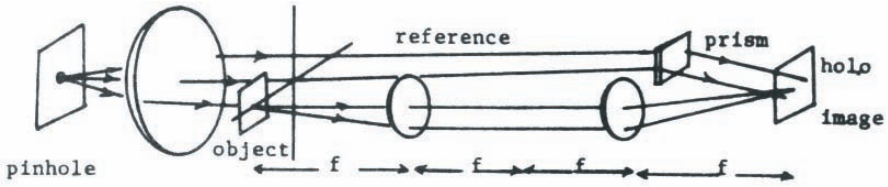

Figure 32.31: Typical setup for recording an image plane hologram.

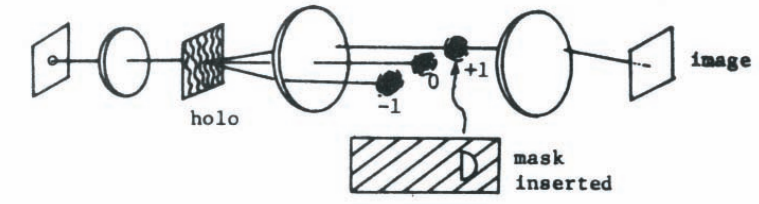

Figure 32.32: Reconstruction of an image plane hologram with the knife edge method (Foucault).

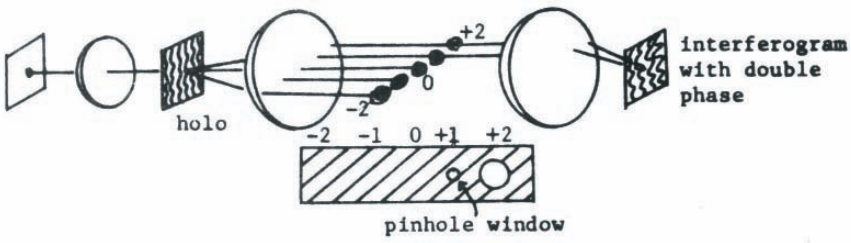

Figure 32.33: Reconstruction with phase amplification from a hologram with higher harmonics due to nonlinear photographic development. All of the +2. order goes through the pinhole; the center of the +1 order goes through the pinhole and provides a plane reference wave.

33 Talbot bands

This chapter is a supplement to the section on coherence. It is a pity that this nice effect is so little known. Maybe it is honestly forgotten, or it is bypassed because it does not fit into the normal teaching pattern, or the authors of textbooks pay attention only to those effects which are useful for making money? Anyway, this effect is worth teaching for three reasons: (a) it gives an unusual but useful insight into the problems of temporal coherence, (b) it demonstrates the powerful "dynamic" approach of multi-wavelength diffraction theory, (c) it shows how easily one may jump to a wrong conclusion when neglecting to distinguish between "necessary" and "sufficient".

Let us start with a "dynamic" description of grating diffraction, which is probably due to Schuster ($\sim$ 1920). The following hypothesis will turn out to be quite useful: White light consists of single pulses (Fig. 33.1). The various monochromatic components in the exit plane of the grating spectroscope are *created* by the grating due to the time delays $\tau(\alpha)$ of partial pulses going through adjacent grating slits. The wavelength is $\lambda = c\tau = \frac{c}{\nu_t} = d\sin\alpha$.

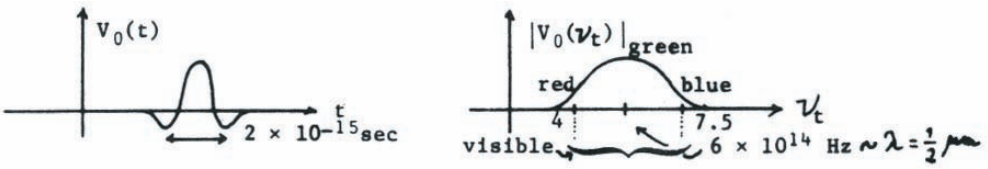

Figure 33.1: The shape of a light pulse and its spectrum.

The unusual aspect of this explanation of the grating spectroscope is that the wavelength λ exists only behind the grating. The newly derived formula $\lambda = d\sin\alpha$ is of course consistent with the standard formula $\sin\alpha = \frac{\lambda}{d}$. For comparison let us sketch how the standard formula is usually derived. An arbitrary light wave function $V_0(t)$ coming from the source can be thought of consisting of purely monofrequency components: $V_0(t) = \int \tilde{V}(\nu_t)e^{-2\pi i\nu_t t}\mathrm{d}t$. First we treat one such monofrequency $e^{-2\pi ni\nu_t t}$ alone. The corresponding wavelength $\lambda = \frac{c}{\nu_t}$ arrives at the exit plane at a point described by $\sin\alpha = \frac{\lambda}{d}$. Next we add up all the contributions from all the other monofrequencies. Since they are arriving at different spots of the exit plane, they cannot interfere (which they could not anyway for other reasons). Hence we observe the intensities $|\tilde{V}(\nu_t)|^2$ at the various places defined by $\sin\alpha = \frac{\lambda}{d} = \frac{c}{\nu_t d}$.

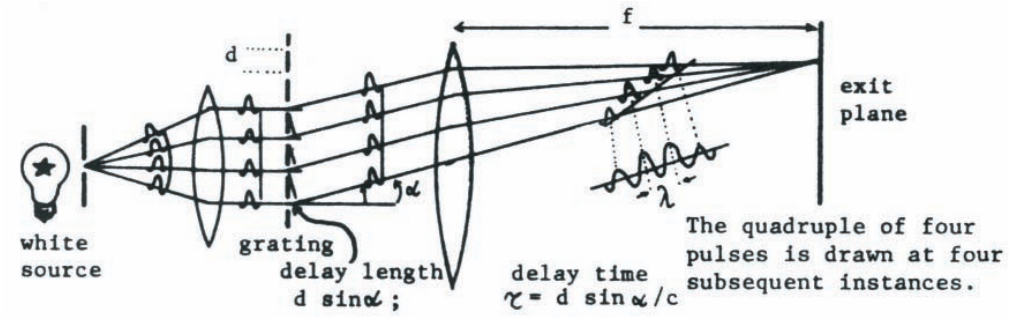

Figure 33.2: Grating diffraction with short ligth pulses.

Now, according to Schuster, we figure as resulting amplitude $V(t,\alpha)$ at place α a sum of delayed light amplitudes $V_0(t-m\tau)$:

$$V(t,\alpha)=\sum_{(m)} V_0(t-m\tau); \qquad \tau = d\frac{\sin\alpha}{c} \tag{33.1}$$

The summation $\sum_{(m)}$ goes over all the grating slits:

$$\sum_{(m)} V_0(t-m\tau)=\sum_{(m)}\int \tilde{V}_0(\nu)e^{-2\pi i\nu(t-m\tau)}\mathrm{d}\nu=\int \tilde{V}_0(\nu)\sum_{(m)} e^{2\pi im\nu\tau}e^{-2\pi i\nu t}\mathrm{d}\nu \tag{33.2}$$

herein: $\sum_{(m)} e^{2\pi im\nu\tau}\approx\sum_{(n)}\delta(\nu\tau-n)$

This expression would contain the straight equality sign $(=)$ if the sum would extend from $m=-\infty$ to $m=+\infty$. But that is unrealistic since all gratings have only a finite number of slits.

$$V(t,\alpha)=\int \tilde{V}_0(\nu)\sum_{(n)}\delta(\nu\tau-n)e^{-2\pi i\nu t}\mathrm{d}\nu= \tag{33.3}$$

$$\frac{1}{\tau}\sum_{(n)}\int \tilde{V}_0(\nu)\delta(\nu\tau-n)e^{-2\pi i\nu t}\mathrm{d}\nu=\frac{1}{\tau}\sum_{(n)}\tilde{V}_0\left(\frac{n}{\tau}\right)e^{-2\pi i\nu t}$$

The receiver in the exit plane observes the time-integrated modulus square.

$$I(\alpha)=\int |V(t,\alpha)|^2\mathrm{d}t=\left(\frac{1}{\tau}\right)^2\sum_{(n)}\sum_{(m)}\tilde{V}_0\left(\frac{n}{\tau}\right)\tilde{V}_0^*\left(\frac{m}{\tau}\right)\int e^{-2\pi i(n-m)\frac{t}{\tau}}\mathrm{d}t \tag{33.4}$$

The integral is τ if $n = m$, and zero if $n \neq m$.

$$I(\alpha) = \frac{1}{\tau^2} \sum_{(n)} \left| \tilde{V}_0 \left(\frac{n}{\tau} \right) \right|^2 ; \qquad \tau = d \sin \frac{\alpha}{c} \tag{33.5}$$

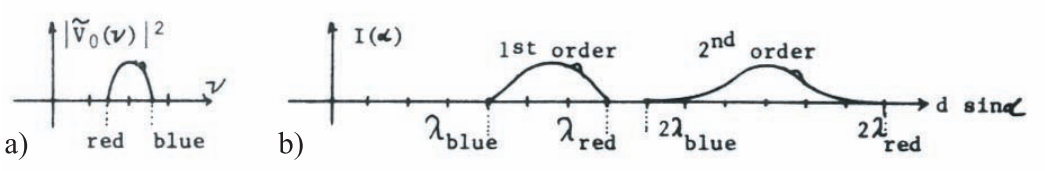

Figure 33.3: a) Spectral width of a pulse $V_0(t)$; b) spatial distribution in the diffraction plane depending of the diffraction angle (order).

In the visible region: $\frac{2}{\nu_{\text{blue}}} > \frac{1}{\nu_{\text{red}}}$; or $2\lambda_{\text{blue}} > \lambda_{\text{red}}$

Now let us use the dynamic approach for the explanation of the Talbot bands. The ordinary approach, where one first computes a monofrequency component $e^{-2\pi i \nu t}$ all the way through the plane of observation, is of course physically correct too, but it leads in this case to an extremely messy mathematical treatment.

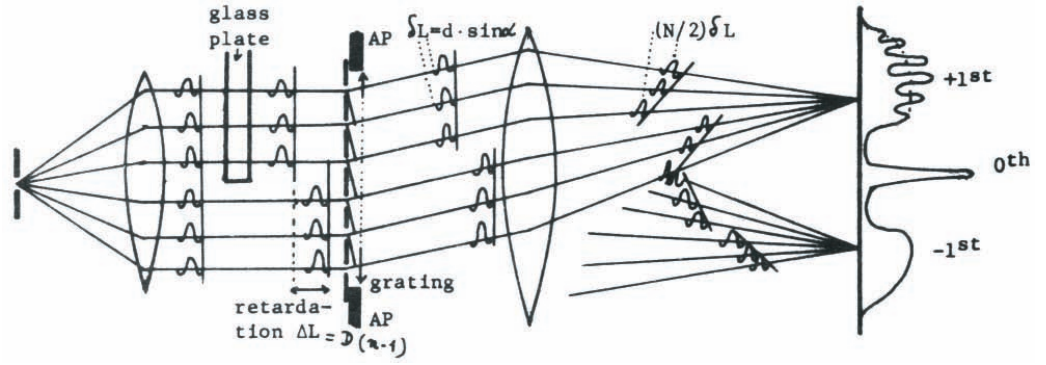

Figure 33.4: The effect of a phase plate in the aperture in front of the diffraction grating.

Plate thickness:	D;
Plate refraction index:	n;
Grating constant:	d;
Grating width or aperture size:	$Nd = B$;
Shift between neighbours:	$\delta L = d \cdot \sin \alpha$;

Shift between the two half-trains: $\Delta L = (n-1)D$ due to retardation in glass;
Length of full train (if no glass plate): $L = N\delta L$.

For the *+1st order* the upper half of the total wave train is delayed so that the lower half can catch up and interfere with the upper half. But in the *-1st order* the upper half is delayed for two reasons: retardation in the glass plate and detour on the way downwards. Hence the two parts cannot overlap. This explains why the Talbot bands appear in the +1st order only.

The most vivid Talbot bands are to be expected if the retardation $(n-1)D$ equals the length of a half-train $\frac{N}{2}\delta L$.

$$\frac{N}{2}\delta L = d\frac{\sin\alpha}{2}N = d\frac{\sin\alpha}{2}\frac{B}{d} = B\frac{\sin\alpha}{2} \tag{33.6}$$

$$\boxed{2(n-1)D = B\sin\alpha = N\lambda} \tag{33.7}$$

Now let us determine the fringe distance of Talbot bands, measured in angular coordinate α. The brightest fringe is at α_0, which is given by $(n-1)D = B\frac{\sin\alpha_0}{2}$. The adjacent fringe maximum occurs where the two half-trains are shifted by one wavelength (Fig. 33.5):

Figure 33.5: Interference of two wavefronts shifted by one wavelength.

$$\begin{aligned} B\frac{\sin\alpha_1}{2} + d\frac{\sin\alpha_1}{2} &= (n-1)D \\ \text{or}: \quad \frac{B}{2}\sin\alpha_1 &= (n-1)D - \lambda_1 \end{aligned} \tag{33.8}$$

We call the angular period $\alpha_0 - \alpha_1 = \delta\alpha$, which can be computed this way:

$$\begin{aligned} B\sin\alpha_1 \quad &+ \quad d\sin\alpha_1 = 2(n-1)D = B\sin\alpha_0; \qquad \alpha_1 = \alpha_0 - \delta\alpha; \\ B\sin(\alpha_0-\delta\alpha) \quad &+ \quad d\sin(\alpha_0-\delta\alpha) \approx B\sin\alpha_0 - B\cos\alpha_0\cdot\delta\alpha + d\sin\alpha_0 \end{aligned} \tag{33.9}$$

By comparison we conclude $B\cos\alpha_0\cdot\delta\alpha_0 = d\sin\alpha_0$;

$$\delta\alpha = \frac{d}{B}\tan\alpha_0 = \frac{d\sin\alpha_0}{B\cos\alpha_2} = \frac{\lambda_0}{B\cos\alpha_0} \tag{33.10}$$

Now follows the quantitative theory: Assume the center slit of the grating, where the edge of the glass plate is to be blocked. Below and above may be $\frac{N}{2}$ slits. At the observation plane is $x = f \tan\alpha$ the total amplitude is:

$$V(t,\alpha) = \sum_{m=-\frac{N}{2}}^{-1} V_0(t - m\tau) + \sum_{m=+1}^{+\frac{N}{2}} V_0(t - m\tau + \Delta t) \tag{33.11}$$

$$= \tilde{V}_0(\nu) \left[\sum_{m=-\frac{N}{2}}^{-1} e^{2\pi i m\tau} + \sum_{m=+1}^{+\frac{N}{2}} e^{2\pi i(m\tau - \Delta t)} \right] e^{-2\pi i\nu t} \mathrm{d}\nu$$

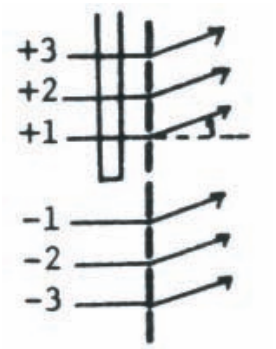

Figure 33.6: Diffraction at a grating with an additional phase shifting plate.

Herein $\tau = \frac{d}{c}\sin\alpha$, and $\Delta t = \frac{D}{c}(n-1)$, and $[\ldots] = \tilde{F}(\nu;\alpha)$.

The observed intensity is:

$$\begin{aligned} I(\alpha) &= \int |V(t,\alpha)|^2 \mathrm{d}t = \\ &= \iint \tilde{V}(\nu')\tilde{F}(\nu',\alpha)\tilde{V}_0^*(\nu'')\tilde{F}^*(\nu'',\alpha)e^{-2\pi i(\nu'-\nu'')t}\mathrm{d}(\nu'\nu''t) \\ &= \int |\tilde{V}_0(\nu)|^2 |\tilde{F}(\nu,\alpha)|^2 \mathrm{d}\nu \end{aligned} \tag{33.12}$$

Notice: the phase of $\tilde{V}_0$ has no influence on the intensity distribution $I(\alpha)$.

$$\tilde{F}(\nu,\alpha) = e^{-i\pi\Delta t\nu} \left[\sum_{-\frac{N}{2}}^{-1} e^{2\pi i\nu\left(m\tau + \frac{\Delta t}{2}\right)} + \sum_{-+1}^{+\frac{N}{2}} e^{2\pi i\nu\left(m\tau - \frac{\Delta t}{2}\right)} \right] = \tag{33.13}$$

$$= 2e^{-i\pi\Delta t\nu} \frac{\sin\left(\pi N\tau\frac{\nu}{2}\right)}{\sin(\pi\tau\nu)} \cos\left[\pi\nu\left(\Delta t - \left(\frac{N}{2}+1\right)\tau\right)\right]$$

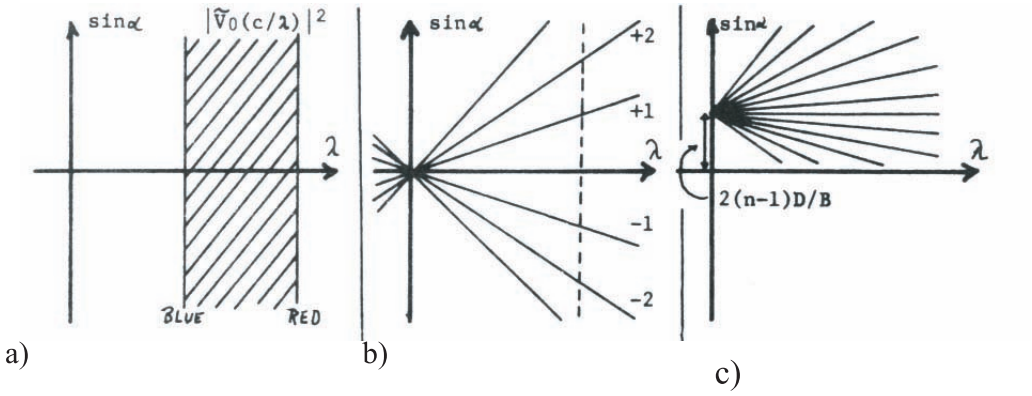

Figure 33.7: Graphical illustration of the three terms in Eq. 33.15 in the $(\lambda, \sin\alpha)$ domain:
a) $|\tilde{V}_0\left(\frac{c}{\lambda}\right)|$; notice: $\lambda_{\rm red} < 2\lambda_{\rm blue}$;
b) $\frac{\sin(\ldots)}{\sin(\ldots)}$; lines at $\tau\nu = 0, \pm1, \pm2, \pm3, \ldots$, or $\sin\alpha = 0, \pm\frac{\lambda}{d}, 2\frac{\lambda}{d}, \ldots$;
c) $\{1 + \cos[\ldots]\}$ maxima at: $\nu\left(\Delta t - \tau\left(\frac{N}{2}+1\right)\right) = 0, \pm1, \pm2, \pm3, \ldots$ or $\sin\alpha = \frac{(n-1)D}{(\frac{N}{2}+1)d} + 0,$ or $\pm\frac{\lambda}{(\frac{N}{2}+1)d},$ or $\frac{2\lambda}{(\frac{N}{2}+1)d}\ldots$;
vertical line distance: $\Delta\sin\alpha = \frac{\lambda}{(\frac{N}{2}+1)d} \approx \frac{2\lambda}{Nd} = \frac{2\lambda}{B}$.

$$|\tilde{F}(\nu,\alpha)|^2 = 2\frac{\sin^2\left(\pi N\tau\frac{\nu}{2}\right)}{\sin^2(\pi\nu\tau)}\left\{1+\cos\left[2\pi\nu\left(\Delta t - \left(\frac{N}{2}+1\right)\tau\right)\right]\right\}; \qquad (33.14)$$

$$\tau = d\frac{\sin\alpha}{c}$$

Now let us discuss $I(\alpha)$ graphically:

$$\begin{aligned} I(\alpha) &= \int |\tilde{V}_0(\nu)|^2 |\tilde{F}(\nu,\alpha)|^2 \mathrm{d}\nu = \qquad (33.15)\\ &= 2\int |\tilde{V}_0(\nu)|^2 \frac{\sin^2\left(\pi N\tau\frac{\nu}{2}\right)}{\sin^2(\pi\nu\tau)}\left\{1+\cos\left[2\pi\nu\left(\Delta t - \left(\frac{N}{2}+1\right)\tau\right)\right]\right\}\mathrm{d}\nu \end{aligned}$$

It is more convenient to use $\lambda = \frac{c}{\nu}$ instead of ν as the variable of integration. The three factors of this integral have the distribution in the $(\lambda, \sin\alpha)$-domain shown in Fig. 33.7.

Only the factor $\{1+\cos[\ldots]\}$ contains the glass plate parameter $\nu\Delta t = \frac{(n-1)D}{\lambda}$. Hence it is primarily responsible for the Talbot bands. The first two factors together describe ordinary grating diffraction. The $\int \ldots \mathrm{d}\lambda$ can be visualized as a collapsing projection of $|\tilde{V}_0|^2\frac{\sin^2}{\sin^2}\{1+\cos\}$ onto the $\sin\alpha$-axis. The question is, in which regions of $\sin\alpha$ will the $\{1+\cos\}$-modulation not be smeared out. This $\{1+\cos\}$-modulation is what creates the Talbot bands

of $I(\alpha)$. Obviously, the most complete modulation is achieved where the $\{1+\cos\}$ fringes in the $(\sin\alpha, \lambda)$ diagram are horizontal, or at least close to it:

$$\sin\alpha_0 = \frac{2(n-1)D}{B} \tag{33.16}$$

This calls for $\sin\alpha_0 > 0$. For $\sin\alpha < 0$ the two stripe-systems $\frac{\sin^2(\ldots)}{\sin^2(\ldots)}$ and $\{1+\cos\}$ are crossing under such a small angle, that everything will be smeared out. Remember the $\{1+\cos\}$-stripes have a width of $\frac{\lambda}{B}$, and adjacent stripes are only $\frac{2\lambda}{B}$ apart.

Another point is of importance here. Since the visible region of the light covers a little bit *less than an octave* ($\lambda_{\rm red} < 2\lambda_{\rm blue}$), it is possible to find conditions such that each spike from the $\{1+\cos\}$-star hits *only once* the spikes of the coarse star $\frac{\sin^2(\ldots)}{\sin^2(\ldots)}$ within the visible region, at least if working in the 1st order (Fig. 33.8).

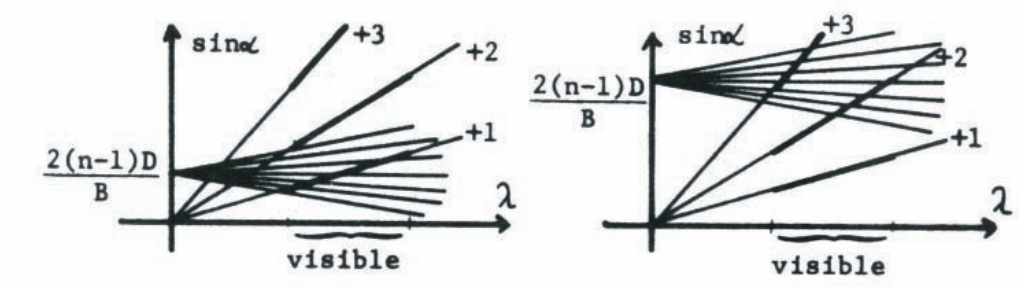

Figure 33.8: Graphical solution of the Talbot bands.

The second grating diffraction order will not exhibit strong Talbot fringes due to overlap of the 3rd order on the $\sin\alpha$-axis. Actually with *normal* dispersion ($\frac{{\rm d}n}{{\rm d}\lambda} < 0$) the situation becomes even better in the +1st order because the $\left\{1+\cos\left[\pi\nu\left(\Delta t - \frac{N}{2}\tau\right)\right]\right\}$ star is slightly bent: $\nu\left(\Delta t - \frac{N}{2}\tau\right) = 0, \pm1, \pm2, \pm3, \ldots$.

$$\begin{aligned} \nu\Delta t &= (n-1)\frac{D}{\lambda}; \\ \nu\tau &= d\frac{\sin\alpha}{\lambda} \longrightarrow \sin\alpha = 2(n-1)\frac{D}{B} + (0, \pm2\frac{\lambda}{B}, \pm4\frac{\lambda}{B}, \ldots) \end{aligned} \tag{33.17}$$

Under unusual circumstances one might expect to see Talbot bands in the -1st order, if $D\frac{{\rm d}n}{{\rm d}\lambda} \geq 0$. Anomalous dispersion appears at wavelengths close to resonance absorption: $\chi(\lambda) \rightarrow \max$. It is also possible to "fake" anomalous dispersion by imbedding a glass plate with $n_{\rm G} > n_{\rm F}$, $|\frac{{\rm d}n_{\rm G}}{{\rm d}\lambda}| < |\frac{{\rm d}n_{\rm F}}{{\rm d}\lambda}|$ into a properly chosen liquid (F). What matters now is $\frac{{\rm d}\frac{n_{\rm G}}{n_{\rm F}}}{{\rm d}\lambda}$, which may be ≥ 0. These "anomalous" Talbot bands have not yet been observed.

Conclusions: The hypothesis that white light has a pulse-like amplitude as a function of time did prove quite useful both for the Schuster explanation of grating diffraction as well as

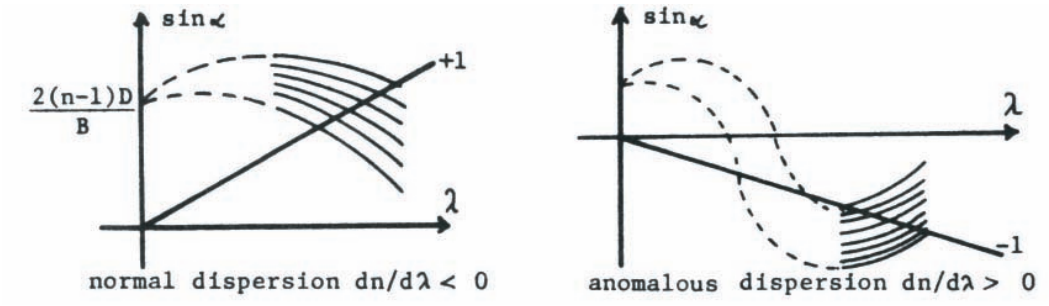

Figure 33.9: Talbot bands at normal and anomalous disperion

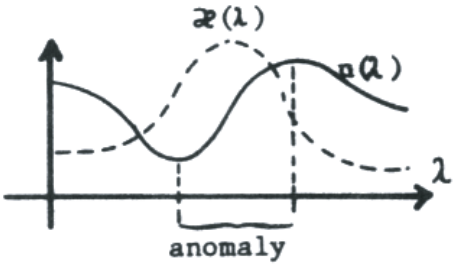

Figure 33.10: Anomolous dispersion close to resonance absorption.

Figure 33.11: Short pulses as a model for white light.

for the ("dynamic") theory of Talbot's bands. Does this prove that white light *is* actually pulse-like? Several well-renowned physicists thought so. However, if a hypothesis is quite useful for explaining a finite number of experiments it simply says that the theory is *not disproven*, but not that is proven. In other words, it was *sufficient* to assume that white light is pulse-shaped in order to derive the right conclusions about Talbot's bands, but this assumption was *not necessary*. In fact, a random-sequence of quasi-monochromatic wave trains would have been another suitable model for our purpose.

The only requirement is that quite different $V_0(t)$ have the same $|\tilde{V}_0(\nu)|^2$, which is possible

since the phase of $\tilde{V}_0(\nu)$ is never explicitly used in the quantitative theory of the observed intensity $I(\alpha)$. The most dramatic case of two functions with the same $|V(\nu)|^2$ is a delta-function and white noise (Fig. 33.12).

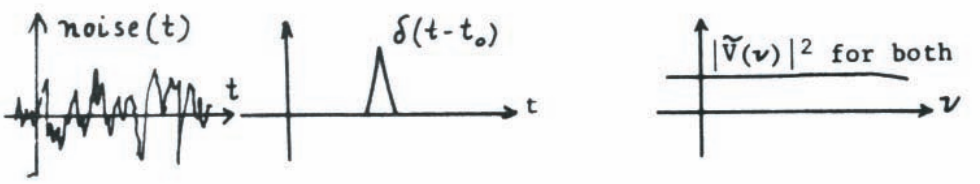

Figure 33.12: "White" noise and a δ-pulse which both have the same power spectrum $|\tilde{V}_0(\nu)|^2$.

34 Influence of the photographic material on spatial data processing

34.1 Effects in a Photographic Emulsion

First let us discuss what happens in a photographic emulsion, then we will compare the three hologram types “Fresnel”, “Fourier”, and “Image” in the context of the photographic materials limitations.

1. The photographic plate is phase-blind. Not u, rather $|u|^2$ is recorded. It is the essence of holography to cope with this difficulty.
2. The photographic plate is polarization-blind (except for the marginal “Weigand” effect). We will discuss later a modified holographic system, which avoids the loss of polarization-information.
3. During recording the incoming light intensity is scattered within the emulsion. Linear (undisturbed) superposition holds for this scattering process. Details will follow shortly.
4. The photochemical development process usually means for the optical signal a point-to-point nonlinearity (also called a “memoryless” nonlinearity).
5. The grain structure of the photographic emulsion causes a spatial noise which is not additive.
6. An adjacency-effect (Eberhard-effect) due to unusual chemical diffusion conditions may introduce a non-linear spread process.

We will now discuss these six effects, though not in sequence listed.

34.2 (3) Light Scattering During Recording

When Eggert & Schmidt and Frieser studied in the nineteen thirties the sound reproduction from the sound track on the movie film they found that the highest acoustical frequencies were reduced in amplitude. As a means of describing this effect they invented the term “spatial frequencies”. When the sound track is scanned with velocity v, the spatial frequency ν_x will be re-converted into temporal sound frequency $\nu_t = v\nu_x$. Since the higher sound frequencies came back with reduced amplitude, they concluded the film must have a low-pass transfer function for spatial frequencies. Frieser recognized scattering as the cause, which was

confirmed theoretically by G. Haase and H. Müller, Optik 17, 3 (1960). Frieser found also that with a sharp line as the aerial image intensity $I_{\mathrm{A}}(x,y) = \delta(x)$ falling upon the film, the effective intensity distribution after scattering has the shape of a two-sided exponential (Fig. 34.1):

$$I_{\mathrm{E}}(x,y) = 2\pi\nu_p e^{-2\pi\nu_p|x|} \tag{34.1}$$

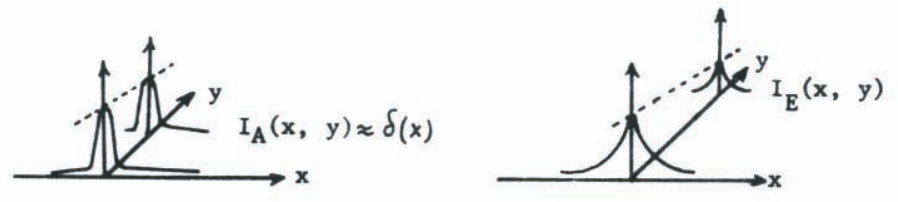

Figure 34.1: The effect of scattering on the recording of a pulse.

Next Frieser verified not only that for $I_{\mathrm{A}} = \delta(x)$ the double-exponent was characteristic, but that for any aerial image I_{A} one gets an effective image

$$I_{\mathrm{E}}(x) = \int I_{\mathrm{A}}(x')2\pi\nu_p e^{-2\pi\nu_p|x-x'|}\mathrm{d}x' \tag{34.2}$$

Herein ν_p is a typical constant, describing the "sharpness" (as it was called at first) of the film. The experiments were not easy, because one had to keep those other effects, described under (4) and (5), under control. The convolution result suggests describing the situation as a linear filtering process:

$$\begin{aligned} I_{\mathrm{E}}(x,y) &= \iint I_{\mathrm{A}}(x,y)F_p(x-x',y-y')\mathrm{d}x'\mathrm{d}y' \\ \tilde{I}_{\mathrm{E}}(\nu,\mu) &= \tilde{I}_{\mathrm{A}}(\nu,\mu)\tilde{F}_p(\nu,\mu) \end{aligned} \tag{34.3}$$

These formulas are two-dimensional, whereas Frieser's experiments cover only the one-dimensional case $\delta(x) \longrightarrow 2\pi\nu_p e^{-2\pi\nu_p|x|}$. However this is enough knowledge for computing F_p and $\tilde{F}_p$, since there is no reason why the scattering should be anisotropic (dependent on the angel within the emulsion plane).

$$\tilde{F}_p(\nu,0) = \iint F_p(x,y)e^{-2\pi ix\nu}\mathrm{d}x\mathrm{d}y = \int \underbrace{\left\{\int F_p(x,y)\mathrm{d}y\right\}}_{2\pi\nu_p e^{-2\pi\nu_p|x|}} e^{-2\pi ix\nu}\mathrm{d}x \quad (34.4)$$

$$\tilde{F}_p(\nu,0) = \frac{1}{1+\left(\frac{\nu}{\nu_p}\right)^2}; \quad \text{or in polar coordinates}$$

$$\nu = \varrho\cos\Theta; \quad \mu = \varrho\sin\Theta; \quad \tilde{F}_p(\varrho,\Theta) = \tilde{F}_p(\varrho) = \tilde{F}(\varrho,0)$$

$$\tilde{F}_p(\varrho) = \frac{1}{1+\left(\frac{\varrho}{\nu_p}\right)^2}; \quad \tilde{F}_p(0)=1; \quad \tilde{F}_p(\nu_p)=\frac{1}{2}$$

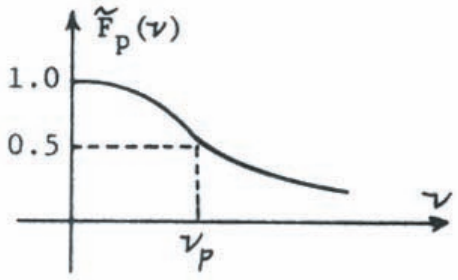

Figure 34.2: Typical frequency response of a holographic film described by Eq. 34.4.

A few typical characteristic frequencies ν_p are:

Polaroid and color film:	$\sim 10-25\ \mathrm{mm}^{-1}$
35 mm film, black-white:	$\sim 50-200\ \mathrm{mm}^{-1}$
Kodak 649:	$\sim 200\ \mathrm{mm}^{-1}$
Agfa Agepan:	$\sim 500\ \mathrm{mm}^{-1}$
Agfa Scientia:	$\sim 1000\ \mathrm{mm}^{-1}$

Usually when selecting a photographic film one has to make a compromise between high "bandwidth" ν_p and "speed" (sensitivity). - For some high resolution films one parameter ν_p is no longer enough for describing the light scattering process in the emulsion. The photographic transfer function $\tilde{F}_p$ curve looks more like

$$\tilde{F}_p(\nu) = \frac{a}{1+\left(\frac{\nu}{\nu_1}\right)^2} + \frac{a}{1+\left(\frac{\nu}{\nu_2}\right)^2} \quad (34.5)$$

Typical data for very high resolution films are like
$\nu_1 \sim 50\ \mathrm{mm}^{-1}$
$\nu_2 \sim 2000\ \mathrm{mm}^{-1}$
$1-a \sim 0.8$

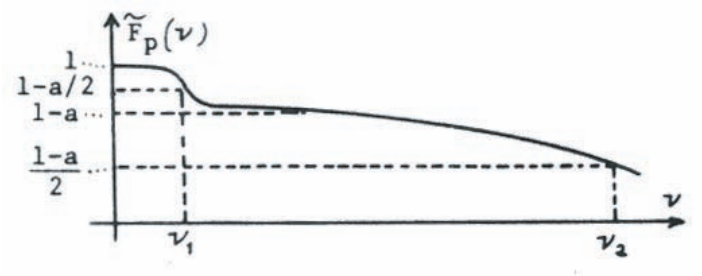

Figure 34.3: Typical frequency response of a high resolution holographic film described by Eq. 34.6.

34.3 (4) The photographic nonlinear effect

It has long been known that the "density" D of a photographic plate after development depends in a nonlinear way on the exposure (effective illuminating intensity times time).

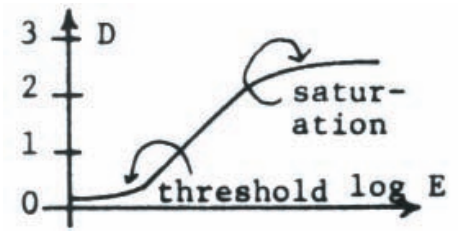

Figure 34.4: Hurter & Druffield (or H&D) curve: Nonlinear dependence of the photographic density of a film after exposure.

Definition:
density $D = -\log_{10}(T^2)$
T^2: intensity transmittance;
$E = I_E \Delta t$: ΔT exposure time.

L. Silberstein gave a statistical explanation for the H&D curve. The chapter 7 in E. O'Neill's Statistical Optics presents Silberstein's ideas in advanced form. Silberstein assumed that each grain (a piece of Ag-halide crystal, many thousands of atoms, but mostly smaller or only a little larger than the wavelength of light) needs, four photons to become activated, i.e. ready to be changed permanently into a black spot due to the action of the photographic developer. Such a model explains nicely the threshold and the steep portion of the H&D curve. If the incoming photons are so diluted that almost no grain gets the minimum of four photons the emulsion is practically unexposed. Also the saturation can be understood in this way. When practically all the grains in the emulsion have had their four or more photons a further increase

of the exposure will have no effect. Although the $D - \log E$ curve (H&D) is quite adequate for describing the nonlinear effect in the context of ordinary photography, it is better to present the same physical effect in non-logarithmic quantities:

$$D = -\log_{10}(T^2) = -2\log_{10}(T) \qquad \log E = \log(I\Delta t) = \log I + \log \Delta t \tag{34.6}$$

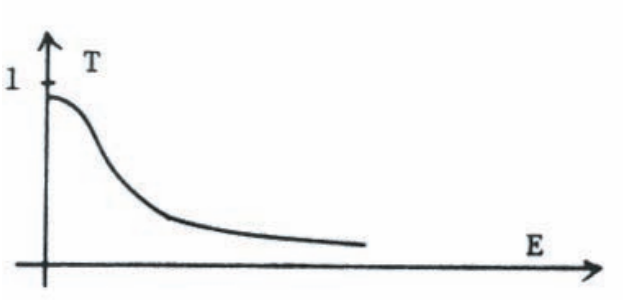

Figure 34.5: Intensity transmittance in dependence of the exposure of a photographic medium

Between $T = 0.8$ and $T = 0.4$ a linear approximation is valid for many films and under many development conditions (type of developer, temperature, duration).

$$T(E) = C_0 + C_1 E; \quad (C_1 < 0) \tag{34.7}$$

However when using also the lower region (fairly dark) of the $T - E$ curve, a more adequate description is a third order polynomial (A. Kozma, 1966; J. W. Goodman):

$$T(E) = \sum_{m=0}^{3} T_m E^m \tag{34.8}$$

$\frac{\mathrm{d}T}{\mathrm{d}E}$ is negative because we assumed a "negative-film" (black-white inversion). Going twice through a photographic process one can achieve in total a $T(E)$ curve with $\frac{\mathrm{d}T}{\mathrm{d}E} > 0$, which however is rarely necessary in holography, only sometimes in in-line holography. For example, whenever we assumed "linear"-development, $v_H(x, y) = I_H(x, y)$, it should have been $v_H(x, y) = T_0 + T_1 I_H(x, y)$. With $I_H = 1 + ue^- + u^* e^+$ we get:

$$v_H = T_0 + T_1 + T_1(ue^- + u^* e^+) = T\left[\frac{T_0 + T_1}{T_1} + ue^- + u^* e^+\right] \tag{34.9}$$

as compared to $v_H = 1 + ue^- + u^* e^+$.

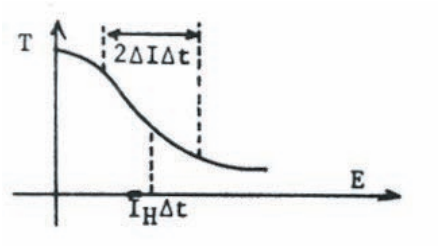

Figure 34.6: Transmittance vs. exposure curve of photographic film.

The difference is merely an overall constant T_1 and a relative constant $\frac{T_0+T_1}{T_1}$, determining the modified ratio of "direct" light versus "true plus conjugate" light. This could be of interest only in terms of energy economy, not in terms of image structure. However for in-line holography the term $\frac{T_0+T_1}{T_1}$ is of importance since the constant part or "strong background" is a genuine part of the object $u_0 = 1 + \Delta u_0$. This point is unimportant since today almost all holograms are off-line.

To keep the film "linear" one has to use a large enough ratio of reference wave to object wave, and chose the exposure time $\Delta t_{\exp}$ properly:

$$I_H = 1 + \tilde{u}e^- + \tilde{u}^* e^+; \qquad E = I_H \Delta t_{\exp}; \qquad |T_H - 1| \leq \Delta I \tag{34.10}$$

34.4 (6) Adjacency Effect

So far we assumed the nonlinear influence of the photographic emulsion upon the photographic signal to be of the point-to-point variety. This variety is called in the temporal domain "memoryless". That means, at any point (x, y) the resulting amplitude transmittance $T(x, y)$ depends only on the exposure $E(x, y)$ at that point. The exposure in turn is the product of exposure time Δt and effective intensity I_E. However strictly speaking this $T - E$ relation is not truly "point-to-point". In general one has to write $T(x, y) = \mathrm{NL}\{E(x - x', y - y')\}\,\mathrm{d}x'\mathrm{d}y'$, where NL stands for "nonlinear Function". For the theoretician, this is a mess, for the experimentalist this so-called adjacency or Eberhard effect is often a delight because it is usually a helpful effect which enhances edge sharpness. The human retina also has such an adjacency effect, which proves that an adjacency effect must be good.

The adjacency effect is an inhibitory effect, whereby during the photochemical process the used developer liquid travels away from the high exposure area and hence reduces action at the low-exposure region. Also un-used developer diffuses from the low-exposure area into the nearby high-exposure area. This causes an edge overshoot of the developed density D. This diffusion process goes on largely outside of the emulsion in a thin liquid layer. Brushing the emulsion during development eliminates the effect almost entirely.

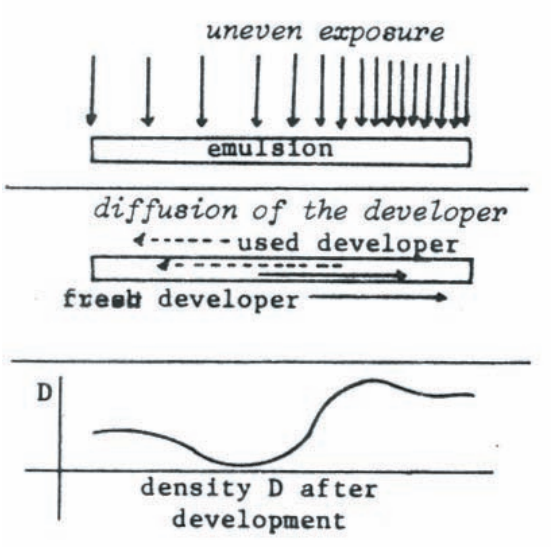

Figure 34.7: Diffusion causing the "adjacency effect" in photographic media

One last of warning: the term linearity is used with different meanings in different books and papers on holography.

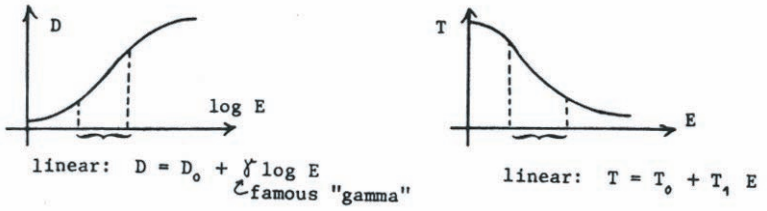

Figure 34.8: Linear $D - \log E$ and $T - E$ curves

The linear portion of the $T - E$ curve is never where $D - \log E$ is linear, but rather at the lower bend of $D - \log E$. "Never" refers to one-step negative-material. In a two-step photographic process the two types of linear regions may correspond, but they do not have to.

34.5 (5) Grain-Noise

It has been found empirically that the density fluctuations are worst where the $T - E$ curve is steepest. Obviously this type of noise is not *additive*, at least if E covers a wide range. The signal-to-noise for a small E range from E to $E + \mathrm{d}E$ is characterized by $\frac{\frac{\mathrm{d}T}{\mathrm{d}E}}{\Delta T(E)}$.

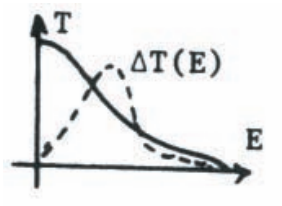

Figure 34.9: The $T - E$ and ΔT-E curves

34.6 The influence of light scattering within the emulsion during holographic recording

As we have seen in the section 34.2, the light scattering within the photographic emulsion can be described as a linear and space-invariant filter process with the aerial image intensity $I_A(x, y)$ as input, and with effective intensity $I_E(x, y)$ (after scattering) as output:

$$\tilde{I}_E(\nu.\mu) = \tilde{I}_A(\nu, \mu)\tilde{F}_P(\nu, \mu); \tag{34.11}$$

Typically, $\tilde{F}_p(\nu, \mu) = \frac{1}{1+\frac{\nu^2+\mu^2}{\nu_P^2}}$.

Now let us investigate how the photographic transfer function $\tilde{F}_P$ (often in the literature abbreviated as MTF, modulation transfer function) influences the flow of data from object to reconstructed image. We assume linear development.

34.6.1 Image holography

Recording the aerial intensity:

$$I_A(x, y) = |u_0(x, y) + e^{-2\pi i x \nu_R}|^2 \approx 1 + u_0 e^+ + u_0^* e^- \tag{34.12}$$

The effective intensity is:

$$I_E = I_A \otimes F_p; \quad \text{or} \quad \tilde{I}_E = \tilde{I}_A \cdot \tilde{F}_p \tag{34.13}$$

$$\begin{aligned}\tilde{I}_A(\nu,\mu) &= \iint I_A(x,y)e^{-2\pi i(x\nu+y\mu)}\mathrm{d}x\,\mathrm{d}y = \\ &= \delta(\nu,\mu)+\tilde{u}_0(\nu-\nu_R,\mu)+\tilde{u}^*(-\nu-\nu_R,\mu)+ \\ &+ \underbrace{\iint \tilde{u}_0(\nu',\mu')\tilde{u}^*(\nu'-\nu,\mu'-\mu)\mathrm{d}\nu'\,\mathrm{d}\mu'}_{\text{intramodulation}}\end{aligned} \tag{34.14}$$

$$\tilde{F}_p(\nu,\mu)=\frac{1}{1+\frac{\nu^2+\mu^2}{\nu_P^2}};\quad \tilde{F}_p(0,0)=1;\quad \tilde{F}_p\geq\frac{1}{2}\quad\text{within}\quad \nu^2+\mu^2\leq\nu_p^2 \tag{34.15}$$

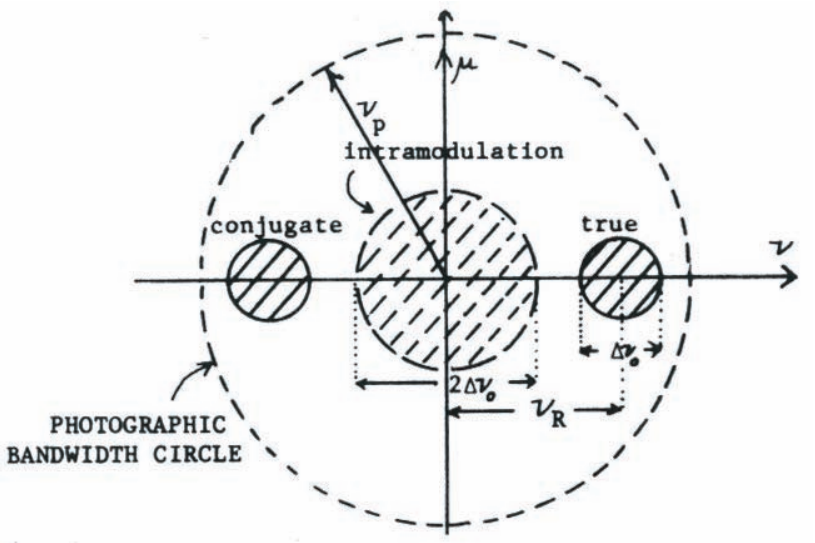

Figure 34.10: Reconstruction plane of an image hologram

In reconstruction, if everything else goes well, the true image will have a spectrum

$$\begin{aligned}\tilde{u}_0(\nu-\nu_R,\mu)\tilde{F}_p(\nu,\mu) &= \tilde{v}_T(\nu,\mu) \\ v_T(x,y) &= \iint \tilde{v}_T(\nu,\mu)e^{2\pi i(x\nu+y\mu)}\mathrm{d}\nu\,\mathrm{d}\mu = \\ &= \iint \tilde{u}_0(\nu-\nu_R,\mu)\tilde{F}_p(\nu,\mu)e^{2\pi i(x\nu+y\mu)}\mathrm{d}\nu\,\mathrm{d}\mu \\ &= \underbrace{e^{2\pi i x\nu_R}}_{\substack{\text{unimportant}\\ \text{phase factor}}} \iint \tilde{u}_0(\nu,\mu)\tilde{F}_p(\nu+\nu_R,\mu)e^{2\pi i(x\nu+y\mu)}\mathrm{d}\nu\,\mathrm{d}\mu\end{aligned} \tag{34.16}$$

The object spectrum $\tilde{u}_0(\nu,\mu)$ will be reduced most severely by $\tilde{F}_p(\nu+\nu_R,\mu)$ at $\nu = +\frac{\Delta\nu_0}{2}, \mu = 0$, that is on its right edge. We demand for this worst case as tolerance $\tilde{F}_p(\frac{\Delta\nu_0}{2}+\nu_R,0) \geq \frac{1}{2}$; $\rightarrow \frac{\Delta\nu_0}{2}+|\nu_R| \leq \nu_p$. The most economical use of the "photographic bandwidth circle" above is when the frequencies of the true (virtual) image $\tilde{u}_0(\nu-\nu_R,\mu)$ are as close as possible to the intramodulation region, which occurs if $\nu_R = 3\frac{\Delta\nu_{\rm obj}}{2}$. If the intramodulation term is neglibly small, one might go to an even smaller reference frequency $\nu_R = \frac{\Delta\nu_0}{2}$. The photographic bandwidth frequency has to be $\nu_p = 2\Delta\nu_0$, or $\nu_p \geq \Delta\nu_0$, respectively.

Remember, overlap of the various terms, which are graphically presented in Fig. 34.10, has to be avoided, because the contents of that figure is actually displayed in the Fourier plane of the image-hologram-reconstruction-plane, where a proper mask eliminates all but the true term, or all but the conjugate term. This can be done only if the various terms do not overlap. The setup in question is shown in Fig. 32.28 and in Fig. 32.31. In summary, the photographic MTF, which changes I_A into T_E (intensities), acts like a filter function $\tilde{F}_p(\nu+\nu_R,\mu)$ for the complex amplitudes $u_0 \rightarrow v_T$. In this sense image holography is a system that is linear in complex amplitude.

34.6.2 Fourier holography

Using the obvious notation the theory of the recording process can be presented very briefly:

$$\begin{aligned} u_0(x,y) \quad &+ \quad \delta(x-x_R,y) \longrightarrow \tilde{u}_0\left(\frac{x}{\lambda f},\frac{y}{\lambda f}\right) + e^{-2\pi i\frac{xx_R}{\lambda f}} \\ \longrightarrow I_A(x,y) \quad &= \quad |\tilde{u}_0+e^-|^2 = 1+\tilde{u}_0e^+ + \tilde{u}_0^*e^- + |\tilde{u}_0|^2 \\ I_E(x,y) \quad &= \quad I_A \otimes F_p \end{aligned} \tag{34.17}$$

Again we replace this convolution integral by its Fourier-reciprocal equivalent counterpart, which is simply a multiplication $\tilde{I}_E(\nu,\mu) = \tilde{I}_A(\nu,\mu)\tilde{F}_p(\nu,\mu)$. Now we have to be alert that we do not get confused by the various Fourier operations. During recording the object $u_0(x,y)$ has been Fourier transformed by a lens into the plane of the Fourier hologram where $\tilde{u}_0\left(\frac{x}{\lambda f},\frac{y}{\lambda f}\right)$ is displayed. Next we calculate the spatial frequency spectrum $\tilde{I}_A(\nu,\mu)$ of the aerial intensity in the hologram plane $I_A(x,y) = |\tilde{u}_0\left(\frac{x}{\lambda f},\frac{y}{\lambda f}\right) + e^{-2\pi i\frac{xx_R}{\lambda f}}|^2$. We do this in order to be able to take into account the influence of the light scattering in the emulsion by multiplying $\tilde{I}_A \cdot \tilde{F}_p = \tilde{I}_E$. From there we go back by another Fourier transform to the effective intensity I_E. After linear development the effective intensity I_E is represented by the amplitude transmittance v_H of the hologram. Yet another Fourier transform describes the influence of the lens used in reconstruction. Now the formulas:

$$\begin{aligned} \tilde{I}_A(\nu,\mu) \quad &= \quad \delta(\nu,\mu) + u_0(x_R-\lambda f\nu,-\lambda f\mu) + u_0^*(x_R+\lambda f\nu,\lambda f\mu) + \\ &+ \quad \iint u_0(x',y')u_0^*(x'-x,y'-y)\mathrm{d}x'\,\mathrm{d}y' \end{aligned} \tag{34.18}$$

$$\begin{aligned} \tilde{I}_E(\nu,\mu) &= \tilde{I}_A(\nu,\mu)\tilde{F}_p(\nu,\mu) \\ I_E(x,y) &= \iint \tilde{I}_E(\nu,\mu)e^{2\pi i(x\nu+y\mu)}\mathrm{d}\nu\ \mathrm{d}\mu \\ v_H(x,y) &= I_E(x,y) \quad \text{(linear development)} \end{aligned} \tag{34.19}$$

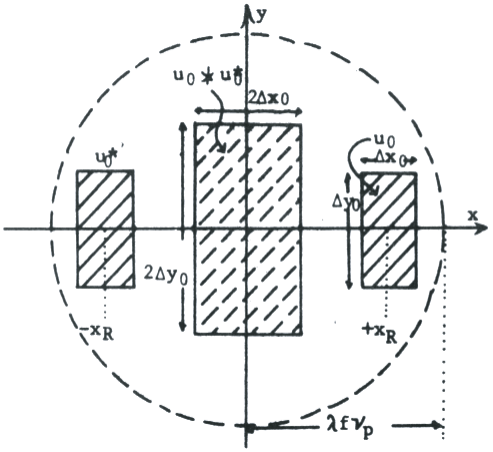

Figure 34.11: Reconstruction plane of a Fourier hologram.

Reconstruction:

$$\begin{aligned} & \iint v_H(x',y')e^{-2\pi i\frac{(xx'+yy')}{\lambda f}}\mathrm{d}x'\ \mathrm{d}y' \\ = & \iint \left\{ \iint \tilde{I}_E(\nu.\mu)e^{2\pi i(\nu x'+\mu y')}\mathrm{d}\nu\ \mathrm{d}\mu \right\} e^{-2\pi i\frac{xx'+yy'}{\lambda f}}\mathrm{d}x'\ \mathrm{d}y' \\ = & \tilde{I}_E\left(\frac{x}{\lambda f},\frac{y}{\lambda f}\right) = \tilde{I}_A\left(\frac{x}{\lambda f},\frac{y}{\lambda f}\right)\tilde{F}_p\left(\frac{x}{\lambda f},\frac{y}{\lambda f}\right) = \\ = & \underbrace{\tilde{F}_p\left(\frac{x}{\lambda f},\frac{y}{\lambda f}\right)}_{\substack{\text{photographic MTF, acting like a greyish mask in the final image plane}}} \cdot \Bigg[\underbrace{\delta\left(\frac{x}{\lambda f},\frac{y}{\lambda f}\right)}_{\text{direct}} + \underbrace{u_0(x_R-x,-y)}_{\text{true}} + \\ + & \underbrace{u_0^*(x_R+x,y)}_{\text{conjugate}} + \underbrace{\iint u_0 u_0^*\mathrm{d}x'\ \mathrm{d}y'}_{\text{intramodulation}} \Bigg] \end{aligned} \tag{34.20}$$

Assume $u_0(x,y) \neq 0$ only in $|x| \leq \frac{\Delta x_0}{2};\ |y| \leq \frac{\Delta y_0}{2}$. In the final image plane of the reconstruction setup we have the display shown in Fig. 34.11. Result: in Fourier holography the photographic MTF does not influence the resolution (or in better language, the spatial spectrum of the reconstructed images) but it limits the image field size to $x^2 + y^2 \leq (\lambda f \nu_p)^2$. The worst case is at $x = x_R + \frac{\Delta x_0}{2};\ y = \frac{\Delta y_0}{2}$.

34.6.3 Fresnel hologram

In Fresnel holography, which in all its properties lies in between image holography and Fourier holography, both results from the image and from the Fourier cases are gradually true. In practice Fresnel holography tends usually to the Fourier case because the corresponding dimensions are more in fashion. We will not pursue Fresnel holography now, but will introduce first the concept of “Space-Bandwidth Product”, which is a very simple and quick tool for understanding many things qualitatively.

35 The Space-Bandwidth-Product SW

On the following pages a report about the SW is reproduced. On the first five pages the general properties are outlined, at first by analogy to the better known Time-Bandwidth Product. On page 5 in Fig. 2 a case of a space-variant SW is sketched, which is no longer a rectangle with axis-parallel edges. Any deviations from such a rectangle indicate space-variance, because then, obviously, the frequency spread in ν_x is not the same for all locations x. On the other hand, a piece of photographic material will always have a rectangular SW, with axis-parallel edges. This will become important later, when the SW concept is applied to Fresnel-holography. Before that, on p. 6 - 7, some SW-generalizations are briefly mentioned. The pages 8 - 14 are not important in this context since they deal with coherence in holography. However from p. 15 on the information storage capacity of holograms is discussed in terms of SW. It turns out that a hologram has no more SW than the same piece of film used for ordinary image recording.

THE SPACE-BANDWIDTH PRODUCT, APPLIED TO SPATIAL FILTERING AND TO HOLOGRAPHY*

A. W. Lohmann

IBM San Jose Research Laboratory
San Jose, California

ABSTRACT: The Space-Bandwidth product SW is the spatial analogy to the Time-Bandwidth product, which is an important term in temporal data processing. First, some fundamental properties of the SW are described. Then the SW concept is applied for investigating the following problems: the influence of imperfect coherence on the performance of spatial filtering systems, and the influence of the film data (size and resolution) on the storage capability of a hologram. Fraunhofer holograms and image holograms can store just as many data as the same piece of film can in the ordinary storage mode. But Fresnel holograms are inferior for data storage.

Research Paper
RJ-438
May 9, 1967

* Lecture at the Summer School of the University of Michigan on "Optical Data Processing" ; Ann Arbor, Michigan, 1966.

INTRODUCTION

In 1914, Max von Laue calculated the number of degrees of freedom in the wave field behind a lens.[1] This is the maximal number of independent parameters in an image formed by that lens. M. von Laue discussed both temporal and spatial variations of the image. The temporal aspect of his results is essentially what is now known under the name "Time-Bandwidth-Product TW." The number of spatial degrees of freedom, which has been discussed in recent years by Gabor,[2] Wolter,[3] Gamo,[4] and others, has several names. However, in the field of data processing, the term "Space-Bandwidth Product SW" seems most appropriate to me.

In this paper, I want to show how convenient the concept of the SW is when dealing with problems in optical data processing. First, I will outline some of the basic properties of the SW. Then I will apply the SW to the study of certain limitations in spatial filtering and in holography. Although most of the final results are known already, it might be worthwhile to see how simply one can obtain them when using the SW concept. Since simplicity is the main virtue of the SW concept, too much mathematical rigor would defeat our purpose. This attitude is justified, if only order-of-magnitude results are sought.

GENERAL PROPERTIES OF THE SW

We want to introduce the term SW by way of analogy to the "Time-Bandwidth-Product TW," which is well established in electrical engineering. The price which must be paid for the transmission of a signal over a communication channel is proportional to the TW, where T refers to the time duration Δt, and W to the bandwidth $\Delta\nu$. One has to buy at least as much TW as the signal contains.

The fact that the TW is closely related to money might prove its significance to some, but not necessarily to everyone. Therefore, I want to show some of the invariance properties of the TW, thus indicating the fundamental nature. Imagine a signal of duration Δt and bandwidth $\Delta\nu$. In the time-frequency domain, it occupies an area of size $\Delta t\,\Delta\nu = TW$, as shown in Fig. 1a. If this signal would have been delayed, its TW would be shifted along the t-axis. See Fig. 1b.

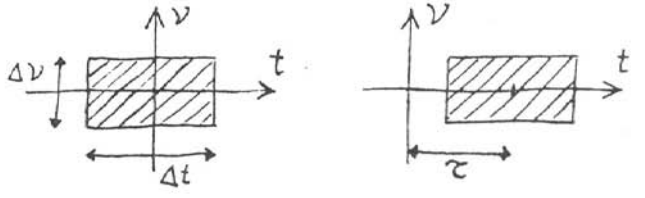

(a) (b)

Figure 1.

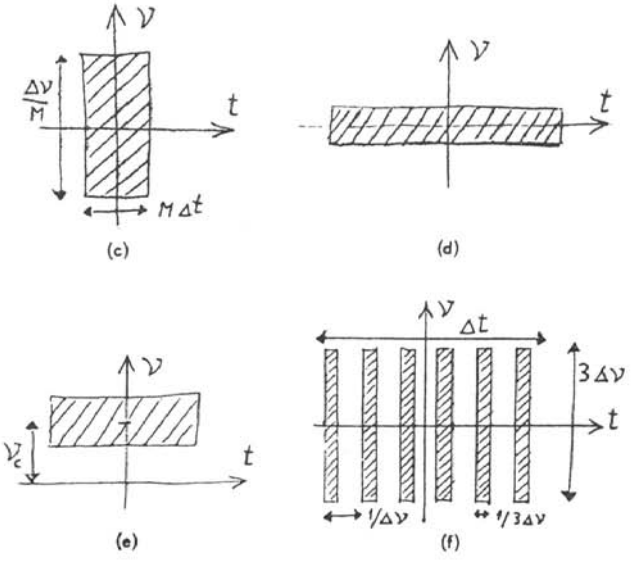

But the size of the TW remains unchanged. If this signal is recorded on tape, and then played back at a higher speed, its duration is compressed, but its bandwidth expanded. The shape of the TW has changed, but not its size, as can be seen in Fig. 1c. The influence of a slower play-back speed is demonstrated in Fig. 1d. Modulation onto a carrier frequency ν_c means a shift of the TW along the ν-axis (Fig. 1e). Also, a sampling procedure for the purpose of pulse-amplitude modulation leaves the size of the TW unchanged, although its shape looks quite different now (Fig. 1f). This sampling procedure does not do any harm to the signal, as can be derived from Cauchy's 125-year-old sampling theorem. At this moment, let me assume that the reader knows the sampling theorem, but I will provide a derivation in the appendix. In qualitative terms, the sampling theorem says: If a signal u(t) is bandlimited within $|\nu| \le \Delta\nu/2$, then the continuous function u(t) is completely known, if one only knows u(t) at the sampling points $t_m = m/\Delta\nu$. Therefore, it should be good enough to record u(t) only during a small fraction of the sampling interval $1/\Delta\nu$, say one-third of it: $(m-1/6)/\Delta\nu \le t \le (m+1/6)/\Delta\nu$; $m = 0, \pm 1, \ldots$ The remaining two-thirds of each sampling interval are now free for other purposes. For example, one could interlace another signal. In other words, we use only one-third of the time duration Δt intermittently (Fig. 1f). However, these pulses of $1/3\,\Delta\nu$ length now occupy a larger frequency band as compared to before, when the signal was not yet cut into these pulses. If the signal u(t) is almost constant during these intervals, we can write

$$u(t) \approx \sum(m)\; u(m/\Delta\nu)\; \mathrm{rect}\left(\frac{t-m/\Delta\nu}{1/3\,\Delta\nu}\right)$$

$$\mathrm{rect}\,(\alpha) = \begin{cases} 1 & \text{if } (\alpha) \le 1/2 \\ 0 & \text{otherwise} \end{cases} \quad ; \quad \mathrm{rect}\left(\frac{t-m/\Delta\nu}{1/3\,\Delta\nu}\right) = 1 \quad \text{in}$$

$$(m-1/6)/\Delta\nu \le t \le (m+1/6)/\Delta\nu \; .$$

Each pulse rect (...) has a bandwidth of about $3\Delta\nu$, as can be seen from the frequency spectrum:

$$\int_{-\infty}^{+\infty} \mathrm{rect}\left(\frac{t-m/\Delta\nu}{1/3\,\Delta\nu}\right) e^{-2\pi i\nu t}\, dt = \frac{e^{-2\pi i m \frac{\nu}{\Delta\nu}}}{3\Delta\nu}\ \mathrm{sinc}\,(\pi\nu/3\Delta\nu)$$

$$\mathrm{sinc}\ \alpha = \sin\alpha/\alpha\ .$$

So each pulse occupies in the (t,ν) domain a stripe of a height $3\Delta\nu$ and of a width $1/3\Delta\nu$, covering an area 1. These stripes (Fig. 1f) follow at intervals $1/\Delta\nu$. Their total number is given by the signal duration Δt divided by the interval $1/\Delta\nu$, which is $\Delta t\,\Delta\nu$. This number of stripes equals the TW area of the signal after sampling, since each stripe covers a unit area. Hence, the TW after sampling has the same size as before sampling.

Since the size of the TW is so resistant against all kinds of operations, the TW is obviously very fundamental. This becomes clear also in the following way: It follows from the sampling theorem that a signal of bandwidth $\Delta\nu$ cannot have pulses shorter than $\delta t = 1/\Delta\nu$. If we want to implement a message as a sequence of pulses, their distance in time has to be at least $\delta t = 1/\Delta\nu$ in order to be able to separate two elementary signals riding on adjacent pulses. If the total duration of the signal is Δt, it cannot contain more than N_t pulses:

$$N_t \le \frac{\Delta t}{\delta t} = \frac{\Delta t}{1/\Delta\nu} = \Delta t\,\Delta\nu = \mathrm{TW}.$$

Hence, the TW determines the number of resolvable pulses, this number being what von Laue called "the temporal degrees of freedom"

Now we are well prepared for the introduction of the new term "Space-Bandwidth Product SW," which is a useful measure for the contents of a spatial signal (= image), and for the data-handling capability of optical instruments.

$$\mathrm{SW} = \iint dx\,dy \iint d\nu_x d\nu_y$$

S refers to the space or area of a signal (= image). Sometimes S might refer to the useful image field of a lens or any other optical instrument. W means the two-dimensional bandwidth in the spatial frequency domain (ν_x, ν_y). If both the image field and the spatial frequency domain have a rectangular shape, the SW is simply

$$\mathrm{SW} = \Delta x\ \Delta y\ \Delta\nu_x\ \Delta\nu_y\ .$$

Typical order of magnitude figures for the SW are as follows:

Microscope, TV	10^5
Slide projector	10^6
Good photo lens F/2; f = 50 mm; used at F/4	10^7
Long focal length lens for aerial reconnaissance	10^8

100 cm^2 Agfa Agepan FF film	10^9
100 cm^2 Kodak 649 F film	10^{10}

The speed ratio of these two films is about 200 to 1.

A simple interpretation of the SW is possible if one concludes that a spatial bandwidth $\Delta\nu_x$ does not allow lines in the image, which are smaller than $\delta x = 1/\Delta\nu_x$. This follows from the sampling theorem. Of course, the same holds for the minimal width δy of lines at right-angular position: $\delta y = 1/\Delta\nu_y$. The smallest image point can be thought of as the corssing of two such lines. Hence, the minimal point size is $\delta x\, \delta y = 1/\Delta\nu_x \Delta\nu_y$. If the image field has a total size of $\Delta x\, \Delta y$, it contains as the maximum of distinguishable image points:

$$N_{xy} = \Delta x\, \Delta y/\delta x\, \delta y = \Delta x\, \Delta y\, \Delta\nu_x\, \Delta\nu_y = SW.$$

Since every distinguishable image point might represent one parameter of the signal to be processed, the SW sets the upper limit N_{IMAGE} of the number of parameters in the image. M. von Laue derived this result for a diffraction-limited lens over fifty years ago. New here is the name SW and the attitude to consider the SW concept not only to find fundamental limitations, but also to apply if for feasibility studies of optical data processing systems.

We want to ask once more about the maximum number of free parameters, this time not for the object or image $u(x, y)$, but for the spatial frequency spectrum $\tilde{u}(\nu_x, \nu_y)$. We assume a finite object region: $|x| \leq \Delta x/2$; $|y| \leq \Delta y/2$. Hence, the spatial frequency spectrum can be written as a sampling sum:

$$\tilde{u}(\nu_x, \nu_y) = \sum_{-\infty}^{+\infty}\sum \tilde{u}(n/\Delta x,\, m/\Delta y)\, \mathrm{sinc}\left\{\pi\Delta x(\nu_x - n/\Delta x)\right\} \mathrm{sinc}\left\{\pi\Delta y(\nu_y - m/\Delta y)\right\}.$$

This means that the function $\tilde{u}(\nu_x, \nu_y)$ is built up from sampling parameters $\tilde{u}(n/\Delta x, m/\Delta y)$, which are separted from each other by $\delta\nu_x = 1/\Delta x$ and $\delta\nu_y = 1/\Delta y$. Within a rectangular area in the frequency domain of size $\Delta\nu_x\, \Delta\nu_y$, there are N_{FREQU} independent parameters or sampling values:

$$N_{FREQU} = \Delta\nu_x \Delta\nu_y/\delta\nu_x \delta\nu_y = \Delta\nu_x \Delta\nu_y\, \Delta x\, \Delta y = SW.$$

In other words, the number of free parameters in the frequency domain (ν_x, ν_y) is given again by the SW.

The SW has several invariance properties quite similar to the ones of the TW considered before. Since it is hard to visualize the SW in its four-dimensional domain (x, y, ν_x, ν_y), we will restrict ourselves to one-dimensional signals or objects (x), which have a SW representation in two dimensions (x, ν_x). Now we can use again the Fig. 1, but with x instead of t, and ν_x instead of ν (or better: ν_t). The transitions from Fig. 1a to Figs. 1b, 1c, 1d, respectively, mean for the image a shift, a minification, and a magnification, respectively.

The size of the SW remains the same, of course. Now imagine that the object u(x) is illuminated by a tilted plane wave, instead of by a plane wave of normal incidence, as assumed in Fig. 1a. The process of tilting (α) the plane wave can be described in the x- and ν_x-domains as follows:

$$\left\{u(x) \multimap u(x)e^{-2\pi i(x \sin\alpha/\lambda)}\right\} = \left\{\tilde{u}(\nu_x) \multimap \tilde{u}(\nu_x - \nu_c)\right\} ;$$

$$\nu_c = \sin\alpha/\lambda \; ; \quad \tilde{u}(\nu_x) = \int u(x)\, e^{-2\pi i x \nu_x}\, dx \; .$$

It corresponds to the modulation with a spatial carrier frequency ν_c, which results in a shift of the SW along the ν_x axis (Fig. 1e). Also, the operation described in Fig. 1f has its spatial analogy in high-speed photography:[7] A black-and-white grating of slit width $1/3\Delta\nu_x$ and slit distance (= grating constat) $1/\Delta\nu_x$ is put in contact with the recording film. After one exposure has been taken, the grating is shifted by one slit width. The next scene falls onto yet unexposed stripes of the film. The number of scences one can take is three, in our example. It is limited by the ratio of grating constant to slit width. The resolution of the film (or its spatial bandwidth) has to be good enough so that no light from one stripe creeps into the adjacent stripe, maybe via scattering on the silver halide grains. Otherwise, it would be impossible to observe single scenes on the film after development, when the same grating is superimposed at a proper position. Lack of film bandwidth leads to "crosstalk" of subsequent scenes. In order to obtain a certain image quality expressed in terms of SW_{IMG}, one needs the same amount of SW_{FILM}, whether one records the scene in the ordinary way (Fig. 1a) or in the sampled fashion (Fig. 1f). The virtue of the sampling-type recording is that the mechanical movement needed between the exposure of two subsequent scenes is only one slit width, as compared to one frame width in ordinary cinematography.

The SW concept is useful also when describing "space-variant image formation."[5] A typical example for this image formation is a lens, which produces a better image quality at the center of the image field, rather than at the edges. One way to express this is to say the bandwidth $\Delta\nu_x$ varies as a function of x across the field. In other words, the SW of this lens is not rectangular any more (Fig. 2).

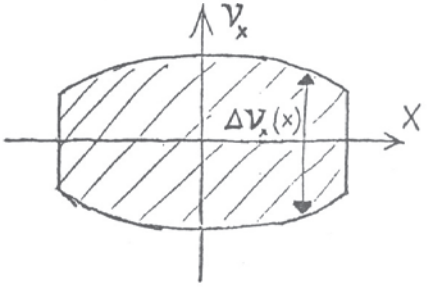

Figure 2.

An extension of the SW concept becomes necessary if the signal does not depend only on the spatial coordinates (x, y), but also on the time t. Obviously, one will combine the SW and TW to form the "Space-Time-Bandwidth-Product STW," as von Laue did in 1914.

$$STW = \Delta x\, \Delta y\, \Delta t\, \Delta\nu_x\, \Delta\nu_y\, \Delta\nu_t .$$

This term is useful if one wants to explain why optics has a good chance to make valuable contributions in the field of data processing. Assume, for example, one may want to perform a sequence of Fourier transformations:

$$u_n(x,y)\ \mathrm{rect}\left(\frac{t-n\delta t}{\delta t/2}\right) \multimap \mathrm{rect}\left(\frac{t-\delta t}{\delta t/2}\right)\tilde{u}_n(\nu_x,\nu_y) \qquad (n=0,1,\ldots N=1/\delta t).$$

The inputs $u_n(x,y)$ might be given as amplitude transmission on a roll of film. A reasonably good lens can perform the Fourier transformation as a Fraunhofer diffraction experiment for input frames $u_n(x,y)$ of up to a $SW = 10^7$. Let us assume a detector, for which an exposure time of $\delta t/2$ is long enough for recording the output $\tilde{u}_n(\nu_x,\nu_y)$ of the n^{th} frame. If the phase of $\tilde{u}_n$ is of interest, one has to superimpose a coherent reference wave $e^{2\pi i\nu_x x_0}$, as one is accustomed to do in interferometry and holography. The film transport from frame to frame might require a time $\delta t/2$, adding up with the processing time $\delta t/2$ to δt. Let us assume $\delta t = 1/1000$ sec., from which follows $\Delta\nu_t = 1000\ \mathrm{sec.}^{-1}$. The total time duration for 1000 frames is then $\Delta t = 1$ sec., yielding $TW = 1000$, and together with $SW = 10^7$:

$$STW = 10^{10}.$$

This is a very high number of data to be processed within one second. The main reason for this high processing capability is that in optics one can handle so many data simultaneously or in parallel as large as the SW of the instrument allows. On the other hand, it should not be forgotten that optical analog computers are not very versatile. Multiplication, addition, Fourier transformations, Fresnel transformations, Hilbert transformations, linear filtering in one and two dimensions, correlations, convolutions, and generation of cross-ambiguity functions are all the operations which are optically possible, as far as I remember.

One can push the generalization of the SW concept one step further by taking the polarization of the light into account. Since there are two independent polarization components, the most general bandwidth product is double the one considered so far for scalar waves STW:

$$STPW = 2\ STW.$$

These generalized bandwidth products STW and STPW are very useful, if one tries to understand the various superresolution experiments published in recent years. They have in common that the STPW of the transmitting instrument is modified in shape (not in size) in order

to match the STPW shape of the signals. Moving masks, spectral prisms, and polarization-type beam splitters are typical components used for the modification of the instrumental STPW. The latest superresolution experiment has been published by W. Lukosz[8]. His paper contains also a good survey of earlier superresolution experiments. It is written in the "SW-language".

One might suspect that the wavelength λ of the light is another parameter, opening up even more degrees of freedom. However, because of the relationship between the wavelength λ and the temporal frequency ν_t, $\lambda \nu_t = c$, the λ-freedom is already covered in the TW. It is well known that the spectral range of the visible light corresponds to an extreme bandwidth of temporal frequencies:

$$\Delta\lambda_{VISIBLE} \sim \Delta\nu_t = 10^{14}\,\text{cps.} \quad ; \quad \text{if } \Delta t = 1\,\text{sec} \rightarrow TW = 10^{14}\,.$$

In order to make use of this wide frequency range, one needs sources with small enough frequency fluctuations:

$$\delta\nu_{FLUCT} < 1/\Delta t_{SIGNAL}\,.$$

The laser is the promising source, of course. However, it deserves to be mentioned that this source stability condition had been achieved before the advent of the laser by P. Connes and his co-workers.[6] They filtered Mercury light with a spherical Fabry-Perot étalon, then amplitude modulated the light by means of a Kerr cell with a signal frequency of several Mega cps. The existence of clearly separated sidebands was demonstrated with a second, scanning Fabry-Perot étalon, also of the spherical type. Another way to express the success of P. Connes is to say that from a thermal source he generated wave trains of several hundred meters in length.

In summarizing this chapter about the general properties of the SW, we can state the following: The SW is of fundamental and practical importance, because it is a convenient measure for the contents of a spatial signal and for processing capability of optical instruments. The SW can be interpreted as the number N_{IMAGE} of free parameters in the image, as well as the number N_{FREQU} of free parameters in the domain of spatial frequencies (ν_x, ν_y).

THE INFLUENCE OF SPATIAL COHERENCE ON SPATIAL FILTERING

Now our lengthy introduction of the SW concept will pay off. You will see how convenient the SW is for evaluating the data processing capability of a spatial filtering system. As our first project, we want to study how the spatial filtering operation is deteriorated by imperfect spatial coherence.

The basic setup is shown in Fig. 3. A monochromatic slit source SOU and a collimator lens L_c provide the illumination of the object u(x), for convenience written only in one dimension. The lens L performs a Fourier transform, displaying the spatial spectrum $\tilde{u}(\nu_x)$ in plane FOU at the coordinate $x_F = \lambda f \nu_x$. There the filter function $F(\nu_x)$ is introduced.

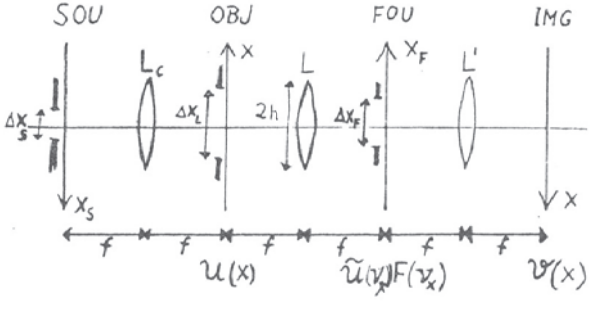

Figure 3.

The lens L' performs another Fourier transform, yielding the image v(x):

$$v(x) = \int \tilde{u}(\nu_x)\, F(\nu_x)\, e^{2\pi i x \nu_x}\, d\nu_x .$$

In the case of perfect spatial coherence, the width of the slit source is very small $\Delta x_s \approx 0$. Now the SW is determined by the quality of the lenses L and L'. The size of the object field, for which a good image can be formed, may be Δx_L. The width of the aperture stop in FOU is Δx_F. It has to be small enough in order to avoid vignetting:

$$\Delta x_L + \Delta x_F \leq 2h.$$

This means that the width 2h of the lens L is wide enough so that the lens L does not block rays going from any object point within $|x| \leq \Delta x$ to any point within the aperture $|x_F| \leq \Delta x_F/2$. In Fig. 4, one sees

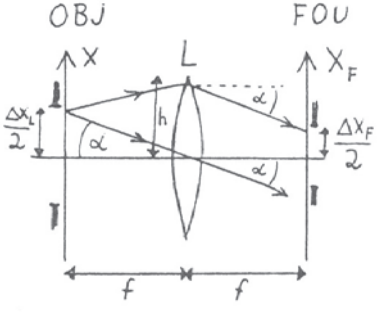

$$tg\,\alpha = \frac{\Delta x_L/2}{f}$$

$$h - f\,tg\,\alpha \geq \frac{\Delta x_F}{2}$$

$$\Delta x_L + \Delta x_F \leq 2h$$

Figure 4.

how the vignetting condition is arrived at by considering the borderline ray, going from $+\Delta x_L/2$ to $+\Delta x_F/2$. Another way to put it is to say: We want to be sure that the finite aperture acts as a space-invariant low pass filter $|\nu_x| \leq \Delta\nu_x/2 = \Delta x_F/2\lambda f$ for all object points within $|x| \leq \Delta x_L/2$. Sometimes the aberrations of the lens L might require an even smaller Δx_F than required by the vignetting condition.

Because the spatial frequencies ν_x of the object u(x) are displayed at the coordinates $x_F = \lambda f \nu_x$ in the plane FOU, the aperture stop acts as a low pass filter:

$$|\nu_x| \leq \Delta\nu_L/2 \; ; \qquad \Delta\nu_L = \Delta x_F/\lambda f.$$

From this, one calculates immediately the SW_L, as far as it is limited by the lens L:

$$SW_L = \Delta x_L \, \Delta\nu_L = \Delta x_L \, \Delta x_F/\lambda f .$$

The maximum of SW_L within the realm of the vignetting condition is achieved with $\Delta x_L = h = \Delta x_F$.

Now we want to show that the SW_L is a relevant measure for the data processing capability of our spatial filteri ng system. One way to look at it is to ask, "How many data of the object can be processed?" Because of the finite bandwidth $\Delta\nu_L$ of our filter, we cannot distinguish points closer together than $\delta x = 1/\Delta\nu_L$ in the image or output plane. Assuming 1:1 magnification, this means that it would be senseless to pack our input data closer together than at intervals δx. Since the input or object domain has the finite extension Δx_L, it cannot accommodat more than N parameters to be processed:

$$N_{INPUT} = \Delta x_L/\delta x = \Delta x_L \, \Delta\nu_L = SW_L.$$

In other words, the maximum number of input data which can be processed by our spatial filtering system is given by the SW_L.

Another way to look at our filtering system is to ask, "How many parameters can our processing filter contain?" We know our input or object u(x) has a finite extension of Δx_L. Hence, its Fourier transform can be written as a sampling sum:

$$\tilde{u}(\nu_x) = \sum_{-\infty}^{+\infty} (m)\, \tilde{u}(m/\Delta x_L) \quad \text{sinc} \left\{ \pi \Delta x_L \, (\nu_x - m/\Delta\nu_x) \right\} .$$

This Fourier transform $\tilde{u}(\nu_x)$ is the complex light amplitude, which falls onto the filter $F(\nu_x)$ in plane FOU (Fig. 3). The sampling representation says that $\tilde{u}(\nu_x)$ has independent parameters only at intervals $\delta\nu_x = 1/\Delta x_L$. This is so, because the sinc-function is essentially different from zero only around $\nu_x = m/\Delta x$, within $\pm 1/2\Delta x$. If the signal $\tilde{u}(\nu_x)$ falling onto the filter $F(\nu_x)$ has independent parameters $\tilde{u}(m/\Delta\nu_x)$ only at intervals $\delta\nu_x = 1/\Delta x_L$, it would not make sense to pack the parameters of the processing filter any closer. Since the filter $F(\nu_x)$ has a finite extension $\Delta\nu_L$, the total number N_{FILTER}

of its parameters is finite as well:

$$N_{FILTER} = \Delta\nu_L/\delta\nu_x = \Delta\nu_L\,\Delta x_L = SW_L.$$

In other words, the maximum sensible number of parameters in our processing filter is given by the SW_L.

So far, we have assumed the slit or pinhole being infinitely narrow $\Delta x_s \approx 0$. But in order to obtain enough light through the system, we want to make Δx_s as large as tolerable. What one suspects, of course, is that the degree of spatial coherence has to be close to unity. This turns out to be right. But to ask for a certain degree of coherence is not the proper question from the viewpoint of data processing, primarily. We ought to ask instead, "How does the $SW(\Delta x_s)$ depend on the slit width Δx_s?" What is the largest tolerable slit width Δx_{sc}, for which the SW does not decrease considerably below its maximum at $\Delta x_s = 0$?

$$SW(\Delta x_{sc}) \approx SW(0) = SW_L.$$

Whereas an illuminating wave, coming from the center point $x_s = 0$, has a constant phase across the object field, this is not true any more for light coming from off-center points $x_s \neq 0$. For example, a ray going from the edge of the slit $(+\Delta x_s/2)$ through the center of the collimating lens L_c is inclined by an angle of about $\Delta x_s/2f$ (Fig. 5). The resulting plane wave, being perpendicular to this ray, is tilted with respect to the x-axis by the same angle. At the edge of the object

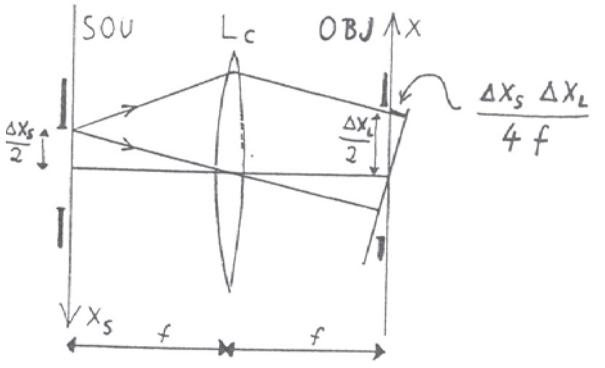

Figure 5.

field at $x = +\Delta x_L/2$, the path difference with respect to the center $(x=0)$ can be calculated by multiplying the distance $\Delta x_L/2$ with the angle $\Delta x_s/2f$, giving $\Delta x_L\,\Delta x_s/4f$. Further multiplication with $2\pi/\lambda$ gives the phase difference, which ought to be smaller than $\pi/2$. Otherwise, the phase of the illuminating waves is not well defined any more. This requirement leads to the well-known coherence condition:

$$\Delta x_s\,\Delta x_L \leq \lambda\, f.$$

If Δx_s is made broader for reasons of image brightness than this condition requires, we cannot use the full object field Δx_L anymore. Otherwise, the phase uniformity would be confused. We reduce the object field to Δx_c, which is smaller than what would be allowed by the

quality of the lens L: Δx_L. The best SW we can achieve, then, is for the largest tolerable object size Δx_c in accordance with the case of the coherence inequality:

$$\Delta x_c = \lambda f/\Delta x_s \ ;$$

$$SW(\Delta x_s) = \Delta x_c \, \Delta \nu_x = \Delta x_c \, \Delta x_F/\lambda f = \Delta x_F/\Delta x_s .$$

In other words, if the slit width Δx_s does not obey the coherence condition any more, we have to reduce the SW to $SW(\Delta x_s) < SW_L$. Its amount is determined by the ratio of aperture size Δx_F versus slit size Δx_s.

The last result can be obtained again in another way, which is more pertinent to data processing. The slit plane SOU (Fig. 3) and the frequency plane FOU are object-image related. Any point source at x'_ξ would form a point image at $x_F = x'_\xi$. If an object u(x) is brought into the plane OBJ between planes SOU and FOU, its Fraunhofer diffraction pattern will replace the point image, yet still centered around x'_s : $\tilde{u}[(x_F - x'_s)/\lambda f]$. Expressed in frequency coordinates $\nu_x = x_F/\lambda f$, the off-center position x'_s of the source point causes a shift of the spatial frequency spectrum in plane FOU by $x'_s/\lambda f$. Such a shift is tolerable for all source points $|x'_s| \leq \Delta x_s/2$, as long as it does not exceed the sampling interval $\delta \nu_x$ of the processing filter $F(\nu_x)$. This sampling interval or minimum distance of adja independent parameters in the frequency domain had been found earlier as being the reciprocal of the object width Δx_L. Hence:

$$\Delta x_s/\lambda f \leq \delta \nu_x = 1/\Delta x_L \longrightarrow \Delta x_s \, \Delta x_L \leq \lambda f .$$

This is again the coherence condition.

If, for reasons of image brightness, the slit width Δx_s exceeds this condition, the position of the frequency spectrum $\tilde{u}(\nu_x - x_s/\lambda f)$ is confused by an amount $\delta_c \nu_x = \Delta x_s/\lambda f$ if $|x_s| \leq \Delta x_s/2$. This is tolerable if the filter function $F(\nu_x)$ varies slowly enough. $F(\nu_x)$ would have to remain practically constant within intervals $\delta_c \nu_x > \delta \nu_x = 1/\Delta x_L$. This, of course, reduces the number N_{FC} of free parameters within the finite range $|\nu_x| \leq \Delta \nu_L$ of the filter function:

$$N_{FC} = \frac{\Delta \nu_L}{\delta_c \nu_x} = \frac{\Delta x_F/\lambda f}{\Delta x_s/\lambda f} = \frac{\Delta x_F}{\Delta x_s} = SW(\Delta x_s) .$$

In other words, a slit width Δx_s, which exceeds the coherence condition $\Delta x_s \leq \lambda f/\Delta x_L$ forces us to reduce the number of free parameters in the filter function $F(\nu_x)$. The object width is still Δx_L.

Earlier, we had derived another counter action required by a too-broad slit. Then we left the requirements for the filter function unchanged, but we reduced the object size below what the quality of lens L would allow, namely Δx_L. In common to both counter actions is that the SW reduces to this

$$SW(\Delta x_s) = \frac{\Delta x_F}{\Delta x_s} < SW_L \quad \text{if} \quad \Delta x_s > \lambda f / \Delta x_L .$$

THE INFLUENCE OF SPECTRAL COHERENCE ON SPATIAL FILTERING

Now we assume the slit source to be infintely small $\Delta x_s \approx 0$. The light source may have a finite spectral region $\Delta\lambda$ around λ_0: $|\lambda - \lambda_0| \leq \Delta\lambda/2$. How does that affect our data processing operation? As we will see, if $\Delta\lambda$ does not obey the condition for spectral coherence, we either have to reduce the number of free parameters in the filter, or we have to reduce the size of the object field.

Our object $u(x)$ is supposed to be a neutral amplitude transmission. "Neutral" means independent of the wavelength λ (in other words, white, grey, or black). The Fraunhofer diffraction pattern $\tilde{u}(x_F/\lambda f)$ in plane FOU has a different scale factor for different wavelengths. This is in contrast to the filter function $F(x_F)$, which is supposed to be λ-neutral. This causes a kind of a λ-dependent mismatch. For example, one particular spatial frequency ν_x of the object falls onto different points x_F in plane FOU, depending on the wavelength:

$$\nu_x \longrightarrow \begin{cases} x_F = (\lambda_0 - \Delta\lambda/2) f \nu_x & \text{for } \lambda_0 - \Delta\lambda/2 \\ x_F = (\lambda_0 + \Delta\lambda/2) f \nu_x & \text{for } \lambda_0 + \Delta\lambda/2 \ . \end{cases}$$

If all light in FOU, which is caused by the particular spatial frequency ν_x of the object $u(x)$, shall be treated equally by the filter $F(x_F)$, then $F(x_F)$ has to be constant within the range of the λ-smear: $\delta x_c = |\Delta\lambda f \nu_x|$. This might not be serious, if the λ-smear is still

smaller than, say, half of the interval $\delta\nu_L$ of free parameters in the filter, which was caused by the finite width Δx_L of the object:

$$|\delta\nu_c| = |\delta x_c/\lambda f| = |\frac{\Delta\lambda}{\lambda_0}\nu_x| \leq \delta\nu_L/2 = 1/2\Delta x_L$$

$$\frac{\Delta\lambda}{\lambda_0}|\nu_x| \leq \frac{\Delta\lambda\Delta\nu_L}{\lambda_0\ 2} \leq \delta\nu_L/2 = \frac{1}{2\Delta x_L}$$

$$\Delta\nu_L\,\Delta x_L = SW_L \leq \lambda_0/\Delta\lambda \ .$$

In other words, the "spectral purity" $\lambda_0/\Delta\lambda$ has to exceed the SW_L, set by the limitations of the lens. If this spectral coherence condition is fulfilled, our spatial filtering process works as if the light were strictly monochromatic.

If the spectral purity is not good enough, and it cannot be improved by a filter, we have to reduce either the object width Δx_L or the aperture width Δx_F. Then the modified

$$\Delta x_L \longrightarrow \Delta x_{Lc} = \frac{\lambda_0/\Delta\lambda}{SW_L}\ \Delta x_L < \Delta x_L$$

$$\Delta x_F \longrightarrow \Delta x_{Fc} = \frac{\lambda_0/\Delta\lambda}{SW_L}\ \Delta x_F < \Delta x_F$$

$$SW_c = \Delta x_{Lc}\,\Delta x_F/\lambda f = \lambda_0/\Delta\lambda = \Delta x_L\,\Delta x_{Fc}/\lambda f$$

space-bandwidth product SW_c is small enough to fulfill the spectral coherence condition.

Another possible counteraction would be to leave the object width Δx_L and the aperture width Δx_F unchanged, but pack the free parameters in the filter less tightly than before. For the low frequencies (small ν_x), the λ-smear $\delta\nu_c = |\nu_x|\,\Delta\lambda/\lambda_0$ is smaller than half of the sampling distance $\delta\nu_L = 1/\Delta x_L$, dictated by the finite width of the object. But for higher frequencies, where $\delta\nu_c > \delta\nu_L/2$, we separate the free parameters of the filter function by $2\delta\nu_c$ or more. For calculating the total number N_{Fc} of free parameters, we define:

$$\delta\nu(\nu_x) = \text{Max}\ \left\{\delta\nu_L\ ;\ 2\delta\nu_c\right\} \ .$$

The parameter density is the inverse of $\delta\nu(\nu_x)$. The total number of parameters is the integrated parameter density:

$$N_{Fc} = \int_{-\Delta\nu_L/2}^{+\Delta\nu_L/2} \frac{d\nu_x}{\delta\nu(\nu_x)} = \lambda_0/\Delta\lambda\left[1 + \log\frac{SW_L}{\lambda_0/\Delta\lambda}\right] \ .$$

One can also obtain an insight into the spectral coherence condition from a more physical point of view. The spectral purity $\lambda_0/\Delta\lambda$ is closely connected with the length Λ of the wave trains, which we will derive in a moment. This length Λ has to be large enough so that it does not prevent interference between any pair of possible wavelets.

The extreme case is discussed in Fig. 6. A spherical wave leaves the

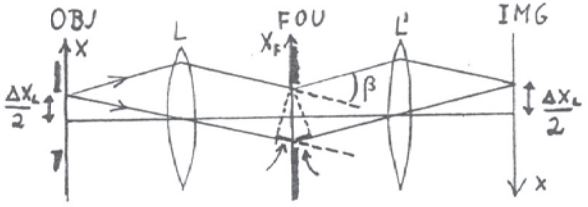

Figure 6.

uppermost point $\Delta x_L/2$ of the object. It hits the filter in FOU as a tilted plane wave. Imagine the filter being a grating with the finest possible grating constant d, being equal to the sampling interval of the filter:

$$d = \lambda f \delta\nu_L = \lambda f/\Delta x_L \ .$$

Such a grating will deflect the light by an angle β of about $\lambda/d = \Delta x_L/f$. The lens L' converts the angular deflection β into a shift βf in the plane IMG. This shift is just equal to the object width Δx_L, hence, within that region of the plane IMG, which we use for the registration of the data processing output. The two rays, which touch the edges of the aperture in FOU at $x_F = \pm \Delta x_F/2$, are delayed by the amount $\Delta x_L \Delta x_F/f$. This delay is indicated in Fig. 6 by two small arrows close to plane FOU. In order not to prevent interference between the two borderline "rays," this delay shall not exceed the length Λ of the wave trains:

$$\Delta x_L \Delta x_F/f \leq \Lambda \ .$$

The length Λ of the wave trains is connected with the spectral purity like $\Lambda/\lambda_0 = \lambda_0/\Delta\lambda$. Hence, our request for interference for any pair of rays reduces to the coherence condition:

$$\Lambda/\lambda_0 = \lambda_0/\Delta\lambda \geq \Delta x_L \Delta x_F/\lambda_0 f = SW_L \ .$$

Now it remains to be shown how the spectral purity $\lambda_0/\Delta\lambda$ and the length of the wave train Λ are related. A range $\Delta\lambda$ of wavelength is related to a range of temporal frequencies like $\Delta\nu_t = \Delta(c/\lambda) = c\,\Delta\lambda/\lambda^2$. A signal of such a range of temporal frequencies has an approximate duration of $\Delta t = 1/\Delta\nu_t$. When propagating with velocity c, the length is $c\Delta t = \Lambda = \lambda_0^2/\Delta\lambda$.

THE DATA STORAGE CAPACITY OF HOLOGRAMS

As you know, in an ordinary photograph one can store only the modulus of the complex light amplitude. But in a hologram, both amplitude and phase are recorded, although indirectly. This is achieved by letting the unknown light wave interfere with a known reference wave. The motivation for making holograms is the desire to reconstruct the original light wave.

In this general formulation of the principle of holography, it is obviously immaterial where the hologram is recorded: at a finite distance behind the object (Fresnel hologram); at infinite distance, that is in the rear focal plane of a lens (Fraunhofer or Fourier hologram); or in the image plane of the object (image hologram). The sequence in which we have mentioned these three types of holograms is the historical one. But for teaching purposes, the opposite sequence is definitely better. We will adapt this sequence when discussing now the data storage capacity of these three types of holograms.

The Image Hologram

The image $u(x)$ might be formed by a lens system with a bandwidth of $|\nu_x| \leq \Delta\nu_L/2$. If the object has a finite extension of $|x| \leq \Delta x_L/2$, the image will have essentially the same extension. Hence, the space-bandwidth product of the image is $SW_L = \Delta x_L \, \Delta\nu_L$. In order to be able to record both amplitude and phase, we superimpose a tilted reference wave $\exp(-2\pi i \nu_r x)$. This yields an intensity on the hologram:

$$I_H(x) = \left| u(x) + e^{-2\pi i \nu_r x} \right|^2 = 1 + u e^{+} + u^{*} e^{-} + |u|^2$$

$$|x| \leq \Delta x_L/2$$

$$\tilde{I}_H(\nu_x) = \int I_H(x)\, e^{-2\pi i \nu_x x}\, dx = \delta(\nu_x) + \tilde{u}(\nu_x - \nu_r) + \tilde{u}^{*}(-\nu_x - \nu_r)$$

$$\tilde{u}(\nu_x - \nu_r) \text{ in } \nu_r - \Delta\nu_L/2 \leq \nu_x \leq \nu_r + \Delta\nu_L/2$$

$$\tilde{u}^{*}(-\nu_x - \nu_r) \text{ in } -\nu_r - \Delta\nu_L/2 \leq \nu_x \leq -\nu_r + \Delta\nu_L/2.$$

The spectrum $\tilde{I}_H(\nu_x)$ is what one observes in the frequency plane of the reconstructing system. In order to be able to single out either u or u^{*}, the two portions $\tilde{u}(\nu_x - \nu_r)$ and $\tilde{u}^{*}(-\nu_x - \nu_r)$ should not overlap. This is achieved by choosing the tilt of the reference wave larger than the largest tilt of any image component in the recording process: $\nu_r \geq \Delta\nu_L/2$.

Now let us find out what space-bandwidth product SW_H of the photographic material is needed. Obviously the width Δx_H has to cover the width of the image to be recorded: $\Delta x_H \geq \Delta x_L$. In order to find the necessary frequency range $\Delta\nu_H$, let us look at the SW_H of the recorded signal $I_H(x)$ with its spectrum $\tilde{I}_H(\nu_x)$. From Fig. 7 follows:

$$\Delta\nu_H = 2\nu_r + \Delta\nu_L$$

$$\Delta\nu_H \geq 2\Delta\nu_L; \text{ due to } \nu_r \geq \Delta\nu_L/2$$

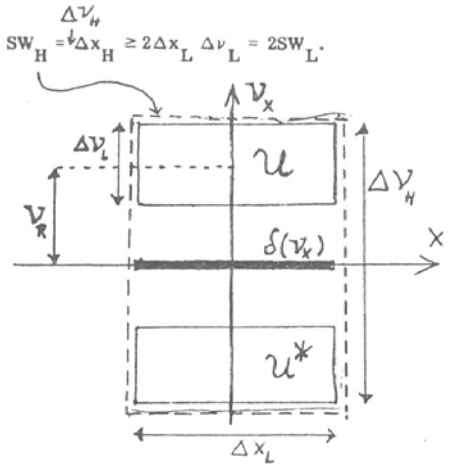

Figure 7.

Even in the most economical case $\nu_r = \Delta\nu_L/2$, one needs twice as much SW_H than the image contains as its SW_L.† Why is that so? Does it have to be that way? Maybe, if the frequency range of the hologram would extend only from 0 to ν_L? Then we would have covered u completely (assuming $u_r = \Delta\nu_L/2$). The loss of u^* is not tragic, because it does not tell us anything new beyond what u can tell us. Unfortunately, we always have to record both u and u^*,

†This case is a good one only if the "quadratic noise" or intermodulation term is very small: $|u|^2 \ll 1$. Otherwise, one would have to make $\nu_r \geq 3\,\Delta\nu_L/2$ in order to leave $|\nu_x| \leq \Delta\nu_L$ free for the quadratic noise.

because the frequency spectrum of the hologram is always symmetrical around the x-axis. This is so because the intensity $I_H(x)$ recorded on the hologram is real:

$$I_H(x) = I_H^*(x) \longrightarrow \left|\tilde{I}_H(\nu_x)\right| = \left|\tilde{I}_H(-\nu_x)\right| .$$

Under perfect recording conditions, this intensity $I_H(x)$ acts later as amplitude transmission in the reconstruction process. But it is still real, which causes the waste of half of the ν_x domain. Well, it is not really a waste, because the SW_L refers to complex degrees of freedom, since u(x) is complex, in general. But SW_H refers to real degrees of freedom, since it represents real intensities or amplitude transmissions. Because a complex number has twice as much freedom as a real number has, this factor 2 in $SW_H \geq 2SW_L$ does not mean a loss or a waste of information.

The Fraunhofer Hologram

The object u(x) may have again an extension $|x| \leq \Delta x_L/2$, and its spectrum $\tilde{u}(\nu_x)$ a bandwidth $|\nu_x| \leq \Delta\nu_L/2$. A lens performs the Fraunhofer diffraction from the object, yielding a complex amplitude in the rear focal plane of the lens: $\tilde{u}(x_F/\lambda f)$. We superimpose a reference wave $\exp(-2\pi i x_r x_F/\lambda f)$ with sufficient tilt: $x_r \geq \Delta x_L/2$. The intensity falling onto the holographic plate is

$$I_H(x_F) = \left| \tilde{u}(x_F/\lambda f) + e^{-2\pi i x_r x_F/\lambda f} \right|^2 = 1 + \tilde{u}e^{+} + \tilde{u}^{*}e^{-} + |\tilde{u}|^2$$

$$\tilde{I}_H(\nu_F) = \int I_H(x_F)\, e^{-2\pi i \nu_F x_F}\, dx_F =$$

$$= \delta(\nu_F) + u(x_r - \lambda f \nu_F) + u^{*}(x_r + \lambda f \nu_r) .$$

The presentation of I_H and $\tilde{I}_H$ in the (x_F, ν_F) domain (Fig. 8) looks very similar, as in the case of the image hologram, shown previously in Fig. 7. But there is a very important difference. Now the necessary

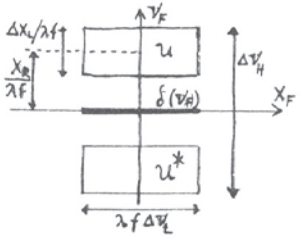

Figure 8.

width Δx_H of the hologram depends on the frequency range $\Delta\nu_L$ of the object:

$$\Delta x_H \geq \lambda f \Delta\nu_L .$$

The frequency range $\Delta\nu_H$ of the material, which records the hologram, is tied to the spatial extension Δx_L of the object:

$$\Delta\nu_H \geq 2x_r/\lambda f + \Delta x_L/\lambda f$$

$$\Delta\nu_H \geq 2\Delta x_L/\lambda f; \text{ due to } x_r \geq \Delta x_L/2$$

$$SW_H = \Delta x_H\, \Delta\nu_H = \Delta\nu_L(2x_r + \Delta x_L) \geq 2\,\Delta\nu_L\, \Delta x_L = 2SW_L .$$

According to this result, Fourier holograms and image holograms are equivalent in terms of storage efficiency, since in both cases the SW_H of the recording material has to be at least twice the SW_L of the objec The physical reason for this factor 2, which was discussed earlier for the image hologram, is the same for the Fourier hologram.

Another important point of view for comparing Fraunhofer and image holograms is the aspect of "data localization". In a Fourier hologram, the data of the object are completely non-localized. In other words, each object point spreads its diffracted light all over the Fraunhofer hologram. In contrast to this, the data in an image hologram are completely localized. Each object element, which is at least as large as the resolution length $\delta x = 1/\Delta\nu_L$, covers an area of the same size on the image hologram.

The feature of the non-localized data distribution in the Fourier hologram is sometimes advantageous, but sometimes not. On one hand, it is the reason for the desirable error insensitivity. Dust, scratches, or film imperfections do not affect very much the quality of an image, reconstructed from a Fraunhofe ogram. On the other hand, it is

impossible to illuminate or address an isolated portion of the image, which is encoded in a Fraunhofer hologram. The full-size image will always appear. This can mean a considerable waste of light.

Finally, we want to emphasize a particular feature of Fraunhofer holograms, which has sometimes been stated wrongly in the literature. The resolution or bandwidth $\Delta\nu_L$ of the reconstructed image does not depend at all on the bandwidth $\Delta\nu_H$ of the film, but only on the size of the film $\Delta x_H \geq \lambda f \Delta\nu_L$. The film bandwidth $\Delta\nu_H$ determines only the permissible object size $\Delta x_L \leq \lambda f \Delta\nu_H/2$. But for image holograms, there are direct relationships: $\Delta x_L \leq \Delta x_H$; $\Delta\nu_L \leq 2\Delta\nu_H$. As we will see, for Fresnel holograms, it is somewhere in between.

The Fresnel Hologram

The configuration is shown in Fig. 9. The object has a width described by $|x_0| \leq \Delta x_0/2$ and a frequency range of $|u_0| \leq \Delta x_0/2$. The widths of the prism and of the holographic plate are equal: $\Delta x_p = \Delta x_H$. The prism, which is directly beside the object, provides a tilted reference wave. The tilt angle $\lambda\nu_r = (\Delta x_0 + \Delta x_H)/2z$ is chosen so that the holographic plate at a distance z is fully illuminated. The hologram is wider than the object $\Delta x_H > \Delta x_0$, in order to catch all spatial frequencies: $(\Delta x_H - \Delta x_0)/2z \geq \lambda \Delta\nu_0/2$ (from every object area).

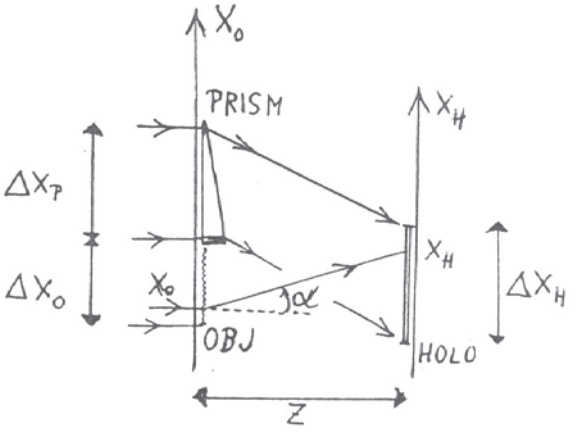

Figure 9.

Our first problem is to find out how the $SW_0 = \Delta x_0\, \Delta\nu_0$ changes its shape while the light propagates from the object plane OBJ to the hologram plane HOLO. We use now a semi-quantitative description, which could be improved in rigour if desired by using an approach similar to the one in Ref. 5. Let us start with a particular "point" in the (x_0, ν_0) domain, but within the SW_0 area: $|x_0| \leq \Delta x_0/2$; $|\nu_0| \leq \Delta\nu_0/2$. This "point" may have an aerial size of one, such representing one degree of freedom, or one free parameter. In more physical terms, this "point" may cover the x_0 region: $x_0 \pm D/2$. If a light bundle passes the object area of size D around x_0, it will

have an angular uncertainty of $\delta\alpha = \lambda/D$. This means a lateral uncertainty at a distance z of $z\lambda/D$. If we want our bundle to stay together, this lateral uncertainty should not exceed the size D of the bundle itself: $z\lambda/D < D$, or $z < D^2/\lambda$. This is the well-known near-field condition, describing the range of FRESNEL diffraction. Hence, our light bundle is a justified model in the realm of Fresnel diffraction.

This particular bundle of width D hits the object under normal incidence, and then interacts with the spatial frequency ν_0. We interpret $\nu_0 = 1/d$ as the inverse of a grating constant d. Then we know the bundle will be deviated due to grating diffraction by an angle $\alpha(\nu_0) = \lambda/d = \lambda\nu_0$. At a distance z, where the hologram is, this results in a lateral shift of $z(\nu_0) = \lambda z\nu_0$. In other words, a light bundle, which interacts at the object point x_0 with the object frequency ν_0, will hit the hologram at $x_H = x_0 + \lambda z\nu_0$. Hence the process of propagation from plane $z = 0$ to plane z can be described as:

$(x_0, \nu_0) \rightarrow (x_0 + \lambda z\nu_0, \nu_0)$.

The spatial frequency ν_0, which determines the angle of inclination, remains of course unchanged while the light propagates from OBJ to HOLO. There the wave will be superimposed by the reference wave $\exp(-2\pi i\nu_r x_H)$, and then recorded together as intensity:

$$\left| e^{2\pi i\nu_0 x_H} + e^{-2\pi i\nu_r x_H} \right|^2 = 2\left[1 + \cos\left\{2\pi(\nu_0 + \nu_H)\, x_H\right\}\right] .$$

This fraction of the recorded intensity contains the spatial frequencies: $0;\ +(\nu_0 + \nu_r);\ -(\nu_0 + \nu_r)$. This statement would have been correct, too, even if we would have included an amplitude factor $a(\nu_0)$ of our light bundle. Anyway, the object frequency ν_0 appears due to the interference process, as three different frequencies on the hologram:

$$\nu_0 \rightarrow \nu_H = \begin{cases} +\nu_0 + \nu_r \\ 0 \\ -\nu_0 - \nu_r . \end{cases} \quad \Big\| \quad x_0 \rightarrow x_H = x_0 + \lambda z\nu_0$$

Now we use both transitions $x_0 \rightarrow x_H$ and $\nu_0 \rightarrow \nu_H$ to find out how the whole rectangular SW_0 of the object is deformed into the SW_H, which has to be recorded on the hologram. As we see in Fig. 10, the

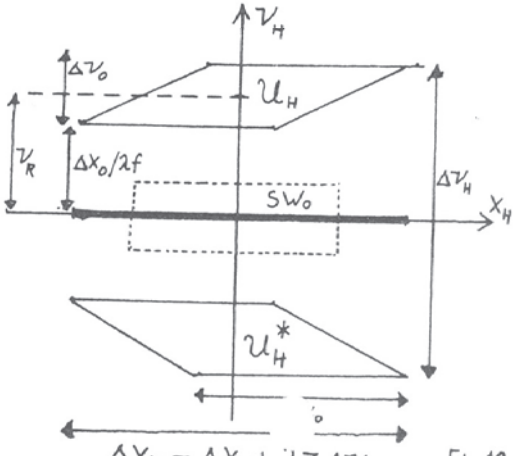

Fig. 10

SW_H consists of a $\delta(\nu_H)$ line and two islands on both sides of the x_H axis, each island representing one of the twin images.

We see also that the shape of these islands is not rectangular any more. On the other hand, the SW of the recording plate is always rectangular, like $|x_H| \leq \Delta x_H/2$ and $|\nu_H| \leq \Delta\nu_H/2$. This means, that some areas of the SW of the film will not be used by the SW_H of the incoming intensity. This indicates an inefficiency of data storage. The only exceptions are the trivial cases $\Delta x_0 = 0$, or $\Delta\nu_0 = 0$. From Fig. 10, we derive:

$$SW_H = (\Delta x_0 + \lambda z \Delta\nu_0)(\Delta\nu_0 + 2\nu_r) .$$

This can be modified by using earlier definitions:

$$SW_0 = \Delta x_0 \, \Delta\nu_0$$

$$2\nu_r = (\Delta x_0 + \Delta x_H)/\lambda z$$

$$(\Delta x_H - \Delta x_0)/z = \lambda \Delta\nu_0$$

$$SW_H = (\Delta x_0 + \lambda z \Delta\nu_0)(2\Delta\nu_0 + 2\Delta x_0/\lambda z)$$

$$= 2SW_0 [2 + \xi + 1/\xi] \geq 8SW_0$$

$$\xi = \lambda z \Delta\nu_0/\Delta x_0; \quad \xi_{OPTIMUM} = 1$$

$\xi = 1$ means $\Delta x_H = 2\Delta x_0$.

Whereas we had found for FOU and IMG:

$$\frac{2SW_0}{SW_H} \leq 1,$$ it is now for FRS:

$$\frac{2SW_0}{SW_H} = \frac{1}{2+\xi+1/\xi} \leq \frac{1}{4} .$$

As we see from these formulae, the SW_H of the recording film has to be considerably larger than the SW_0 of the object. The reason is that the intensity arriving at the recording film has an SW of such a crummy shape (see Fig. 10), which is badly suited for being embraced by the rectangular SW_H of the hologram. In other words, the SW_H of the film is very inefficiently used for storing data in the form of a Fresnel hologram.

CONCLUSIONS

The space-bandwidth product is of fundamental and practical importance in data processing. With only little mathematics, it gives a good understanding of many situations, for example, in spatial filtering and in holography. The coherence requirements for the recording and reconstruction of holograms are also amenable to an SW study.

The applicability of the SW concept is based on the linearity of the process to be considered. But this requirement is not very critical. For example, quadratic processes do not cause any trouble, as we have

seen. Space-invariance of the system is not required. But noise problems are beyond the realm of this type of study.

On several occasions, the mathematics was sloppy. For example, an image cannot have a sharply limited finite extension in x, if it formed by a lens with sharply limited bandwidth. This is true, even if the object might have been sharply limited in x. However, this mathematical finesse is of no practical concern, if the SW is large compared to one. But it should be mentioned that Wolter and others have found some superresolution methods based on analytical extrapolation.[3,9] Their approach makes essential use of those small data which were neglected due to our approximation. Wolter's method is certainly very exciting, but useful only if one is willing to do a lot of a-*posteriori* data processing. Even then the unavoidable noise might keep the success small.

A newer and more accurate form of these "Space Bandwidth Product" considerations is called "Structural Information Theory".[10]

APPENDIX: DERIVATION OF THE SAMPLING THEOREM

Assume a function $f(\alpha)$, which is zero outside of the interval $|\alpha| \leq \Delta\alpha/2$. Hence, $f(\alpha) = f(\alpha)\ \mathrm{rect}\ (\alpha/\Delta\alpha)$; whereby

$$\mathrm{rect}\ (x) = \begin{cases} 1 & \text{if } |x| \leq 1/2 \\ 0 & \text{otherwise} \end{cases} .$$

We can add at the right-hand side of the equality many shifted functions $f(\alpha - n\Delta\alpha)$ without disturbing the equality, because the $\mathrm{rect}(\alpha/\Delta\alpha)$ eliminates all terms $n \neq 0$ anyway:

$$f(\alpha) = \mathrm{rect}\ (\alpha/\Delta\alpha) \sum (n)\ f(\alpha - n\Delta\alpha) .$$

From this identity we will derive the sampling theorem by performing a Fourier transformation on both sides of the equality sign. On the left-hand side, one simply gets:

$$\int f(\alpha)\, e^{-2\pi i\alpha\beta}\, d\alpha = g(\beta) .$$

Before transforming the right-hand side, we modify the sum:

$$\sum (n)\ f(\alpha - n\Delta\alpha) = \sum \int g(\gamma)\, e^{2\pi i\gamma(\alpha - n\Delta\alpha)}\, d\gamma$$

$$= \int g(\gamma) \left[\sum_{-\infty}^{+\infty} (n)\, e^{-2\pi i\gamma n\Delta\alpha} \right] e^{2\pi i\gamma\alpha}\, d\gamma$$

$$\left[\sum_{-\infty}^{+\infty}(n)\ldots\right] = \sum_{-\infty}^{+\infty}(m)\ \delta(\gamma\,\Delta\alpha - m) = \frac{1}{\Delta\alpha}\sum\delta(\gamma - \frac{m}{\Delta\alpha}) \ .$$

This is so because for $\gamma\,\Delta\alpha$ = integer (or m), all exponentials in $\sum_{-\infty}^{+\infty}(n)$ add up, whereas for non-integer values they will cancel each other. Now the integration over γ can be performed, giving:

$$\sum(n)\ f(\alpha - n\Delta\alpha) = \frac{1}{\Delta\alpha}\sum(m)\ g(\frac{m}{\Delta\alpha})\ e^{2\pi i m\frac{\alpha}{\Delta\alpha}} \ .$$

The rect-function does nothing but limit the range of integration over α:

$$\int_{-\infty}^{+\infty} \text{rect}\,(\alpha/\Delta\alpha)\ldots d\alpha = \int_{-\Delta\alpha/2}^{+\Delta\alpha/2}\ldots d\alpha \ .$$

Hence, the Fourier transform

$$\int_{-\infty}^{+\infty}\ldots e^{-2\pi i\alpha\beta}\ d\alpha$$

of the right-hand side of our identity yields:

$$\sum_{-\infty}^{+\infty}(m)\ g(\frac{m}{\Delta\alpha})\quad \text{sinc}\left\{\pi\ \Delta\alpha(\beta - \frac{m}{\Delta\alpha})\right\} = g(\beta) \ .$$

This equation, the so-called sampling theorem, says that the function $g(\beta)$ of the continuous variable β can be calculated for very β, if $g(\beta)$ is known only at its sampling points $\beta_m = m/\Delta\alpha$. In order to prove it, we had to assume that the Fourier transform

$$f(\alpha) = \int g(\beta)\ e^{2\pi i\alpha\beta}\ d\beta$$

was zero outside of $-\Delta\alpha/2 \leq \alpha \leq +\Delta\alpha/2$.

References

1. M. von Laue, Ann. der Phys. 44, 1197 (1914).

2. D. Gabor, Progr. in Optics I, 109 (1961).

3. H. Wolter, Progr. in Optics. I, 155 (1961).

4. H. Gamo, Progr. in Optics III, 189 (1964).

5. A.W. Lohmann and D.P. Paris, J. Opt. Soc. Am. 55, 1007 (1965).

6. P. Connes, Duong Hong Tuan and J. Pinard, J. Physique Radium 23, 173 (1962).

7. J.S. Courtney - Pratt, J.S.M.P.T.E. 72, 876 (1963).

8. W. Lukosz, J. Opt. Soc. Am. 56, 1463 (1966).

9. J.L. Harris, J. Opt. Soc. Am. 54, 931 (1964);
R.A. Williams, W.S.C. Chang, J. Opt. Soc. Am. 56, 167 (1966);
C.W. Barnes, J. Opt. Soc. Am. 56,575, 1421A (1966).

10. J.T. Winthrop, IBM J.R. & D. 14, 501 (1970);
J. Opt. Soc. Am. 61, 15 (1971).

Whoever likes the space bandwidth product, will enjoy also the WIGNER distribution function, introduced into information optics by M.J. Bastiaans. As first reading we recommend:"The Wigner distribution function and its optical production", by H.O.Bartelt, K.-H.Brenner, A.W.Lohmann; Opt.Comm.32(1980)32.